

**Some pages of this thesis may have been removed for copyright restrictions.**

If you have discovered material in AURA which is unlawful e.g. breaches copyright, (either yours or that of a third party) or any other law, including but not limited to those relating to patent, trademark, confidentiality, data protection, obscenity, defamation, libel, then please read our [Takedown Policy](#) and [contact the service](#) immediately

# **THE DEVELOPMENT AND APPLICATIONS OF THE COMBINED USE OF NMR AND ULTRASOUND**

**Claire Louise Burrows**

**Doctor of Philosophy**

**The University of Aston in Birmingham**

**February 2002**

**This copy of the thesis has been supplied on condition that anyone who consults it is understood to recognise that its copyright rests with its author and that no quotation from the thesis and no information derived from it may be published without proper acknowledgement.**

## Acknowledgements

I would like to express my sincere gratitude to my supervisor Professor John Homer and, after his retirement, Dr. Martin Beevers and also my co-supervisor Dr. Michael Perry for their continued advice and support during the period of this PhD. I am also grateful to my colleague Paul Douglas who has helped to keep me sane during the long days working in the laboratory.

I would also like to thank a number of other support staff; Denise Ingram for the loan of equipment and chemicals and most of all for listening, Mike Lea for his technical skills with the temperamental NMR spectrometer and to Roger Wheeler for his help in designing and constructing equipment.

My thanks are also due to Bruker for their funding and continual support and to the E.P.S.R.C. for their award of a studentship.

Finally, thanks to my family and my partner Stephen Whetton for their love and support during the course of my PhD.

## Abstract

The objective of the research carried out in this report was to observe the first ever in-situ sonochemical reaction in the NMR Spectrometer in the megahertz region of ultrasound. Several reactions were investigated as potential systems for a sonochemical reaction followed by NMR spectroscopy.

The primary problem to resolve when applying ultrasound to a chemical reaction is that of heating. Ultrasound causes the liquid to move and produces 'hot spots' resulting in an increase in sample temperature. The problem was confronted by producing a device that would counteract this effect and so remove the need to account for heating. However, the design of the device limited the length of time during which it would function. Longer reaction times were required to enable observations to be carried out in the NMR spectrometer.

The first and most obvious reactions attempted were those of the well-known ultrasonic dosimeter. Such a reaction would, theoretically, enable the author to simultaneously observe a reaction and determine the exact power entering the system for direct comparison of results. Unfortunately, in order to monitor the reactions in the NMR spectrometer the reactant concentrations had to be significantly increased, which resulted in a notable increase in reaction time, making the experiment too lengthy to follow in the time allocated.

The Diels-Alder Reaction is probably one of the most highly investigated reaction systems in the field of chemistry and it was this to which the author turned her attention. Previous authors have carried out ultrasonic investigations, with considerable success, for the reaction of anthracene with maleic anhydride. It was this reaction in particular that was next attempted. The first ever sonochemically enhanced reaction using a frequency of ultrasound in the megahertz (MHz) region was successfully carried out as bench experiments. Due to the complexity of the component reactants the product would precipitate from the solution and because the reaction could only be monitored by its formation, it was not possible to observe the reaction in the NMR spectrometer.

The solvolysis of 2-chloro-2-methylpropane was examined in various solvent systems; the most suitable of which was determined to be aqueous 2-methylpropan-2-ol. The experiment was successfully enhanced by the application of ultrasound and monitored in-situ in the NMR spectrometer. The increase in product formation of an ultrasonic reaction over that of a traditional thermal reaction occurred. A range of 1.4 to 2.9-fold improvement was noted, dependent upon the reaction conditions investigated.

An investigation into the effect of sonication upon a large biological molecule, in this case aqueous lysozyme, was carried out. An easily observed effect upon the sample was noted but no explanation for the observed effects could be established.

## Contents Page

<b>Chapter 1</b>	<b>The Theory of Nuclear Magnetic Resonance Spectroscopy .....</b>	<b>22</b>
1.1	The Basic Theory of NMR Spectroscopy .....	23
1.2	Relaxation.....	28
1.2.1	Introduction .....	28
1.2.2	Nuclear Relaxation .....	29
1.3	Pulse Fourier Transform Spectroscopy .....	30
1.4	The Chemical Shift.....	31
1.4.1	Nuclear Shielding .....	31
1.4.2	The $\delta$ -Scale and Reference Materials .....	34
1.4.3	The Origin of the Chemical Shift .....	36
1.4.4	The Ring Current Effects in Arenes .....	39
1.4.5	The Effect of Magnetic Anisotropy of Neighbouring Groups.....	40
1.4.6	Intermolecular and Intramolecular Interactions.....	42
1.4.7	Solvent Effects.....	44
1.5	The Distortionless Enhancement by Polarisation Transfer (DEPT).....	44
<b>Chapter 2</b>	<b>The Theory of Ultrasound .....</b>	<b>48</b>
2.1	Cavitation .....	50
2.2	Parameters Affecting Cavitation .....	57
2.3	The Generation of Ultrasonic Waves .....	60
2.4	Power Ultrasonic Equipment.....	64
2.5	The Measurement of Ultrasonic Power.....	66
2.5.1	The Physical Measurement of Ultrasonic Power.....	66
2.5.2	The Chemical Measurement of Ultrasonic Power.....	67
2.6	The Combination of NMR Spectroscopy and Ultrasound .....	71

<b>Chapter 3</b>	<b>The Theory of S<sub>N</sub>1 and S<sub>N</sub>2 Mechanisms.....</b>	<b>72</b>
3.1	Types of Mechanisms.....	73
3.2	The S <sub>N</sub> 1 Mechanism.....	73
3.2.1	Kinetic Evidence for the S <sub>N</sub> 1 Mechanism .....	74
3.2.2	Stereochemical Evidence for the S <sub>N</sub> 1 Mechanism.....	76
3.3	The S <sub>N</sub> 2 Mechanism.....	80
3.3.1	Kinetic Evidence for the S <sub>N</sub> 2 Mechanism .....	81
3.3.2	Stereochemical Evidence for the S <sub>N</sub> 2 Mechanism.....	82
3.4	Factors Affecting the Rates of S <sub>N</sub> 1 and S <sub>N</sub> 2 Reactions.....	83
3.4.1	The Role of the Solvent in S <sub>N</sub> 1 and S <sub>N</sub> 2 Reactions .....	84
3.4.2	The Effect of Temperature upon Reaction Rate .....	86
3.4.3	The Effect of the Substrate Structure.....	87
3.4.4	The Effect of the Leaving Group.....	90
3.5	Summary of the Overall Factors Affecting Reaction Rate.....	90
<b>Chapter 4</b>	<b>The Diels-Alder Reaction.....</b>	<b>92</b>
4.1	The Diels-Alder Reaction Mechanism .....	93
4.1.1	Orbital Symmetry Requirements of Pericyclic Reactions.....	97
4.1.2	Alternative Mechanisms for the Diels-Alder Reaction.....	102
4.2	The Study of The Diels-Alder Reaction of Maleic Anhydride with Anthracene	103
4.3	The Reversibility of the Diels-Alder Reaction.....	104
4.4	Factors Affecting the Rates of Diels-Alder Reactions .....	105
4.5	The Sonochemical Modification of the Diels-Alder Reaction .....	106
4.6	Monitoring the Progress of the Reaction by Ultraviolet Spectroscopy .....	110
4.7	The Treatment of Kinetic Data for the Diels-Alder System.....	111
<b>Chapter 5</b>	<b>The Solvolysis Reaction of 2-Chloro-2-Methylpropane.....</b>	<b>115</b>
5.1	The Reaction Mechanism of 2-Chloro-2-Methylpropane .....	116

5.2	The Effects of the Solvent on the Reaction Rate.....	121
5.3	The Ultrasonically Enhanced Solvolysis of t-BuCl.....	127
5.4	The Treatment of Kinetic Data for the t-BuCl System.....	131
<b>Chapter 6</b>	<b>The Construction of an Experimental Thermal Dissipation Device to Reduce Sample Heating Caused by Sonication.....</b>	<b>135</b>
6.1	Eliminating the Temperature Increase Induced by the Application of Ultrasonic Energy by a Glass Adapter .....	136
6.2	Eliminating the Temperature Increase Induced by the Application of Ultrasonic Energy by a PTFE Adapter .....	137
6.3	The Reduction of Sample Heating Employing a PTFE Adapter.....	138
6.4	Discussion and Conclusions.....	141
<b>Chapter 7</b>	<b>The Chemical Dosimeter as an in-situ Ultrasonic Reaction in the Nuclear Magnetic Resonance Spectrometer. ....</b>	<b>143</b>
7.1	The Ultrasonic Irradiation of 4-Nitrophenol in Aqueous Solution .....	144
7.1.1	The Ultrasonic Reaction of 4-Nitrophenol Outside the NMR Spectrometer.....	145
7.1.2	The Ultrasonic Reaction of 4-Nitrophenol in the NMR Spectrometer.....	146
7.2	The Ultrasonic Irradiation of Terephthalic Acid in Aqueous Solution .....	148
7.2.1	The Ultrasonic Reaction of Terephthalic Acid in the NMR Spectrometer..	148
7.3	Discussion and Conclusions.....	150
<b>Chapter 8</b>	<b>The Investigation of the Ultrasonically Induced Diels-Alder Reaction of Maleic Anhydride with Anthracene .....</b>	<b>151</b>
8.1	Confirmation of the Existence of Cavitation.....	152
8.2	The Formation of 9,10-Dihydroanthracene-endo- $\alpha,\beta$ -succinic Anhydride .....	152
8.2.1	Proving the Identity of the 9,10-Dihydroanthracene-endo- $\alpha,\beta$ -succinic Anhydride .....	152
8.3	Following the Progress of the Diels-Alder Reaction of Maleic Anhydride with Anthracene .....	154
8.4	The Calibration of the UV/Vis Spectrometer with Respect to the Concentration of Anthracene .....	155

8.5	The Thermal Diels-Alder Reaction of Maleic Anhydride with Anthracene in Toluene.....	156
8.5.1	Identification of the Precipitate Produced During Reaction.....	160
8.6	The Diels-Alder Reaction of Maleic Anhydride with Anthracene in o-Xylene. ....	162
8.6.1	The Thermally Induced Diels-Alder Reaction of Maleic Anhydride with Anthracene in o-Xylene.....	163
8.6.2	The Ultrasonically Induced Diels-Alder Reaction of Maleic Anhydride with Anthracene in o-Xylene.....	166
8.6.3	Comparison of the Thermally and Ultrasonically Induced Diels-Alder Reaction of Maleic Anhydride with Anthracene in o-Xylene.....	168
8.6.4	The Effect of Changing the Solvent on the Thermodynamic Parameters on the Thermally Induced Diels-Alder Reaction of Maleic Anhydride with Anthracene.....	170
8.7	The NMR Spectroscopic Analysis of the Diels-Alder Reaction of Maleic Anhydride with Anthracene in o-Xylene.....	170
8.8	Discussion and Conclusions.....	174
<b>Chapter 9</b>	<b>The Ultrasonically Induced Solvolysis of 40% (v/v) t-BuCl in Propan-2-ol with 40% (w/w) Aqueous Propan-2-ol.....</b>	<b>183</b>
9.1	Determination of a Suitable Solvent System for the Solvolysis of t-BuCl.....	184
9.2	The Construction of a Novel Conductivity Cell.....	185
9.3	The Bench Top Reaction of 40% (v/v) t-BuCl/Propan-2-ol with 40% (w/w) Propan-2-ol/Water.....	187
9.3.1	The Thermally Induced Bench Top Reaction.....	187
9.3.2	The Ultrasonically Induced Bench Top Reaction of 40% (v/v) t-BuCl/Propan-2-ol with 40% (w/w) Propan-2-ol/Water.....	190
9.3.3	Comparison of the Thermally- and Ultrasonically-Induced Bench Top Reactions.....	193
9.4	The Reaction of 40% (v/v) t-BuCl/Propan-2-ol with 40% (w/w) Propan-2-ol/Deuterated Water in the NMR Spectrometer.....	195
9.4.1	Analysis of the Combined Propan-2-ol/2-Methylpropan-2-ol in the NMR Spectrometer.....	195
9.4.2	Analysis of the Thermally Induced Reaction of t-BuCl in the NMR Spectrometer.....	197
9.4.3	Analysis of the Ultrasonically Induced Reaction of t-BuCl in the NMR Spectrometer.....	201
9.4.4	Comparison of the Thermally and Ultrasonically Induced Reaction of 2-Chloro-2-methylpropane in the NMR Spectrometer.....	205



9.5	Discussion and Conclusions.....	207
9.6	The Chemical Shift of the Water Peak for the Reaction of 40% (v/v) t-BuCl/Propan-2-ol with 40% (w/w) Propan-2-ol/Deuterated Water in the NMR Spectrometer.....	216
9.6.1	Analysis of the Chemical Shift of the Water Peak for the Thermally Induced Reaction in the NMR Spectrometer.....	216
9.6.2	Analysis of the Chemical Shift of the Water Peak for the Ultrasonically Induced Reaction in the NMR Spectrometer.....	220
9.6.3	The Comparison of the Chemical Shift of the Water Peak for the Thermally and Ultrasonically Induced Reaction in the NMR Spectrometer.....	222
<b>Chapter 10</b>	<b>The Effects of Ultrasonic Irradiation upon an Aqueous Solution of Lysozyme .....</b>	<b>224</b>
10.1	The Structure of Lysozyme .....	225
10.2	Analysis of the Effects of Ultrasonic Irradiation Upon an Aqueous Solution of Lysozyme .....	227
10.3	Establishing an External Standard.....	230
10.4	Conclusions and Discussion.....	235
<b>Chapter 11</b>	<b>Conclusions and Further Work.....</b>	<b>237</b>
11.1	The Elimination of Sample Heating Caused by Ultrasonic Irradiation.....	238
11.2	The Chemical Dosimeter as an in-situ Ultrasonic Reaction in the NMR Spectrometer.....	240
11.3	The Diels Alder Reaction of Maleic Anhydride with Anthracene .....	241
11.4	The Ultrasonically Induced Solvolysis of 40% (v/v) t-BuCl in Propan-2-ol with 40% (w/w) Aqueous Propan-2-ol.....	245
11.5	Comparison of the Diels-Alder Reaction of Maleic Anhydride with Anthracene to the Solvolysis of t-BuCl .....	250
11.6	The Sonication of Aqueous Lysozyme.....	251

## List of Equations

Equation 1:	Spin Angular Momentum.....	23
Equation 2:	The Magnetic Moment.....	24
Equation 3:	The Larmor Frequency.....	25
Equation 4:	The Boltzmann Distribution.....	25
Equation 5:	The Net Magnetisation.....	26
Equation 6:	The Angular Frequency.....	27
Equation 7:	The Pulse Angle.....	27
Equation 8:	The Three Components of the Bulk Magnetisation.....	29
Equation 9:	The Exponential Decay of spin-lattice Relaxation.....	29
Equation 10:	Magnetisation Along the y'-axis Immediately After Applying a RF Pulse.....	30
Equation 11:	The Exponential Decay of spin-spin Relaxation.....	30
Equation 12:	The Magnetic Field Experienced as a Result of Shielding of a Nucleus.....	32
Equation 13:	The Resonance Condition Incorporating the Shielding Constant.....	32
Equation 14:	The Chemical Shift.....	34
Equation 15:	The Chemical Shift Simplified.....	35
Equation 16:	The Shielding Constant.....	37
Equation 17:	The Overall Shielding Constant.....	39
Equation 18:	The Shielding due to the Magnetic Anisotropy of Neighbouring Groups.....	41
Equation 19:	The Sensitivity of a Nucleus.....	44
Equation 20:	The Total Pressure in a Liquid upon Application of a Sound Wave.....	50
Equation 21:	The Applied Acoustic Pressure.....	51
Equation 22:	The Variation of Intensity with Respect to Distance from the Source.....	51
Equation 23:	Ultrasonic Intensity as a Function of Liquid Density and Velocity.....	51
Equation 24:	Experimental Evaluation of Intensity.....	52
Equation 25:	Experimental Evaluation of Power.....	52
Equation 26:	The Maximum Temperature Attained Upon Collapse of a Cavity.....	55
Equation 27:	The Maximum Pressure Attained Upon Collapse of a Cavity.....	55
Equation 28:	Estimate of the Maximum Temperature Caused by a Stable Cavity.....	56
Equation 29:	The Simple Rate Equation of a First-order Reaction.....	74
Equation 30:	The Complete Rate Equation of a First-order Reaction.....	75

Equation 31: The Rate Equation of a Second-order Reaction.....	82
Equation 32: The Rate Equation of a Pseudo First-order Reaction. ....	82
Equation 33: The Gibb's Free Energy Change of Activation. ....	85
Equation 34: The Arrhenius Equation.....	86
Equation 35: The Logarithmic form of the Arrhenius Equation. ....	87
Equation 36: The Second-order Rate Equation for the Diels-Alder Reaction. ....	111
Equation 37: The Natural Logarithmic Arrhenius Equation for the Diels-Alder Reaction. . .....	112
Equation 38: The Second-order Rate Constant. ....	112
Equation 39: The Wynne-Jones Eyring Equation for the Diels-Alder Reaction.....	112
Equation 40: The Enthalpy of Activation with Respect to the Change in Energy and Volume for the Reaction.....	112
Equation 41: The Change in Enthalpy of Activation with respect to Activation Energy. .... .....	113
Equation 42: The Wynne-Jones Eyring Equation Expressed with respect to Activation Energy.....	113
Equation 43: Calculation of the Entropy of Activation, $\Delta S^\ddagger$ .....	113
Equation 44: Calculation of the Activation Energy, $E_a$ .....	114
Equation 45: The Grunwald Equation.....	125
Equation 46: The Integrated Rate Equation for the Solvolysis of t-BuCl.....	131
Equation 47: Molar Conductance with Respect to the Cell Constant, Conductance and concentration of $H^+Cl^-$ at time, t. ....	132
Equation 48: Molar Conductance in a Dilute Solution. ....	132
Equation 49: The Integrated Rate Equation in Terms of Conductivity.....	133
Equation 50: The First Order Rate Equation of Absorption Peak Integral versus Time.	198
Equation 51: The Entropy Change of Activation.....	209
Equation 52: The Enthalpy Change of Activation. ....	209
Equation 53: Calculation of Enthalpy Change.....	242
Equation 54: The Wynne-Jones Eyring Equation with respect to Activation Energy. ...	251

## List of Figures

Figure 1:	The Generation of the Magnetic Moment $\mu$ from the Spin I.....	24
Figure 2:	The Precession of Identical Spins in a Magnetic Field $B_0$ .....	25
Figure 3:	The Net z-Magnetisation in the Rotating Frame. ....	26
Figure 4:	The Effect of the Application of a Radio Frequency Pulse upon the Net z-Magnetisation .....	27
Figure 5:	The Effects of the Secondary Field upon the Applied Field $B_0$ .....	32
Figure 6:	Chemically Shifted Compounds According to their Shielding.....	33
Figure 7:	The Reduced Effect of $B_0$ by an Opposing Field $B_{app}$ . ....	37
Figure 8:	The Effect of the Induced Ring Current on Shielding. ....	39
Figure 9:	The Effect of Magnetic Anisotropy of Neighbouring Groups.....	42
Figure 10:	<i>o</i> -hydroxyacetophenone.....	43
Figure 11:	Acetylacetone (enol). ....	44
Figure 12:	The DEPT Pulse Sequence .....	46
Figure 13:	The Formation of Cavities by the Irradiation of a Liquid with Ultrasound....	52
Figure 14:	The Mechanical and Chemical Effects from the Implosion of a Cavity.....	53
Figure 15:	The Sonication of Water. ....	54
Figure 16:	Schematic Diagram of a Liquid Whistle.....	61
Figure 17:	The Piezoelectric Transducer. ....	62
Figure 18:	The Magnetostrictive Transducer. ....	63
Figure 19:	A Flat-Bottomed Flask in an Ultrasonic Bath. ....	64
Figure 20:	The Iodine Dosimeter Reaction with Hydrogen Peroxide.....	68
Figure 21:	The Sonolysis of Aqueous $CCl_4$ . ....	68
Figure 22:	Reaction Mechanism for the Weissler Reaction.....	68
Figure 23:	The Reaction of the Terephthalate Dosimeter .....	69
Figure 24:	The Reaction of the Nitrophenol Dosimeter.....	69
Figure 25:	The Reaction of the Fricke Dosimeter.....	70
Figure 26:	Scavenging of Hydrogen Atoms by Molecular Oxygen in the Iodine Dosimeter.....	71
Figure 27:	The Two-Stage $S_N1$ Mechanism.....	73
Figure 28:	Nucleophilic Aliphatic Substitution by Solvolysis. ....	73

Figure 29:	Hypothetical Energy Diagrams for the S <sub>N</sub> 1 Mechanism. ....	74
Figure 30:	The Competing Reaction in the Solvolysis S <sub>N</sub> 1 Mechanism. ....	75
Figure 31:	The Ion Pair Theory. ....	77
Figure 32:	The Substitution and Elimination Products from the Solvolysis S <sub>N</sub> 1 Reaction. ....	78
Figure 33:	All Possible Products Which Result from the S <sub>N</sub> 1 Solvolysis Reaction. <sup>38</sup> ....	79
Figure 34:	The S <sub>N</sub> 2 Mechanism by <i>Backside</i> Attack of the Nucleophile. ....	81
Figure 35:	Hypothetical Energy Diagrams for the S <sub>N</sub> 2 Mechanism. ....	81
Figure 36:	The Walden Inversion of l(-)-Hydroxybutanedioic Acid. ....	83
Figure 37:	Boltzmann Distribution of Energies. ....	86
Figure 38:	The Relative Solvolysis Rates of Various Cyclic Compounds with Respect to 2-Chloro-2-methylpropane. <sup>48</sup> ....	89
Figure 39:	The Diels-Alder Reaction to Form the Required Reactant for Synthetic Reserpine Production. ....	93
Figure 40:	The General Diels-Alder Reaction. ....	94
Figure 41:	The Stabilisation of the Transition State by Secondary Interactions. ....	97
Figure 42:	Absence of Stabilisation of the Transition State by Secondary Interactions. .	97
Figure 43:	A Symmetry Forbidden [2+2] Thermal Reaction. ....	99
Figure 44:	A Symmetry Allowed [4+2] Thermal Reaction. ....	99
Figure 45:	Twisting of a Symmetry Forbidden [2+2] Thermal Reaction to Enable Reaction. ....	100
Figure 46:	Photochemical Promotion of an Electron in the Ground State, from the HOMO to the LUMO, to Form of the Excited State Molecule. ....	100
Figure 47:	A Symmetry Allowed [2+2] Photochemical Reaction. ....	101
Figure 48:	The Diels-Alder Reaction via a Diradical Transition State. ....	103
Figure 49:	The Resonance Structures of Maleic Anhydride. ....	104
Figure 50:	The Reaction of Anthracene with Maleic Anhydride to form 9,10-Dihydroanthracene-9,10-endo- $\alpha,\beta$ -succinic anhydride. ....	104
Figure 51:	The Double Bond Rule Applied to a Typical Maleic Anhydride Adduct. ...	105
Figure 52:	The Diels-Alder Reaction via a Radical Cation. ....	106
Figure 53:	The Ultrasonic Reaction of a Vinylcyclohexene with an <i>o</i> -quinone. ....	107

Figure 54:	The Effect of Ultrasonic Irradiation on the Reaction of Maleic Anhydride with Anthracene. <sup>81</sup> .....	109
Figure 55:	The S <sub>N</sub> 1 Solvolysis Reaction of t-BuCl. ....	117
Figure 56:	The Substitution and Elimination Products from the Solvolysis S <sub>N</sub> 1 Reaction of t-BuCl. ....	118
Figure 57:	<i>Backside</i> and <i>Frontside</i> Nucleophilic Attack of the <i>tert</i> -Butyl Carbocation. ....	119
Figure 58:	The Energy Profile for the Three-Step S <sub>N</sub> 1 Reaction for the Solvolysis of t-BuCl with Water. ....	119
Figure 59:	The Assistance of Hydrogen Bonding in the Weakening and Ultimate Cleavage of the C-Cl Bond. ....	120
Figure 60:	The Production of the Carbocation from Alkanes in Superacid. ....	121
Figure 61:	The Effect of Changing Aqueous Solvent Composition upon the Enthalpy Change $\Delta H^\ddagger$ for the Solvolysis of t-BuCl. ....	124
Figure 62:	The Absorption Properties of Various Aqueous Alcohols. ....	127
Figure 63:	Concentrations of the Components of the t-BuCl Throughout the Reaction	131
Figure 64:	The Possible Products for the Solvolysis of t-BuCl. ....	132
Figure 65:	The Glass Adapter for the Reduction of Sample Heating. ....	136
Figure 66:	The PTFE Adapter for the Reduction of Sample Heating. ....	138
Figure 67:	The Heating of a 10 cm <sup>3</sup> Water Sample Resulting from Ultrasonic Irradiation using a 3 MHz Transducer. ....	139
Figure 68:	The Heating of a 10 cm <sup>3</sup> Water Sample Resulting from Ultrasonic Irradiation using a 5 MHz Transducer. ....	140
Figure 69:	The Heating of a 10 cm <sup>3</sup> Water Sample Caused by Ultrasonic Irradiation using a 10 MHz Transducer. ....	141
Figure 70:	Absorption Spectra Evolution for the 4-Nitrophenol Reaction. <sup>23</sup> .....	144
Figure 71:	The UV Absorbance Spectra of Sonicated 4-Nitrophenol. ....	145
Figure 72:	The Spectrum of 4-Nitrophenol in Phosphate Buffer (pH 5). ....	146
Figure 73:	The Structure of 4-Nitrophenol. ....	147
Figure 74:	The Spectrum of Terephthalic Acid in Phosphate Buffer (pH 7.4). ....	149
Figure 75:	The <sup>1</sup> H NMR Spectrum of the Synthesised 9,10-Dihydroanthracene-endo- $\alpha,\beta$ -succinic Anhydride. ....	153

Figure 76:	The Structure of 9,10-Dihydroanthracene-endo- $\alpha,\beta$ -succinic Anhydride....	153
Figure 77:	The Ultraviolet Spectrum of Anthracene.....	155
Figure 78:	Calibration Plot for the Absorbance of Anthracene on the UV Spectrometer....	156
Figure 79:	The Apparatus for Ultrasonic Irradiation. ....	157
Figure 80:	The Thermal Diels-Alder Reaction of Maleic Anhydride with Anthracene in Toluene at 342 K. ....	158
Figure 81:	Plot of $\ln k_2$ versus $1/T$ ( $K^{-1}$ ) for the Thermal Diels-Alder Reaction in Toluene on the Bench. ....	159
Figure 82:	The Infrared Spectrum of the Unknown Precipitate.....	161
Figure 83:	The Infrared Spectrum of 9,10-Dihydroanthracene-endo- $\alpha,\beta$ -succinic Anhydride. ....	162
Figure 84:	The Thermal Diels-Alder Reaction of Maleic Anhydride with Anthracene in <i>o</i> -Xylene at 342 K.....	164
Figure 85:	Plot of $\ln k_2$ versus $1/T$ ( $K^{-1}$ ) for the Thermal Diels-Alder Reaction in <i>o</i> -Xylene on the Bench. ....	165
Figure 86:	The Ultrasonic Diels-Alder Reaction of Maleic Anhydride with Anthracene in <i>o</i> -Xylene at 339 K.....	166
Figure 87:	The Ultrasonic Diels-Alder Reaction of Maleic Anhydride in <i>o</i> -Xylene. ....	167
Figure 88:	Plot of $\ln k_2$ versus $1/T$ ( $K^{-1}$ ) for the Comparison of the Ultrasonic and Thermal Diels-Alder Reaction of Maleic Anhydride with Anthracene.....	168
Figure 89:	$^{13}C$ NMR PENDANT Spectrum of the Diels-Alder Reaction Mixture.....	170
Figure 90:	$^{13}C$ NMR DEPT Spectra of an Ultrasonic Diels-Alder Reaction. ....	173
Figure 91:	$^{13}C$ NMR DEPT Spectra of a Thermal Diels-Alder Reaction. ....	173
Figure 92:	Compensation Diagram of the Linear Relationship between $\Delta H^\ddagger$ and $T\Delta S^\ddagger$ for the Diels-Alder Reactions.....	178
Figure 93:	Compensation Diagram of the Linear Relationship between $\Delta H^\ddagger$ and $T\Delta S^\ddagger$ for the Thermally Induced Diels-Alder Reactions. ....	179
Figure 94:	Compensation Diagram of the Linear Relationship between $\Delta H^\ddagger$ and $T\Delta S^\ddagger$ for the Ultrasonically Induced Diels-Alder Reactions. ....	180
Figure 95:	The General Trend Observed for the Ultrasonic and Thermal Solvolysis Reactions. ....	181

Figure 96: A Novel Conductivity Cell .....	186
Figure 97: Conductivity Cell Equipment. ....	186
Figure 98: The Bench Reaction Equipment Set-up.....	187
Figure 99: The Thermal Solvolysis Bench Reaction of t-BuCl.....	188
Figure 100: Plot of $\ln k_1$ versus $1/T$ ( $K^{-1}$ ) for the Thermally Induced Solvolysis Bench Reactions of t-BuCl. ....	189
Figure 101: The Ultrasonic Bench Reaction of t-BuCl at 285 K. ....	191
Figure 102: Plot of $\ln k_1$ versus $1/T$ ( $K^{-1}$ ) for the Ultrasonic Solvolysis Bench Reactions of t-BuCl. ....	192
Figure 103: Plot of $\ln k_1$ versus $1/T$ ( $K^{-1}$ ) for the Comparison of the Ultrasonic and Thermal Solvolysis Bench Reactions of t-BuCl. ....	193
Figure 104: The NMR Reaction Equipment Set-up.....	195
Figure 105: Comparison of the Ultrasonic and Thermal Reactions by the Increase of the Combined Propan-2-ol/2-Methylpropan-2-ol Absorption Peak in the NMR Spectrometer.....	197
Figure 106: Staggered Plot of Spectra for the Thermally Induced Solvolysis Reaction of t-BuCl at 298 K.....	198
Figure 107: The Thermal Solvolysis Reaction of t-BuCl in the NMR Spectrometer. ....	199
Figure 108: Plot of $\ln k_1$ versus $1/T$ ( $K^{-1}$ ) for the Thermal Solvolysis Reactions of t-BuCl in the NMR Spectrometer.....	200
Figure 109: Staggered Plot of Spectra for the Ultrasonically Induced Solvolysis Reaction of t-BuCl at 302 K. ....	202
Figure 110: The Ultrasonic Solvolysis Reaction of t-BuCl in the NMR Spectrometer at 310 K. ....	203
Figure 111: Plot of $\ln k_1$ versus $1/T$ ( $K^{-1}$ ) for the Comparison of the Ultrasonic and Thermal Solvolysis Reactions of t-BuCl in the NMR Spectrometer. ....	204
Figure 112: Plot of $\ln k_1$ versus $1/T$ ( $K^{-1}$ ) for the Comparison of the Ultrasonic and Thermal Solvolysis Reactions of t-BuCl in the NMR Spectrometer. ....	205
Figure 113: Compensation Diagram of the Linear Relationship between $\Delta H^\ddagger$ and $T\Delta S^\ddagger$ for the Solvolysis of t-BuCl.....	211
Figure 114: Compensation Diagram of the Linear Relationship between $\Delta H^\ddagger$ and $T\Delta S^\ddagger$ for the Thermally Induced Solvolysis of t-BuCl. ....	213



Figure 115: Compensation Diagram of the Linear Relationship between $\Delta H^\ddagger$ and $T\Delta S^\ddagger$ for the Ultrasonically Induced Solvolysis of t-BuCl. ....	214
Figure 116: Overlay Plot of Spectra for the Thermally Induced Solvolysis Reaction of t-BuCl at 298 K.....	217
Figure 117: The Rate of Change of the Chemical Shift of Water, for the Thermally Induced Solvolysis of t-BuCl, in the NMR Spectrometer. ....	218
Figure 118: The Rate of Change of the Chemical Shift of the Water Peak, for the Thermal Solvolysis of t-BuCl, in the NMR Spectrometer. ....	219
Figure 119: Overlay Plot of Spectra for the Ultrasonically Induced Solvolysis Reaction of t-BuCl at 302 K.....	220
Figure 120: The Rate of Change of the Chemical Shift of the Water Peak, for the Ultrasonic Solvolysis of t-BuCl, in the NMR Spectrometer. ....	221
Figure 121: Plot of $\ln k_1$ versus $1/T$ ( $K^{-1}$ ) for the Rate of Change of the Chemical Shift of the Water Absorption Peak for the Comparison of the Thermal and Ultrasonic Solvolysis Reactions of t-BuCl in the NMR Spectrometer. ....	222
Figure 122: Space-filling Model of Lysozyme. ....	225
Figure 123: The Covalent Structure of Lysozyme. ....	226
Figure 124: The Hairpin Turn of the Main Chain of Lysozyme. <sup>125</sup> ....	227
Figure 125: The Spectrum of Lysozyme in Aqueous Solution in the Bruker WM300....	228
Figure 126: The Spectrum of Lysozyme in Aqueous Solution in the Bruker WM250....	229
Figure 127: The Effect of Ultrasound upon the Chemical Shift of the Lysozyme System. ....	230
Figure 128: Establishing an External Standard. ....	231
Figure 129: $^1H$ Spectrum of a Sample of Water with the External Standard. ....	233
Figure 130: $^1H$ Spectrum of a Sample of Aqueous Ethanol with the External Standard. ....	234

## List of Tables

Table 1:	δ-values for the Protons in Methyl Halides CH <sub>3</sub> X. ....	33
Table 2:	Reference Chemical Shifts (δ <sub>H</sub> ) in Aqueous Solution. ....	36
Table 3:	δ-values of Hydrocarbons .....	40
Table 4:	Elimination Product Distributions in Various Solvent Systems. ....	78
Table 5:	Hughes-Ingold Rules for Predicting Solvent Effects on Reaction Rates. <sup>44</sup> ....	84
Table 6:	The Rates of Hydrolysis of t-alkyl Chlorides, at 298 K, in 80% Aqueous Ethanol. <sup>47</sup> .....	88
Table 7:	Summary of Effects upon S <sub>N</sub> 1 Reaction Rates. ....	90
Table 8:	Summary of Effects upon S <sub>N</sub> 2 Reaction Rates. ....	91
Table 9:	Additions of Vinylcyclohexenes to <i>o</i> -Quinones. <sup>79</sup> .....	107
Table 10:	The Dependence of Adduct Formation upon Reaction Conditions. <sup>83</sup> .....	108
Table 11:	Ultraviolet Absorbances of some Conjugated Organic Compounds. ....	111
Table 12:	The Hydrolysis of t-BuCl in 70% Aqueous Ethanol at Various Concentrations of t-BuCl. <sup>85</sup> .....	116
Table 13:	Rate Constants and Thermodynamic Parameters for the Solvolysis of t-BuCl in Various Pure Solvents at 298 K. <sup>98,99</sup> .....	121
Table 14:	The Hydrolysis of t-BuCl in Various Concentrations of Aqueous Ethanol. <sup>85</sup> ....	122
Table 15:	The Dielectric Constants for Various Concentrations of Aqueous Ethanol. ....	123
Table 16:	Y-values for Binary Mixtures. ....	126
Table 17:	m Values for Various Substrates with Respect to t-BuCl. ....	126
Table 18:	The Effect of Ultrasound on the Rates of Solvolysis of t-BuCl at 298 K. <sup>114</sup> .....	129
Table 19:	The Effect of Sonication on the Solvolysis of t-BuCl at Various Ethanol Concentrations and Temperatures. <sup>115</sup> .....	130
Table 20:	The Reaction Conditions for the Ultrasonic Degradation of 4-Nitrophenol. ....	147
Table 21:	The Reaction Conditions for the Ultrasonic Reaction of Terephthalic Acid. ....	149
Table 22:	The Thermodynamic Parameters for the Diels-Alder Reaction in Toluene over the Temperature Range 333 K to 352 K. ....	159

Table 23:	The Thermodynamic Parameters for the Diels-Alder Reaction in Toluene over the Temperature Range 333 K to 352 K. ....	160
Table 24:	Infrared Frequencies of Organic Groups. ....	161
Table 25:	The Thermodynamic Parameters for the Diels-Alder Reaction in <i>o</i> -Xylene over the Temperature Range 335 K to 354 K. ....	165
Table 26:	The Thermodynamic Parameters for the Diels-Alder Reaction in <i>o</i> -Xylene over the Temperature Range 335 K to 354 K. ....	165
Table 27:	The Thermodynamic Parameters for the Diels-Alder Reaction in <i>o</i> -Xylene over the Temperature Range 339 K to 349 K. ....	167
Table 28:	The Thermodynamic Parameters for the Diels-Alder Reaction in <i>o</i> -Xylene over the Temperature Range 339 K to 349 K. ....	168
Table 29:	Relative Increase in the Rate Constant as a Consequence of Ultrasonic Irradiation Employing a 3 MHz Transducer Operating at 7W. ....	169
Table 30:	The Thermodynamic Parameters at 343 K for the Toluene System. ....	169
Table 31:	The Thermodynamic Parameters at 343 K for the <i>o</i> -Xylene System. ....	170
Table 32:	Assignment of Resonances in the PENDANT Spectrum of the Diels-Alder Reaction Mixture. ....	171
Table 33:	Rate Constant Increase of the Ultrasonic over the Thermal Diels-Alder Reaction. ....	176
Table 34:	Comparison of the Thermodynamic Parameters Established for the Diels-Alder Reactions. ....	177
Table 35:	Linear Relationship between $\Delta H^\ddagger$ and $T\Delta S^\ddagger$ . ....	178
Table 36:	Establishing a Suitable Solvent System for the Solvolysis of t-BuCl. ....	184
Table 37:	The Thermodynamic Parameters for the Solvolysis Reaction of t-BuCl over the Temperature Range 275 K to 319 K. ....	189
Table 38:	The Thermodynamic Parameters for the Solvolysis Reaction of t-BuCl over the Temperature Range 275 K to 319 K. ....	189
Table 39:	The Thermodynamic Parameters for the Solvolysis Reaction of t-BuCl at the bench over the Temperature Range 275 K to 319 K. ....	192
Table 40:	The Thermodynamic Parameters for the Solvolysis Reaction of t-BuCl at the bench for the Temperature Range 275 K to 319 K. ....	192

Table 41:	Relative Increase in the Rate Constant as a Consequence of Ultrasonic Irradiation Using a 3 MHz Transducer Operating at 7W.....	194
Table 42:	The Thermodynamic Parameters for the Bench Solvolysis of t-BuCl at 308K.....	194
Table 43:	The Thermodynamic Parameters for the Thermally Induced Solvolysis Reaction of t-BuCl in the NMR Spectrometer over the Temperature Range 298 K to 319 K.....	200
Table 44:	The Thermodynamic Parameters for the Thermally Induced Solvolysis Reaction of t-BuCl in the NMR Spectrometer over the Temperature Range 298 K to 319 K.....	201
Table 45:	The Thermodynamic Parameters for the Ultrasonically Induced Solvolysis Reaction of t-BuCl in the NMR Spectrometer for the Temperature Range 298 K to 319 K.....	204
Table 46:	The Thermodynamic Parameters for the Ultrasonically Induced Solvolysis Reaction of t-BuCl in the NMR Spectrometer for the Temperature Range 298 K to 319 K.....	204
Table 47:	Relative Increase in the Rate Constant as a Consequence of Ultrasonic Irradiation Using a 3 MHz Transducer Operating at 7 W.....	206
Table 48:	The Thermodynamic Parameters for the Solvolysis of t-BuCl in the NMR Spectrometer at 308 K.....	206
Table 49:	Rate Constant Increase of the Ultrasonic over the Thermal Solvolysis Reaction.....	207
Table 50:	Comparison of the Thermodynamic Parameters Established for the Bench and NMR Experiments of 2-Chloro-2-methylpropane in Aqueous Propan-2-ol.	208
Table 51:	Linear Relationship between $\Delta H^\ddagger$ and $T\Delta S^\ddagger$ .....	210
Table 52:	The Thermodynamic Parameters for the Thermally Induced Solvolysis of t-BuCl, according to the water peak shift, at 308 K.....	219
Table 53:	The Thermodynamic Parameters for the Ultrasonically Induced Solvolysis of t-BuCl, according to the water peak shift, at 308 K.....	221
Table 54:	The Thermodynamic Parameters at 308 K for all t-BuCl Solvolysis Reactions.....	223

Table 55:	The Change in Chemical Shift for Sonicated Aqueous Lysozyme.....	229
Table 56:	Identity of the $^1\text{H}$ Resonances for Establishing an External Standard.....	232
Table 57:	Identity of the $^1\text{H}$ Resonances for Aqueous Ethanol Containing the External Standard.....	234
Table 58:	Comparison of the Reaction Conditions for the Two Dosimeter Systems. ..	241
Table 59:	Comparison of Traditional Pericyclic Thermodynamic Parameters with those of an Ultrasonically Enhanced Reaction.....	242
Table 60:	Comparison of the Author's results for the reaction of 2-Chloro-2-methylpropane in aqueous Propan-2-ol with those of Winstein and Fainberg <sup>98,99</sup> in various pure solvents.....	246

## Appendices

Appendix 1:	The Thermally Induced Diels-Alder Reaction of Maleic Anhydride with Anthracene in Toluene.....	254
Appendix 2:	The Least Mean Square Computer Programme <sup>120</sup> .....	264
Appendix 3:	The Analysis of Precipitate by Infra-Red Spectroscopy.....	286
Appendix 4:	The Thermally Induced Diels-Alder Reaction of Maleic Anhydride with Anthracene in <i>o</i> -Xylene.....	287
Appendix 5:	The Ultrasonically Induced Diels-Alder Reaction of Maleic Anhydride with Anthracene in <i>o</i> -Xylene.....	293
Appendix 6:	The DEPT Pulse Programme.....	297
Appendix 7:	The Thermally Induced Reaction of 40% (v/v) t-BuCl/IPA with 40% (w/w) IPA/H <sub>2</sub> O.....	298
Appendix 8:	The Thermally and Ultrasonically Induced Reaction of 40% (v/v) t-BuCl/IPA with 40% (w/w) IPA/H <sub>2</sub> O.....	305
Appendix 9:	Microprogramme for the in-situ detection of the Reaction of 40% (v/v) t-BuCl/IPA with 40% (w/w) IPA/H <sub>2</sub> O by <sup>1</sup> H NMR Spectroscopy. ....	309
Appendix 10:	The Thermally Induced Reaction in the NMR Spectrometer of 40% (v/v) t-BuCl/IPA with 40% (w/w) IPA/D <sub>2</sub> O.....	310
Appendix 11:	The Ultrasonically Induced Reaction in the NMR Spectrometer of 40% (v/v) t-BuCl/IPA with 40% (w/w) IPA/D <sub>2</sub> O.....	316
Appendix 12:	The Thermally Induced Reaction in the NMR Spectrometer of 40% (v/v) t-BuCl/IPA with 40% (w/w) IPA/D <sub>2</sub> O.....	321
Appendix 13:	The Ultrasonically Induced Reaction in the NMR Spectrometer of 40% (v/v) t-BuCl/IPA with 40% (w/w) IPA/D <sub>2</sub> O.....	327
Appendix 14:	The Rate of Change of the Chemical Shift of Water for the Thermally Induced Reaction in the NMR Spectrometer of 40% (v/v) t-BuCl/IPA with 40% (w/w) IPA/D <sub>2</sub> O.....	332
Appendix 15:	The Rate of Change of the Chemical Shift of Water for the Ultrasonically Induced Reaction in the NMR Spectrometer of 40% (v/v) t-BuCl/IPA with 40% (w/w) IPA/D <sub>2</sub> O.....	338

# Chapter 1 The Theory of Nuclear Magnetic Resonance Spectroscopy

NMR Spectroscopy is a classic example of an innovative discovery developed to become a routine analytical technique used in all areas of chemical science. It was a Dutch physicist called Gorter who in 1936 first predicted the phenomenon now known as Nuclear Magnetic Resonance (NMR). However, the system was not developed as an analytical tool until 1946 when two American physicists furthered the technique independently.

The first NMR signals were observed by two groups of physicists independently in 1945: Bloch, Hansen and Packard<sup>1</sup> at Stanford University detected a signal from the protons of water, and Purcell, Torrey and Pound<sup>2</sup> at Harvard University observed the protons of paraffin wax. Bloch and Purcell were jointly awarded the Nobel Prize for Physics in 1952 as a result of their discovery.

Nuclear Magnetic Resonance Spectroscopy now occupies a very important position in chemistry. It is an enormously powerful and versatile technique for investigating the structure and dynamics of molecules; illustrated by the award of the Nobel Prize for Chemistry in 1991 to R. R. Ernst for his innovative research on NMR methods. The emergence of new NMR techniques during the last few years has proven that developments in NMR spectroscopy are still far from coming to an end.

NMR spectroscopy was dominated by continuous wave techniques for many years (1945-1970). In continuous wave (CW) spectroscopy the applied magnetic field  $B_0$  is varied at a given frequency or the frequency is varied and  $B_0$  is held constant to bring about resonance. The technique has now almost completely been superseded by pulse Fourier transform techniques. Pulse Fourier transform spectroscopy employs a short pulse of radio frequency RF irradiation of  $t$  seconds duration, which simultaneously excites all of the frequencies.

## 1.1 The Basic Theory of NMR Spectroscopy

NMR spectroscopy is based on the fact that a nucleus has both charge and spin so displaying distinct behaviour when placed in a magnetic field  $B_0$ .

When a nucleus is placed in a magnetic field  $B_0$  the angular momentum  $I$  (Equation 1), whose magnitude is quantised in units of  $\hbar$  ( $= h/2\pi$ ), of a spin- $I$  (*spin quantum number*  $I = 0, \frac{1}{2}, 1, 1\frac{1}{2}$ , etc). The nucleus has  $(2I+1)$  allowed orientations on an arbitrarily chosen axis; in the absence of a magnetic field, the spin angular momentum has no preferred direction.

**Equation 1:** Spin Angular Momentum.



$$I = [I(I+1)]^{1/2} \hbar$$

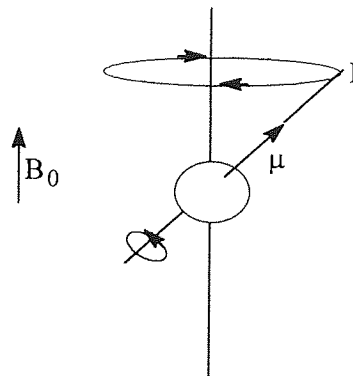
In the presence of a static magnetic field  $B_0$  a magnetic moment  $\mu$  arises as a result a nucleus having both charge and spin. The magnetic moment  $\mu$  (a vector quantity) is directly proportional to the angular momentum  $I$  by Equation 2. The gyromagnetic ratio  $\gamma$ , the proportionality constant, determines the resonant frequency of the particular nucleus.

**Equation 2:** The Magnetic Moment.

$$\mu = \gamma I$$

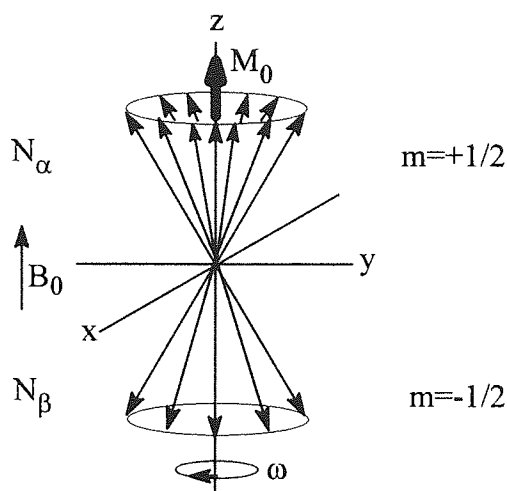
As illustrated in Figure 1 the magnetic moment  $\mu$  precesses around and parallel to the direction of the magnetic field  $B_0$  (anti-parallel for nuclei with negative  $I$ ).

**Figure 1:** The Generation of the Magnetic Moment  $\mu$  from the Spin  $I$ .



At equilibrium a large number of identical nuclei, for example spin- $I = 1/2$ , precess in exactly the same manner as that of the nucleus described above (Figure 2).

**Figure 2:** The Precession of Identical Spins in a Magnetic Field  $B_0$ .



All of the spins precess in the  $xy$  plane at the Larmor frequency  $\omega_0$ , which is dependent upon the strength of the static magnetic field  $B_0$  and on the intrinsic properties reflected in the gyromagnetic ratio  $\gamma$  (Equation 3).

**Equation 3:** The Larmor Frequency.

$$\omega_0 = -\gamma B_0$$

The stronger the magnetic field  $B_0$  the greater the Larmor frequency and the value of the frequency itself is different for nuclei in different environments. Thus, different nuclei, even of the same element come into resonance at distinct frequencies.

The sign of  $\gamma$  dictates whether rotation of the spins is clockwise, or anti-clockwise, which is always the same for a particular nucleus.

The phases of the individual spins of identical energy in the  $xy$  plane are random because there is no transverse magnetic field to align them; thus their vector sum in the  $xy$  plane vanishes.

Spins of parallel orientation along the field direction have a lower energy than those that are antiparallel to  $B_0$ . According to the Boltzmann distribution, magnetic nuclei distribute themselves amongst the available  $2I+1$  energy levels.

**Equation 4:** The Boltzmann Distribution.

$$\frac{N_{\beta}}{N_{\alpha}} = e^{-\Delta E/kT}$$

Where:  $N_{\beta}$  = Number of nuclei in higher energy level  
 $N_{\alpha}$  = Number of nuclei in lower energy level  
 $\Delta E$  = Energy separation =  $h\nu = \hbar\gamma B_0$   
 $k$  = Boltzmann constant =  $1.38 \times 10^{-23} \text{ JK}^{-1}$   
 $T$  = Absolute temperature (K)

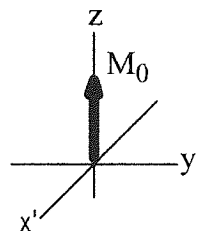
At thermal equilibrium  $N_{\alpha} > N_{\beta}$  resulting in a population difference equal to  $\Delta N_{\text{eq}}$ . The sample therefore has a net magnetisation  $M_0$  as observed in Figure 2, where each spin contributes  $\pm m\gamma \hbar$  to the total z magnetisation of the sample.

**Equation 5:** The Net Magnetisation.

$$M_0 = m\gamma \hbar \Delta N_{\text{eq}}$$

Thus far the description employed is referred to as the laboratory frame of reference. Rotating the x- and y-axis around the z-axis of the laboratory frame of reference at the Larmor frequency results in spins appearing to become static and coincide with the magnetic field  $B_0$  as in Figure 3.

**Figure 3:** The Net z-Magnetisation in the Rotating Frame.



The magnetic behaviour is fully described by the bulk magnetisation vector acting along  $B_0$ . Employment of the rotating frame of reference simplifies the description of effects resulting from the application of a RF pulse.

Application of a constant radio frequency pulse, at the resonant frequency, along the x'-axis in the laboratory frame of reference is the equivalent to applying an additional static field  $B_1$  to the system. The introduction of  $B_1$  to the system causes  $M_0$  to tilt in a clockwise direction and so precesses in the y'z plane at an angular frequency  $\omega$  according to Equation 6.

**Equation 6:** The Angular Frequency.

$$\omega = \gamma B_1$$

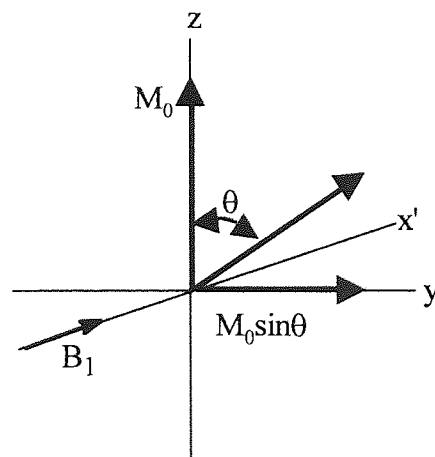
If the radio frequency pulse is applied for a known duration of  $\tau_p$  seconds then  $M_0$  is rotated through the angle  $\theta$ , known as the pulse angle.

**Equation 7:** The Pulse Angle.

$$\theta = \gamma B_1 \tau_p \frac{360}{\pi}$$

Tilting the bulk magnetisation through the  $\theta$  produces a component of  $M_0$  along the y'-axis as displayed in Figure 4. The y'-axis is used for the detection of signals in NMR spectroscopy. The pulse angle may be increased in size in one of two ways, either by increasing the amplitude of  $B_1$  or by increasing the pulse duration  $\tau_p$ .

**Figure 4:** The Effect of the Application of a Radio Frequency Pulse upon the Net z-Magnetisation



It is the vector  $M_0$ , which plays an important role in the description of all types of pulsed NMR experiment.

## 1.2 Relaxation

### 1.2.1 Introduction

In 1946 Felix Bloch derived a set of equations (the Bloch equations), which allowed relaxation to be correlated with the magnetisation vector. Resolution was specified along the  $x'$ ,  $y'$  and  $z$ -axes, and also that the direction of  $B_0$  is directed along the  $z$ -axis.

In an NMR experiment the result of irradiating a system at the resonance frequency is the disturbance of thermal equilibrium of the spin system effected by a change in the detectable magnetisation  $M_z$ . Consequently, the population ratios are altered, and the transverse magnetic components  $M_x$  and  $M_y$  arise.

On cessation of the perturbation the relaxation of the system occurs until it once again reaches its original equilibrium position.

Bloch identified two particular processes by which this relaxation occurs, the first being that which takes place in the applied field direction and is known as the *spin-lattice* (or *longitudinal*) *relaxation time*  $T_1$ . The second is the *spin-spin* (also known as the *transverse*) *relaxation time*  $T_2$  that is perpendicular to the field direction: unlike  $T_1$ ,  $T_2$  does not influence the energy level populations.

The relaxation of nuclear systems is very slow compared with other types of excited states such as those associated with molecular rotation and vibrations. A particularly slow relaxing nuclear system is one having a spin number  $I = \frac{1}{2}$  where relaxation can take anything from a few seconds to a few hours.

High resolution  $^1\text{H}$  NMR spectra are very complex and for this reason make the measurement of  $T_1$ 's laborious, coupled with the fact that such spin-lattice relaxation times tend to be of the order of a second and do not vary significantly for different bonding systems.

For  $^{13}\text{C}$  the variation of  $T_1$  between large and small molecules is of the order of milliseconds to several hundred seconds. As a result of the large  $T_1$  difference for  $^{13}\text{C}$  nuclei, this additional information has become an important spectral parameter for the chemist.

### 1.2.2 Nuclear Relaxation

After a pulse of radio frequency of duration  $\tau_p$  the bulk magnetisation vector  $M_0$  is tilted through a pulse angle  $\theta$  as illustrated Figure 4.

Immediately after application of the pulse, the bulk magnetisation has the components described in Equation 8 in all three axes of the rotating frame.

**Equation 8:** The Three Components of the Bulk Magnetisation.

$$\begin{aligned}M_x &= 0 \\M_y &= M_0 \sin\theta \\M_z &= M_0 \cos\theta\end{aligned}$$

At the instant the radio frequency pulse is switched off the perturbed spin system relaxes towards its equilibrium position ( $M_0$  aligned along the z-axis) via two separate processes.

The first of these processes is characterised by a relaxation time  $T_1$ . The magnetisation component along the z-axis relaxes back via an exponential decay, along the z-axis, to its original value  $M_0$ . The process of relaxation is referred to as spin-lattice relaxation. Relaxation occurs by the loss of energy from the excited nuclear spins to the nuclear lattice surrounding them, thus,  $T_1$  is known as the *spin-lattice relaxation time*.

Initially, the magnetisation along the z-axis is  $M_0$ . At a time  $t$  seconds after application of the pulse the corresponding magnetisation equals  $M_z$  and immediately begins returning to  $M_0$ , thus, the component of  $M$  along the y'-axis decays so when  $M_z = M_0$ ,  $M_y = 0$ . (This process is, in fact, the limiting condition and  $M_y$  decays before  $M_z$  returns to  $M_0$ .) Mathematically, the exponential decay can be expressed as

**Equation 9:** The Exponential Decay of spin-lattice Relaxation.

$$(M_0 - M_z) = M_0 (1 - \cos\theta) \exp\left(-\frac{t}{T_1}\right)$$

If, immediately after the pulse, the value of  $M$  along the  $y$ -axis is set at  $M_{y'(0)}$ , any relaxation occurring during the pulse will be negligible as the time which it takes to apply is so short, so

**Equation 10:** Magnetisation Along the  $y'$ -axis Immediately After Applying a RF Pulse.

$$M_{y'(0)} = M_0 \sin \theta$$

*Spin-spin* (also known as the *transverse*) relaxation  $T_2$  is the second process by which relaxation occurs. Nuclear spins exchange energy with each other causing some to precess faster than  $\omega_0$  while others precess slower, thus, losing phase coherence. Every nucleus producing a signal along the positive  $y'$ -axis has a corresponding signal produced by a nucleus in the negative direction along the same axis. Signals will cancel; subsequently no detectable signal is observed along either the  $y'$ - or  $x'$ -axis. An exponential decay in the signal also occurs, so that  $T_1$  and  $T_2$  relaxation happens simultaneously yet independently of each other.

**Equation 11:** The Exponential Decay of spin-spin Relaxation.

$$M_{y'(t)} = M_{y'(0)} \exp(-t/T_2)$$

When relaxation is complete along the  $z$ -axis there can be no residual component in the  $x'y'$  plane, i.e.  $T_2 \leq T_1$ . As a result of signal detection in the  $x'y'$  plane, regardless of the  $T_1$  value, no signal can be obtained from the spin system after a time  $5T_1$ .

### 1.3 Pulse Fourier Transform Spectroscopy

Pulse Fourier Transform spectroscopy began to replace the continuous wave (CW) technique in 1970. The continuous wave spectrometers functioned in a similar manner to optical absorption instruments; the sample is placed in a field of constant strength and the frequency scanned or vice versa.

Pulse Fourier Transform Spectroscopy employs a short pulse of radio frequency irradiation of frequency ( $F$ ) for duration of  $\tau_p$  seconds, simultaneously exciting all of the frequencies

in the range  $F \pm \tau_p^{-1}$ . The use of a short pulse can excite all the nuclei of a given species, but it is important that the power to accomplish this is sufficient, taking into account the time available. It must therefore satisfy the condition  $\gamma B_1 \gg 2\pi\Delta$ , where  $\Delta$  is the spectral width required.

## 1.4 The Chemical Shift

The Chemical shift is nowadays represented by the symbol  $\delta$ , although it used to be referred to by the symbol  $\tau$ . It is the relative difference in shielding of nuclei brought about by their different electronic environments, i.e., it is expressed as a molecular parameter dependent only upon sample conditions (solvent, concentration, temperature) and not on spectrometer frequency. NMR spectroscopy is an attractive analytical technique due to effects resulting in the chemical shift.

### 1.4.1 Nuclear Shielding

The chemist is concerned with molecules in which nuclei are surrounded by electrons and other atoms.

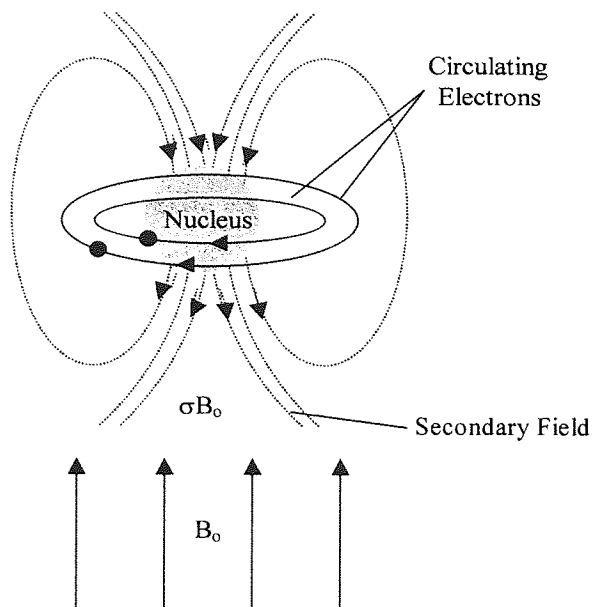
Resonances, which are produced by NMR spectroscopy, are influenced in characteristic ways by the electronic environment surrounding the nuclei under observation.

Chemical shifts occur as a result of secondary magnetic fields generated by the circulation of electrons in the observed molecule. The secondary field produced may either decrease or enhance the field to which a given nucleus responds.

Under the influence of a magnetic field electrons bonding the nucleus are inclined to precess around the nucleus in a plane perpendicular to the magnetic field (See Figure 5). The secondary field developed opposes that of the primary field, thus, the nucleus experiences an effective field  $B_{\text{eff}}$ , which is somewhat smaller than the applied field  $B_0$ .



**Figure 5:** The Effects of the Secondary Field upon the Applied Field  $B_0$ .



The nucleus is *shielded* from the full effect of the primary field.

**Equation 12:** The Magnetic Field Experienced as a Result of Shielding of a Nucleus.

$$B_{\text{eff}} = B_0 - B_0\sigma = B_0(1 - \sigma)$$

The effect of shielding is small but measurable and is represented by the symbol  $\sigma$  known as the *shielding constant*. The shielding constant is a dimensionless quantity of the order of  $10^{-5}$  for protons. It has a greater value than this for heavier atoms due to their larger number of electrons. The shielding constant is not dependent upon the magnetic field, as it is a molecular constant that is determined only by the magnetic and electronic environment of the nucleus being examined.

As a result of the shielding of a nucleus, the resonance condition becomes Equation 13.

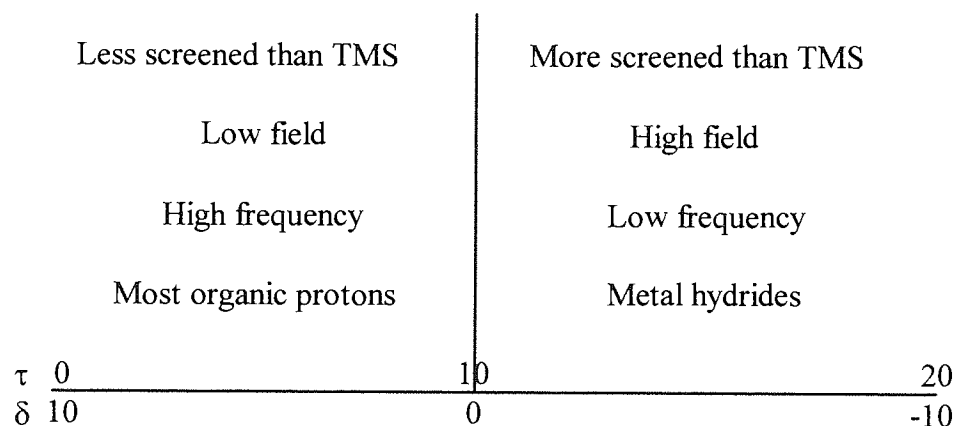
**Equation 13:** The Resonance Condition Incorporating the Shielding Constant.

$$\nu_1 = \frac{\gamma}{2\pi} B_0(1 - \sigma)$$

It can be seen from Equation 13 that  $\nu_1 \propto B_0$  and more importantly  $\nu_1 \propto (1-\sigma)$ . Two significant conclusions can be deduced from these facts. Nuclei, which are chemically non-equivalent, are shielded to different extents and as a result give separate resonance signals in a spectrum.

The convention employed universally for the measurement of resonance signals in NMR spectroscopy is such that  $\sigma$  increases from left to right on a spectrum (see Figure 6).

**Figure 6:** Chemically Shifted Compounds According to their Shielding.



There have been many attempts made at calculating  $\sigma$  theoretically but none of the approaches have yielded exact values. However, it has been established from theory and experimental work that a reduction in the field  $B_0$  and of the associated resonance frequency is determined mainly by the distribution of electron density in the molecule under inspection. It has been noted that chemical shifts are considerably affected by molecular substituents, which specifically influence this electron distribution. Since the shielding effect experienced by the observed nucleus is directly related to the electron density surrounding it, an absence of any other influences would be expected to cause  $\sigma$  to decrease with increased electronegativity of adjacent groups. This effect is illustrated by the  $\delta$ -values for the protons in methyl halides  $\text{CH}_3\text{X}$  in Table 1.

**Table 1:**  $\delta$ -values for the Protons in Methyl Halides  $\text{CH}_3\text{X}$ .

X	$\delta$ -value
I	2.16
Br	2.68
Cl	3.05
F	4.26

The iodine molecule is the least electronegative of the halogens listed. It has the least deshielding effect because it is the least effective at withdrawing electrons from the protons. The position of tetramethylsilane TMS can also be explained using this model; silicon is relatively electropositive.

Although inductive and mesomeric shielding effects are transmitted through chemical bonds, through space interactions are also possible, for example, if the nuclei under observation have magnetically anisotropic neighbours such as C=C, C $\equiv$ C, a carbonyl group or a phenyl ring. Another contribution to shielding is that of intermolecular interactions. These effects are discussed in section 1.4.6.

### 1.4.2 The $\delta$ -Scale and Reference Materials

Nuclei can occupy various magnetic sublevels and the frequency required to effect nuclear transitions is different for each isotope or element. The resonance frequency varies in direct proportion to the applied field; the larger the magnetic field, the higher the frequency required to initiate resonance. That is  $\nu \propto B_0$ .

As a consequence of the resonance condition (Equation 13) there is no absolute spectral scale in NMR spectroscopy due to the fact that the resonance frequency  $\nu_1$  and magnetic flux density  $B_0$  are independent. The result is the implementation of a relative scale in which the frequency difference  $\Delta\nu$  is measured between the resonance signals of a sample and that of a reference material.

Unlike  $\nu_1$ ,  $\Delta\nu$  is dependent upon  $B_0$ , consequently the chemical shift  $\delta$  is a dimensionless quantity.

**Equation 14:** The Chemical Shift.

$$\delta \text{ (ppm)} = \frac{(\nu_{\text{sample}} - \nu_{\text{ref.}}) \text{ (Hz)}}{\nu_{\text{ref}} \text{ (Hz)}} \times 10^6 \text{ ppm}$$

The figure of  $10^6$  is introduced in order to simplify numerical values, thus  $\delta$  is always expressed in numbers of parts per million (ppm). However, ppm is not a dimensioned quantity and so is not written when quoting  $\delta$  values. Thus, chemical shifts are usually written in terms of ppm. For ease of calculation Equation 14 can be expressed as Equation 15.

**Equation 15:** The Chemical Shift Simplified.

$$\delta \text{ (ppm)} = \frac{\text{Shift } \Delta\nu \text{ (Hz)}}{\text{Operating Frequency (MHz)}}$$

The substitution of  $\nu_{\text{ref}}$  for the operating frequency of the machine introduces no significant error. For the purpose of this research the  $^1\text{H}$  operating frequency of the spectrometer is 250 MHz.

Since measurement of  $\delta$  is a relative term, it is only possible to define a chemical shift scale for a nucleus by employment of a reference material.

There are two methods by which a reference material may be employed

- i) As an *external reference* where the material is placed in a capillary tube, which is itself then placed in the sample tube.
- ii) As an *internal reference* where the material is added directly to the sample being investigated.

However, in calculations using data obtained in such a manner it must be taken into account that nuclei at the position of the reference standard experience a different shielding from those in the sample due to bulk magnetic susceptibility differences.

The only universally accepted standard for use in proton NMR is TMS. The  $\delta$ -value for the reference compound TMS is zero as  $\Delta\nu = 0$ . According to Equation 15 the  $\delta$ -values to the left of TMS are positive and those to the right of it are negative (see Figure 6).

The success of TMS as a reference material can be attributed to its following characteristics

- TMS contains twelve equivalent, highly shielded protons providing it with three advantages as a reference material in NMR spectroscopy
  - i) Addition to the sample of only a small amount is required.
  - ii) It gives a single, sharp peak.
  - iii) The narrow, singlet resonance produced does not interfere with most other proton resonances.
- TMS is magnetically isotropic, non-associating, miscible with most organic solvents, chemically inert in most systems and is also highly volatile (boiling point =  $26.5^{\circ}\text{C} = 299.7\text{K}$ ) thus allowing easy sample recovery after analysis.

However, TMS is insoluble in water, which can pose problems, especially in biological investigations. Fortunately, alternative reference materials are available (See Table 2) and  $\delta$  values are unchanged for acid or alkaline solutions.

**Table 2:** Reference Chemical Shifts ( $\delta_{\text{H}}$ ) in Aqueous Solution.

TSP	<sup>t</sup> Bu-OH	CH <sub>3</sub> CN <sup>a</sup>	Acetone <sup>a</sup>	DMSO <sup>b</sup>	Me <sub>4</sub> N <sup>+</sup> Br <sup>-</sup>	Dioxan
0.0	1.231	2.059	2.216	2.710	3.178	3.743

<sup>a</sup>Exchanges in alkaline solution.

<sup>b</sup>Unsuitable for acid solution.

TSP = Sodium Phosphate, dibasic dodecahydrate (Na<sub>2</sub>HPO<sub>4</sub>·12H<sub>2</sub>O)

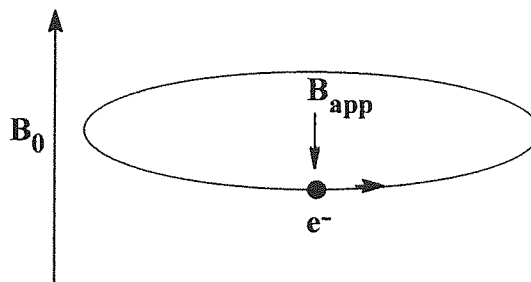
DMSO = Dimethyl Sulphoxide

### 1.4.3 The Origin of the Chemical Shift

The shells of electrons surrounding the nucleus determine its magnetic shielding.

The assumption is made that the magnetic field  $B_0$  induces an electron current in the electron shell resulting in the production of an opposing field  $B_{\text{app}}$  at the position of the nucleus, which reduces the effective  $B_0$  according to Equation 14.

**Figure 7:** The Reduced Effect of  $B_0$  by an Opposing Field  $B_{app}$ .



The magnetic field  $B_0$  induces two forms of electric current in a molecule: diamagnetic and paramagnetic.

Diamagnetism is the ability of a substance to cause it to repel a magnetic field. The effect originates from the interaction of the electronic charge with the field, an additive property of the atoms and the groups present.

Paramagnetism is associated with the presence of unpaired electrons and occurs when such a substance is placed in a magnetic field. The result is a greater concentration of the lines of magnetic force within itself than the surrounding field.

Diamagnetic currents give rise to nuclear shielding  $\sigma_{dia}$  i.e. an upfield shift and paramagnetic to deshielding  $\sigma_{para}$  i.e. a downfield shift. The overall shielding constant  $\sigma$  is therefore equal to the sum of these contributions where  $\sigma_{dia}$  and  $\sigma_{para}$  have positive and negative values respectively. Although, the order of diamagnetism is  $10^{-3}$  that of paramagnetism so that the effect is swamped by the presence of unpaired electrons.

**Equation 16:** The Shielding Constant.

$$\sigma = \sigma_{para} + \sigma_{dia}$$

For the hydrogen atom containing one electron (and other nuclei with spherically symmetric charge distributions) the contribution to shielding, known as the *diamagnetic shielding term*  $\sigma_{dia}$  is calculated using the *simple classical model* of an electron in a circular orbit (Lamb formula<sup>3</sup>). However, the simple classical model fails for electrons in *p-orbitals* and all non-spherical molecules where the charge distribution is not usually spherically symmetric. The *paramagnetic shielding term*  $\sigma_{para}$  aims to correct such discrepancies by

taking into account the effect of non-spherical charge distribution, and has the opposite sign to  $\sigma_{\text{dia}}$ , a diamagnetic shift causing a move upfield, whereas the paramagnetic shift (deshielding) produces a low-field shift.  $\sigma_{\text{para}}$  is small for  $^1\text{H}$  but has a much larger effect for atoms such as  $^{19}\text{F}$  and  $^{13}\text{C}$ .

In order to calculate  $\sigma_{\text{para}}$  the wave functions of excited states are required but these are only known for a few exceptional cases. Exact calculations can only be achieved for small molecules such as  $\text{H}_2$  and  $\text{LiH}$ .

A greater contribution to the overall shielding  $\sigma$  is made by the shielding  $\sigma_{\text{para}}$  as the value for the average electronic excitation energy  $\Delta E$  decreases, where

$$\sigma_{\text{para}} \propto \Delta E^{-1} \left( \frac{1}{\Delta E} \right)$$

For the hydrogen atom  $\Delta E$  is very large, which means  $\sigma_{\text{para}}$  plays a minor role in  $^1\text{H}$  NMR spectroscopy. For heavy atoms, including  $^{13}\text{C}$ , which have low-lying excited states  $\Delta E$  is small, implying that  $\sigma_{\text{para}}$  is an important factor in the calculation of shielding.  $\sigma_{\text{para}}$  is never greater in magnitude than  $\sigma_{\text{dia}}$ ; thus net shielding always remains positive.

It is such theoretical calculations, which assist in the understanding of the basic differences between  $^1\text{H}$  and  $^{13}\text{C}$  NMR spectroscopy.

In the absence of molecular motion, shielding constants and thus chemical shifts are generally anisotropic quantities. This is a result of the fact that distribution of electron density in a molecule is not in general spherically symmetrical. As a consequence of this fact  $\sigma$  (and also the resonance frequency of the nucleus being observed, according to Equation 13) is dependent upon the orientation of the molecule relative to the external magnetic field  $B_0$ .

The equation used to calculate  $\sigma_{\text{para}}$  is not adequate for obtaining an overall shielding constant  $\sigma$  for large molecules. Further terms are required to account for intermolecular contributions and the effects induced by neighbouring groups. The most important contributions experienced are

- $\sigma_N$  magnetic anisotropy of neighbouring groups.
- $\sigma_R$  ring current effects in arenes.
- $\sigma_e$  electric field effects.
- $\sigma_i$  intermolecular interactions, such as hydrogen bonding and solvent effects.

Equation 16 can therefore be replaced with Equation 17

**Equation 17:** The Overall Shielding Constant.

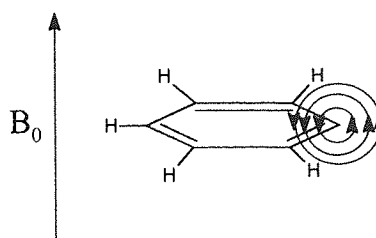
$$\sigma = \sigma_{para}^{local} + \sigma_{dia}^{local} + \sigma_R + \sigma_e + \sigma_i + \sigma_N$$

$\sigma_{para}^{local}$  is essentially the same as  $\sigma_{para}$ , taking into account contributions of electrons in the immediate vicinity of the observed nucleus. In  $^1\text{H}$  NMR the most important contributions are  $\sigma_R$  and  $\sigma_N$ .

#### 1.4.4 The Ring Current Effects in Arenes

The protons in arenes such as benzene are generally less shielded than those of alkenes. When a molecule with delocalised  $\pi$ -electrons is placed in a magnetic field  $B_0$ , an induced ring current is set up. An additional magnetic field is formed which opposes  $B_0$  at the centre of the aromatic ring. The effect of the ring current is greatest when the arene is perpendicular to  $B_0$ .

**Figure 8:** The Effect of the Induced Ring Current on Shielding.





The hydrogen atoms are in the region of the molecule where the induced ring current enhances the external field  $B_0$  i.e. they are in an area of reduced shielding. No ring current effect occurs when the arene molecule is aligned parallel to  $B_0$ , because the magnetic field does not pass through the centre of the ring. In practise when the molecules are in solution they experience continual rapid motion and an average value is measured.

The effect of ring currents is less important in  $^{13}\text{C}$  NMR spectroscopy as it makes only a small contribution to the total shielding of the molecule. The reason for the small contribution can be explained simply, using the benzene model, by the fact that the carbon atoms are located in the centre of the current ring where there is zero induced field.

### 1.4.5 The Effect of Magnetic Anisotropy of Neighbouring Groups

It is evident from inspection of spectra that for molecules containing double and triple bonds local diamagnetic effects do not fully explain certain peak positions. Examples of hydrocarbons displaying these anomalies are listed in Table 3.

**Table 3:**  $\delta$ -values of Hydrocarbons

Hydrocarbon	$\delta$ -value
$\text{H}_3\text{C}-\text{CH}_3$	0.9
$\text{H}_2\text{C}=\text{CH}_2$	5.8
$\text{HC}\equiv\text{HC}$	2.9
RCHO	$\sim 10.0$
$\text{C}_6\text{H}_6$	$\sim 7.3$

Chemical bonds are generally magnetically anisotropic; they have different susceptibilities along the cartesian axes in space. The result is that magnetic moments  $\mu$  induced by  $B_0$  are not equal for the different directions. The shielding constant  $\sigma$  for the observed nucleus is dependent upon its geometrical position with respect to the rest of the molecule.

The deviation of theoretical relationships is fairly straightforward for groups with axially symmetrical charge distribution. In such instances two magnetic susceptibilities exist, the first, is perpendicular to the bond axis and is represented by the symbol  $\chi_{\perp}$ , the second  $\chi_{\parallel}$  is

parallel to it. It was McConnell<sup>4</sup> who, using Equation 18, calculated the effect on shielding of the magnetic anisotropy of neighbouring groups.

**Equation 18:** The Shielding due to the Magnetic Anisotropy of Neighbouring Groups.

$$\overline{\sigma_N} = \frac{1}{3r^3 4\pi} (\chi_{\parallel} - \chi_{\perp}) (1 - 3\cos^2 \theta)$$

With the aid of the McConnell model, Equation 18 displays  $\overline{\sigma_N}$ , the averaged contribution to the shielding of the observed nucleus, as a function of the distance  $r$  to the point dipole's centre  $Z$  and  $\theta$ , the angle between the line joining  $Z$  to the observed nucleus and  $A$ , the direction of the induced magnetic field.

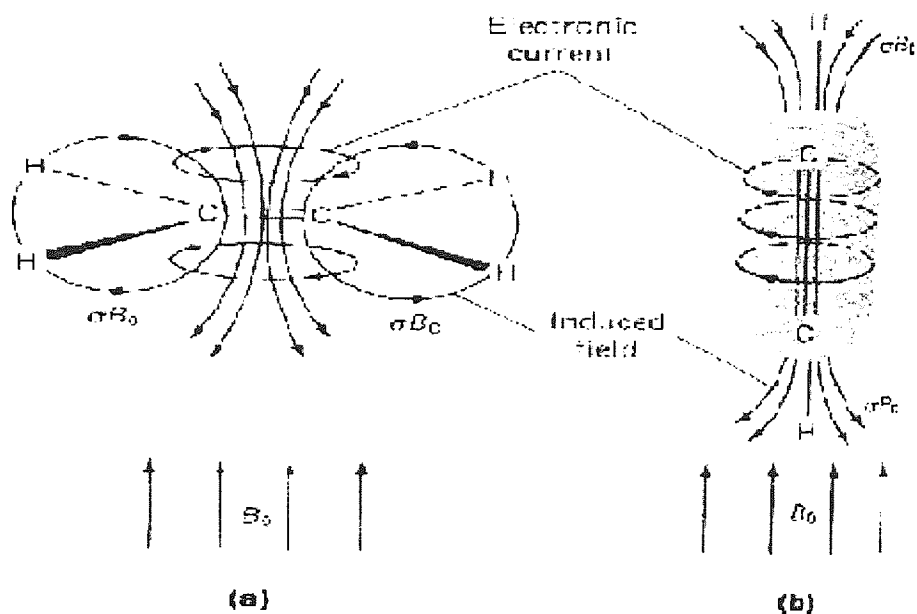
Two important properties are recognised from the equation

- $\overline{\sigma_N}$  is *only* dependent upon geometry and susceptibilities. The magnitude of the effect is the same whether for  $^{13}\text{C}$  or  $^1\text{H}$ .
- $\overline{\sigma_N} = 0$  when  $\theta = 54.7^\circ$  the magic angle, the essence of solid state NMR spectroscopy. A double cone can be defined around the magnetically anisotropic group, which separates the areas of positive and negative shielding contribution.  $\overline{\sigma_N} = 0$  at the surface of the cone.

Illustration of the effect can be afforded using those examples in Table 3.

For ethylenic or carbonyl double bonds the circulation of  $\pi$  electrons can be visualised in a plane along the axis of the bond when the molecule is oriented to the field (See Figure 2.4a). The secondary field produced acts upon the proton reinforcing the applied field. The resulting deshielding effect shifts the peak to a larger  $\delta$  value i.e. downfield. For an aldehyde, the effect observed for an ethylenic or carbonyl double bond also occurs, however, it is combined with deshielding caused by the electronegative nature of the carbonyl and a very large  $\delta$  value arises.

**Figure 9:** The Effect of Magnetic Anisotropy of Neighbouring Groups



The classical example of a magnetic anisotropic group is that of acetylene. The hydrogen atom lies on the molecular axis and the symmetrical distribution of  $\pi$  electrons about this permits their circulation around the bond (comparison with Figure 9a shows such motion is prohibited by the nodal plane in the electron distribution of the double bond). Figure 9b illustrates the shielding experienced by the protons in this particular orientation to the field. The effect of magnetic anisotropy is sufficient to counteract the deshielding due to proton acidity and the electronic currents perpendicular to the bond.

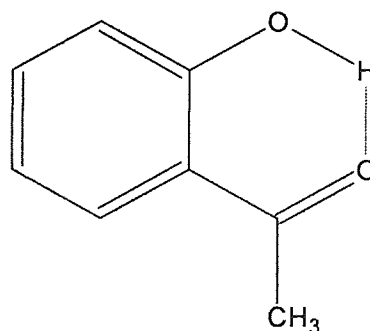
#### 1.4.6 Intermolecular and Intramolecular Interactions

*Hydrogen bonding* is responsible for some of the most significant deshielding effects in  $^1\text{H}$  NMR spectroscopy. Formation of a hydrogen bond ( $A-H\cdots B$ ) normally occurs when A and B are electronegative, usually halides, O or N. The hydrogen bond may be approximated as electrostatic in character. The attractive energy of the molecule is determined by its charge distribution  $\overset{\delta^-}{A}-\overset{\delta^+}{H}\cdots\overset{\delta^-}{B}$ , which is slightly enhanced upon the formation of a hydrogen bond. The result is that the hydrogen atom becomes more positive and A and B become more negative, thereby deshielding the proton.

It is difficult to state exact chemical shift values for compounds capable of forming intermolecular hydrogen bonds (e.g. ROH, RNH<sub>2</sub>), as they are critically dependent on several factors including concentration, temperature and solvent type. For example, the chemical shift of the hydroxyl proton in pure ethanol is 5.28 $\delta$ , although it shifts upfield on dilution in CCl<sub>4</sub> by the separation of the hydrogen-bonded complexes. In dilute CCl<sub>4</sub> the hydroxyl proton appears at 0.7 $\delta$ , high field of the methyl protons.

Compounds, which undergo *intramolecular* hydrogen bonding, show less dependence of the chemical shift on dilution; however, the chemical shift of the hydroxyl proton will be to the lower field of the analogous compound. For example, the hydroxyl proton in phenol moves from 7.45 $\delta$  to 4.37 $\delta$  when increasing dilution in CCl<sub>4</sub>, however, the analogous proton of *o*-hydroxyacetophenone (see Figure 10) appears at 12.0 $\delta$  altering little on dilution in CCl<sub>4</sub>.

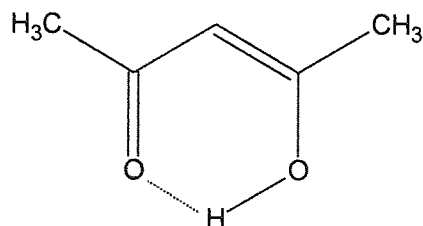
**Figure 10:** *o*-hydroxyacetophenone.



*o*-hydroxyacetophenone

Particularly strong *intramolecular* hydrogen bonding is observed in enols, where the hydroxyl proton is detected at extremely low fields (ca. 12-16 $\delta$ ) e.g. acetylacetone (enol form, see Figure 11) using chloroform as a solvent,  $\delta = 15.5$ . The electron withdrawing effect of the two oxygen atoms probably causes the profound downfield shift.

**Figure 11:** Acetylacetonone (enol).



Acetylacetonone (enol)

### 1.4.7 Solvent Effects

Often there are interactions between dissolved molecules and the solvent. This can cause shifts in signal positions that are difficult to predict and as a consequence reduce the accuracy of the measurements by an unknown quantity. Chemical shifts take place especially if the solvent molecules arrange themselves into a preferred orientation around the solute molecule, or if hydrogen bonding can occur. Visible shifts may be observed in non-polar (CCl<sub>4</sub>, hydrocarbons), polar (DMSO-d<sub>6</sub>) and magnetically anisotropic (benzene-d<sub>6</sub> or other aromatic compounds) solvents. However, the most extreme solvent effects are achieved when a spectrum is first measured in a non-polar solvent then in one causing large magnetic anisotropic effects.

On the basis of such effects, while a nuisance to those interested solely in structure determination, solvents may be used to assist signal assignment since they help explain the weak interactions between solvent and solute.

## 1.5 The Distortionless Enhancement by Polarisation Transfer (DEPT)

The acquisition of <sup>13</sup>C NMR spectra is often difficult because of the lack of sensitivity of the nucleus of interest. The <sup>13</sup>C nucleus has a low sensitivity with respect to hydrogen because of its low natural abundance and small magnetic moment. The magnetic moment  $\mu$  may be substituted by the gyromagnetic ratio  $\gamma$  since the two are proportional according to Equation 2.

**Equation 19:** The Sensitivity of a Nucleus.

$$\text{Sensitivity of nucleus X} = \left[ \frac{\gamma \text{ of X}}{\gamma \text{ of } ^1\text{H}} \right]^3 \times \frac{(I+1)/I^2 \text{ for X}}{(I+1)/I^2 \text{ for } ^1\text{H}}$$

The spin quantum number  $I$  for both the carbon and the hydrogen atom is equal to  $\frac{1}{2}$  so  $\frac{(I+1)/I^2 \text{ for } ^{13}\text{C}}{(I+1)/I^2 \text{ for } ^1\text{H}} = 1$ . The relative sensitivity of  $^{13}\text{C}$  with respect to  $^1\text{H}$  is  $1.59 \times 10^{-2}$ .

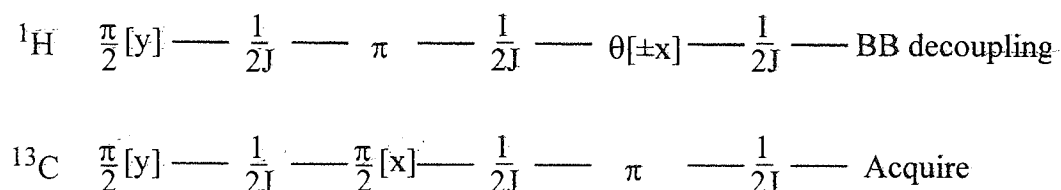
Multiplying this value by the natural abundance gives a value for the absolute sensitivity at natural abundance relative to the proton of  $1.76 \times 10^{-4}$ .

Polarisation transfer techniques such as the DEPT<sup>5</sup> pulse sequence can help to solve some of the problems encountered as a result of the low sensitivity of the  $^{13}\text{C}$  nucleus. The magnetism from the highly magnetic proton can be transferred, by a double irradiation technique, to the  $^{13}\text{C}$  thus increasing its sensitivity. The same method can also be employed for other nuclei, which also have low sensitivities. The main advantages of this technique are an improved signal-to-noise ratio of difficult nuclei as a result of the irradiation of the protons to which they are coupled. It can also manipulate the phase employed to produce spectra where all signals are positive, selected resonance signals as negative or eliminate unwanted peaks.

When interpreting  $^{13}\text{C}$  NMR spectra it is very useful to be able to distinguish between peaks produced by quaternary, CH, CH<sub>2</sub> and CH<sub>3</sub> carbon nuclei, so the number of hydrogens attached to each carbon atom may be determined. The DEPT experiment allows such distinctions to be made using the pulse program shown in Figure 12.

Spectra obtained have the same characteristics of 'normal' spectra (all signals are positive but at higher sensitivities) with the exception of the ability to separate signals with various multiplets.

**Figure 12:** The DEPT Pulse Sequence



The intensities of the CH, CH<sub>2</sub> and CH<sub>3</sub> signals are dependent upon the pulse angle  $\theta$ .

- CH carbons exhibit a maximum enhancement of  $\gamma_{\text{H}}/\gamma_{\text{C}}$  at  $\theta=\pi/2=90^\circ$ .
- CH<sub>2</sub> carbons exhibit a maximum enhancement of  $\gamma_{\text{H}}/\gamma_{\text{C}}$  at  $\theta=\pi/4=45^\circ$ .
- CH<sub>3</sub> carbons exhibit a maximum enhancement of  $1.15\gamma_{\text{H}}/\gamma_{\text{C}}$  at  $\theta=0.196\pi$ .

The signal enhancement can be uniformly varied by altering the value of  $\theta$  which itself has the following mathematical dependencies:

- CH =  $\sin\theta$ .
- CH<sub>2</sub> =  $2\sin\theta$ .
- CH<sub>3</sub> =  $\sin\theta+\sin3\theta$ .

In order to differentiate between the various carbon nuclei three DEPT spectra at pulse angles of  $45^\circ$ ,  $90^\circ$  and  $135^\circ$  and a BB decoupled spectrum must be acquired.

- The CH sub-spectrum may be obtained directly by the application of a  $90^\circ$  pulse angle i.e. DEPT (90).
- The CH<sub>2</sub> sub-spectrum is obtained by subtracting the spectrum recorded at  $135^\circ$  from that at  $45^\circ$  i.e. DEPT (45)-DEPT (135).
- Finally, combining all three DEPT experiments provides the CH<sub>3</sub> sub-spectrum i.e. DEPT (45)+DEPT (135)-0.707DEPT(90).

The identity of the quaternary of the carbon nuclei, using the DEPT program, may only be determined by a process of elimination; once the nuclei already described have been established the only unidentified peaks left in the BB decoupled spectrum must result from the quaternary carbons. The more recent PENDANT<sup>6</sup> technique could also be used to establish the signals produced as the result of the presence of quaternary carbons.

According to the pulse sequence (Figure 12) a delay time of  $1/2J$  is required so it is necessary to know the value(s) of the coupling constant  $J(C,H)$ . In practice, results are not greatly influenced by the delay time so the DEPT pulse sequence can be employed for systems containing a wide variety of coupling constants.

However, for most situations, two DEPT experiments are sufficient for  $\theta$  at  $90^\circ$  and  $135^\circ$ . The DEPT (90) provides a CH spectrum directly, whereas the DEPT (135) assigns negative signals to  $CH_2$  nuclei and positive signals to CH and  $CH_3$  groups. The  $CH_3$  carbons are the remaining positive peaks in DEPT (135) when all the CH peaks have been identified from the DEPT (90) spectrum. The quaternary carbons can then be identified as the remaining unassigned peaks in a broadband-decoupled spectrum when all the peaks from the DEPT 135 and DEPT 90 spectra have been identified.



## **Chapter 2    The Theory of Ultrasound**

Historically, the generation of ultrasound dates back to work carried out by F. Galton<sup>7</sup> to establish the frequency limits of human and animal hearing in 1883. Determination of the limit was achieved using a whistle with an adjustable resonant cavity, which created sound of a known frequency thus, establishing the upper limit of human hearing at around 16-20 kHz. The hearing threshold of other animal species differs to that of humans. Dog whistles operate at frequencies above that of human hearing so are silent to humans. Bats also employ ultrasound, at frequencies >50 MHz, for navigation.

In 1917 Langevin developed the technique of echo sounding for the estimation of water depth. The first commercial application of ultrasonics was proposed as the result of a competition following the sinking of the White Star liner the Titanic. Further improvements were made to the system over the subsequent 40-year period leading to the advent of SONAR (Sound Navigation And Ranging).

Ultrasonics is the study of the effects of sound waves having frequencies higher than those to which the human ear responds (>20 kHz). It is only relatively recently that interest in the use of ultrasound has increased in the research area known as *sonochemistry*. The effects of ultrasound on chemical and biological systems have been observed over the last 80 years, yet it's employment by the synthetic chemist dates back little further than 1980. Since then ultrasonic research has been fairly constant, although not to the extent of other fields of chemistry.

The advantage of using ultrasound as a tool for inducing chemical reactions lies in the extremely mild reaction conditions, on a macroscopic scale, under which they may be carried out. However, as will become clear later, on a microscopic scale reaction conditions are relatively harsh. There is also no need for very complicated and expensive apparatus and in fact most reactions can be carried out in an ultrasonic cleaning bath, something most laboratories have as a standard item.

The classification of ultrasound as sound, having a frequency between 20 kHz and 100 MHz, can be divided into two main areas of interest:

- 1) Diagnostic ultrasound (2-10 MHz)
- 2) Power ultrasound (20-100 kHz)

### Diagnostic Ultrasound

Diagnostic ultrasound relies upon the release of a pulse of sonic energy through a medium and detection of the reflected signal from an interfering surface or boundary. Changes in the medium, or an obstruction within it, alter the velocity at which the sound travels through it.

Medical imaging, for example foetal imaging, and non-destructive testing rely upon the same system as that of SONAR. However, the introduction of complex computer equipment and the employment of high frequency ultrasound (usually above 5MHz) of much shorter wavelength allow the detection of changes in much smaller areas, thereby improving definition.

Other diagnostic techniques include the detection of flaws in materials, ultrasonic welding and SONAR.

It is generally believed that the application of diagnostic ultrasound to analytical chemistry causes only temporary physical changes to the medium, through which it passes and does not influence chemical reactivity. However, the author has carried out experiments, which indicate that for frequencies in the low diagnostic region this is not strictly true.

### Power Ultrasound

The uses of power ultrasound include cleaning, degassing, defoaming and emulsification. A less well-known application is that of sonochemistry where the frequency range normally employed is in the range 20 kHz to 2 MHz. Recent advances in ultrasonic engineering have given rise to an increasing interest in the area.

## **2.1 Cavitation**

The total pressure  $P_T$  in a liquid at time =  $t$  when a sound wave passes through it may be expressed as the combination of the applied acoustic pressure  $P_A$  and the experimental (hydrostatic) pressure  $P_h$ .

**Equation 20:** The Total Pressure in a Liquid upon Application of a Sound Wave.

$$P_T = P_h + P_A$$

A sinusoidal sound wave creates an applied acoustic pressure  $P_A$ , as it moves through the medium, which is coupled with an ambient hydrostatic pressure  $P_h$ .  $P_A$  is time dependent as described by Equation 21 where  $\nu$  = frequency of ultrasound and  $P_{MAX}$  = the maximum pressure amplitude of the wave.

**Equation 21:** The Applied Acoustic Pressure.

$$P_A = P_{MAX} \sin 2\pi \nu t$$

Sonic energy is dissipated as it moves further away from the emitting source. The variation in intensity with respect to the distance from the source is defined in Equation 22.

**Equation 22:** The Variation of Intensity with Respect to Distance from the Source.

$$I = I_0 \exp(-2\alpha d)$$

The intensity  $I$ , as a result of dissipation effects reducing the initial intensity  $I_0$ , is dependent upon the distance  $d$  from the source and the absorption coefficient  $\alpha$ , which is itself dependent on the viscosity and the thermal conductivity of the solvent system that the sound passes through. In order for attenuation to be larger at higher frequencies the value of  $\alpha/\nu^2$  needs to be constant at constant temperature.

As is also applied to electrical waves, the intensity (energy transmitted per metre square of the medium per unit time) ultrasound may be expressed as Equation 23 where,  $\rho$  = density of the medium and  $c$  = velocity ( $\text{ms}^{-1}$ ) of sound in the medium of interest.

**Equation 23:** Ultrasonic Intensity as a Function of Liquid Density and Velocity.

$$I = \frac{(P_{MAX})^2}{2\rho c}$$

Experimentally, the equation is of no use as it is very difficult to measure  $P_{MAX}$ . Intensity may be measured practically when both the power entering the system and area of the ultrasonic source are known and substituting the values Equation 24.

**Equation 24:** Experimental Evaluation of Intensity.

$$\text{Intensity (Wcm}^{-2}\text{)} = \frac{\text{Power entering the system (W)}}{\text{Area of the ultrasonic face (cm}^2\text{)}}$$

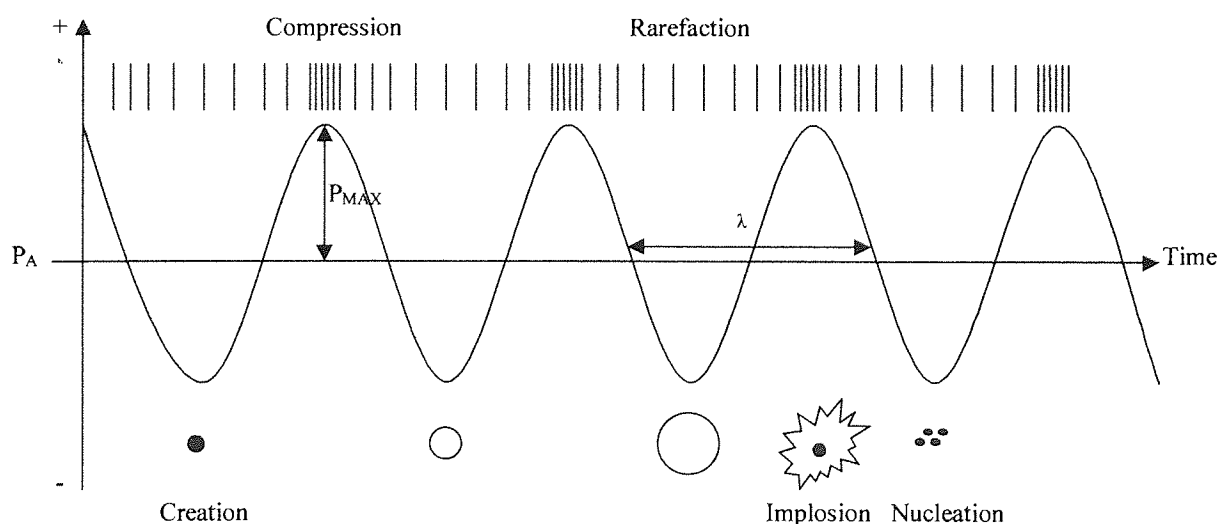
The actual ultrasonic power entering the system may be obtained by application of Equation 25 where,  $C_p$  = the heat capacity of the medium ( $\text{JK}^{-1}\text{mol}^{-1}$ ) and  $M$  = mass of the solvent used (kg).

**Equation 25:** Experimental Evaluation of Power.

$$\text{Power (W)} = \left(\frac{dT}{dt}\right) C_p M$$

Sonication causes enhanced molecular motion due to a mismatch occurring between the sound and the solvent leading to liquid-liquid phase boundary disruption, efficient emulsification, mass transfer and mixing. These factors can improve many chemical reactions although the origin of the majority of enhancements is a result of cavitation effects. It was as early as 1894 that Sir John Thorncroft and Sidney Barnaby first observed the effect of cavitation due to the motion of an incorrectly set ship's propeller.

**Figure 13:** The Formation of Cavities by the Irradiation of a Liquid with Ultrasound.

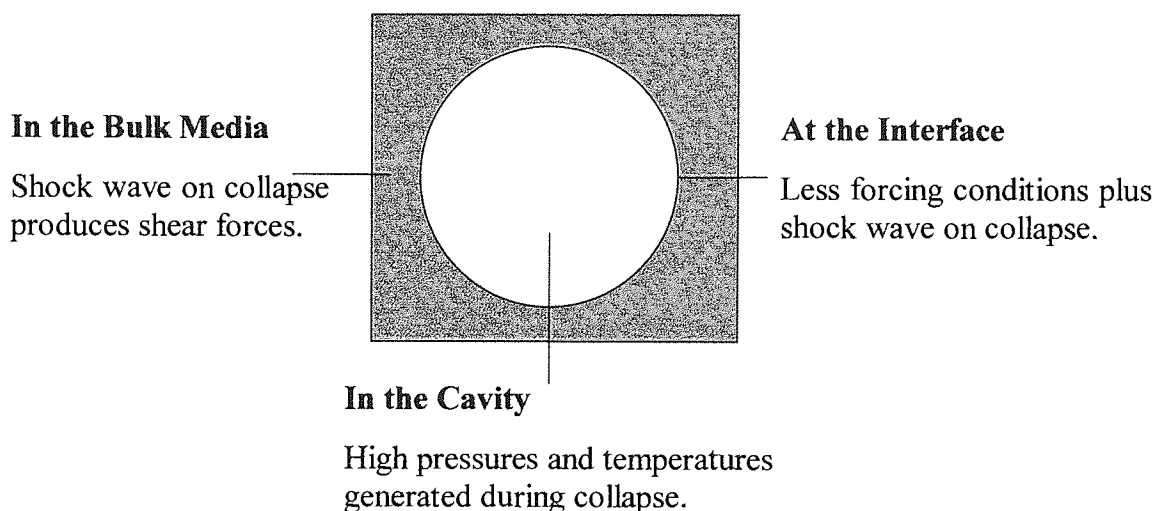


The application of high intensity ultrasound to liquids generates a sinusoidal acoustic pressure  $P_A$  that is superimposed upon the steady ambient pressure  $P_h$  and it is this that

induces cavitation. During the rarefaction phase of the acoustic cycle a negative pressure is developed which has the strength to overcome intermolecular forces binding the medium and 'ripping' it apart, thus, producing cavitation bubbles as displayed in Figure 13.

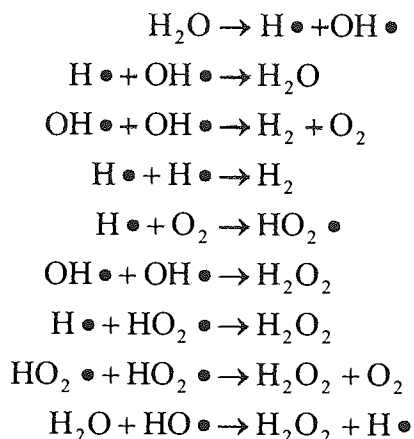
The positive acoustic pressure during the compression phase of the acoustic cycle causes a cavity to collapse, producing both mechanical and chemical effects that are experienced in three specific areas of the bubble.

**Figure 14:** The Mechanical and Chemical Effects from the Implosion of a Cavity.



*In the cavity* - The cavity contains vapour from the solvent, which enters when the bubble forms. Collapse of the bubble causes the vapour to undergo an increase in temperature and pressure resulting in homolytic bond breakage of the solvent and/or reagent generating reactive species such as radicals. An example of such a reaction is that of the sonication of water producing the gases oxygen and hydrogen by the reactions described in Figure 15.

**Figure 15:** The Sonication of Water.



The presence of the species hydrogen peroxide  $\text{H}_2\text{O}_2$  would expose anything dissolved in the water to chemical reaction with it.

*At the bubble interface* - This is where species produced in the bubble first begin to react with chemicals contained in the bulk liquid. A Reaction occurs as the result of large gradients of temperature and pressure, high shear forces produce shock waves, which cause solvent molecule motion around collapsing bubbles.

*In the bulk media* - On collapse of the bubble, liquid rushes into the space it occupied, so causing a shock wave creating huge shear forces. No ultimate sonochemical activity exists in this area, although it may react with intermediates formed due to ultrasonic irradiation. An additional effect of bubble collapse occurs near a solid surface<sup>8</sup>, where collapse is non-spherical and causes jets of liquid to approach it at speeds of up to  $100\text{ms}^{-1}$ .

Two forms of cavitation bubble exist, the transient (inertial) and the stable (non-inertial). The transient bubble, illustrated in Figure 13, has a short lifetime usually no more than one acoustic cycle. If the negative acoustic pressure is large enough these cavities expand to many times their original size. Upon collapse in the positive half of the acoustic cycle many smaller bubbles are produced which may become sites for nucleation of further bubbles. Stable bubbles have a lifetime of many cycles and oscillate, often non-linearly, about some equilibrium size. Initially it was thought that these stable cavities did not contribute greatly to the overall effects of cavitation, however, it is now believed that their oscillation does

have an effect upon cavitation. Stable cavities can themselves absorb ultrasonic energy. If enough of these stable cavities are present they can prevent further enhancement to ultrasonically induced reactions.

In a pure liquid, cavities may not be produced until a large enough negative pressure is applied to overcome the natural forces of cohesion. Degassed liquids may withstand very high negative pressures before cavitation occurs.

The increase in pressure during the compression cycle of the acoustic wave causes almost instantaneous violent collapse of the bubbles formed producing shock waves, high temperatures and pressures. The most widely accepted theory describes the energy released upon bubble implosion is the qualitative 'hot spot'<sup>9</sup> approach. Cavities implode so rapidly that little heat escapes and the surrounding liquid remains 'cold', quickly quenching the heated cavity. It is these imploding cavities that became known as 'hot spots'. Assuming that the bubble collapses adiabatically it was established that the maximum temperatures  $T_{MAX}$  and pressures  $P_{MAX}$  generated might be calculated using Equation 26 and Equation 27.

$T_0$  = The experimental temperature of the bulk liquid.

$P_M$  = Pressure in the liquid at the moment of collapse (generally assumed to be  $P_h + P_A = P_T$ ).

$P$  = Pressure in the cavity before collapse (usually equal to the vapour pressure of the liquid medium).

$\gamma$  = The ratio of specific heats of the gas (or gas-vapour pressure).

**Equation 26:** The Maximum Temperature Attained Upon Collapse of a Cavity.

$$T_{MAX} = T_0 \left[ \frac{P_M (\gamma - 1)}{P} \right]$$

**Equation 27:** The Maximum Pressure Attained Upon Collapse of a Cavity.

$$P_{MAX} = P \left[ \frac{P_M (\gamma - 1)}{P} \right]^{\gamma/(\gamma-1)}$$

An imploding cavity behaves like a localised micro-reactor generating instantaneous temperatures of several thousand degrees and pressure in the region of 1000 atmospheres,



dependent upon the conditions of the system involved. However, in order to solve the equations certain assumptions were made:

- The liquid is incompressible.
- The gas content of the bubble remains constant over its lifetime.
- The applied ultrasonic pressure wave is exactly sinusoidal as displayed in Figure 13. Changes in the volume of the bubble must distort the pressure wave around it to some extent.
- The diameter of the cavity is  $\lll \lambda$ .

As with transient cavitation, an estimate was made by Griffing *et al*<sup>10</sup> for the maximum temperatures and pressures produced by stable bubbles as they oscillate in resonance with the applied acoustic field (Q = damping factor equal to the ratio of the resonance amplitude to the static amplitude of bubble vibration).

**Equation 28:** Estimate of the Maximum Temperature Caused by a Stable Cavity.

$$\frac{T_0}{T_{MAX}} = \left\{ 1 + Q \left[ \left( \frac{P_h}{P_M} \right)^{1/3\gamma} - 1 \right] \right\}^{3(\gamma-1)}$$

It is the 'hot spot'<sup>9</sup>, which is widely believed to be the centre of sonochemical reactions. There is much evidence to support the 'hot spot' theory although Margulis<sup>11</sup> and Lepoint *et al*<sup>12</sup> proposed an alternative 'electric' theory as an explanation for the effect of ultrasound in chemical reactions. Electrical phenomena in cavitation are said to be the result of an electrical double layer formation in any liquid on the surface of the cavitation bubble boundary. This charge distribution of dipoles in the solvent and their dispersal about the cavity are considered. The boundary of electrical charge is continually renewed as the bubble moves and grows. An electrical microdischarge occurs upon the implosion of the cavity and is accompanied by excitation and decomposition of vapour within the cavity. The implosion results in sonoluminescence and sonochemical reactions. It was noted that formation and collapse of a bubble generates electric field gradients of about  $10^{11} \text{ Vm}^{-1}$  and shock waves causing bond breaking and chemical activity.

It is difficult to define the nature and intensities of the phenomena governing sonochemical reactions but whatever the effects are due to, energy is provided to molecules to promote reactions that are difficult to achieve 'normally'.

## **2.2 Parameters Affecting Cavitation**

Many factors<sup>13</sup> influence the results of ultrasonic irradiation in chemical solutions.

### Solvent Viscosity

Shear forces are produced from the formation and subsequent collapse of cavitation bubbles. The viscosity of a liquid is a measure of resistance to shear forces; the more viscous a liquid is, the more difficult it is for cavitation to take place.

### Solvent Surface Tension

A gas-liquid interface is generated upon formation of cavities, a solvent of low surface tension causes a reduction in the cavitation threshold i.e. less energy is required in order to create cavities as it is easier to 'tear apart' the liquid. This can be shown where the addition of a surfactant encourages cavitation in aqueous solution.

### Solvent Vapour Pressure<sup>14</sup>

Cavitation bubbles do not take the form of a vacuum but contain vapour of the solvent in which they develop. A pressure occurs inside the bubble reducing the difference between it and that of the bulk media. Formation of cavities is difficult in solvents of low vapour pressure since little vapour will enter the bubble. A solvent with a high vapour pressure allows cavitation at lower energies as more vapour is admitted into the bubble cavity, however, the collapse of the bubbles is then cushioned and thus, less energetic.

### Bubbled (Entrained) Gas

Any gas present at the commencement of reaction produces a rate enhancement since it may behave as nucleation sites for cavitation. However, as the reaction continues liquids become degassed as a result of sonication and enhancement ceases. It is for this reason that many researchers introduce a gas into a sonochemical reaction to maintain uniform cavitation. The nature of the gas dissolved in a system can greatly affect the rate at which sonochemical reactions take place. Based on the 'hot spot' theory<sup>9</sup>, it is accepted that gases with the greatest ratio of specific heats  $C_p/C_v$  such as monoatomic gases He, Ar and Ne are preferred to diatomic gases like air, O<sub>2</sub> and N<sub>2</sub>. Exceptions do occur, for example CF<sub>4(g)</sub><sup>15</sup> proves to be better than Ar<sub>(g)</sub> so it is perhaps not such a good idea to make use of the theory exclusively for effects due to ultrasonic irradiation.

### Irradiation Frequency

The frequency of ultrasound with which the sample is irradiated is an important function of cavitation. At low frequencies bubbles are larger than at higher frequencies and collapse with a greater force. Therefore, the intensity of the shock waves produced by the collapsing cavity decrease as frequency increases.

### Intensity (Power)

There are limits to the ultrasonic energy that can be input into a system. A minimum intensity is required to reach the cavitation threshold and is dependent upon the frequency. However, there appears to be an upper limit at which this general trend ceases and, in fact, the reaction rate decreases. A possible reason for this observation is that beyond this intensity the bubble may grow so large during the rarefaction cycle that the time in which collapse may occur is too short. If a sufficient amount of such bubbles are created they can form a bubble 'cushion' and so reduce the energy transfer from the ultrasonic source to the system.

There are two extremes, which must be considered with respect to intensity.

- 1) The threshold intensity must be exceeded so that cavitation takes place.
- 2) An optimum intensity exists beyond which further increase in intensity has no effect on reaction rate.

Decoupling of the source to the liquid may happen at high vibrational amplitudes reducing the efficiency of sonication. It is most pronounced when a large number of bubbles build up on or near the surface of the transducer. A further problem for transducers operating at high powers is fracturing.

#### The Application of External Pressure

The effects of increasing static pressure are unclear, but what is clear is that changes in it will influence the cavitation process. It could be reasoned that if the total pressure  $P_T$  of the system were to increase, the effective intensity of cavitation collapse would also increase.<sup>16</sup> However, such an increase means that the formation of cavities becomes simultaneously more difficult and so the intensity of the ultrasonic irradiation must also be increased to achieve cavitation.

#### Temperature

A temperature increase results in increased vapour pressure leading to easier cavitation but accompanied by their less violent collapse. An increase in temperature also leads to a reduction in the viscosity and the surface tension of the reaction solution thus, reducing the cavitation threshold.

Luche and co-workers<sup>17</sup> observed the existence of an optimum temperature for reaction rate increase due to sonication. A general increase in reaction rate was noted, however, upon approaching the boiling point of the solvent there is a significant increase in the number of cavities, which absorb ultrasonic energy and prevent further rate enhancement. Strictly though these were the results for one reaction only.

#### Sound Attenuation

As sound passes through a medium the intensity is attenuated (decreased) and the extent of the attenuation is inversely related to ultrasonic frequency ( $\alpha/v^2$ ). In order to gain the same intensity at a particular distance from the ultrasonic source, a higher initial power is required at higher frequencies.

## 2.3 The Generation of Ultrasonic Waves

The generation of ultrasonic waves is based on the action of a device called a transducer. A transducer is “any device for converting a signal from one medium of transmission to another”<sup>18</sup>. The simplest example of such a device is a whistle, which converts gas motion into sound.

There are three main types of transducer that are capable of converting mechanical or electrical energy into high frequency sound.

- Gas driven transducers
- Liquid driven transducers
- Electromechanical transducers

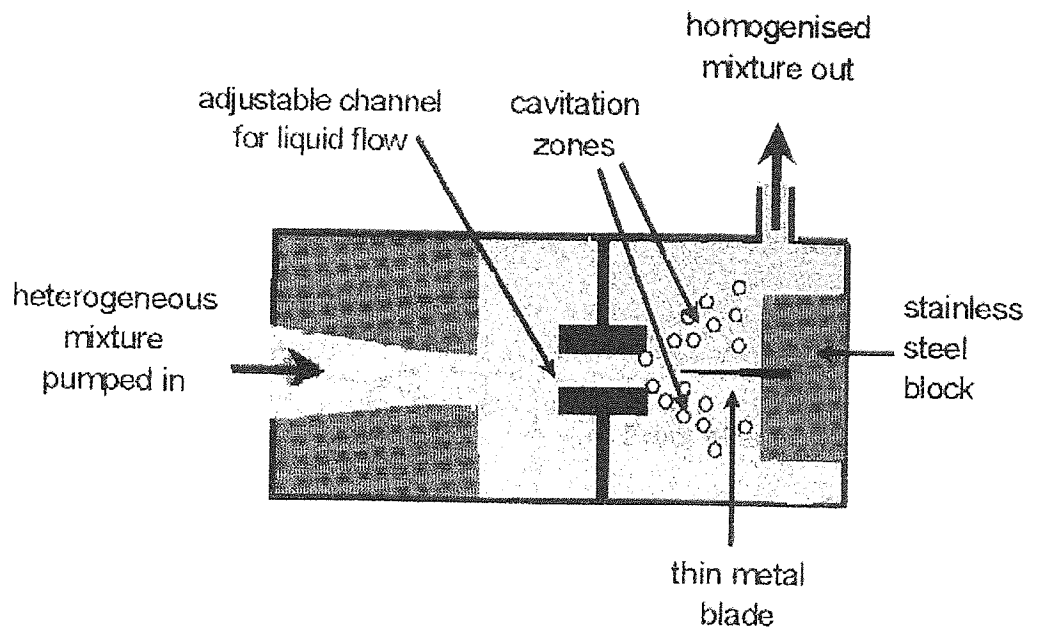
### Gas-driven Transducers

Explained simply gas-driven transducers are whistles with a high frequency output. However, no significant chemical application has yet been discovered for their use. The Galton<sup>7</sup> whistle is an example of such a transducer. It functions by passing a gas jet through an orifice into a resonating cavity and altering the size of the cavity changes the frequency of the sound produced.

### Liquid-driven Transducers

A ‘liquid whistle’ (Figure 16 reproduced from Mason, T. J., “Sonochemistry”, Oxford Chemistry Primers, Oxford University Press, 1999, P26.) produces cavitation by the rapid movement of a blade caused by a liquid flowing across it. The frequency of the blade is dependent upon the flow rate of the liquid.

**Figure 16:** Schematic Diagram of a Liquid Whistle.



The liquid whistle finds its main application in the food industry for immiscible liquid homogenisation (e.g. mayonnaise).

### Electromechanical Transducers

The transducer used in Sonochemistry converts electrical energy into sonic energy. The two main types of electromechanical transducers function according to either the piezoelectric or magnetostrictive effect.

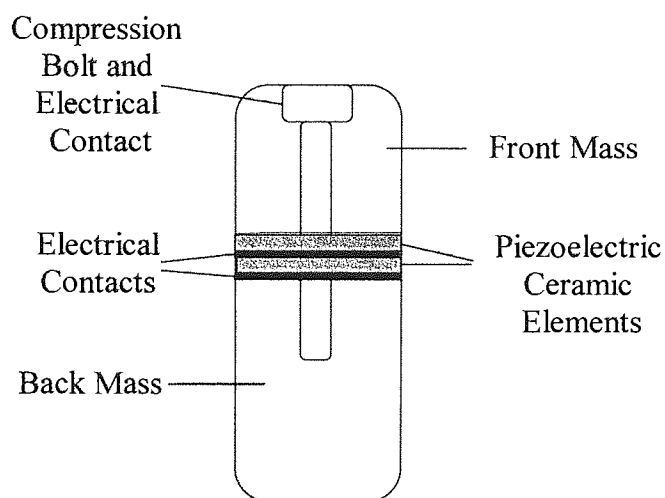
#### *Piezoelectric transducers*

The piezoelectric effect is based on the production of a potential difference across opposite faces of a mechanically compressed crystal. Transducers employed in the present day make use of the inverse of the effect. Rapid alternation of the potential difference across the crystal results in the corresponding, alternating changes in dimension converting electrical energy into sound. Piezoelectric transducers are the most commonly employed, normally powering the bath- and probe-type sonicator systems.

Almost without exception modern transducers are based on the pre-stressed piezoelectric design. Large piezoelectric elements have inherent weakness when power is supplied to them. It is for this reason that a transducer normally consists of a number of thin

piezoelectric elements (typically two or four) bolted together, and so kept under compression, between a pair of acoustically low loss metal end masses, generally titanium or aluminium (Figure 17). The assembly is designed so that the overall length corresponds to one-half wavelength ( $\lambda/2$ ) at the required frequency of operation.

**Figure 17:** The Piezoelectric Transducer.



The piezoelectric elements are made up of prepolarised lead zirconium titanate (PZT), ideal for an efficient and resilient transducer.

Other suitable piezoelectric materials can be manufactured or occur naturally. Quartz is found naturally although it is very fragile, which makes it difficult to machine. The 'electrostrictive materials' can be manufactured from various synthetic compounds such as lead metaniobate ( $\text{PbNb}_2\text{O}_6$ ) and barium titanate ( $\text{BaTiO}_3$ ).<sup>19</sup>

The transducer operates by application of a rapidly reversing charge to the piezoelectric material causing fluctuations in its dimensions. The vibrations of the crystal transmit ultrasonic waves through any medium with which the transducer is in contact.

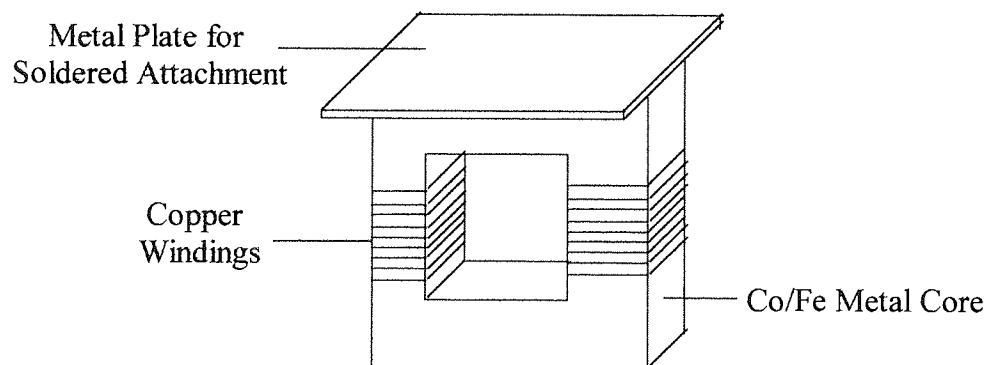
Piezoelectric transducers constructed in this manner have a potential efficiency of 98%<sup>20</sup> when converting electrical energy to acoustic energy and can handle power transfers of up to 1kW when operated continuously. However, the transducer described has a low vibrating motion, too small for its practical application in sonochemistry, so amplification of the motion is required. It is for this reason that horns are used, which, like transducers, also have a resonant element in the compression mode. The horn is normally half-wavelength ( $\lambda/2$ ) in length, however, in instances where longer assemblies are required

they are produced in multiples of this distance. Suitable materials for the construction of horns include titanium alloy, aluminium and stainless steel, as they have high dynamic fatigue strength, low acoustic loss, are chemically unreactive and resist erosion due to cavitation. The titanium alloy is far more efficient than the other materials with respect to its suitability in the four characteristic requirements.

### *Magnetostrictive Transducers*

Magnetostrictive transducers operate by dimensional changes in suitable ferromagnetic materials on the application of a magnetic field. Examples of such materials include iron, cobalt, nickel and their alloys. Normally a bar, acting as a magnetic core, is surrounded by a coil through which a varying current is applied, resulting in the production of ultrasonic energy.

**Figure 18:** The Magnetostrictive Transducer.



Although the magnetostrictive transducer is very robust and can withstand temperatures up to 453 K (180°C) they are not very efficient in their consumption of electrical energy. This problem has been improved with the advent of new, non-metallic, ceramic-based, ferrite materials. The employment of these materials reduces the frequency range to less than 100 kHz and as a consequence they find no application in the area of medicine, as this requires the frequency to be in the diagnostic ultrasound region i.e. above 2 MHz.



## 2.4 Power Ultrasonic Equipment

Within the laboratory environment there are two basic methods for the application of ultrasonic energy to a liquid reaction system.

- A low intensity system, typically the ultrasonic cleaning bath is used.
- A single transducer system coupling acoustic power to the reaction by using a direct immersion probe.

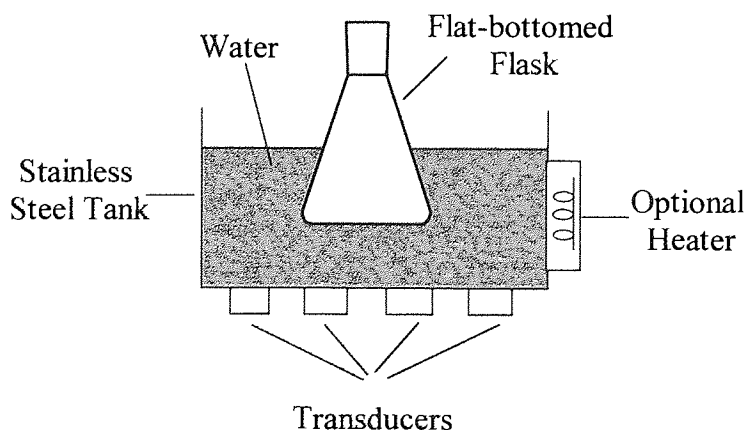
In each case a generator powers the transducer. However, in order to gain reproducible results both systems require that their reaction temperature and irradiation power intensity (Equation 24) be controlled.

A cleaning bath, using a modern piezoelectric transducer, has a power intensity in the region of  $1-5 \text{ Wcm}^{-2}$ . In order to obtain high powers a number of transducers are required for a bath. A horn operates at much greater powers, in the order of several hundred  $\text{Wcm}^{-2}$ .

### Ultrasonic Bath

The ultrasonic bath is the most widely used, inexpensive source of ultrasound available, providing a relatively even distribution of energy to the reaction vessel. No specialised reaction vessel is required, although, there is an advantage to using flat-bottomed glassware which allows more efficient transfer of the ultrasonic energy, whereas round-bottomed vessels tend to reflect a large portion of it.

**Figure 19:** A Flat-Bottomed Flask in an Ultrasonic Bath.



Although the ultrasonic bath is the most widely available source of ultrasonic energy, it has several disadvantages:

- Due to the low energy provided by the equipment (normally  $1-5 \text{ Wcm}^{-2}$ ), most heterogeneous reactions require agitation.
- Comparison studies using the bath are difficult since different models operate at frequencies and powers dependent upon the type of transducer employed.
- The use of water within the bath limits the temperature of its operation to under  $373\text{K}$  ( $100^\circ\text{C}$ ). The medium may be changed to allow a greater range, but this affects energy transfer from the transducer to the reaction vessel.
- The system has poor temperature control and it is important to record the temperature inside the reaction vessel, as this becomes a few degrees higher than the bath, due to ultrasonic heating.
- The precise position of the reaction vessel in the bath is very important as different areas within it produce slight variations in ultrasonic energy.
- The same vessel should be used for every reaction because the slightest difference in the thickness of the glass base alters the transfer of ultrasound into the reaction system.

#### Ultrasonic Horn (Probe)

The ultrasonic horn is the most efficient equipment employed to ultrasonically irradiate a system. A wide variety of ultrasonic horns are available, using different probes, most of which operate at around  $20 \text{ kHz}$ . The greatest advantage of the probe over the bath is that much higher ultrasonic powers, up to a maximum of a few hundred  $\text{Wcm}^{-2}$ , can be easily achieved. The power entering the system may be regulated by control of the power input to the horn and the power delivered by the horn is directly related to the magnitude of the vibration of the probe tip. A Vectronics VC300DLP antenna tuner measured the power entering any system investigated during these experiments. Reproducible results can be obtained because modern instruments have an automatic frequency regulator, in the case of the work carried out by the author a Yaesu FT-757GX transceiver was used. The Miroset PT135 was also used to provide a stabilised DC power supply. Finally, agitation of the

system is not required as ultrasonic streaming from the tip of the probe can cause effective bulk mixing.

However, the probe does have some disadvantages; it is more expensive than the ultrasonic bath and is less convenient in terms of the glassware required. As with the bath there is a problem with temperature control of the system and operation at a fixed frequency. In addition to these problems, erosion of the tip due to cavitation occurs causing contamination of the reaction by metal particles, which results in a reduction in the horn efficiency. Probe tips must be regularly replaced. Radical species can also be produced due to the high intensity irradiation from the tip of the probe, which is itself another source of reaction contamination.

Both types of equipment have their advantages, but for research the direct immersion probe is superior as it attains greater vibrational amplitudes and much greater power densities are achievable. The control of the power density within the reaction sample may also be achieved.

## **2.5 The Measurement of Ultrasonic Power**

There are two methods to measure ultrasonic power in a reaction system. As previously discussed there are various types of ultrasonic equipment available to the chemist for sonochemical reactions; the most commonly employed sources of ultrasonic irradiation are the ultrasonic cleaning bath and the horn (or probe). The horn transmits ultrasonic energy directly into the reaction sample whereas the bath conveys the energy via the water contained in the bath through the reaction vessel until it finally makes contact with the reaction mixture.

### **2.5.1 The Physical Measurement of Ultrasonic Power**

The most common method for the physical measurement of ultrasound entering a reaction mixture is calorimetry. The temperature rise is measured every few seconds using a thermocouple and temperature  $T$  versus time  $t$  plotted. The construction of a tangent to the curve at time zero or fitting a polynomial equation and obtaining the first differential from

its equation represents the rate of change of temperature with respect to time  $t$ . The power can be estimated using Equation 25.

If the calculated power is dissipated from a probe tip of area  $\text{cm}^2$  into a reaction sample, Equation 24 may be used to establish the intensity of power entering the sample.

### 2.5.2 The Chemical Measurement of Ultrasonic Power

Chemical measurements may be carried out using dosimeters. A chemical dosimeter measures only those products of a chemical reaction, which are produced as the result of sonication. However, this chemical measurement does not reflect the total energy entering the reaction system as not all events occurring inside the cavitation bubble result in the formation of observable reaction products; in the case of the sonication of water the  $\text{H}^\bullet$  and  $^\bullet\text{OH}$  radicals can recombine to form water again. There are four commonly used types of chemical dosimeter

- The Iodine Dosimeter
- The Terephthalate Dosimeter
- The Nitrophenol Dosimeter
- The Fricke Dosimeter

The nitrophenol and terephthalate dosimeters detect only the production of hydroxyl radicals as a result of the application of ultrasonic irradiation. However, the iodine and Fricke dosimeters are less specific and are oxidised by  $\text{HO}_2^\bullet$ ,  $\text{H}_2\text{O}_2$  or any other oxidising agent present.

#### The Iodine Dosimeter

The Iodine dosimeter utilises the homolytic fission of water to hydrogen, hydroxyl radicals and, in particular, hydrogen peroxide  $\text{H}_2\text{O}_2$  (see Figure 15). The hydrogen peroxide then oxidises potassium iodide to liberate iodine  $\text{I}_2$ .

By measurement of the absorbance of iodine in the UV/Vis spectrometer at 355nm a Beer-Lambert calibration line may be plotted for the addition of known quantities of hydrogen

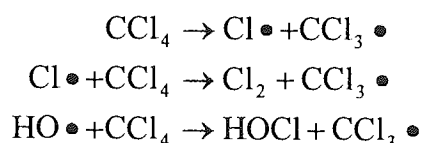
peroxide. The amount of peroxide can be ascertained from the calibration plot for a sonication reaction.

**Figure 20:** The Iodine Dosimeter Reaction with Hydrogen Peroxide.



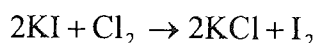
The rate of iodine liberated in the reaction can be enhanced by the addition of carbon tetrachloride ( $\text{CCl}_4$ ) to the iodine dosimeter and is known as the Weissler reaction<sup>21</sup>. The addition of a quantity of  $\text{CCl}_4$  increases the rate of the reaction by the production of chlorine  $\text{Cl}_2$ . The sonolysis of aqueous  $\text{CCl}_4$  is believed to proceed via the pathway in Figure 21.

**Figure 21:** The Sonolysis of Aqueous  $\text{CCl}_4$ .



The chlorine reacts with the potassium iodide to improve the rate of iodine liberation as displayed in Figure 22.

**Figure 22:** Reaction Mechanism for the Weissler Reaction.



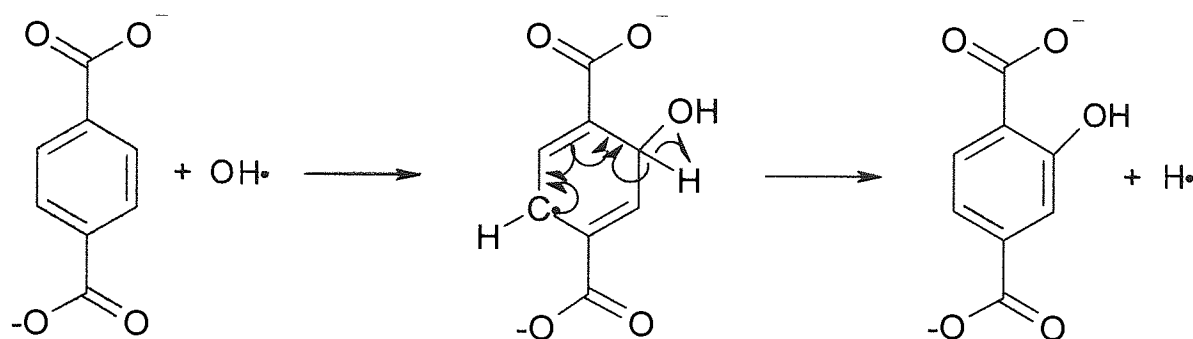
In the presence of  $\text{CCl}_4$ , the iodine is not entirely due to the existence of  $\text{H}_2\text{O}_2$  because of the possible side reactions. The chlorine **and** the hydrogen peroxide react to liberate iodine.

### The Terephthalate Dosimeter<sup>22</sup>

The Terephthalate Dosimeter is prepared by dissolving terephthalic acid and NaOH in a phosphate buffer of pH 7.4. In solution terephthalic acid generates terephthalate anions that

react with hydroxyl radicals to produce the highly fluorescent hydroxyterephthalate ions. This is a particularly sensitive method for the measurement of hydroxyl radicals produced as the result of sonication.

**Figure 23:** The Reaction of the Terephthalate Dosimeter

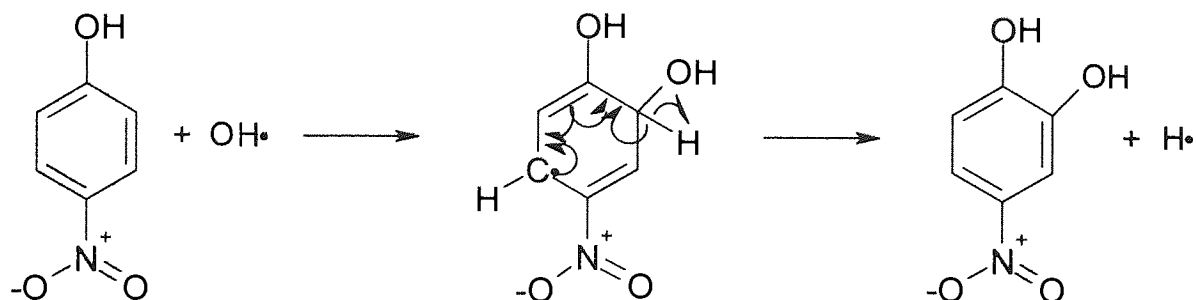


The hydroxyterephthalic acid produced by the reaction may be observed by fluorescence spectroscopy and it provides very good linearity for the plot of concentration against absorbance.

#### The Nitrophenol Dosimeter<sup>23</sup>

Hydroxyl free radicals may react with other aromatic compounds including 4-nitrophenol (*p*-nitrophenol) by the reaction scheme shown in Figure 24 to produce 4-nitrocatechol.

**Figure 24:** The Reaction of the Nitrophenol Dosimeter



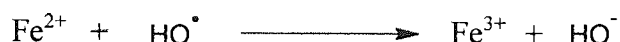
4-nitrophenol is used in an aqueous solution at pH 5 and the consumption of the 4-nitrophenol and the production of the nitrocatechol can be observed simultaneously by ultraviolet spectroscopy at wavelengths 401nm and 512nm respectively. The main

disadvantage of the system is that the hydroxyl radicals can continue to add to the 4-nitrocatechol leading to other products with different absorbances. A calibration curve for 4-nitrocatechol is constructed in the same manner as that for the terephthalate dosimeter.

#### The Fricke Dosimeter

Miller<sup>24</sup> studied the oxidation of  $\text{Fe}^{2+}$  to  $\text{Fe}^{3+}$  under ultrasonic conditions at a frequency of 500 kHz.

**Figure 25:** The Reaction of the Fricke Dosimeter

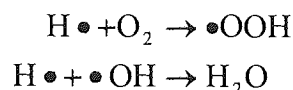


Miller<sup>24</sup> noted that the reaction occurred linearly for the production of the ferric ion over the first ten minutes of the reaction at, which point the linearity ceased. This was believed to be the result of the reaction mixture becoming degassed. When the solution was aerated the linearity was re-established. The energy input was estimated according to the increasing concentration of the ferric ion  $\text{Fe}^{3+}$  by ultraviolet spectroscopy at 304nm using a Beer-Lambert plot. The ferrous ion  $\text{Fe}^{2+}$  may not be observed as it has very poor ultraviolet absorption. This is both an advantage and disadvantage for the reaction; an advantage as there is no differentiation required between the two ions and a disadvantage since only the rate of production of the ferric ion may be followed.

It is important to be aware that the dosimeter reactions are highly frequency dependent, for example Luche and co-workers<sup>25</sup> have shown that the iodine dosimeter reaction using air-saturated KI solution is about six times faster at a frequency of 514 kHz than at 20 kHz. The increase in reaction rate was the result of the increased ultrasonic irradiation frequency employed. Increasing frequency has two effects: a cavity collapses in a shorter time producing less energy as it does so. At the higher frequency the  $\bullet\text{OH}$  radicals, formed as the result of water sonolysis, are released from the bubble before they can react. The formation of  $\text{H}_2\text{O}_2$  and  $\text{I}^{-}$  oxidation only occurs when the radical reaches the bubble interface and ultimately the reaction solution. When low frequency ultrasound of 20 kHz is employed the radicals begin to react within the cavity, forming amongst other things oxygen, in a manner

similar to that of flame chemistry. The molecular oxygen scavenges hydrogen atoms as shown in Figure 26 so lowering the recombination of the  $\bullet\text{OH}$  and  $\bullet\text{H}$  radicals.

**Figure 26:** Scavenging of Hydrogen Atoms by Molecular Oxygen in the Iodine Dosimeter.



Consequently, at 514 kHz more  $\bullet\text{OH}$  radicals are available since they escape from the cavity so do not undergo this reaction thus  $\text{H}_2\text{O}_2$  and  $\text{I}_3^-$  formation is greater at the higher ultrasonic irradiation frequency. Luche and co-workers further proved this fact as  $\text{H}_2\text{O}_2$  and  $\text{I}_3^-$  formation was more effective under argon than air saturated conditions for the same reason.

Miller<sup>24</sup> has also shown that the dissolved gas content of a reaction mixture is also a key reaction condition that must be considered when employing chemical dosimeters for power measurements. Degassing of the sample occurs as a reaction proceeds and the gas provides nucleation sites for the formation of cavities, the source of the effects of ultrasound on the reaction. It is for this reason that many reactions are saturated with a gas.

## 2.6 The Combination of NMR Spectroscopy and Ultrasound

For the chemist the most familiar use of ultrasound is in the area known as Sonochemistry. However, it has recently been used in conjunction with the analytical technique of NMR spectroscopy. Homer *et al*<sup>26</sup> have carried out investigations in several areas involving the combination of ultrasound with NMR spectroscopy, in particular the effects of sonication on the spin-lattice relaxation times  $T_1$  of liquids and the sonically induced narrowing of solid state NMR spectra (SINNMR).



## Chapter 3    The Theory of $S_N1$ and $S_N2$ Mechanisms

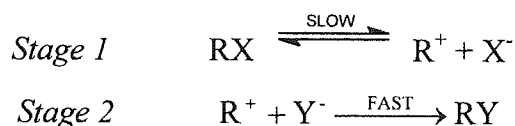
### 3.1 Types of Mechanisms

The mechanisms for aliphatic nucleophilic substitution reactions are dependent upon the substrate, leaving group, nucleophile and reaction conditions. However, in all such reactions the attacking species carries the electron pair. The most common mechanisms of this type are the  $S_N1$  and  $S_N2$ .

### 3.2 The $S_N1$ Mechanism

In an ideal situation the  $S_N1$  mechanism (*substitution nucleophilic unimolecular*) comprises two stages.

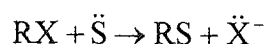
**Figure 27:** The Two-Stage  $S_N1$  Mechanism.



The initial stage is that of the ionisation of the substrate, which constitutes the rate-determining step. The remaining stage involves the prompt reaction of the intermediate carbocation with the nucleophile. The nucleophile in an  $S_N1$  reaction does not have to be a negative ion  $Y^-$  as will be shown later.

Nucleophilic aliphatic substitution has for many years been one of the most widely studied areas of organic chemistry and the subject of many disputes. Of particular interest is the system in which the solvent (S) is the nucleophile i.e. *solvolysis*.

**Figure 28:** Nucleophilic Aliphatic Substitution by Solvolysis.

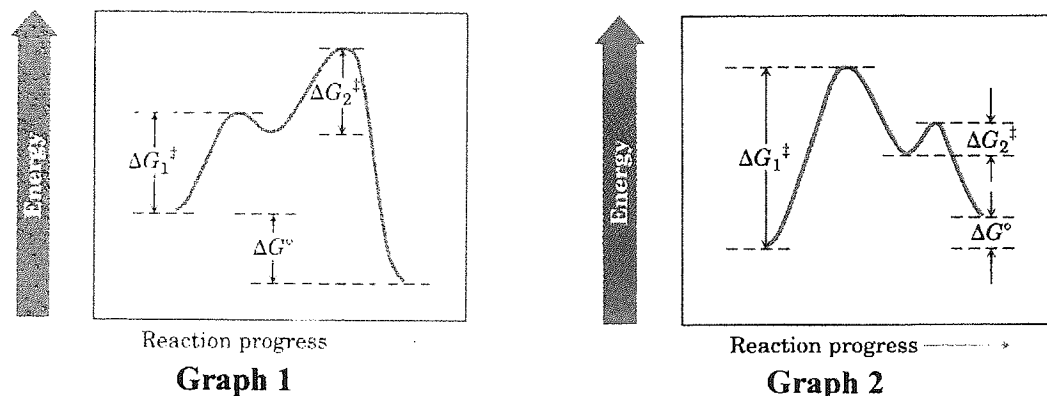


The solvolysis of many substrates occurs via the  $S_N1$  mechanism. It is the formation of the organic cation as an intermediate during this reaction, which requires investigation of its character, how it is produced and how it reacts. The study of the solvolysis system covers, in essence, all  $S_N1$  reactions and all reactions involving an intermediate carbocation.

### 3.2.1 Kinetic Evidence for the S<sub>N</sub>1 Mechanism

The hypothetical reaction energy diagrams displayed in Figure 29 (reproduced from McMurray, J. "Organic Chemistry" p 170, 4<sup>th</sup> ed. Brooks/Cole Publishing) represent the S<sub>N</sub>1 system for such two-stage reactions.

**Figure 29:** Hypothetical Energy Diagrams for the S<sub>N</sub>1 Mechanism.



Where:  $\Delta G^\ddagger$  = Free Activation Energy,  $E_a$  and  $\Delta G^\circ$  = Overall Gibb's Free Energy.

Graph 1 represents an exergonic reaction for which the Gibb's free energy change  $\Delta G^\circ$  has a negative value.

Graph 2 represents an endergonic reaction for which the Gibb's free energy change  $\Delta G^\circ$  has a positive value.

In a reaction system, the rate of the reaction is a measure of the disappearance of a reactant(s) or appearance of a product(s). However, the rate is not always proportional to the concentration of all reactants. Studying which reactants affect the rate of the overall reaction yields information on the possible mechanism.

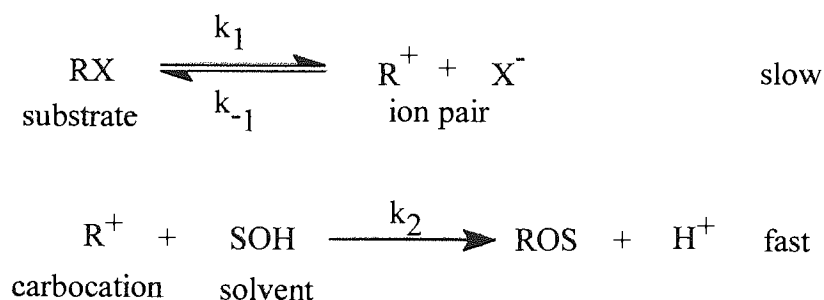
Kinetic evidence for the S<sub>N</sub>1 mechanism is indicated by a first-order reaction, where  $k$  is the rate constant in Equation 29.

**Equation 29:** The Simple Rate Equation of a First-order Reaction.

$$\text{Rate} = k[\text{RX}]$$

The rate-determining step involves only the substrate and the rate should be dependent only upon the concentration of the substrate. Even though the solvent assists in the ionisation of the substrate, because it is in excess, it is not inserted into the rate expression. However, this simplified version of the rate law does not account for all that occurs within the reaction. There are many cases in which more complicated kinetics take place and these too must be evaluated. The  $X^-$  produced as a result of the ionisation step competes with the nucleophile, Y, and consequently the simple rate law must be modified.

**Figure 30:** The Competing Reaction in the Solvolysis  $S_N1$  Mechanism.



**Equation 30:** The Complete Rate Equation of a First-order Reaction.

$$\text{Rate} = \frac{k_1 k_2 [\text{RX}][\text{SOH}]}{k_{-1} [\text{X}^-] + k_2 [\text{SOH}]}$$

When the reaction first commences the concentration of  $X^-$  is very small, i.e.  $k_{-1}[X^-]$  is negligible with respect to  $k_2[\text{SOH}]$  thus, the rate law may be represented by Equation 29.  $S_N1$  reactions do actually exhibit such simple first order kinetics during the preliminary stages of the process. Subsequently, during the latter stages of  $S_N1$  solvolyses,  $[X^-]$  increases, and according to Equation 30, it is predicted that the rate should decrease. Although this is the case for reactions of diarylmethyl halides,<sup>27</sup> it has been observed that t-butyl halides follow the simple rate equation (Equation 29) for the entire reaction.<sup>28</sup> One explanation for this disparity is the fact that t-butyl cations are less selective than that of the fairly stable diarylmethyl cation. Even though water is a much weaker nucleophile than the halide ion, ( $X^-$ ), it is present in much larger quantities since it is the solvent.<sup>29</sup> This means that the diarylmethyl cation endures many collisions with solvent molecules before it reacts

with a halide ion, whereas the less selective t-butyl cation reacts with the more abundant solvent.

According to the *common-ion effect*, the addition of  $X^-$  causes a decrease in the rate of the reaction. Once again this is true for the reaction of the diarylmethyl but not for that of the t-butyl halides, due to the less selective nature of t-butyl halides. The t-butyl halide is more likely to react with the excess solvent than the added ion  $X^-$ .

The *salt effect* further complicates matters and so must also be considered for such reactions. The rate of an  $S_N1$  reaction may be increased, by increasing the ionic strength of the solution. When the substrate  $RX$  and the nucleophile  $Y$  are both neutral,  $X$  is negatively charged. Most solvolyses involve this combination of charge character, so the ionic strength increases, thereby resulting in an increase in rate. It is this fact that must also be accounted for when studying the kinetics of such a system.

It is worth noting that the pseudo-first-order rate equation for an  $S_N2$  reaction, where  $Y$  is in excess, is the same as that for a simple  $S_N1$  reaction (Equation 29). It is therefore not possible to tell the two reactions apart through the use of simple kinetic measurements. The common-ion effect may be employed to discriminate between  $S_N1$  and  $S_N2$  reactions. The rate of an  $S_N2$  reaction will not be greatly affected by the addition of a common ion. Again, an exception to this is with the t-butyl  $S_N1$  system, which also does not exhibit the common-ion effect.

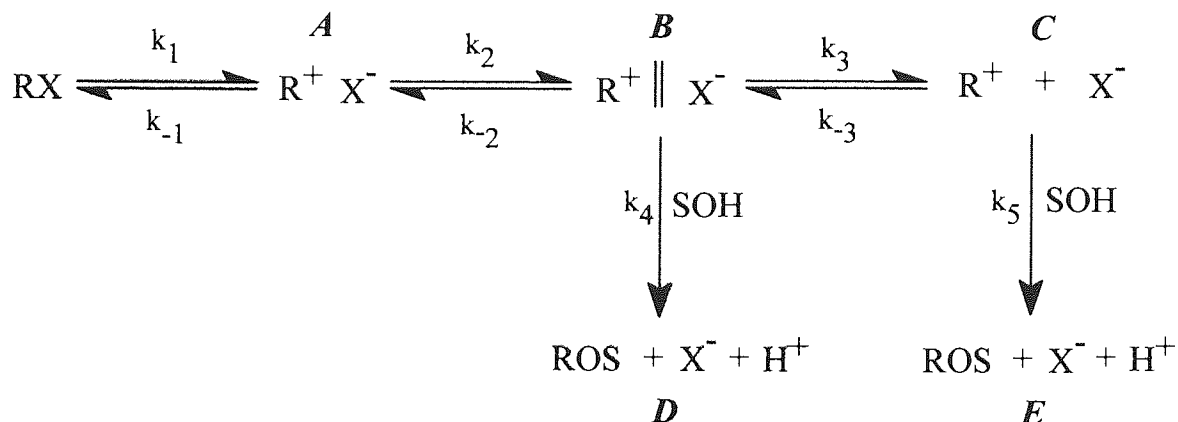
### 3.2.2 Stereochemical Evidence for the $S_N1$ Mechanism

The stereochemical evidence for the  $S_N1$  mechanism is as ambiguous as that of the kinetic evidence. It has been shown that some products are formed from *ion pairs* rather than from the free carbocation.

The ion pair is important for a number of reasons, which includes the mechanism and stereochemistry of solvolysis<sup>30, 31</sup> and the conductivity of triarylmethyl chlorides.<sup>32</sup>

A free carbocation has a planar structure and it is this that allows an attacking nucleophile to attack it from either side, consequently leading to racemic products. However, a little of the product does retain its configuration. It is this observation that led to the concept first proposed by Hammett<sup>33</sup> in 1940, then further developed by Winstein<sup>34</sup> *et al*, that the reaction proceed via *ion pairs*.<sup>35</sup>

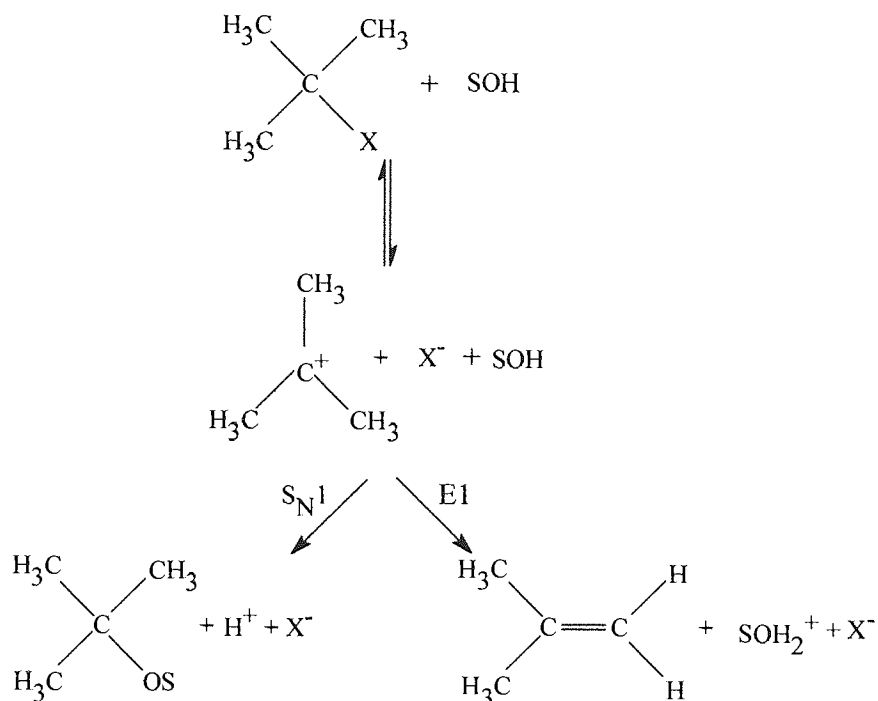
**Figure 31:** The Ion Pair Theory.



The reaction demonstrates the production of ROS from the solvent separated ion pair **B** and the dissociated ion **C** with rate constants  $k_4$  and  $k_5$  respectively. It is observed that the intimate ion pair **A** may also form ROS in reactions such as the solvolysis of  $\alpha,\alpha$ -dimethylallyl chloride and *t*-BuCl.<sup>6</sup> It should be noted that, at any stage, any of the ions **A**, **B** or **C** might return to their original RX form.

The existence of the intermediate ion pair may be demonstrated by the ratio of final products.<sup>36</sup> A solvolysis reaction often yields a mixture of substitution and elimination products (Figure 32).

**Figure 32:** The Substitution and Elimination Products from the Solvolysis  $S_N1$  Reaction.



If the mechanism of these reactions occurs via the free carbocation, being completely dissociated from the leaving group then the nature of that leaving group should have no affect upon subsequent reactions. Thus, the two products should form in proportions determined by the medium and should be independent of the nature of the leaving group. The results obtained by Winstein<sup>10</sup> for the product distributions of the solvolysis of a series of t-butyl derivatives, measured in various different solvent systems, are displayed in Table 4.

**Table 4:** Elimination Product Distributions in Various Solvent Systems.

X in t-BuX	Mole percent alkene		
	H <sub>2</sub> O 75°C (348K)	C <sub>2</sub> H <sub>5</sub> OH 75°C (348K)	CH <sub>3</sub> COOH 75°C (348K)
Cl	7.6	44.2	73
Br	6.6	36.0	69.5
I	6.0	32.3	—
S <sup>+</sup> (CH <sub>3</sub> ) <sub>3</sub> ClO <sub>4</sub> <sup>-</sup>	6.5	17.8	11.7

For water, the most ionising of solvents, the products are independent of the leaving group. The remaining solvents in the table display a marked dependence of product distribution on the leaving group indicating that the intermediate is an ion pair where  $X^-$  is still closely associated with the cation. The result of this close association is that the leaving group influences the course of the subsequent reactions.

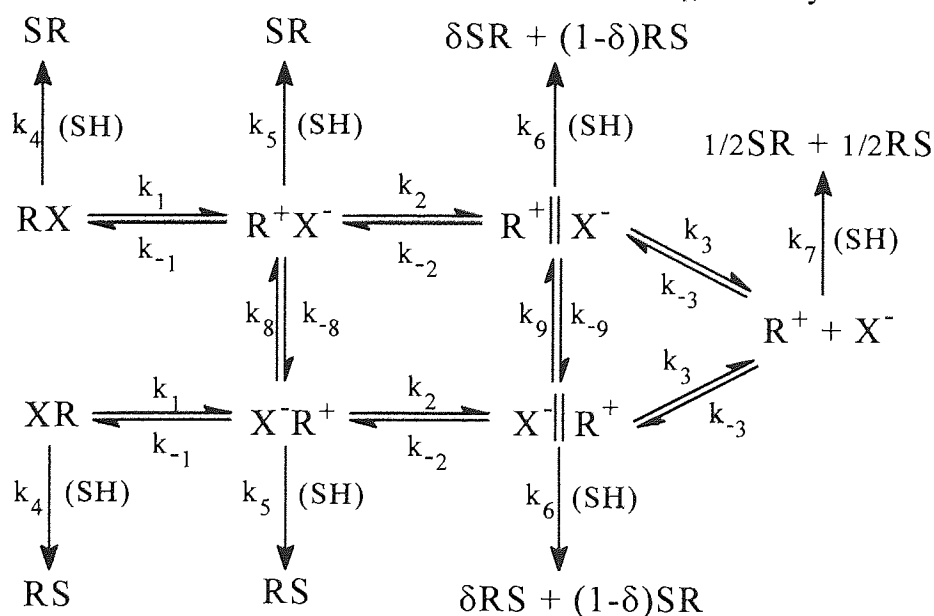
This accounts for the observations made by Hammett<sup>9</sup>, which were that substitution, or elimination, from an ion-pair instead of the free ion affects the partition of the alternative pathways since the departing group is sufficiently associated with the carbocation. Furthermore, complete racemisation cannot be achieved because the ion-pair, in contrast to the free ion, is still chiral.

Changing the structure of the starting material to make the carbocation less reactive, or, varying the solvent to aid ion separation, thus favouring the dissociation step relative to direct reactions of the ion-pairs, leads to results more characteristic of the free ion.

The evidence supporting the existence of the various types of ion pairs was derived from the observations made on the special salt effect by Winstein.<sup>37</sup>

In 1971 Shiner and Fisher<sup>38</sup> prepared a more comprehensive version of the reactions of solvolysis in the solvent SH. However, their scheme did not account for the obvious additional complications, which included elimination, rearrangement and other such processes.

**Figure 33:** All Possible Products Which Result from the  $S_N1$  Solvolysis Reaction.<sup>38</sup>



Where,  $0 \leq \delta \leq 1$



It was suggested that the initial reactant might also, in some cases, undergo attack from the nucleophile ( $k_4$ ). SR represents the enantiomeric partner of RS and  $\delta$  represents a fraction of the overall reactant. It should also be noted that the ion pairs required the solvent molecule to be present at the reverse of  $R^+$ . In each case  $k_4$ ,  $k_5$ ,  $k_6$  and  $k_7$  it is assumed that they pass directly via a transition state, with no intermediates, although such intermediates may be possible under certain conditions.

The aim of the diagram shown in Figure 33 is to ascertain which steps are rate determining and which step forms the product(s). The four main possibilities considered are:

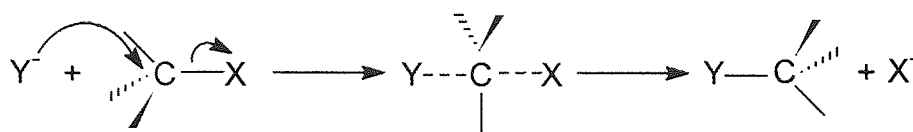
- SH reacts directly via an  $S_N2$  process ( $k_4$ ) with complete inversion to give SR.
- The solvent may attack at the intimate pair stage, via  $k_5$ , leading to complete inversion, or, if  $k_8$  occurs, the reactions compete and a combination of inversion and racemisation arises.
- The solvent separated ion pair undergoes a similar attack by the solvent to that of the intimate ion pair ( $k_6$ ). Due to the reduced proximity of the leaving group to the carbon, increased racemisation is anticipated and in some cases may be complete.
- Finally, production of the planar, free carbocation  $R^+$  gives rise to total racemisation ( $k_7$ ).

The behaviour described by the ion pair hypothesis is observed extensively and is proof that they are involved in many  $S_N1$  reactions resulting in total racemisation or partial inversion.

### 3.3 The $S_N2$ Mechanism

The  $S_N2$  mechanism (*substitution nucleophilic bimolecular*) consists of a one-step process passing through a transition state, not via an intermediate. The system involves *backside attack* of the nucleophile with respect to the position of the leaving group and does not involve the formation of an intermediate.

**Figure 34:** The  $S_N2$  Mechanism by *Backside* Attack of the Nucleophile.

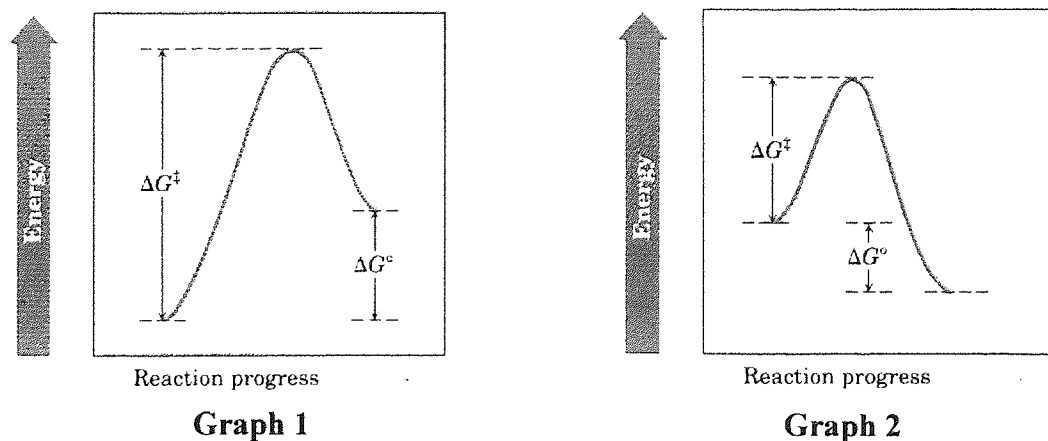


It is the simultaneous formation of the C-Y bond that produces the energy required in order to initiate the breaking of the C-X bond. At no point during this process does the carbon atom possess more than eight electrons in its outer shell. At the transition state the carbon has converted to an  $sp^2$  system from the initial  $sp^3$  hybrid with a near perpendicular p orbital, the lobes of which overlap with the nucleophile at one end and the leaving group at the other. It is for this reason that a front side attack for an  $S_N2$  mechanism has never been observed.

### 3.3.1 Kinetic Evidence for the $S_N2$ Mechanism

The hypothetical reaction energy diagrams displayed in Figure 35 (reproduced from McMurray, J. "Organic Chemistry" p 167, 4<sup>th</sup> ed. Brooks/Cole Publishing) represent a one-step reaction following an  $S_N2$  mechanism.

**Figure 35:** Hypothetical Energy Diagrams for the  $S_N2$  Mechanism.



Where:  $\Delta G^\ddagger$  = Free Activation Energy,  $E_a$  and  $\Delta G^\circ$  = Overall Gibb's Free Energy.

Graph 1 represents a 'slow' endogonic reaction, which has a positive Gibb's free energy of activation  $\Delta G^\ddagger$  value and large activation energy  $E_a$ .

Graph 2 represents a 'slow' exogonic reaction, which has a negative Gibb's free energy of activation  $\Delta G^\ddagger$  value and large activation energy  $E_a$ .

In order for either reaction to be 'fast' the activation energy value needs to be reduced.

Both the nucleophile and the substrate participate in the rate-determining step, since there is only one step in the reaction. Consequently, the reaction is first-order with respect to each constituent. Thus, Equation 31 is satisfied.

**Equation 31:** The Rate Equation of a Second-order Reaction.

$$\text{Rate} = k[\text{RX}][\text{Y}]$$

Although, as the name suggests, the mechanism for the  $S_N2$  reaction is bimolecular, this does not necessarily mean that such a reaction is always second-order. It may be that the nucleophile is present in excess and the reaction presents first-order kinetics. This is known as a pseudo first-order reaction and has the same rate equation as that of a first-order reaction.

**Equation 32:** The Rate Equation of a Pseudo First-order Reaction.

$$\text{Rate} = k[\text{RX}]$$

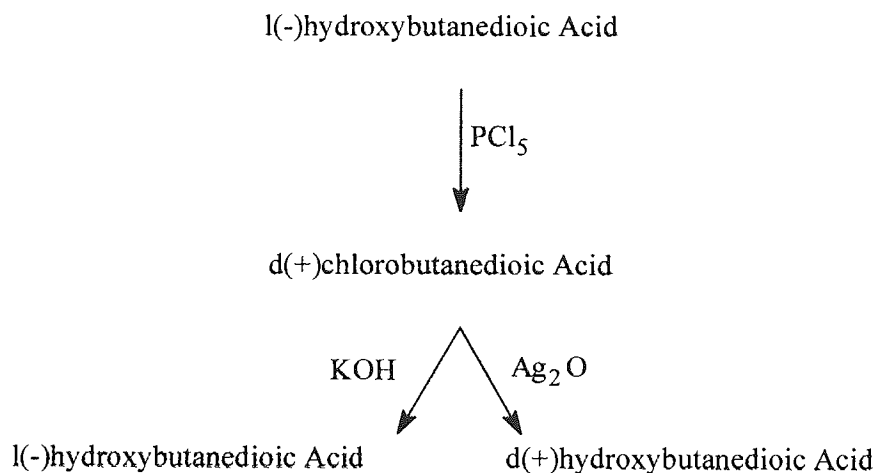
As a result of this effect, it is not sufficient to observe only the kinetic effects of an  $S_N2$  mechanism reaction; erroneous conclusions may follow if this simple approach is adopted.

### 3.3.2 Stereochemical Evidence for the $S_N2$ Mechanism

The  $S_N2$  mechanism predicts an inversion of configuration upon substitution at a chiral carbon and is known as the *Walden inversion*.<sup>39,40,41</sup> Hughes and Ingold observed The Walden inversion, named after its discoverer, long before the formulation of the  $S_N2$

mechanism.<sup>42</sup> Walden proffered various examples of reactions<sup>39,40,41</sup> in which inversion must have occurred, including that shown in Figure 36.<sup>40</sup>

**Figure 36:** The Walden Inversion of l(-)Hydroxybutanedioic Acid.



The reaction displays a system that produces the same compound of opposite configuration, or, by conducting a displacement under two different conditions; the products formed have opposite signs. However, a change in sign does not necessarily coincide with a change in configuration. Walden, unfortunately, did not establish exactly where the inversion happened.

Work carried out by Philips<sup>43</sup> and co-workers in 1923 proved that inversion was indeed taking place during the process of S<sub>N</sub>2 reactions.

### 3.4 Factors Affecting the Rates of S<sub>N</sub>1 and S<sub>N</sub>2 Reactions

It has been observed in many S<sub>N</sub>1 and S<sub>N</sub>2 experiments that a number of factors affect their relative rates. The most important factors being the role of the solvent, the effect of temperature, the nature of the leaving group, the substrate structure and the concentration and reactivity of the nucleophile (applicable to bimolecular reactions only).

### 3.4.1 The Role of the Solvent in S<sub>N</sub>1 and S<sub>N</sub>2 Reactions

Hughes and Ingold<sup>44</sup> carried out investigations into the interactions of solvents during aliphatic nucleophilic substitution and elimination reactions. They divided reactions of this type into groups according to the charge type of the reacting species, neutral, positive or negative. In passing from reactants via a transition state a change in charge magnitude of the reactant will have certain consequences for solvation: an increase in charge magnitude results in an increase in solvation, an increase in charge dispersal or destroying the charge decreases solvation. The effect of this upon nucleophilic substitution and elimination reactions is summarised in Table 5.

**Table 5:** Hughes-Ingold Rules for Predicting Solvent Effects on Reaction Rates.<sup>44</sup>

Reaction Type	Ground State Charge Distribution	Transition State Charge Distribution	Effect of Increasing Solvent Polarity upon Reaction Rate
S <sub>N</sub> 1 1	R-Z	$\delta^+$ R ----- $\delta^-$ Z	Large Acceleration
S <sub>N</sub> 1 2	R-Z <sup>+</sup>	$\delta^+$ R ----- $\delta^+$ Z	Small Deceleration
S <sub>N</sub> 2 3	X <sup>-</sup> + RZ	$\delta^-$ X ----- R ----- $\delta^-$ Z	Small Deceleration
S <sub>N</sub> 2 4	X + RZ	$\delta^+$ X ----- R ----- $\delta^-$ Z	Large Acceleration
S <sub>N</sub> 2 5	X <sup>-</sup> + RZ <sup>+</sup>	$\delta^-$ X ----- R ----- $\delta^+$ Z	Large Acceleration
S <sub>N</sub> 2 6	X + RZ <sup>+</sup>	$\delta^+$ X ----- R ----- $\delta^+$ Z	Small Deceleration

For an increase in solvent polarity it is suggested that increases in reaction rate occur when a decrease in charge density occurs in moving from reactants to transition state and a decrease in rate following an increase in charge density. Negligible effect is observed when little or no change in charge density takes place in the system. Thus, for the reactions of occurring via the S<sub>N</sub>1 and S<sub>N</sub>2 mechanism, qualitative predictions regarding the effect of solvent polarity may be made.

The conclusions of Hughes and Ingold have been confirmed in many substitution reactions. However, there are several limitations to the rules formulated. One assumption was that an increase in solvation usually results in a relatively small decrease of entropy  $\Delta S^\ddagger$  thus, its contribution at constant temperature to the Gibb's free energy of activation  $\Delta G^\ddagger$  would be negligible according to Equation 33.

**Equation 33:** The Gibb's Free Energy Change of Activation.

$$\Delta G^\ddagger = \Delta H^\ddagger - T\Delta S^\ddagger$$

This suggests that the expression is controlled by changes in enthalpy ( $\Delta H^\ddagger$ ) of the system. In practise this assumption is not entirely true, although most reactions are governed in this way. It is noteworthy that Pearson<sup>45</sup> reported several reactions, which exhibited a dominance of entropy  $\Delta S^\ddagger$  in the Gibb's free energy of activation  $\Delta G^\ddagger$ .

As the reaction name suggests solvents play a very important role during the solvolysis process,  $S_N1$  in reaction. The separation of the reactant, via the intimate and solvent separated ion pairs, to ultimately form the free carbocation  $R^+$  constitutes the rate-determining step. Due to the large increase in charge density in conversion from the neutral reactants to ion pairs in the transition state, a change in solvent polarity has a significant effect upon the rate of such reactions. The use of polar protic solvents greatly increases the rate at which this process takes place for any alkyl halide in *any*  $S_N1$  reaction because such solvents have the ability to solvate cations *and* anions, and as a consequence, the reaction has a lower energy of activation,  $E_a$ . So, by increasing the polarity of the solvent the activation energy should decrease and the rate increase for a transition state having a higher charge density than the starting material. It is anticipated that the reverse would also be true.

In contrast small or even negligible effects of solvent polarity are displayed in pericyclic reactions including the Cope rearrangement and Diels-Alder cycloadditions, since the change in charge density is minimal or non-existent.

### 3.4.2 The Effect of Temperature upon Reaction Rate

According to the *collision theory* molecules must collide with sufficient energy and in the correct orientation in order to effect a reaction, which explains why reaction rates increase for increased concentration and pressure.

The Maxwell-Boltzmann distribution of molecular energies describes how the fraction of molecules of given energy alters with a change in reaction temperature. An exponential relationship occurs in this situation illustrated by the Arrhenius equation.

**Equation 34:** The Arrhenius Equation.

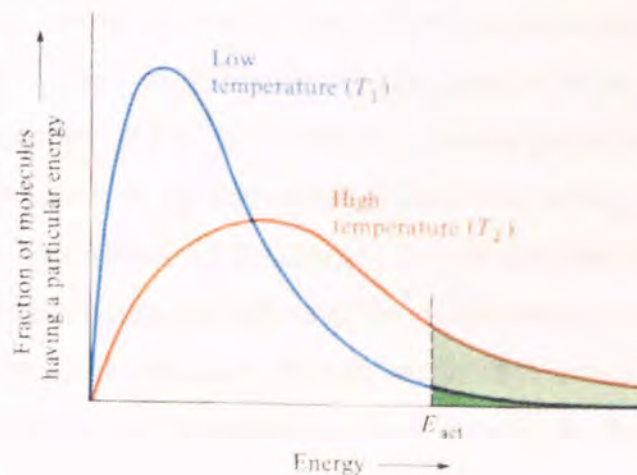
$$k = pz \exp^{-E_a/RT}$$

Equation 34 demonstrates the dependence of a reaction upon three factors: steric factor  $p$ , the collision-rate  $z$  and finally the fraction of collisions with sufficient energy ( $\geq E_a$ ) to react. In general the factors  $p$  and  $z$  are replaced by the pre-exponential factor  $A$

$$k = A \exp^{-E_a/RT}$$

The distribution is such that the fraction of molecules having energies greater than the activation energy  $E_a$  is given by  $\exp^{-E_a/RT}$ , where  $R$  = gas constant and  $T$  = temperature (K).

**Figure 37:** Boltzmann Distribution of Energies.



It is noted from Figure 37 (reproduced from Carey, F. A. "Organic Chemistry" p86, McGraw Hill, 2<sup>nd</sup> ed.) that the fraction of molecules with an energy greater than the activation energy increases greatly with increasing temperature.

The pre-exponential factor A (independent of temperature, or nearly), and the activation energy  $E_a$  can be determined by plotting  $\ln k$  against  $1/T$ .

**Equation 35:** The Logarithmic form of the Arrhenius Equation.

$$\ln k = \ln A - \frac{E_a}{RT}$$

The graph has an intercept of  $\ln A$  and a slope equal to  $-E_a/R$  and a reaction giving a straight line is described as showing Arrhenius-type behaviour. Once the activation energy of any reaction is determined it is a simple matter to predict how the rate would respond to a change in temperature.

### 3.4.3 The Effect of the Substrate Structure

The effect of the structure of the substrate upon the rate of a reaction is dependent upon the mechanism by which a particular reaction occurs.

In systems following the  $S_N1$  mechanism the reactivity is determined by the stability of the intermediate carbocation. Those reactions producing such carbocations capable of undergoing an  $S_N1$  mechanism include tertiary alkyl, allylic and benzylic halides. In such reactions  $\alpha$ -branching, i.e. the number of alkyl groups bound to the carbon atom to which the functional group is attached, increases the rate, usually in the order of alkyl cation stability; tertiary > secondary > primary > methyl. A tertiary cation is the most stable due to the positive inductive effect of the three-alkyl groups surrounding the positively charged central carbon atom thus dispersing its charge. Stabilisation reduces the free energy of activation in the rate-determining step allowing the overall reaction to occur at a reasonable rate. The reduced stability of secondary, primary and methyl carbocations, with respect to the tertiary form, means that the free energies of activation  $E_a$  for the  $S_N1$  mechanism have



the order methyl > primary > secondary. As a consequence the rates of reaction are slow and the  $S_N1$  mechanism does not compete with that of the  $S_N2$ .

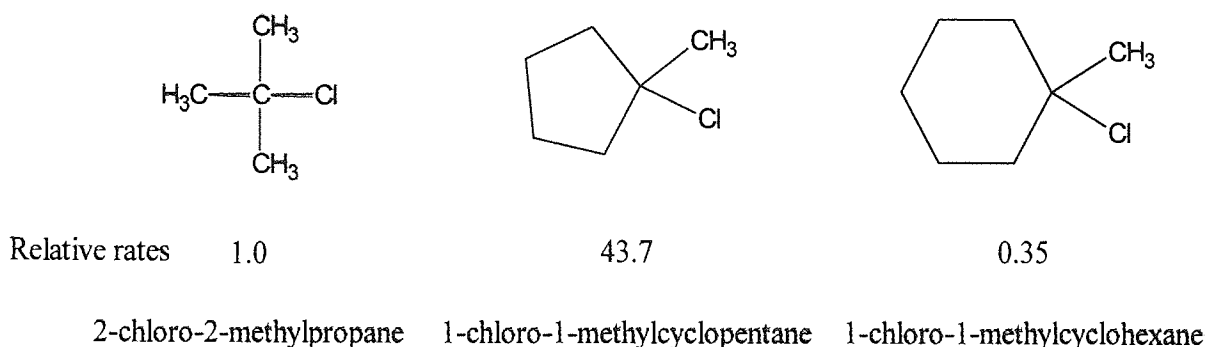
An additional explanation for the increase in reaction rates, due to increased  $\alpha$ -branching, is based on the effects of strain on reactivity. The rate-determining step involves the ionisation of the alkyl halide,  $sp^3$  hybridised with bond angles of around  $109.5^\circ$ , to the carbocation, which is  $sp^2$  hybridised with bond angles of around  $120^\circ$ . If the three-alkyl groups of the tertiary halide are large enough they will be pushed together by the enforced angle of the tetrahedral state resulting in B-strain (back strain). This strain is relieved by formation of the trigonal state when it becomes a carbocation.<sup>46</sup> In situations where B-strain is present the rate of carbocation formation and thus of the overall reaction is greater than when there is none. Work carried out by Brown and Fletcher<sup>47</sup> displayed this effect by examining the hydrolysis rate of t-alkyl halides under identical conditions (Table 6).

**Table 6:** The Rates of Hydrolysis of t-alkyl Chlorides, at 298 K, in 80% Aqueous Ethanol.<sup>47</sup>

Halide	Rate
$Me_3CCl$	0.033
$Me_2EtCCl$	0.055
$MeEt_2CCl$	0.086
$Et_3CCl$	0.099

Similarly, the reaction rate of cyclic compounds is affected by I-strain (internal strain) as a result of changes in ring strain in moving from a carbon atom with tetrahedral structure to that of trigonal planar. Using the reaction rate of t-BuCl as a reference, the eclipsing strain of 1-chloro-1-methylcyclopentane is alleviated, resulting in a 43.7 fold increase in solvolysis rate<sup>48</sup> under the conditions outlined in Table 6.

**Figure 38:** The Relative Solvolysis Rates of Various Cyclic Compounds with Respect to 2-Chloro-2-methylpropane.<sup>48</sup>



Eclipsing strain, however, does not exist in the compound 1-chloro-1-methylcyclohexane hence the rate with respect to the reference compound is not increased. The reason for the decrease in rate experienced by this compound is unclear.

Since any transition state has an almost zero lifetime it may not be directly detected. Consequently, a theory was constructed which permitted the geometry of such states to be predicted. In 1955 G. S Hammond<sup>49</sup> postulated that for any single reaction step '*the geometry of the transition state for that step resembles the side to which it is closer in free energy*'. According to the postulate, the transition state in an exogonic reaction (Figure 35, graph 2) that has a negative value of  $\Delta G^\ddagger$  has geometry resembling that of the reactants. The postulate is of most use in reactions during which an intermediate is formed. For reactions having free energy diagrams such as those displayed in Figure 29, both the first and second transition states are shown to resemble the geometry of the intermediate rather than that of the products or reactants. This is generally true of very reactive intermediates.

In systems following the  $S_N2$  mechanism branching of either  $\alpha$  or  $\beta$  carbons causes a reduction in the rate of a reaction. For example, simple alkyl halides follow the general order of reactivity, methyl > primary > secondary > tertiary, methyl being the most reactive. However, the reaction of a tertiary alkyl halide is so slow that it seldom follows an  $S_N2$  mechanism.<sup>50</sup>

The order of reactivity is mainly due to steric effects. Steric hindrance of large, bulky groups causes an increase in the potential energy of the transition state, which increases the activation energy, thus, reducing the overall reaction rate.

### 3.4.4 The Effect of the Leaving Group

A suitable leaving group is required to be stable upon departure from the reacting molecule. Most leaving groups possess a negative charge and those able to effectively stabilise this charge prove to be the most suitable, for example weak bases. At the transition stage during  $S_N1$ ,  $S_N2$  and  $E1$  reactions, the leaving groups attain a negative charge. The overall reaction rate increases since the potential energy and thus the activation energy of the transition state may be lowered by an increase in the ability of the leaving group to stabilise itself upon departure. The stabilisation ability of the halogens follows the trend  $I^- > Br^- > Cl^- \gg F^-$ , the opposite to that of basicity. One of the best-known leaving groups is the anion of the exceedingly strong acid  $CF_3SO_3H$ , the trifluoromethanesulphonate ('triflate') ion  $CF_3SO_3^-$ .

Strong bases, such as the hydroxide ion  $OH^-$ , rarely behave as leaving groups. However, dissolution of an alcohol in a strong acid causes the protonation of the  $-OH$  group forming a water molecule as a leaving group, a much weaker base than the hydroxide ion. Extremely powerful bases, which include the hydride  $H^-$  and alkanide  $R^-$  ions, may never operate as leaving groups.

### 3.5 Summary of the Overall Factors Affecting Reaction Rate

A summary of the overall effects of the factors, discussed in section 4.4, upon reaction rates are displayed in Table 7 and Table 8.

**Table 7:** Summary of Effects upon  $S_N1$  Reaction Rates.

	Type	Result	Effect upon reaction rate, $k_1$
<b>Solvent</b>	Polar	Stabilises carbocation via solvation.	Increases
<b>Nucleophile</b>	Reactive nucleophiles	Must be non-basic to prevent $E_2$ elimination.	No Change
<b>Temperature</b>	Increase in temperature	Increases number of molecules with correct $E_a$ for reaction to occur.	Increase
<b>Substrate</b>	Steric hindrance	$3^\circ$ , benzylic and allylic form most stable cations.	Increase
<b>Leaving Group</b>	Stable anions	Decrease the $E_a$ of the transition state.	Increase

**Table 8:** Summary of Effects upon  $S_N2$  Reaction Rates.

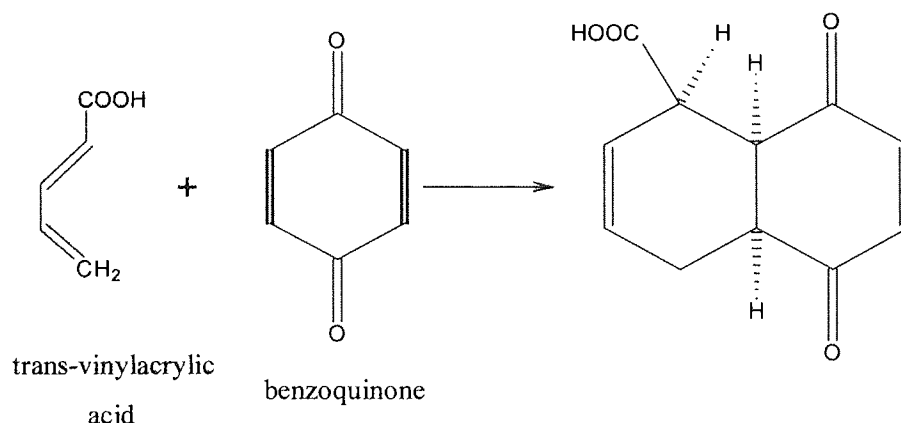
	Type	Result	Effect upon reaction rate, $k_2$ .
<b>Solvent</b>	Protic	Form $-OH$ bonds with nucleophile decreasing its energy, so increasing $E_a$ .	Decrease
	Polar aprotic	Surround cation not nucleophilic anion, increasing anion energy, decreasing $E_a$ .	Increase
<b>Nucleophile</b>	Reactive nucleophiles	$E_a$ decreased	Increase
<b>Temperature</b>	Increase in temperature	Increases number of molecules with correct $E_a$ for reaction to occur.	Increase
<b>Substrate</b>	Steric hindrance	Increase in $E_a$ due to steric hindrance methyl and $1^\circ$ are best.	Decrease
<b>Leaving Group</b>	Stable anions	Decrease in $E_a$ .	Increase

## Chapter 4    The Diels-Alder Reaction

In 1928 two German chemists, Kurt Alder and his chief instructor at the University of Kiel, Otto Diels, developed a 1,4-cycloaddition reaction of dienes<sup>51</sup>, which has now become widely known as the Diels-Alder reaction. However, it was Zincke and Günther<sup>52</sup> who made the initial discovery of the Diels-Alder type diene synthesis reactions. It was not until two decades later, in 1950, that Diels and Alder were jointly awarded the Nobel Prize in chemistry. Their work, which proved to be of such great versatility and synthetic utility as a route to six-membered, carbocyclic compounds, was finally recognised.

The Diels-Alder reaction is particularly important since it can be employed in the synthesis of cyclic and heterocyclic structures of naturally occurring compounds such as reserpine. It has tranquillising properties so is used for the treatment of mental disorders and the reduction of hypertension. Reserpine is an alkaloid found, with others, in the roots of the plant genus *Rauwolfia*, a source of various drugs. The Diels-Alder reaction in Figure 39 represents the reaction, which yields the compound required for synthetic reserpine production.<sup>53</sup>

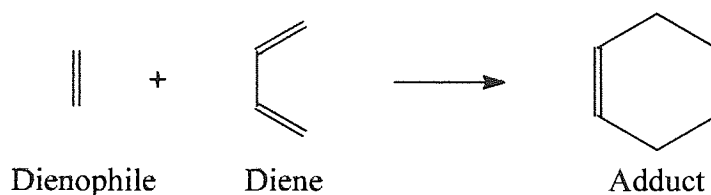
**Figure 39:** The Diels-Alder Reaction to Form the Required Reactant for Synthetic Reserpine Production.



#### 4.1 The Diels-Alder Reaction Mechanism

In general terms, a Diels-Alder reaction occurs between a conjugated *diene* (a  $4\pi$ -electron system) and a compound, containing a double or a triple bond, called a *dienophile* (diene + Greek; *philein*, to love). The reaction takes place by way of an  $S_N2$  mechanism producing a compound generally referred to as an *adduct*.

**Figure 40:** The General Diels-Alder Reaction.



As may be noted from the general equation in Figure 40 the reaction results in the creation of a ring not originally present in the reactants. The Diels-Alder reaction is therefore a member of a group of reactions referred to as **pericyclic reactions**. These are systems proceeding via a cyclic transition state. A Diels-Alder reaction is only pericyclic when bonds are simultaneously formed and broken. A zwitterionic or diradical system is therefore not classified as a member of the pericyclic group.

Pericyclic reactions have certain characteristics:

- i) The entropy of activation  $\Delta S^\ddagger$  is large and negative consistent with the loss of translational energy when two molecules combine forming a transition state. Bimolecular reactions inherently require additional organisation in order to align in the correct orientation to allow simultaneous bond formation. A value typically in the range  $-150 \text{ JK}^{-1}\text{mol}^{-1}$  to  $-200 \text{ JK}^{-1}\text{mol}^{-1}$  is observed.
- ii) The enthalpy of activation  $\Delta H^\ddagger$  is often small; consequently rates are large even at modest temperatures. This reflects the exothermic nature of the reaction.
- iii) Reactions are usually stereospecific.
- iv) Reversible Reactions are those involving two molecules reacting to produce one molecule which may then be reversed at high temperatures, since the  $T\Delta S^\ddagger$  term becomes increasingly important.

The most impressive evidence, although it only suggests and does not prove the ultimate pericyclic nature of any single reaction, is that there are an extraordinary number of reactions, which obey these very strict stereochemical rules. This is no coincidence and it supports the theory that almost all of the pericyclic reactions occur via a concerted mechanism. More often than not, if a reaction is believed to be pericyclic it usually is.

Most dienophiles employed in the Diels-Alder reaction are of the form  $\text{CH}_2=\text{CHZ}$  or  $\text{ZHC}=\text{CHZ}$  and in the case of  $\text{H}_2\text{C}=\text{CH}_2$  it is itself a diene. Other double and triple bonded compounds may also behave as dienophiles, including  $\text{N}\equiv\text{C}-$ ,  $-\text{N}=\text{C}-$ ,  $-\text{N}=\text{N}-$ ,  $\text{O}=\text{N}-$  and  $\text{C}=\text{O}$  compounds, producing heterocyclic compounds. With few exceptions there are six categories into which these dienophiles may be placed<sup>54</sup>.

- $\text{H}_2\text{C}=\text{CHZ}$   
 $\text{Z} = \text{H}, \text{X}, \text{CHO}, \text{CO}_2\text{H}, \text{CO}_2\text{CH}_3, \text{CO}_2\text{C}_2\text{H}_5, \text{COCl}, \text{COCH}_3, \text{CH}_2\text{X}, \text{CH}_2\text{NH}_2, \text{CH}_2\text{CN}, \text{CH}_2\text{CO}_2\text{H}, \text{CH}_2\text{NCS}, \text{OCOCH}_3, \text{SC}_6\text{H}_4\text{CH}_3, \text{SO}_2\text{R}.$
- $\text{C}_6\text{H}_5\text{CH}=\text{CHZ}$   
 $\text{Z} = \text{CHO}, \text{CO}_2\text{H}, \text{CO}_2\text{CH}_3, \text{CO}_2\text{C}_2\text{H}_5, \text{COCH}_3, \text{COC}_6\text{H}_5.$
- $\text{H}_2\text{C}=\text{CZ}_2$   
 $\text{Z} = \text{X}, \text{CO}_2\text{C}_2\text{H}_5, \text{CN}, \text{COCH}_3.$
- $\text{ZHC}=\text{CHZ}$   
 $\text{Z} = \text{X}, \text{CO}_2\text{H}, \text{COCl}, \text{CO}_2\text{CH}_3, \text{CO}_2\text{C}_2\text{H}_5, \text{COCH}_3, \text{COC}_6\text{H}_5.$
- Quinones e.g. Benzoquinone
- $\text{ZC}\equiv\text{CZ}$   
 $\text{Z} = \text{H}, \text{CO}_2\text{H}, \text{CO}_2\text{CH}_3, \text{CO}_2\text{C}_2\text{H}_5, \text{COC}_6\text{H}_5, \text{C}_6\text{H}_5.$

Such diversity as observed for the dienophiles is also noted for the dienes.

- Aliphatic Conjugates.
- Alicyclic Conjugates.
- Completely alicyclic systems
- Bicyclic systems
- Alicyclic-Aliphatic systems
- Aromatic Conjugates.
- Completely aromatic systems
- Aromatic-aliphatic systems
- Aromatic-alicyclic systems
- Heterocyclic Conjugates.



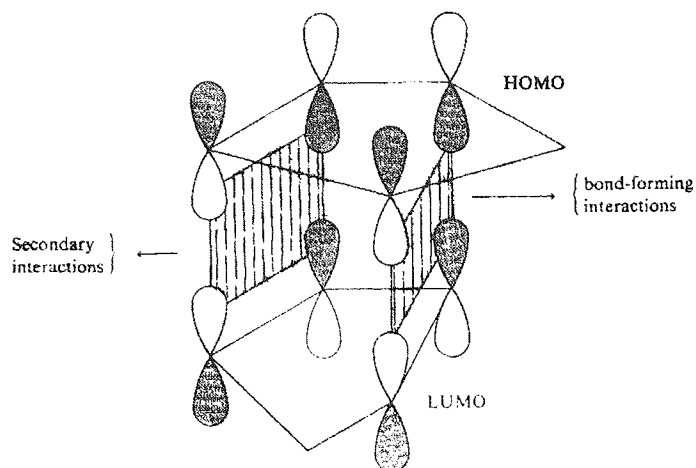
During the Diels-Alder reaction two new  $\sigma$  bonds are formed from two  $\pi$  bonds of the diene and dienophile. Since  $\sigma$  bonds are normally stronger than  $\pi$  bonds, adduct formation is favoured energetically, although *most Diels-Alder reactions are reversible*.

The Diels-Alder reaction is highly stereospecific: The reaction is a *syn* addition where orbital overlap is only achieved if the diene and dienophile approach with their molecular planes parallel. The configuration of the dienophile is retained in the product as  $sp^2$  hybridised orbitals effect rehybridisation to an  $sp^3$  structure i.e. a CIS dienophile forms a CIS product and a TRANS dienophile forms a TRANS adduct.

The diene of necessity may only react in the *s-cis* conformation. If a reaction of the *trans* conformation occurred, a highly strained *trans* double bond would be formed, but such a Diels-Alder reaction has never been observed.

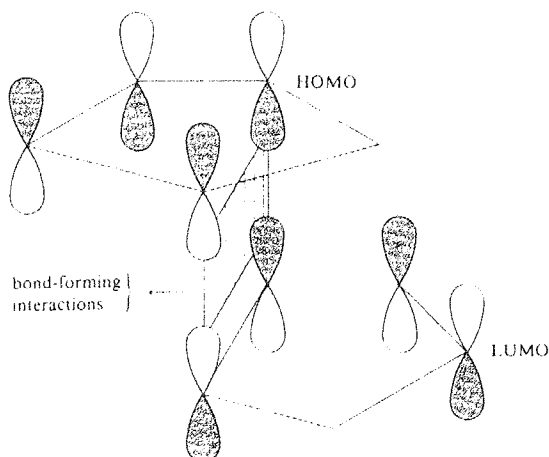
Diels-Alder reactions are also stereoselective: In the case of aromatic dienes, for example anthracene, when kinetically controlled the Diels-Alder reaction occurs primarily in an *endo* rather than an *exo* manner, although exceptions do exist in which mixtures of both do occur.<sup>55</sup> This follows according to the *Alder Rule* or the *rule of maximum accumulation of unsaturation*.<sup>56</sup> The *endo* adduct predominates since it is thermodynamically less stable than the product of an *exo* addition. This arises due to favourable secondary interactions between the  $\pi$  electrons of the developing double bond of the diene and the  $\pi$  electrons of the unsaturated groups. These 'like orbitals' of the dienophile help to stabilise the transition state of the reaction (Figure 41 reproduced from Norman, R. O. C. "Principles of Organic Synthesis" p293 2<sup>nd</sup> Ed. Chapman and Hall Ltd. 1978.).

**Figure 41:** The Stabilisation of the Transition State by Secondary Interactions.



An exo product, as shown in Figure 42 (reproduced from Norman, R. O. C. "Principles of Organic Synthesis" p293 2<sup>nd</sup> Ed. Chapman and Hall Ltd. 1978.), which is thermodynamically more stable, does not possess secondary interactions but may sometimes be formed in circumstances where the kinetically favoured adduct is reversible.

**Figure 42:** Absence of Stabilisation of the Transition State by Secondary Interactions.



#### 4.1.1 Orbital Symmetry Requirements of Pericyclic Reactions

It was not until 1965 that the mechanism and stereochemistry of pericyclic reactions were explained and as a result it was noted that they had orbital symmetry requirements. Woodward and Hoffmann, and Fukui have stated that this may be explained by the

*principle of conservation of orbital symmetry*<sup>57</sup> predicting those reactions that are symmetry allowed or *symmetry forbidden*. Hoffmann and Fukui were awarded the Nobel Prize in 1981 for their work in this area.

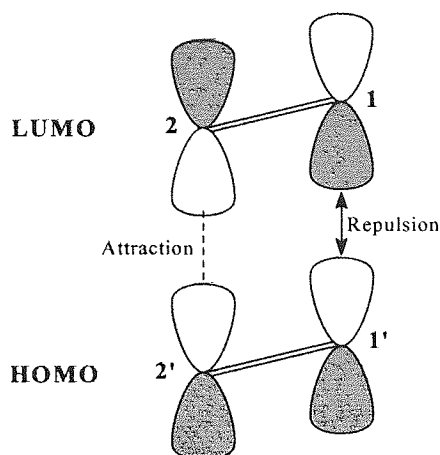
The Woodward-Hoffmann Rules, also termed orbital symmetry rules, are based on the hypothesis: *Only in concerted reactions*, for example the mechanism shown in Figure 40, *is maximum bonding maintained throughout the course of the reaction*. Although a reaction may be *symmetry forbidden*, in that it has a high energy of activation  $E_a$ , it may still occur via a different path, which is *symmetry allowed*, or via a non-concerted pathway ( $S_N1$  mechanism). There are several applications for the principle devised by Woodward and Hoffmann to cycloadditions, including that of the Diels-Alder reaction. The simplest approach is based on a method devised by Fukui<sup>58</sup> called the *Frontier Orbital Method*.

The highest occupied molecular orbital (HOMO) is the key to the reactivity of a molecule and is described as the *frontier orbital*. According to the Pauli Exclusion Principle no orbital may contain more than two electrons, whose spins are paired, and since almost all molecules contain an electron pair in the HOMO this cannot be the only orbital involved in bonding interactions. In fact, the HOMO of one reactant interacts with the lowest unoccupied molecular orbital (LUMO) of another. The LUMO and HOMO are closest in energy and make a disproportionate contribution, thus lowering the energy of the transition state as they interact.

The frontier orbital method may be used to explain the reason why common thermally induced reactions have  $(4n+2)$  electrons involved in their transition states i.e.  $[4+2]$ ,  $[8+2]$  and  $[6+4]$ . Cycloadditions involving  $4n$  electrons i.e.  $[2+2]$ ,  $[4+4]$  and  $[6+6]$  are almost exclusively photochemically induced reactions. Comparing the frontier orbitals of a  $[2+2]$  system with that of a  $[4+2]$  system illustrates the reason for this chemical behaviour.

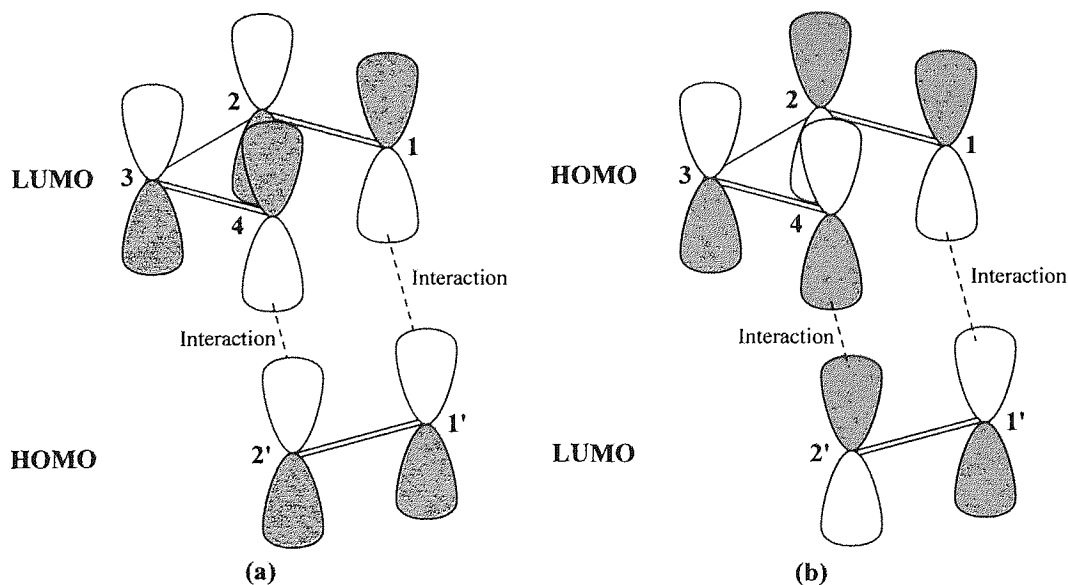
Figure 43 represents a  $[2+2]$  reaction system, which does not actually take place thermally as it is *symmetry forbidden*. Bonding may only occur between lobes of 'like phase' known as a bonding interaction, however, if the lobes are of opposite phase (dark and clear respectively) repulsion is experienced and is known as an antibonding interaction. A barrier is present to concerted bond formation; however, since no barrier exists for the formation of a bond between carbons 2 and 2' a stepwise reaction is possible.

**Figure 43:** A Symmetry Forbidden [2+2] Thermal Reaction.



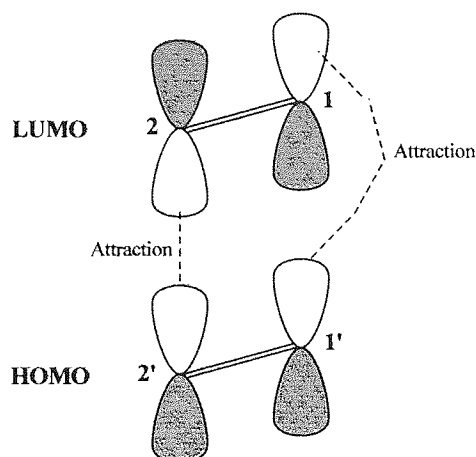
The [4+2] thermal reaction is *symmetry allowed*, as displayed in Figure 44. Both lobes have 'like phase' upon suprafacial approach and so bonding interactions are observed between both carbons 1 and 1' and 4 and 2'. This remains true no matter which way, (a) or (b), the orbitals approach each other.

**Figure 44:** A Symmetry Allowed [4+2] Thermal Reaction.



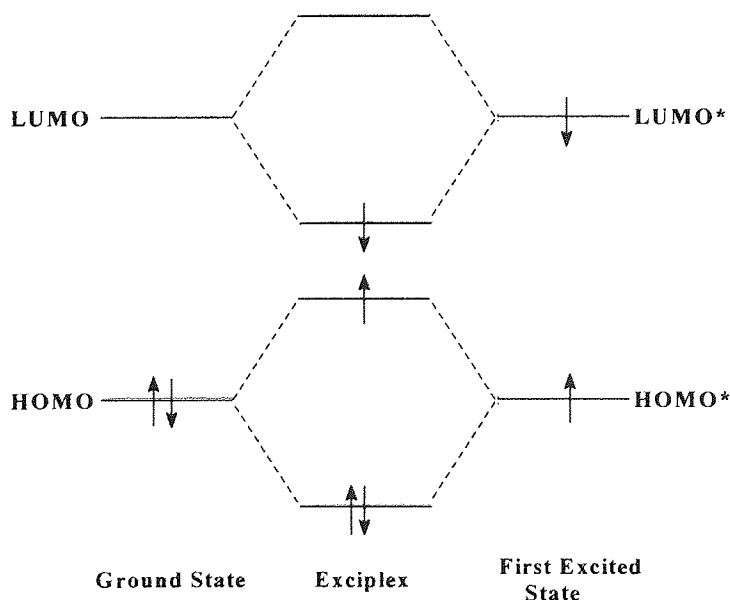
The explanation why some reactions, involving  $4n$  electrons, do proceed thermally is based on the fact that a long conjugated molecule may allow twisting so that bonding interactions may occur between two 'like phase' lobes.

**Figure 45:** Twisting of a Symmetry Forbidden [2+2] Thermal Reaction to Enable Reaction.



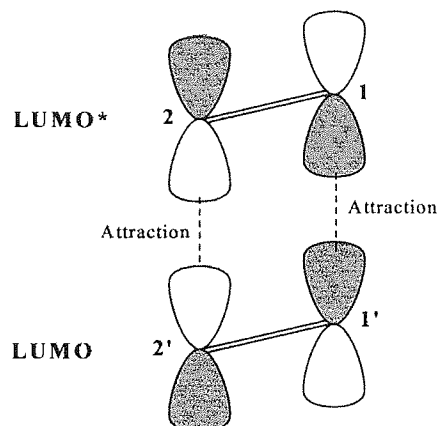
Certain reactions are photochemically induced rather than thermally because an electron may be promoted from the HOMO to the LUMO allowing the excited state molecule to react. As a result, the most efficient orbitals interact the LUMO of the ground state and the LUMO\* of the excited state (or alternatively the HOMO with the HOMO\*) thus lowering the energy of the transition state. The intermediate formed via such a photochemically induced bonding interaction is known as an *exciplex*.

**Figure 46:** Photochemical Promotion of an Electron in the Ground State, from the HOMO to the LUMO, to Form of the Excited State Molecule.



The energy of the two interacting frontier orbitals is close or almost identical causing the two molecules to be positively attracted (Figure 47) instead of being slightly repelled as observed in thermally induced reactions.

**Figure 47:** A Symmetry Allowed [2+2] Photochemical Reaction.



A similar argument can be applied to thermal cycloadditions in which a concerted [4+2] reaction may not occur photochemically as this has one bonding and one antibonding interaction.

There are two basic systems to which the Woodward-Hoffmann rules for cycloadditions can be applied. The first rule is based on thermal reactions and the other on photochemical systems.

**The Thermal Reaction Rule** – *'A ground state pericyclic change is symmetry-allowed when the total number of  $(4q+2)_s$  and  $(4r)_a$  components is odd'*<sup>59</sup>, where a = antarafacial addition and s = suprafacial addition and q and r are integers.

The example of a [4+2] system in Figure 44 is employed in order to explain the thermal rule. In a Diels-Alder reaction both reactants react in a suprafacial manner. The diene has four electrons involved in the reaction therefore may be represented as a  $(4r)_s$  component where  $r = 0$  and as a result no  $(4r)_a$  components exist for the system i.e.  $(4r)_a = 0$ . The dienophile has two electrons taking part corresponding to the  $(4q+2)_s$  component where  $q = 0$ . Since,  $(4q+2)_s = 1$  and  $(4r)_a = 0$  the total number of components = 1, which is an odd

number, thus it is a symmetry allowed system. As is observed for a thermal reaction the  $(4q+2)_a$  and  $(4r)_s$  components are ignored.

Since both the diene and dienophile involved in the Diels-Alder reaction are  $\pi$  systems it is more correctly described as a  $[\pi 4_s + \pi 2_s]$  cycloaddition. However, other systems may be annotated in the same manner and so the reaction still needs to be referred to as a Diels-Alder reaction.

**The Pericyclic Reaction Rule** – ‘A pericyclic change in the first electronically excited state is symmetry-allowed when the total number of  $(4q+2)_s$  and  $(4r)_a$  components is even’.<sup>60</sup>

The example of a  $[\pi 2_s + \pi 2_s]$  system in Figure 47 is employed in order to explain the photochemical rule. Both reactants have two electrons involved in the photochemical system which are both represented by  $(4q+2)_s$ , where  $q=0$  and there are no  $(4r)_a$  components. Having an even number of components means that the system is symmetry allowed.

It must also be noted that this system may also undergo thermal reaction if one reactant has a long enough chain to allow twisting in a  $[\pi 2_s + \pi 2_a]$  manner (Figure 45). Applying the same Woodward-Hoffmann photochemical rule to this exception again shows that no  $(4r)_a$  component is present and there is only one  $(4q+2)_s$  component. The other remaining component is that of a  $(4q+2)_a$  but according to the pericyclic reaction rule this is ignored in this situation, so the total number of components is odd and is not allowed to proceed photochemically.

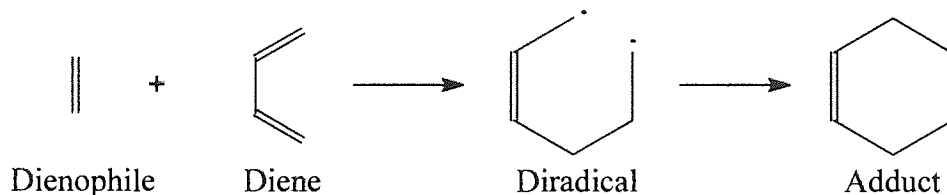
It is not possible to conclude which photochemical reactions are true pericyclic systems and exceptions do occur.

#### 4.1.2 Alternative Mechanisms for the Diels-Alder Reaction

There is great interest in the mechanism of the Diels-Alder reaction, in particular the precise timing of the formation of the new carbon-carbon bonds. Does their formation occur simultaneously or consecutively? In Figure 40 the reaction proceeds in a single

concerted step via a cyclic, six-membered transition state with no intermediate. However, there are two other possible routes by which the reaction may proceed. The second potential mechanism is via a diradical, as observed in Figure 48.

**Figure 48:** The Diels-Alder Reaction via a Diradical Transition State.



The first step of the reaction involves one end of the diene fastening itself to one end of the dienophile in order to form a diradical. During the second step the two diradical ends form the last remaining bond. The final mechanism is another stepwise system in which the intermediate is a zwitterion, formed in a similar manner to that of the diradical, except the initial and final bonds are created by the movement of electron pairs instead of single electrons. Both the diradical<sup>61</sup> and the zwitterion<sup>62</sup> systems have been observed.

Evidence suggests that most Diels-Alder reactions occur by way of the concerted one-step cyclic mechanism.<sup>63</sup> If a true diradical or diion situation were present the retention of configuration in both the diene and the dienophile would not be feasible. The rates of Diels-Alder reactions are independent of the nature of the solvent employed, ruling out the possibility of the presence of a zwitterion. A polar solvent would cause an increase in reaction rate of reactions in which the transition state develops a charge (see Table 5).

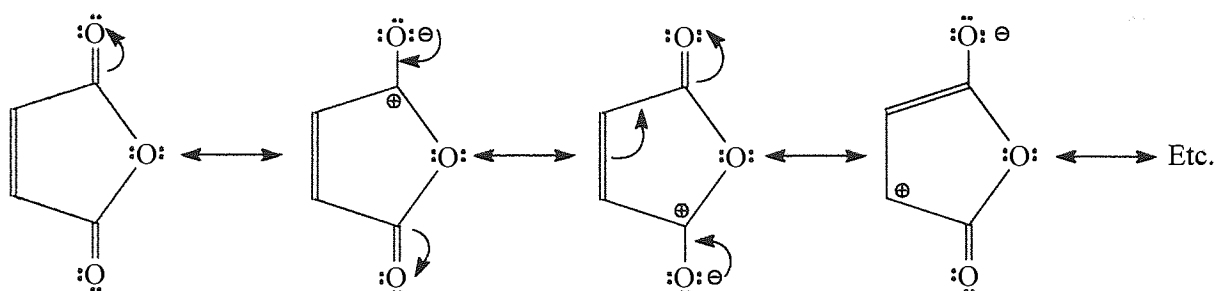
## 4.2 The Study of The Diels-Alder Reaction of Maleic Anhydride with Anthracene

In this study the Diels-Alder reaction investigated was that of the diene anthracene and the dienophile maleic anhydride in the solvents toluene and the more polar *o*-xylene.

Maleic anhydride is one of the most widely employed dienophiles in the Diels-Alder system: two carbonyl C=O groups on carbon atoms adjacent to a double bond withdraw electrons and it also has several resonance structures (Figure 49) contributing to the hybrid.

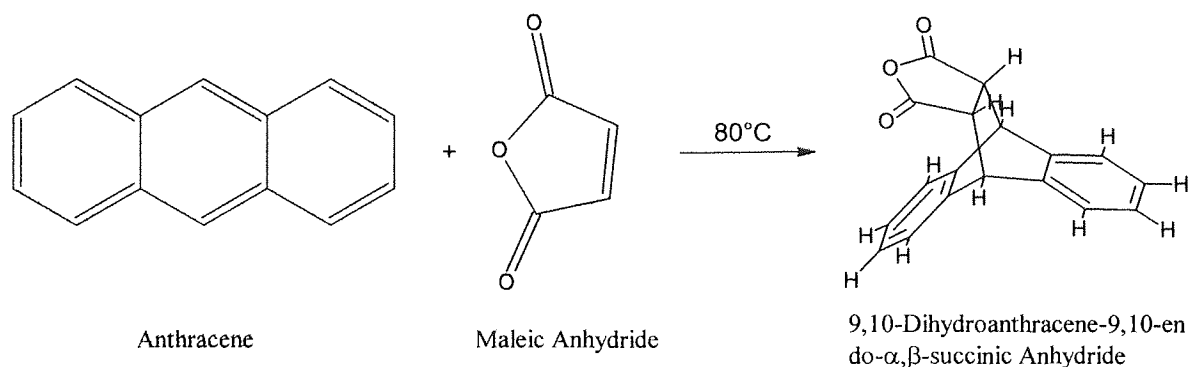


**Figure 49:** The Resonance Structures of Maleic Anhydride.



Anthracene, with its characteristic diene system, reacts with maleic anhydride almost quantitatively at  $80^{\circ}\text{C}^{64}$  (353 K) to produce the adduct 9,10-dihydroanthracene-9,10-endo- $\alpha,\beta$ -succinic anhydride. As a result of this reaction both the outer rings of the anthracene system become truly aromatic in character. Clar<sup>65</sup> observed the unmistakable absorption spectrum of a simple benzene derivative.

**Figure 50:** The Reaction of Anthracene with Maleic Anhydride to form 9,10-Dihydroanthracene-9,10-endo- $\alpha,\beta$ -succinic anhydride.

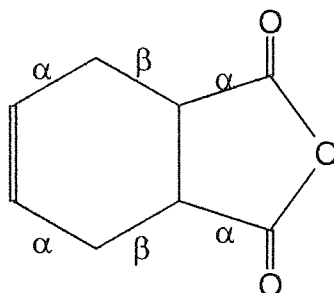


### 4.3 The Reversibility of the Diels-Alder Reaction

An adduct produced as the result of a Diels-Alder reaction is often thermally unstable. Systems involving two molecules reacting to form one final molecule may be reversed by what is known as a *retro-cycloaddition*. A *retro-cycloaddition* occurs when there is a large increase in temperature  $T$  causing the  $T\Delta S^{\ddagger}$  term of Equation 33 to become increasingly more important. In particular, those adducts with an endo-bridge show a pronounced tendency to revert to their components.<sup>66</sup> A number of reactions between maleic anhydride and several polycyclic hydrocarbons containing the anthracene nucleus have been observed

as being truly reversible.<sup>67</sup> The bonds one removed from unsaturation, not those adjacent, in the maleic anhydride undergo pyrolytic rupture (double bond rule). In a typical maleic anhydride adduct, such as that displayed in Figure 51, it is observed, according to the double bond rule, that  $\alpha$  is a strong bond and  $\beta$  is a weak bond.

**Figure 51:** The Double Bond Rule Applied to a Typical Maleic Anhydride Adduct.



The pyrolytic reversal of the Diels-Alder reaction between maleic anhydride and anthracene has been suggested as a method for the purification of anthracene.<sup>68</sup>

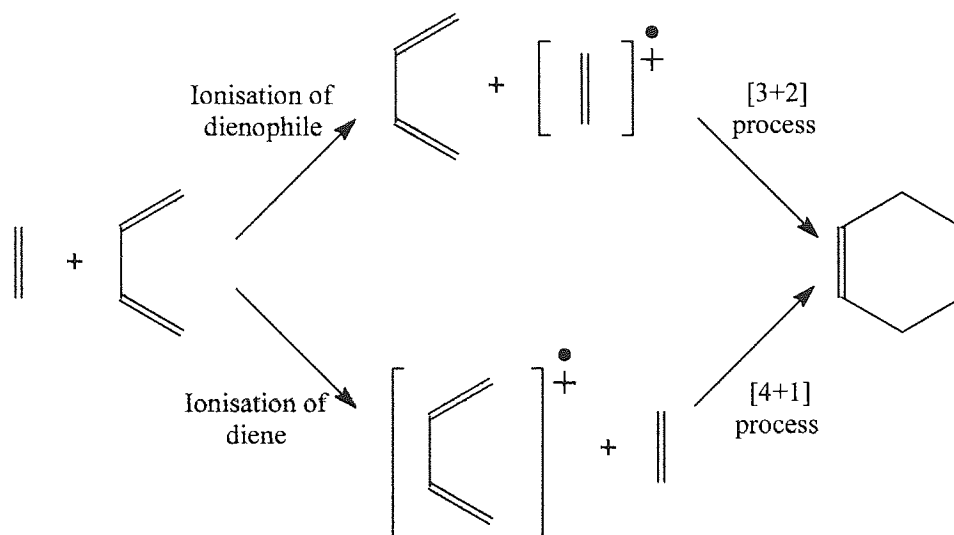
#### 4.4 Factors Affecting the Rates of Diels-Alder Reactions

In order to cause acceleration of the rate of a Diels-Alder reaction the presence of electron-withdrawing substituents in the dienophile and electron-releasing substituents in the diene are required. Electron-withdrawing groups attached to the diene and electron-donating groups attached to the dienophile cause a reduction in the reaction rate of a Diels-Alder system.

Various techniques for increasing the reaction rate of Diels-Alder reactions have been reported and include the use of an ultracentrifuge<sup>69</sup> (achieving reaction at high pressures), a microwave oven<sup>70</sup>, employing water to create a hydrophobic effect<sup>71</sup> or  $\text{LiClO}_4$  in  $\text{Et}_2\text{O}$ <sup>72</sup> and the absorption of reactants on chromatographic absorbents.<sup>73</sup>

Another method to induce a Diels-Alder reaction is by transforming a non-, or poorly reactive species into a closely related, much more reactive species, a radical cation for example (Figure 52)<sup>74</sup>.

**Figure 52:** The Diels-Alder Reaction via a Radical Cation.



Since the Diels-Alder reaction is known to be very sensitive to the effects of temperature and pressure, according to the 'hot spot' theory<sup>75</sup> it should also be sensitive to sonication.

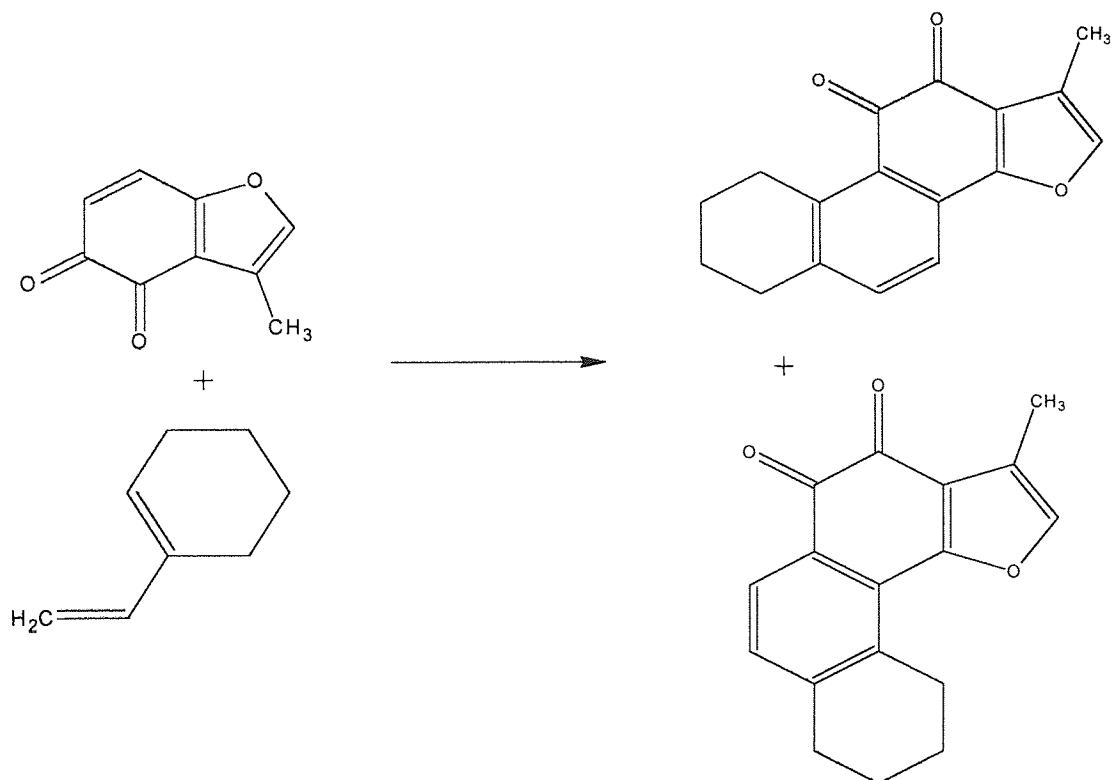
#### 4.5 The Sonochemical Modification of the Diels-Alder Reaction

Diels-Alder reactions have been researched over many decades and their mechanistic pathways well documented. As a result, it is particularly interesting to observe their modification during ultrasonic irradiation. However, the numbers of papers published concerning sonochemical Diels-Alder additions are few. Papers<sup>76</sup> have been published for reactions in which no enhancement of reaction rate due to sonication was observed.

Luche<sup>77</sup> proposed that a 'true' sonochemical reaction should only occur if a single electron transfer takes place. Thus, ionic and two electron transfer systems would be insensitive to the phenomena of cavitation. However, a few reactions do arise that are not normally accelerated by sonication since they are ionic processes. Such systems include cycloadditions.

One of the best examples of an ultrasonically induced Diels-Alder reaction describes additions of vinylcyclohexenes to *o*-quinones.<sup>78</sup>

**Figure 53:** The Ultrasonic Reaction of a Vinylcyclohexene with an *o*-quinone.



Numerous cases of such reactions have been cited and in each case the dienophile was *o*-quinone, a few examples are displayed in Table 9.<sup>79</sup> In each case the yield could be increased using high pressures or sonication in a cleaning bath. Both methods produce high yields of adduct.

**Table 9:** Additions of Vinylcyclohexenes to *o*-Quinones.<sup>79</sup>

Reaction Conditions	% Yield of Adduct
110°C, benzene, 12h, sealed tube	<10
Reflux, MeOH, 16h	40
11kBar, MeOH, 2h, RT	67
Eu(fod) <sub>3</sub> , 0.08 eq, benzene	31
Eu(fod) <sub>3</sub> , 0.08 eq, MeOH	20
Sonicate, neat, 45°C, 2h	65

Using the classical method of heating a benzene solution in a sealed tube produces a yield of <10% after a 12-hour period. However, irradiation in a cleaning bath, without the use of a solvent, forms adduct in up to 65% yield. It is interesting that in most cases the reactivity

of an ultrasonically induced system is reduced by the addition of an aromatic solvent such as toluene or benzene, whereas alcohols cause it to remain high.

Recently, Villacampa *et al*<sup>80</sup> obtained impressive results for the ultrasonic enhancement of the Diels-Alder reaction using N,N-dimethylhydrazones to produce six-membered nitrogen heterocycles. For example, the thermal reaction of dimethyl acetylenedicarboxylate with methacrolein N,N-dimethylhydrazone is not normally possible, but upon sonication produced 60% yield for the adduct after 50 hours at 50°C (323 K).

It is the Diels-Alder reaction of maleic anhydride with anthracene that the author has examined at high frequency, 3MHz. There has been much controversy with respect to the effects of ultrasonic irradiation upon this system. In 1992 Low<sup>81</sup> reported an overall enhancement due to sonication for the addition and that it probably still occurred via a concerted pathway, although in 1996 Luche *et al*<sup>82</sup> contested these results in an unpublished experiment, but did not actually state the frequency at which their experiments were carried out. Da Cunha and Garrigues<sup>83</sup> re-examined the work carried out by Low and Luche who studied the Diels-Alder reaction of maleic anhydride with anthracene in solution in toluene using a 20 kHz direct immersion probe. In all cases an equimolar homogeneous system was employed and all experiments, thermal and sonicated, were carried out under identical conditions (i.e. power, concentration, temperature, volume of toluene and time) in the temperature range 40-85°C (313-358 K). The final product solution was characterised by <sup>1</sup>H NMR spectroscopy. A significant acceleration in reaction rate due to sonication over that of thermal was observed, the maximum effect observed at 60°C (333 K) during the first hour of reaction (Table 10).

**Table 10:** The Dependence of Adduct Formation upon Reaction Conditions.<sup>83</sup>

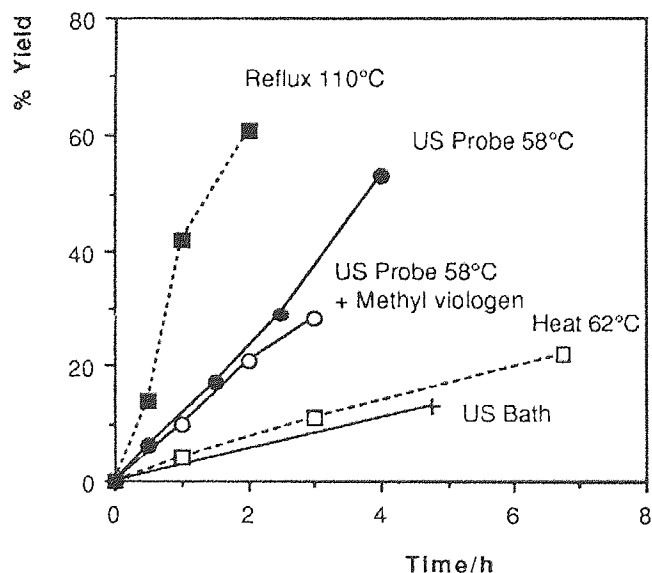
Exp. No.	Concentration (mol dm <sup>-3</sup> )	Temperature (°C)	Reaction Time (hour)	% Adduct Produced		Ratio $\left(\frac{\text{Sonicated}}{\text{Thermal}}\right)$
				Thermal	Sonicated	
1	0.03	40	3	Traces	3	3.0
2	0.05	60	1	2	12	6.0
3	0.05	60	3	7	36	2.1
4	0.08	75	1	5	14	2.8
5	0.08	75	3	14	49	3.5
6	0.15	85	1	18	41	2.3
7	0.15	85	3	36	80	2.2

It was also noted that no modification was observed when the ultrasonic source was replaced with a cleaning bath, thereby confirming the findings of Low<sup>81</sup>.

Toluene was chosen as a solvent since it was relatively inert to the effects of ultrasound and a homogeneous system ensured the elimination of the mechanical effects of ultrasound. Both Low<sup>81</sup> and Da Cunha/Garrigues<sup>83</sup> clearly showed that the transfer of an electron in the mechanism was not possible and that the reaction most likely followed a concerted mechanism. Addition of the electron transfer agent methyl viologen had no effect on the rate of the sonochemical reaction and no colour change was observed. If the transfer of an electron had taken place the production of a bright red intermediate and a further increase in reaction rate would have been observed.

The results of Low<sup>81</sup> are displayed in Figure 54 (reproduced from "Current Trends in Sonochemistry" Ed. G. J. Price, Royal Society of Chemistry Cambridge, 1992, P67.).

**Figure 54:** The Effect of Ultrasonic Irradiation on the Reaction of Maleic Anhydride with Anthracene.<sup>81</sup>



The thermal reaction was observed to be considerably slower than that of the ultrasonic reaction using a direct immersion probe. The extent of the thermal reaction was only 11% after a 4-hour period but the sonicated system had reached completion by this time. However, the traditional method of refluxing the reaction is still observed to be much faster than either method. The advantage of using sonication is that it involves milder conditions,

on a macroscopic scale, which may be advantageous for reactions involving substrates of low thermal stability.

The results observed by Da Cunha and Garrigues<sup>83</sup> and by Low<sup>81</sup> do not follow the rules set out by Luche<sup>77</sup> for 'true' sonochemical reactions. It would therefore be irresponsible to adopt these guidelines as an ultimate rule for predicting sonochemical reactions, whilst the understanding of the operation of sonochemical systems remains, at present, incomplete.

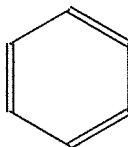
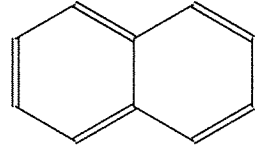
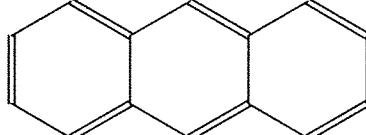
#### **4.6 Monitoring the Progress of the Reaction by Ultraviolet Spectroscopy**

When a conjugated organic molecule such as anthracene is irradiated with electromagnetic energy in the ultraviolet region (200-400nm) the energy absorbed is equal to the amount required to promote an electron from one orbital to another.

Anthracene absorbs ultraviolet energy ( $h\nu$ ) and a  $\pi$  electron is promoted from the HOMO to the LUMO. The electron is promoted from the bonding  $\pi$  molecular orbital to the antibonding  $\pi^*$  molecular orbital, that is a  $\pi \rightarrow \pi^*$  excitation. The magnitude of the energy gap over which this occurs is dependent upon the nature of the conjugated molecule. The energy gap between the HOMO and the LUMO for anthracene requires that ultraviolet light of wavelength 352.2nm is necessary to effect the  $\pi \rightarrow \pi^*$  electronic transition.

The extent of conjugation in an organic molecule is an important factor upon which the wavelength of ultraviolet light absorbed is dependent. The degree of separation between the HOMO and LUMO decreases as conjugation increases where a longer wavelength corresponds to reduced energy (Table 11).

**Table 11:** Ultraviolet Absorbances of some Conjugated Organic Compounds.

Name of organic compound	Structure of organic compound	$\lambda_{\text{max}}$ (nm)
Benzene		254
Naphthalene		275
Anthracene		359.3*

\*Determined experimentally by the author. Anthracene was examined in chloroform and the position of the largest of the five absorption peaks observed is provided.

The reduction in the concentration of anthracene will be monitored as the reaction runs its course and this will be employed to measure the rate of the reaction.

#### 4.7 The Treatment of Kinetic Data for the Diels-Alder System

The Diels-Alder reaction of maleic anhydride with anthracene occurs by way of an  $S_N2$  mechanism, following a second-order rate equation where  $[MA]$  represents the concentration of maleic anhydride and  $[A]$  that of anthracene at time  $t$ .

**Equation 36:** The Second-order Rate Equation for the Diels-Alder Reaction.

$$\text{Rate} = k_2[MA][A]$$

However, the reaction may be forced to follow pseudo first-order kinetics by addition of excess of one reaction component. The resulting equation takes into account the changing concentration of anthracene but assumes that any changes occurring to the maleic anhydride are negligible since it is present in excess.



**Equation 37:** The Natural Logarithmic Arrhenius Equation for the Diels-Alder Reaction.

$$\ln [A]_t = \ln [A]_0 - k_2 [MA]_0 t$$

In the case of the author's studies of the maleic anhydride/anthracene system, maleic anhydride was placed in excess whilst observing the reduction of anthracene by UV/Visible spectrophotometric analysis. A plot of  $\ln [A]_t$  vs.  $t$  should yield a straight-line graph, thus enabling an evaluation of the rate constant  $k_2$ .

**Equation 38:** The Second-order Rate Constant.

$$k_2 = \frac{-\text{gradient}}{[MA]_0}$$

Where  $[MA]_0$  is the concentration of maleic anhydride at time  $t=0$ s.

Various thermodynamic parameters may then be calculated using the Wynne-Jones Eyring equation (Equation 39) established and named after the authors in 1936.<sup>84</sup>

**Equation 39:** The Wynne-Jones Eyring Equation for the Diels-Alder Reaction.

$$k_2 = \frac{kT}{h} e^{\Delta S^\ddagger/R} e^{-\Delta H^\ddagger/RT}$$

However, it is a more convenient form to express the equation for  $k_2$  in terms of the activation energy  $E_a$ , instead of the enthalpy  $\Delta H^\ddagger$ .

**Equation 40:** The Enthalpy of Activation with Respect to the Change in Energy and Volume for the Reaction.

$$\Delta H^\ddagger = \Delta E^\ddagger + P\Delta V^\ddagger$$

$\Delta V^\ddagger$  is equal to the change in volume in passing from the initial reactants to the activated state and is almost equal to zero for all reactions occurring in solution, thus Equation 40 becomes

$$\Delta H^\ddagger = \Delta E^\ddagger$$

Since

$$E_a = RT + \Delta E^\ddagger$$

This equation may also be used to calculate the enthalpy for the reaction once the activation energy has been determined for the process.

**Equation 41:** The Change in Enthalpy of Activation with respect to Activation Energy.

$$\Delta H^\ddagger = E_a - RT$$

Finally, substituting Equation 41 into the Wynne-Jones Eyring equation, and with a little rearranging and taking natural logarithms of both sides of the equation, an equation is produced which incorporates the activation energy for the system (Equation 42).

$$k_2 = \frac{kT}{h} e^{\Delta S^\ddagger/R} e^{-(E_a - RT)/RT}$$

$$k_2 = e \frac{kT}{h} e^{\Delta S^\ddagger/R} e^{-E_a/RT}$$

**Equation 42:** The Wynne-Jones Eyring Equation Expressed with respect to Activation Energy.

$$\ln k_2 = \ln \frac{kT}{h} + \frac{\Delta S^\ddagger}{R} - \frac{E_a}{RT}$$

According to Equation 42 the 'constant' part of the equation is temperature dependent and strictly speaking a plot of  $\ln k_2$  versus  $1/T$  should produce a curve. However,  $\ln T$  varies to a lesser degree than the  $E_a/RT$  term when the value of  $E_a$  is significantly large that it acts as a multiplier outweighing any changes in the  $\ln kT/h$  term caused by temperature.

From Equation 42 a plot of  $\ln k_2$  versus  $1/T$  ( $K^{-1}$ ) yields the following information to allow calculation of entropy (Equation 43) and activation energy (Equation 44) for the system.

**Equation 43:** Calculation of the Entropy of Activation,  $\Delta S^\ddagger$ .

$$\text{Intercept} = \left( \ln \frac{kT}{h} + \frac{\Delta S^\ddagger}{R} \right)$$

**Equation 44:** Calculation of the Activation Energy,  $E_a$ .

$$\text{gradient} = -\frac{E_a}{R}$$

The Gibb's Free energy change of activation  $\Delta G^\ddagger$  may also be established at various temperatures using the well-known equation previously defined as Equation 33.

From the data obtained from the equations discussed, it is possible to assess the effect of ultrasonic irradiation upon the Diels-Alder reaction of maleic anhydride with anthracene.

## Chapter 5    The Solvolysis Reaction of 2-Chloro-2-Methylpropane

## 5.1 The Reaction Mechanism of 2-Chloro-2-Methylpropane

As previously discussed in chapter 3, several distinct mechanisms are possible for aliphatic nucleophilic substitution reactions, which depend on the nature of the substrate, nucleophile, leaving group and upon the reaction conditions. However, all the systems are related by the fact that the attacking species retains a lone pair of electrons.

Hughes and Ingold<sup>44</sup> carried out extensive studies with respect to the solvolysis reaction of alkyl halides. It was established that the hydrolysis of methyl and ethyl halides is bimolecular and that those of the ethyl are slower than the methyl whilst, in contrast, *tert*-butyl halides are hydrolysed very rapidly. This is consistent with the fact that there is a change in mechanism between the ethyl and *tert*-butyl group. Hughes<sup>85</sup> has proven that the solvolysis of 2-chloro-2-methylpropane, which from now on will be referred to as t-BuCl, is a unimolecular reaction, where the measured rate is that of the ionisation of the halide since this is the rate-determining step. Hughes<sup>85</sup> carried out experiments containing excess t-BuCl in dilute KOH<sub>(aq)</sub> and found that the reaction rate was constant and independent of the concentration of the alkyl halide. Even when all the alkali was neutralised by hydrochloric acid formation, the reaction continued at the same velocity. As illustrated in Table 12, it was also noted that at the lower concentrations the rate was independent of the initial concentration of the t-BuCl.

**Table 12:** The Hydrolysis of t-BuCl in 70% Aqueous Ethanol at Various Concentrations of t-BuCl.<sup>85</sup>

Experiment Number	[t-BuCl] (mol dm <sup>-3</sup> )	[KOH] (mol dm <sup>-3</sup> )	k <sub>1</sub> (hr <sup>-1</sup> )
1	0.0510	0.0571	0.145
2	0.0465	0.0571	0.147
3	0.0824	0.0571	0.145
4	0.1322	0.0571	0.141
5	0.1746	0.0571	0.137

A decrease in rate occurred for experiment 5 in Table 12 for a system containing 2cm<sup>3</sup> t-BuCl in 100cm<sup>3</sup> of reaction mixture. The change in rate was attributed to the fact that the reaction is particularly sensitive to solvent effects.

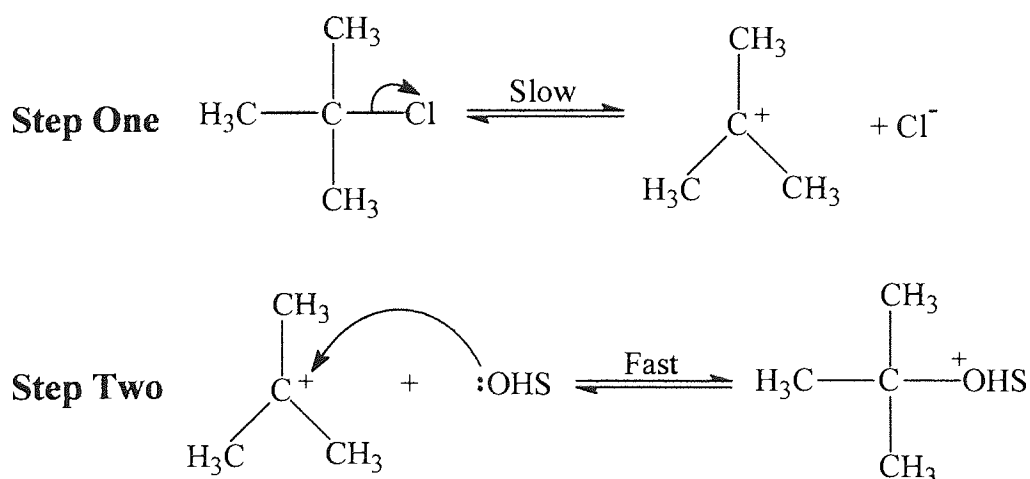
In order to confirm the limiting S<sub>N</sub>1 mechanism for the solvolysis of t-BuCl, Schleyer and co-workers<sup>86</sup> compared the solvolysis rates of t-BuCl and 1-bromoadamantane in a large

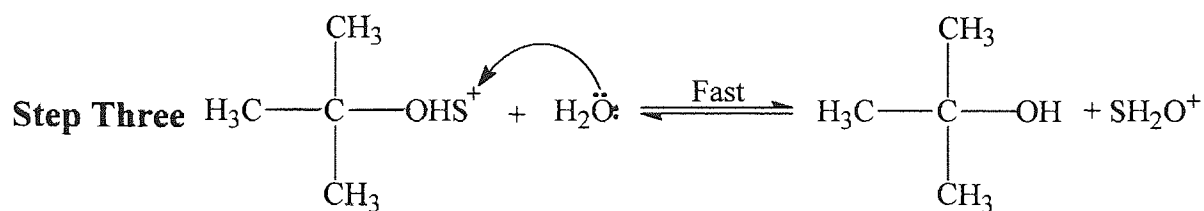
series of solvents. They reasoned that any rate determining elimination or nucleophilic solvent assistance in t-BuCl solvolysis would result in a failure to correlate with 1-bromoadamantane. In 1-bromoadamantane backside nucleophilic solvent attack and elimination are both impossible. An excellent correlation was found between solvolysis data for t-BuCl and 1-bromoadamantane, indicating that t-BuCl solvolyses via a limiting S<sub>N</sub>1 mechanism, free from nucleophilic solvent participation and from rate determining elimination. Similar correlations have been observed between t-BuCl and 1-adamantyl tosylate<sup>87</sup> as well as 2-adamantyl tosylate<sup>88</sup>. In most cases, an S<sub>N</sub>1 process best explains the solvolysis rate data of t-butyl substrates with electrophilic solvent assistance of the leaving group in protic solvents forming strong hydrogen bonds. In other words the ionisation rates of t-butyl halides should be mainly dependent upon solvent polarity and electrophilicity, but not upon nucleophilicity<sup>89</sup>.

Further evidence for the S<sub>N</sub>1 mechanism is observed for the reaction, or lack of reaction, under S<sub>N</sub>1 conditions of bridgehead carbon atoms. The lack of reaction is no surprise since carbocations require a planar (sp<sup>2</sup>) structure, which bridgehead carbon atoms cannot adopt.

The work described indicated that the solvolysis of t-BuCl is a kinetically first-order nucleophilic displacement reaction, S<sub>N</sub>1, in which, as the name suggests, the solvent acts as the nucleophile, where S = H or isopropyl group.

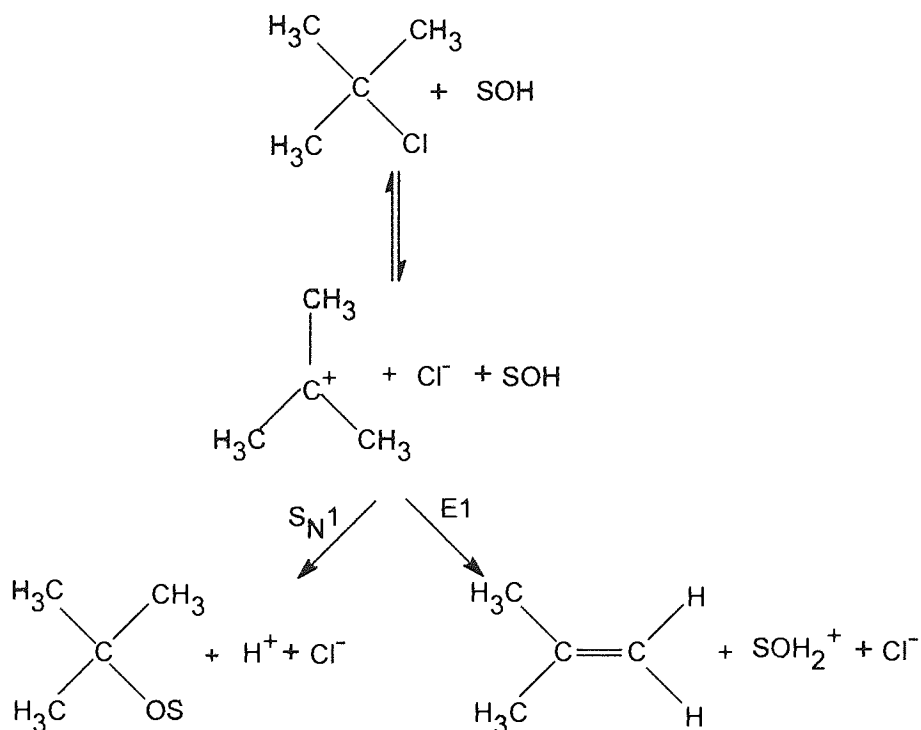
**Figure 55:** The S<sub>N</sub>1 Solvolysis Reaction of t-BuCl.





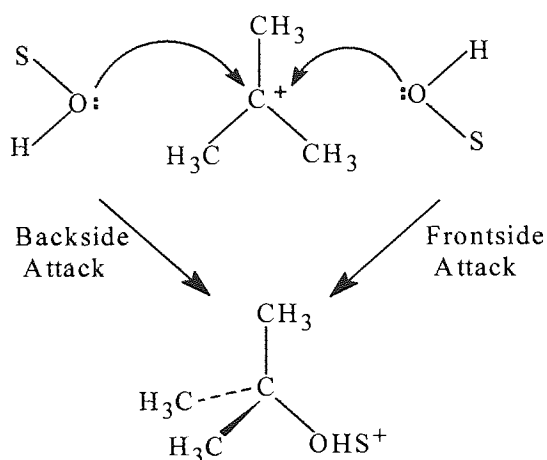
The most likely products result from the competing substitution  $\text{S}_{\text{N}}1$  and elimination  $\text{E}1$  reactions for the system.

**Figure 56:** The Substitution and Elimination Products from the Solvolysis  $\text{S}_{\text{N}}1$  Reaction of t-BuCl.



In the case of the solvolysis of t-BuCl the initial step (rate determining step) involves the cleavage of the C-Cl bond forming the carbocation in the transition state, via the ion pairs previously discussed in chapter 3. Formation of the reaction products occurs by solvent attack of the carbocation. The carbocation formed from the tetrahedral  $\text{sp}^3$  t-BuCl has a trigonal planar  $\text{sp}^2$  structure and the nucleophile may attack from either side.

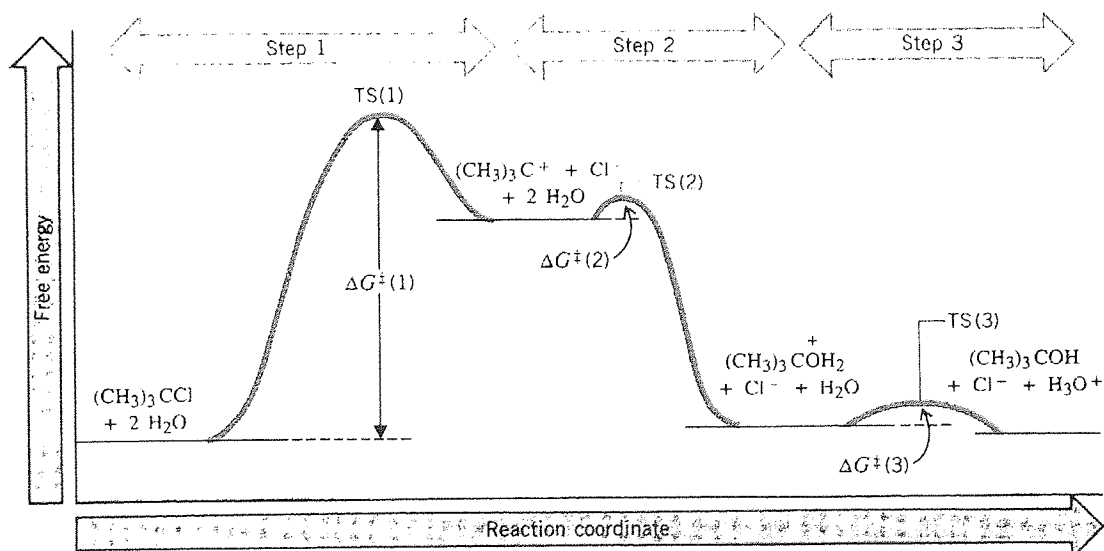
**Figure 57:** *Backside and Frontside Nucleophilic Attack of the tert-Butyl Carbocation.*



However, unlike some cations where different products are prepared as a result of the two possible modes of attack, the *tert*-butyl cation always forms the same compound.

The energy profile for the three-step  $S_N1$  reaction for the solvolysis of *t*-BuCl with water is illustrated in Figure 58 (reproduced from Solomons, T. W. G. *Organic Chemistry*, 5<sup>th</sup> ed. John Wiley and Sons, Inc. 1992, P228).

**Figure 58:** The Energy Profile for the Three-Step  $S_N1$  Reaction for the Solvolysis of *t*-BuCl with Water.

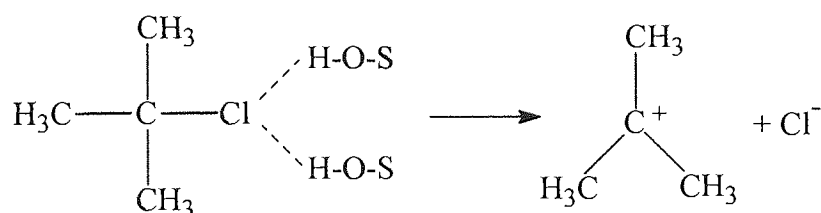




The initial transition state is of greatest importance for this reaction, where the C-Cl bond of the t-BuCl is breaking and ions begin to develop via ion pairs. This ionisation always requires solvent assistance<sup>90</sup> in the form of solvation of the carbocation. Solvation recovers a large portion of the energy required to break the bond. For example, the energy required to induce the ionisation of t-BuCl in the gas phase (without a solvent) is 630 kJmol<sup>-1</sup> and normally this reaction would only occur at very high temperatures. The same reaction in water only requires 84 kJmol<sup>-1</sup> of energy and can take place readily at room temperature. The fast, second step involves the conversion of the carbocation into the *tert*-butyloxonium ion, the second intermediate, which then quickly loses a proton to finally form *tert*-butyl alcohol. According to the Hammond postulate, both the first and second transition states, TS(1) and TS(2) respectively, have geometry resembling that of the intermediate carbocation since they are closest in energy to it. The third transition state TS(3) most resembles the sp<sup>3</sup> structure of the *tert*-butyloxonium ion to which it is closest in energy.

Kinetic and other evidence<sup>91</sup> suggests that the presence of two hydrogen-bonded OH groups act on the Cl thus, weakening its bond with the carbon atom and ultimately assisting in the cleavage of that bond.

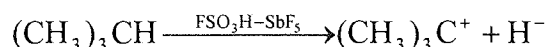
**Figure 59:** The Assistance of Hydrogen Bonding in the Weakening and Ultimate Cleavage of the C-Cl Bond.



The existence of 'free' OH groups in water has been observed in the near infrared region by spectroscopic investigation.<sup>92,93</sup> During the studies it was also observed<sup>92,93</sup> that upon the addition of co-solvents, scavenging of the 'free' OH groups in the water occurred. Evidence for the existence of the carbocation is displayed by the fact that the solvolysis rates of alkyl chlorides in ethanol resemble carbocation stabilities determined by

measurement of the heats of ionisation in superacids.<sup>94</sup> The *tert*-butyl carbocation can itself be produced from alkanes in superacid SO<sub>2</sub> by the loss of H<sup>-</sup>.<sup>95</sup>

**Figure 60:** The Production of the Carbocation from Alkanes in Superacid.



The carbocation has a very short lifetime and therefore it is difficult to observe. Nevertheless, photolytic induction of 3,4-dimethoxydiphenylmethyl acetate<sup>96</sup> in a polar solvent, allowed ultraviolet detection of the intermediate carbocation and it has also been observed by <sup>13</sup>C NMR spectroscopy<sup>97</sup> thus providing further evidence for the S<sub>N</sub>1 mechanism.

## 5.2 The Effects of the Solvent on the Reaction Rate

Numerous studies have been carried out observing the effect of the solvent upon the rate of the solvolysis reaction, all of which have noted extreme changes as a result of modifying the reaction medium.

Winstein and Fainberg<sup>98,99</sup> carried out the solvolysis of *t*-BuCl in various pure solvents of increasing polarity (Table 13). The solvolysis of *t*-BuCl was 335,000 times faster in water and nine times faster in pure methanol relative to the less polar solvent ethanol. The marked difference in the rate of the reaction is also evident for various other solvents.

**Table 13:** Rate Constants and Thermodynamic Parameters for the Solvolysis of *t*-BuCl in Various Pure Solvents at 298 K.<sup>98,99</sup>

Solvent	Dielectric Constant, $\epsilon_r$	$k_1^{\text{rel}*}$	$\Delta G^\ddagger$ (kJmol <sup>-1</sup> )	$\Delta H^\ddagger$ (kJmol <sup>-1</sup> )	$\Delta S^\ddagger$ (JK <sup>-1</sup> mol <sup>-1</sup> )
C <sub>2</sub> H <sub>5</sub> OH	24.55	1	113.0	109.0	-13
C <sub>2</sub> H <sub>3</sub> CO <sub>2</sub> H	6.15	2.5	111.0	108.0	-10
CH <sub>3</sub> OH	32.7	9	108.0	104.0	-13
HCONH <sub>2</sub>	111.0	430	98.3	93.6	-16
HCO <sub>2</sub> H	58.5	12200	90.0	87.9	-7
H <sub>2</sub> O	78.3	335000	82.0	97.2	+51 (!)

\*The examples are only relative rate constants,  $k_1^{\text{rel}}$ , with respect to the slowest.

The effect of changing the solvent upon the thermodynamic parameters for the solvolysis of t-BuCl is quite different from the effect it has upon the rate of the reaction. All six solvents investigated displayed a tendency to increase the rate of reaction and decrease the  $\Delta G^\ddagger$  value as their polarity increased. However, the first five solvents examined showed fairly constant values for the entropy  $\Delta S^\ddagger$  of the reaction of about  $12 \text{ kJmol}^{-1}$  thus, the overall solvent effect is dominated by the effect of enthalpy  $\Delta H^\ddagger$  which is in agreement with the assumption of Hughes and Ingold. However, a large  $\Delta S^\ddagger$  value of  $+51 \text{ JK}^{-1}\text{mol}^{-1}$  was found for the reaction in water suggesting that changes of entropy have a huge effect upon the solvolysis, due in part to the highly ordered, three-dimensional nature of the solvent.

The dielectric constant  $\epsilon$  is a rough estimate of the polarity of a solvent and is a measure of the ability of a solvent to shield opposite charges from each other. The higher the dielectric constant a particular solvent possesses, the smaller the electrostatic attraction and repulsion within that medium. However,  $\epsilon$  values give little information regarding the solvating ability of the solvent molecules. Although, the polarity obviously plays a role in the solvolysis reaction the ability of the solvent to solvate the system is of greatest importance, as is observed by the effect of water with respect to the other solvents investigated.

Whilst water is the most effective solvent for promoting ionisation most organic compounds are not appreciably soluble in it. The addition of a co-solvent, often an alcohol, is required to enable dissolution.

Hughes<sup>85</sup> carried out experiments in aqueous ethanol solutions and upon increasing the water content, thus the polarity of the medium, an increase in the rate of reaction was noted.

**Table 14:** The Hydrolysis of t-BuCl in Various Concentrations of Aqueous Ethanol.<sup>85</sup>

EtOH (% v/v)	90	80	70	60	50	40
[t-BuCl] ( $\times 10^{-3} \text{ mol dm}^{-3}$ )	75.5	76.2	82.4	73.5	81.0	30.6
$k_1$ ( $\times 10^{-3} \text{ hr}^{-1}$ )	6.16	32.9	145	453	132	466

If the solvent remains of the same general type, for example, the solvolysis of t-BuCl in aqueous ethanol/water the trends in Table 15 are observed. The rates of solvolysis increase by more than six hundred fold as the reaction medium is changed from 90% aqueous ethanol to the more polar solvent water.

**Table 15:** The Dielectric Constants for Various Concentrations of Aqueous Ethanol.

25°C (298 K) $k_1 \times 10^{-5} \text{ s}^{-1}$	% Aqueous EtOH (v/v)	25°C (298 K) Dielectric Constant, $\epsilon$
—	100	24.5
17.1	90	29.5
91.4	80	35.0
403	70	40.5
1260	60	46.5
3760	50	52.0
12540	0	78.0

A rough quantitative relationship is observed between  $k$  and  $1/\epsilon$  for a series of alcohols. For a solvent series having a common functional group, however, this no longer holds if one of the alcohols is replaced by, for example, a nitrile having the same  $\epsilon$  value (e.g.  $\text{CH}_3\text{CN}/\text{H}_2\text{O}$  and  $\text{CH}_3\text{OH}/\text{H}_2\text{O}$ ).

The rate of solvolysis of t-BuCl is found to be less in aqueous alcohols compared to that in aqueous acetonitrile. The reason for this is due to the hydrogen bonding that occurs in the alcoholic solvent system. For a reaction to advance further, the ‘solvent shell’ surrounding the nucleophile must be removed if it is to form a new bond with the substrate. The energy required to break the hydrogen bonds to the solvent will contribute to, and so increase the total energy required to reach the transition state.

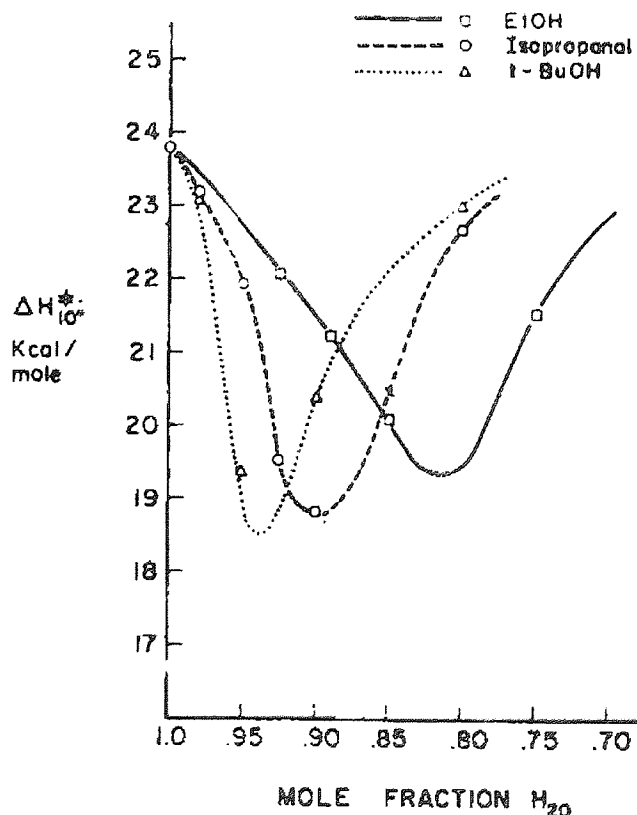
Robertson and Sougamori<sup>100,101</sup> reported the results for the solvolysis of t-BuCl in a series of alcohol-water solutions in the high water concentration range where the mole fraction of the alcohol  $x_2$  was in the region 0 to 0.2. It was reported that the enthalpy and entropy values for the solvolysis of t-BuCl in ethanol-water mixtures where  $x_2 = 0$  to 0.2 followed the trend of that previously reported by Winstein and Fainberg.<sup>99</sup>

The behaviour of the system observed changes as the amount of alcohol added to it is increased. Initially pure water has a three-dimensional hydrogen-bonded structure, which

can accommodate a certain quantity of alcohol by forming a quasi-aqueous structure. The hydrophilic  $-OH$  group of the alcohol forms hydrogen bonds with the water and fits into the three-dimensional structure and the hydrophobic alkyl group surrounded by the rest of the water network.<sup>13</sup> This apparent enhancement in the structure of water for the mole fraction of alcohol content over the range 0 to 0.15 is reflected by various physical properties including viscosity<sup>102</sup>, partial molar volume<sup>103</sup>, abnormal absorption of ultrasound<sup>104</sup>, and the heat of a solution<sup>105</sup>.

The effect of increasing the temperature opposes such structure formation<sup>105,106</sup> as too does the addition of further quantities of alcohol which puts additional strain on a structure, that already has a limited capacity to accommodate a weakly polar group whilst attempting to maintain a three-dimensional structure. The plot in Figure 61 (reproduced from Robertson, R. E. and Sougamori, S E, Can. J. Chem. Soc. 1972, **50**, 1353) displays the general trend expected for the ethanol-water solution when moving from a solvent system with a three-dimensional structure to one that is more two-dimensional.

**Figure 61:** The Effect of Changing Aqueous Solvent Composition upon the Enthalpy Change  $\Delta H^\ddagger$  for the Solvolysis of *t*-BuCl.



A similar plot arises for aqueous propan-2-ol and 2-methylpropan-2-ol systems. Arnett *et al*<sup>105</sup> verified the trend. Their research supported the theory that the amount of alcohol compatible with a three-dimensional, quasi aqueous structure is dependent upon the size of the hydrophobic alkyl group; the larger the alkyl group the lower the concentration of alcohol the water can accommodate before the structure becomes two-dimensional. In the high water range studied it is entropy  $\Delta S^\ddagger$  rather than enthalpy  $\Delta H^\ddagger$  that is the limiting factor of the solubility of weakly polar molecules, such as alcohols, in the much more polar water molecules.<sup>107</sup> It has also been shown that the addition of a third component, such as t-BuCl, to alcohol/water systems at low temperatures is still dominated by the effect of the solvent structure<sup>102</sup>.

Since solvent polarity strongly affects reaction rates, Winstein and co-workers attempted to correlate reaction rates with empirical parameters of solvent polarity<sup>98,99,108,109,110</sup>. They discovered that the S<sub>N</sub>1 solvolysis of t-BuCl is strongly accelerated by polar, especially protic, solvents. Grunwald and Winstein defined a solvent 'ionising power' parameter Y, characteristic of the given solvent based on the solvolysis of t-BuCl.

**Equation 45:** The Grunwald Equation.

$$Y = \log k_A^{t\text{-BuCl}} - \log k_0^{t\text{-BuCl}}$$

$k_0^{t\text{-BuCl}}$  represents the first order rate constant for the solvolysis of t-BuCl at 298 K in aqueous ethanol (80% (v/v) ethanol/water; Y=0) and was employed as a reference solvent. The parameter  $k_A^{t\text{-BuCl}}$  therefore corresponds to the rate constant in another solvent system. The solvolysis reaction of t-BuCl was chosen, as it is believed to occur by an essentially pure S<sub>N</sub>1 mechanism. Choosing a standard reaction and a reference solvent, a linear Gibb's energy relation would yield

$$\log k_A - \log k_0 = \log \left( \frac{k_A}{k_0} \right) = mY$$

m is the substrate parameter and is a measurement of sensitivity of the starting materials to changes in Y of the solvent system.

Scales of  $Y$  and  $m$  were established by taking  $Y = 0$  for the reference solvent 80% (v/v) aqueous ethanol and  $m = 1$  for the solvolysis of  $t\text{-BuCl}$ . It is expected that this equation can be applied to reactions very similar to the standard reaction, that is reactions occurring via an  $S_N1$  mechanism. The similarity between  $Y$  and  $m$  and  $\sigma$  and  $\rho$  of the Hammett equation is obvious.  $Y$ -values are known for some pure, mainly protic, solvents and for various binary mixtures of various organic solvents with water or a second organic solvent<sup>98,99,108,109</sup>.

**Table 16:**  $Y$ -values for Binary Mixtures.<sup>111,112</sup>

Solvent	$Y$
Water	3.493
Methanol/Water [80% (v/v)]	0.381
Ethanol/Water [80% (v/v)]	0.000
Acetone/Water [80% (v/v)]	-0.673
Methanol	-1.090
Acetic acid	-1.675
Ethanol	-2.033

Table 17 gives some values of  $m$ . Those substrates having a value greater than unity suggests that it is more sensitive to the solvent 'ionising power'  $Y$  than  $t\text{-BuCl}$  (i.e. the transition state to which it gives rise is more 'ion pair-like' in character).

**Table 17:**  $m$  Values for Various Substrates with Respect to  $t\text{-BuCl}$ .

Halide	Temperature (°C)	$m$ Value
$\text{Me}_3\text{CCl}$	25	1.00
$\text{Me}_3\text{CBr}$	25	0.94
$\text{EtMe}_2\text{CBr}$	25	0.90
$\text{PhCH}(\text{Me})\text{Br}$	50	1.20
$\text{CH}_2=\text{CHCH}(\text{Me})\text{Cl}$	25	0.89
$\text{EtBr}$	75	0.34
$\text{Me}(\text{CH}_2)_3\text{Br}$	75	0.33

The Grunwald equation (Equation 45) is fairly successful in a large number of cases where it exhibits a good linear relationships between  $\log k_1$  and  $Y$  for the solvolysis of various tertiary halogenoalkanes and secondary sulphonates; reactions proceeding via an  $S_N1$  mechanism as for the standard reaction. For reactions of borderline  $S_N1/S_N2$  and  $S_N2$

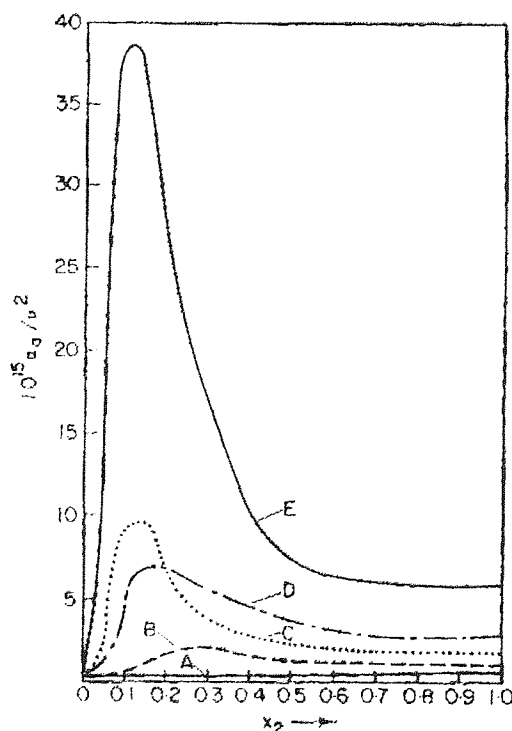
mechanisms, the application of this equation is less satisfactory and a variation upon it has been postulated for a gradual change in mechanism moving from  $S_N2$  (one stage) through  $S_N2$  (intermediate) to  $S_N1$  (limiting)<sup>88,89</sup>.

### 5.3 The Ultrasonically Enhanced Solvolysis of t-BuCl

A considerable amount of research has been carried out with respect to the ultrasonically induced solvolysis reaction of t-BuCl in aqueous alcoholic media. All those reactions investigated were in the kHz region of sound, above the upper limit of human hearing (>16kHz). The rate enhancements observed for the system have been attributed to the effects of cavitation.

Blandamer and co-workers<sup>113</sup> investigated the absorption properties of ultrasound<sup>104</sup> when aqueous solutions contain certain co-solvents, such as alcohols. A trend was observed; as the alkyl group of the alcohol gets larger the absorption maximum  $\alpha/v^2$  increases and occurs at a lower mole fraction of alcohol as displayed by Figure 62 (reproduced from Blandamer, M. J. "Introduction to Chemical Ultrasonics" Academic Press, New York, 1973, 109).

**Figure 62:** The Absorption Properties of Various Aqueous Alcohols.





The plots on the graph represent the following alcohols:

A = Methanol

D = Propan-2-ol

B = Ethanol

E = 2-Methylpropan-2-ol

C = Propan-1-ol

Although the intensity of the maximum is dependent upon temperature, increasing with a decrease in temperature, the mole fraction of alcohol at which it occurs is not notably temperature dependent. The plot noted by Blandamer would be very different if another organic co-solvent replaced the water, as a consequence of the unique three-dimensional structure of water. The intense maximum is only observed for co-solvents with a large degree of hydrophobic character, for example alcohols with only a single –OH group. Co-solvents containing more than two hydrophilic groups, for example diols and glycerol, experience a smooth increase in the absorption coefficient  $\alpha/v^2$  with an increase in concentration of the added co-solvent.

Franks and Wen<sup>111</sup> subdivided binary aqueous mixtures into two groups those typically aqueous and typically non-aqueous. The basis of this subdivision is the thermodynamic properties of the mixture where, for a typically aqueous solution, the sign and magnitude of the free energy of mixing  $\Delta G$  is controlled by the entropy change  $\Delta S$ , such that  $T|\Delta S| > |\Delta H|$ . The reverse is also true for typically non-aqueous systems that are governed by the enthalpy change  $\Delta H$ .

Mason and co-workers<sup>114,115,116,117</sup> have carried out significant research into ultrasonically enhanced solvolysis reactions of t-BuCl in aqueous alcohols. Research includes

- Effects of ultrasonic irradiation at various concentrations of three different alcohols, propan-2-ol, ethanol and 2-methylpropan-2-ol.<sup>114</sup>
- Effects of ultrasonic irradiation at various concentrations and temperatures of aqueous ethanol.<sup>115,116</sup>
- Effects of ultrasonic irradiation at various concentrations of ethanol upon the heat capacity of activation  $\Delta C_p$ .<sup>117</sup>

The work carried out on the three different alcohols, at various concentrations.<sup>114</sup> A cup-horn device operating at 45kHz was employed at room temperature 25°C (298 K). The results of Blandamer<sup>113</sup> and Burton<sup>118</sup> were confirmed as the largest increase in rate, due to ultrasonic irradiation, was observed for the most structured region for the quasi-aqueous solution (Table 18).

**Table 18:** The Effect of Ultrasound on the Rates of Solvolysis of t-BuCl at 298 K.<sup>114</sup>

Solvent	Mole Fraction of Alcohol	$k_{US}/k_{therm}$
Aqueous Ethanol	0.089	1.22
	0.144	1.15
	0.207	1.47
	0.281	2.13
	0.307	1.89
Aqueous Propan-2-ol	0.070	0.93
	0.144	0.89
	0.167	1.44
	0.231	1.92
Aqueous 2-Methylpropan-2-ol	0.057	0.89
	0.094	1.04
	0.139	1.07
	0.196	1.33

It can be seen that the largest enhancement occurs when the mole fraction of ethanol is 0.3, although no enhancement is observed in systems occurring in the highly aqueous regions. Continuing the investigations, the effects of sonication at a lower frequency than in the previous research paper of 20kHz on various concentrations of aqueous ethanol mixtures at a range of temperatures<sup>115</sup> were studied. It was noted that a reduction in the activation energy  $E_a$  took place compared with the conventional thermal reaction. For a reaction to advance further, the 'solvent shell' surrounding the nucleophile must be removed if it is to form a new bond with the substrate. The energy required to break the hydrogen bonds within the aqueous alcohol will contribute to, and so increase the total energy required to reach the transition state. However, ultrasonic irradiation destroys these strong solvent-solvent interactions so reducing the activation energy  $E_a$  as displayed in Table 19.

**Table 19:** The Effect of Sonication on the Solvolysis of t-BuCl at Various Ethanol Concentrations and Temperatures.<sup>115</sup>

Mole Fraction of Alcohol	Temperature (°C)	$k_{US}/k_{therm}$	$E_a$ (kJmol <sup>-1</sup> )	
			Ultrasonic	Thermal
0.089	6.0	2.4	69	92
	15.9	1.5		
	23.4	1.2		
0.144	6.3	4.8	30	87
	14.5	2.3		
	23.3	1.2		
0.207	7.7	7.9	19	91
	14.4	4.0		
	25.0	1.3		
0.281	9.1	12.2	~0	93
	15.0	5.5		
	24.3	1.4		

As the alcohol content increased the overall activation energy  $E_a$  decreased. The energy of activation was found to be almost equal to zero for the most structured region of the solvent containing a mole fraction of ethanol equal to 0.3. An increase in rate with decreasing temperature was noted for all solvent compositions. It was theorised, in a further paper<sup>116</sup> that this trend was due to an increase in the volatility of the solvent so an increased amount of vapour fills the cavities reducing the intensity of cavitation collapse. The effects of sonication on the heat capacity of activation  $\Delta C_p$  were also studied<sup>117</sup> confirming the results of the conventional thermal solvolysis reaction. It was assumed that the main contribution to heat capacity  $\Delta C_p$  was due to solvent-solvent interactions and that any decrease in these interactions, such as that caused by an increase in the mole fraction of alcohol, leads to the reduction of the parameter. In general the  $\Delta C_p$  value was positive for sonicated reactions and decreased with increasing concentration of alcohol. It was believed that sonication destroyed the weak solute-solvent interactions in the ground state and some of the strong solvent-solvent interactions. However, the stronger solvent-solute interactions of the transition state, occurring as a result of the greater electrical dissymmetry, cannot be destroyed by sonication and thus produce a positive  $\Delta C_p$  value.

## 5.4 The Treatment of Kinetic Data for the t-BuCl System

It has been shown<sup>28</sup> that the solvolysis of t-BuCl follows pure first-order kinetics for the duration of the reaction.

**Figure 63:** Concentrations of the Components of the t-BuCl Throughout the Reaction

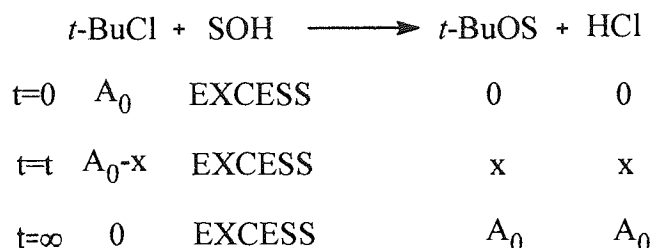


Figure 63 shows the rate of consumption of the t-BuCl, at time t, with respect to time, where

$$\frac{-d[t\text{-BuCl}]}{dt} = k_1[t\text{-BuCl}]$$

The equation may be rearranged and integrated in order to obtain a rate equation (Equation 46) that enables the rate constant  $k_1$  for the reaction to be calculated.

$$\begin{aligned} \frac{-d[t\text{-BuCl}]}{[t\text{-BuCl}]} &= k_1 dt \\ -\int_{A_0}^{A_0-x} \frac{d[t\text{-BuCl}]}{[t\text{-BuCl}]} &= k_1 \int_{t=0}^{t=t} dt \\ -[\ln(t\text{-BuCl})]_{A_0}^{A_0-x} &= k_1 [t]_0^t \\ -[\ln(A_0 - x) - \ln(A_0)] &= k_1 t \end{aligned}$$

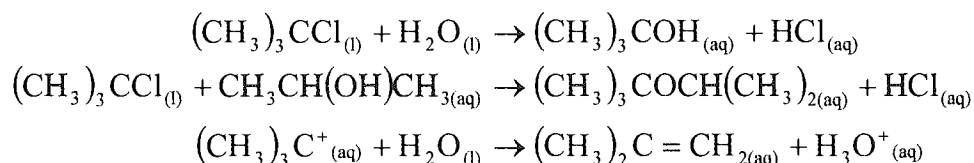
**Equation 46:** The Integrated Rate Equation for the Solvolysis of t-BuCl.

$$\ln(A_0 - x) = \ln(A_0) - k_1 t$$

Since the solvolysis of t-BuCl is an  $S_N1$  first-order reaction then the plot of  $\ln (A_0-x)$  against time (t) yield a straight line where the gradient =  $-k_1$  and intercept =  $\ln (A_0)$ .

There are four products formed in this reaction system.

**Figure 64:** The Possible Products for the Solvolysis of t-BuCl.



It is assumed that  $\text{H}^+\text{Cl}^-$  is the only product, which is conducting. However, other side reactions might occur as sometimes they do in sonochemical reactions. Any side products would be visible when the reaction was analysed in the NMR spectrometer but no such products were observed. Let the concentration of  $\text{H}^+\text{Cl}^-$  at any time, t, be equal to x. Since the conductance G is related to the conductivity  $\chi$  by the equation

$$\chi = \frac{Gl}{A}$$

Where:  $-\frac{l}{A}$  = cell constant, and since molar conductance  $\Lambda = \frac{\chi}{x}$ . Then,

**Equation 47:** Molar Conductance with Respect to the Cell Constant, Conductance and concentration of  $\text{H}^+\text{Cl}^-$  at time, t.

$$G \frac{\left(\frac{l}{A}\right)}{x} = \Lambda$$

In general

$$\Lambda = \Lambda_\infty - A\sqrt{x}$$

where  $\Lambda_\infty$  represents the molar conductance at infinite dilution and A is a constant for a given solvent system.

For a very dilute solution  $x = 0$ , so

**Equation 48:** Molar Conductance in a Dilute Solution.

$$\Lambda = \Lambda_\infty$$

Substituting Equation 48 into Equation 47 gives: -

$$G \frac{\left(\frac{1}{A}\right)}{x} = \Lambda_{\infty} = c$$

$c = \text{constant}$

$$G = \frac{\Lambda_{\infty} A}{l} = cx$$

It can be seen that  $G \propto x$

On completion of the reaction one mole of HCl is produced for every mole of t-BuCl consumed, regardless of the quantity of alcohol, ether or alkene formed. Thus

$$A_0 \propto (G_{\infty} - G_t)$$

$$x \propto (G_t - G_0)$$

$$(A_0 - x) \propto (G_{\infty} - G_t)$$

Equation 46 may then be expressed in terms of conductivity.

**Equation 49:** The Integrated Rate Equation in Terms of Conductivity.

$$\ln (G_{\infty} - G_t) = \ln (G_{\infty} - G_0) - k_1 t$$

Plotting a graph of  $\ln (G_{\infty} - G_t)$  against time,  $t$ , will give a straight-line graph from which the rate constant may be ascertained.

The thermodynamic parameters discussed in chapter 5 may also be evaluated for this system. From a graph of  $\ln (G_{\infty} - G_t)$  vs.  $t$  the experimental rate constants may be calculated from the following, previously defined, equations.

**Equation 42:** The Wynne-Jones Eyring Equation Expressed with respect to Activation Energy.

$$\ln k_1 = \ln \frac{kT}{h} + \frac{\Delta S}{R} - \frac{E_a}{RT}$$

From Equation 42 an Arrhenius plot of  $\ln k_1$  versus  $1/T$  ( $K^{-1}$ ) allows calculation of entropy (Equation 43) and activation energy (Equation 44) from

**Equation 43:** Calculation of the Entropy of Activation,  $\Delta S^\ddagger$ .

$$\text{intercept} = \left( \ln \frac{kT}{h} + \frac{\Delta S^\ddagger}{R} \right)$$

**Equation 44:** Calculation of the Activation Energy,  $E_a$ .

$$\text{gradient} = -\frac{E_a}{R}.$$

The change in enthalpy of activation for the solvolysis reaction of t-BuCl may be determined using Equation 41.

**Equation 41:** The Change in Enthalpy of Activation with respect to Activation Energy

$$\Delta H^\ddagger = E_a - RT$$

The Gibb's Free energy of activation  $\Delta G^\ddagger$  may also be established at various temperatures using the well-known equation.

**Equation 33:** The Gibb's Free Energy Change of Activation.

$$\Delta G^\ddagger = \Delta H^\ddagger - T\Delta S^\ddagger$$

From the data obtained from the equations discussed, it is possible to assess the effect of ultrasonic irradiation upon the  $S_N1$  solvolysis reaction of t-BuCl in 40% (v/v) aqueous propan-2-ol solution.

**Chapter 6      The Construction of an Experimental Thermal Dissipation  
Device to Reduce Sample Heating Caused by Sonication.**

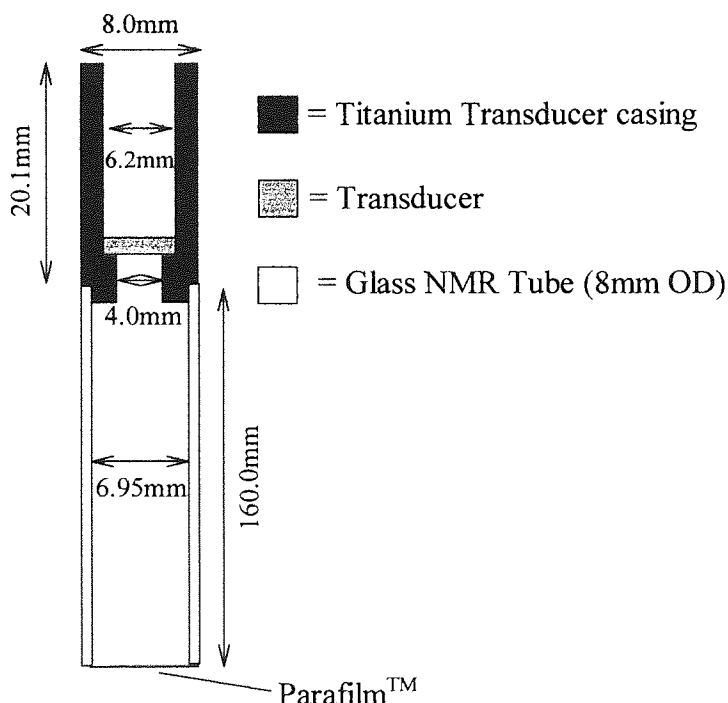


The application of ultrasonic energy brings about the movement of molecules resulting in heating of the sample. Heating induces changes in the sample, which alter any spectra obtained by NMR spectroscopy. Experiments that experience an increase in reaction temperature undergo a reduction in the  $T_1$  of the sample. Thus, the problem of heating within a sample that is subjected to NMR spectroscopic determination must be eliminated to ensure meaningful results.

### 6.1 Eliminating the Temperature Increase Induced by the Application of Ultrasonic Energy by a Glass Adapter

A device was designed and constructed to reduce the heating of samples exposed to sonication. An 8mm OD NMR tube was secured around the transducer casing of the ultrasonic apparatus as illustrated in Figure 65.

**Figure 65:** The Glass Adapter for the Reduction of Sample Heating.



The glass NMR tube was bonded to the transducer casing using titanium putty, for extra strength, to enable the tube to withstand vibrations caused by the movements of the piezoelectric transducer. The tube was filled with a coupling fluid of degassed water and

the end sealed with Parafilm™. The Parafilm™ was employed to act as a lossless drum so that the ultrasonic energy could be transferred from one medium to another with a minimal loss of energy.

The employment of a glass tube posed several significant problems for the system.

- Glass is fragile and thus, must be handled with care.
- The glass tube experienced cracking around the bonded area, due to heating and vibration caused by the transducer.
- The tube was permanently bound to the transducer casing, preventing its removal.

However, the use of glass also had one advantage.

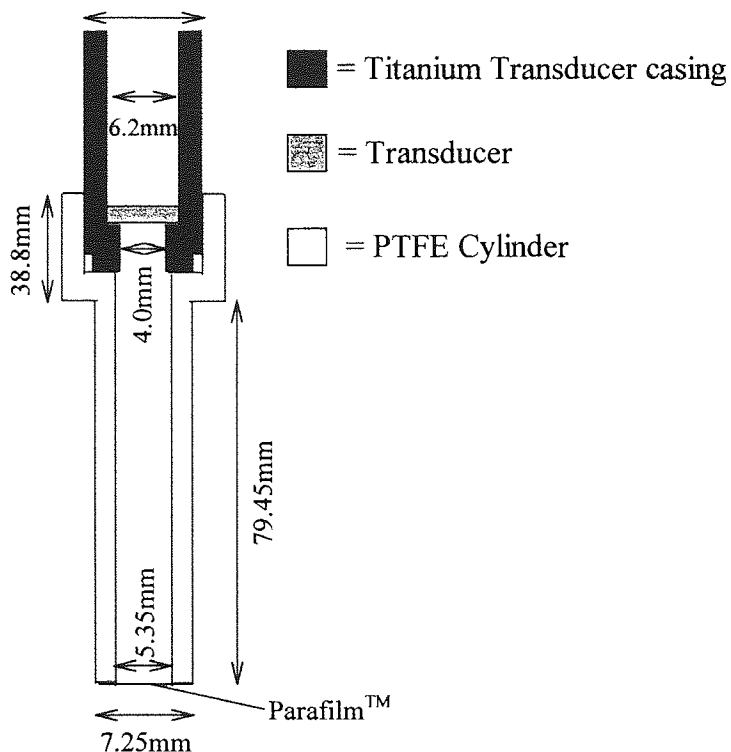
- Glass allowed observation of the degassed water contained within the tube.

The disadvantages of using the glass tube to reduce heating of samples far outweighed the single advantage, although that was not truly an advantage for if the apparatus was to be employed within the NMR spectrometer it would be impossible to observe anyway. An alternative material needed to be established. The key difficulty with using glass attached directly or indirectly to the transducer casing was its fragility, being easily fractured by the natural vibrations of an ultrasonic transducer.

## **6.2 Eliminating the Temperature Increase Induced by the Application of Ultrasonic Energy by a PTFE Adapter**

An alternative adapter to the glass device, as shown in Figure 66 (not to scale), was constructed from polytetrafluoroethylene (PTFE) to overcome the difficulties encountered with the glass tube. As previously, the tube was filled with degassed water and the device sealed at the end with parafilm™.

**Figure 66:** The PTFE Adapter for the Reduction of Sample Heating.



A disadvantage associated with the use of the PTFE adapter was that the water could not be observed during a reaction. The PTFE is an opaque material; however, this was not a great disadvantage as observation was not possible when the system was held within the NMR spectrometer.

The new PTFE adapter has many advantages compared to the glass device.

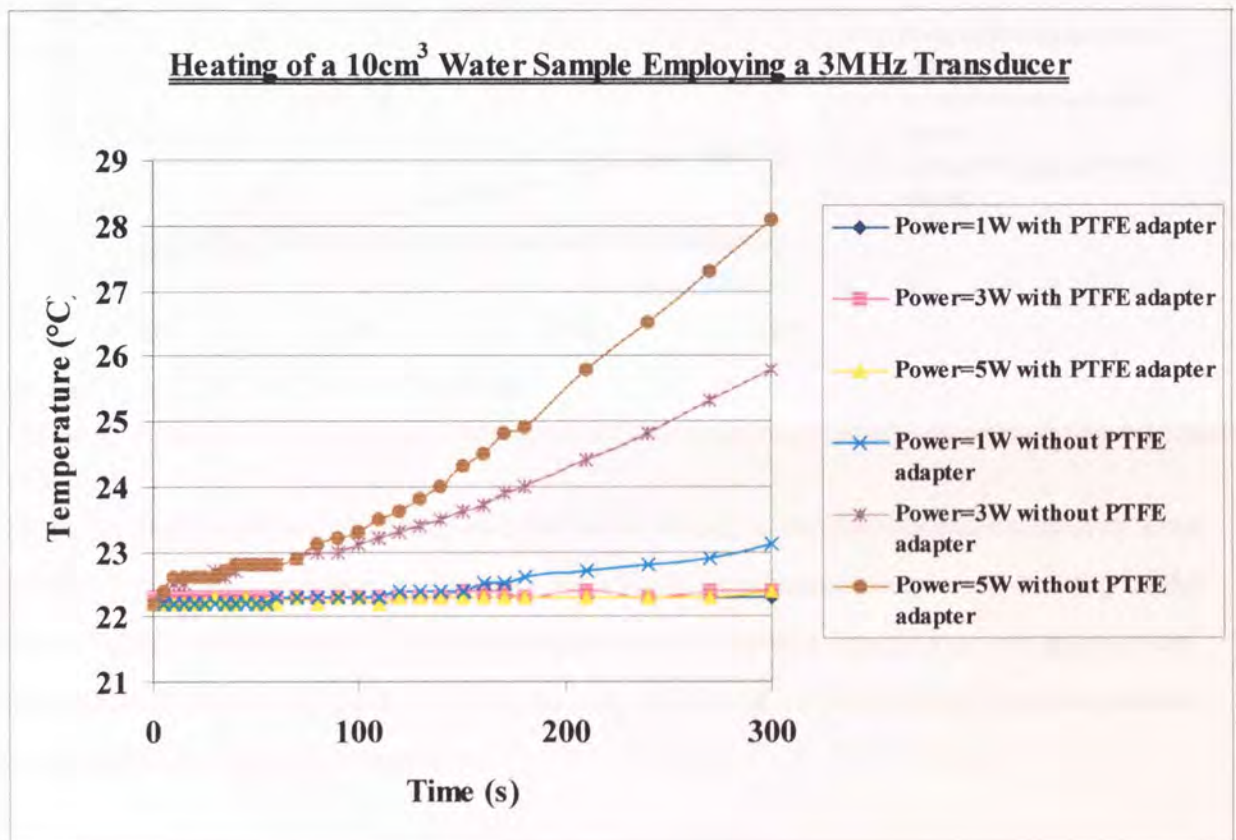
- The unit is not permanently bound to the transducer casing (the two interfaces are wedged together using PTFE tape to fill the gap), so it is easily removed when required.
- PTFE is a robust material and damage as a result of vibration and heating is eliminated.

### 6.3 The Reduction of Sample Heating Employing a PTFE Adapter

Degassed distilled water ( $10 \text{ cm}^3$ ) was placed in a test tube and the transducer with the adapter was placed at a depth of  $2.5 \text{ cm}^3$  into it. The temperature of the sample was

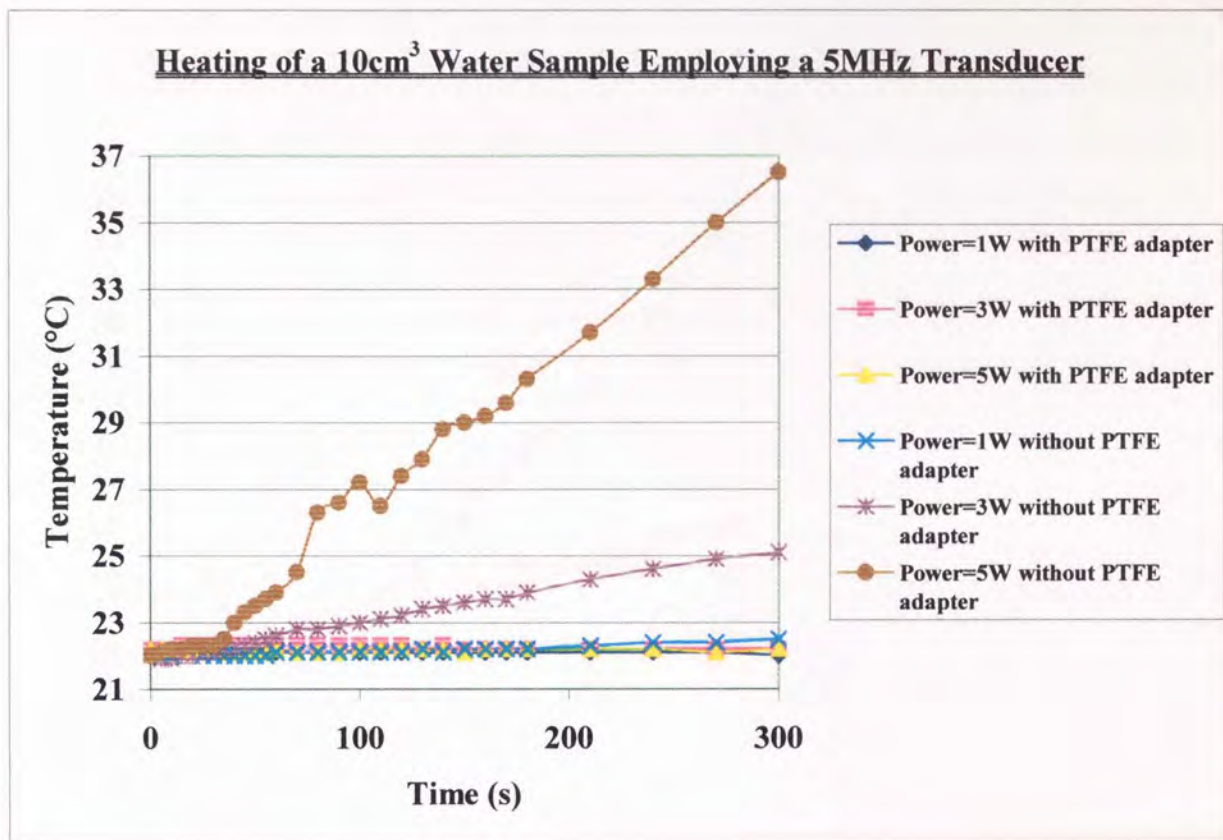
measured at regular intervals, using a Digitron Type K thermocouple having an operating range of  $-200^{\circ}\text{C}$  to  $1350^{\circ}\text{C}$  (73 K to 1623 K), for a total time of five minutes. Comparison of the temperature changes occurring at different power inputs (1 W, 3 W and 5 W) and using different transducers (2 MHz, 5 MHz and 10 MHz) was made against systems without the PTFE adapter. The effects of the employment of the adapter over those systems where it is not used are shown in Figure 67 to Figure 69.

**Figure 67:** The Heating of a  $10\text{ cm}^3$  Water Sample Resulting from Ultrasonic Irradiation using a 3 MHz Transducer.



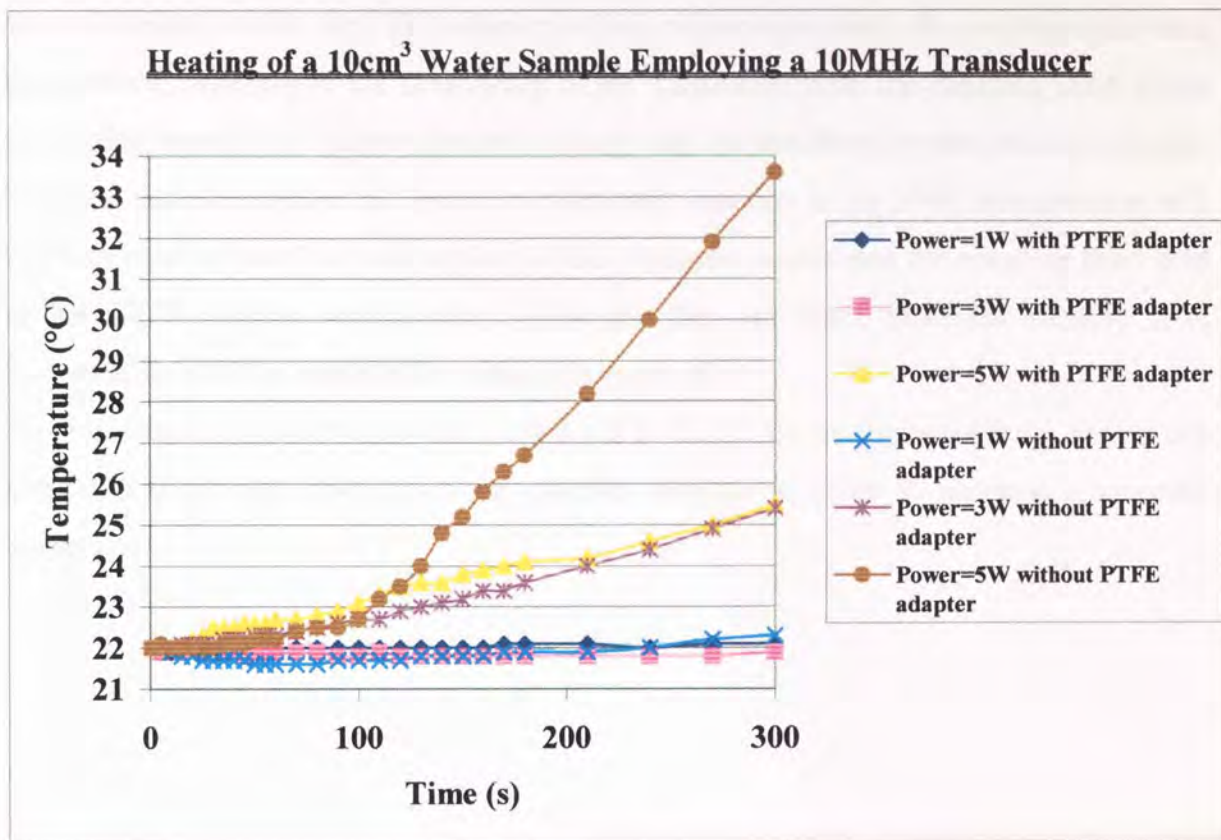
It is clear that experiments, which utilised a transducer of frequency 3 MHz experienced a significant reduction in heating of the  $10\text{ cm}^3$  water sample over a five-minute period of ultrasonic irradiation. All three tests upon the sample with the PTFE adapter experienced an almost negligible increase in temperature compared to those systems where the transducer was directly coupled to the liquid sample. The increases in temperature were as large as 6 K.

**Figure 68:** The Heating of a 10 cm<sup>3</sup> Water Sample Resulting from Ultrasonic Irradiation using a 5 MHz Transducer.



At the higher transducer frequency of 5 MHz the 10 cm<sup>3</sup> water sample experienced an even greater temperature increase up to about 14.5 K. A significant reduction in heating of the 10 cm<sup>3</sup> water sample over a five-minute period of ultrasonic irradiation was again noted. The experiments where the PTFE adapter was employed suffered little from temperature increase due to ultrasonic irradiation.

**Figure 69:** The Heating of a 10 cm<sup>3</sup> Water Sample Caused by Ultrasonic Irradiation using a 10 MHz Transducer.



Finally, the highest frequency transducer (10 MHz) examined displayed the same general trends as those of the 3 MHz and 5 MHz transducers. The heating of the 10 cm<sup>3</sup> water sample was almost entirely suppressed by the use of the PTFE adapter.

As a precaution the temperature of each sample was checked after ten minutes irradiation and was found to have altered little from the temperature acquired at five minutes.

## 6.4 Discussion and Conclusions

It is apparent from the data obtained that the PTFE adapter successfully suppressed the heating of a 10 cm<sup>3</sup> water sample caused by the ultrasonic irradiation of the system when direct coupling is carried out.

There is one important factor that must be considered before the PTFE adapter is employed in the prevention of temperature increases of ultrasonic reactions carried out in the NMR spectrometer. For a reaction that is to be observed in the NMR spectrometer it would have to take place over a relatively long period of time i.e. greater than 1 hour. The PTFE

adapter must therefore be able to function for these intervals without experiencing any problems. Unfortunately, the PTFE adapter cannot fulfil such a requirement because the water contained within the PTFE adapter suffers evaporation due to the continued elevated temperature, resulting in the decoupling of the transducer from the coupling fluid. Once decoupling occurs, no further ultrasonic energy can be transferred to the reaction sample. The time periods required to observe an ultrasonic reaction in the NMR spectrometer will be of an hour or more thus decoupling of the ultrasonic source and the coupling fluid held in the PTFE adapter would occur. Although the unit itself functions suitably it is incompatible with the reaction for which it is required.

All subsequent sonicated reactions carried out in the NMR spectrometer were carried out using liquid nitrogen cooling of the reaction samples in order to maintain a constant temperature.

**Chapter 7    The Chemical Dosimeter as an in-situ Ultrasonic Reaction  
in the Nuclear Magnetic Resonance Spectrometer.**

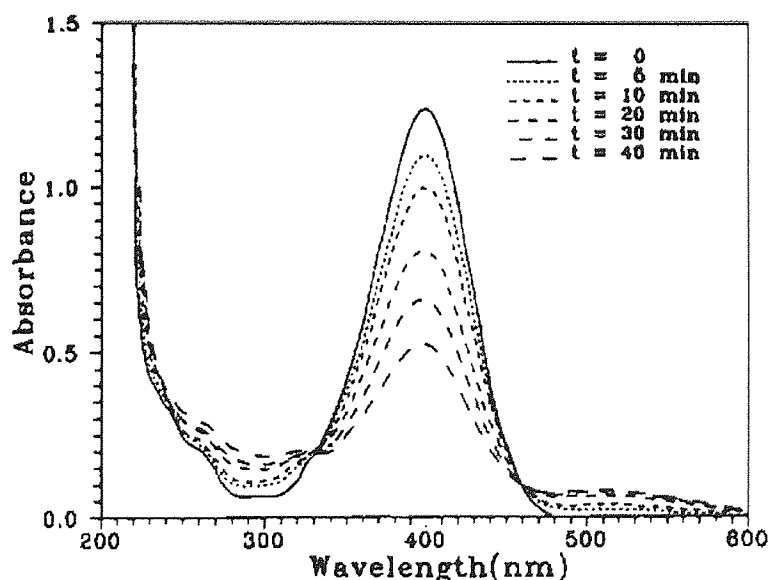


It was hypothesised that the most suitable system for the first ever in-situ ultrasonic reaction in the NMR spectrometer was a chemical dosimeter as it could simultaneously be employed to establish the ultrasonic power entering the reaction mixture. Neither the Fricke nor the iodine dosimeter could be utilised since their reactants or products could not be observed in the NMR spectrometer, however, the nitrophenol and terephthalic dosimeters are both possible reaction systems for analysis.

## 7.1 The Ultrasonic Irradiation of 4-Nitrophenol in Aqueous Solution

The ultrasonic irradiation of 4-nitrophenol in aqueous solution was successfully observed by Kotronarou *et al*<sup>23</sup> (20 kHz, 84W), determining both the kinetics and mechanism for the reaction. The reaction observed by Kotronarou of 4-nitrophenol was clearly visible over a 40-minute reaction period and this was considered a suitable time for the NMR investigation to be attempted.

Figure 70: Absorption Spectra Evolution for the 4-Nitrophenol Reaction.<sup>23</sup>

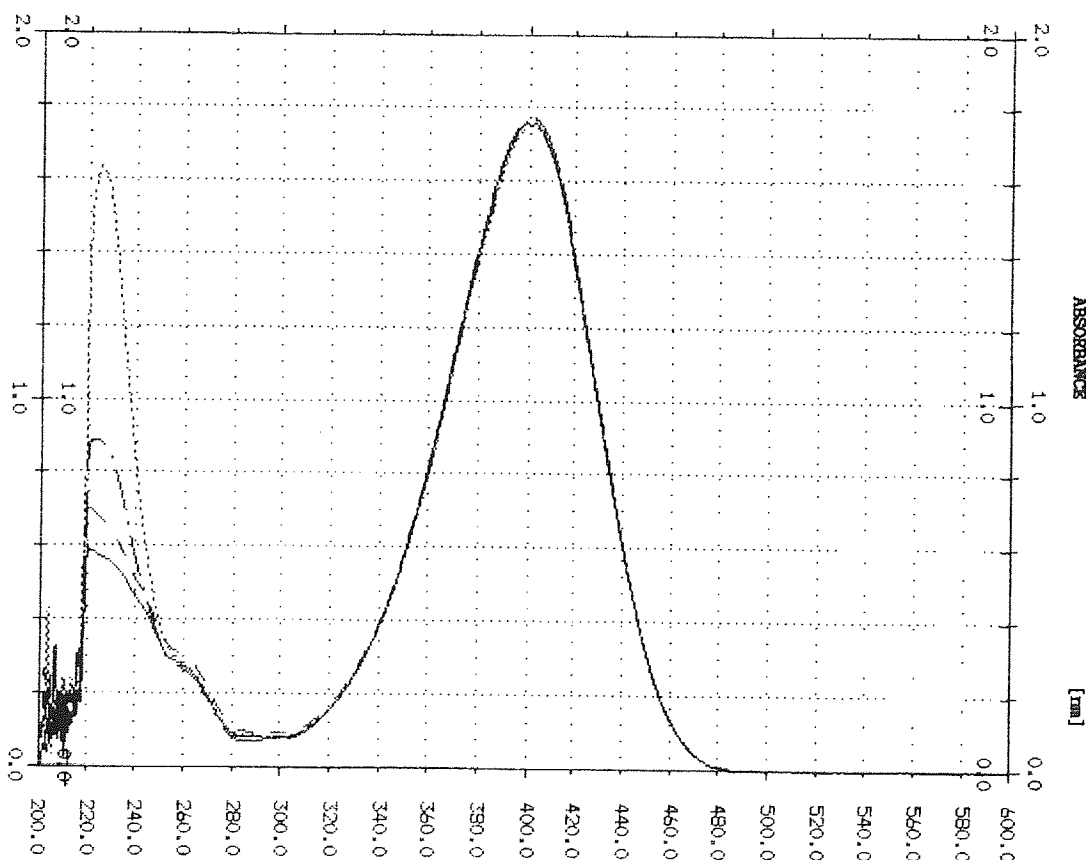


The following experiments were based upon the reactions carried out by Kotronarou although the concentration of 4-nitrophenol was increased in order to permit NMR spectroscopic analysis.

### 7.1.1 The Ultrasonic Reaction of 4-Nitrophenol Outside the NMR Spectrometer

A quantity of 4-nitrophenol (0.74 g) was added to 100 cm<sup>3</sup> of phosphate buffer (pH 5). A 7cm<sup>3</sup> aliquot of the solution was placed in a 10 mm NMR tube and irradiated using a 3MHz transducer at a power of 3W. The reaction mixture was tested at equal time intervals for the reduction in the 4-nitrophenol absorbance peak at 401 nm and the appearance of an absorbance peak at 512 nm due to the formation of 4-nitrocatechol.

**Figure 71:** The UV Absorbance Spectra of Sonicated 4-Nitrophenol.



It was observed in Figure 71, and in subsequent repeated ultrasonically irradiated reactions, that very little or no decrease in the concentration of the reactant 4-nitrophenol took place. No UV absorbance peak was observed at 512nm, which would indicate the formation of 4-nitrocatechol, though this may not necessarily appear because 4-nitrocatechol can react with further hydroxyl radicals and the absorbance of the various possible products would

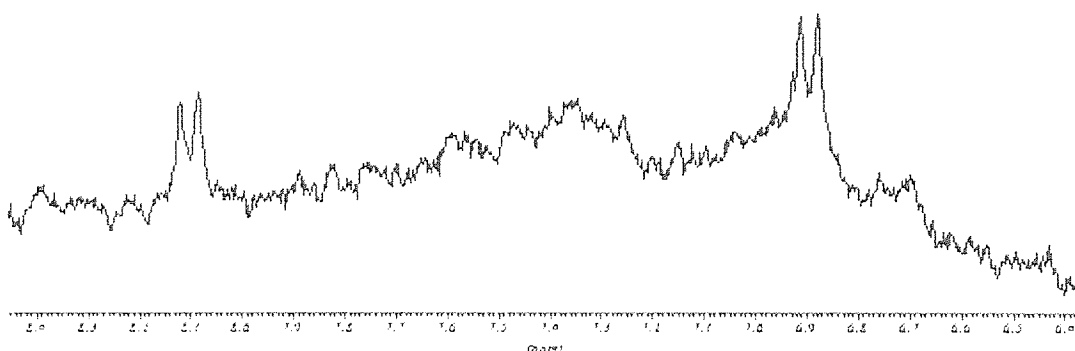
appear at different wavelengths. However, it was noted that a significant UV absorbance peak occurs at about 225nm and then disappears during the course of the reaction, this suggested the presence of a reaction intermediate.

Although it appeared that little or no reaction occurred in the bench reactions, it is noted that something may be happening as a UV absorbance peak was observed at 225nm. The NMR spectroscopic experiments were carried out in an attempt to establish the reason for the UV peak observed.

### 7.1.2 The Ultrasonic Reaction of 4-Nitrophenol in the NMR Spectrometer

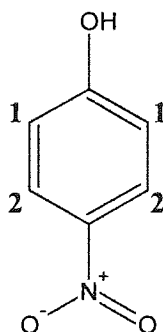
The reaction mixture was made up according to the method for the reactions carried out at the bench and a few drops of DMSO-d<sub>6</sub> were added to obtain a lock signal. The solution was analysed in a 5mm NMR tube to ensure that the 4-nitrophenol was present in large enough concentrations for the NMR signal to be observable. Unfortunately, an extremely large signal at 4.6ppm, due to the protons of water, dwarfs the signals of the reactant preventing its observation. As a result of the poor dynamic range of the 4-nitrophenol reaction system a 1-3-3-1 pulse programme<sup>119</sup> was employed to suppress the resonance of the solvent thus permitting the observation of the 4-nitrophenol by <sup>1</sup>H NMR spectroscopy (see Figure 72).

**Figure 72:** The Spectrum of 4-Nitrophenol in Phosphate Buffer (pH 5).



A single resonance was still observed for residual water protons not completely suppressed and two doublets for the signals of the protons at position 1 and 2 (refer to Figure 73) on the aromatic ring were also observed for the 4-nitrophenol at chemical shifts of 8.1ppm and 6.9ppm respectively. An additional signal was noted at about 1.6ppm and it was assigned to the protons of the  $\text{KH}_2\text{PO}_4$  and  $\text{Na}_2\text{HPO}_4$  in the buffer solution.

**Figure 73:** The Structure of 4-Nitrophenol.



No significant reaction occurred when observed in the ultraviolet spectrometer but the suggestion was made that something was happening to the reaction mixture as an absorbance peak was observed in the UV spectrometer but could not be identified by the technique. NMR spectroscopic experiments were completed to try to identify the source of the absorbance noted in the ultraviolet method. The reaction mixture ( $6 \text{ cm}^3$ ) was irradiated in an ultrasonic cleaning bath at a low frequency, since the reaction of Kotronarou<sup>23</sup> had proven successful when irradiated with a low frequency source. If the application of low frequency ultrasound did not yield a reaction, the final approach was to continually aerate the mixture and add a small quantity of  $\text{CCl}_4$ , both well-known techniques for improving ultrasonic reaction rates.

**Table 20:** The Reaction Conditions for the Ultrasonic Degradation of 4-Nitrophenol.

Reaction Conditions	Result
Sonicated for 1½ hours.	No reaction products observed.
Sonicated for 4 hours whilst continually aerated and a small amount of $\text{CCl}_4$ added.	No reaction products observed.

Once again, the NMR spectra obtained did not display any additional signals to those observed previously in Figure 72. It is most probable that under the conditions shown in

Table 20 then the reaction either takes place so slowly that no product could be observed in the time, or the reaction does not occur at all using the increased concentration of reactants. An alternative dosimeter, the terephthalic dosimeter, would be investigated.

## **7.2 The Ultrasonic Irradiation of Terephthalic Acid in Aqueous Solution**

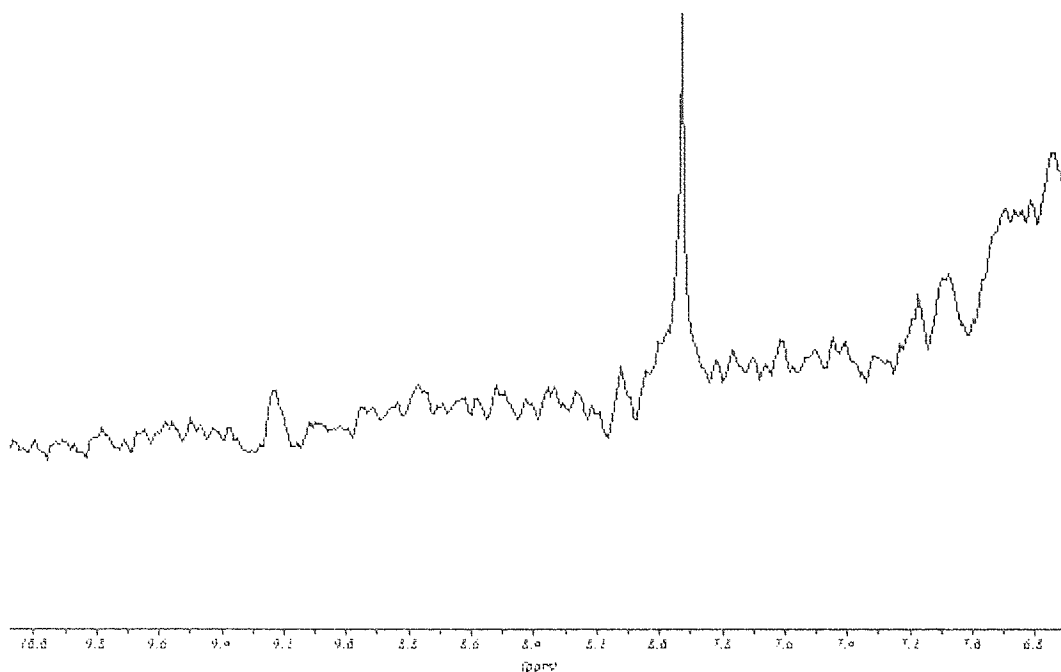
The terephthalic dosimeter was the second potential reaction system for the in-situ observation of an ultrasonically induced reaction in the NMR spectrometer. 'Bench reactions' could not be carried out, because a fluorimeter was not available for use so all reactions were carried out in the NMR spectrometer.

### **7.2.1 The Ultrasonic Reaction of Terephthalic Acid in the NMR Spectrometer**

Terephthalic acid (0.6 g) and sodium hydroxide (0.4 g) were added to the phosphate buffer of pH 7.4 (100 cm<sup>3</sup>), increasing the suggested<sup>120</sup> concentration of terephthalic acid 20 fold compared to that normally used for the dosimeter reaction. A few drops of DMSO-d<sub>6</sub> were added to the sample to obtain a field lock signal. The reaction solution (6 cm<sup>3</sup>) was placed in a 10mm NMR tube and irradiated using a 2 MHz transducer operating at 3 W. The reaction sample was not spun because the ultrasonic equipment required was placed in the top of the tube preventing it from spinning.

As for the nitrophenol dosimeter, the NMR spectra of the reaction mixture were obtained using the 1-3-3-1 pulse sequence<sup>119</sup> to suppress the water absorption signal. An example of a spectrum obtained over the range 6.8-10 ppm is shown in Figure 74.

**Figure 74:** The Spectrum of Terephthalic Acid in Phosphate Buffer (pH 7.4).



In the spectra that were obtained of the reaction sample no products were observed during the one-hour reaction period. The only signal observed was at a chemical shift of about 7.95ppm representing the four chemically equivalent protons on the benzene ring of the terephthalic acid.

It had to be established whether the reaction was functioning. A possible reason that it might not be occurring could be because it had been irradiated with a high frequency source of ultrasound. This was confirmed by the irradiation of a reaction sample in an ultrasonic cleaning bath for a period of one hour and then examined by NMR spectroscopy in a spinning 5mm NMR tube to which had been added a few drops of DMSO-d<sub>6</sub>. No signals for the products were noted in the resulting spectrum obtained using the 1-3-3-1 solvent suppression program.

Two further reactions were attempted, using the 2 MHz source of ultrasonic energy operating at a higher power of 5W. As for the nitrophenol reaction the sample was saturated with air and CCl<sub>4</sub> was added in an attempt to increase reaction rates.

**Table 21:** The Reaction Conditions for the Ultrasonic Reaction of Terephthalic Acid.

Reaction Conditions	Results
Air continuously bubbled through the reaction mixture. 47 minutes reaction time.	No reaction products observed.
Two drops of CCl <sub>4</sub> added and air continuously bubbled through the reaction mixture. 31 minutes reaction time.	No reaction products observed.

No reaction products were observed, by NMR spectroscopic examination, for any of the experiments carried out on the terephthalic system.

### 7.3 Discussion and Conclusions

The detection sensitivity of ultraviolet and fluorescence spectroscopy techniques far exceeds that of NMR spectroscopy. With the aid of a solvent suppression pulse programme it was established that the reactants could also be observed by NMR spectroscopy when the concentration of the reactants was increased significantly.

Both systems were examined by <sup>1</sup>H NMR spectroscopy in the high frequency region (2 or 3 MHz) and in the low frequency region in an ultrasonic cleaning bath and neither yielded observable products.

Employing well-known techniques such as saturation with air and dissolution of CCl<sub>4</sub>, for improving ultrasonic reaction rates, also proved that neither reaction would take place during the time investigated.

The results suggest that, at the concentrations required to carry out NMR observation of dosimeter reactions, the reaction either does not take place or it occurs at such a slow rate it could not be observed in these experimental times. It was hypothesised that if the latter were true, the reaction would still not be a suitable system, because of the long length of time over which the reaction occurs.

**Chapter 8    The Investigation of the Ultrasonically Induced Diels-Alder  
Reaction of Maleic Anhydride with Anthracene**



## 8.1 Confirmation of the Existence of Cavitation

The existence of cavitation within a reaction sample can be confirmed by the Weisser reaction.<sup>21</sup> Stock solutions of potassium iodide  $\text{KI}_{(\text{aq})}$  ( $1.2 \text{ mol dm}^{-3}$ ) and 1% starch solution were prepared freshly for each experiment. The power required by a 3MHz and a 2MHz transducer to guarantee inducing a reaction in  $6.5 \text{ cm}^3$  of solution ( $4 \text{ cm}^3 \text{ KI}_{(\text{aq})} + 2 \text{ cm}^3 \text{ starch}_{(\text{aq})} + \frac{1}{2} \text{ cm}^3 \text{ CCl}_{4(\text{l})}$ ) was established as being 7W for both frequencies, noted by a change in the colour of the sample from colourless to blue/black, caused by the iodine formed, reacting with the starch indicator.

## 8.2 The Formation of 9,10-Dihydroanthracene-endo- $\alpha,\beta$ -succinic Anhydride

In order to confirm the production of adduct formation from the reaction of anthracene with maleic anhydride, the adduct itself was produced by a traditional reflux reaction.

Anthracene (2.0g), maleic anhydride (1.0g) and toluene ( $25 \text{ cm}^3$ ) were placed in a  $50 \text{ cm}^3$  round-bottomed flask and fitted with a reflux condenser. The reaction mixture was refluxed for a period of  $4\frac{1}{2}$  hours and then allowed to cool. A solid precipitate was observed and a recrystallisation was performed on the mixture.

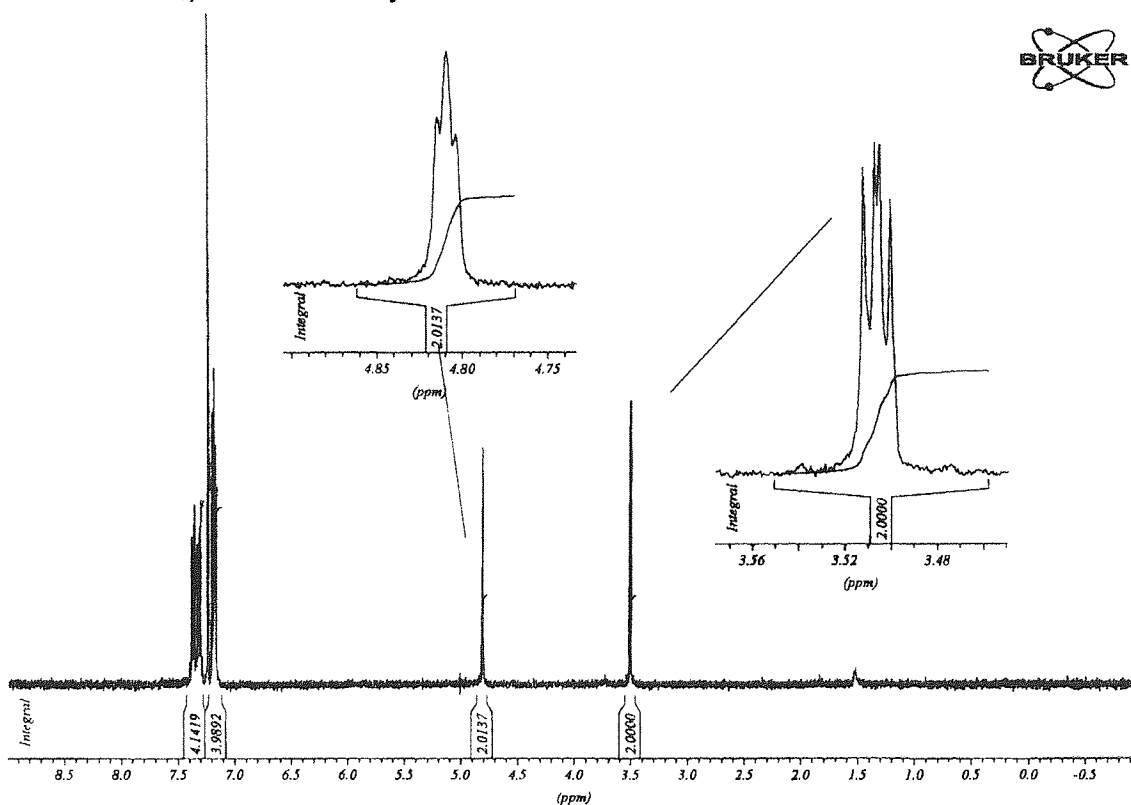
The identity of the precipitate had to be confirmed as that of the adduct 9,10-dihydroanthracene-endo- $\alpha,\beta$ -succinic anhydride.

### 8.2.1 Proving the Identity of the 9,10-Dihydroanthracene-endo- $\alpha,\beta$ -succinic Anhydride

A preliminary investigation using thin layer chromatography (TLC) was carried out to confirm the presence of a compound in the reaction mixture, not due to either of the two reactants, anthracene or maleic anhydride. The eluent employed for the TLC analysis consisted of four parts hexane and one part ethyl acetate and samples of the refluxed mixture were held on silica gel plates. An additional spot due to neither of the reactants was observed in UV light, confirming the formation of a new compound.

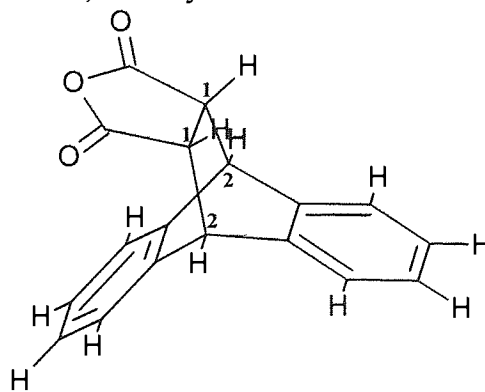
A small quantity of the product of the reflux reaction was dissolved in some  $\text{CDCl}_3$  and analysed further by  $^1\text{H}$  NMR spectroscopy.

**Figure 75:** The  $^1\text{H}$  NMR Spectrum of the Synthesised 9,10-Dihydroanthracene-endo- $\alpha,\beta$ -succinic Anhydride.



The resonances located between 7 ppm and 7.5 ppm are due to the aromatic protons. The large resonance at about 7.2ppm is due to the aromatic protons of the adduct. The remaining two signals are the result of aliphatic protons found only in the adduct.

**Figure 76:** The Structure of 9,10-Dihydroanthracene-endo- $\alpha,\beta$ -succinic Anhydride.



9,10-Dihydroanthracene-9,10-endo- $\alpha,\beta$ -succinic Anhydride

The resonance at 3.5 ppm is caused by the aliphatic hydrogens shown at position 1, adjacent to the carbonyl group of the adduct in Figure 76. The signal is split into two doublets representing the fact that the two protons are non-equivalent i.e. they are in slightly different environments. The absorption peak downfield at 4.8 ppm is assigned to the hydrogens at position 2. The two equivalent protons are split into a triplet by the two neighbouring protons. The identity of the precipitate was proven to be that of the compound 9,10-dihydroanthracene-endo- $\alpha,\beta$ -succinic anhydride. Finally, the melting point of the solid was established as being in the range 261-263°C.

Da Cunha and Garrigues<sup>83</sup> also characterised the adduct by its melting point of 265°C and <sup>1</sup>H NMR (in DMSO-d<sub>6</sub>) where 7.23ppm (m, 8H); 4.81ppm (t, 2H, HCC=C) and 3.5ppm (t, 2H, HCCO) confirming the results obtained in CDCl<sub>3</sub>.

### 8.3 Following the Progress of the Diels-Alder Reaction of Maleic Anhydride with Anthracene

In order to establish that the Diels-Alder reaction of maleic anhydride experienced an enhancement due to sonication, bench top experiments were undertaken using a water bath before pursuing the more difficult experiments in the NMR spectrometer.

A method for following the progress of the Diels-Alder reaction had to be established for the bench reactions. Initially gas liquid chromatography was tested as a method for tracking the formation of the adduct and also the consumption of reactants under the following conditions: -

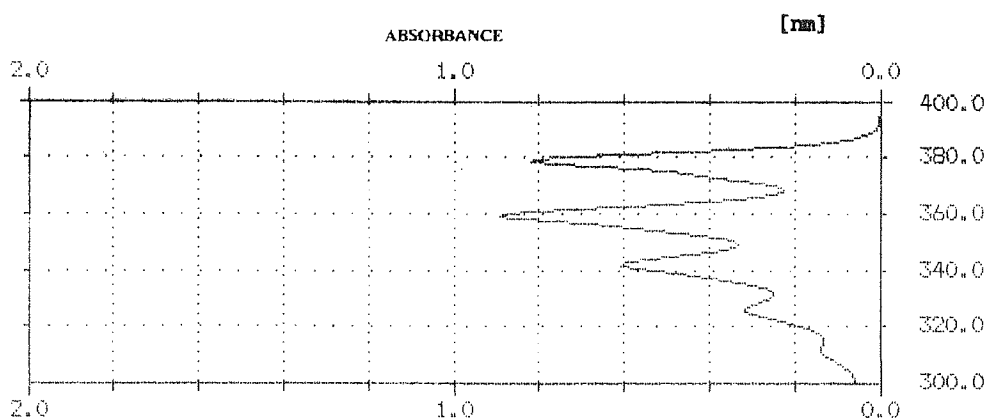
- N<sub>2</sub> carrier gas at 30cm<sup>3</sup>/min
- H<sub>2</sub>/air fuel for the flame ionization detector
- 25% Si grease on diatomite column

The temperature was increased from 200°C to 325°C (473-598 K) and maintained at this temperature for a period of ten minutes. Unfortunately, adducts with an endo-bridge undergo a *retro-cycloaddition* reaction and a number of reactions between maleic anhydride and several polycyclic hydrocarbons containing the anthracene nucleus have been observed as being truly reversible.<sup>67</sup> At the temperatures required for the GC analysis

of the reaction products, the technique was proven unsuitable for this type of Diels-Alder reaction as it too experiences a *retro-cycloaddition* reaction.

Ultraviolet spectroscopy employing the Perkin Elmer Lambda 12 UV/Vis spectrometer was investigated as an alternative method for monitoring the system. Although the formation of the adduct could not be tracked, as it is visible in the infrared region, the consumption of the anthracene could be observed. The largest absorption peak of those observed was used to monitor the reaction at wavelength 359.3nm (see Figure 77).

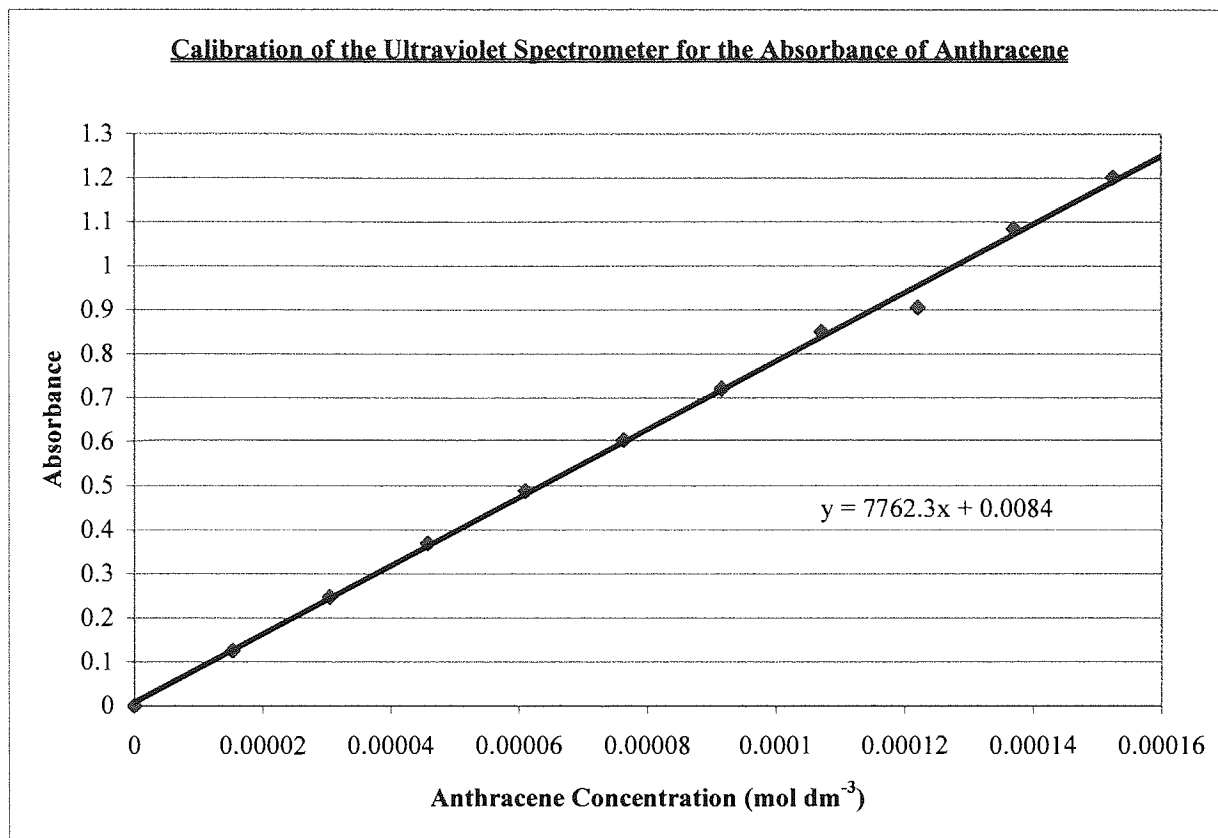
**Figure 77:** The Ultraviolet Spectrum of Anthracene.



#### 8.4 The Calibration of the UV/Vis Spectrometer with Respect to the Concentration of Anthracene

A calibration curve (Figure 78) of absorbance versus concentration ( $\text{mol dm}^{-3}$ ) for anthracene was constructed using a freshly prepared stock solution of known concentration.

**Figure 78:** Calibration Plot for the Absorbance of Anthracene on the UV Spectrometer.



The resulting calibration plot takes the form of a straight-line graph for the concentrations under investigation during the observed Diels-Alder reaction. The consumption of the anthracene during the progress of the reaction could be used to follow the reaction as it proceeded. The graph allows interpolation of concentrations with respect to the absorbance for measurements made for the duration of the reaction.

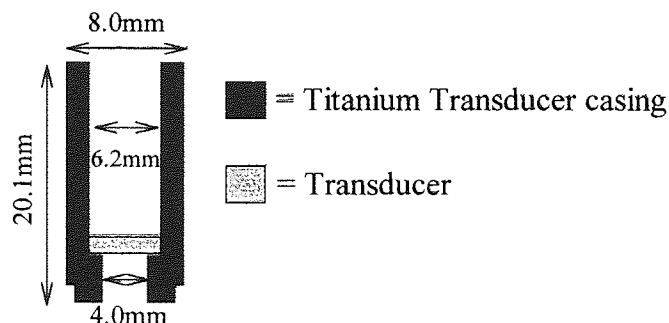
### 8.5 The Thermal Diels-Alder Reaction of Maleic Anhydride with Anthracene in Toluene

Stock solutions of maleic anhydride ( $0.63\text{mol dm}^{-3}$ ) and anthracene ( $0.12\text{mol dm}^{-3}$ ) were prepared separately using toluene as a solvent and warmed to aid dissolution. Toluene- $d_8$   $1\text{cm}^3$  was placed in the test tube held in a water bath and allowed to reach thermal equilibrium. The warmed maleic anhydride ( $1\frac{1}{2}\text{cm}^3$ ) and anthracene ( $3\frac{1}{2}\text{cm}^3$ ) solutions were then added to the solution.

The apparatus employed as the source of ultrasonic irradiation was constructed by Dr. A. Weekes<sup>121</sup> and is illustrated in Figure 79 (not to scale). The author machined the step at the

base of the casing in order to accommodate the glass tube adapter of the heat dissipation device.

**Figure 79:** The Apparatus for Ultrasonic Irradiation.

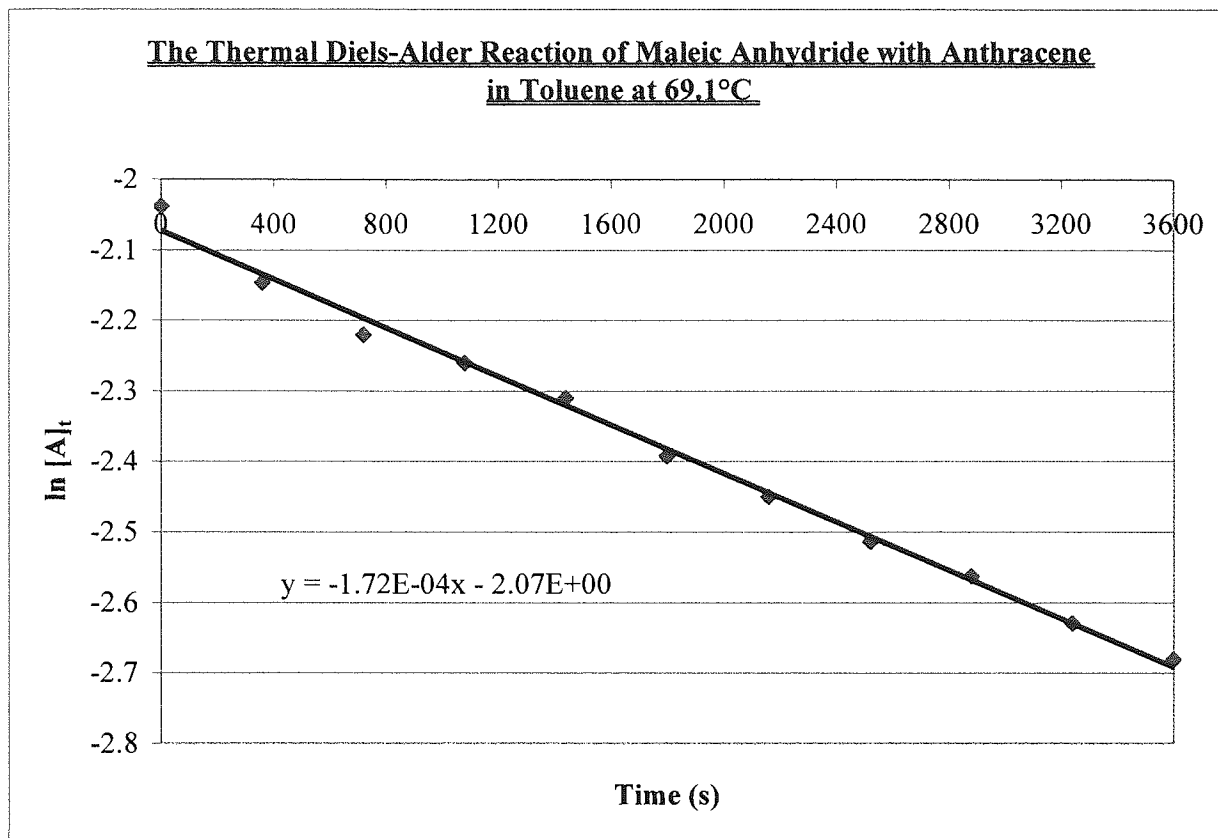


For all thermal and sonicated reactions carried out on the bench, a transducer was placed at a depth of 2cm in the reaction mixture with a thermocouple set at a distance of 2.5cm below the base of the transducer casing. The reactions could only be carried out at temperatures at or above 333 K, the temperature of the system at which dissolution of the anthracene occurred. For this reason all reactions were carried out in the range 333-353 K. The temperature of the sample was measured directly using a thermal couple at equal intervals throughout the course of the reaction.

Over a one-hour period 100 $\mu$ l aliquots were removed at six-minute intervals, quenched in 900 $\mu$ l of chloroform and stored in the refrigerator until required. At the end of reaction the samples were further diluted (100 $\mu$ l made up to 10cm<sup>3</sup> with chloroform) and analysed in the UV spectrometer using a chloroform reference. The UV absorbance of anthracene of each sample was observed at a wavelength of 359.3nm.

The concentration of anthracene in each sample was deduced by interpolation from the calibration graph and the results were plotted according to Equation 37, an example of such a reaction plot is given in Figure 80. Additional plots for all the experiments carried out are available in Appendix 1.

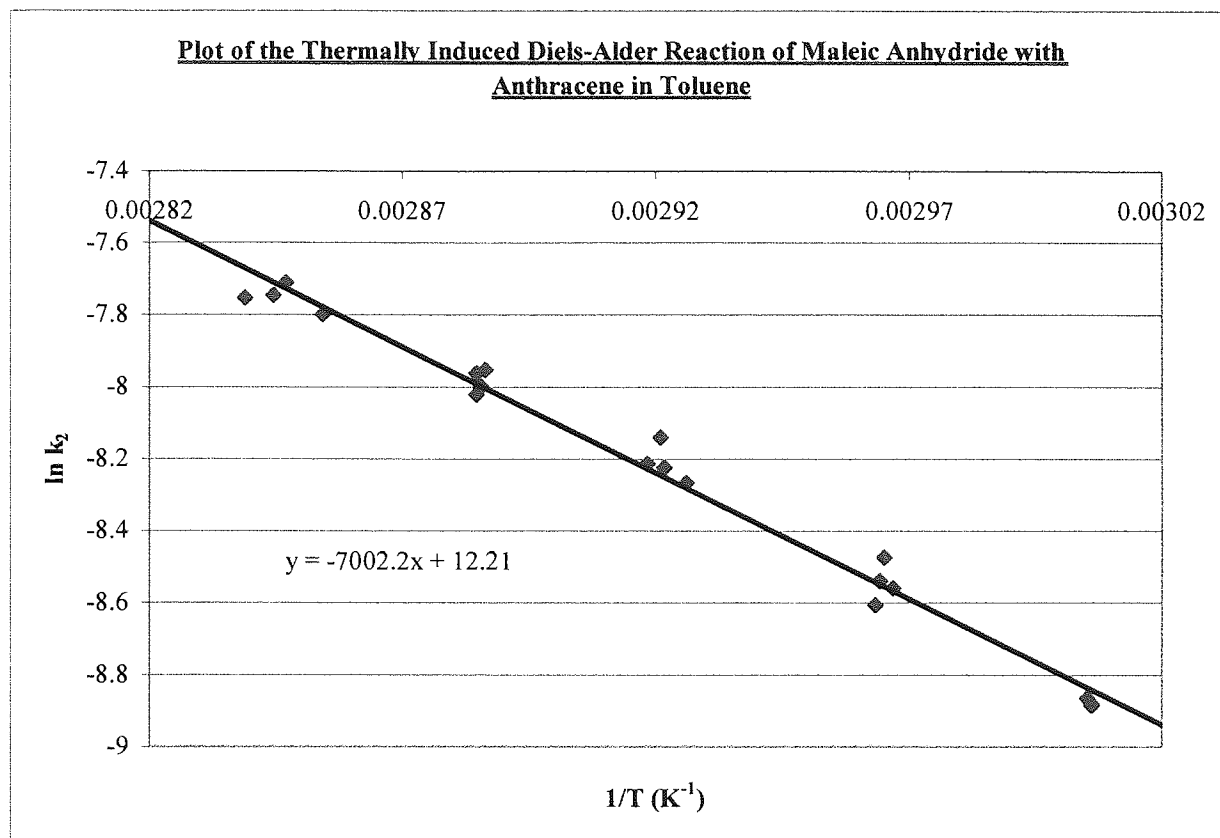
**Figure 80:** The Thermal Diels-Alder Reaction of Maleic Anhydride with Anthracene in Toluene at 342 K.



The rate constant  $k_2$  was calculated using the change in concentration of anthracene  $[A]_t$  for each reaction from Equation 37 for which the gradient of the graph is equal to  $-k_2$ .

According to the modified Wynne-Jones Eyring equation (Equation 42) a plot of  $\ln k_2$  versus  $1/T$  (see Figure 81) yields the thermodynamic parameters of entropy  $\Delta S^\ddagger$ , enthalpy  $\Delta H^\ddagger$ , activation energy  $E_a$  and free energy change  $\Delta G^\ddagger$  using Equation 33, Equation 41, Equation 43 and Equation 44. Errors were calculated using a linear regression computer program provided by Dr. M. Beevers<sup>122</sup> (see Appendix 2).

**Figure 81:** Plot of  $\ln k_2$  versus  $1/T$  ( $K^{-1}$ ) for the Thermal Diels-Alder Reaction in Toluene on the Bench.



The thermodynamic parameters determined for the thermal experiments carried out on the bench top over the temperature range 333-352 K are shown in Table 22 and Table 23.

**Table 22:** The Thermodynamic Parameters for the Diels-Alder Reaction in Toluene over the Temperature Range 333 K to 352 K.

Reaction Conditions	Gradient (K)	Intercept	$\Delta S^\ddagger$ at 333 K ( $JK^{-1}mol^{-1}$ )	$\Delta S^\ddagger$ at 352 K ( $JK^{-1}mol^{-1}$ )
Thermally Induced	$-7002.2 \pm 140.91$	$12.21 \pm 0.41$	$-144.32 \pm 2.90$	$-144.79 \pm 2.91$



**Table 23:** The Thermodynamic Parameters for the Diels-Alder Reaction in Toluene over the Temperature Range 333 K to 352 K.

Reaction Conditions	$\Delta H^\ddagger$ at 333 K (kJmol <sup>-1</sup> )	$\Delta H^\ddagger$ at 352 K (kJmol <sup>-1</sup> )	$\Delta G^\ddagger$ at 333 K (kJmol <sup>-1</sup> )	$\Delta G^\ddagger$ at 352 K (kJmol <sup>-1</sup> )	$E_a$ (kJmol <sup>-1</sup> )
Thermally Induced	55.5±1.12	55.3±1.11	103.0±2.08	106.0±2.14	58.2±1.17

The thermodynamic parameters are not significantly affected by a change in temperature for the range over which this reaction was carried out. For this reason comparisons of the thermodynamic parameters will be made at 343 K.

It was noted, during the course of the reaction, that a large amount of precipitate was produced and its identity had to be established prior to continuing further investigations of the reaction. If the precipitate proved to be the product or reactants then their formation or consumption cannot be observed in the NMR spectrometer.

### 8.5.1 Identification of the Precipitate Produced During Reaction

The precipitate formed during the thermal Diels-Alder reactions in toluene was examined by infrared spectroscopy and compared with the reactants and the adduct, produced by the traditional reflux reaction, to establish its identity. Each sample was made into a KBr<sub>(s)</sub> disc and examined in the Perkin Elmer 1710 Fourier Transform infrared spectrometer. The infrared spectra produced as a result of this analysis are shown in Figure 82 and Figure 83 and also in Appendix 3. Comparison of the infrared spectra for anthracene and maleic anhydride clearly shows that the precipitate is not due to either of the reactants. However, examination of the infrared spectrum of the adduct shows that the precipitate is unmistakably due to the formation of the product (see Table 24).

**Table 24:** Infrared Frequencies of Organic Groups.

Bond	Type of Compound	Frequency (cm <sup>-1</sup> ) <sup>123</sup>	Anthracene	Maleic Anhydride	Adduct	Unknown precipitate
C-H	Alkanes	2850-2970 1340-1470			×	×
C-H	Alkenes	3010-3095 675-995		×		
C-H	Aromatic rings	3010-3100 690-900	×		×	×
C=C	Alkenes	1610-1680		×		
C=C	Aromatic rings	1500-1600	×		×	×
C-O	Anhydrides <i>Normal-</i> <i>Cyclic-</i>	1700-1780 1780-1900. 1750-1820 1820-1950		×	×	×
C=O	Anhydrides	1600-1900		×	×	×

**Figure 82:** The Infrared Spectrum of the Unknown Precipitate.

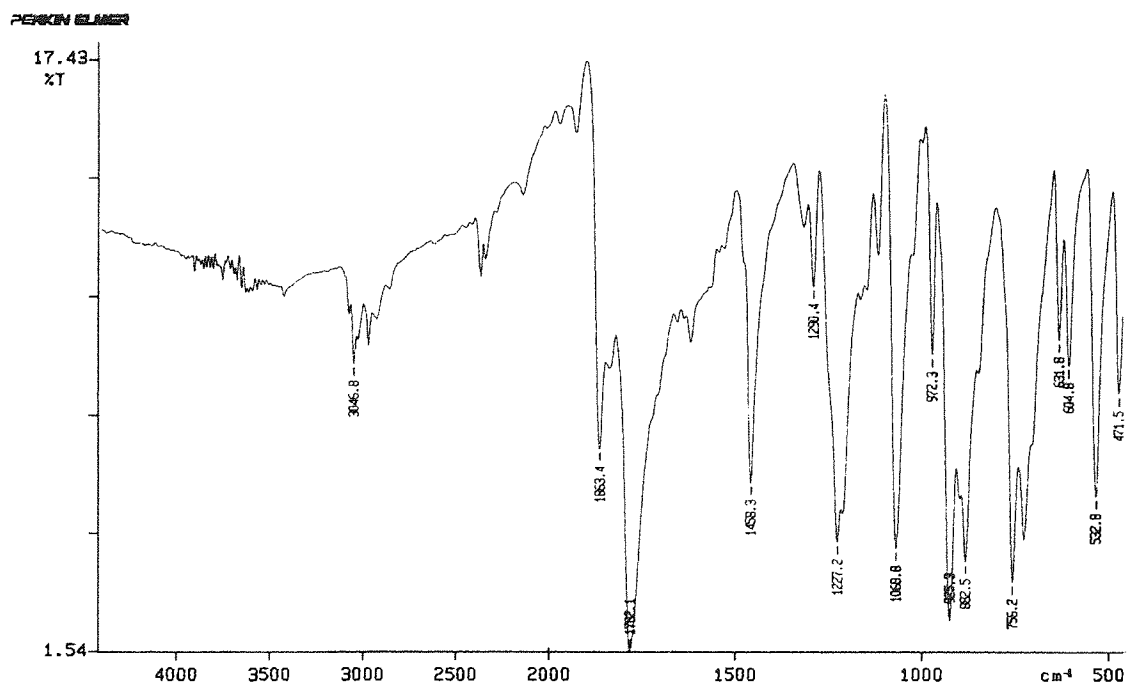
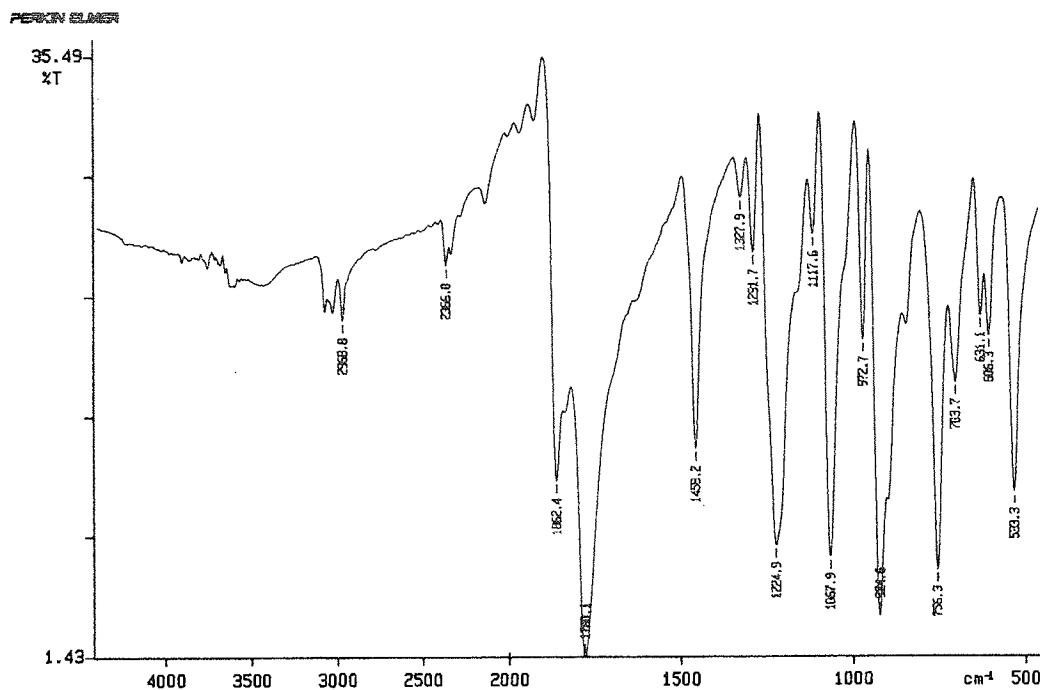


**Figure 83:** The Infrared Spectrum of 9,10-Dihydroanthracene-endo- $\alpha,\beta$ -succinic Anhydride.



The results from the infrared spectra using a KBr disc of the 9,10-dihydroanthracene-endo- $\alpha,\beta$ -succinic anhydride confirms those results obtained by Da Cunha and Garrigues<sup>83</sup> who also noted absorption peaks at  $1860\text{ cm}^{-1}$  (C=O) and  $1780\text{ cm}^{-1}$  (C=O).

As a consequence of the adduct precipitating out of the reaction mixture, any reactions carried out in the NMR spectrometer using the same conditions could only be monitored by the consumption of reactants. Thus an alternative solvent had to be employed to prevent this.

## 8.6 The Diels-Alder Reaction of Maleic Anhydride with Anthracene in *o*-Xylene

The alternate solvent system employed was that of the more polar *o*-xylene (b.p. 418 K) which, in comparison, dissolved a greater amount of both reactants and adduct and also had a higher boiling point than that of toluene (383 K). The employment of *o*-xylene also had an advantage with respect ultrasound. The increased boiling point of *o*-xylene means that, at a particular temperature, the vapour pressure is lower than that of toluene, thus less

vapour enters the cavity produced by ultrasonic irradiation so it collapses with a greater force so producing more energy than those cavities formed in toluene.

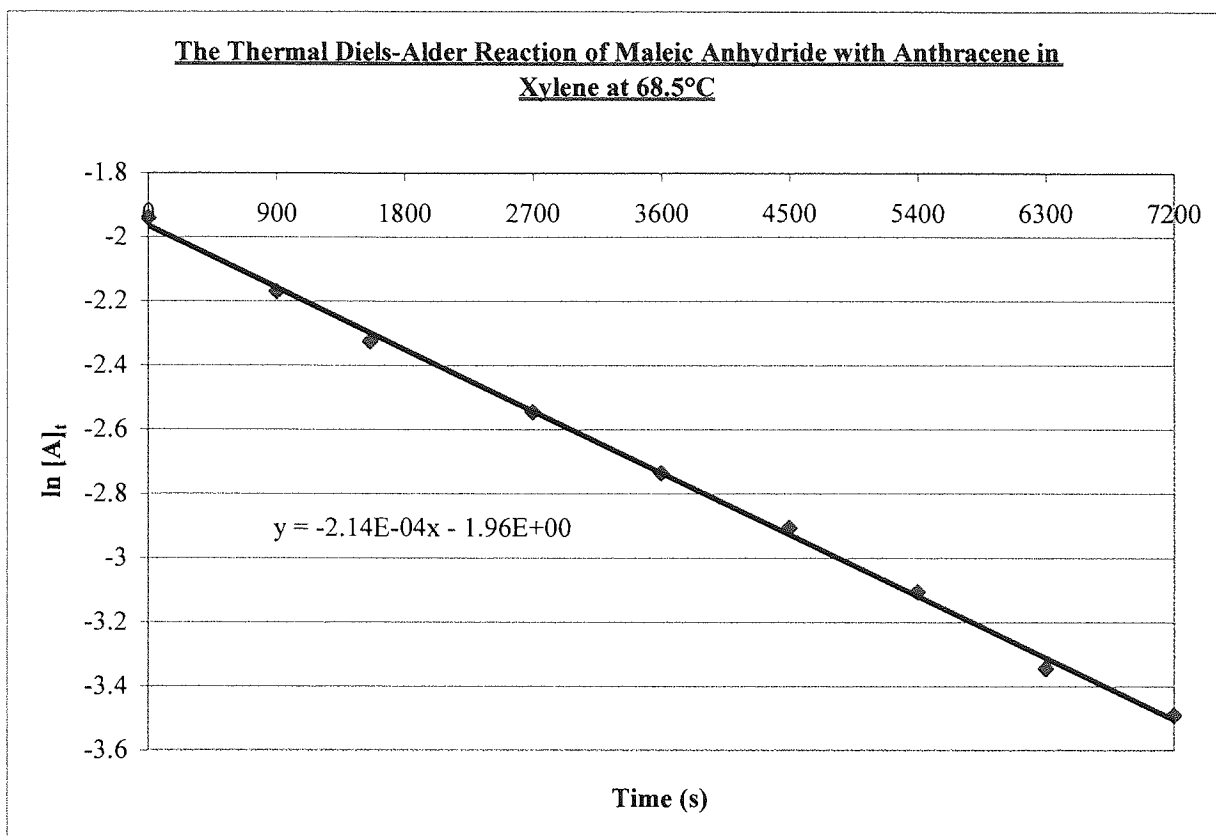
### 8.6.1 The Thermally Induced Diels-Alder Reaction of Maleic Anhydride with Anthracene in *o*-Xylene

Stock solutions of maleic anhydride ( $0.9 \text{ mol dm}^{-3}$ ) and anthracene ( $0.2 \text{ mol dm}^{-3}$ ) were prepared in spectrophotometric grade *o*-xylene. The maleic anhydride was in excess so that the reaction would follow a pseudo-first-order plot for the reaction. Deuterated *o*-xylene- $\text{d}_{10}$  ( $1 \text{ cm}^3$ ) was placed in a test tube held in a water bath and allowed to reach thermal equilibrium. Maleic anhydride ( $2 \text{ cm}^3$ ) and anthracene ( $3 \text{ cm}^3$ ) solution were added.

Over a two-hour period  $100 \mu\text{l}$  aliquots were removed at fifteen-minute intervals and quenched in  $900 \mu\text{l}$  of chloroform and stored in the refrigerator until completion of the reaction. The temperature was measured directly at equal intervals using a thermocouple.

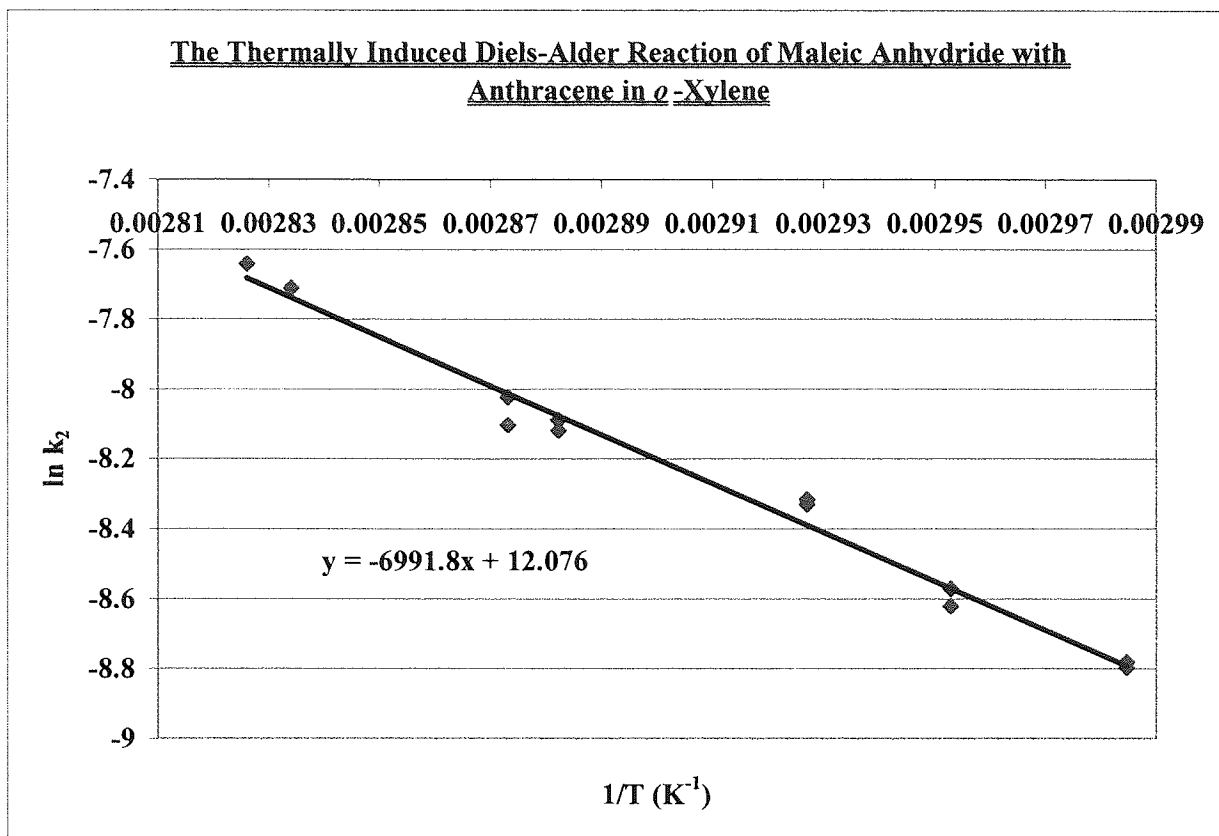
The samples were further diluted ( $100 \mu\text{l}$  made up to  $10 \text{ cm}^3$  with chloroform) and analysed in the UV spectrometer at  $\lambda = 359.3 \text{ nm}$  using a chloroform reference. The concentration of anthracene in each sample was used to plot graphs according to Equation 37, an example of which is displayed in Figure 84. The remainder of the experimental results are shown in Appendix 4.

**Figure 84:** The Thermal Diels-Alder Reaction of Maleic Anhydride with Anthracene in *o*-Xylene at 342 K.



The gradient of each graph at the various temperatures gives a direct value for the rate constant since it equals  $-k_2$ . A plot of  $\ln k_2$  versus  $1/T$  produced the graph in Figure 85 from which the thermodynamic parameters were calculated.

**Figure 85:** Plot of  $\ln k_2$  versus  $1/T$  ( $K^{-1}$ ) for the Thermal Diels-Alder Reaction in *o*-Xylene on the Bench.



The thermodynamic parameters established for the thermal experiments in *o*-xylene over the temperature range 335 K to 354 K are shown in Table 25 and Table 26.

**Table 25:** The Thermodynamic Parameters for the Diels-Alder Reaction in *o*-Xylene over the Temperature Range 335 K to 354 K.

Reaction Conditions	Gradient (K)	Intercept	$\Delta S^\ddagger$ at 335 K ( $JK^{-1}mol^{-1}$ )	$\Delta S^\ddagger$ at 354 K ( $JK^{-1}mol^{-1}$ )
Thermally Induced	$-6991.8 \pm 193.15$	$12.076 \pm 0.56$	$-145.49 \pm 4.02$	$-145.94 \pm 4.03$

**Table 26:** The Thermodynamic Parameters for the Diels-Alder Reaction in *o*-Xylene over the Temperature Range 335 K to 354 K.

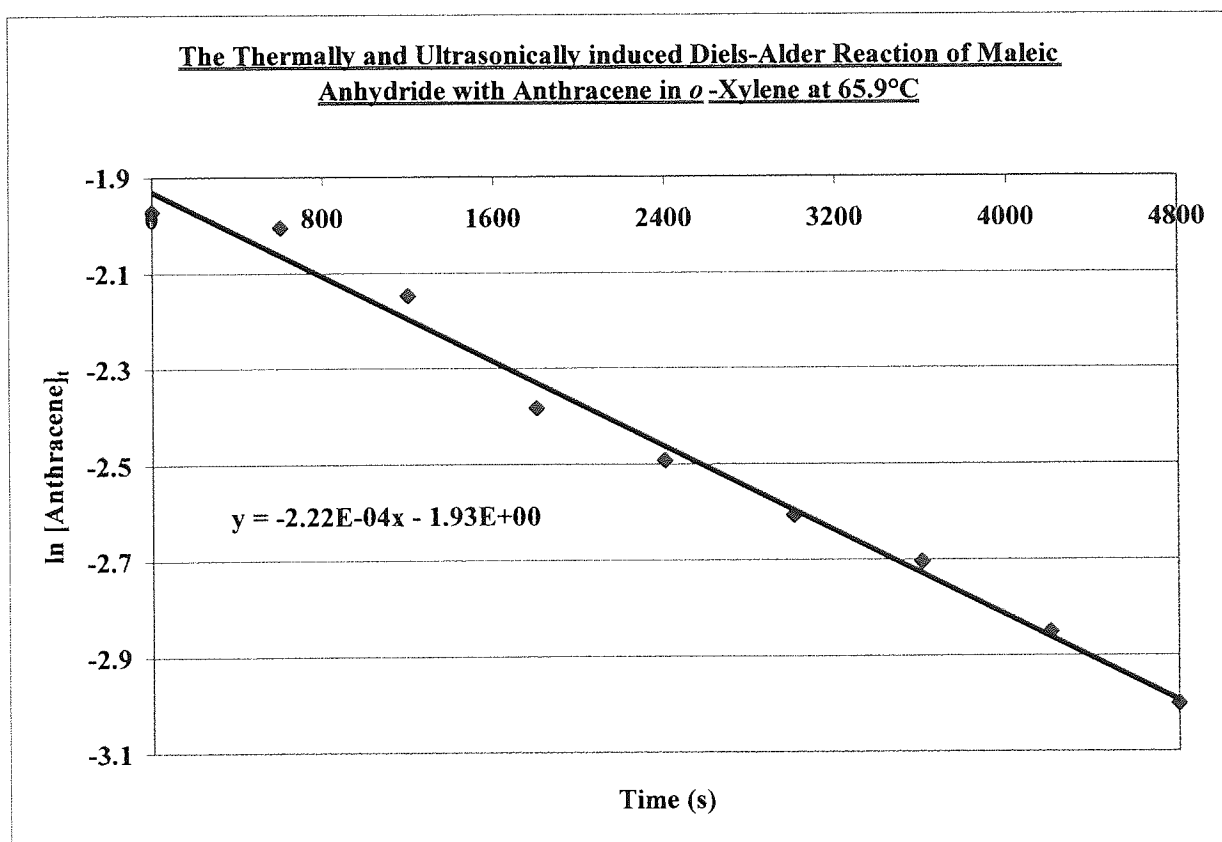
Reaction Conditions	$\Delta H^\ddagger$ at 335 K ( $kJmol^{-1}$ )	$\Delta H^\ddagger$ at 354 K ( $kJmol^{-1}$ )	$\Delta G^\ddagger$ at 335 K ( $kJmol^{-1}$ )	$\Delta G^\ddagger$ at 354 K ( $kJmol^{-1}$ )	$E_a$ ( $kJmol^{-1}$ )
Thermally Induced	$55.3 \pm 1.53$	$55.2 \pm 1.52$	$104.0 \pm 2.88$	$107.0 \pm 2.95$	$58.1 \pm 1.61$

## 8.6.2 The Ultrasonically Induced Diels-Alder Reaction of Maleic Anhydride with Anthracene in *o*-Xylene

The ultrasonically induced reactions were carried out using the same method as the thermally induced reactions; however, liquid nitrogen cooling of the sample was employed to prevent the heating of the sample by the effects of irradiation. The ultrasound was switched on at the commencement of the reaction period using a 2MHz transducer operating at a power of 7W.

The concentration of anthracene present in each sample was used to plot graphs according to Equation 37, an example of which is displayed in Figure 86. The rest of the experimental results are in Appendix 5.

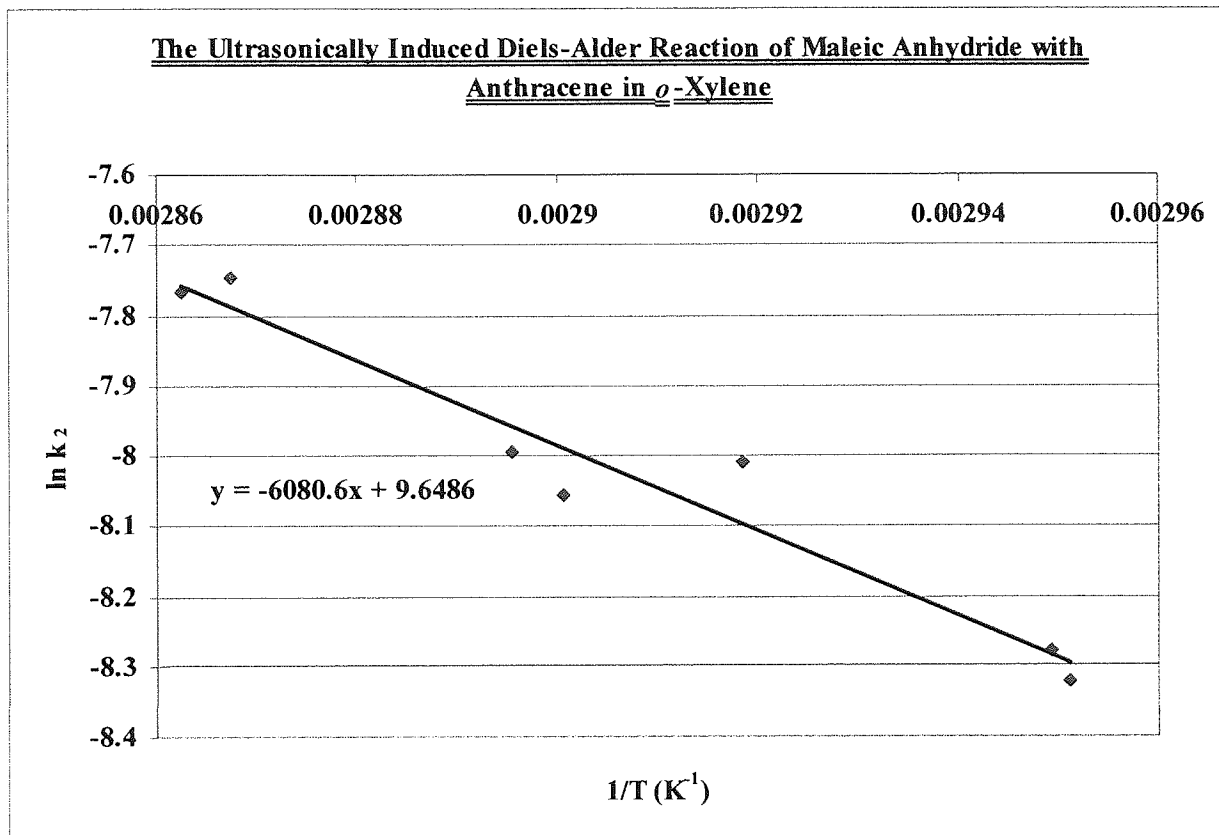
**Figure 86:** The Ultrasonic Diels-Alder Reaction of Maleic Anhydride with Anthracene in *o*-Xylene at 339 K.



The rate constant  $k_2$  was established directly from each experiment because it was equal to the negative of the gradient. An Arrhenius plot of  $\ln k_2$  versus  $1/T$  was constructed to

determine the thermodynamic parameters for the ultrasonic Diels-Alder reaction over the temperature range 339 K to 349 K.

**Figure 87:** The Ultrasonic Diels-Alder Reaction of Maleic Anhydride in *o*-Xylene.



The thermodynamic parameters for the ultrasonically induced reaction of maleic anhydride with anthracene in *o*-xylene were calculated over the temperature range 339 K to 349 K (see Table 27 and Table 28).

**Table 27:** The Thermodynamic Parameters for the Diels-Alder Reaction in *o*-Xylene over the Temperature Range 339 K to 349 K.

Reaction Conditions	Gradient (K)	Intercept	$\Delta S^\ddagger$ at 339 K (JK <sup>-1</sup> mol <sup>-1</sup> )	$\Delta S^\ddagger$ at 349 K (JK <sup>-1</sup> mol <sup>-1</sup> )
Ultrasonically Induced	-6080.6±456.68	9.6486±1.33	-165.77±12.45	-166.02±12.47



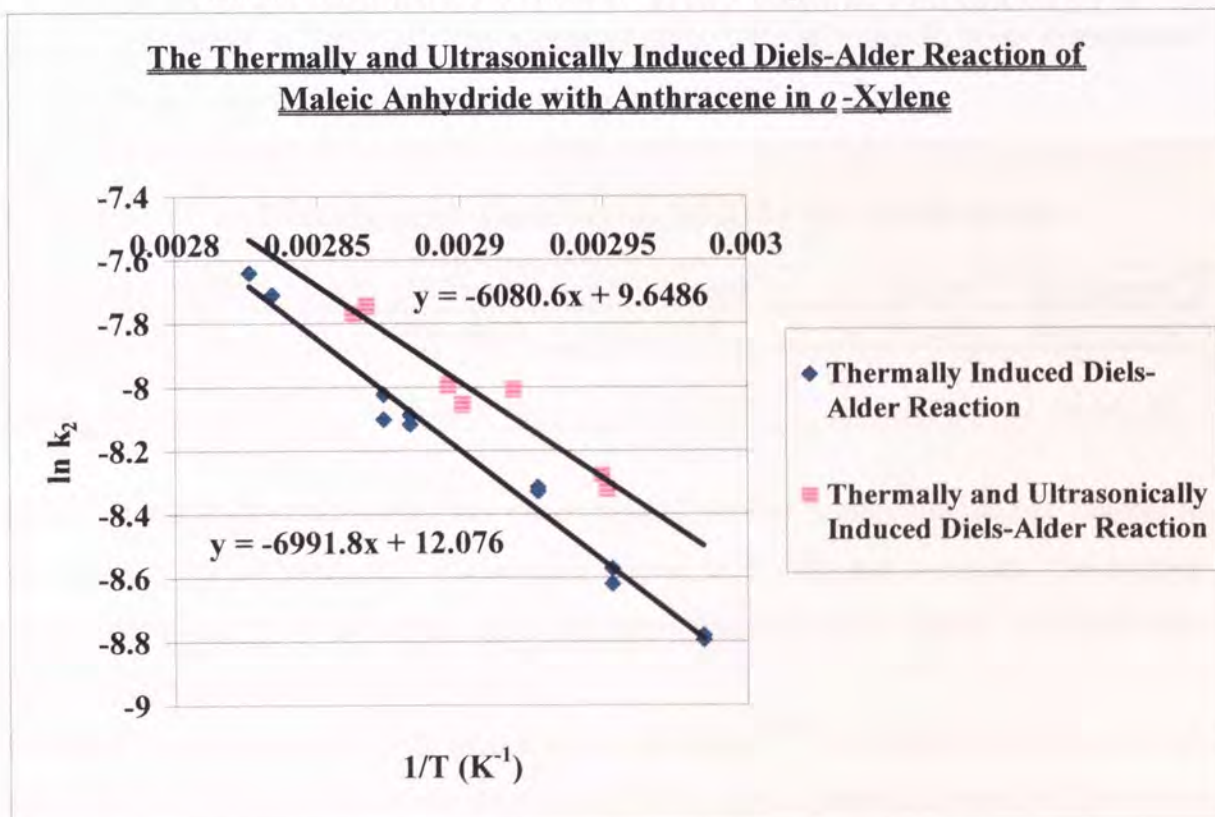
**Table 28:** The Thermodynamic Parameters for the Diels-Alder Reaction in *o*-Xylene over the Temperature Range 339 K to 349 K.

Reaction Conditions	$\Delta H^\ddagger$ at 339 K (kJmol <sup>-1</sup> )	$\Delta H^\ddagger$ at 349 K (kJmol <sup>-1</sup> )	$\Delta G^\ddagger$ at 339 K (kJmol <sup>-1</sup> )	$\Delta G^\ddagger$ at 349 K (kJmol <sup>-1</sup> )	$E_a$ (kJmol <sup>-1</sup> )
Ultrasonically Induced	47.7±3.59	47.7±3.58	104.0±7.80	106.0±7.93	50.6±3.8

### 8.6.3 Comparison of the Thermally and Ultrasonically Induced Diels-Alder Reaction of Maleic Anhydride with Anthracene in *o*-Xylene

A comparison of data for the thermal and ultrasonic Diels-Alder reactions of maleic anhydride with anthracene (Figure 85 and Figure 87) indicate an enhancement in the reaction rate of those systems that were subjected to ultrasonic irradiation (Figure 88).

**Figure 88:** Plot of  $\ln k_2$  versus  $1/T$  (K<sup>-1</sup>) for the Comparison of the Ultrasonic and Thermal Diels-Alder Reaction of Maleic Anhydride with Anthracene.



Rate constants  $k_2$  were extrapolated from the line of best-fit for each system over the temperature range studied. Table 29 displays the upper and lower limits within experimental error.

**Table 29:** Relative Increase in the Rate Constant as a Consequence of Ultrasonic Irradiation Employing a 3 MHz Transducer Operating at 7W.

Temperature (K)	$k_2^{therm}$ ( $\times 10^{-6}$ )	$k_2^{US}$ ( $\times 10^{-6}$ )	$k_2^{US} / k_2^{therm}$		
			Lower	Mean	Upper
333.15	135±1.94	183±19.3	1.20	1.36	1.53
338.15	184±2.65	241±25.4	1.15	1.31	1.46
343.15	249±3.58	313±32.9	1.11	1.26	1.41
348.15	334±4.80	404±42.5	1.07	1.21	1.36
353.15	442±6.35	515±54.2	1.03	1.17	1.31

It can be seen from the results shown in Table 29 that there is an overall increase in the rate constant for the sonicated Diels-Alder reactions over that of the thermally induced systems. However, it is important to establish the basis for the increase in rate constant for sonicated systems; it is either due to a change in the activation energy for the reaction or changes in the pre-exponential factor. The thermodynamic parameters for the thermal and sonicated systems are shown in Table 30. The values of  $\Delta S^\ddagger$ ,  $\Delta H^\ddagger$ ,  $\Delta G^\ddagger$  and  $E_a$  were extrapolated from the line of best fit for each of the reaction conditions.

**Table 30:** The Thermodynamic Parameters at 343 K for the Toluene System.

Reaction Conditions	$\Delta S^\ddagger$ ( $\text{JK}^{-1}\text{mol}^{-1}$ )	$\Delta H^\ddagger$ ( $\text{kJmol}^{-1}$ )	$\Delta G^\ddagger$ ( $\text{kJmol}^{-1}$ )	$E_a$ ( $\text{kJmol}^{-1}$ )
Thermally induced	-145.69±4.02	55.3±1.53	105.0±2.91	58.1±1.61
Thermally and Ultrasonically induced	-165.87±12.46	47.7±3.58	105.0±7.86	50.6±3.80

All of the thermodynamic parameters except that of the free energy change  $\Delta G^\ddagger$ , appear to alter slightly for the sonicated systems with respect to the thermal reactions. The entropy change decreases by about  $20 \text{ JK}^{-1}\text{mol}^{-1}$ , enthalpy decreases by  $8 \text{ kJmol}^{-1}$  and activation energy is also reduced by about  $8 \text{ kJmol}^{-1}$ .

The results are in agreement with Mason and co-workers<sup>115,117</sup> who believed that sonication destroyed the weak solute-solvent interactions in the ground state and some of the strong solvent-solvent interactions. When the solute-solvent interaction is weakened results an increase in enthalpy H, thereby a decrease of  $\Delta H^\ddagger$  takes place. An increase in the freedom of vibration and rotation of the solvent molecules results in an increased entropy S and thus decreased  $\Delta S^\ddagger$ . For the reaction to advance further, the 'solvent shell' surrounding the

nucleophile must be removed if it is to form a new bond with the substrate. The energy required to break the hydrogen bonds within the solvent will contribute to, and so increase the total energy required to reach the transition state. However, the destruction of these solute-solvent interactions by ultrasonic irradiation results in a reduction in the activation energy  $E_a$  as also occurred for a different reaction displayed by the results of Mason in Table 19.

#### 8.6.4 The Effect of Changing the Solvent on the Thermodynamic Parameters on the Thermally Induced Diels-Alder Reaction of Maleic Anhydride with Anthracene

For the experimental reasons outlined in the previous section the solvent employed in the Diels-Alder reaction of maleic anhydride with anthracene was changed from toluene to *o*-xylene. The data shown in Table 31 proves that changing the solvent in this particular  $S_N2$  Diels-Alder reaction does not alter the thermodynamic parameters of the reaction. All of the parameters appear to remain almost identical in magnitude no matter whether the solvent is toluene, or the more polar *o*-xylene.

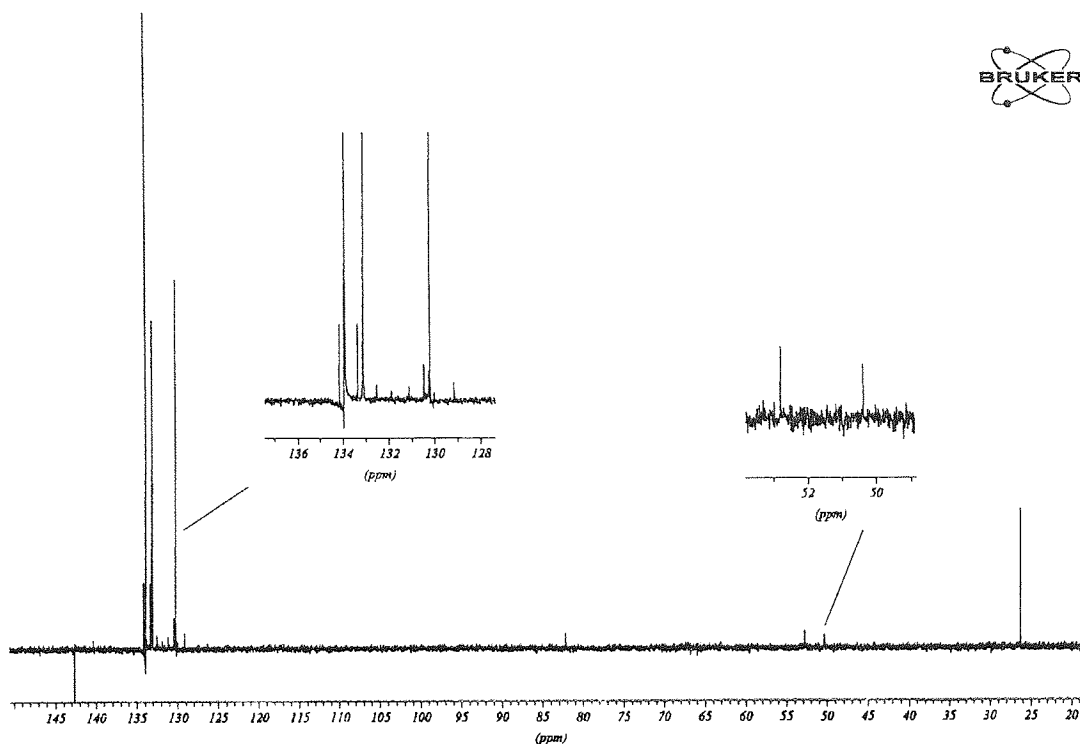
**Table 31:** The Thermodynamic Parameters at 343 K for the *o*-Xylene System.

Reaction Conditions	$\Delta S^\ddagger$ (JK <sup>-1</sup> mol <sup>-1</sup> )	$\Delta H^\ddagger$ (kJmol <sup>-1</sup> )	$\Delta G^\ddagger$ (kJmol <sup>-1</sup> )	$E_a$ (kJmol <sup>-1</sup> )
Thermal-toluene	-144.57±2.91	55.4±1.11	105.0±2.11	58.2±1.17
Thermal- <i>o</i> -xylene	-145.69±4.02	55.3±1.53	105.0±2.91	58.1±1.61

#### 8.7 The NMR Spectroscopic Analysis of the Diels-Alder Reaction of Maleic Anhydride with Anthracene in *o*-Xylene

Investigation of the Diels-Alder reaction by <sup>1</sup>H NMR was not possible due to the large amount of *o*-xylene used in the experiment causing significant problems observing the significantly smaller absorption peaks of interest. Thus, <sup>13</sup>C NMR spectroscopy was investigated as a possible technique to monitor the progress of the Diels-Alder reaction. A PENDANT<sup>6</sup> (Polarisation Enhancement During Attached Nucleus Testing) spectrum of the reaction mixture was obtained in a spinning 5mm NMR tube (see Figure 89).

**Figure 89:** <sup>13</sup>C NMR PENDANT Spectrum of the Diels-Alder Reaction Mixture.



The resonances were assigned to establish the best method for the monitoring the progress of the reaction by  $^{13}\text{C}$  NMR spectroscopy.

**Table 32:** Assignment of Resonances in the PENDANT Spectrum of the Diels-Alder Reaction Mixture.

Absorption peak position (ppm)	Carbon Environment	Source
~26.3	-CH <sub>3</sub>	<i>o</i> -xylene
~50.5	CH-CO	Adduct
~53.0	CH-CH	Adduct
~82.0	CH-CO	Maleic Anhydride
~130.2	-CH (arom next to CH <sub>3</sub> )	<i>o</i> -xylene
~133.1	-CH (arom)	<i>o</i> -xylene
~133.8	-CH (arom)	Anthracene
~134.0	Quaternary C	<i>o</i> -xylene
~142.7	Quaternary C	Anthracene

The signals observed in the  $^{13}\text{C}$  PENDANT spectrum were also observed by Da Cunha and Garrigues<sup>83</sup> when they carried out a  $^{13}\text{C}$  spectrum in DMSO-*d*<sub>6</sub>. They also noted resonances (ppm) at 170.5 (C=O); 140.6 (arom); 136.1 (arom); 127.7 (arom); 127.0 (arom.); 125.2 (arom.); 124.4 (arom.); 48.0 (CH-CH); 45.4 (CH-CO).

Due to the limited resolution in a non-spinning 10mm OD NMR tube the system could not be monitored by way of the aromatic resonances in the region 130-135ppm. This ruled out observation of the system by the consumption of either of the reactants, maleic anhydride or anthracene. In fact, the maleic anhydride is actually present in excess in order to effect a pseudo-first order reaction and the magnitude of this peak will differ little as the reaction progresses. The only available option was to observe the formation of the 9,10-dihydroanthracene-endo- $\alpha,\beta$ -succinic anhydride by way of the two absorption peaks, resulting from the two protons adjacent to the carbonyl groups, occurring between 50-53ppm. It was considered that the most suitable technique to carry out the analyses was by using the DEPT<sup>5</sup> pulse program. The DEPT technique allows the preferential detection of the <sup>13</sup>C absorption peaks of -CH and improves the signal-to-noise ratio by increasing the sensitivity of carbon-13 by a factor of about 4. The <sup>13</sup>C PENDANT spectrum showed how small the resonances of the adduct were, with respect to the other components in the reaction mixture.

To conserve time the ultrasonic NMR experiments were carried out first to check that there were no problems with the reaction conditions set up on the bench when compared with an equivalent thermal reaction.

A modified DEPT pulse programme was specially written for the purpose of this experiment and is given in Appendix 6. The programme allows the automatic sampling, at set time intervals, of the reaction mixture over the course of the experiment. An example of the spectra obtained as the result of such experiments is shown in Figure 90 and Figure 91, where each set of absorption peaks has been slightly offset to allow their comparison. The absorption peaks represent those of the -CH protons adjacent to the carbonyl groups of the product. They have slightly different values as their electronic environments are dissimilar, oriented at different angles to the carbonyl groups (see Figure 76).

**Figure 90:**  $^{13}\text{C}$  NMR DEPT Spectra of an Ultrasonic Diels-Alder Reaction.

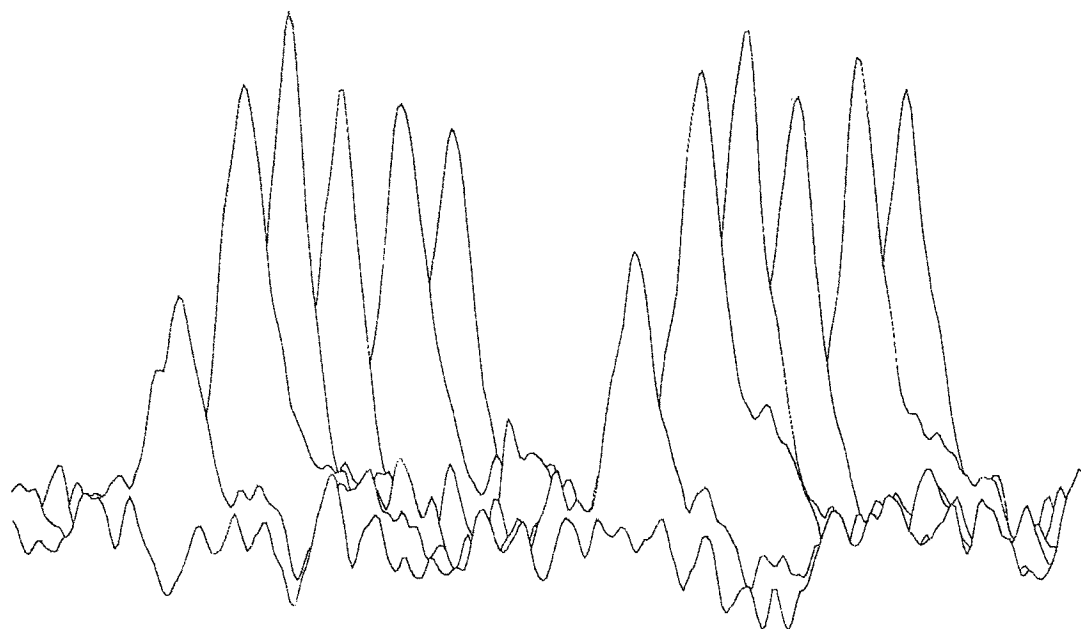
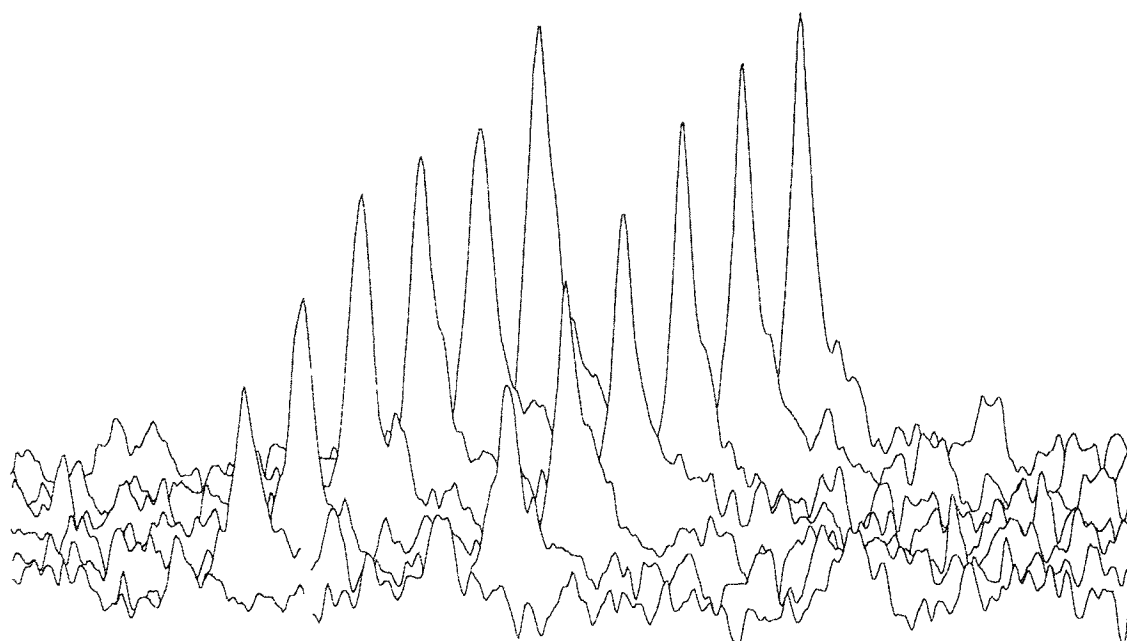


**Figure 91:**  $^{13}\text{C}$  NMR DEPT Spectra of a Thermal Diels-Alder Reaction.



During the course of the reaction under thermal conditions a small quantity of precipitate was observed on the transducer casing, however, when irradiated with ultrasound a much greater amount was created. The solution was becoming saturated at a rate that meant it

was not possible to observe the progress of the reaction. Figure 91 displays a smooth trend of increasing peak size as the reaction progresses. In comparison, the ultrasonic reaction showed in Figure 90 displays a large increase in peak size at the very beginning of the experiment but no further increase occurs as the product is 'dropping out' of the sample preventing its observation.

## 8.8 Discussion and Conclusions

The Diels-Alder reaction of maleic anhydride with anthracene was, for several reasons, an unsuitable system for the in-situ observation of an ultrasonically induced reaction in the NMR spectrometer.

- The reaction could not be observed by  $^1\text{H}$  NMR spectroscopy due to the limited resolution of the NMR spectrometer as a result of the equipment being placed in the top of a 10mm OD NMR tube preventing it from being spun.
- Monitoring the system by way of the carbons in positions 1 and 2 highlighted in Figure 76 using the DEPT pulse sequence for  $^{13}\text{C}$  NMR spectroscopy was the only method available. Unfortunately, the product experienced precipitation out of the mixture prohibiting DEPT examination of the rate of production of the adduct.
- The quantities of reactants required for spectroscopic analysis were dissolved almost to saturation in the solvent employed. Anthracene does not dissolve at temperatures lower than 331 K. The dissolution of the quantities of adduct produced in sonicated reactions was inhibited as the mixture either became saturated or because of mechanical effects caused by the application of ultrasonic energy.

Although the Diels-Alder reaction was an unsuccessful system to study in the NMR spectrometer, it has proven to be the first ever reaction enhanced by the application of ultrasound in the high frequency, megahertz region. A great deal of information has still been obtained from the bench experiments carried out in toluene and *o*-xylene.

Pericyclic reactions traditionally display certain characteristics, which are in agreement with the findings obtained in this study.

- Pericyclic reactions typically have an exceptionally high entropy change of activation  $\Delta S^\ddagger$  normally in the range  $-150$  to  $-200 \text{ JK}^{-1}\text{mol}^{-1}$ . The values obtained for the bench experiments carried out on the Diels-Alder reaction of maleic anhydride with anthracene are in the range  $-145 \text{ JK}^{-1}\text{mol}^{-1}$  to  $-165 \text{ JK}^{-1}\text{mol}^{-1}$ . This is consistent with the loss of translational energy when two molecules combine forming a transition state. Bimolecular reactions inherently require additional organisation in order to align in the correct orientation to allow simultaneous bond formation and breaking.
- The enthalpy of activation  $\Delta H^\ddagger$  is small, being in the range of  $47$ - $55 \text{ kJmol}^{-1}$  reflecting the endothermic nature of the reaction.
- As observed during GLC analysis of the system, the Diels-Alder reaction investigated is reversible at high temperatures, as the  $T\Delta S^\ddagger$  term in Equation 33 becomes increasingly more important.

There are several pieces of information, which can be drawn upon as proof that the Diels-Alder reaction occurs by the way of a concerted, one-step pathway as suggested by Low<sup>81</sup>.

- A retention of configuration is observed in the  $^1\text{H}$  (Figure 75) and  $^{13}\text{C}$  (Figure 89) NMR spectra of the adduct. As a consequence of this observation the mechanism cannot occur via a true diradical or zwitterionic situation.
- It is noted in Table 31 that the use of the more polar solvent *o*-xylene in the place of toluene does not cause an increase in reaction rate, ruling out the presence of a charged transition state. If a zwitterionic intermediate were involved it would be of greater polarity than the reactants and a more polar solvent would result in better solvation causing an increase in the rate of the reaction. No increase in reaction rate was noted. The reaction cannot take place via a stepwise ionic pathway.

The ultrasonically induced reaction on the bench does cause an enhancement in the rate constant as displayed in Table 33 where the rate increase of the ultrasonic reactions at a



particular temperature were compared to that of the thermal reactions. The greatest improvement occurred at the lowest temperature investigated 298K.

**Table 33:** Rate Constant Increase of the Ultrasonic over the Thermal Diels-Alder Reaction.

Temperature (K)	Bench-top Reaction $k_2^{US} / k_2^{therm}$ (mean)
298	1.36±0.16
303	1.31±0.15
308	1.26±0.15
313	1.21±0.14
318	1.17±0.14

Other workers, examining another ultrasonic reaction system, also observed a similar trend,<sup>115,116</sup> where it was believed that the decrease in reaction rate was the result of increasing vapour pressure with increasing temperature. It was surmised that the vapour fills the cavities and causes them to implode less violently as more vapour enters at higher temperatures the implosion of the cavities is cushioned, so less energy is produced to initiate a rate enhancement.

Analysis of the reaction in the NMR spectrometer by either <sup>1</sup>H or <sup>13</sup>C NMR spectroscopy was found to be an impossible task. The placement of the metal transducer equipment and thermocouple meant that extensive shimming had to be carried out to compensate for their presence in the magnet of the NMR spectrometer. The limited resolution of the spectrometer for the <sup>1</sup>H NMR spectroscopy due to any extremely large resonance of the solvent meant that the only technique that could be employed was <sup>13</sup>C NMR spectroscopy of the product. Signals for the reactants in the aromatic region could not be suitably resolved to follow their consumption. The product 'dropping out' of the reaction mixture prevented the reaction being monitored using the <sup>13</sup>C DEPT technique. Employing the more polar solvent *o*-xylene slowed the rate at which the product precipitated out of solution. However, when the ultrasonic energy was applied the product was formed much more quickly and as a consequence it 'dropped out' of solution more quickly, which lead to problems in the observation of the rate of the reaction. Due to the low sensitivity of <sup>13</sup>C

nuclei and the increased relaxation time  $T_1$  each NMR spectrum took 15 minutes to acquire during this time the precipitate began to appear.

The thermodynamic quantities established are with respect to the formation of the activated complex. In order to establish those for the reaction the reverse reaction would also have to be carried out to obtain values for the 'product side' of the Gibb's free energy profile.

Table 34 lists the thermodynamic parameters calculated for each of the three different reaction conditions investigated and their associated errors.

**Table 34:** Comparison of the Thermodynamic Parameters Established for the Diels-Alder Reactions.

Reaction Conditions	$\Delta S^\ddagger$ ( $\text{JK}^{-1}\text{mol}^{-1}$ )	$\Delta H^\ddagger$ ( $\text{kJmol}^{-1}$ )	$\Delta G^\ddagger$ ( $\text{kJmol}^{-1}$ )	$E_a$ ( $\text{kJmol}^{-1}$ )
Thermal - toluene	-144.57±2.91	55.4±1.11	105.0±2.11	58.2±1.17
Thermal - <i>o</i> -xylene	-145.69±4.02	55.3±1.53	105.0±2.91	58.1±1.61
Thermally and Ultrasonically induced - <i>o</i> -xylene	-165.87±12.46	47.7±3.58	105.0±7.86	50.6±3.80

The activation energy  $E_a$  represents the minimum amount of energy required by the reacting species to form the activated complex or transition state before proceeding to the final products. For both of the thermal reactions the activation energy remains the same at about  $58 \text{ kJmol}^{-1}$ . However, the activation energy  $E_a$  experiences a reduction of nearly  $8 \text{ kJmol}^{-1}$ . The 'solvent shell' surrounding the nucleophile needs to be removed if it is to form a new bond with the substrate. The energy required to break the hydrogen bonds within the solvent contributes to the total energy required to reach the transition state. However, the ultrasonic irradiation assists with this solute-solvent interaction destruction thus reducing the  $E_a$  for the reaction.

The Gibb's free energy for any reaction involving an enthalpy change  $\Delta H$  and an entropy change  $\Delta S$  may be defined by

$$\Delta G = \Delta H - T\Delta S$$

$\Delta G$  is the maximum amount of useful work that may be obtained from the reaction. For any system, the value and sign of  $\Delta G$  describes the position of the equilibrium for a reaction; at

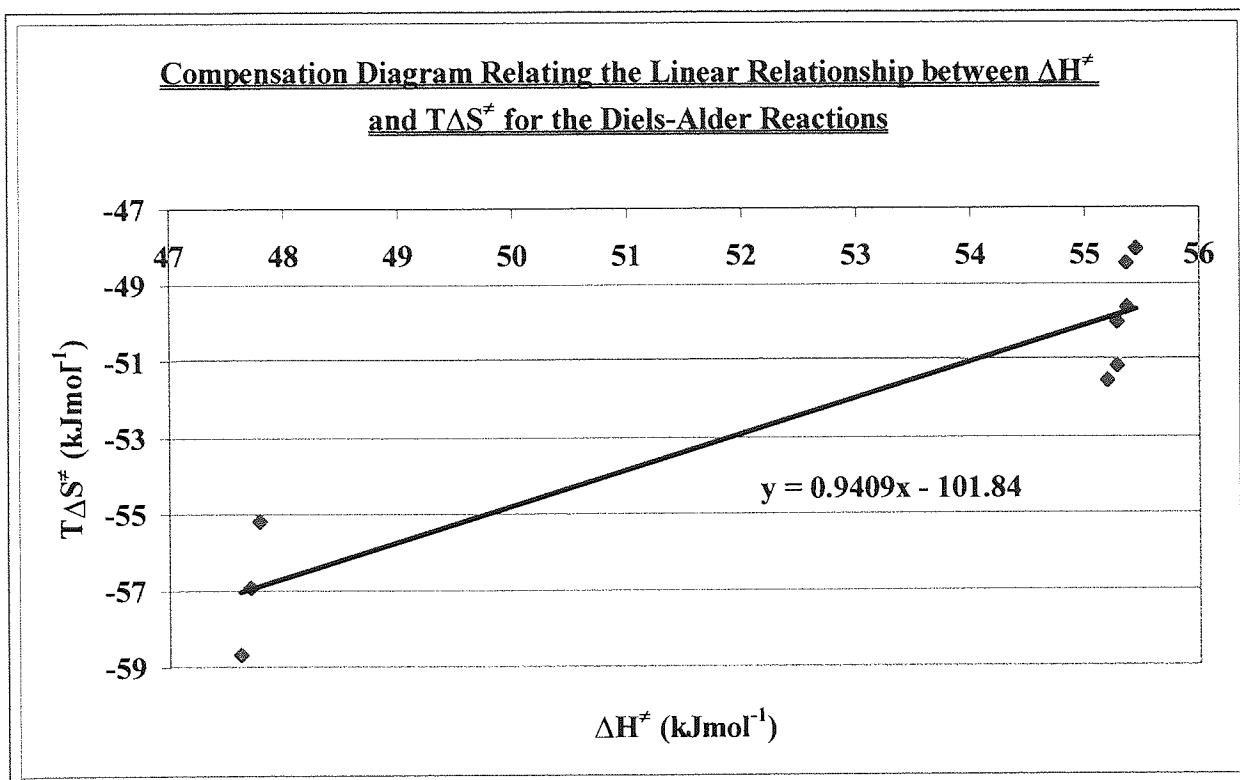
equilibrium,  $\Delta G$  is equal to zero. Under standard conditions  $\Delta G$  must be negative in order for the reaction to be feasible. However, the free energy change determined in the experiments was that for the development of the activated complex  $\Delta G^\ddagger$ , not for the progress of the entire reaction. The values of  $\Delta G^\ddagger$  for the thermal and sonicated reaction systems are constant at  $105 \text{ kJmol}^{-1}$ . The value of  $\Delta G^\ddagger$  is positive because the formation of the activated complex requires energy in order for it to occur.

According to Equation 33 a linear relationship exists between the  $T\Delta S^\ddagger$  and  $\Delta H^\ddagger$ , the gradient of a plot of the two parameters is equal to unity when no variation of  $\Delta G^\ddagger$  occurs. Values of  $\Delta H^\ddagger$  and  $T\Delta S^\ddagger$  extrapolated from the line of best fit obtained for the bench top Diels-Alder reactions at 333 K, 343 K and 353 K are shown in Table 35.

**Table 35:** Linear Relationship between  $\Delta H^\ddagger$  and  $T\Delta S^\ddagger$ .

Temperature (K)	Reaction Conditions	$\Delta H^\ddagger$ ( $\text{kJmol}^{-1}$ )	$T\Delta S^\ddagger$ ( $\text{kJmol}^{-1}$ )
333	Thermal Diels-Alder in Toluene	$55.45 \pm 1.12$	$-48.08 \pm 0.97$
333	Thermal Diels-Alder in <i>o</i> -xylene	$55.36 \pm 1.53$	$-48.45 \pm 1.34$
333	Ultrasonic Diels-Alder in <i>o</i> -xylene	$47.79 \pm 3.59$	$-55.18 \pm 4.14$
343	Thermal Diels-Alder in Toluene	$55.37 \pm 1.11$	$-49.61 \pm 1.00$
343	Thermal Diels-Alder in <i>o</i> -xylene	$55.28 \pm 1.53$	$-49.99 \pm 1.38$
343	Ultrasonic Diels-Alder in <i>o</i> -xylene	$47.70 \pm 3.58$	$-56.92 \pm 4.28$
353	Thermal Diels-Alder in Toluene	$55.28 \pm 1.11$	$-51.14 \pm 1.03$
353	Thermal Diels-Alder in <i>o</i> -xylene	$55.20 \pm 1.52$	$-51.54 \pm 1.42$
353	Ultrasonic Diels-Alder in <i>o</i> -xylene	$47.62 \pm 3.58$	$-58.66 \pm 4.41$

**Figure 92:** Compensation Diagram of the Linear Relationship between  $\Delta H^\ddagger$  and  $T\Delta S^\ddagger$  for the Diels-Alder Reactions.



The slope in Figure 92 for the plot of  $T\Delta S^\ddagger$  vs  $\Delta H^\ddagger$  was equal to  $0.9409 \pm 0.094$  within experimental errors. The changes in the Gibb's free energy of activation  $\Delta G^\ddagger$  for the reaction conditions investigated is almost equal to zero within experimental error and confirmed by the fact that the slope of the compensation diagram is almost equal to unity. The very small variation in  $\Delta G^\ddagger$  is due to a compensation effect occurring between  $\Delta H^\ddagger$  and  $T\Delta S^\ddagger$ .

The data examined may also be divided into those reactions that were ultrasonically and those that were thermally induced. Figure 93 displays the data for the thermally induced and the ultrasonically induced reactions Figure 94. However, no such trend was observed when the two sets of data were separated and further investigations are needed here in order to obtain further data points and explain the effect.

This could be the result of over saturation of the solvent system employed.

**Figure 93:** Compensation Diagram of the Linear Relationship between  $\Delta H^\ddagger$  and  $T\Delta S^\ddagger$  for the Thermally Induced Diels-Alder Reactions.

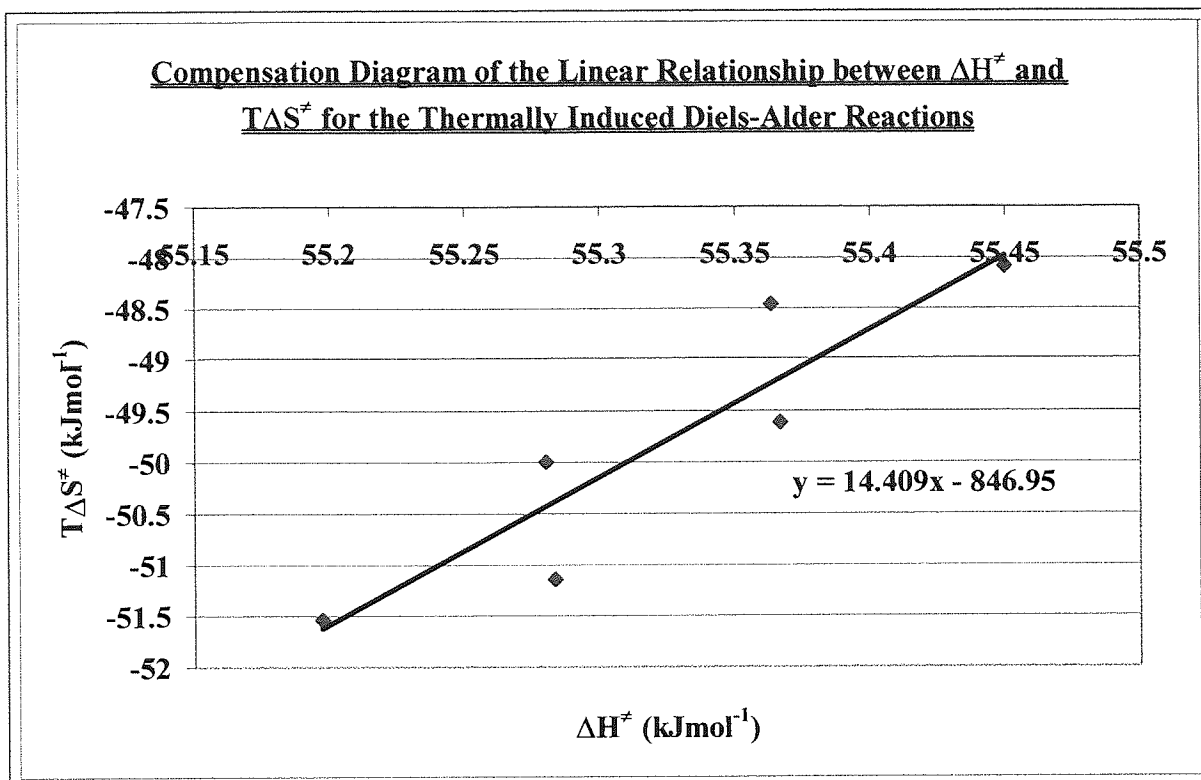
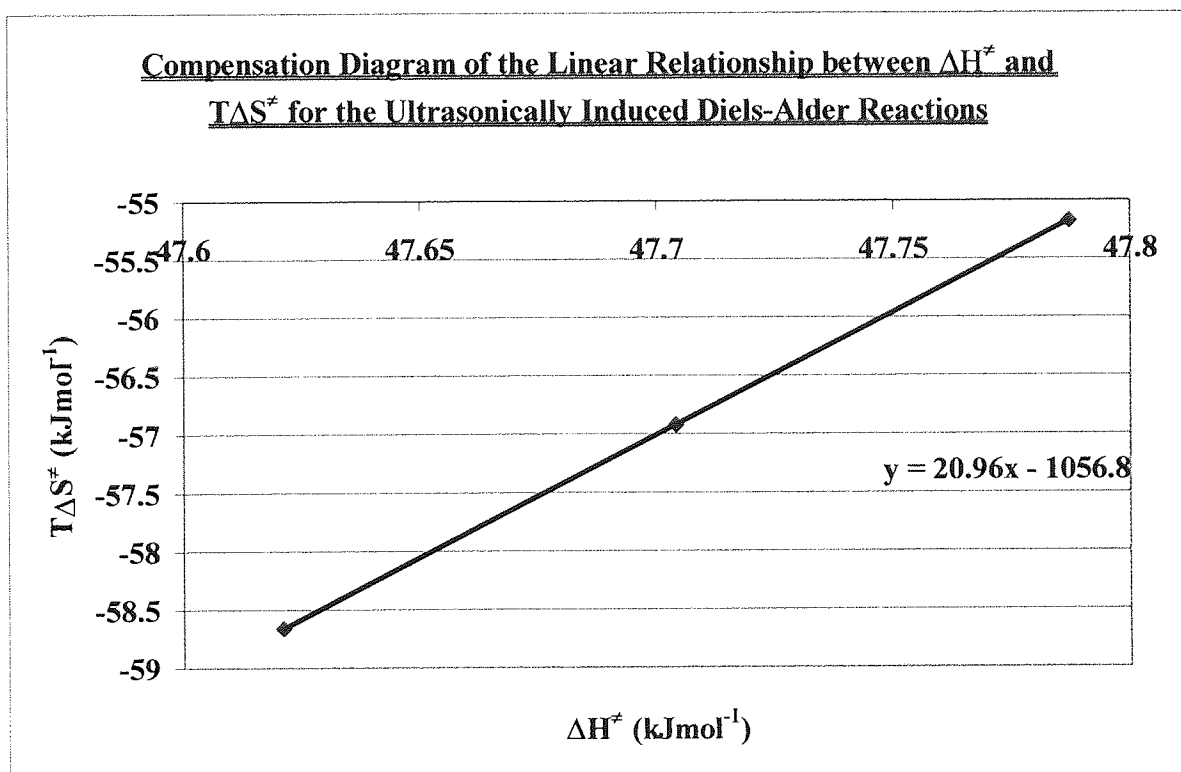


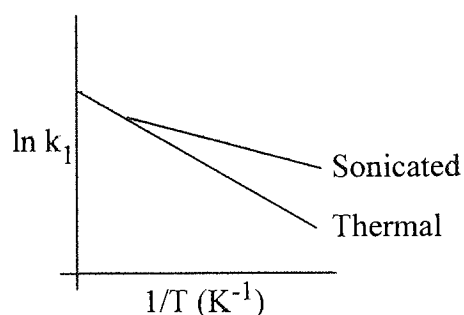
**Figure 94:** Compensation Diagram of the Linear Relationship between  $\Delta H^\ddagger$  and  $T\Delta S^\ddagger$  for the Ultrasonically Induced Diels-Alder Reactions.



The entropy change of activation for each reaction is calculated using the value of the intercept on the y-axis of the extrapolated Arrhenius plot, making the assumption that the

graph can be extrapolated linearly. However, although the assumption is founded for the thermal experiments it is not strictly true for sonicated reactions where the gradient usually crosses the thermal trend line at some point before it meets the y-axis. At the temperature where the two trend lines meet, the ultrasonic enhancement has no further effect and the thermal effects are dominant (Figure 95), above this temperature the data derived from the thermal experiments and from thermal-ultrasonic experiments are described by the same single trend.

**Figure 95:** The General Trend Observed for the Ultrasonic and Thermal Solvolysis Reactions.



The ultrasonically induced reactions are actually a combination of thermal and ultrasonic effects. However, there is a temperature at which the sonicated reaction becomes dominated by thermal effects and experiences no further enhancement due to sonication. The temperature at which the effect occurs can be established by solving simultaneous equations of the thermal and sonicated reactions.

$$\text{Thermal } y_1 = -6991.8x_1 + 12.076$$

$$\text{Sonicated } y_1 = -6080x_2 + 9.6486$$

At the point where the two lines cross  $y_1=y_2$  thus,

$$-6080.6x_2 + 9.6486 = -6991.8x_1 + 12.076$$

And  $x_1=x_2$  so the value of  $x$  at which the two trend lines cross can be calculated

$$\frac{12.076 - 9.6486}{6991.8 - 6080.6} = x_1 = x_2 = 2.664 \times 10^{-3} \text{ K}$$

From the experimental data gathered the two trend lines should cross at a temperature of 375 K. At the temperature calculated the sonicated reaction would effect no further enhancement over and above that which would normally occur for a thermal reaction at the same temperature.

**Chapter 9    The Ultrasonically Induced Solvolysis of 40% (v/v) t-BuCl  
in Propan-2-ol with 40% (w/w) Aqueous Propan-2-ol**



In the previous chapter there were several problems which, when combined, resulted in an unsuitable reaction system for the in-situ detection by NMR spectroscopy of an ultrasonically enhanced chemical reaction.

As a result of the problems encountered in the Diels-Alder system it was established that a reaction requires certain characteristics in order to be observable in a NMR spectrometer.

- Homogeneous liquid system.
- Observable by  $^1\text{H}$  NMR spectroscopy because the proton is almost 100% abundant compared with the 1.1% abundance of the  $^{13}\text{C}$  carbon atom, which corresponds to a 62.9 factor increase in sensitivity.
- Ensure reactants and products are not prone to precipitate out of solution.

The well-documented, ultrasonically enhanced, solvolysis of t-BuCl appeared to be an ideal reaction to investigate.

### 9.1 Determination of a Suitable Solvent System for the Solvolysis of t-BuCl

In order to obtain a suitable reaction rate to permit the observation of the reaction, the best solvent system had to be established. The solvolysis system had to allow the dissolution of sufficient t-BuCl for NMR spectroscopic observation and react over a period that was neither too short nor too long. Table 36 shows the solvents examined as possibilities for a practical reaction medium.

**Table 36:** Establishing a Suitable Solvent System for the Solvolysis of t-BuCl.

Solvent System	Experimental Results
Ethanol/Water	Reaction was too slow due to the larger amounts of t-BuCl required.
Methanol/Water	No observable product after three hours at room temperature. Reaction too slow.
Acetone/Water	
DMSO/Water	
DMF/Water	
1,4-Dioxane/Water	t-BuCl immiscible at the volumes required for NMR spectroscopic observation.
Propan-2-ol/Water	A suitable quantity of product was present after three hours at room temperature. This was the system chosen for the solvolysis reaction.

DMSO = Dimethyl Sulphoxide

DMF = Dimethyl Furan

From Table 36 it can be seen that the most suitable solvent system for the solvolysis reaction of t-BuCl was aqueous propan-2-ol. A 40% (w/w) propan-2-ol/water medium provided a reaction of adequate length to enable the study of the reaction in the NMR spectrometer. The t-BuCl was present in a solution of 40% (v/v) t-BuCl/propan-2-ol in which the propan-2-ol was employed as a co-solvent.

## 9.2 The Construction of a Novel Conductivity Cell

A standard conductivity probe was too large for the simultaneous measurement of conductivity and application of ultrasonic irradiation to the relatively small sample volumes. When larger sample volumes were used the ultrasonic energy was dissipated and higher powers were required to effect an enhancement of the reaction by sonication. Unfortunately very high powers resulted in the fracturing of transducers.

Thus, a great deal of time was expended on the design and construction of a conductivity cell, which had to fulfil certain requirements.

- i) Permits continuous sonication of small reaction samples (about 6 cm<sup>3</sup>).
- ii) Allow simultaneous measurement of conductivity and temperature.
- iii) The electrodes had to be rigid to maintain a constant distance between them to ensure consistent conductivity readings.
- iv) The positioning of the transducer had to be the identical at all times to preserve the consistent reaction conditions.
- v) All materials, which come into contact with the reaction samples had to be resistant to the chemicals used.

A Teflon™ locator was created which would position the transducer, thermocouple and electrodes in the same position at all times. However, because of the small scale on which the cell had to be constructed the copper wires, to which the stainless steel electrode plates were attached, were too flexible to maintain a constant distance between them. Thus, a

Teflon™ plug was made to go in the bottom of the test tube and keep the electrodes in the same position at all times. Finally, the whole cell was placed on a rigid holder, which could be clamped into position to prevent any further movement of the equipment. The final cell set up is shown in Figure 96.

**Figure 96:** A Novel Conductivity Cell

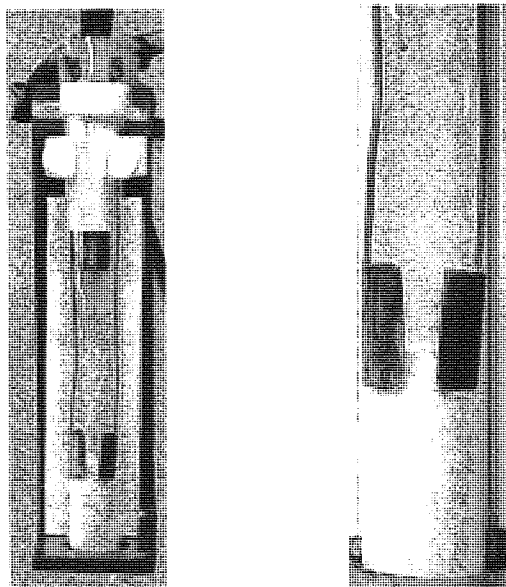
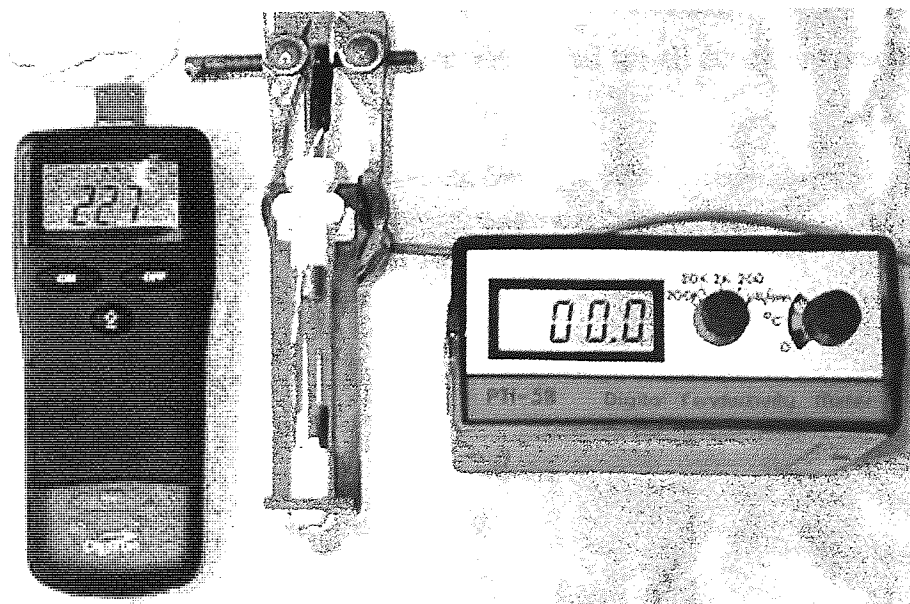


**Figure 97:** Conductivity Cell Equipment.



The cell functioned effectively for samples in which concentrations of t-BuCl and H<sup>+</sup>Cl<sup>-</sup> product were low. Unfortunately, at the concentrations essential for acceptable signal-to-

noise ratios in the NMR experiments, the detection limits of the meters available were too low. For this reason an alternative sampling technique was formulated.

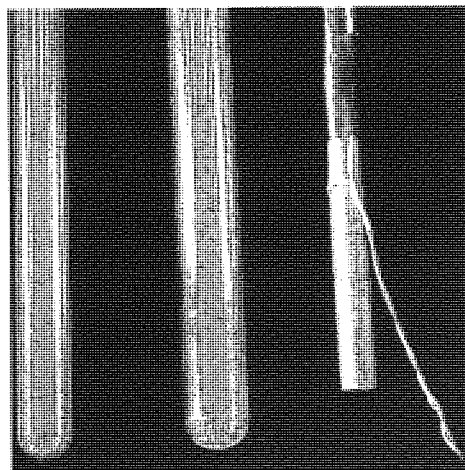
### 9.3 The Bench Top Reaction of 40% (v/v) t-BuCl/Propan-2-ol with 40% (w/w) Propan-2-ol/Water

In order to establish that the reaction of 40% (v/v) t-BuCl in propan-2-ol with 40% (w/w) aqueous propan-2-ol experienced an enhancement due to ultrasonic irradiation, bench top experiments were undertaken using a water bath, before pursuing the more difficult experiments in the NMR spectrometer.

#### 9.3.1 The Thermally Induced Bench Top Reaction

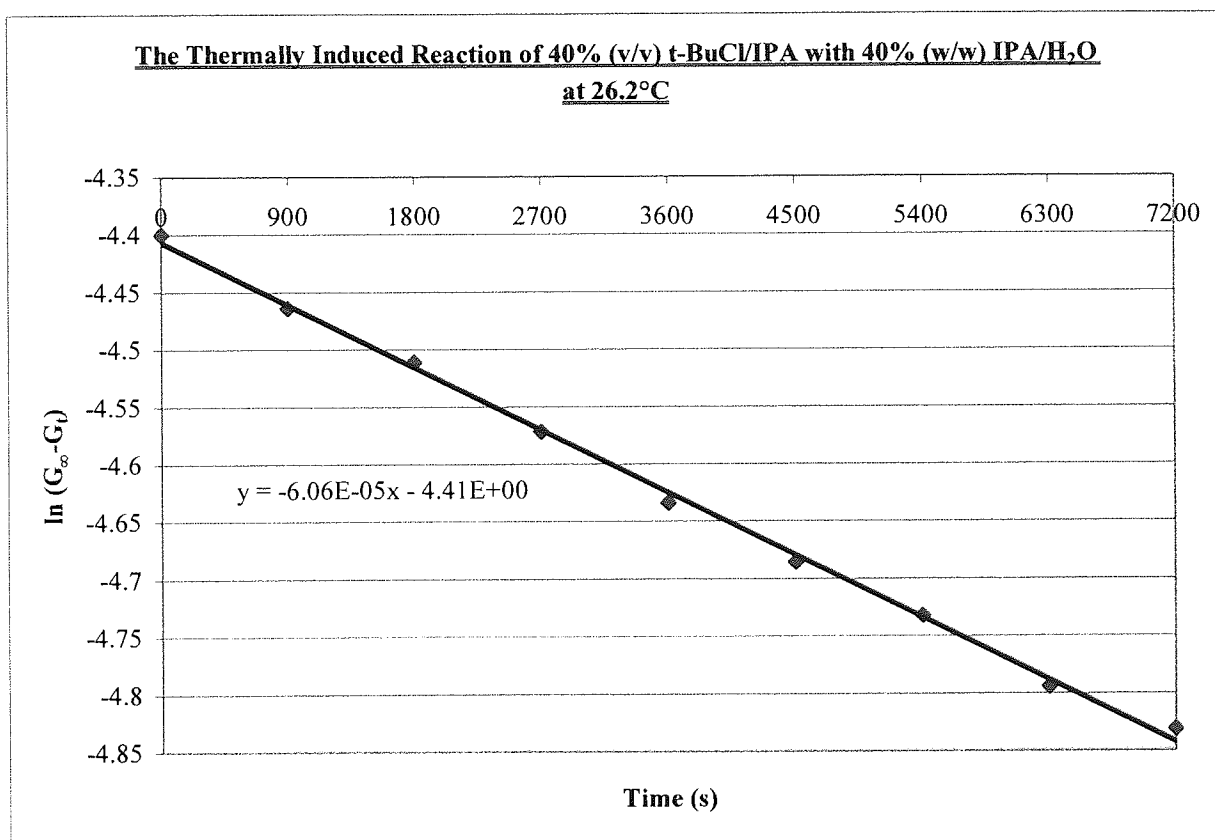
Stock solutions of 40% (v/v) t-BuCl in propan-2-ol and 40% (w/w) aqueous propan-2-ol, were freshly prepared. Aqueous propan-2-ol ( $4 \text{ cm}^3$ ) was placed in a test tube held in a water bath and allowed to reach thermal equilibrium. A  $2 \text{ cm}^3$  aliquot of t-BuCl solution was then added. The transducer<sup>121</sup> was placed at a depth of 2 cm in the reaction solution with a thermocouple held at a distance of 2.5 cm below the bottom of the transducer. The temperature of the sample solution was measured directly at equal intervals through by the thermocouple. Figure 98 shows the equipment employed for all bench top reactions.

**Figure 98:** The Bench Reaction Equipment Set-up.



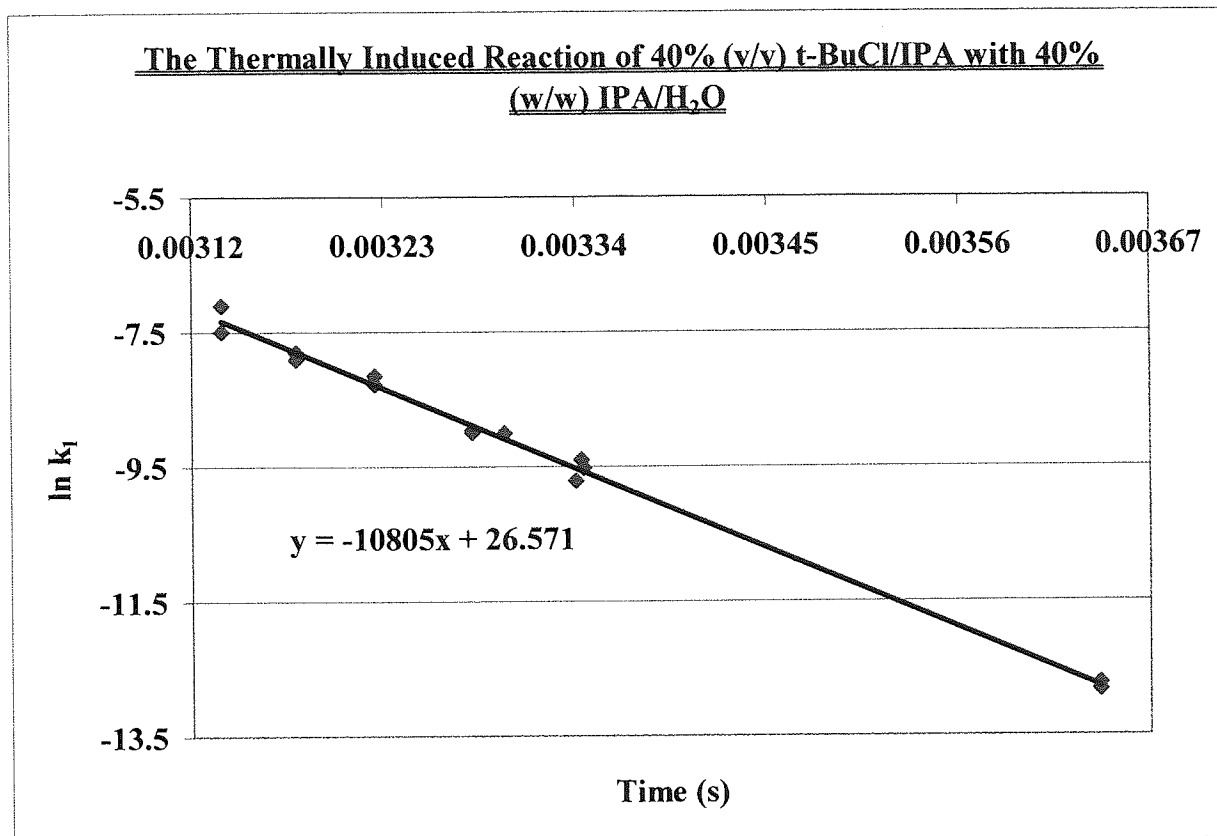
An initial conductivity measurement was made on a solution made by adding a 100 $\mu$ l aliquot of the reaction mixture to 10 cm<sup>3</sup> of propan-2-ol. The conductivity was measured at room temperature for the initial and all subsequent samples. Samples were extracted at equal intervals during the two-hour reaction. The reaction solution was maintained at room temperature for 24 hours in order to provide an 'infinity' value for the conductivity. The results were plotted according to Equation 49 and a typical example of such a plot is displayed in Figure 99, where  $G_{\infty}$  = conductivity at infinity and  $G_t$  = conductivity at time t. Additional plots are available in Appendix 7.

**Figure 99:** The Thermal Solvolysis Bench Reaction of t-BuCl at 299 K.



The negative of the gradient of each thermal graph yields the rate constant  $k_1$  directly. Constructing an Arrhenius plot of  $\ln k_1$  versus  $1/T$  (K<sup>-1</sup>), as shown in Figure 100, enabled the determination of a number of thermodynamic parameters entropy  $\Delta S^\ddagger$  (Equation 43), enthalpy  $\Delta H^\ddagger$  (Equation 41), free energy  $\Delta G^\ddagger$  (Equation 33) and activation energy  $E_a$  (Equation 44).

**Figure 100:** Plot of  $\ln k_1$  versus  $1/T$  ( $K^{-1}$ ) for the Thermally Induced Solvolysis Bench Reactions of t-BuCl.



The various thermodynamic parameters are given in Table 37 and Table 38.

**Table 37:** The Thermodynamic Parameters for the Solvolysis Reaction of t-BuCl over the Temperature Range 275 K to 319 K.

Reaction Conditions	Gradient (K)	Intercept	$\Delta S^\ddagger$ at 275 K ( $JK^{-1}mol^{-1}$ )	$\Delta S^\ddagger$ at 319 K ( $JK^{-1}mol^{-1}$ )
Thermally Induced	$-10805 \pm 155.37$	$26.571 \pm 0.51$	$-23.32 \pm 0.34$	$-24.56 \pm 0.35$

**Table 38:** The Thermodynamic Parameters for the Solvolysis Reaction of t-BuCl over the Temperature Range 275 K to 319 K.

Reaction Conditions	$\Delta H^\ddagger$ at 275 K ( $kJmol^{-1}$ )	$\Delta H^\ddagger$ at 319 K ( $kJmol^{-1}$ )	$\Delta G^\ddagger$ at 275 K ( $kJmol^{-1}$ )	$\Delta G^\ddagger$ at 319 K ( $kJmol^{-1}$ )	$E_a$ ( $kJmol^{-1}$ )
Thermally Induced	$87.6 \pm 1.26$	$87.2 \pm 1.25$	$94.0 \pm 1.35$	$95.0 \pm 1.37$	$89.8 \pm 1.29$

According to Equation 39  $\Delta H^\ddagger$  is assumed to be temperature independent but this is not true in this case, as illustrated by the values obtained for the thermal reaction: Thus, for an

increase of 44 K,  $\Delta H^*$  decreases by only  $400 \text{ Jmol}^{-1} \pm 5.8 \text{ Jmol}^{-1}$ . However, due to the relatively narrow temperature range employed for the study, the derived thermodynamic parameters are not very sensitive to changes in reaction temperature.

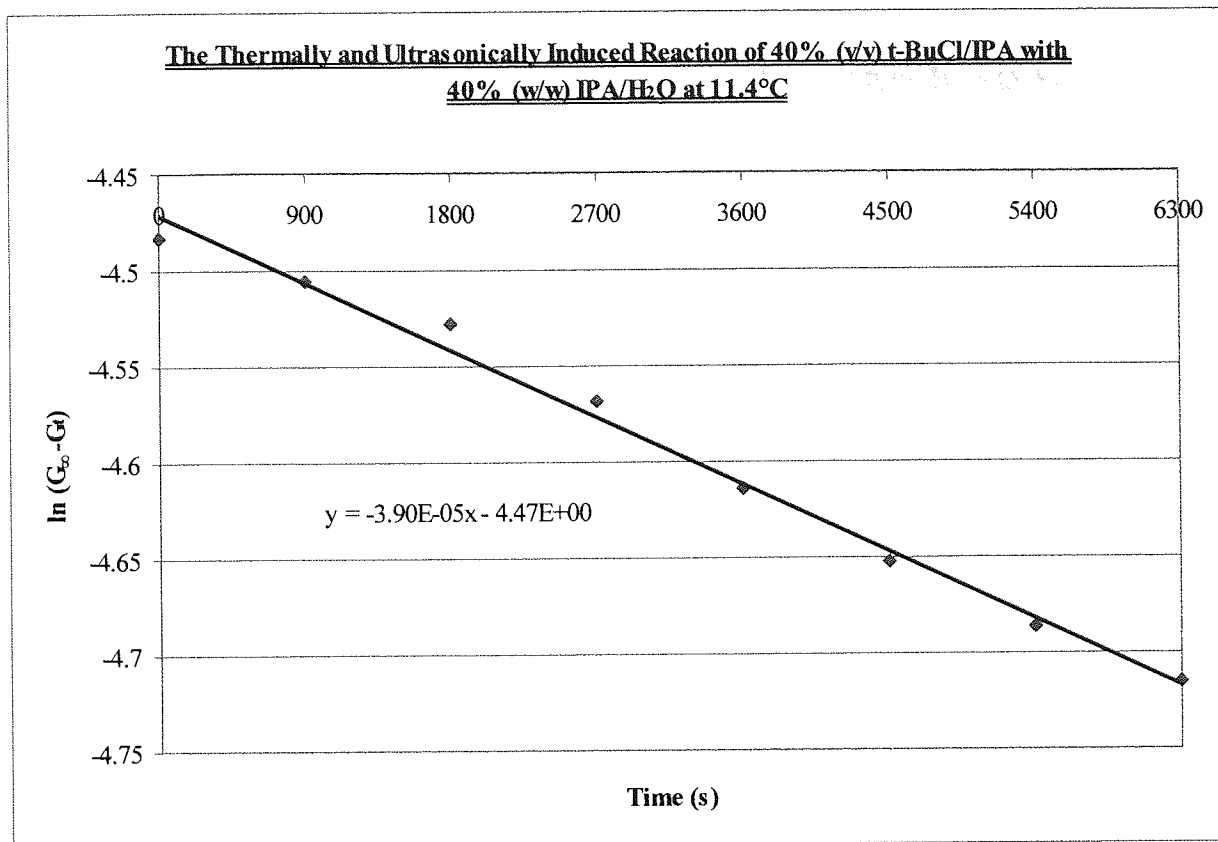
### **9.3.2 The Ultrasonically Induced Bench Top Reaction of 40% (v/v) t-BuCl/Propan-2-ol with 40% (w/w) Propan-2-ol/Water**

In reality, ultrasonically promoted reactions are a combination of ultrasonic and thermal contributions. The bulk of the contribution is usually attributed to thermal effects; however, cavitation effects generate a further perceptible increase.

The ultrasonic experiments were carried out using the same method and calculations as those employed for the thermal investigations. Each reaction sample was irradiated using a 3MHz transducer operating at a power of 7W.

Plotting data in the form  $\ln (G_{\infty}-G_t)$  against Time (s) yields a graph for each reaction from which the rate constant  $k_1$  may be determined (see Figure 101). Additional graphs for the other experimental conditions investigated are provided in Appendix 8.

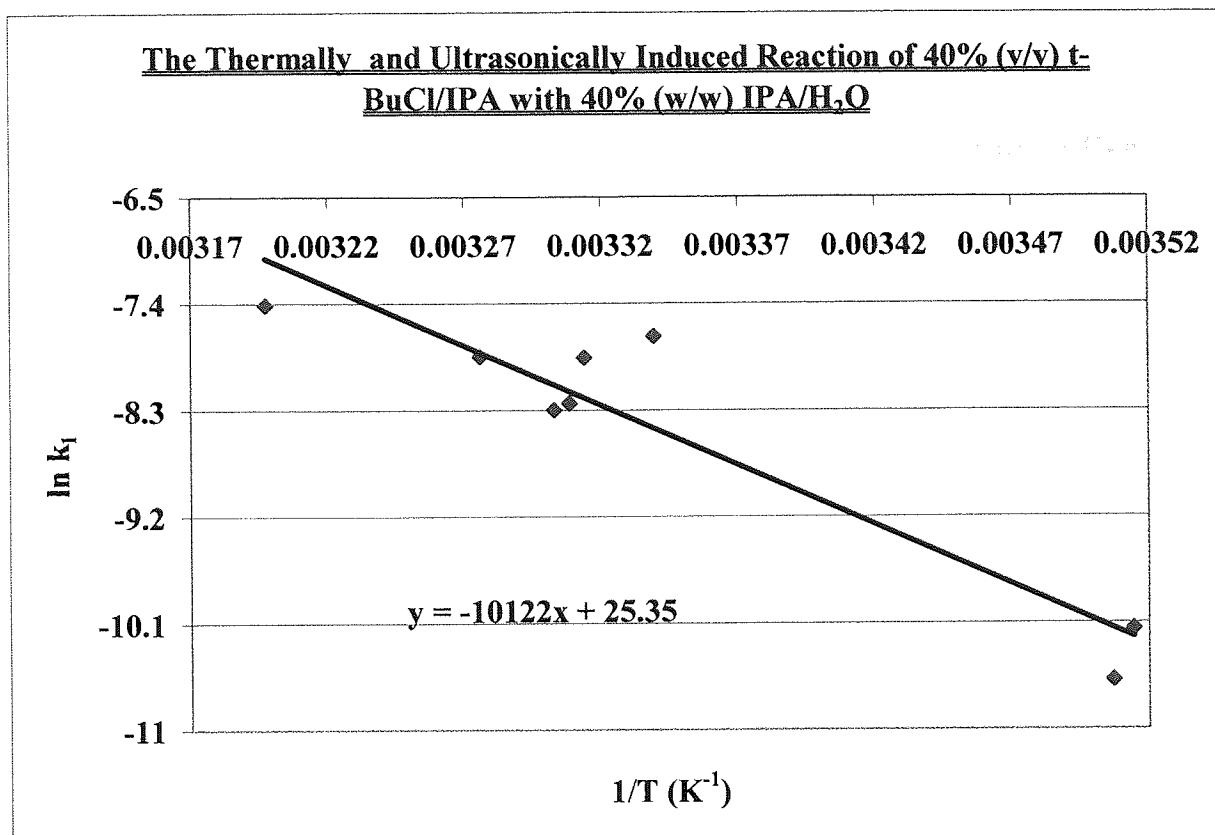
Figure 101: The Ultrasonic Bench Reaction of t-BuCl at 285 K.



A plot (Figure 102) of  $\ln k_1$  against  $1/T$  ( $K^{-1}$ ) was obtained and the thermodynamic parameters for the ultrasonic solvolysis reaction were calculated for the range of temperatures investigated.



**Figure 102:** Plot of  $\ln k_1$  versus  $1/T$  ( $K^{-1}$ ) for the Ultrasonic Solvolysis Bench Reactions of t-BuCl.



The derived thermodynamic parameters are given in Table 39 and Table 40 along with their associated errors.

**Table 39:** The Thermodynamic Parameters for the Solvolysis Reaction of t-BuCl at the bench over the Temperature Range 275 K to 319 K.

Reaction Conditions	Gradient (K)	Intercept	$\Delta S^\ddagger$ at 275 K ( $JK^{-1}mol^{-1}$ )	$\Delta S^\ddagger$ at 319 K ( $JK^{-1}mol^{-1}$ )
Thermally and Ultrasonically Induced	$-10122 \pm 1066.51$	$25.35 \pm 3.57$	$-33.47 \pm 3.53$	$-34.71 \pm 3.66$

**Table 40:** The Thermodynamic Parameters for the Solvolysis Reaction of t-BuCl at the bench for the Temperature Range 275 K to 319 K.

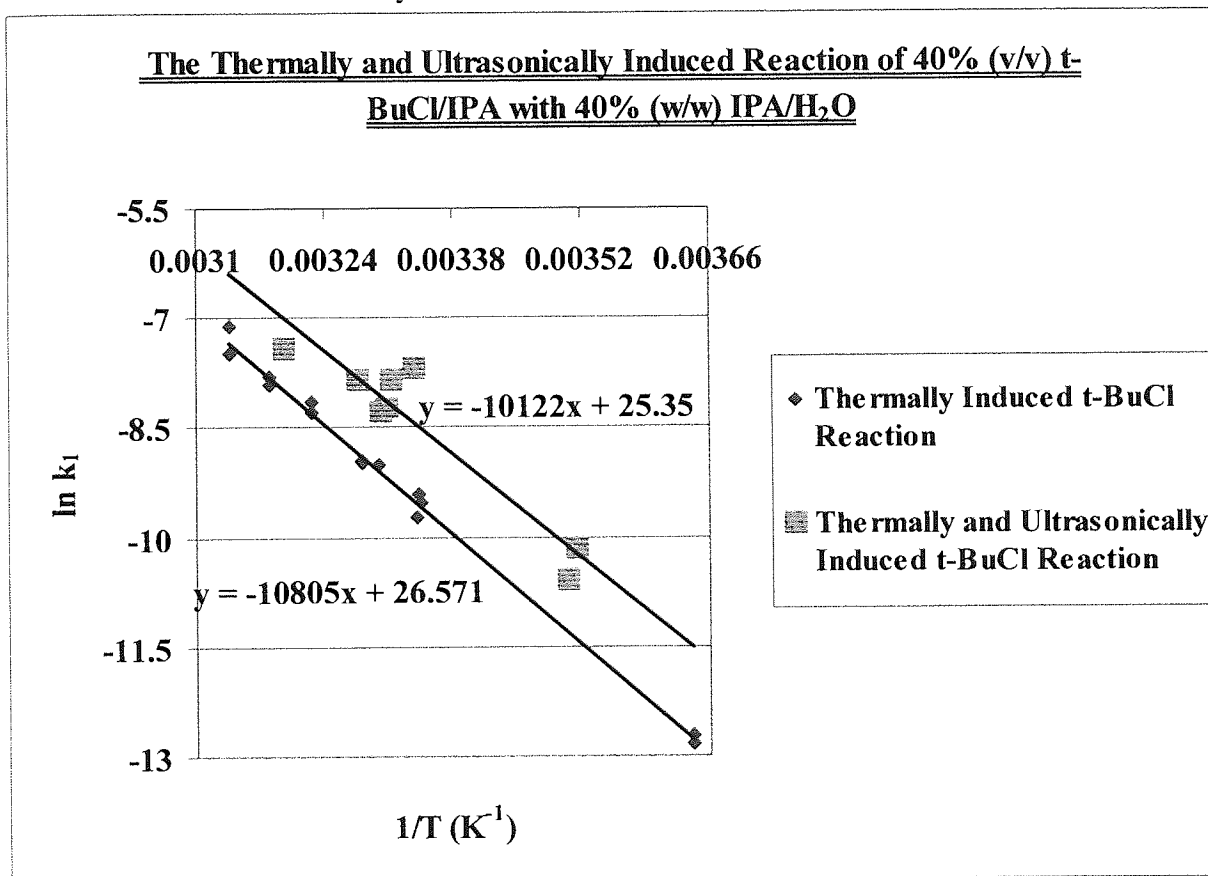
Reaction Conditions	$\Delta H^\ddagger$ at 275 K ( $kJmol^{-1}$ )	$\Delta H^\ddagger$ at 319 K ( $kJmol^{-1}$ )	$\Delta G^\ddagger$ at 275 K ( $kJmol^{-1}$ )	$\Delta G^\ddagger$ at 319 K ( $kJmol^{-1}$ )	$E_a$ ( $kJmol^{-1}$ )
Thermally and Ultrasonically Induced	$81.9 \pm 8.63$	$81.5 \pm 8.59$	$91.1 \pm 9.6$	$92.6 \pm 9.75$	$84.2 \pm 8.87$

The values of the thermodynamic parameters calculated alter little over the narrow range of temperatures investigated.

### 9.3.3 Comparison of the Thermally- and Ultrasonically-Induced Bench Top Reactions

A comparison (see Figure 103) of reaction data for the thermally induced solvolysis reaction and the ultrasonically induced systems, shows a visible increase in the reaction rate due to the application of ultrasonic irradiation.

**Figure 103:** Plot of  $\ln k_1$  versus  $1/T$  ( $K^{-1}$ ) for the Comparison of the Ultrasonic and Thermal Solvolysis Bench Reactions of t-BuCl.



The rate constants were extrapolated from the line of best fit for each system. Table 41 displays the maximum and minimum increase in the rate constants for each temperature, within the limits of the errors calculated for each individual value.

**Table 41:** Relative Increase in the Rate Constant as a Consequence of Ultrasonic Irradiation Using a 3 MHz Transducer Operating at 7W.

Temperature (K)	$k_1^{\text{therm}}$ ( $\times 10^{-6}$ )	$k_1^{\text{US}}$ ( $\times 10^{-6}$ )	$k_1^{\text{US}} / k_1^{\text{therm}}$ (lower)	$k_1^{\text{US}} / k_1^{\text{therm}}$ (mean)	$k_1^{\text{US}} / k_1^{\text{therm}}$ (upper)
298	63.2±0.909	184±19.4	2.57	2.91	3.27
303	115±1.65	322±33.9	2.48	2.81	3.15
308	205±2.95	555±58.5	2.39	2.71	3.03
313	360±5.18	940±99.1	2.30	2.61	2.93
318	618±8.89	15600±164	2.23	2.52	2.83

Although it has been established that an increase in the rate constant has taken place it is important to explain whether this is due to a change in activation energy or to a change in the pre-exponential factor in the expression for the rate constant. The thermodynamic parameters for the two systems (thermal and thermal + ultrasonic) and all subsequent solvolysis reactions are compared at a temperature of 308 K. The values of  $\Delta S^\ddagger$ ,  $\Delta H^\ddagger$ ,  $\Delta G^\ddagger$  and  $E_a$  are those calculated from the line of best fit for each system analysed.

**Table 42:** The Thermodynamic Parameters for the Bench Solvolysis of t-BuCl at 308K.

Reaction Conditions	$\Delta S^\ddagger$ ( $\text{JK}^{-1}\text{mol}^{-1}$ )	$\Delta H^\ddagger$ ( $\text{kJmol}^{-1}$ )	$\Delta G^\ddagger$ ( $\text{kJmol}^{-1}$ )	$E_a$ ( $\text{kJmol}^{-1}$ )
Thermally Induced	-24.27±0.35	87.3±1.25	94.8±1.36	89.8±1.29
Thermally and Ultrasonically Induced	-34.43±3.63	81.6±8.6	92.2±9.72	84.2±8.87

The only thermodynamic parameter that appears to have experienced a significant change is the entropy change for the reaction. The reaction undergoes a reduction in the entropy change of activation of about  $10 \text{ JK}^{-1}\text{mol}^{-1}$  when sonicated compared to the thermally induced system. All the other parameters calculated remain reasonably constant, within experimental error, when compared to each other under the two different experimental conditions.

## 9.4 The Reaction of 40% (v/v) t-BuCl/Propan-2-ol with 40% (w/w) Propan-2-ol/Deuterated Water in the NMR Spectrometer

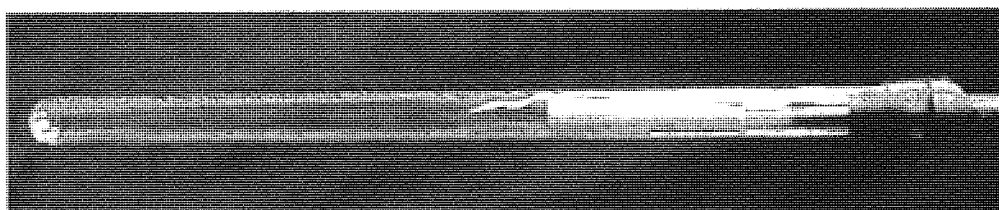
The aim of this experiment was to carry out the first in-situ, ultrasonically enhanced reaction in the NMR spectrometer.

### 9.4.1 Analysis of the Combined Propan-2-ol/2-Methylpropan-2-ol in the NMR Spectrometer

Stock solutions of 40% (v/v) t-BuCl in propan-2-ol and 40% (w/w) propan-2-ol in heavy water D<sub>2</sub>O, were freshly prepared. The deuterated water was employed in order to obtain a signal on the NMR spectrometer for field locating.

Aqueous propan-2-ol (4 cm<sup>3</sup>) was placed in a 10mm OD NMR tube to which was added 250 µl of 1,4-dioxane. The reaction solution was 'spiked' with a known quantity of 1,4-dioxane in all of the NMR experiments in order to enable accurate comparisons to be made of the various resonances because its concentration did not alter. Finally, a 2 cm<sup>3</sup> quantity of the t-BuCl solution was added. For both the thermal and ultrasonically induced reactions the transducer was placed in the NMR tube at a depth of 9.5 cm and the thermocouple 2.5 cm below the transducer, as shown in Figure 104.

**Figure 104:** The NMR Reaction Equipment Set-up.



The temperature of the sample solution was measured at equal intervals throughout the duration of the reaction using the thermocouple inserted directly into the solution. The solution was cooled with liquid nitrogen to maintain a constant temperature.

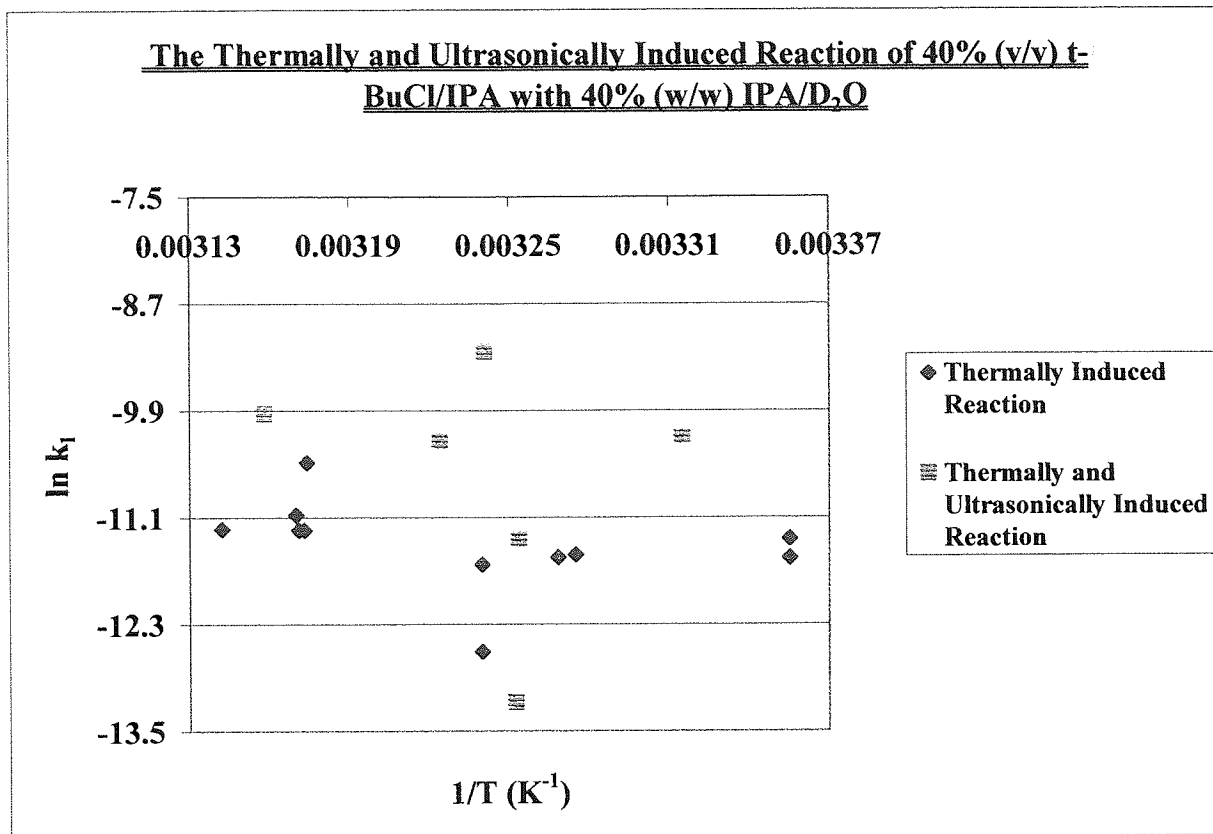
An NMR sequence programme (Appendix 9) was written to enable the first ever in-situ detection of the ultrasonically enhanced solvolysis of the t-BuCl. The programme allowed automatic acquisition of <sup>1</sup>H NMR spectra of the reaction system at ten-minute intervals, for

the duration of the reaction. A Gaussian<sup>124</sup> transformation was performed on the FID of each spectrum prior to Fourier transformation, in order to obtain deconvolution of the absorption peaks to assist in their resolution.

Formation of the final product 2-methylpropan-2-ol can be observed under normal circumstances i.e. in a spinning NMR tube. However, in this instance the spinning of the sample was prevented due to the insertion of equipment in the top of the tube. The resolution required for observation of the alcohol absorption was not attainable because the alcohol resonance merges into that of the solvent propan-2-ol. The integrals, from both the thermal and sonicated reactions, of the combined peaks of propan-2-ol and 2-methylpropan-2-ol were established and the rate constant determined for each. It could be assumed that the concentration of the propan-2-ol remained constant as it was in large excess so any change in the integral of the peak would be due solely to the production of the product 2-methylpropan-2-ol. Thus, the increase in the integral of the peak would be a measure of the rate of production of the 2-methylpropan-2-ol. A comparison of the rate of production of the 2-methylpropan-2-ol under thermal and ultrasonic conditions was then made in order to assess whether ultrasonic irradiation enhanced the reaction .

A plot of the  $\ln k_1$  against  $1/T$  ( $K^{-1}$ ) was obtained (Figure 105) and from the graph it could clearly be seen that no obvious trend had occurred. Due to the very large integral for the absorption peak of the solvent propan-2-ol any small addition caused by the formation of the 2-methylpropan-2-ol would be insignificant with respect to the total solvent concentration and so difficult to observe.

**Figure 105:** Comparison of the Ultrasonic and Thermal Reactions by the Increase of the Combined Propan-2-ol/2-Methylpropan-2-ol Absorption Peak in the NMR Spectrometer.



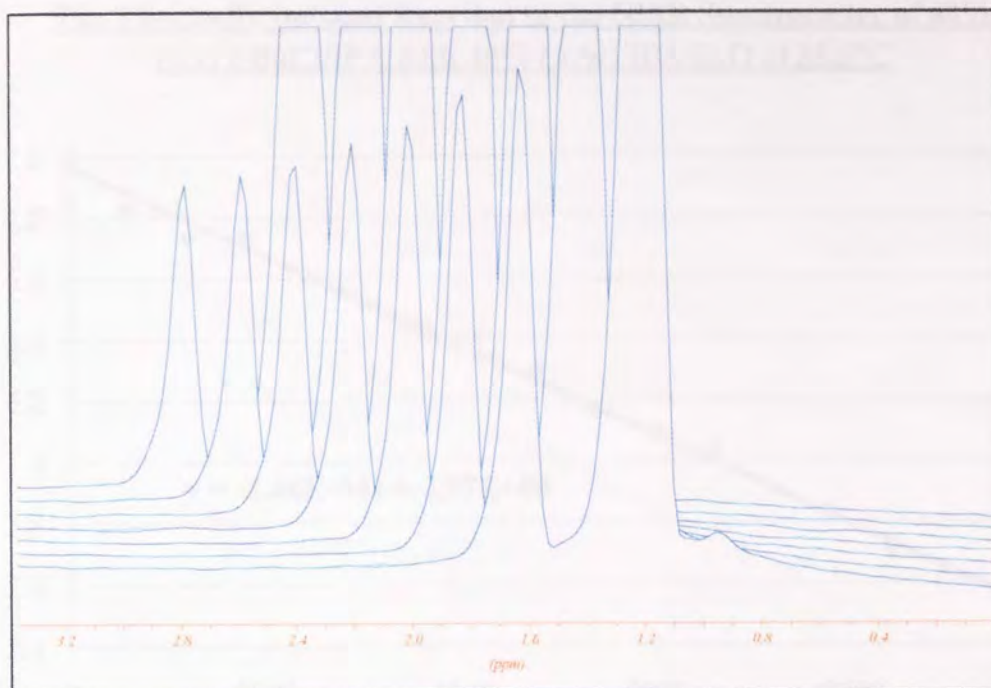
As a consequence of the uncertainties involved in monitoring the progress of the reaction by the formation of the product of the reaction, only the consumption of the t-BuCl reactant could be used for this purpose.

#### 9.4.2 Analysis of the Thermally Induced Reaction of t-BuCl in the NMR Spectrometer

The stock solutions and method as previously described in section 9.3.4 were employed. The integrated value of the t-BuCl absorption peak was normalised to that of the 1,4-dioxane spike and was used to evaluate its concentration at time t.

The rate of the reaction was monitored as the reduction in the integrated value (Int)<sub>t</sub> of the absorption peak at time t of the nine protons of the -CH<sub>3</sub> groups of the t-BuCl. Figure 106 shows the staggered plot of the t-BuCl resonance as it reacts and thus reduces over time.

**Figure 106:** Staggered Plot of Spectra for the Thermally Induced Solvolysis Reaction of t-BuCl at 298 K.



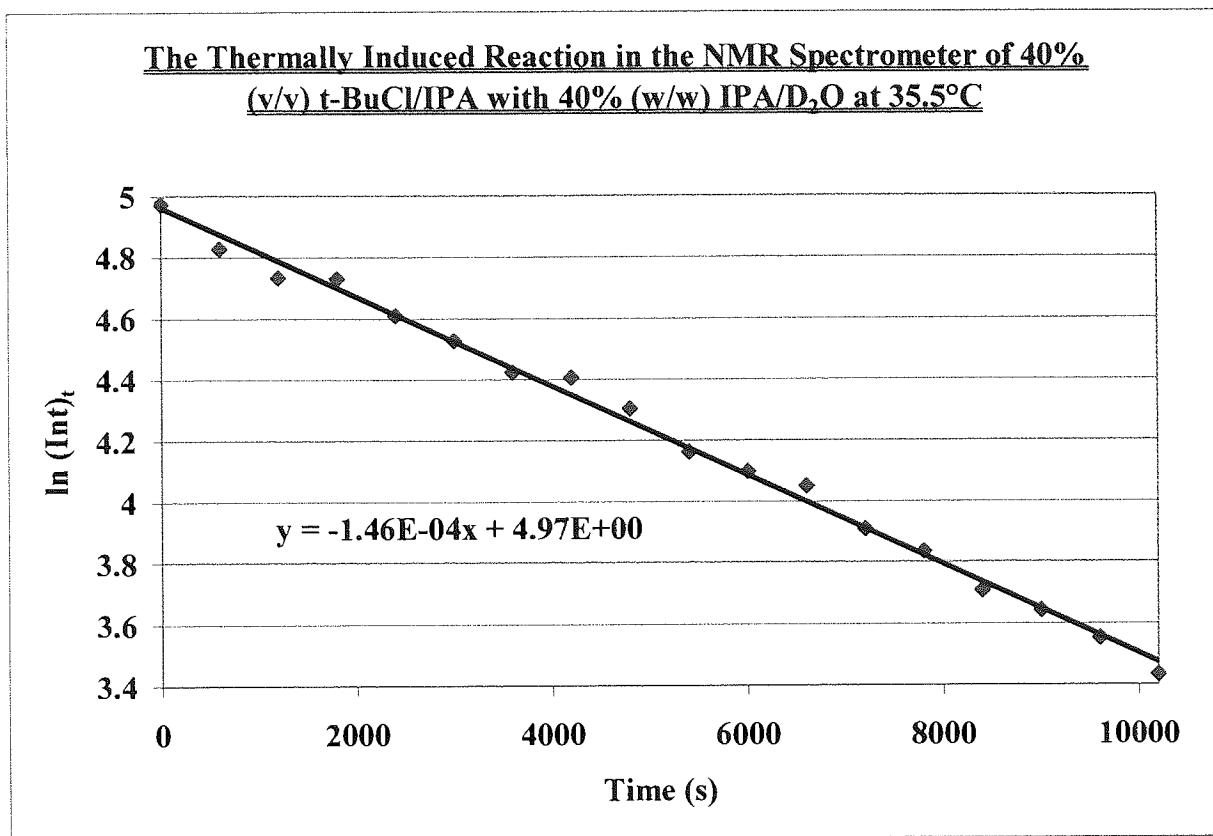
The results were plotted according to Equation 50 and an example of such a plot is displayed in Figure 107. Additional plots for further experiments are available in Appendix 10.

**Equation 50:** The First Order Rate Equation of Absorption Peak Integral versus Time.

$$\ln(\text{Int})_t = \ln(\text{Int})_0 - k_1 t$$

The reactions were carried out over the temperature range 298 K to 319 K. It was assumed that at infinity  $(\text{Int})_\infty = 0$  since all of the t-BuCl had reacted.

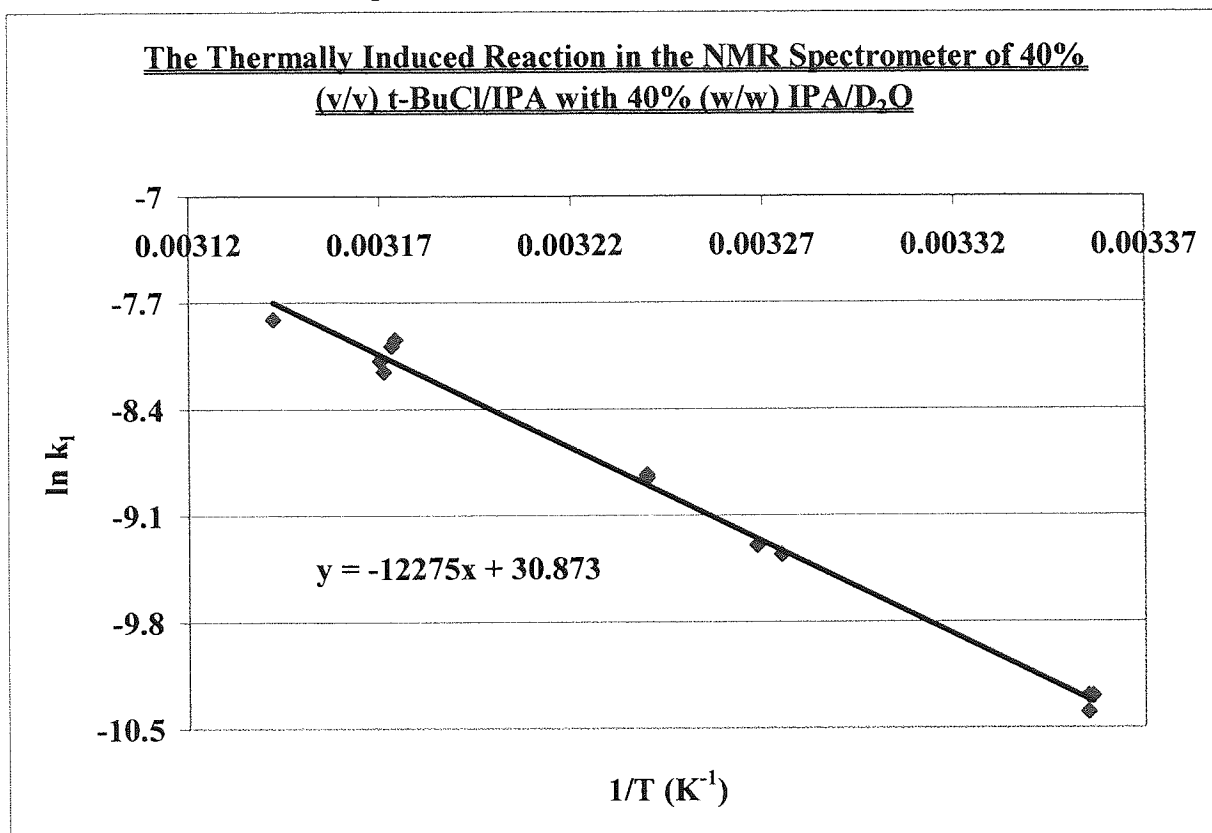
Figure 107: The Thermal Solvolysis Reaction of t-BuCl in the NMR Spectrometer.



A plot of  $\ln k_1$  versus  $1/T$  ( $K^{-1}$ ), shown in Figure 108, enabled the determination of the various thermodynamic parameters under investigation,  $\Delta S^\ddagger$ ,  $\Delta H^\ddagger$ ,  $\Delta G^\ddagger$  and  $E_a$ .



**Figure 108:** Plot of  $\ln k_1$  versus  $1/T$  ( $K^{-1}$ ) for the Thermal Solvolysis Reactions of t-BuCl in the NMR Spectrometer.



The thermodynamic parameters for the thermal solvolysis reaction in the NMR spectrometer were calculated using the equations as applied to the bench top experiments over the range of temperatures investigated. The thermodynamic parameters are given in Table 43 and Table 44.

**Table 43:** The Thermodynamic Parameters for the Thermally Induced Solvolysis Reaction of t-BuCl in the NMR Spectrometer over the Temperature Range 298 K to 319 K.

Reaction Conditions	Gradient (K)	Intercept	$\Delta S^\ddagger$ at 298 K ( $JK^{-1}mol^{-1}$ )	$\Delta S^\ddagger$ at 319 K ( $JK^{-1}mol^{-1}$ )
Thermally Induced	$-12275 \pm 224.49$	$30.873 \pm 0.73$	$11.77 \pm 0.22$	$11.21 \pm 0.20$

**Table 44:** The Thermodynamic Parameters for the Thermally Induced Solvolysis Reaction of t-BuCl in the NMR Spectrometer over the Temperature Range 298 K to 319 K.

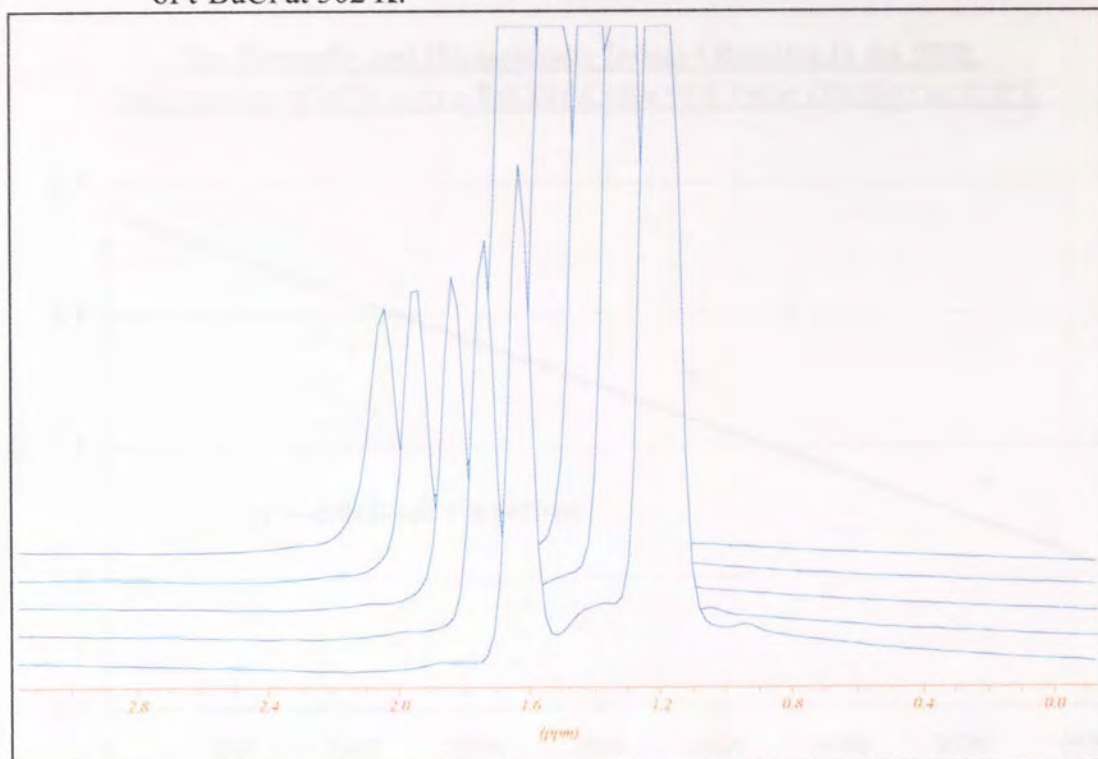
Reaction Conditions	$\Delta H^\ddagger$ at 298 K (kJmol <sup>-1</sup> )	$\Delta H^\ddagger$ at 319 K (kJmol <sup>-1</sup> )	$\Delta G^\ddagger$ at 298 K (kJmol <sup>-1</sup> )	$\Delta G^\ddagger$ at 319 K (kJmol <sup>-1</sup> )	$E_a$ (kJmol <sup>-1</sup> )
Thermally Induced	99.6±1.82	99.4±1.82	96.1±1.76	95.8±1.75	102.0±1.87

As a consequence of the relatively narrow temperature range employed for the study, the thermodynamic parameters derived for the reaction in the NMR spectrometer are relatively insensitive to changes in reaction temperature.

### 9.4.3 Analysis of the Ultrasonically Induced Reaction of t-BuCl in the NMR Spectrometer

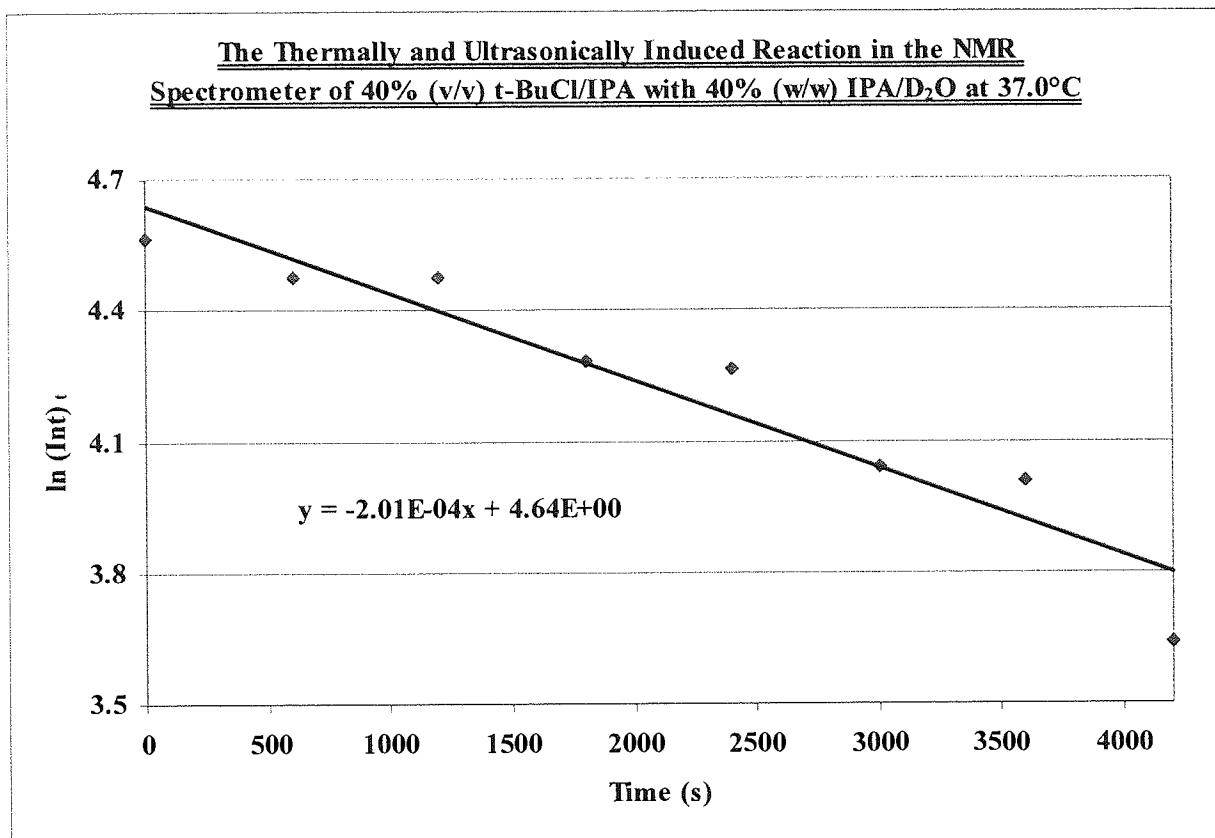
The ultrasonic experiments were carried out using the same method and calculations as previously employed for the thermal investigations in the NMR spectrometer. Each reaction sample was irradiated using a 3MHz transducer operating at a power of 7W and the temperature of the reaction medium was monitored throughout the duration of the reaction using a thermocouple. An example of a staggered plot of spectra for the ultrasonically induced solvolysis reaction is shown in Figure 109.

**Figure 109:** Staggered Plot of Spectra for the Ultrasonically Induced Solvolysis Reaction of t-BuCl at 302 K.



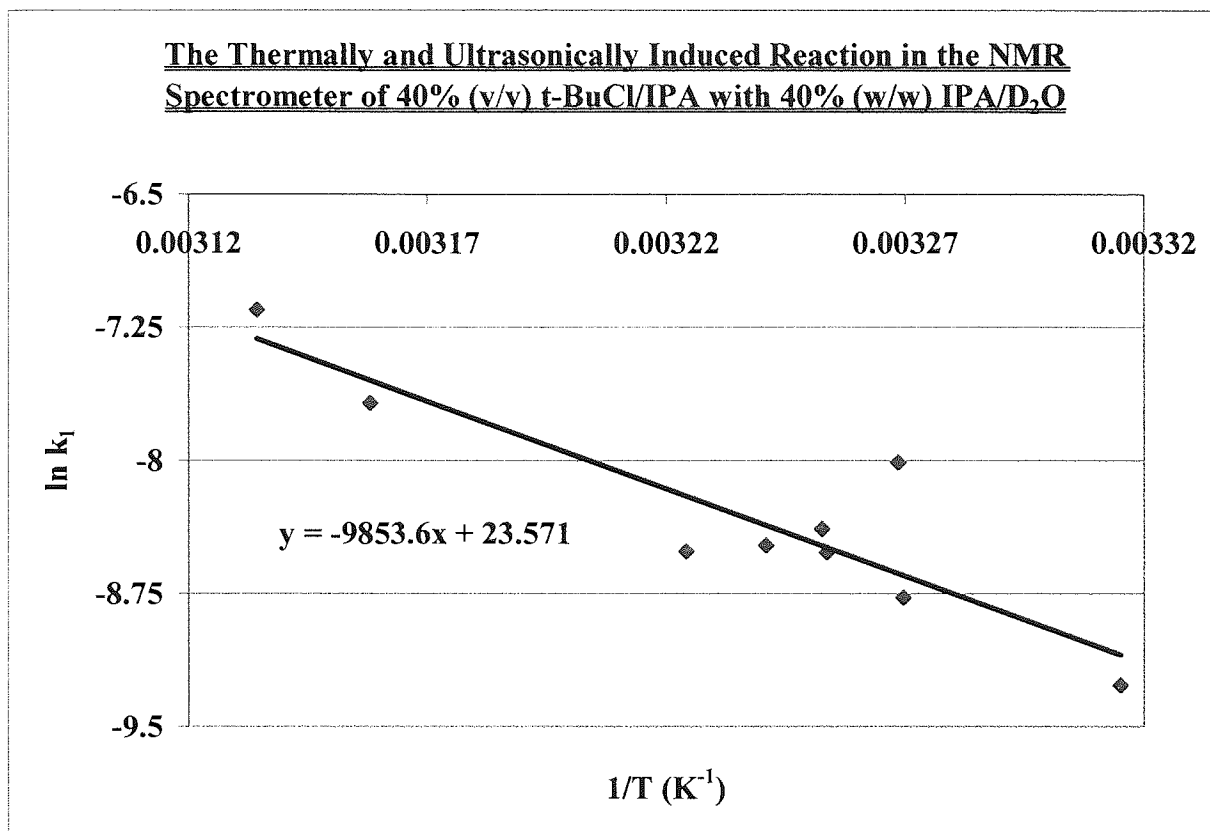
Plotting data in the form  $\ln(\text{Int})_t$  against time (s) yields a graph for each reaction for which the gradient equals  $-k_1$  (see Figure 110). Additional graphs plotted for other experimental conditions are presented in Appendix 11.

**Figure 110:** The Ultrasonic Solvolysis Reaction of t-BuCl in the NMR Spectrometer at 310 K.



A plot of the  $\ln k_1$  against  $1/T$  ( $K^{-1}$ ) was obtained (Figure 111) and the thermodynamic parameters for the ultrasonic solvolysis reaction in the NMR spectrometer were calculated.

**Figure 111:** Plot of  $\ln k_1$  versus  $1/T$  ( $K^{-1}$ ) for the Comparison of the Ultrasonic and Thermal Solvolysis Reactions of t-BuCl in the NMR Spectrometer.



The thermodynamic parameters are given in Table 45 and Table 46.

**Table 45:** The Thermodynamic Parameters for the Ultrasonically Induced Solvolysis Reaction of t-BuCl in the NMR Spectrometer for the Temperature Range 298 K to 319 K.

Reaction Conditions	Gradient (K)	Intercept	$\Delta S^\ddagger$ at 298 K ( $JK^{-1}mol^{-1}$ )	$\Delta S^\ddagger$ at 319 K ( $JK^{-1}mol^{-1}$ )
Thermally and Ultrasonically Induced	$-9853.6 \pm 1296.62$	$23.571 \pm 4.2$	$-48.94 \pm 6.44$	$-49.51 \pm 6.51$

**Table 46:** The Thermodynamic Parameters for the Ultrasonically Induced Solvolysis Reaction of t-BuCl in the NMR Spectrometer for the Temperature Range 298 K to 319 K.

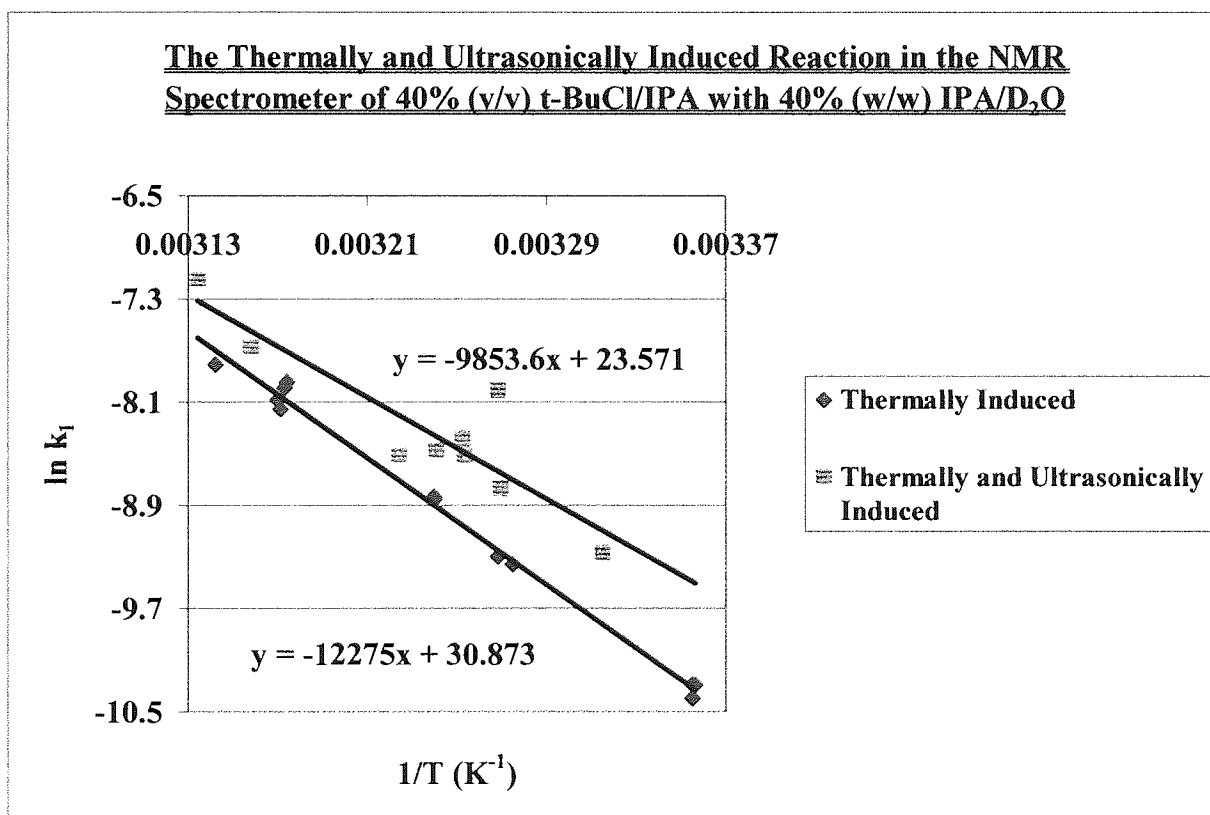
Reaction Conditions	$\Delta H^\ddagger$ at 298 K ( $kJmol^{-1}$ )	$\Delta H^\ddagger$ at 319 K ( $kJmol^{-1}$ )	$\Delta G^\ddagger$ at 298 K ( $kJmol^{-1}$ )	$\Delta G^\ddagger$ at 319 K ( $kJmol^{-1}$ )	$E_a$ ( $kJmol^{-1}$ )
Thermally and Ultrasonically Induced	$79.5 \pm 10.5$	$79.3 \pm 10.4$	$94.0 \pm 12.4$	$95.1 \pm 12.5$	$81.9 \pm 10.8$

The effect on the thermodynamic parameters as a consequence of a change in reaction temperature is again relatively small as a result of the narrow range of temperatures employed.

#### 9.4.4 Comparison of the Thermally and Ultrasonically Induced Reaction of 2-Chloro-2-methylpropane in the NMR Spectrometer

A comparison of the reaction data (Figure 108 and Figure 111) for the thermally induced solvolysis reaction and the ultrasonically induced systems respectively, indicates a significant increase in the reaction rate for those samples subjected to ultrasonic irradiation (Figure 112).

**Figure 112:** Plot of  $\ln k_1$  versus  $1/T$  ( $K^{-1}$ ) for the Comparison of the Ultrasonic and Thermal Solvolysis Reactions of t-BuCl in the NMR Spectrometer.



The rate constants were extrapolated from the line of best fit for each system. Table 47 displays the maximum and minimum increase in rate constant for each temperature within the limits of the errors calculated for each individual value.

**Table 47:** Relative Increase in the Rate Constant as a Consequence of Ultrasonic Irradiation Using a 3 MHz Transducer Operating at 7 W.

Temperature (K)	$k_1^{\text{therm}}$ ( $\times 10^{-6}$ )	$k_1^{\text{US}}$ ( $\times 10^{-6}$ )	$k_1^{\text{US}} / k_1^{\text{therm}}$		
			Lower	Mean	Upper
298	33.7 $\pm$ 0.617	76.5 $\pm$ 1.40	2.19	2.27	2.35
303	66.2 $\pm$ 1.210	132.0 $\pm$ 2.41	1.91	1.99	2.06
308	129.0 $\pm$ 2.350	224.0 $\pm$ 4.10	1.68	1.74	1.81
313	243.0 $\pm$ 4.450	374.0 $\pm$ 6.84	1.48	1.54	1.59
318	450.0 $\pm$ 8.220	612.0 $\pm$ 11.50	1.31	1.36	1.41

The thermodynamic parameters for the two different experimental conditions, thermal and ultrasonic, of the NMR systems are compared at a temperature of 308 K. The comparison was made using values extrapolated from the line of best fit for each system analysed.

**Table 48:** The Thermodynamic Parameters for the Solvolysis of t-BuCl in the NMR Spectrometer at 308 K.

Reaction Conditions	$\Delta S^\ddagger$ ( $\text{JK}^{-1}\text{mol}^{-1}$ )	$\Delta H^\ddagger$ ( $\text{kJmol}^{-1}$ )	$\Delta G^\ddagger$ ( $\text{kJmol}^{-1}$ )	$E_a$ ( $\text{kJmol}^{-1}$ )
Thermally Induced	11.49 $\pm$ 0.21	99.5 $\pm$ 1.82	96.0 $\pm$ 1.75	102.0 $\pm$ 1.87
Thermally and Ultrasonically Induced	-49.22 $\pm$ 6.48	79.4 $\pm$ 10.4	94.5 $\pm$ 12.4	81.9 $\pm$ 10.8

The thermodynamic parameters all appear to undergo a change in their values except the Gibb's free energy of activation  $\Delta G^\ddagger$ , which remains constant with a value of about +94  $\text{kJmol}^{-1}$ . The thermally induced reaction yields an entropy change of activation of 11.49  $\text{JK}^{-1}\text{mol}^{-1}$  whereas the sonicated system requires a lower entropy change of activation, by about 61  $\text{JK}^{-1}\text{mol}^{-1}$ , of -49.22  $\text{JK}^{-1}\text{mol}^{-1}$ .

## 9.5 Discussion and Conclusions

**Table 49:** Rate Constant Increase of the Ultrasonic over the Thermal Solvolysis Reaction.

Temperature (K)	$\frac{k_1^{US}}{k_1^{therm}}$	
	Bench-top Reaction (mean)	NMR Reaction (mean)
298	2.27±0.08	2.91±0.34
303	1.99±0.07	2.81±0.34
308	1.74±0.07	2.71±0.32
313	1.54±0.05	2.61±0.31
318	1.36±0.05	2.52±0.31

As the temperature of both the bench and NMR reaction systems increased, a reduction in the overall ultrasonic enhancement of the reaction was noted, thus confirming the previous findings of Mason and co-workers<sup>115,116</sup>. It was theorised by Mason and co-workers that this decrease in rate was due to an increase in the vapour pressure for the reaction. As the amount of vapour filling the cavities formed increases, their implosion is less violent and so less energy is produced to enhance the reaction rate. The differences were probably a result of the change in the reaction vessel employed; bench-top experiments were carried out in a test tube because samples had to be removed for analysis using a syringe and the test tube was considerably wider than that of the 10mm NMR tube. The energy within the NMR tube is more focussed and less dissipated since it is narrower than the test tube, thus having a greater effect (i.e. more enhanced) upon the reaction.

Analysis of the formation of the 2-methylpropan-2-ol was shown to be impossible due to the limited resolution of the NMR spectrometer. The extremely large propan-2-ol absorption peak swamped the relatively small absorption peak resulting from the alcohol product. The reaction was monitored by observation of the rate of consumption of t-BuCl. The thermodynamic quantities established are with respect to the formation of the activated complex. There are several obvious trends observed in the thermodynamic parameters for the experiments carried out both in the NMR spectrometer and in the water bath on the bench. Table 50 lists the thermodynamic parameters and their associated errors. The values



have a similar magnitude to those established by Winstein and Fainberg<sup>98,99</sup> for the reaction of t-BuCl in various pure solvents (Table 13).

**Table 50:** Comparison of the Thermodynamic Parameters Established for the Bench and NMR Experiments of 2-Chloro-2-methylpropane in Aqueous Propan-2-ol.

Reaction Conditions	$\Delta S^\ddagger$ (JK <sup>-1</sup> mol <sup>-1</sup> )	$\Delta H^\ddagger$ (kJmol <sup>-1</sup> )	$\Delta G^\ddagger$ (kJmol <sup>-1</sup> )	$E_a$ (kJmol <sup>-1</sup> )
Bench top - Thermally Induced	-24.27±0.35	87.3±1.25	94.8±1.36	89.8±1.29
Bench top – Thermally and Ultrasonically Induced	-34.43±3.63	81.6±8.6	92.2±9.72	84.2±8.87
NMR - Thermally Induced	11.49±0.21	99.5±1.82	96.0±1.75	102.0±1.87
NMR - Thermally and Ultrasonically Induced	-49.22±6.48	79.4±10.4	94.5±12.4	81.9±10.8

The activation energy  $E_a$  represents the minimum amount of energy required by the reacting species to form the activated complex or transition state before proceeding to the final products. For the particular reactions described the activation energy remains in the region of 80-90 kJmol<sup>-1</sup> with the exception of the thermally induced reaction which is not significantly altered at only 10 kJmol<sup>-1</sup> higher in value. It is inferred that despite the change in the reaction conditions the mechanism remains the same. However, it is possible that the reaction may occur by way of another mechanism of identical activation energy, but this is believed to be unlikely.

The entropy  $S$  is a measure of the degree of disorder within any system. As the entropy value for any system becomes larger so too does the degree of disorder within it, for example  $S_{\text{gas}} > S_{\text{liquid}} > S_{\text{solid}}$ .

Since the activation energy remains fairly constant it is assumed that both reactions occur by way of the same mechanism and that both systems pass through an activated complex possessing the same entropy  $S^\ddagger$ . According to Equation 51 the change in entropy  $\Delta S^\ddagger$  is equal to the entropy of the activated complex  $S^\ddagger$  less the sum of the entropy of the reactants  $S_r^\ddagger$ .

**Equation 51:** The Entropy Change of Activation.

$$\Delta S^\ddagger = S^\ddagger - \sum S_r$$

It is assumed that  $S^\ddagger$  is identical for both reactions so the change must be due to a change in the entropy of the initial reactants  $S_r$ . The entropy change of activation  $\Delta S^\ddagger$  for the sonicated reaction is more negative than that of the thermal reaction thereby suggesting that the entropy of the initial reactants has increased. Since an increase in the entropy of a system is the result of it becoming more disordered i.e. less structured, it seems reasonable to deduce that the ultrasound is disrupting the structure of the reactants and so allowing them to react more quickly.

A more negative change in entropy  $\Delta S^\ddagger$  of about  $60 \text{ kJmol}^{-1}$  between the thermal and sonicated systems was observed in the NMR experiment compared to the bench top experiment where a decrease of about  $10 \text{ kJmol}^{-1}$  occurred. This difference was most likely due to the different reaction vessels employed. The ultrasonic energy within the NMR tube was believed to be more focussed and less dissipated than that in the test tube, and therefore produced a greater enhancement of the reaction rate.

Enthalpy H, is defined as  $H = U + PV$ , where U is the internal energy and P and V the pressure and volume respectively. For any process at a constant pressure the heat evolved or absorbed during the process is equal to the change in enthalpy  $\Delta H$  i.e.  $\Delta H = \Delta U + P\Delta V$ . The change of enthalpy value measured corresponds to the formation of the activated complex  $\Delta H^\ddagger$ .

**Equation 52:** The Enthalpy Change of Activation.

$$\Delta H^\ddagger = H^\ddagger - \sum H_r$$

The calculated values for the change in enthalpy  $\Delta H^\ddagger$  are all positive numbers as expected. Since a positive activation energy is noted, the reactions require energy in order to force the reactants to form an activated complex. Thus, according to Equation 52 the enthalpy of the activated complex  $H^\ddagger$  is greater than the sum of the enthalpies of the reactants  $H_r$ .

No change in  $\Delta H^\ddagger$  was observed for the thermal bench top experiments, perhaps the result of the reduced focussing of ultrasound when employing the larger reaction vessel. However, for the reactions conducted in the NMR spectrometer there was a decrease in the

change in enthalpy for ultrasonic reactions compared to thermal reactions. This difference ( $20 \text{ kJmol}^{-1}$ ) shows that the sonicated system is less endothermic than the thermal reaction i.e.  $\Delta H_{\text{US}}^{\ddagger} < \Delta H_{\text{therm}}^{\ddagger}$ . Three possible explanations may be offered to account for these observations.

- The system obtains the energy from elsewhere i.e. the additional stirring effect (ultrasonic streaming) caused by the movement of sound waves within the sample.
- The ultrasonic energy is more focussed within the narrower NMR tube i.e. higher energy density.
- The increased disorder of the system induced by sonication results in a lower enthalpy change of activation.

The final thermodynamic function to be considered is the Gibb's free energy of activation  $\Delta G^{\ddagger}$ . Under standard conditions  $\Delta G$  must be negative in order for the reaction to be feasible. However, the free energy change determined in these experiments is that for the development of the activated complex, not for the progress of the entire reaction. The values of  $\Delta G^{\ddagger}$  for the thermally or ultrasonically promoted reaction systems do not vary within experimental error and are essentially constant at around  $+94 \text{ kJmol}^{-1}$ . The value of  $\Delta G^{\ddagger}$  is positive because the formation of the activated complex requires an input of energy, however, for the overall reaction  $\Delta G$  should be negative, because it is feasible i.e. it forms products without much difficulty.

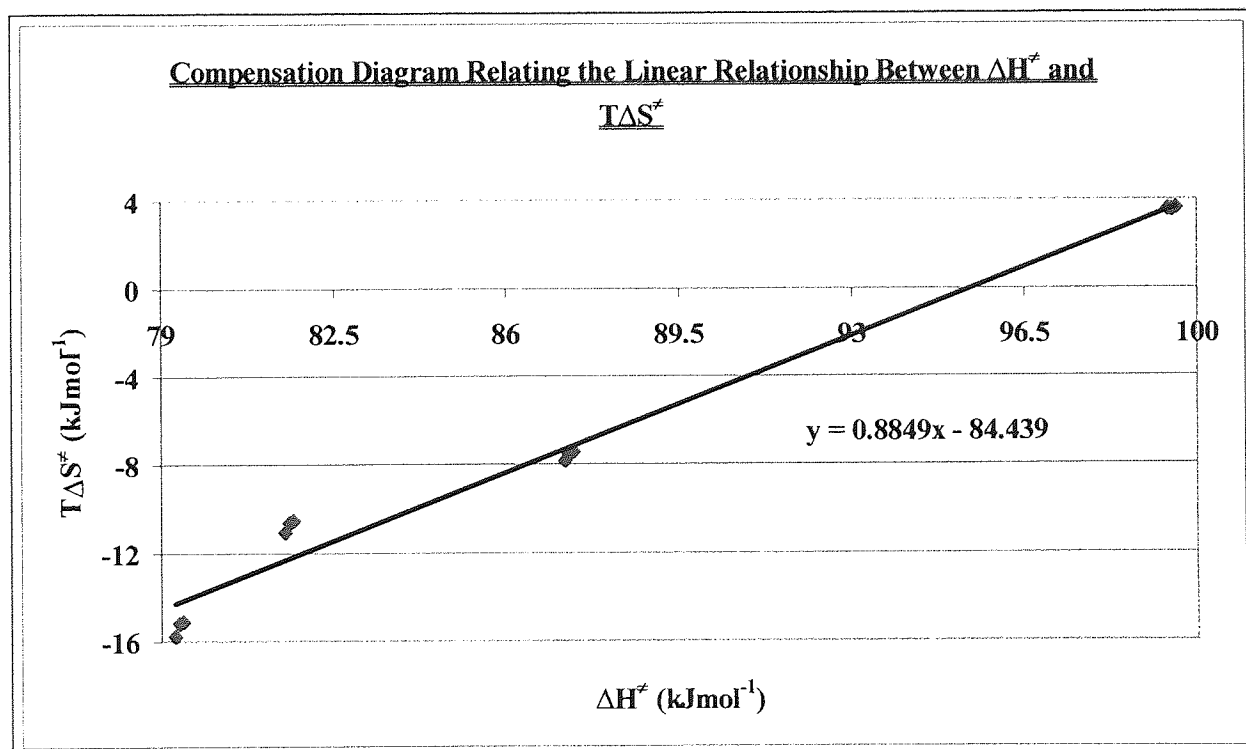
According to Equation 33 a linear relationship exists between the  $T\Delta S^{\ddagger}$  and  $\Delta H^{\ddagger}$  when a graph of  $T\Delta S^{\ddagger}$  vs.  $\Delta H^{\ddagger}$  is plotted. If the gradient of the plot is equal to unity no variation of  $\Delta G^{\ddagger}$  occurs.

Values of  $\Delta H^{\ddagger}$  and  $\Delta S^{\ddagger}$  obtained for the bench top and NMR experiments at 298 K, 308 K and 318 K (Table 51) are plotted in Figure 113.

**Table 51:** Linear Relationship between  $\Delta H^\ddagger$  and  $T\Delta S^\ddagger$ .

Temperature (°C)	Reaction Conditions	$\Delta H^\ddagger$ (kJmol <sup>-1</sup> )	$T\Delta S^\ddagger$ (kJmol <sup>-1</sup> )
298	Bench top – Thermally Induced	87.36±1.26	-7.40±0.10
298	Bench top – Thermally and Ultrasonically Induced	81.68±8.61	-10.52±1.07
298	NMR – Thermally Induced	99.58±1.82	3.63±0.06
298	NMR – Thermally and Ultrasonically Induced	79.45±10.50	-15.08±1.92
308	Bench top – Thermally Induced	87.28±1.25	-7.48±0.11
308	Bench top – Thermally and Ultrasonically Induced	81.60±8.60	-10.61±1.12
308	NMR – Thermally Induced	99.50±1.82	3.54±0.06
308	NMR – Thermally and Ultrasonically Induced	79.37±10.40	-15.17±2.00
318	Bench top – Thermally Induced	87.19±1.25	-7.81±0.11
318	Bench top – Thermally and Ultrasonically Induced	81.51±8.59	-11.04±1.16
318	NMR – Thermally Induced	99.42±1.82	3.57±0.07
318	NMR – Thermally and Ultrasonically Induced	79.28±10.40	-15.74±2.07

**Figure 113:** Compensation Diagram of the Linear Relationship between  $\Delta H^\ddagger$  and  $T\Delta S^\ddagger$  for the Solvolysis of t-BuCl.

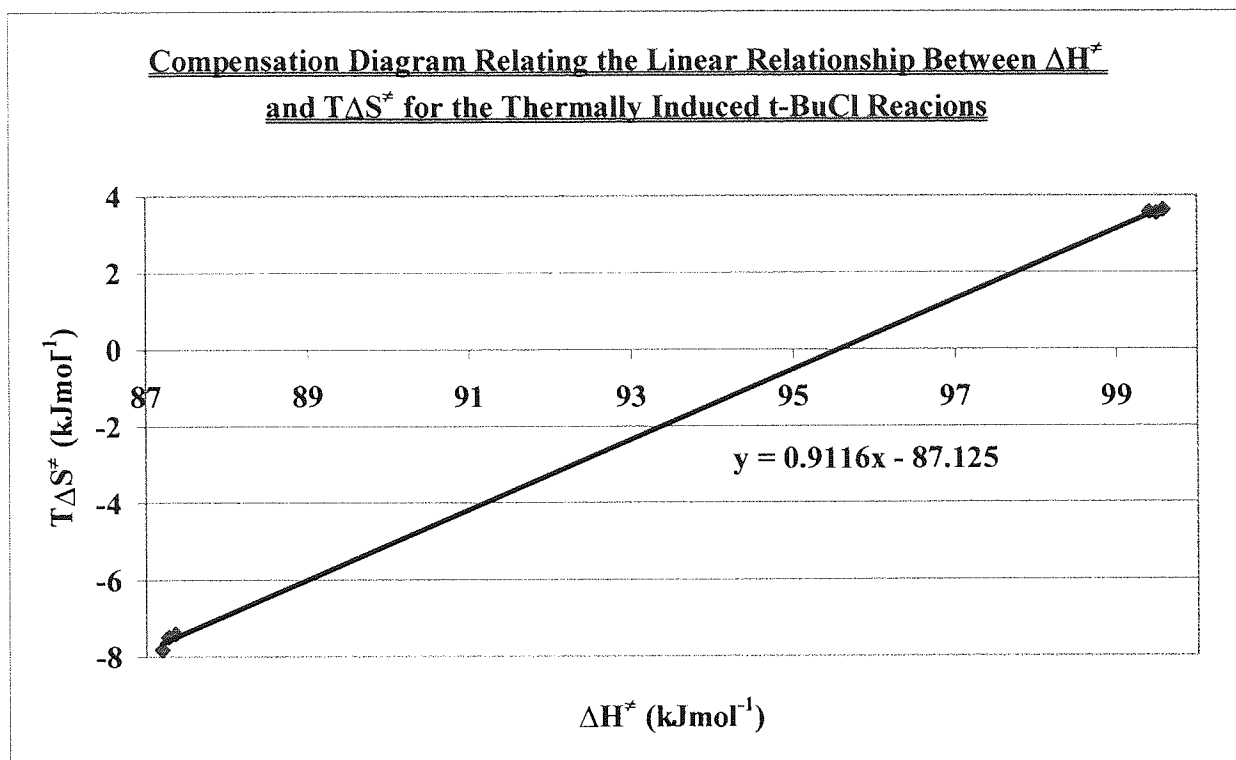


It has been found in many cases that the slope of the plot is often close to unity, particularly for a given reaction in a series of solvents and also for homologous reactions in which substituents are added to a reactant. Robertson and Sougamori<sup>100</sup> observed such a correlation for the solvolysis of t-BuCl in a series of alcohols where two linear plots of different slopes were noted. According to Figure 61 the minimum mole fraction of water in aqueous propan-2-ol, for which a three-dimensional quasi-aqueous structure may occur, is about 0.9. For the experiment conducted in this study aqueous propan-2-ol contained a mole fraction of water equal to 0.83, outside that required for a three-dimensional, quasi-aqueous structure. If the same experiments were to be conducted using higher mole fractions of water a second line of greater gradient should be observed. However, this would not be possible in practice because increasing the mole fraction of water with respect to the alcohol would prevent the complete dissolution of the amount of t-BuCl required for NMR spectroscopic observation.

If the slope in Figure 113 for the plot of  $T\Delta S^\ddagger$  versus  $\Delta H^\ddagger$  was exactly equal to unity, the change in the free energy change  $\Delta G^\ddagger$  should be equal to zero, thus for a slope which is close to unity the variation in  $\Delta G^\ddagger$  is very small. For the compensation diagram of the solvolysis reactions observed a slope of  $0.8849 \pm 0.0273$  was noted. The very small variation in  $\Delta G^\ddagger$  is due to a compensation effect occurring between  $\Delta H^\ddagger$  and  $T\Delta S^\ddagger$ . The explanation for the compensation effect is due to solute-solvent and solvent-solvent interactions. A reaction where the binding of the solute to the solvent weakens resulting in an increase in enthalpy H, thereby a decrease of  $\Delta H^\ddagger$ . It has been suggested<sup>117</sup> that ultrasound weakens these solute-solvent interactions. There is also an increase in the freedom of vibration and rotation of the solvent molecules, which increases the entropy S and decreases  $\Delta S^\ddagger$ , this is the result of the destruction of some of the strong solvent-solvent interactions by ultrasonic irradiation as observed by Mason and co-workers<sup>117</sup>.

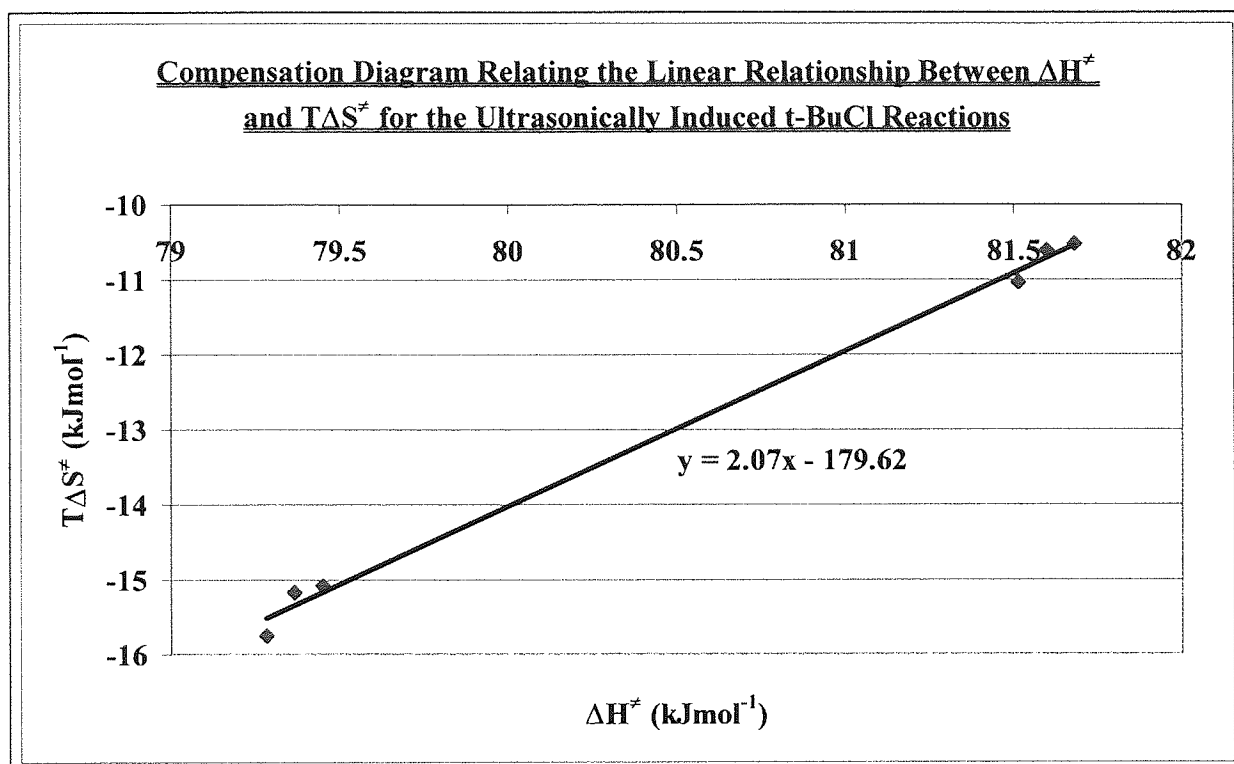
The data examined may also be divided into those reactions that were ultrasonically and those that were thermally induced. Figure 114 displays the data for the thermally induced solvolysis reactions carried out at the bench experiments and in the NMR spectrometer. Again the slope produced for the compensation diagram is close to unity, suggesting that there is very small variation of  $\Delta G^\ddagger$ .

**Figure 114:** Compensation Diagram of the Linear Relationship between  $\Delta H^\ddagger$  and  $T\Delta S^\ddagger$  for the Thermally Induced Solvolysis of t-BuCl.



However, the same is not true for those reactions carried out under the influence of ultrasound. Figure 115 displays a much larger slope, having a value of about 2. This suggests that a change is occurring in the Gibbs free energy change of activation  $\Delta G^\ddagger$  for the reaction.  $\Delta G^\ddagger$  changes due to the effect of ultrasound on the solute-solvent interactions. The binding of the solute to the solvent is weakened by the ultrasound passing through the sample causing an increase in enthalpy H, thereby a decrease of  $\Delta H^\ddagger$ . There is also an increase in the freedom of vibration and rotation of the solvent molecules, which increases the entropy S and decreases  $\Delta S^\ddagger$ . Although the data in Table 50 only depicts a slight change in  $\Delta G^\ddagger$  a large error is observed compared to that for the thermal reactions. The entropy change of activation  $\Delta S^\ddagger$  does experience a large variation in its value for which  $\Delta H^\ddagger$  cannot compensate hence the doubling of the gradient between the two different reaction conditions. The effect of the increase in the freedom of vibration and rotation of the solvent molecules, caused by the destruction by ultrasonic irradiation of some of the strong solvent-solvent interactions so increasing the entropy S and decreasing  $\Delta S^\ddagger$ , must be far greater than the effect of weakening the solute-solvent interaction.

**Figure 115:** Compensation Diagram of the Linear Relationship between  $\Delta H^\ddagger$  and  $T\Delta S^\ddagger$  for the Ultrasonically Induced Solvolysis of t-BuCl.



Like the Diels-Alder reaction carried out previously, the thermal effects should become dominant at a temperature where no further enhancement may be effected by the application of ultrasonic irradiation. The temperature at which this occurs for the bench experiments may be established by solving the simultaneous equations of the thermal and sonicated reactions.

$$\text{Bench Thermal } y_1 = -10805x_1 + 26.571$$

$$\text{Bench Sonicated } y_2 = -10122x_2 + 25.35$$

At the point where the two lines cross  $y_1=y_2$  thus,

$$-10122x_2 + 25.35 = -10805x_1 + 26.571$$

and  $x_2=x_1$  so the value of x at which the two trend lines cross can be calculated

$$\frac{26.571 - 25.35}{-10122 - (-10805)} = x = 1.788 \times 10^{-3} \text{ K}^{-1}$$

Theoretically the two trend lines for the bench reactions cross at a temperature of 559 K although this is not practically feasible since it is much greater than the boiling points of any of the components of the reaction. This result suggests that the reaction should experience an enhancement in rate due to ultrasonic irradiation no matter what the temperature of the reaction, however, this cannot occur and further investigations would need to be carried out to prove the theory.

The temperature at which the crossover point occurs for the reactions in the NMR spectrometer can also be established using the same method.

$$\begin{aligned} \text{NMR Thermal } y_1 &= -12275x_1 + 30.873 \\ \text{NMR Sonicated } y_2 &= -9853.6x_2 + 23.571 \end{aligned}$$

At the point where the two lines cross  $y_1=y_2$  thus,

$$-9853.6x_2 + 23.571 = -12275x_1 + 30.873$$

and  $x_2=x_1$  so the value of  $x$  at which the two trend lines cross can be calculated

$$\frac{30.873 - 23.571}{-9853.6 - (-12275)} = x = 3.016 \times 10^{-3} \text{ K}^{-1}$$

Theoretically the sonicated reaction in the NMR spectrometer would effect no further enhancement at a temperature of 332 K or above where thermal effects predominate, although further reactions around this temperature would need to be carried out to prove the theory.

Since the values of the crossover points for the bench experiments compared to those carried out in the NMR spectrometer are 559 K and 332 K respectively. It seems more reasonable to suggest that the crossover temperature calculated for the bench reactions should be of a similar value to that noted in the NMR spectrometer, if the trend truly resulted from the vapour pressure effect described earlier.

In conclusion, ultrasonic irradiation of the reaction system affects both the entropy and enthalpy of the system, but that they compensate for one another. The ultrasound disrupts both the solute-solvent and solvent-solvent interactions thus reducing the enthalpy change



of activation  $\Delta H^\ddagger$  and entropy change of activation  $\Delta S^\ddagger$  as experienced in the reactions investigated by the author.

Although the compensation effect is a fairly simple explanation of the effects of  $\Delta H^\ddagger$  and  $T\Delta S^\ddagger$  on  $\Delta G^\ddagger$ , the effects of changing substituents and solvent have very complex influences upon enthalpy and entropy separately. According to Franks and Wen<sup>111</sup>, for a typically aqueous structure, such as the aqueous propan-2-ol solution employed in these investigations, the sign and magnitude of the free energy of mixing  $\Delta G$  is controlled by the entropy change  $\Delta S$ , such that  $T|\Delta S| > |\Delta H|$ . This is consistent with the idea that ultrasound disrupts the quasi-aqueous structure causing the solvent to become more disordered.

## **9.6 The Chemical Shift of the Water Peak for the Reaction of 40% (v/v) t-BuCl/Propan-2-ol with 40% (w/w) Propan-2-ol/Deuterated Water in the NMR Spectrometer**

Initially, the solvent system tends to have a fairly quasi-aqueous, three-dimensional hydrogen bonded structure that accommodates the alkyl group of the propan-2-ol molecule. As the t-BuCl reacts it produces t-BuOH. This increase in alcohol content causes the solvent structure to become more two-dimensional and less able to accommodate the alkyl group. As a consequence of the changes of the solvent structure the water peak experiences an increasing chemical shift downfield as the reaction progresses.

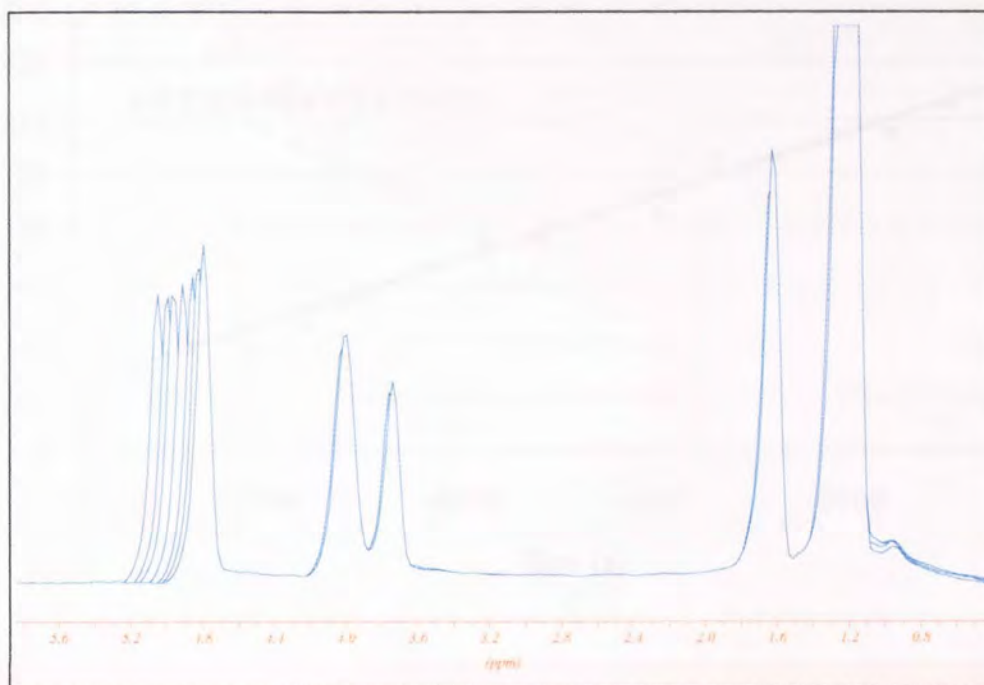
A change in the disruption of the structure of the reactants, that is the quasi-aqueous structure, may be established by the evaluation of the rate of change of the chemical shift of the absorption peak produced by water in the NMR spectra.

### **9.6.1 Analysis of the Chemical Shift of the Water Peak for the Thermally Induced Reaction in the NMR Spectrometer**

The experimental technique was the same as that in all the previous NMR investigations reported in this study. The change in the chemical shift was evaluated with respect to the position of the peak of the reference 1,4-dioxane. An example of the spectra obtained during the course of a thermally induced solvolysis reaction is illustrated in Figure 116.

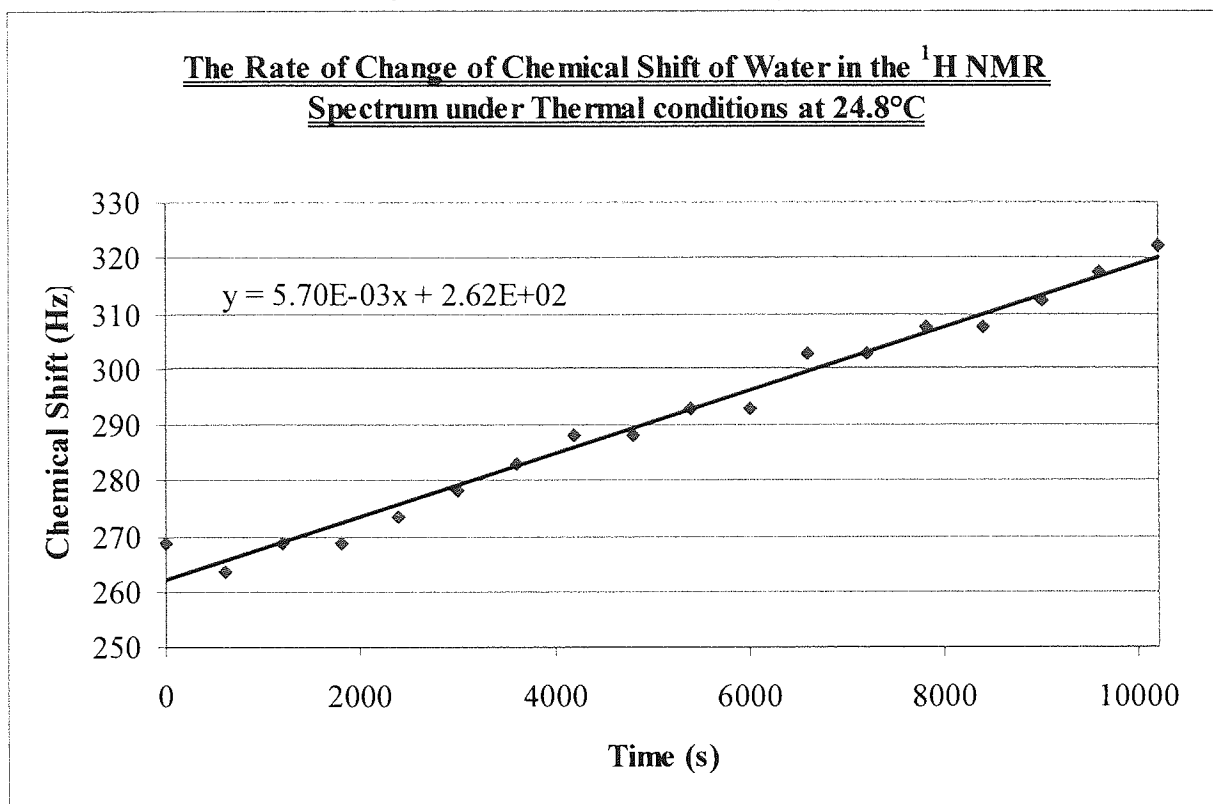
The shift in water peak is a consequence of a change in the solvent structure caused by the production of increasing quantities of 2-methylpropan-2-ol as the reaction progresses.

**Figure 116:** Overlay Plot of Spectra for the Thermally Induced Solvolysis Reaction of t-BuCl at 298 K.



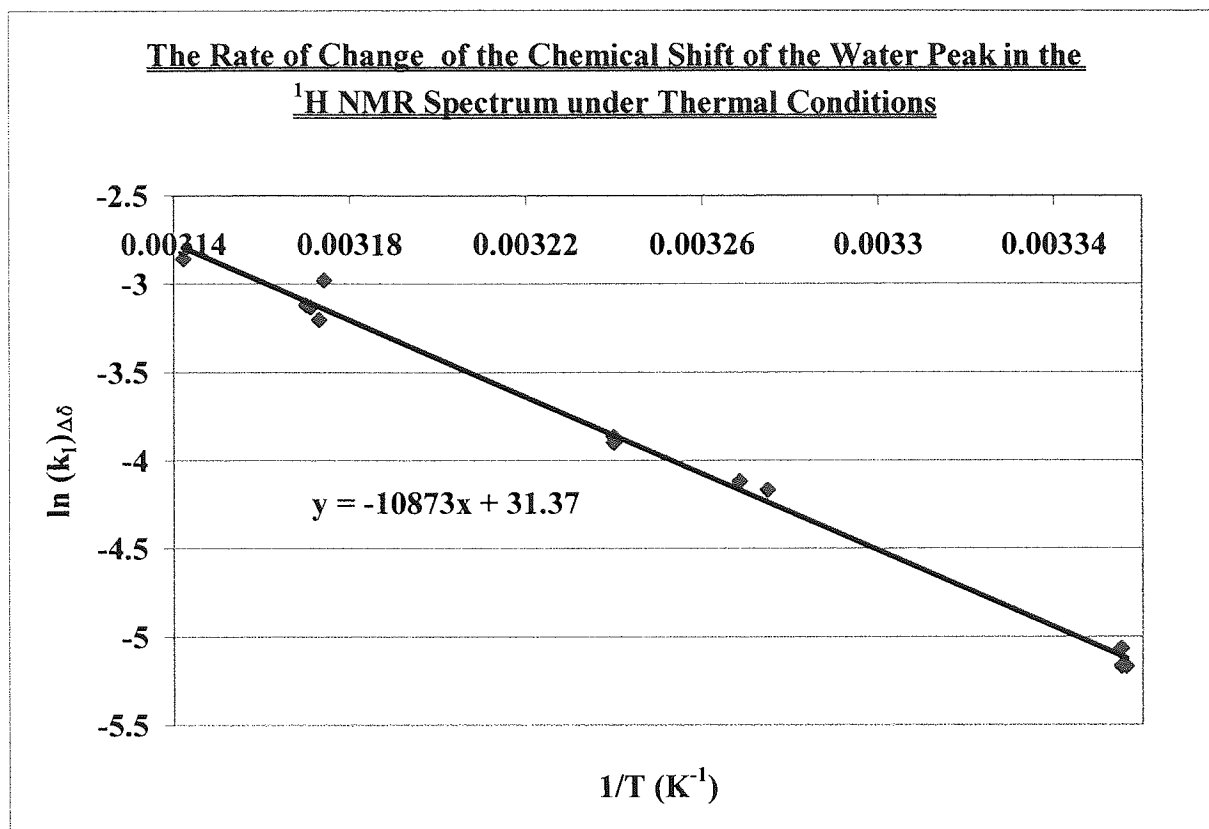
A plot of the change of the chemical shift  $\Delta\delta$  (Hz) against time  $t$  was made for each reaction such as that displayed in Figure 117.

**Figure 117:** The Rate of Change of the Chemical Shift of Water, for the Thermally Induced Solvolysis of t-BuCl, in the NMR Spectrometer.



The remaining plots are available in Appendix 14 and from these plots, the rate constant  $k_1$  for each was determined and used to construct Arrhenius plots (see Figure 118).

**Figure 118:** The Rate of Change of the Chemical Shift of the Water Peak, for the Thermal Solvolysis of t-BuCl, in the NMR Spectrometer.



The thermodynamic parameters for the thermally induced solvolysis of t-BuCl, according to the water peak shift, at 308 K were calculated from the best-fit line in Figure 118 and are shown in Table 52.

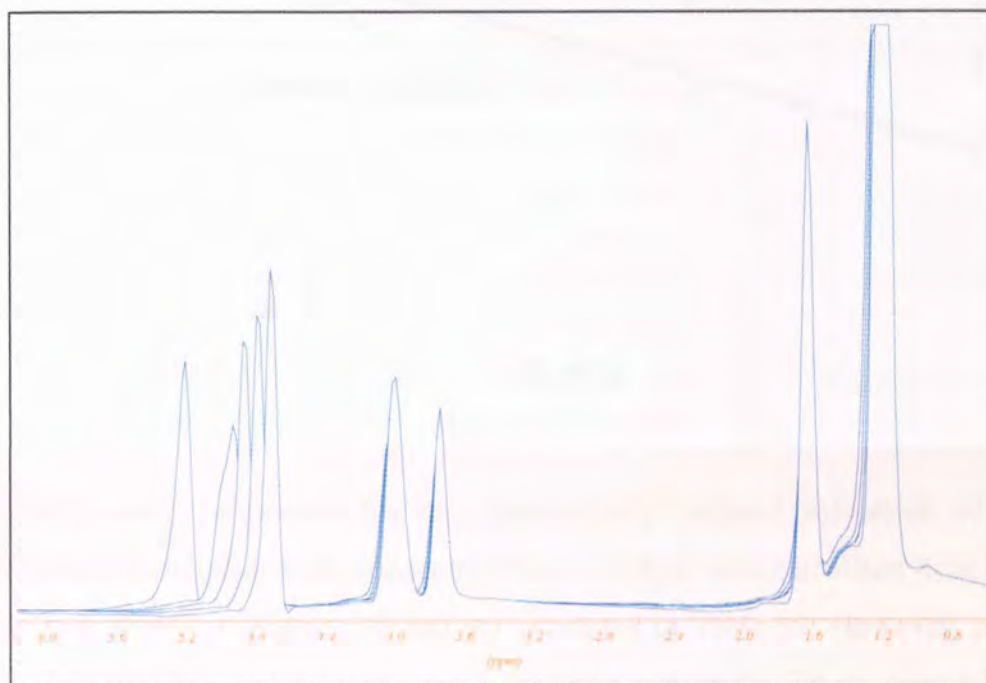
**Table 52:** The Thermodynamic Parameters for the Thermally Induced Solvolysis of t-BuCl, according to the water peak shift, at 308 K.

Reaction Conditions	$\Delta S^\ddagger$ (JK <sup>-1</sup> mol <sup>-1</sup> )	$\Delta H^\ddagger$ (kJmol <sup>-1</sup> )	$\Delta G^\ddagger$ (kJmol <sup>-1</sup> )	$E_a$ (kJmol <sup>-1</sup> )
NMR Water Shift – Thermally Induced	15.63±0.28	87.8±1.58	83.0±1.49	90.4±1.63

### 9.6.2 Analysis of the Chemical Shift of the Water Peak for the Ultrasonically Induced Reaction in the NMR Spectrometer

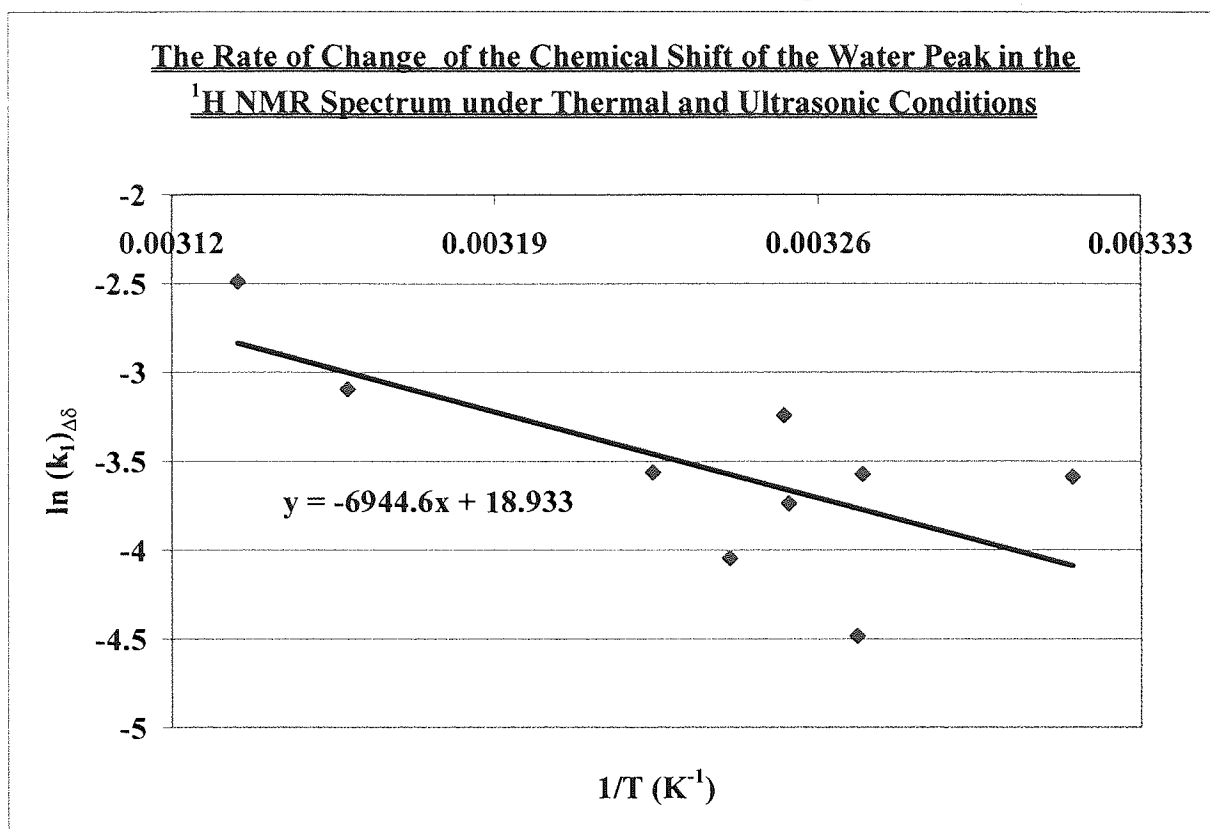
The reaction as carried out for the thermal system was repeated under ultrasonic conditions using a 3MHz transducer operating at a power of 7W. The types of spectra obtained are illustrated in Figure 119.

**Figure 119:** Overlay Plot of Spectra for the Ultrasonically Induced Solvolysis Reaction of t-BuCl at 302 K.



The data was plotted using the methodology employed in the analysis of data obtained for the thermal reactions (Appendix 15). The derived thermodynamic parameters determined from the Arrhenius plot are shown in Figure 120.

**Figure 120:** The Rate of Change of the Chemical Shift of the Water Peak, for the Ultrasonic Solvolysis of t-BuCl, in the NMR Spectrometer.



The thermodynamic parameters for the ultrasonically induced solvolysis of t-BuCl, according to the water peak shift, at a temperature of 308 K were calculated from the best-fit line to data shown in Figure 120 and are presented in Table 53. However, as can be observed from that line and the data, errors are large and so the figures cannot be relied upon.

**Table 53:** The Thermodynamic Parameters for the Ultrasonically Induced Solvolysis of t-BuCl, according to the water peak shift, at 308 K.

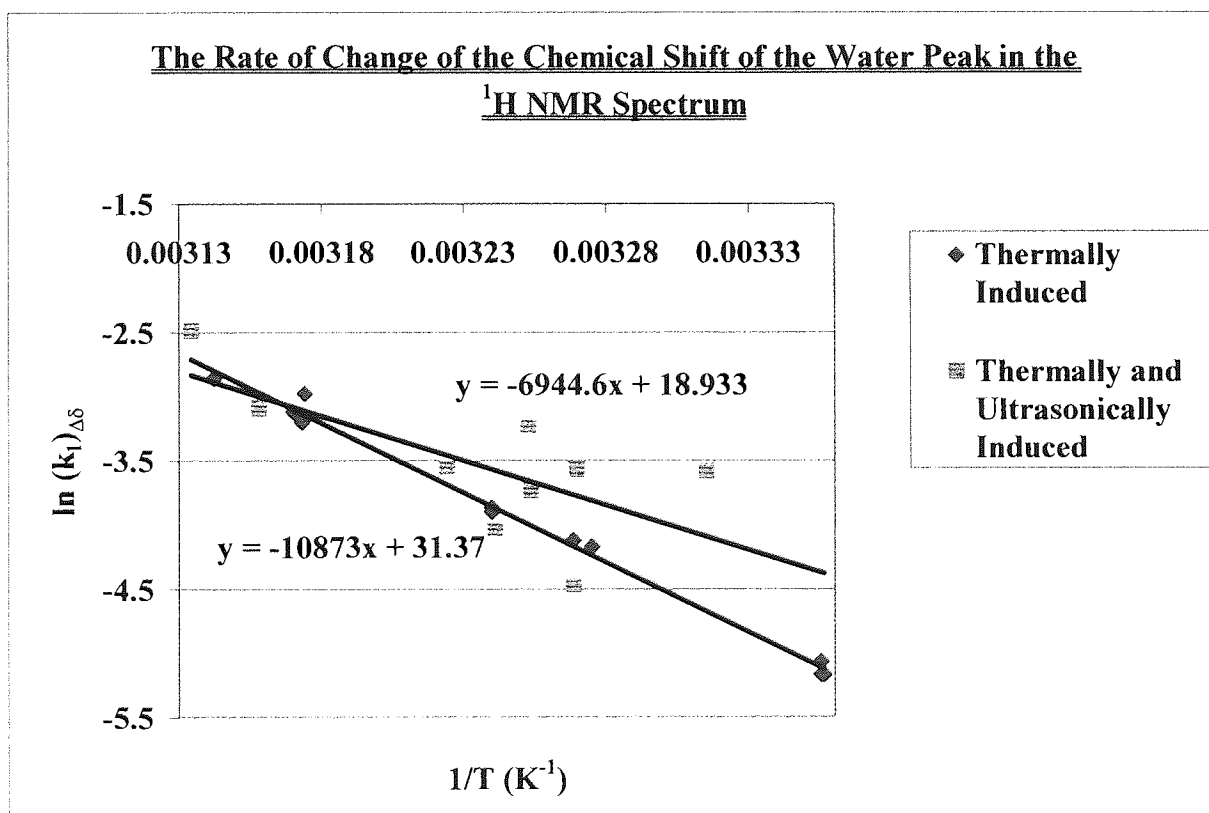
Reaction	$\Delta S^\ddagger$ (JK <sup>-1</sup> mol <sup>-1</sup> )	$\Delta H^\ddagger$ (kJmol <sup>-1</sup> )	$\Delta G^\ddagger$ (kJmol <sup>-1</sup> )	$E_a$ (kJmol <sup>-1</sup> )
NMR Water Shift – Thermally and Ultrasonically Induced	-87.78±24.51	55.2±15.4	82.2±23.0	57.7±16.1

### 9.6.3 The Comparison of the Chemical Shift of the Water Peak for the Thermally and Ultrasonically Induced Reaction in the NMR Spectrometer

It is clearly visible from the overlay plots illustrated in Figure 116 and Figure 119, for the thermal and ultrasonic solvolysis reactions respectively, that a larger shift of the absorption peak of water occurs for the ultrasonic reaction compared with the thermally induced system over the same period of time.

Figure 121 shows a comparison of the respective thermal and sonicated reactions. A significantly enhanced rate of change is observed for the chemical shift of the water peak, during the in-situ reaction of t-BuCl, in the NMR spectrometer.

**Figure 121:** Plot of  $\ln k_1$  versus  $1/T$  ( $K^{-1}$ ) for the Rate of Change of the Chemical Shift of the Water Absorption Peak for the Comparison of the Thermal and Ultrasonic Solvolysis Reactions of t-BuCl in the NMR Spectrometer.



The change in the rate of the chemical shift for the thermal reaction follows a good linear trend. The sonicated reactions appear to be quite random and although a trend line has been

included in the graph for the purposes of comparison it cannot be said that this is an accurate representation of a trend. The trend has a very large standard deviation of 0.44 compared to a value of 0.073 obtained for the thermal data.

**Table 54:** The Thermodynamic Parameters at 308 K for all t-BuCl Solvolysis Reactions.

Reaction Conditions	$\Delta S^\ddagger$ (JK <sup>-1</sup> mol <sup>-1</sup> )	$\Delta H^\ddagger$ (kJmol <sup>-1</sup> )	$\Delta G^\ddagger$ (kJmol <sup>-1</sup> )	$E_a$ (kJmol <sup>-1</sup> )
Bench top - Thermally Induced	-24.27±0.35	87.3±1.25	94.8±1.36	89.8±1.29
Bench top – Thermally and Ultrasonically Induced	-34.43±3.63	81.6±8.6	92.2±9.72	84.2±8.87
NMR - Thermally Induced	11.49±0.21	99.5±1.82	96.0±1.75	102.0±1.87
NMR - Thermally and Ultrasonically Induced	-49.22±6.48	79.4±10.4	94.5±12.4	81.9±10.8
NMR Water Shift – Thermally Induced	15.63±0.28	87.8±1.58	83.0±1.49	90.4±1.63
NMR Water Shift – Thermally and Ultrasonically Induced	-87.78±24.51	55.2±15.4	82.2±23.0	57.7±16.1

The enthalpy and entropy changes observed for the chemical shift of the water peak display the largest decrease in their values, at around 103 kJmol<sup>-1</sup> and 33 kJmol<sup>-1</sup> respectively, compared to those obtained for the thermal and sonicated reactions followed according to the consumption of t-BuCl. However, due to the large standard deviation of the water shift under ultrasonic conditions this is not a conclusive result displaying an increase in the disorder of reactants although it is a good indication.

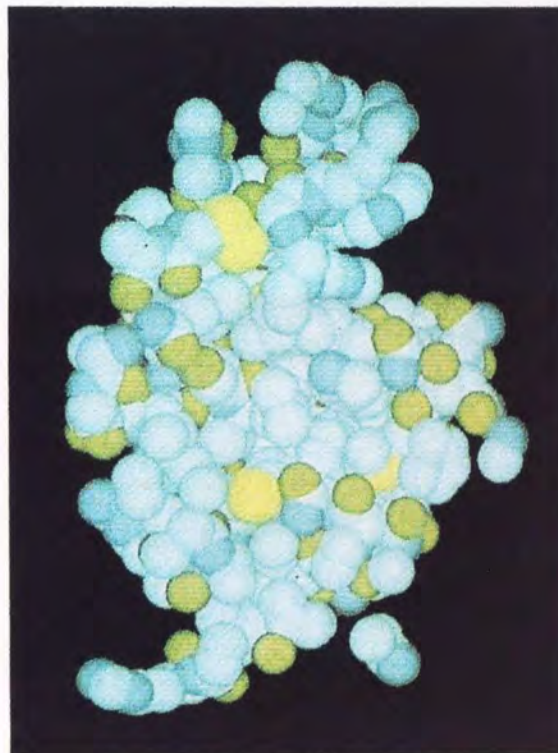


**Chapter 10    The Effects of Ultrasonic Irradiation upon an Aqueous  
Solution of Lysozyme**

## 10.1 The Structure of Lysozyme

Lysozyme is a relatively small enzyme, which is present in nasal mucosa, egg white, plant latex and various animal tissues. Alexander Fleming discovered Lysozyme in 1922, during his quest for a substance that would kill harmful bacteria. Lysozyme was so named from *lyso* because of its ability to lyse i.e. dissolve bacteria and *zyme* as it was an enzyme. In 1965, David Philips and his colleagues determined the three-dimensional structure of lysozyme by x-ray analysis. The high-resolution image obtained was the first of its kind for an enzyme molecule.

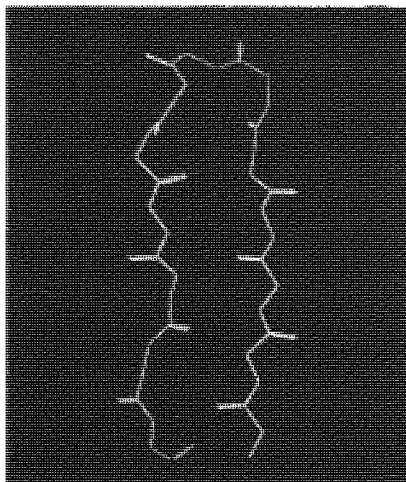
**Figure 122:** Space-filling Model of Lysozyme.<sup>125</sup>



Lysozyme is highly stable and consists of 129 amino acid residues, cross-linked by four disulphide bridges as displayed in Figure 123.



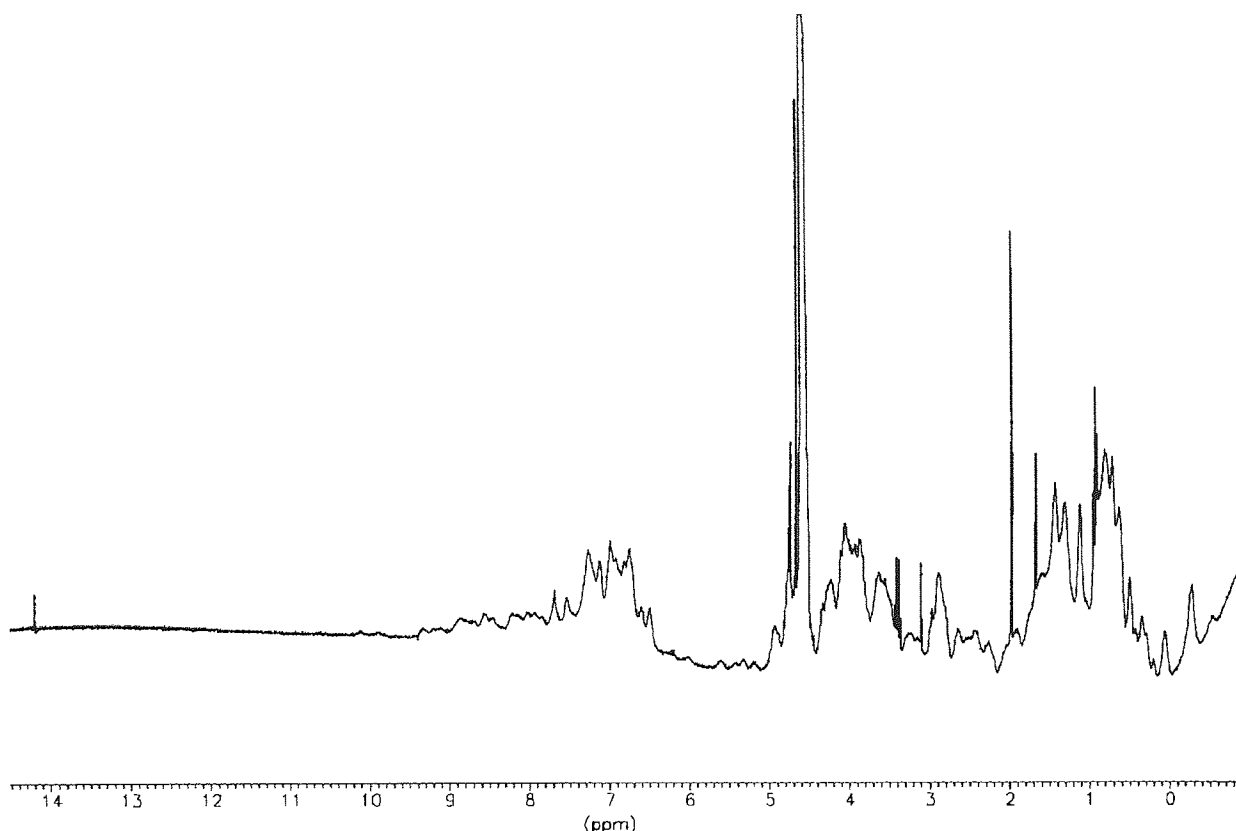
**Figure 124:** The Hairpin Turn of the Main Chain of Lysozyme.<sup>125</sup>



## **10.2 Analysis of the Effects of Ultrasonic Irradiation Upon an Aqueous Solution of Lysozyme**

A saturated aqueous solution of lysozyme was made, with the addition of a few drops of  $\text{DCl}_{(l)}$  to aid the dissolution of the protein in larger quantities, and an example  $^1\text{H}$  NMR spectrum obtained in a 300 MHz NMR spectrometer in a spinning 5 mm OD NMR tube with the resulting spectrum displayed in Figure 125.

**Figure 125:** The Spectrum of Lysozyme in Aqueous Solution in the Bruker WM300.

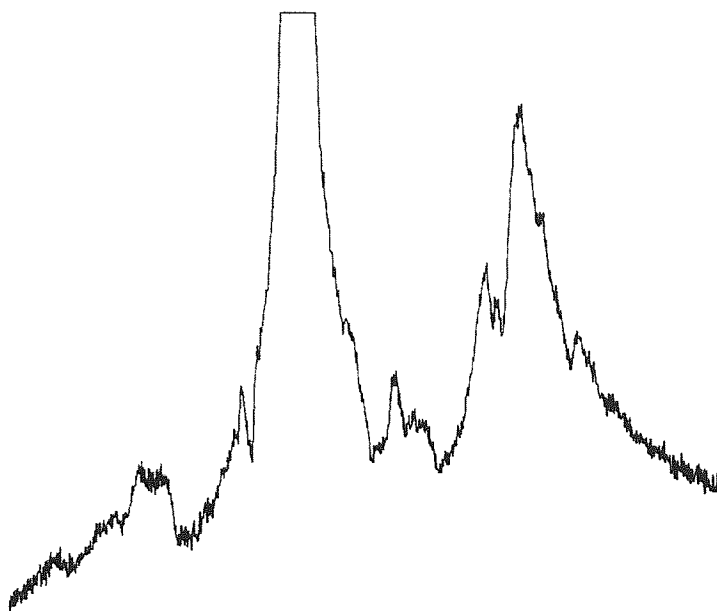


Due to the size of the molecule the proton spectrum of lysozyme is extremely complex. The large signal noted at about 4.6ppm is due to the protons of the water molecule.

All of the following experiments were carried out using the thermal dissipation device as previously described in Chapter 6.

A 6 cm<sup>3</sup> sample of the aqueous lysozyme solution was placed in a 10 mm OD non-spinning NMR tube and irradiated with various frequencies of ultrasound operating at a range of different powers for a period of five minutes in the NMR spectrometer. The <sup>1</sup>H spectrum was obtained in the Bruker WM250 at the end of the five minutes whilst the sample was still being irradiated with ultrasonic energy. An initial reference <sup>1</sup>H spectrum was attained for each sample set without the application of ultrasound. An example of a <sup>1</sup>H spectrum acquired is shown in Figure 126.

**Figure 126:** The Spectrum of Lysozyme in Aqueous Solution in the Bruker WM250.



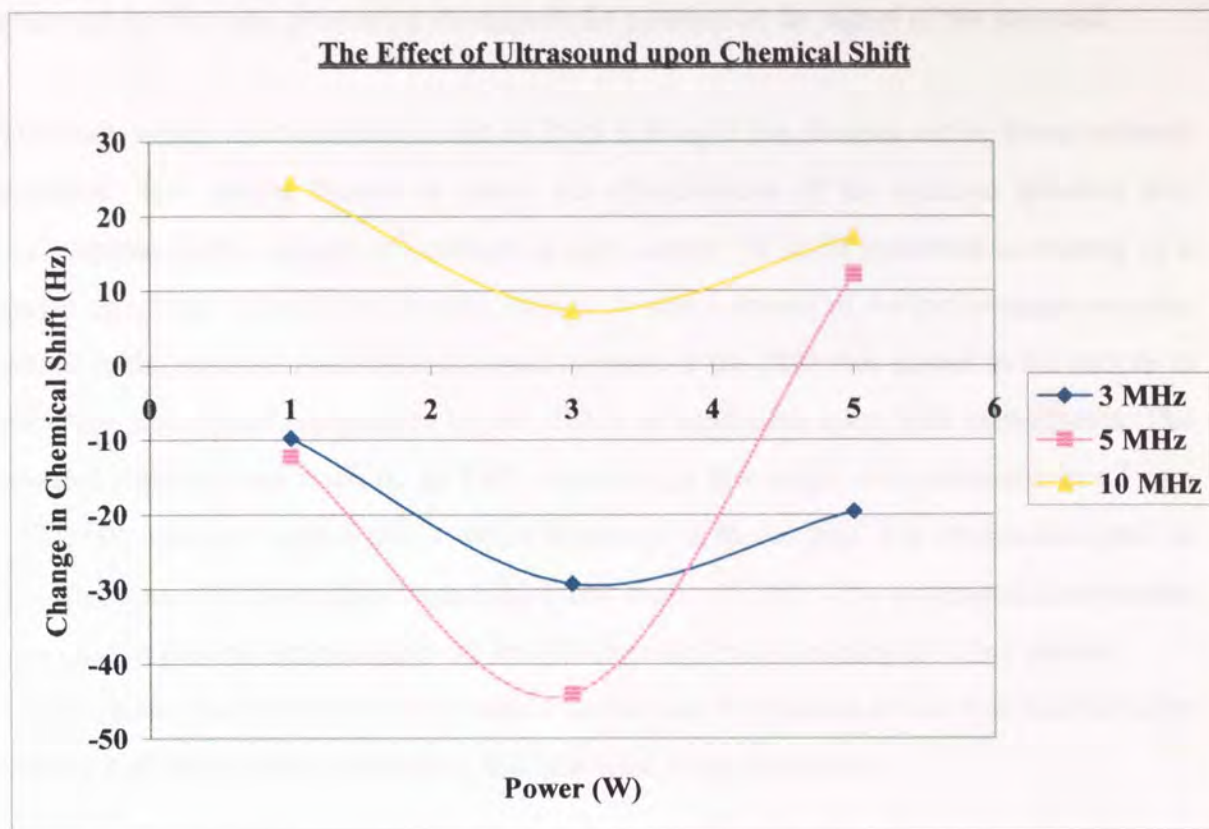
The chemical shifts observed between the two largest proton signals, as in the spectrum above, were determined for each of the experiments carried out upon the aqueous lysozyme sample and are given in Table 55.

**Table 55:** The Change in Chemical Shift for Sonicated Aqueous Lysozyme.

Transducer Frequency (MHz)	Input Power (W)	Intensity ( $\text{Wcm}^{-2}$ )	Chemical Shift (Hz)	Change in Chemical Shift (Hz)
Reference	Reference	Reference	976.6	0
3	1	8	966.8	-9.8
3	3	24	947.3	-29.3
3	5	40	957.0	-19.6
Reference	Reference	Reference	964.4	0
5	1	8	952.2	-12.2
5	3	24	920.4	-44.0
5	5	40	976.6	+12.2
Reference	Reference	Reference	949.7	0
10	1	8	974.1	+24.4
10	3	24	957.0	+7.3
10	5	40	966.8	+17.1

The effect of sonication upon the chemical shift between the two proton signals is best displayed in graphical form.

**Figure 127:** The Effect of Ultrasound upon the Chemical Shift of the Lysozyme System.



The same general trend occurs for all three different frequencies of ultrasound 3 MHz, 5 MHz and 10 MHz. For the experiments in which the 3 MHz and 5 MHz transducers were used the chemical shift between the two signals observed generally decreased when ultrasonic energy was applied compared to that of the reference without ultrasound. However, the reactions using a 10 MHz transducer displayed an increase to the overall chemical shift.

It had to be established that the change in chemical shift was the result of either one or both of the proton signals analysed. This was attempted using a standard for comparison.

### 10.3 Establishing an External Standard

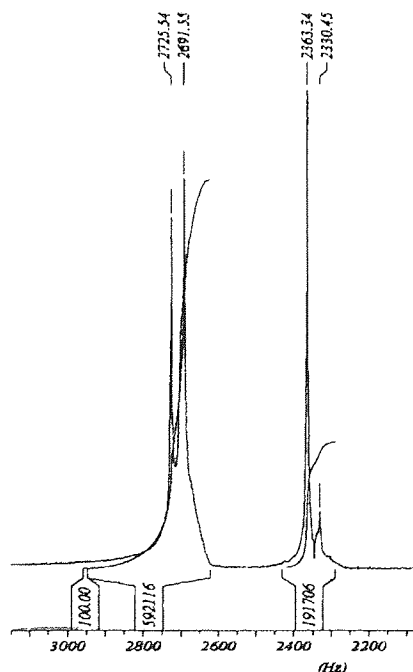
An external standard is required as opposed to an internal standard because of the fact that ultrasound is being applied. Any internal standard would be affected by the ultrasound in a similar manner to the sample, as it would be directly coupled to the source. It was theorised

that if the standard were placed in a tube held in the sample any ultrasound would be absorbed by that tube preventing changes in the position of the signal of the standard.

The most widely used standard is that of TMS making it the obvious choice for an external standard. The sample chosen to assess the effectiveness of the external standard was cyclohexane  $C_6H_{12}$  because it produces a very simple  $^1H$  NMR spectrum consisting of a single signal due to the 12 equivalent protons. A small amount of the cyclohexane was also placed in the external standard and a small amount of the TMS was placed in the sample to carry out a complete comparison of the effects of sonication upon both components. The external standard was made up as TMS containing a few drops of cyclohexane in a 5 mm OD NMR tube cut short so that it would submerge in the sample. The sample consisted of a 1:1 mixture of  $C_6D_{12}$ : $C_6H_{12}$  containing a few drops of TMS. The deuterated cyclohexane was used to prevent the resonance of the cyclohexane from dwarfing the other signals. Unfortunately the Parafilm<sup>TM</sup> skin used on the thermal dissipation device was soluble in the sample used and so household cling film was used as an alternative.

Figure 128 shows the spectrum obtained when the system previously described was examined by  $^1H$  NMR spectroscopy.

**Figure 128:** Establishing an External Standard.





The identity of each resonance is given in Table 56 where each signal has been assigned to either a component of the sample or the external standard.

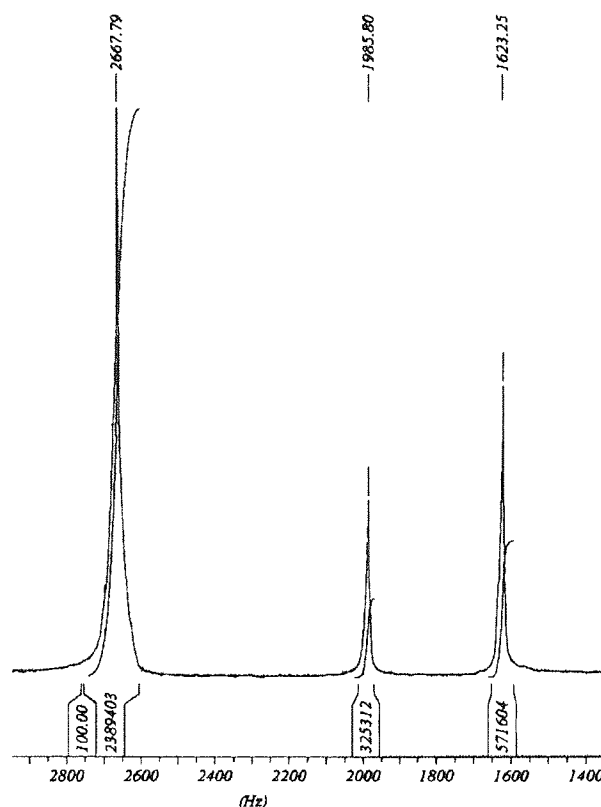
**Table 56:** Identity of the  $^1\text{H}$  Resonances for Establishing an External Standard.

Identity of the $^1\text{H}$ Resonance	Frequency (Hz)
$\text{C}_6\text{H}_{12}$ in External Standard	2725.54
$\text{C}_6\text{H}_{12}$ in Sample	2691.55
TMS in External Standard	2363.34
TMS in Sample	2330.45

When the samples were analysed with and without the application of ultrasound no visible change in either the sample or the external standard was observed. There are two possible reasons for no chemical shifting of signals occurring, the first being that the clingfilm does not sufficiently transfer the ultrasonic energy to the sample itself. The second reason is that the ultrasound simply has no effect on the system that was observed. The lysozyme system must have been experiencing some kind of change to its physical environment and the cyclohexane does not exhibit the same effect because it does not exist in the same kind of physical environment.

It was hypothesised that the lysozyme solution might have experienced a disruption of the hydrogen bonding, so a system involving it had to be designed in order to prove the theory. The compound with the greatest amount of hydrogen bonding known is water. The external standard previously designed was placed in a 1:1  $\text{H}_2\text{O}:\text{D}_2\text{O}$  sample and the Parafilm<sup>TM</sup> skin used on the thermal dissipation device. The sample was irradiated using a 5 MHz transducer operating at powers of 1 W, 3 W and 5 W producing spectra such as that shown in Figure 129.

**Figure 129:**  $^1\text{H}$  Spectrum of a Sample of Water with the External Standard.



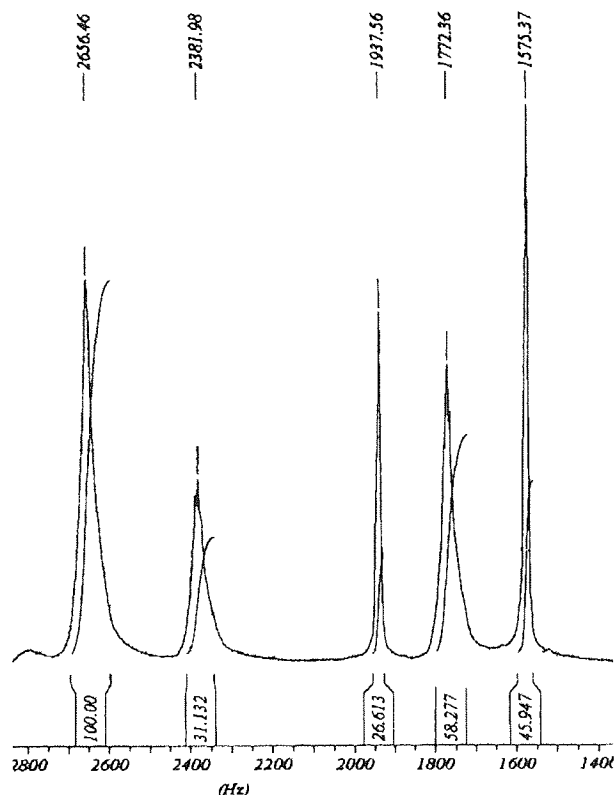
The signal at 2667.79 Hz was due to the protons of the water whilst the remaining two resonances at 1985.80 Hz and 1623.25 Hz were the result of the  $\text{C}_6\text{H}_{12}$  and TMS respectively in the external standard.

Although the previous results suggest otherwise, the author's hypothesis remained that the ultrasonic waves interacted with the bonding in a manner so as to effect a change in the NMR spectra obtained. However, water is known to have a highly ordered three-dimensional hydrogen bonded structure and this could be the explanation for the absence of any reaction of the sample when irradiated with ultrasound.

An alternative sample composition still involving hydrogen bonding was examined. As previously noted for the solvolysis reaction of 2-chloro-2-methylpropane forming 2-methylpropan-2-ol, the addition of increasing amounts of alcohol to water leads to a sample with a more two-dimensional structure and it was for this reason that a sample consisting of a 2:1:1 mixture of  $\text{C}_2\text{H}_5\text{OH}:\text{D}_2\text{O}:\text{H}_2\text{O}$  was produced. The same external standard mixture

of TMS and cyclohexane was utilised as in the water experiments. Individual samples were irradiated using both the 3 MHz and 5 MHz transducers running at 1W, 3W and 5W to produce spectra such as that shown in Figure 130.

**Figure 130:**  $^1\text{H}$  Spectrum of a Sample of Aqueous Ethanol with the External Standard.



The identities of the signals observed in the spectrum are given in the table below. A quantity of  $\text{D}_2\text{O}$  was added to prevent the water signal from being so large that it obscured those due to ethanol.

**Table 57:** Identity of the  $^1\text{H}$  Resonances for Aqueous Ethanol Containing the External Standard.

Identity of the $^1\text{H}$ Resonance	Frequency (Hz)
Water	2656.46
$\text{C}_6\text{H}_{12}$ in External Standard	2381.98
$-\text{CH}_2-$ of Ethanol	1937.56
TMS in External Standard	1772.36
$-\text{CH}_3$ of Ethanol	1575.37

Once again, no effect upon the spectra acquired was noted for the irradiated aqueous ethanol samples.

#### 10.4 Conclusions and Discussion

The main problem with the lysozyme experiment was establishing a method by which the signals obtained could be referenced to a standard, for example TMS, in the same manner as would normally be carried out for NMR spectroscopic studies.

A general trend was detected for the change in chemical shift between the two largest proton signals for the  $^1\text{H}$  spectra of the aqueous lysozyme solution analysed when compared to a reference where no ultrasound had been applied. Employing both the 3 MHz and 5 MHz transducers a distinct decrease in chemical shift between the resonances examined occurred for all powers investigated. The largest decrease appeared to take place at an applied power of around 3 W. However, this would have to be further established by completing more in depth studies of the power region in question as only three points were obtained in the study.

At a transducer frequency of 10 MHz a slightly different trend was observed. An increase in the chemical shift between resonances was witnessed. Nevertheless, upon plotting of the trend of change in chemical shift again a trough was noted for the region of 3 W.

It is impossible to state whether the changes in chemical shift are due to the movement of *either* signal or a combination of them both. If a movement of the signal due to the protons of water had occurred then this would truly be an interesting discovery for the biologist who has to analyse most samples in water, as they are not soluble in other solvents. All that can be conclusively stated is that something is occurring to bring about the change. It was for the reason outlined here that the use of a standard had to be pursued. An internal standard was not considered as an option due to the fact that it would obviously be liable to the same effects as that of the sample itself. The only remaining alternative was that of an external standard, which could itself be shielded from the effects of sonication by the tube in which it was held.

After the investigation of a non-hydrogen bonded system, it was hypothesised that the sample underwent a change in the hydrogen bonding of the system bringing about the chemical shift changes noted. Initially a sample of water, well known for its hydrogen bonding, was examined with reference to an external standard but to no avail. It was suggested that the system might be too strongly bonded, having a highly ordered three-dimensional structure and so ethanol was added to form a more two-dimensional structure. Once more no effect upon the spectra attained was displayed.

There was one significant difference between the initial experiments carried out on the sample of aqueous lysozyme compared to those using an external standard. The external standard involved the use of a glass tube placed directly in the sample under investigation, which although prevented the reference from experiencing an effect caused by the ultrasound could have absorbed a large quantity of the energy entering the solution and thus precluded any change in the spectra.

The sample did not appear to be experiencing any reaction upon application of the ultrasound but this still remains a possibility. The proton spectrum due to lysozyme is very complex and so would make it difficult to observe any product formation which may take place as a result of any ultrasonically induced reaction.

Unfortunately, due to time constraints the findings of these experiments could not be investigated further and may perhaps hold the key to an explanation of sonochemically enhanced reactions.

## **Chapter 11 Conclusions and Further Work**

In general it has been theorised that the application of diagnostic ultrasound to analytical chemistry causes only temporary physical changes to the medium, through which it passes and does not influence chemical reactivity. However, the results obtained from the experiments carried out during the course of this work, suggest that for frequencies in the low diagnostic region, 3 MHz this is not strictly true.

### **11.1 The Elimination of Sample Heating Caused by Ultrasonic Irradiation**

The main problem when considering the effects of ultrasound upon a reaction sample is accounting for the heating produced as a result of sample irradiation. A device was therefore designed and constructed to reduce the heating of samples exposed to ultrasound. The initial device was proven to be unsuitable for the task at hand as it was constructed of glass, which fractured due to the natural vibrations during the operation of the transducer. The design was modified and the glass piece of the device replaced with a PTFE component thus eliminating the problem of fracturing, however, the coupling fluid could no longer be observed. This was not a significant disadvantage since it could not be observed when placed in the NMR spectrometer.

The effects of heating using 3, 5 and 10 MHz transducers operating at powers of 1 W, 3 W and 5 W were investigated using a 10 cm<sup>3</sup> sample of degassed distilled water. The test was carried out in the same test tube for all the experiments in order to enable a direct comparison of the results: varying the vessel causes differences in the transfer of ultrasound to the sample. The device was placed at a depth of 2.5 cm in the liquid for all experiments to ensure comparable conditions. The temperature of the bulk sample was measured at regular intervals over a five-minute period. It was instantly obvious from the result obtained that the device almost entirely suppressed sample heating compared to that of the directly coupled traditional system.

The traditional irradiation of the water experienced an increase in temperature of anything between 1 K for the 3 MHz transducer operating at a power of 1 W and 14.5 K for the 5 MHz transducer operating at a power of 5 W. In comparison, the heating in samples tested with the device experienced very little increase in temperature over the same period.

There was, however, one significant disadvantage relating to the device. The PTFE component was filled with  $D_2O_{(l)}$  that acted as a coupling medium between the ultrasonic source and the sample limiting the operating time of the device as the water was prone to evaporation, causing the source to become decoupled from the sample. This factor prevented the employment of the device for chemical reactions carried out in the NMR spectrometer, which would be of the order of two or three hours in duration. All reactions carried out by the author therefore had to be completed using a transducer directly coupled to the reaction sample and an outside source i.e. a water bath or liquid nitrogen cooling in the NMR spectrometer controlled sample temperature.

Further work would need to be carried out redesigning the device to overcome the problems of evaporation of the coupling fluid. Investigations to determine an alternative medium with a higher boiling point is suggested but of course such a liquid must satisfy the following requirements for a suitable medium to transmit ultrasound:

- A solvent with high viscosity is more resistant to cavitation.
- A solvent with high surface tension reduces cavitation.
- A solvent with low vapour pressure prevents cavitation at lower energies.

The coupling fluid needs to transmit ultrasound as efficiently as possible with the least energy lost during its transmission to the reaction sample. If the fluid allows cavitation energy will be lost and the resulting cavities will also absorb further ultrasonic energy reducing sample irradiation.

According to Equation 22 the attenuation of sound occurs as it moves away (distance  $d$ ) from the ultrasonic source so a certain amount of energy will have been lost in the coupling fluid and upon passing through a Parafilm™ or cling film drum before it finally enters the sample. If cavitation occurs in the coupling fluid there is also the risk that those bubbles formed would also absorb ultrasonic energy. It is for this reason that any reaction carried out would be of little use. The exact power entering the sample would need to be calculated for direct comparison of any results obtained using the device and still that energy would



only be an average value of ultrasonic intensity as it continually changes with distance  $d$  from the source.

## 11.2 The Chemical Dosimeter as an in-situ Ultrasonic Reaction in the NMR Spectrometer

The chemical dosimeter is a well-known reaction in the field of sonochemistry and was believed to be the most suitable reaction to attempt in the NMR spectrometer. The dosimeter also had the added advantage that it could also be used to simultaneously measure the power entering the system enabling direct comparison of reactions.

The two systems investigated were those of the nitrophenol and the terephthalic dosimeters. In order to monitor the reaction in the NMR spectrometer the concentrations of the reactants had to be significantly increased and this was the ultimate problem for the systems.

The reactions of the 4-nitrophenol were completed using a 3 MHz transducer operating at a power of 3 W in both bench and NMR spectroscopic reactions. The solvent resonance was suppressed using the 1-3-3-1 pulse programme allowing observation of the reactant by  $^1\text{H}$  NMR spectroscopy.

No notable reaction was observed for the bench experiments. However, the appearance and disappearance of an absorbance peak at about 220 nm suggested the presence of an intermediate. NMR spectroscopic analyses did not provide any evidence to indicate a reaction when the sample was irradiated at either 3 MHz or in an ultrasonic bath. Even the addition of a small quantity of  $\text{CCl}_4$ , a well-known chemical used for improving ultrasonic reaction rates, and continual aeration did not result in product formation.

The terephthalic dosimeter was also examined and like the nitrophenol dosimeter required a large increase in reactant concentration for NMR analysis. The sample was irradiated using a 2 MHz transducer operating at 3W. Again, the 1-3-3-1 pulse programme was used to suppress the solvent signal. No products were noted during the reaction period and so the sample was continually aerated and irradiated in a water bath with a small amount of  $\text{CCl}_4$ . A higher power of 5 W was also employed using a 2 MHz transducer but without success.

**Table 58:** Comparison of the Reaction Conditions for the Two Dosimeter Systems.

Reaction Conditions	Result
<b>4-Nitrophenol</b> - Sonicated for 1½ hours.	No reaction products observed.
<b>4-Nitrophenol</b> - Sonicated for 4 hours whilst continually aerated and a small amount of CCl <sub>4</sub> added.	No reaction products observed.
<b>Terephthalic</b> - Air continuously bubbled through the reaction mixture. 47 minutes reaction time.	No reaction products observed.
<b>Terephthalic</b> - Two drops of CCl <sub>4</sub> added and air continuously bubbled through the reaction mixture. 31 minutes reaction time.	No reaction products observed.

There were two possible reasons for the lack of results

1. As a result of the greatly increased concentration of the reactants required to enable NMR analysis, the reactions simply could not take place under the different reaction conditions.
2. The reactions may occur so slowly that over the duration of the experiment insufficient product was formed and so could not be detected. If this was true the duration of the experiment is too lengthy for the criteria of the investigation.

Further work would need to be carried out to establish if these theories are correct. The reactions could be completed over a much longer experimental period and those of the terephthalic dosimeter could be analysed using a fluorimeter, which was not available to the author at the time of the experiment. The fluorimeter and the UV spectrometer both have far superior sensitivity to that of the NMR spectrometer, as they can detect compounds present in much smaller quantities. If any reaction takes place the fluorimeter and the UV spectrometer should record the presence of products sooner than the NMR spectrometer.

### 11.3 The Diels Alder Reaction of Maleic Anhydride with Anthracene

For the reasons previously discussed in chapter 8 the Diels-Alder reaction of maleic anhydride with anthracene was proved an unsuitable system for the in-situ observation of an ultrasonically induced reaction in the NMR spectrometer.

The Diels-Alder reaction has become the first ever ultrasonically enhanced reaction employing ultrasound in the high frequency, megahertz region. Although, it could not be used to achieve the first ever in-situ NMR spectroscopic analysis a great deal of information has still been obtained from the bench experiments carried out in toluene and *o*-xylene. The findings obtained in this study are in agreement with those displayed by traditional pericyclic reactions.

**Table 59:** Comparison of Traditional Pericyclic Thermodynamic Parameters with those of an Ultrasonically Enhanced Reaction.

Reaction Type	$\Delta S^\ddagger$ ( $\text{JK}^{-1}\text{mol}^{-1}$ )	$\Delta H^\ddagger$ ( $\text{kJmol}^{-1}$ )	Reversible Reaction
Traditional Pericyclic	-150 to -200	Small and exothermic	Yes
Author's Results	-145 to -165	+47 to +55	Yes

The entropy change is consistent with the loss of translational energy when two molecules combine forming a transition state. Bimolecular reactions inherently require additional organisation in order to align in the correct orientation to allow simultaneous bond formation and breaking. The value obtained by the author is actually that of the enthalpy of activation which is endothermic in nature for the reaction although the overall enthalpy change for the reaction may well be exothermic for the reaction. The enthalpy change could be acquired by determining experimentally  $K^\ddagger$  and using Equation 53.

**Equation 53:** Calculation of Enthalpy Change.

$$\Delta H = -RT \ln K^\ddagger$$

The Diels-Alder reaction investigated was reversible at high temperatures, proven by the HPLC experiment carried out on the product formed, as the  $T\Delta S^\ddagger$  term becomes increasingly more important.

The ultrasonically enhanced Diels-Alder reaction occurs by the way of a concerted, one-step pathway as suggested by Low<sup>81</sup>. The reaction cannot occur via a true diradical or zwitterionic mechanism because retention of configuration is observed in the <sup>1</sup>H (Figure

75) and  $^{13}\text{C}$  (Figure 89) NMR spectra of the adduct. It was also noted that the use of the more polar solvent *o*-xylene in the place of toluene did not cause an increase in reaction rate, ruling out the presence of a charged transition state. If a zwitterionic intermediate were involved it would be of greater polarity than the reactants and the employment of a more polar solvent would result in better solvation causing an increase in the rate of the reaction. No increase in reaction rate was noted therefore, the reaction could not have taken place via a stepwise ionic pathway.

The ultrasonically induced reaction on the bench does cause an enhancement in the rate constant, the greatest improvement occurring at the lowest temperature investigated where an almost 1.4 fold increase in rate over the thermal reaction was observed. Other workers<sup>115,116</sup> also experienced the same trend and hypothesised that the decrease in reaction rate was the result of increasing vapour pressure with increasing temperature. The explanation is that the vapour produced fills the cavities and causes them to implode less violently as more vapour enters cushioning their implosion, so less energy is produced to initiate a rate enhancement.

The values for the thermodynamic parameters and their associated errors for the mid-point in the temperature range investigated are given in Table 34 for each of the three different reaction conditions.

**Table 34:** Comparison of the Thermodynamic Parameters Established for the Diels-Alder Reactions.

Reaction Conditions	$\Delta S^\ddagger (\text{JK}^{-1}\text{mol}^{-1})$	$\Delta H^\ddagger (\text{kJmol}^{-1})$	$\Delta G^\ddagger (\text{kJmol}^{-1})$	$E_a (\text{kJmol}^{-1})$
Thermal - toluene	-144.57±2.91	55.4±1.11	105.0±2.11	58.2±1.17
Thermal - <i>o</i> -xylene	-145.69±4.02	55.3±1.53	105.0±2.91	58.1±1.61
Thermally and Ultrasonically induced – <i>o</i> -xylene	-165.87±12.46	47.7±3.58	105.0±7.86	50.6±3.80

For both of the thermal reactions the activation energy remained the same at about 58  $\text{kJmol}^{-1}$ . However, the activation energy  $E_a$  experiences a reduction of nearly 8  $\text{kJmol}^{-1}$  under sonication. This suggests that the ultrasound assists the reaction thus reducing the activation energy. The reaction still occurs by way of a concerted, one-step mechanism for

the reasons stated earlier. The free energy change determined in the experiments was that for the development of the activated complex  $\Delta G^\ddagger$ , not for the progress of the entire reaction. The values of  $\Delta G^\ddagger$  for the thermal and sonicated reaction systems are constant at  $105 \text{ kJmol}^{-1}$ .

According to Equation 33 a linear relationship exists between the  $T\Delta S^\ddagger$  and  $\Delta H^\ddagger$ , the gradient of a plot of the two parameters is equal to unity when no variation of  $\Delta G^\ddagger$  occurs.

It has been found in many cases that the slope of the plot is often close to unity. The slope obtained for this particular system for the plot of  $T\Delta S^\ddagger$  vs.  $\Delta H^\ddagger$  was equal to  $0.9409 \pm 0.094$  within experimental errors. The change in the free energy change  $\Delta G^\ddagger$  for the reaction conditions investigated is almost equal to zero within experimental error and confirmed by the fact that the slope of the compensation diagram is almost equal to unity. The very small variation in  $\Delta G^\ddagger$  is due to a compensation effect occurring between  $\Delta H^\ddagger$  and  $T\Delta S^\ddagger$ . It was noted that the data could be further separated into those reactions which, were thermally induced and those which, were ultrasonically induced and examined using the compensation theory. However, no such trend was observed when the two sets of data were separated and further investigations are required in order to obtain further data points and explain the effect. It could be the result of over saturation of the solvent system employed.

The assumption is made when calculating the thermodynamic parameters that the sonicated reactions follow the straight-line trend of an Arrhenius plot but this is not strictly true. The gradient usually crosses the thermal trend line at some point before it meets the y-axis. At the temperature where the two trend lines meet, the ultrasonic enhancement has no further effect and thermal effects are dominant (Figure 95), above this temperature the data derived from the thermal experiments and from ultrasonic experiments are described by the same single thermal trend line. Ultrasonically induced reactions are actually a combination of thermal and ultrasonic effects. However, there is a temperature at which the sonicated reaction becomes dominated by thermal effects and experiences no enhancement due to sonication. The author suggested that the temperature at which the effect occurs could be established by solving simultaneous equations of the thermal and sonicated reactions. However, the results obtained imply that for the thermal and sonicated reactions the two lines crossover at a temperature of 375 K, a rather high temperature: above the boiling

point of the components of the system. This suggests that perhaps the reaction does not follow a straight-line trend.

A wider range of temperatures should be investigated to ascertain the actual temperature at which sonication of the system no longer enhances the reaction and if the trend is truly linear. It would also be interesting to ascertain if the cross over point occurs at the same temperature for reactions carried out at different powers and frequencies.

#### 11.4 The Ultrasonically Induced Solvolysis of 40% (v/v) t-BuCl in Propan-2-ol with 40% (w/w) Aqueous Propan-2-ol

As shown in Table 49 as the temperature of both the bench and NMR reaction systems increased, a reduction in the overall ultrasonic enhancement of the reaction was noted.

**Table 49:** Rate Constant Increase of the Ultrasonic over the Thermal Solvolysis Reaction..

Temperature (K)	$\frac{k_1^{US}}{k_1^{therm}}$	
	Bench-top Reaction (mean)	NMR Reaction (mean)
298	2.27±0.08	2.91±0.34
303	1.99±0.07	2.81±0.34
308	1.74±0.07	2.71±0.32
313	1.54±0.05	2.61±0.31
318	1.36±0.05	2.52±0.31

Mason and co-workers<sup>115,116</sup> also observed such a trend and theorised that the decrease in rate was due to an increase in the vapour pressure for the reaction. As the amount of vapour filling the cavities formed increases, their implosion is less violent and so less energy is available to enhance the rate of the reaction. The large differences in the magnitude of the enhancement of NMR reactions over the bench experiments were probably a result of the fact that two types of reaction vessel were employed. The bench experiments were carried out in a test tube because samples had to be removed for analysis using a syringe and the test tube was considerably wider than that of the 10mm NMR tube used for the NMR reactions. The energy within the NMR tube would be more focussed and less dissipated

due to the fact that it was narrower than the test tube, thus having a greater effect (i.e. more enhanced) upon the reaction.

Several obvious trends occurred in the thermodynamic parameters (Table 50) for the experiments carried out in the NMR spectrometer and in the water bath on the bench. The values obtained are similar in magnitude to those established by Winstein and Fainberg<sup>98,99</sup> for the reaction of t-BuCl in various pure solvents (Table 13). A comparison of these values is shown in Table 60.

**Table 60:** Comparison of the Author's results for the reaction of 2-Chloro-2-methylpropane in aqueous Propan-2-ol with those of Winstein and Fainberg<sup>98,99</sup> in various pure solvents.

Reaction Conditions	$\Delta S^\ddagger$ (JK <sup>-1</sup> mol <sup>-1</sup> )	$\Delta H^\ddagger$ (kJmol <sup>-1</sup> )	$\Delta G^\ddagger$ (kJmol <sup>-1</sup> )	$E_a$ (kJmol <sup>-1</sup> )
Bench top - Thermally Induced	-24.27±0.35	87.3±1.25	94.8±1.36	89.8±1.29
Bench top – Thermally and Ultrasonically Induced	-34.43±3.63	81.6±8.6	92.2±9.72	84.2±8.87
NMR - Thermally Induced	11.49±0.21	99.5±1.82	96.0±1.75	102.0±1.87
NMR - Thermally and Ultrasonically Induced	-49.22±6.48	79.4±10.4	94.5±12.4	81.9±10.8
Solvent – Pure C <sub>2</sub> H <sub>5</sub> OH	-13*	109.0*	113*	No data
Solvent – Pure C <sub>2</sub> H <sub>3</sub> CO <sub>2</sub> H	-10*	108.0*	111.0*	No data
Solvent – Pure CH <sub>3</sub> OH	-13*	104.0*	108.0*	No data
Solvent – Pure HCONH <sub>2</sub>	-16*	93.6*	98.3*	No data
Solvent – Pure HCO <sub>2</sub> H	-7*	87.9*	90.0*	No data
Solvent – Pure H <sub>2</sub> O	+51*	97.2*	82.0*	No data

\* Values established by Winstein and Fainberg<sup>98,99</sup>

For the two reactions conditions examined on the bench the activation energy remained similar within experimental error. However, there is a reduction of the activation energy for the ultrasonic reaction carried out in the NMR spectrometer over that of the thermal reaction under the same conditions. For a reaction to advance the 'solvent shell' surrounding the nucleophile must be removed to enable it to bond with the substrate. As suggested by Mason and co-workers<sup>117</sup> ultrasound assists with this process and so reduces the activation energy  $E_a$ .

The entropy change of activation  $\Delta S^\ddagger$  for the sonicated reaction is more negative than that of the thermal reaction, suggesting that the entropy of the initial reactants has increased. An

increase in the entropy of a system is the result of it becoming more disordered i.e. less structured, it seems reasonable to deduce that the ultrasound has initiated this disruption.

A more negative change in entropy of activation  $\Delta S^\ddagger$  of about  $60 \text{ kJmol}^{-1}$  between the thermal and sonicated systems was observed in the NMR experiment compared to the bench top experiments where a decrease of about  $10 \text{ kJmol}^{-1}$  between the two different systems occurred. The ultrasound is disrupting the structure of the solvent and solute, so allowing them to react more quickly. The difference between bench and NMR experiments is most likely the result of a change in the reaction vessel employed. The ultrasonic energy within the NMR tube, believed to be more focussed and less dissipated than that in the test tube, produces a greater enhancement of the reaction rate.

The enthalpy changes of activation are all positive as expected; because a positive activation energy is noted, the reactions require energy in order to force the reactants to form an activated complex. No change in  $\Delta H^\ddagger$  was observed for the thermal bench top experiments, perhaps the result of employing a larger reaction vessel. However, for the reactions conducted in the NMR spectrometer there was a decrease in the change in enthalpy for ultrasonic reactions compared to thermal reactions. A difference of  $20 \text{ kJmol}^{-1}$  shows that the sonicated system is less endothermic than the thermal reaction i.e.  $\Delta H_{US}^\ddagger < \Delta H_{therm}^\ddagger$ . Several explanations are offered to account for this drop in the energy required by the system to initiate the reaction.

- The reaction is assisted by the stirring effect of ultrasonic irradiation.
- The sample has a higher energy density due to the ultrasonic energy being more focussed in the narrower NMR tube.
- According to the compensation diagrams shown in Figure 113, Figure 114 and Figure 115 changes in  $\Delta H^\ddagger$  are compensated for by  $\Delta S^\ddagger$  and vice versa. The bench reactions experience a much smaller change in  $\Delta S^\ddagger$  (about  $-10 \text{ kJmol}^{-1}$ ) and so the compensation required by  $\Delta H^\ddagger$  is minimal so it is not noticed. Conversely, the NMR experiments show a reduction of around  $60 \text{ kJmol}^{-1}$ , which demands a greater compensation on the part of the enthalpy. The explanation for the compensation effect is due to solute-solvent interactions. A reaction where the binding of the solute to the solvent weakens increases the enthalpy H, thereby decreases  $\Delta H^\ddagger$ .



There is also an increase in the freedom of vibration and rotation of the solvent molecules, which increases the entropy  $S$  and decreases  $\Delta S^\ddagger$  (the system becomes more disordered making reaction easier, thus a lower energy input is needed from the enthalpy component). This is the most probable theory suggesting that the ultrasound destroys the solute-solvent interactions and some of the strong solvent-solvent interactions<sup>117</sup>.

The values of  $\Delta G^\ddagger$  for all of the systems do not vary within experimental error and are essentially constant at around  $+94 \text{ kJmol}^{-1}$ . The value of  $\Delta G^\ddagger$  is positive because the formation of the activated complex requires an input of energy to take place.

Like the Diels-Alder reaction the thermal effects should become dominant at a temperature where no further enhancement may be effected by the application of ultrasonic irradiation. The temperature at which this occurs for the experiments was established as 560 K for the bench experiments and 332 K for those carried out in the NMR spectrometer. Again the different reaction vessels employed for the reactions can explain this, where the energy is more focussed in the NMR tube than the test tube.

It is concluded that ultrasonic irradiation of the reaction system affects both the entropy and enthalpy of the systems, but that they attempt to compensate for one another. The ultrasound destroys solute-solvent interactions and some of the solvent-solvent interactions so bringing about a reduction in the change in enthalpy of activation  $\Delta H^\ddagger$  and entropy of activation  $\Delta S^\ddagger$  as experienced in the reactions investigated by the author.

The compensation effect is a fairly simple explanation of the effects of  $\Delta H^\ddagger$  and  $T\Delta S^\ddagger$  on  $\Delta G^\ddagger$  but the effects of changing substituents and solvent has very complex influences upon enthalpy and entropy separately. According to Franks and Wen<sup>111</sup>, the sign and magnitude of the free energy of mixing  $\Delta G$  is controlled by the entropy change  $\Delta S$ , such that  $T|\Delta S| > |\Delta H|$ . This is consistent with the idea that ultrasound disrupts the quasi-aqueous structure causing the solvent to become more disordered.

The slope produced for the compensation diagram of the thermal reactions of *t*-BuCl is close to unity, suggesting that there is very small variation of  $\Delta G^\ddagger$ . However, the same is not true for those reactions carried out under the influence of ultrasound. Figure 115

displays a much larger slope, having a value of about 2 suggesting that a change occurred in the Gibb's free energy change of activation  $\Delta G^\ddagger$  for the reaction.  $\Delta G^\ddagger$  alters due to the effect of ultrasound on the solute-solvent interactions. The binding of the solute to the solvent is destroyed by the ultrasound passing through the sample causing an increase in enthalpy H, thereby a decrease of  $\Delta H^\ddagger$ . Ultrasound also destroys some of the strong solvent-solvent interactions resulting in an increase in their freedom of vibration and rotation, which increases the entropy S and decreases  $\Delta S^\ddagger$ . Although the data in Table 50 only depicts a slight change in  $\Delta G^\ddagger$  a large error is observed compared to that for the thermal reactions. The entropy change of activation  $\Delta S^\ddagger$  does experience a large variation in its value for which  $\Delta H^\ddagger$  cannot compensate hence the doubling of the gradient between the two different reaction conditions. It suggests that the increase in the freedom of vibration and rotation of the solvent molecules increases the entropy S thus decreases  $\Delta S^\ddagger$ , which is far greater than the effect of destroying the solute-solvent interactions. The effect could be further investigated at different powers and frequencies to ascertain if the same trend occurs under these altered conditions.

There are several reactions, which could still be carried out in order to further the investigations already completed by the author.

- According to Mason and co-workers<sup>114</sup> the smaller the alkyl group in the alcohol, the greater the rate of reaction. The experiments were completed using a 45 kHz transducer at room temperature but what would happen if the same experiments were carried out in the MHz region. Although, some of these experiments may occur over too short a period of time to observe in the NMR spectrometer they could still be followed on the bench.
- The lower the irradiation frequency the greater the force of cavitation collapse. There is a limit to the size of the transducer that can be placed in the NMR spectrometer but the theory can be tested in the MHz region under identical reaction conditions to see if this occurs in the high frequency range.
- Every sonochemical reaction has a cavitation threshold: determine that for the t-BuCl reaction by increasing the irradiation power in equal increments.

- According to Luche and co-workers<sup>17</sup> there is an optimum reaction temperature for sonochemical reactions. Complete further reactions at increasing temperatures to ascertain if such a temperature exists for the t-BuCl experiment. The results of Luche were that of one experiment only and so cannot be relied upon as occurring for all systems. These results could also be employed as additional points on the compensation diagrams for further clarification.
- The salt effect states that the rate of an S<sub>N</sub>1 reaction can be increased, by increasing the ionic strength of the solution. Initially, the substrate RX and the nucleophile Y are both neutral, as for the t-BuCl reaction, but as the reaction proceeds X becomes negatively charged. As the reactions proceeds the overall ionic strength of the system increases so increasing the reaction rate. This increase in ionic strength must also be accounted for when studying the kinetics of such a system. Initially, the ultrasound kick starts the reaction but as increased quantities of X<sup>-</sup> are formed the reaction becomes partially thermally induced, partially ultrasonic induction and partially due to increasing ionic strength. The enhancement due to ultrasonic irradiation over thermal induction has already been accounted for by the experiments already carried out by the author. All that remains to be accounted for is the enhancement due to increasing ionic strength, albeit due to an initial ultrasonic induction.

### 11.5 Comparison of the Diels-Alder Reaction of Maleic Anhydride with Anthracene to the Solvolysis of t-BuCl

When compared to the results obtained for the Diels-Alder reaction, the solvolysis of t-BuCl experienced a greater enhancement as a result of sonication. However, the temperature range over which the experiments were carried out, 298 K to 318 K (25-45°C) was lower compared to the Diels-Alder reaction, 333 to 353 K (60-80°C). As shown by Mason and co-workers<sup>115,116</sup> the effect of increased vapour pressure is once again invoked to account for the difference between the results of the two systems. At the higher temperatures used in the Diels-Alder reaction the solvent vapour pressure increased and the vapour filled the cavities thus cushioning their implosion and so released less energy upon doing so.

The data obtained could be better evaluated by modifying the version of the Wynne-Jones Eyring expression (Equation 42) employed here. By moving the temperature term from the constant part of the equation as shown in Equation 54 a true straight line equation is produced.

**Equation 54:** The Wynne-Jones Eyring Equation with respect to Activation Energy.

$$\ln \frac{k_1}{T} = \frac{k}{h} + \frac{\Delta S^\ddagger}{R} - \frac{E_a}{RT}$$

## 11.6 The Sonication of Aqueous Lysozyme

The investigation of the effect of ultrasound upon large biological molecules was carried out. A general trend was detected, for the change in chemical shift, between the two largest proton signals (one due to the protons of the water, used as a solvent, and the other resulting from the lysozyme itself). The change was observed when the  $^1\text{H}$  spectra of the aqueous lysozyme solution was compared to a reference where no ultrasound had been applied. The experiments using the 3 MHz and 5 MHz transducers displayed a distinct decrease in chemical shift between the resonances examined at all the powers examined. The largest decrease appeared to take place at an applied power of around 3W.

At a transducer frequency of 10 MHz a slightly different trend was observed. An increase in the chemical shift between resonances was witnessed. Nevertheless, upon plotting of the trend of change in chemical shift again a trough was noted for the region of 3W.

It was not possible to state whether the changes in chemical shift were due to the movement of *either* signal or a combination of them both. If a movement of the signal due to the protons of water had occurred then this would truly be an interesting discovery for the biologist who has to analyse most samples in water, as they are insoluble in other solvents.

An external standard was employed as it was theorised that the tube in which it was held would shield the reference from the effects of sonication. After numerous investigations to establish whether this was the case, no definitive conclusions were ascertained.

It was hypothesised that the sample underwent a change in the hydrogen bonding of the system bringing about the chemical shift changes noted. This was based on the previous

idea that the ultrasound was destroying some of the strong solvent-solvent interactions in the solvolysis of t-BuCl, hydrogen bonding being the dominant interaction. Initially a sample of water, well known for its hydrogen bonding, was examined with reference to an external standard but to no avail. It was suggested that the system might be too strongly bonded, having a highly ordered three-dimensional structure and so ethanol was added to form a more two-dimensional structure. Once more no effect upon the spectra attained was displayed.

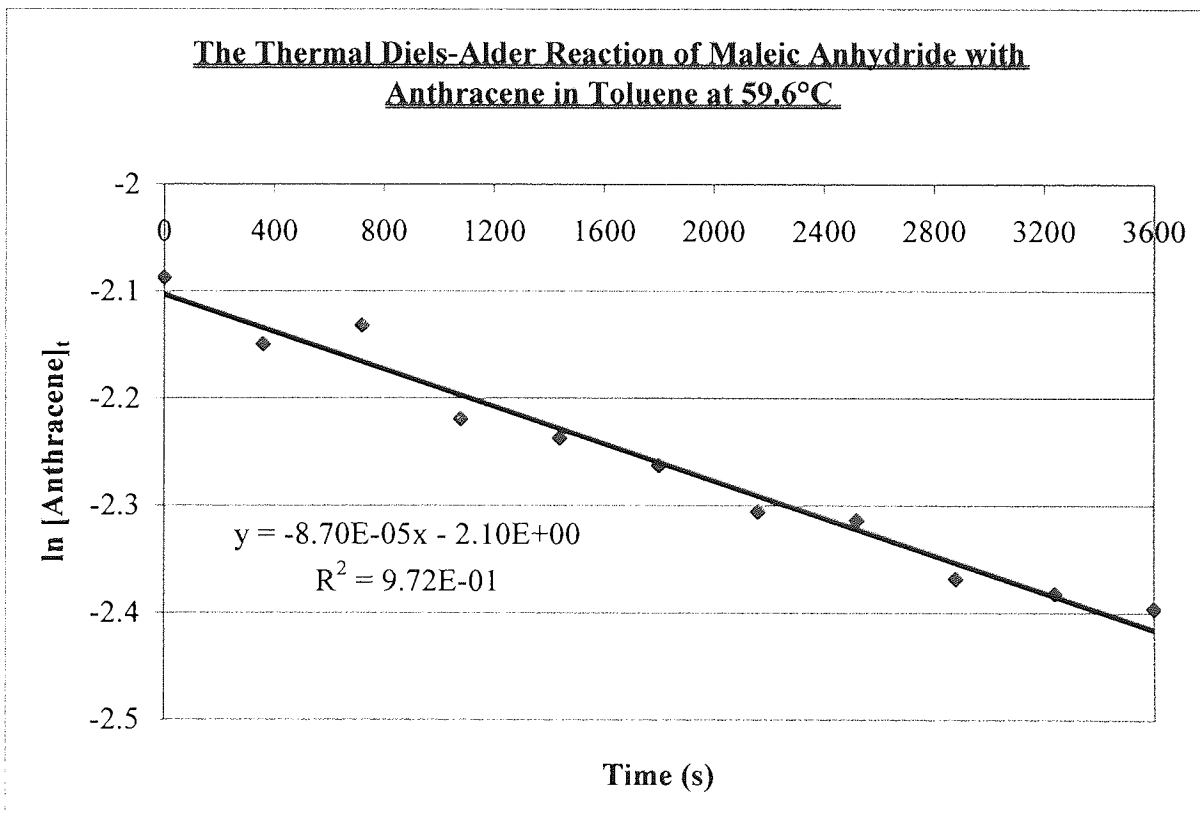
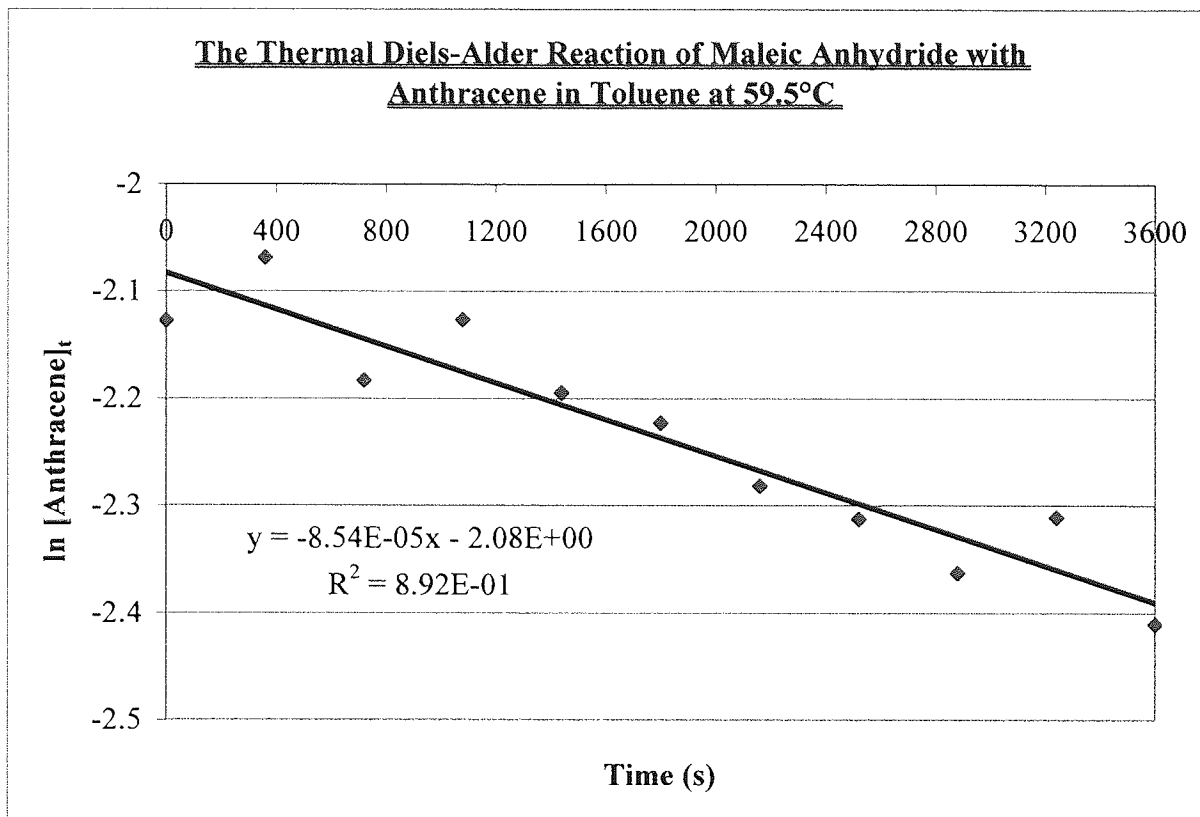
The possibility that the sample was actually undergoing a reaction still remains. Due to the complexity of the lysozyme spectrum it would make the observation of any product, particularly in small amounts, very difficult.

Unfortunately, due to time constraints the findings of these experiments could not be investigated further and may perhaps hold the key to an explanation of sonochemically enhanced reactions.

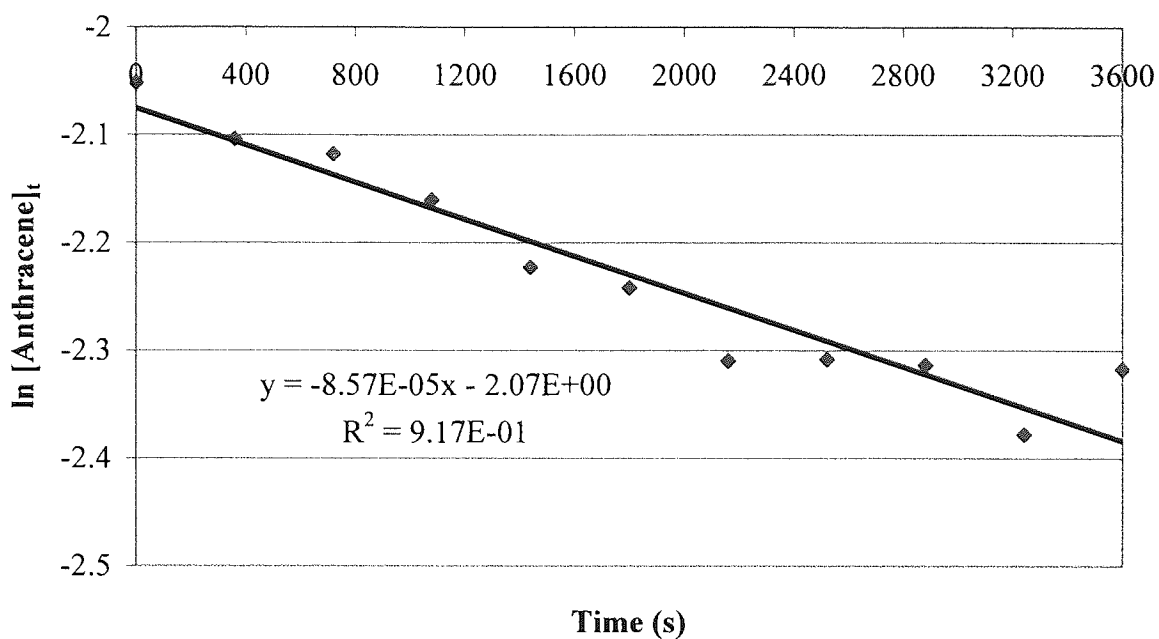
An alternative method needs to be formulated to establish the true reason for the chemical shift changes observed in the aqueous lysozyme solution when irradiated with ultrasound. A reliable procedure for comparing a sample resonance against a reference needs to be determined. The reference itself must be isolated so that it does not experience the effects of irradiation with ultrasound. Such a reference could also be employed to evaluate the water shift in the solvolysis reaction of t-BuCl.

## Appendices

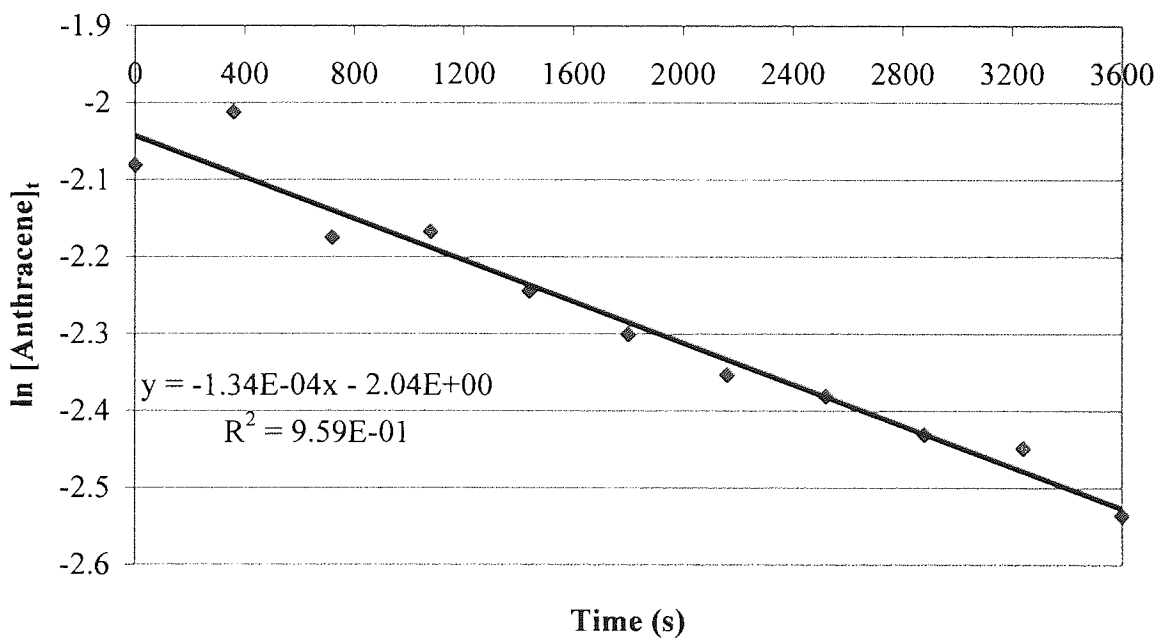
**Appendix 1:** The Thermally Induced Diels-Alder Reaction of Maleic Anhydride with Anthracene in Toluene.



The Thermal Diels-Alder Reaction of Maleic Anhydride with Anthracene in Toluene at 59.5°C

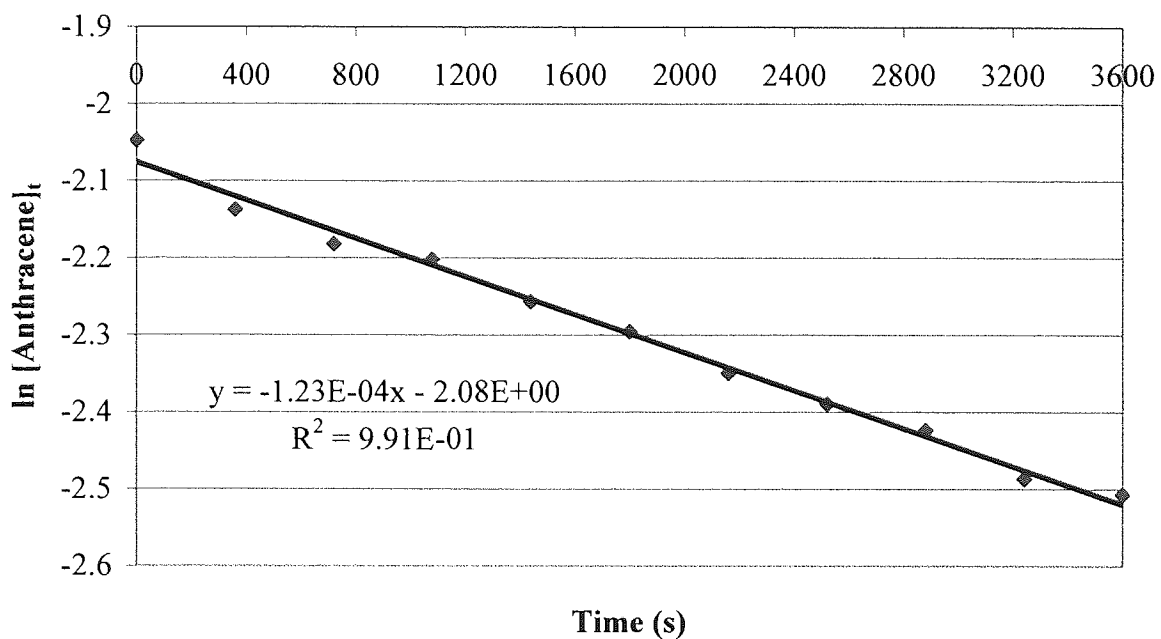


The Thermal Diels-Alder Reaction of Maleic Anhydride with Anthracene in Toluene at 64.1°C

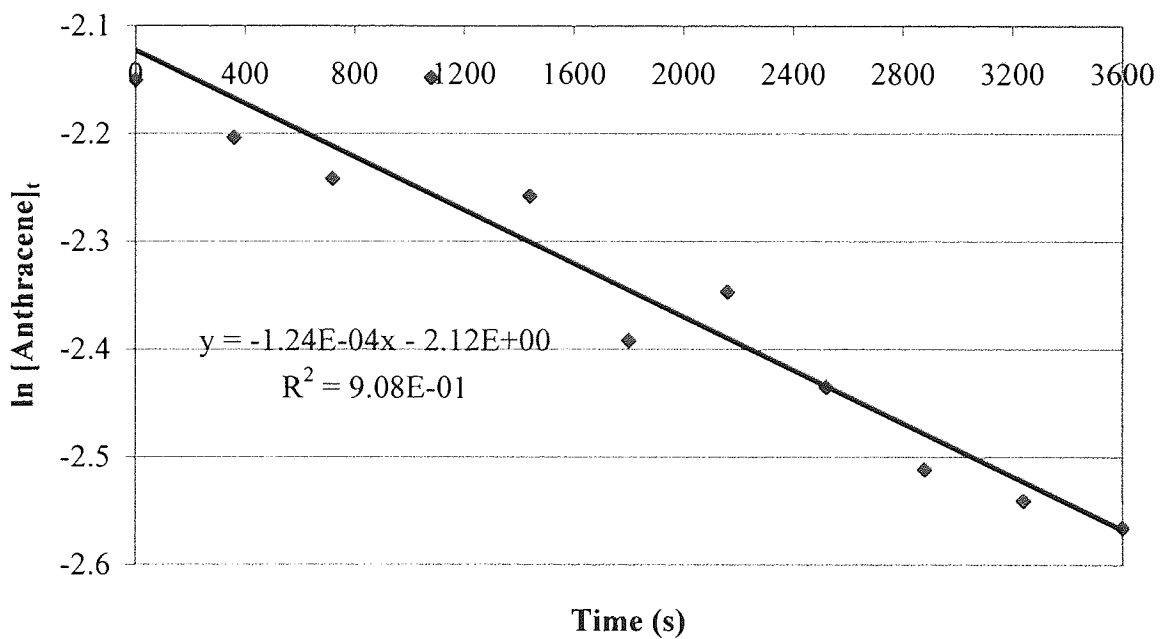




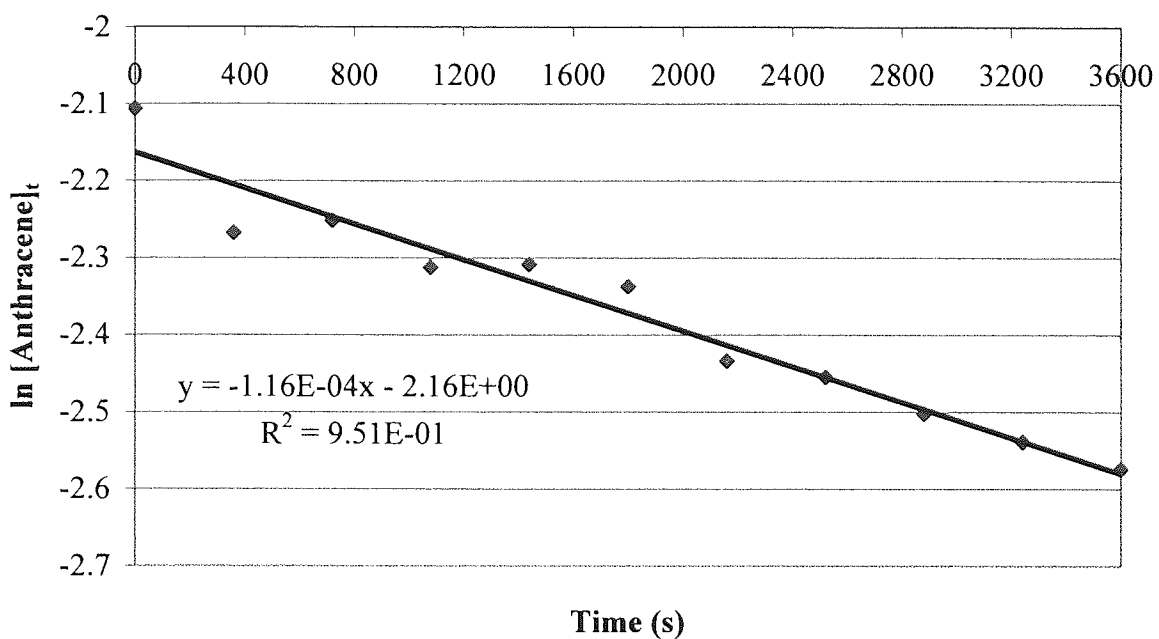
**The Thermal Diels-Alder Reaction of Maleic Anhydride with Anthracene in Toluene at 63.9°C**



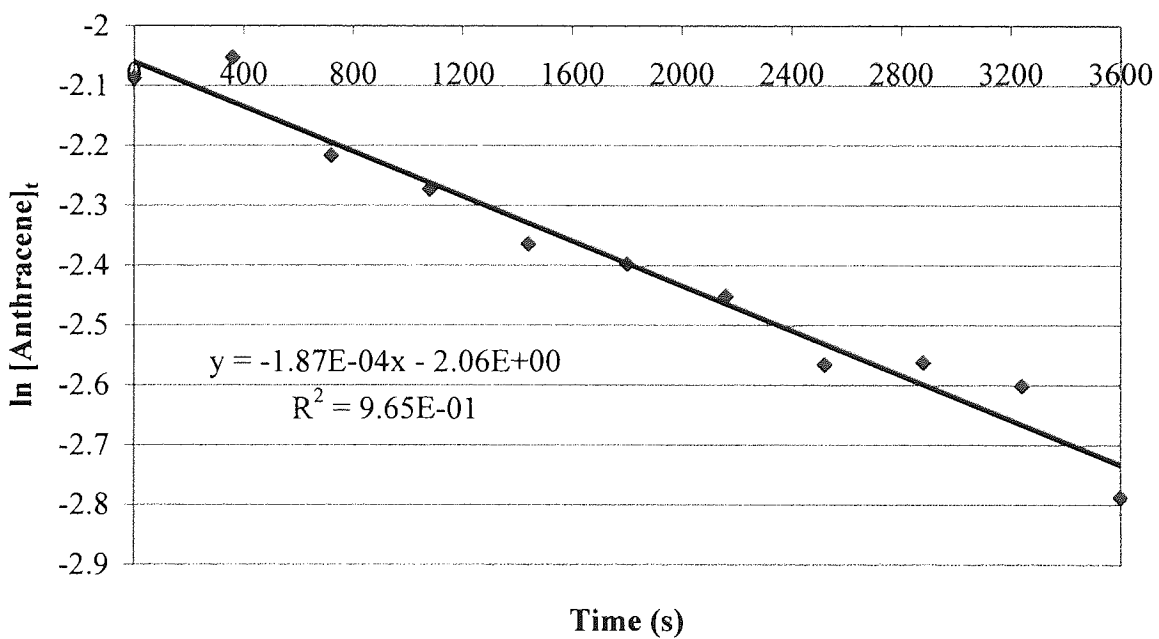
**The Thermal Diels-Alder Reaction of Maleic Anhydride with Anthracene in Toluene at 64.2°C**



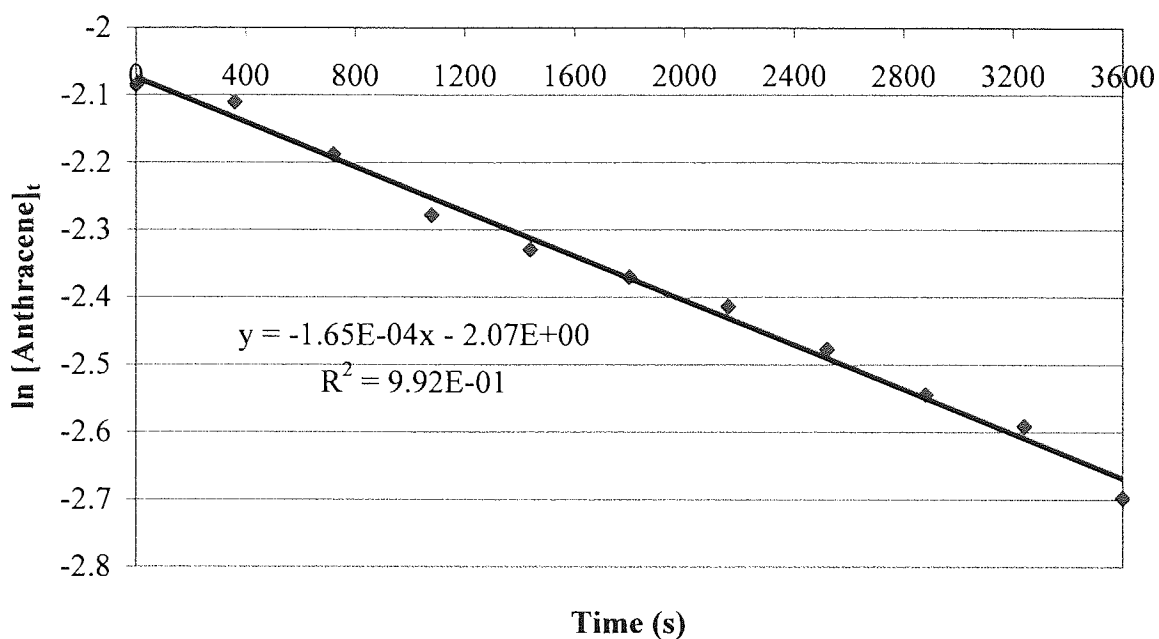
**The Thermal Diels-Alder Reaction of Maleic Anhydride with Anthracene in Toluene at 64.3°C**



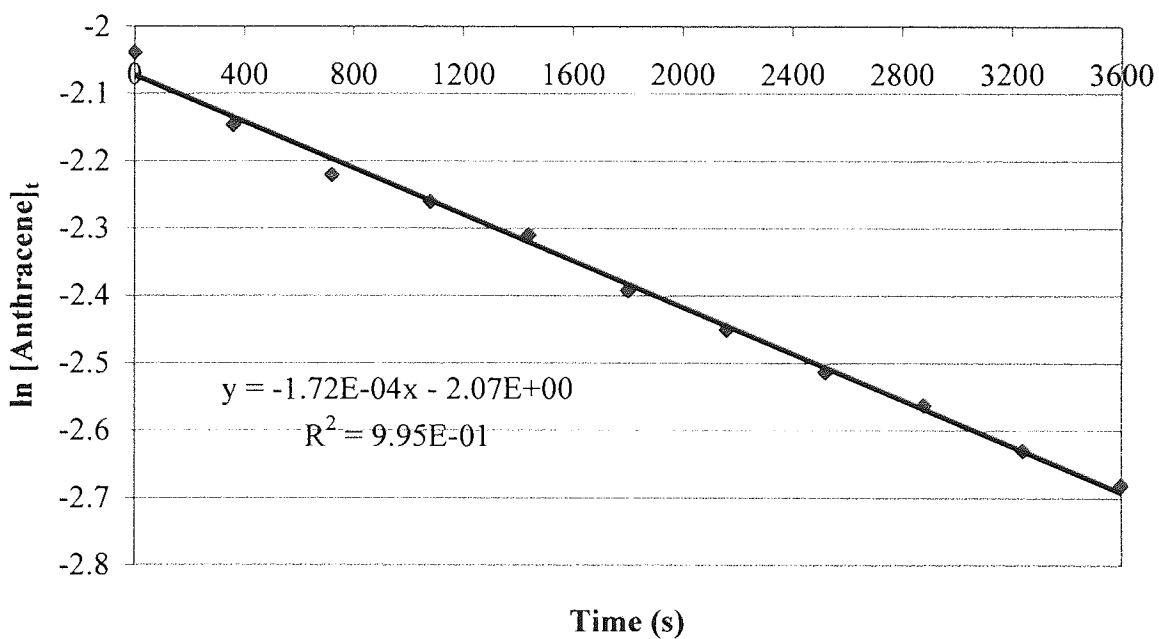
**The Thermal Diels-Alder Reaction of Maleic Anhydride with Anthracene in Toluene at 69.2°C**



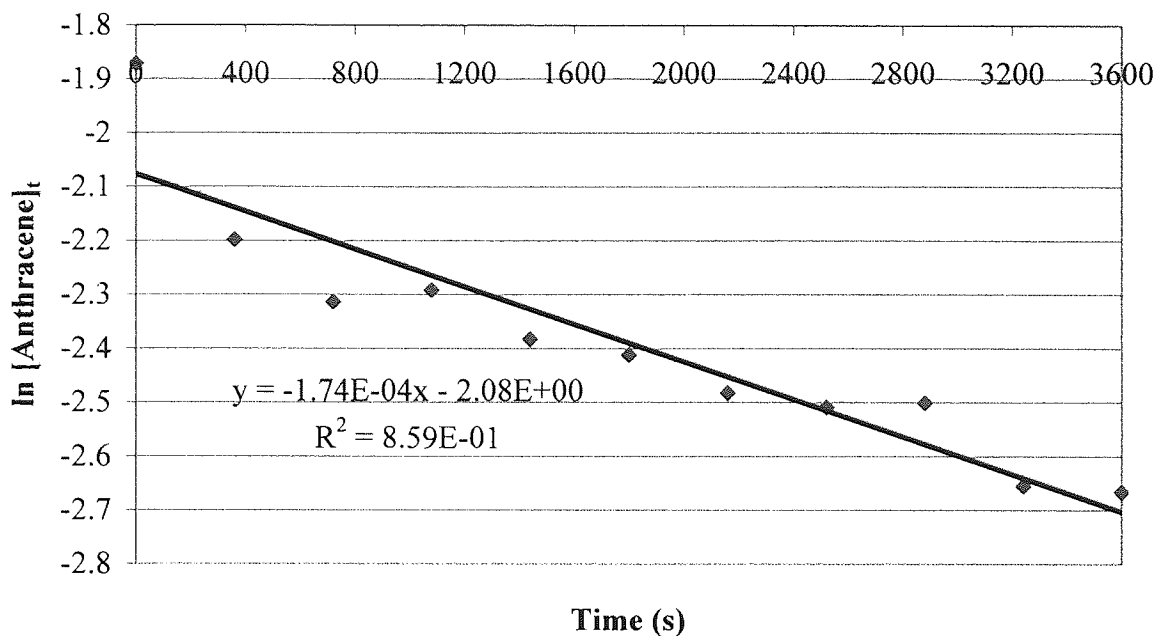
The Thermal Diels-Alder Reaction of Maleic Anhydride with Anthracene in Toluene at 68.6°C



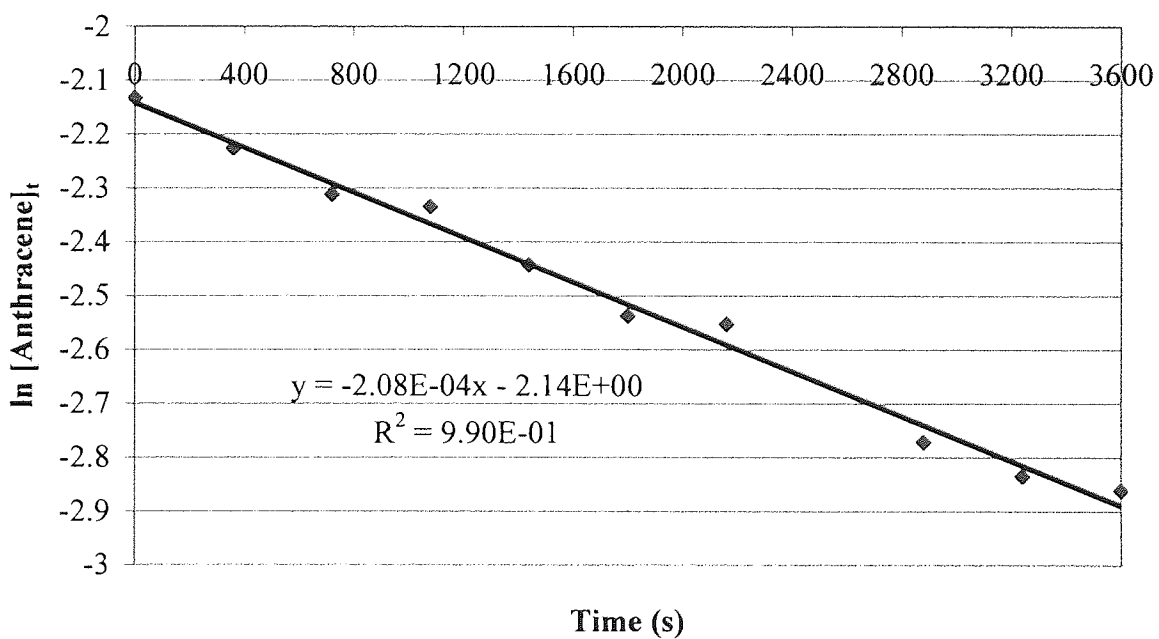
The Thermal Diels-Alder Reaction of Maleic Anhydride with Anthracene in Toluene at 69.1°C



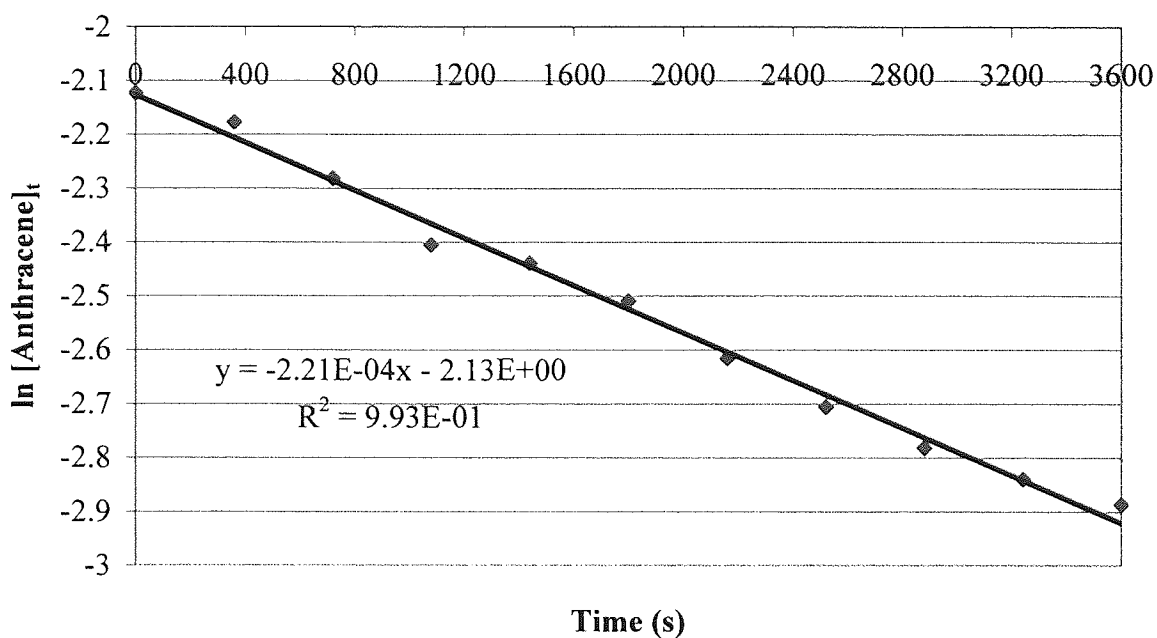
The Thermal Diels-Alder Reaction of Maleic Anhydride with Anthracene in Toluene at 69.5°C



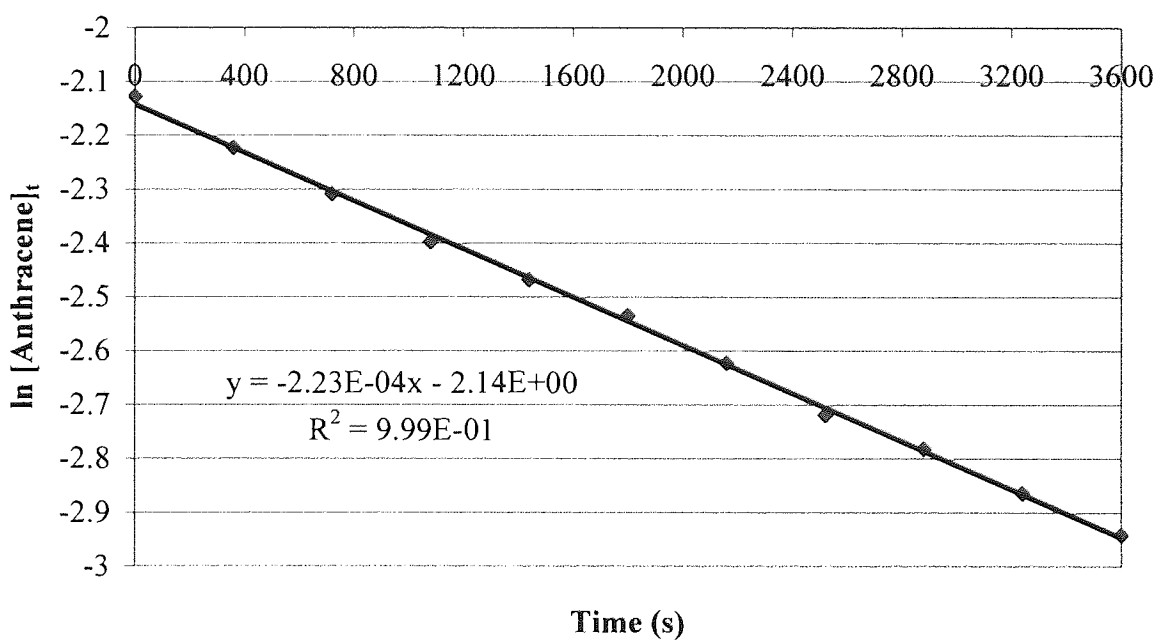
The Thermal Diels-Alder Reaction of Maleic Anhydride with Anthracene in Toluene at 73.5°C



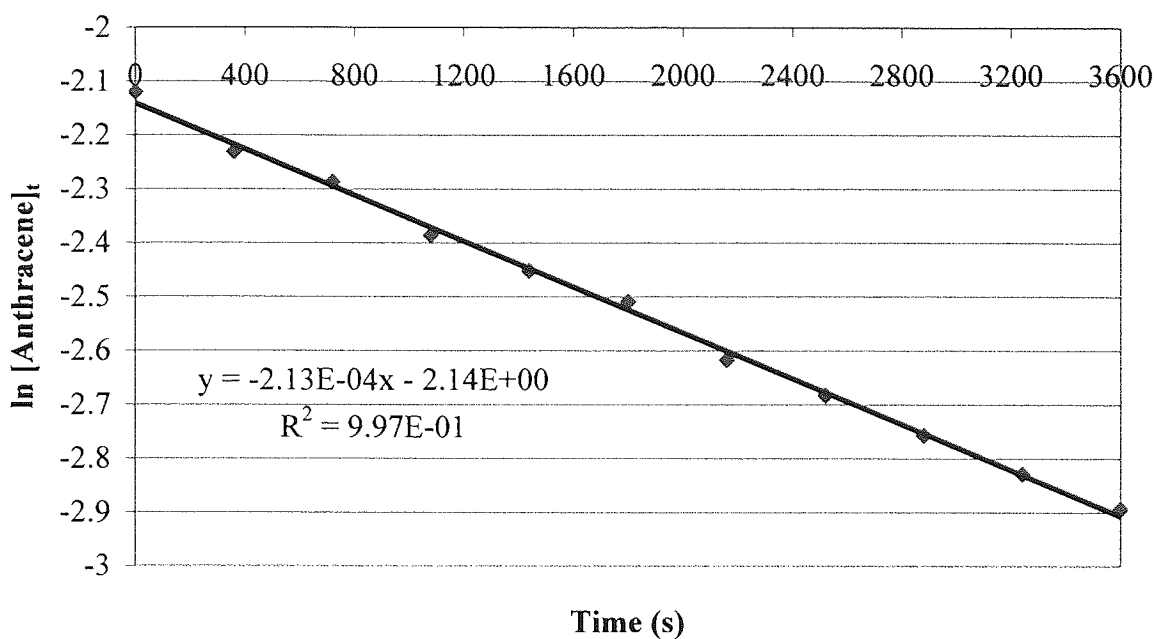
**The Thermal Diels-Alder Reaction of Maleic Anhydride with Anthracene in Toluene at 73.5°C**



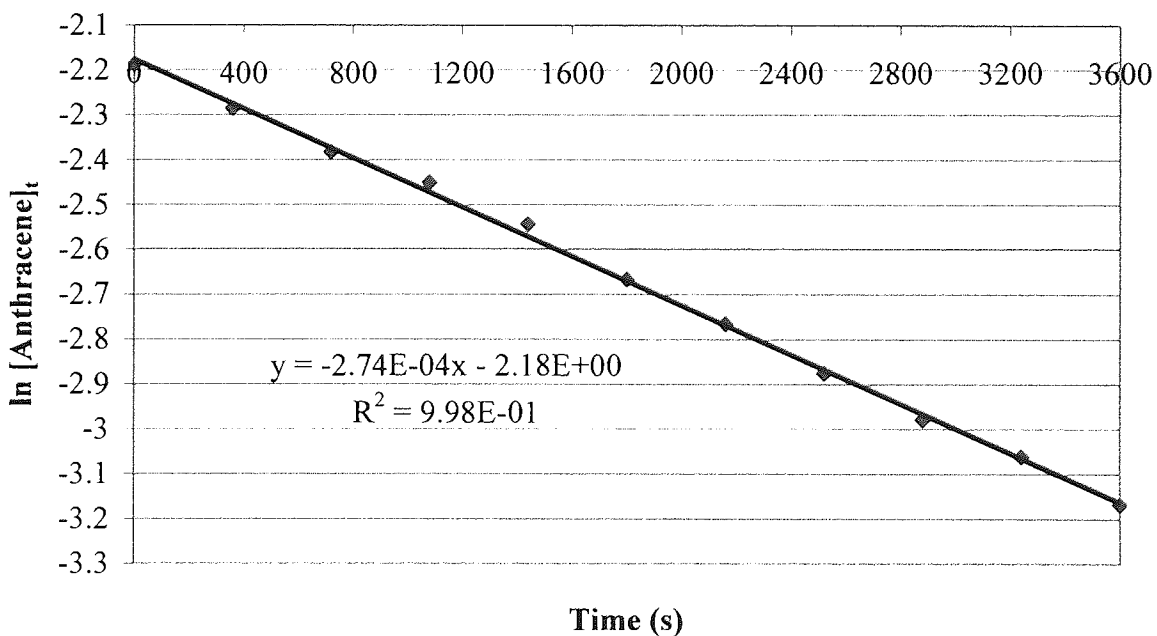
**The Thermal Diels-Alder Reaction of Maleic Anhydride with Anthracene in Toluene at 73.3°C**



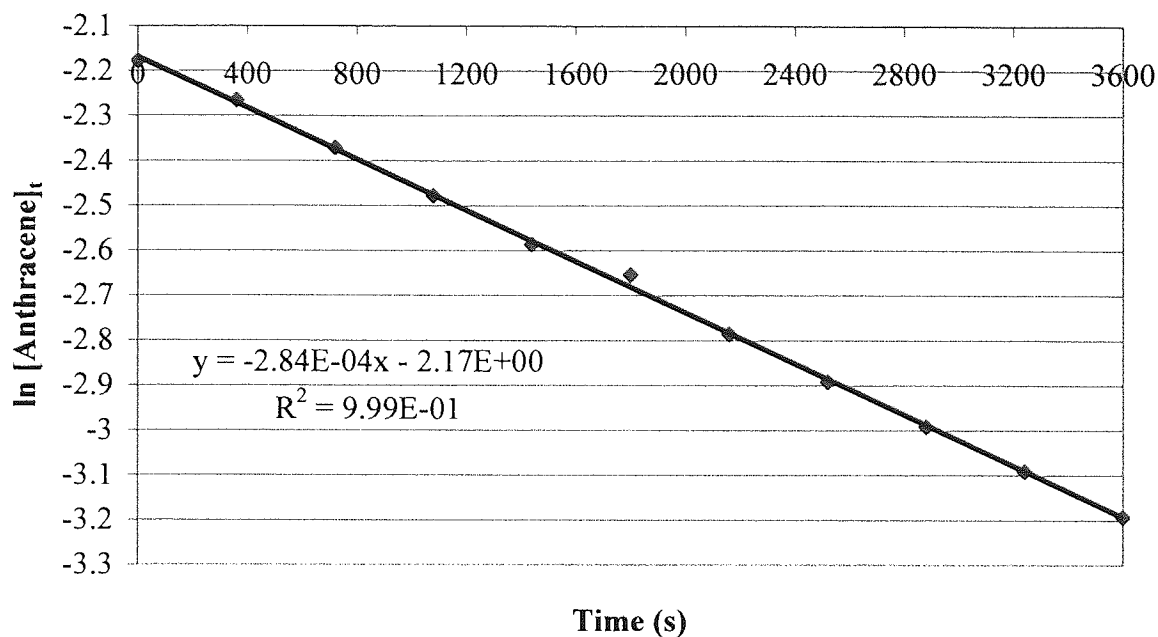
The Thermal Diels-Alder Reaction of Maleic Anhydride with Anthracene in Toluene at 73.4°C



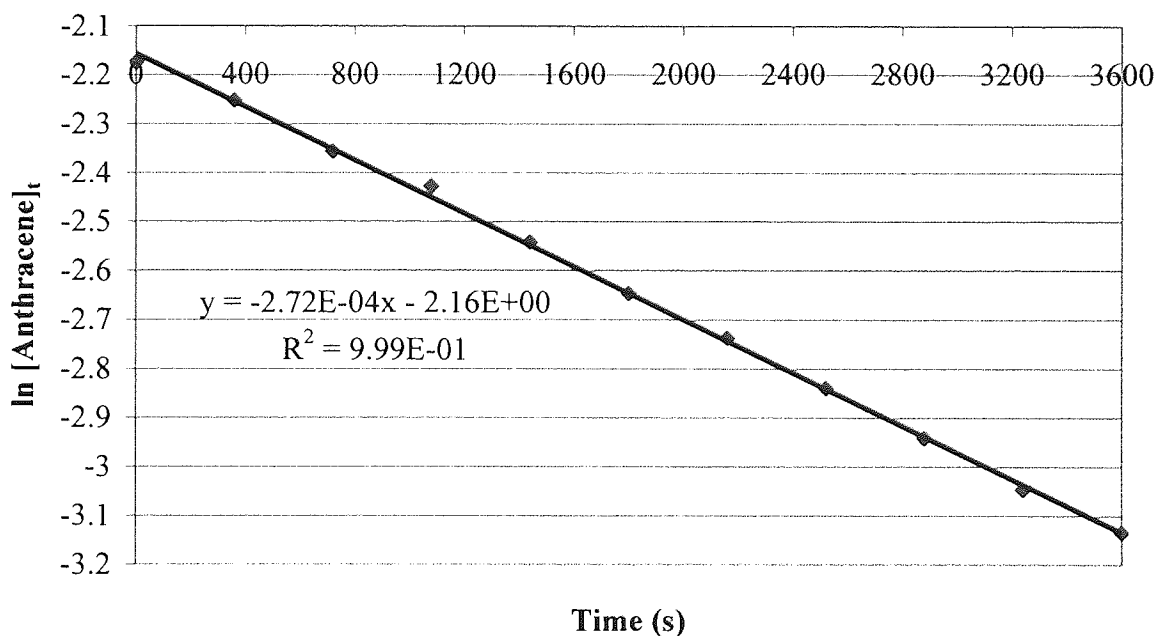
The Thermal Diels-Alder Reaction of Maleic Anhydride with Anthracene in Toluene at 78.4°C



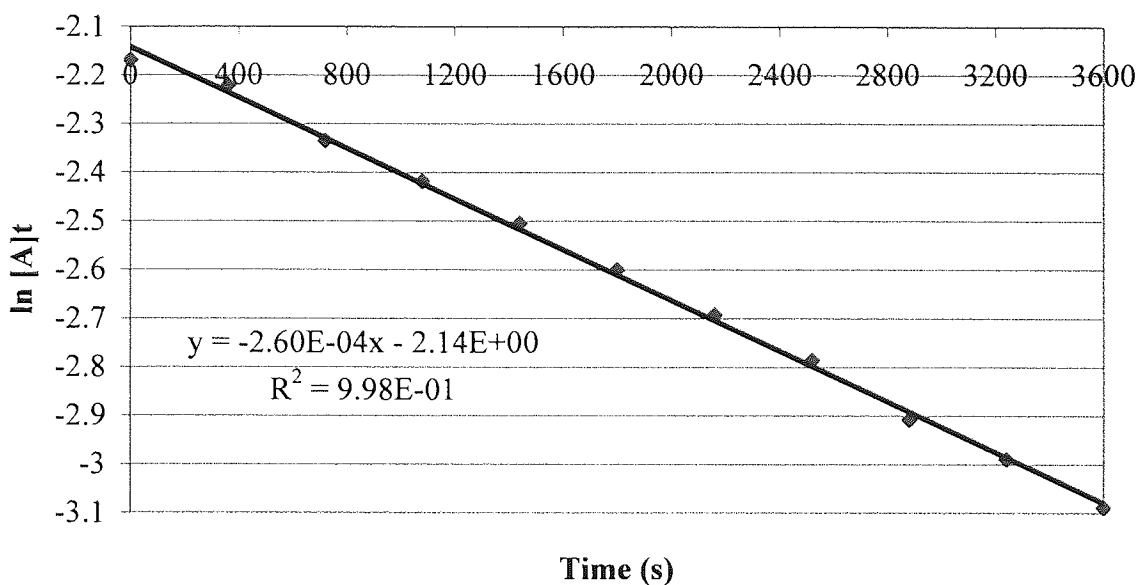
The Thermal Diels-Alder Reaction of Maleic Anhydride with Anthracene in Toluene at 78.1°C



The Thermal Diels-Alder Reaction of Maleic Anhydride with Anthracene in Toluene at 79.1°C



The Thermal Diels-Alder Reaction of Maleic Anhydride with Anthracene in Toluene at 77.2°C









```

WHILE Active$ = "Active"
CALL MainMenu 'Main control Menu of options
WEND

```

```
'Data for t-table
```

```
DATA
```

```
1.00,0.816,.765,.741,.727,.718,.711,.706,.703,.700,.697,.695,.694,.692,.691,.690,.689,.688,
.688,.687,.674
```

```
DATA
```

```
6.34,2.92,2.35,2.13,2.02,1.94,1.90,1.86,1.83,1.81,1.80,1.78,1.77,1.76,1.75,1.75,1.74,1.73,1
.73,1.72,1.64
```

```
DATA
```

```
12.71,4.30,3.18,2.78,2.57,2.45,2.36,2.31,2.26,2.23,2.20,2.18,2.16,2.14,2.13,2.12,2.11,2.10,
2.09,2.09,1.96
```

```
DATA
```

```
31.82,6.96,4.54,3.75,3.36,3.14,3.00,2.90,2.82,2.76,2.72,2.68,2.65,2.62,2.60,2.58,2.57,2.55,
2.54,2.53,2.33 187
```

```
DATA
```

```
63.66,9.92,5.84,4.60,4.03,3.71,3.50,3.36,3.25,3.17,3.11,3.06,3.01,2.98,2.95,2.92,2.90,2.88,
2.86,2.84,2.58
```

```
END 'of main body of LMS program
```

```

*****
*****

```

```
SUB AddLine
```

```
REM - ADD A NEW LINE of data
```

```
N = N + 1
```

```
LOCATE 23, 8: PRINT "Type in X value, then press [Enter]";
```

```
INPUT x$
```

```
x(N) = VAL(x$)
```

```
LOCATE 23, 8: PRINT "Now the Y value, then press [Enter]";
```

```
INPUT y$
```

```
y(N) = VAL(y$)
```

```
IF (x$ = "" OR y$ = "") THEN N = N - 1: EXIT SUB
```

```
IF (x$ <> "" AND y$ <> "") THEN CalcFlag$ = "Not Done": PrintFlag$ = "Disabled"
```

```
END SUB
```

```
SUB CentreString (msg$, linelength%)
```

```
' Centres message string passed in a line of length passed.
```

```
SPaCe% = (linelength% - LEN(msg$)) / 2
```

```
LOCATE CSRLIN, SPaCe%: PRINT msg$
```

END SUB

SUB ChooseAxes

```
SHARED xstart, xend, ystart, yend
SHARED xdivs%, ydivs%
fullscreen% = 80
margin% = 10
```

```
COLOR 14, 1: CLS          ' 14 = yellow text: 1 = blue background
PRINT STRING$(fullscreen%, CHR$(196))
LOCATE CSRLIN - 1, 1: CALL CentreString(" CHOOSE AXES ", fullscreen%)
```

```
LOCATE CSRLIN + 2, margin%:
PRINT "Type a new value, or press `Enter` to keep current value..."
LOCATE CSRLIN + 2, margin%:
PRINT "Start of x axis ["; xstart; "]: "; : INPUT ans$
IF (ans$ <> "") THEN xstart = VAL(ans$)
LOCATE CSRLIN + 1, margin%:
PRINT "End of x axis ["; xend; "]: "; : INPUT ans$
IF (ans$ <> "") THEN xend = VAL(ans$)
LOCATE CSRLIN + 1, margin%:
PRINT "Divisions on x axis ["; xdivs%; "]: "; : INPUT ans$
IF (ans$ <> "") THEN xdivs% = VAL(ans$)
```

```
LOCATE CSRLIN + 1, margin%:
PRINT "Start of y axis ["; ystart; "]: "; : INPUT ans$
IF (ans$ <> "") THEN ystart = VAL(ans$)
LOCATE CSRLIN + 1, margin%:
PRINT "End of y axis ["; yend; "]: "; : INPUT ans$
IF (ans$ <> "") THEN yend = VAL(ans$)
LOCATE CSRLIN + 1, margin%:
PRINT "Divisions on y axis ["; ydivs%; "]: "; : INPUT ans$
IF (ans$ <> "") THEN ydivs% = VAL(ans$)
```

END SUB

SUB ClearKeyboard

' Removes any characters in the keyboard buffer.

```
key$ = INKEY$
DO WHILE (key$ <> "")
  key$ = INKEY$
LOOP
```

END SUB

## SUB DataEditor

```
1330 REM **** SUBROUTINE TO CHECK DATA ARE CORRECT & ALTER IF
NECESSARY"
1340 REM PRINT : PRINT TAB(15); "ARE THESE DATA VALUES CORRECT ?
(Y/N) ";

1360 A4 = 15: REM - A4 EQUALS NO. LINES ON VDU

1390 COLOR 14, 0: CLS : LOCATE 3, 20: COLOR 14, 4: PRINT "Data Editor - ":
COLOR 14, 0
1395 PRINT
1400 LOCATE 5, 15: PRINT " LINE NUMBER "; : PRINT TAB(35); " X VALUE"; :
PRINT TAB(48); " Y VALUE ";
1410 FOR i = 1 TO N
1420 PRINT TAB(20); i; : PRINT TAB(35); x(i); : PRINT TAB(48); y(i)
1430 IF INT(i / (A4 - 1)) * (A4 - 1) <> i THEN 1470
1440 PRINT "PRESS [Enter] FOR REST OF DATA & MENU";
1450 k$ = INKEY$: IF k$ = "" THEN 1450
1470 NEXT i: COLOR 14, 4
1480 LOCATE 19, 15: PRINT "  R  TO REPLACE, ";
1510 IF N = 100 THEN 1560
1520 LOCATE 20, 15: PRINT "  A  TO ADD,  ";
1550 IF N = 1 THEN 1590
1560 LOCATE 21, 15: PRINT "  D  TO DELETE, ";
1590 LOCATE 22, 15: PRINT "  L  TO LIST,  ";
1620 LOCATE 23, 15: PRINT "OR C  TO CONTINUE ";
1650 Q$ = INKEY$: IF Q$ = "" THEN 1650
1660 IF Q$ = "R" OR Q$ = "r" THEN CALL ReplaceLine
1670 IF N = 100 THEN 1700
1680 IF Q$ = "A" OR Q$ = "a" THEN CALL AddLine
1690 IF N = 1 THEN 1710
1700 IF Q$ = "D" OR Q$ = "d" THEN CALL DeleteLine
1710 IF Q$ = "L" OR Q$ = "l" THEN 1390
1720 IF Q$ = "C" OR Q$ = "c" THEN EXIT SUB
1730 FOR TD = 1 TO 1000: NEXT TD
1740 GOTO 1390
END SUB
```

## SUB DeleteLine

```
REM - DELETE A LINE of data
```

```
LOCATE 23, 10: PRINT TAB(16); "Type LINENUMBER to be deleted";

INPUT J$
J = VAL(J$)
IF J < 1 OR J > N THEN
```

```

LOCATE 23, 1: PRINT "Must be 1 - "; N; " Press a key to continue ";
k$ = ""
WHILE k$ = ""
k$ = INKEY$
WEND
EXIT SUB
END IF

```

```

IF J = 1 AND N = 1 THEN N = 0: DataFlag$ = "No Data": CalcFlag$ = "Not Done":
EXIT SUB

```

```

2000 FOR i = J + 1 TO N
2010 x(i - 1) = x(i)
2020 y(i - 1) = y(i)
2030 NEXT i
2040 N = N - 1
2050
CalcFlag$ = "Not Done"
PrintFlag$ = "Disabled"

```

```

END SUB

```

```

SUB DrawFrame

```

```

SHARED backcol%, framecol%, plotcol%
SHARED Xaxis$, Yaxis$, Comment$
SHARED MaxX%, MaxY%, GX1%, GY1%, GX2%, GY2%
SHARED xstart, xend, ystart, yend
SHARED xdivs%, ydivs%
SHARED mx, cx, my, cy
SHARED funcname1$, funcname2$
SHARED Pressure
dottedline% = &H1111 ' dotted line pattern

```

```

CLS 1

```

```

LINE (1, 1)-(MaxX% - 1, MaxY% - 1), backcol%, BF
LINE (0, 0)-(MaxX%, MaxY%), framecol%, B
LINE (2, 2)-(MaxX% - 2, MaxY% - 2), framecol%, B

```

```

LINE (GX1%, GY1%)-(GX2%, GY2%), , B ' draw graph frame
xstep! = (GX2% - GX1%) / xdivs% ' do dotted x divisions
FOR i = 1 TO xdivs% - 1
LINE (GX1% + i * xstep!, GY1%)-(GX1% + i * xstep!, GY2%), , , dottedline%
NEXT i
ystep! = (GY2% - GY1%) / ydivs% ' do dotted y divisions
FOR i = 1 TO ydivs% - 1
LINE (GX1%, GY1% + i * ystep!)-(GX2%, GY1% + i * ystep!), , , dottedline%
NEXT i

```

```

                ' Now label the axes.....
singlerow = MaxY% / 30
singlecol = MaxX% / 80
COLOR plotcol%:
row = GY1% / singlerow - 1: col = 1 + GX1% / singlecol
LOCATE row, col - 7: COLOR plotcol% + 1: PRINT Yaxis$; : PRINT " "; Comment$; :
COLOR plotcol%
row = 3 + GY2% / singlerow: col = .5 + (GX1% + GX2%) / (2 * singlecol)
LOCATE row, col: PRINT Xaxis$;
row = (GY2% + GY1%) / (2 * singlerow):
col = 1 + GX1% / (2 * singlecol)
REM LOCATE row, col: PRINT "Y"; : COLOR plotcol% + 1
row = 2 + GY2% / singlerow
col = GX1% / singlecol
LOCATE row, col: PRINT xstart
col = GX2% / singlecol - LEN(STR$(xend)) / 2
LOCATE row, col: PRINT xend
row = .5 + GY1% / singlerow
col = GX1% / singlecol - LEN(STR$(yend))
LOCATE row, col: PRINT yend
row = .5 + GY2% / singlerow
LOCATE row, col: PRINT ystart

```

```

                ' Now draw & label zero axes if on scale...
IF (xstart < 0) AND (xend > 0) THEN
  LINE (cx, GY1%)-(cx, GY2%)
  row = 2 + GY2% / singlerow: col = .5 + cx / singlecol
  LOCATE row, col: PRINT "0"
END IF
IF (ystart < 0) AND (yend > 0) THEN
  LINE (GX1%, cy)-(GX2%, cy)
  row = .5 + cy / singlerow: col = GX1% / singlecol - 1
  LOCATE row, col: PRINT "0"
END IF

```

END SUB

```

SUB EpsonVGA (left%, top%, right%, bottom%)
' Prints the region of the VGA graphics screen defined by (left, top)
' to (right, bottom) on 9-pin printer (only uses pins 1 to 8).
' Based on a routine by Ben Ezzell, "Graphics Programming in Turbo C++",
' page 273.
' Provides small image by using mode 1 (120 dots per inch across), and
' reading vertical pixels in pairs switching pin on if either pixel is on
' (i.e., not the background colour).
' This version was written 19th November 1993.

```

```

SHARED backcol%
DEFINT I-K
Mode% = 1                ' 120 dots per inch

CALL PrintHeader        ' print user name, date, etc.

Lsb% = 1 + (right% - left%) MOD 256
Msb% = (right% - left%) \ 256
setgraphicsmode$ = CHR$(27) + "*" + CHR$(Mode%) + CHR$(Lsb%) +
CHR$(Msb%)
WIDTH LPRINT 255        ' set printer line width
LPRINT CHR$(27) + "A" + CHR$(8)    ' sets line spacing to 8/72"

FOR J = top% TO bottom% - 1 STEP 16    ' in vertical steps of 16 pixels
  LPRINT setgraphicsmode$;    ' set each line to graphics
  FOR i = left% TO right%    ' scan across a line
    byte% = 0    ' initialise byte each time
    FOR k = 0 TO 15 STEP 2    ' read 16 pixels in pairs
      byte% = byte% * 2    ' always shift left one bit
      ' Switch bit on if EITHER screen pixel not background colour...
      IF (J + k + 1) <= bottom% THEN
        IF (POINT(i, J + k) <> backcol%) OR (POINT(i, J + k + 1) <> backcol%)
        THEN
          byte% = byte% + 1
        END IF
      END IF
    NEXT k
    IF (byte% = 26) THEN byte% = 28    ' replace "substitute" code
    LPRINT CHR$(byte%);    ' now print 8-bit pattern
  NEXT i
  LPRINT    ' start a new line
  IF (INKEY$ <> "") THEN EXIT SUB    ' stop printout with keypress
NEXT J
LPRINT CHR$(27) + CHR$(64)    ' resets printer (#64 = @)
WIDTH LPRINT 80    ' restore printer line width

```

END SUB

DEFSNG I-K

SUB FunctionPlot

```

' Program : based on PLOTTER.BAS (only uses original subroutines)
' Authors : M. S. Beevers (modifier) (original code by S. J. Moss)
' Date   : 23rd March 1995

```

```

' A sub program to plot a function on the VGA high-resolution
' graphics (640 x 480 pixels) screen in 16 colours:

```



```
' 0 = black 1 = blue 2 = green 3 = cyan 4 = red 5 = magenta
' 6 = brown 7 = dark grey 8 = light grey 9 = light blue
' 10 = light green 11 = light cyan 12 = light red
' 13 = light magenta 14 = yellow 15 = white
```

```
SHARED backcol%, framecol%, plotcol%
SHARED MaxX%, MaxY%, GX1%, GY1%, GX2%, GY2%
SHARED xstart, xend, ystart, yend
SHARED mx, cx, my, cy
SHARED Pressure
SHARED y1, S
singlerow = MaxY% / 30
singlecol = MaxX% / 80
```

```
COLOR 15, backcol%
SCREEN 12 ' High-resolution VGA screen (640 x 480)
CALL GetScaleFactors
CALL DrawFrame
```

```
' Now plot the function.....
xstep! = (xend - xstart) / (GX2% - GX1%)
x = xstart + xstep
FOR i = 1 TO N '
  x = x(i): y = y(i)' get x,y experimental values
  xp = mx * x + cx ' convert to screen position
  yp = my * y + cy ' convert to screen position
  ' now plot point if on screen...
  IF (yp > GY1%) AND (yp < GY2%) THEN PSET (xp, yp), plotcol%
  IF (yp + 1 > GY1%) AND (yp + 1 < GY2%) THEN PSET (xp - 1, yp + 1), plotcol%
  IF (yp + 1 > GY1%) AND (yp + 1 < GY2%) THEN PSET (xp, yp + 1), plotcol%
  IF (yp + 1 > GY1%) AND (yp + 1 < GY2%) THEN PSET (xp + 1, yp + 1), plotcol%
  IF (yp > GY1%) AND (yp < GY2%) THEN PSET (xp - 1, yp), plotcol%
  IF (yp > GY1%) AND (yp < GY2%) THEN PSET (xp + 1, yp), plotcol%
  IF (yp - 1 > GY1%) AND (yp - 1 < GY2%) THEN PSET (xp - 1, yp - 1), plotcol%
  IF (yp - 1 > GY1%) AND (yp - 1 < GY2%) THEN PSET (xp, yp - 1), plotcol%
  IF (yp - 1 > GY1%) AND (yp - 1 < GY2%) THEN PSET (xp + 1, yp - 1), plotcol%

  REM x = x + xstep
NEXT i
```

```
IF LMSFlag$ = "yes" THEN
  x2 = xstart + xstep:
  FOR i = GX1% + 1 TO GX2% - 1 ' plot at every pixel along x axis
    y2 = S * x2 + y1 ' calculate function
    xp2 = mx * x2 + cx ' convert to screen position
    yp2 = my * y2 + cy ' convert to screen position
    ' now plot point if on screen...
    IF (yp2 > GY1%) AND (yp2 < GY2%) THEN PSET (xp2, yp2), plotcol% + 1
```

```

    x2 = x2 + xstep
NEXT i
END IF

```

```

COLOR 12
row = MaxY% / singlerow - 1: col = GX1% / singlecol
msg$ = "Press `P' to print screen, or another key for Menu..."
LOCATE row, col:
PRINT msg$;
key$ = INPUT$(1)
IF (key$ = "P") OR (key$ = "p") THEN
    LOCATE row, col
    PRINT SPACES$(LEN(msg$));
    BEEP
    msg$ = "Set printer, then press a key..."
    LOCATE row, col
    PRINT msg$;
    key$ = INPUT$(1)
    LOCATE row, col
    PRINT SPACES$(LEN(msg$));
    CALL EpsonVGA(0, 0, MaxX%, MaxY%)      ' print full graphics screen
    LOCATE row, col
    PRINT "Press a key for Menu...";
    key$ = INPUT$(1)
END IF

```

```

SCREEN 0
END SUB

```

```

SUB GetScaleFactors

```

```

    SHARED GX1%, GY1%, GX2%, GY2%
    SHARED xstart, xend, ystart, yend
    SHARED mx, cx, my, cy

    mx = CSNG(GX2% - GX1%) / (xend - xstart)
    cx = GX1% - mx * xstart
    my = CSNG(GY1% - GY2%) / (yend - ystart)
    cy = GY1% - my * yend

```

```

END SUB

```

```

SUB HELP

```

```

COLOR 14, 0: CLS : COLOR 14, 1: LOCATE 5, 16: PRINT " Type X & Y values (X
value first) separated by "
LOCATE 7, 16: PRINT " a comma, followed by the [Enter] key.      ":
LOCATE 9, 16: PRINT " Then type in the next pair of values, etc.  "

```

```

LOCATE 11, 16: PRINT " You can edit the data at any stage, in order to "
LOCATE 13, 16: PRINT " - correct an incorrect data entry "
LOCATE 15, 16: PRINT " - delete data that is obviously 'bad' "
LOCATE 17, 23: COLOR 14, 4: PRINT " Press any key to continue "; : COLOR 14, 0
WHILE k$ = ""
k$ = INKEY$
WEND
END SUB

```

#### SUB InitialiseTable

```
' data for t-table (see DATA statements at end of main program)
```

```

FOR J = 1 TO 5
FOR i = 1 TO 21
READ ST(i, J)
NEXT
NEXT

```

```
END SUB
```

#### SUB InputData

```
COLOR 14, 0: CLS : COLOR 14, 4
```

```
LOCATE 10, 20: COLOR 14, 1: PRINT " How many pairs of data (Max = 100) "; :
COLOR 14, 4: INPUT N$: PRINT : COLOR 14, 1
```

```
IF VAL(N$) = 0 THEN CLS : EXIT SUB
```

```
IF VAL(N$) < 3 THEN EXIT SUB
```

```
N = VAL(N$)
```

```
COLOR 0, 6
```

```
FOR i = 1 TO N
```

```
PRINT
```

```
LOCATE 12, 20: COLOR 0, 0: PRINT SPC(50);
```

```
LOCATE 12, 20: COLOR 14, 1: PRINT " X,Y for data pair No."; i; : COLOR 14, 4:
```

```
INPUT x(i), y(i): COLOR 14, 1
```

```
NEXT i
```

```
DataFlag$ = "Data Present"
```

```
CalcFlag$ = "Not Done"
```

```
PrintFlag$ = "Disabled"
```

```
END SUB
```

#### SUB InputYesNoCheck

```
1230 REM *** SUBROUTINE TO CHECK REPLIES ***
```

```
flag$ = "": Q$ = ""
```

```
WHILE flag$ = ""
```

```
Q$ = INKEY$
```

```
IF Q$ = "Y" OR Q$ = "y" THEN Q$ = "Y": flag$ = "1": EXIT SUB
```

```

IF Q$ = "N" OR Q$ = "n" THEN Q$ = "N": flag$ = "1": EXIT SUB

WEND
END SUB

SUB LMS
  SHARED N
  IF N < 3 THEN EXIT SUB

  REM *** SUBROUTINE TO CALCULATE LMS ***

  850 REM - ARRAYS X & Y CONTAIN N DATA POINTS
  860 REM - CALC. SUM OF X VALUES & SUM OF Y VALUES

  REM - SET INITIAL VALUES TO ZERO

  C = 1: S2 = 0: S3 = 0: x2 = 0: y2 = 0: S4 = 0: E2 = 0

  870 FOR i = 1 TO N
  880 S2 = S2 + x(i)
  890 S3 = S3 + y(i)
  900 NEXT i
  910 REM - CALC. AVERAGE X & AVERAGE Y
  920 A1 = S2 / N
  930 A2 = S3 / N
  935 SX = 0
  940 FOR i = 1 TO N
  950 X9 = x(i) - A1
  960 Y9 = y(i) - A2
  970 x2 = x2 + X9 * X9
  980 y2 = y2 + Y9 * Y9
  990 S4 = S4 + X9 * Y9
  992 SX = SX + (A1 - x(i)) * (A1 - x(i))
  1000 NEXT i
  1010 PRINT
  1020 IF x2 <> 0 THEN 1070
  1030 PRINT "  RUN ABANDONED BECAUSE ALL OF THE "
  1040 PRINT "  X-COORDINATES ARE THE SAME ! ":
    PRINT : PRINT : PRINT TAB(10); "Any key to continue";
    k$ = ""
    WHILE k$ = ""
    k$ = INKEY$
    WEND
  1050 EXIT SUB
  1060 REM - CALC. THE SLOPE"
  1070 S = S4 / x2
  1080 REM - CALC. INTERCEPT ON Y-AXIS & X-AXIS
  1090 y1 = (x2 * S3 - S2 * S4) / (N * x2)

```

```

1095 XI = -y1 / S
1100 IF y2 = 0 THEN 1140
1110 REM CALC. CORRELATION COEFFICIENT
1120 C = S4 / SQR(x2 * y2)
1130 REM - CALC. SUM OF ERRORS SQUARED
1140 FOR i = 1 TO N
1150 E1 = (y(i) - A2) - S * (x(i) - A1)
1160 E2 = E2 + E1 * E1
1170 NEXT i
1180 REM - CALC. STANDARD DEVIATION
1190 S1 = SQR(E2 / (N - 2)): EY = S1 * SQR((1 / N) + (A1 * A1) / SX): ES = S1 /
SQR(SX)
1195 EX = (S1 / SQR(S * S)) * SQR(1 + (1 / N) + (A2 * A2) / (S * S * SX))
1200 IF N < 30 THEN 1220
1210 S1 = SQR(E2 / N)
1220 REM

```

```

CalcFlag$ = "Done"
PrintFlag$ = "Enabled"

```

```

END SUB

```

```

SUB MainMenu

```

```

COLOR 14, 0: CLS

```

```

COLOR 14, 4

```

```

LOCATE 1, 8

```

```

PRINT " Linear Regression Analysis - Gradient plus both intercepts ": COLOR 14, 0

```

```

PRINT

```

```

"

```

---

```

____": COLOR 14, 1

```

```

LOCATE 4, 12: PRINT " [D/T] D=Input your Data T=Example data "; : COLOR 14, 4:

```

```

PRINT " < "; DataFlag$; " > "; : COLOR 14, 1

```

```

LOCATE 6, 12: PRINT " [N] Name & Axis Labels / Comment "

```

```

LOCATE 8, 21: COLOR 15, 4: PRINT " "; username$; " "; Xaxis$; " "; Yaxis$; " ";

```

```

LOCATE 9, 21: PRINT " "; Comment$; " "; : COLOR 14, 1

```

```

LOCATE 11, 12: PRINT " [E] Edit current data "; : COLOR 14, 4: PRINT " < ";

```

```

DataFlag$; " > "; : COLOR 14, 1

```

```

LOCATE 13, 12: PRINT " [V] View current results "; : COLOR 14, 4: PRINT " < ";

```

```

PrintFlag$; " > "; : COLOR 14, 1

```

```

LOCATE 15, 12: PRINT " [C] Calculate/view results "; : COLOR 14, 4: PRINT " < ";

```

```

CalcFlag$; " > "; : COLOR 14, 1

```

```

LOCATE 17, 12: PRINT " [G/O] View/Print Graph G=points+line O=points only "; :

```

```

COLOR 14, 4: PRINT " < "; PrintFlag$; " > "; : COLOR 14, 1

```

```

LOCATE 19, 12: PRINT " [P] Print results "; : COLOR 14, 4: PRINT " < "; PrintFlag$;

```

```

" > "; : COLOR 14, 1

```

```

LOCATE 21, 12: PRINT " [H] Help - data input format ";

```

```

LOCATE 23, 12: COLOR 14, 4: PRINT " [Q] Quit the program ( Reversible ! ) ";

```

```

k$ = "": Choice$ = ""

```

```

WHILE k$ = "" AND Choice$ = ""
k$ = INKEY$
IF k$ = "D" OR k$ = "d" THEN Choice$ = "D"
IF k$ = "T" OR k$ = "t" THEN Choice$ = "T"
IF k$ = "N" OR k$ = "n" THEN Choice$ = "N"
IF (k$ = "E" OR k$ = "e") AND DataFlag$ = "Data Present" THEN Choice$ = "E"
IF (k$ = "V" OR k$ = "v") AND CalcFlag$ = "Done" THEN Choice$ = "V"
IF (k$ = "C" OR k$ = "c") AND DataFlag$ = "Data Present" THEN Choice$ = "C"
IF (k$ = "G" OR k$ = "g") AND CalcFlag$ = "Done" THEN Choice$ = "G": LMSFlag$ =
"yes"
IF (k$ = "O" OR k$ = "o") AND CalcFlag$ = "Done" THEN Choice$ = "G": LMSFlag$ =
"no"
IF (k$ = "P" OR k$ = "p") AND CalcFlag$ = "Done" THEN Choice$ = "P"
IF k$ = "H" OR k$ = "h" THEN Choice$ = "H"
IF k$ = "Q" OR k$ = "q" THEN Choice$ = "Q"
WEND

```

```

IF Choice$ = "D" THEN CALL InputData: CALL MinMaxXandY
IF Choice$ = "T" THEN CALL TestData: CALL MinMaxXandY
IF Choice$ = "N" THEN CALL NamesLabels
IF Choice$ = "E" THEN CALL DataEditor: CALL MinMaxXandY
IF Choice$ = "V" THEN CALL OutputToScreen
IF Choice$ = "G" THEN CALL FunctionPlot
IF Choice$ = "C" THEN CALL LMS: CALL OutputToScreen
IF Choice$ = "P" THEN CALL OutputToPrinter
IF Choice$ = "H" THEN CALL HELP
IF Choice$ = "Q" THEN CALL Quit

```

END SUB

SUB MinMaxXandY

SHARED MinX, MaxX, MinY, MaxY, xstart, xend, ystart, yend, N

'find minimum and maximum values in the experimental data

MinX = x(1): MaxX = x(N): MinY = y(1): MaxY = y(N)

FOR i = 1 TO N

IF x(i) < MinX THEN MinX = x(i)

IF x(i) > MaxX THEN MaxX = x(i)

IF y(i) < MinY THEN MinY = y(i)

IF y(i) > MaxY THEN MaxY = y(i)

NEXT i

xstart = MinX: xend = MaxX

ystart = MinY: yend = MaxY

END SUB

## SUB NamesLabels

```
SHARED Xaxis$, Yaxis$, username$, Comment$
CLS
LOCATE 8, 5
PRINT "Your name ?(Press [Enter] to accept) "
LOCATE 10, 7: PRINT "<"; username$; " > "; : INPUT k$
IF k$ <> "" THEN username$ = k$
CLS
LOCATE 8, 5
PRINT "Enter a brief comment ? (Press [Enter] to accept) "
LOCATE 10, 7: PRINT "<"; Comment$; " > "
LOCATE 12, 7: INPUT k$
IF k$ <> "" THEN Comment$ = LEFT$(k$, 45)
CLS
LOCATE 8, 5
PRINT "Enter label for x-axis ? (Press [Enter] to accept)"
LOCATE 10, 7: PRINT "<"; Xaxis$; " > "; : INPUT k$
IF k$ <> "" THEN Xaxis$ = LEFT$(k$, 25)
CLS
LOCATE 8, 5
PRINT "Enter label for y-axis? (Press [Enter] to accept) "
LOCATE 10, 7: PRINT "<"; Yaxis$; " > "; : INPUT k$
IF k$ <> "" THEN Yaxis$ = LEFT$(k$, 20)
```

END SUB

## SUB NoDataMessage

```
COLOR 0, 6
LOCATE 21, 8
PRINT "No data ! Press a key to continue";
k$ = ""
WHILE k$ = ""
k$ = INKEY$
WEND
LOCATE 21, 8
PRINT "          ";
```

END SUB

## SUB OutputToPrinter

```
5000 REM PRINTER ROUTINE
5020 CLS : PRINT
5030 PRINT TAB(20); "Send OUTPUT TO PRINTER ? (Y/N)";
5040 CALL InputYesNoCheck
5050 IF Q$ = "N" THEN EXIT SUB
```

```

5070 CLS : LOCATE 10, 3: PRINT "Put paper in EPSON printer (press ON-LINE button)
& then [Enter]"
k$ = ""
WHILE k$ = ""
  k$ = INKEY$
WEND
5390 CLS : LPRINT "  LEAST-MEAN-SQUARES ANALYSIS OF DATA:-"
5400 LPRINT
5410 LPRINT " GRADIENT = "; INT(1000 * S) / 1000
5415 LPRINT " GRADIENT ERROR = "; INT(1000 * ES) / 1000; " *T (=1 FOR 60%
CONFIDENCE)"
5420 LPRINT
5425 LPRINT " Y-AXIS INTERCEPT = "; INT(1000 * y1) / 1000
5427 LPRINT " Y-AXIS INTERCEPT ERROR = "; INT(1000 * EY) / 1000; " ( * T)"
5430 LPRINT : LPRINT " X-AXIS INTERCEPT = "; INT(1000 * XI) / 1000
5435 LPRINT " X-AXIS INTERCEPT ERROR = "; INT(1000 * EX) / 1000; " ( * T)"
5441 LPRINT : LPRINT "  VALUES OF T FOR CONFIDENCE LIMITS OF:-":
LPRINT TAB(5); "50%"; : LPRINT TAB(15); "90%"; : LPRINT TAB(25); "95%"; :
LPRINT TAB(35); "98%"; : LPRINT TAB(45); "99%"
5442 IF N - 2 <= 20 THEN LPRINT TAB(5); ST(N - 2, 1); : LPRINT TAB(15); ST(N - 2,
2); : LPRINT TAB(25); ST(N - 2, 3); : LPRINT TAB(35); ST(N - 2, 4); : LPRINT
TAB(45); ST(N - 2, 5)
5443 IF N - 2 > 20 THEN LPRINT TAB(5); ST(21, 1); : LPRINT TAB(15); ST(21, 2); :
LPRINT TAB(25); ST(21, 3); : LPRINT TAB(35); ST(21, 4); : LPRINT TAB(45); ST(21,
5)
5450 LPRINT : LPRINT " PEARSON'S CORRELATION COEFF. = "; INT(1000 * C) /
1000
5460 LPRINT
5470 LPRINT " STANDARD DEVIATION OF THE POINTS": LPRINT " FROM THE
BEST LINE = "; INT(1000 * S1) / 1000

5480 LPRINT
5490 PRINT : PRINT " Print calculated Y values & errors ? (Y/N)";
5500 CALL InputYesNoCheck
5510 IF Q$ = "N" THEN CLS : EXIT SUB
5520 REM - CALCULATE & PRINT ERROR FOR EACH DATA POINT
5525 REM
5530 LPRINT
5540 CLS : LPRINT " ERROR IN Y VALUE FOR EACH DATA POINT"
5545 LPRINT
5550 LPRINT TAB(5); "X"; : LPRINT TAB(17); "Y OBS."; : LPRINT TAB(27); " Y
CALC."; : LPRINT TAB(40); "ERROR"
5555 LPRINT
5560 FOR i = 1 TO N
5565 IF ((i - 1) / 10 - INT((i - 1) / 10)) < .05 AND i <> 1 THEN PRINT "PRESS [Enter]
FOR REST OF DATA & MENU"; : INPUT k$

```



```

5570 LPRINT TAB(5); INT(1000 * x(i)) / 1000; TAB(17); INT(1000 * y(i)) / 1000;
TAB(27); INT(1000 * (A2 + S * (x(i) - A1))) / 1000; TAB(40); INT(1000 * ((y(i) - A2) - S
* (x(i) - A1))) / 1000;
5580 NEXT i
5590 LPRINT : LPRINT : LPRINT " SUM OF ERRORS SQUARED = "; INT(1000 *
E2) / 1000: LPRINT
5595

END SUB

SUB OutputToScreen
SHARED N
IF N < 3 THEN EXIT SUB

6000 REM view results on screen
6390 LOCATE 1, 5: COLOR 14, 0: CLS : COLOR 14, 4: PRINT "  LEAST-MEAN-
SQUARES ANALYSIS OF DATA:-": COLOR 14, 1
6400 PRINT
6410 PRINT " GRADIENT = "; INT(1000 * S) / 1000
6415 PRINT " GRADIENT ERROR = "; INT(1000 * ES) / 1000; " (*T)"
6420 PRINT
6425 PRINT " Y-AXIS INTERCEPT = "; INT(1000 * y1) / 1000
6427 PRINT " Y-AXIS INTERCEPT ERROR = "; INT(1000 * EY) / 1000; " ( * T)"
6430 PRINT : PRINT " X-AXIS INTERCEPT = "; INT(1000 * XI) / 1000
6435 PRINT " X-AXIS INTERCEPT ERROR = "; INT(1000 * EX) / 1000; " ( * T)"
6441 PRINT : PRINT "  VALUES OF T FOR CONFIDENCE LIMITS OF:-": PRINT
TAB(5); "50%"; : PRINT TAB(15); "90%"; : PRINT TAB(25); "95%"; : PRINT TAB(35);
"98%"; : PRINT TAB(45); "99%"
6442 IF N - 2 <= 20 THEN PRINT TAB(5); ST(N - 2, 1); : PRINT TAB(15); ST(N - 2, 2);
: PRINT TAB(25); ST(N - 2, 3); : PRINT TAB(35); ST(N - 2, 4); : PRINT TAB(45);
ST(N - 2, 5)
6443 IF N - 2 > 20 THEN PRINT TAB(5); ST(21, 1); : PRINT TAB(15); ST(21, 2); :
PRINT TAB(25); ST(21, 3); : PRINT TAB(35); ST(21, 4); : PRINT TAB(45); ST(21, 5)
6450 PRINT : PRINT "  PEARSON'S CORRELATION COEFF. = "; INT(1000 * C) /
1000
6460 PRINT
6470 PRINT " STANDARD DEVIATION OF THE POINTS": PRINT " FROM THE
BEST LINE = "; INT(1000 * S1) / 1000
6480 PRINT

6490 COLOR 14, 4: PRINT : PRINT "    View calculated Y values & errors ? (Y/N)"; :
COLOR 14, 1
6500 CALL InputYesNoCheck
6510 IF Q$ = "N" THEN CLS : EXIT SUB
6520 REM - CALCULATE & PRINT ERROR FOR EACH DATA POINT
6525 REM
6530 PRINT

```

```

6540 COLOR 14, 0: CLS : COLOR 14, 4: PRINT : PRINT " ERROR IN Y VALUE FOR
EACH DATA POINT": COLOR 14, 1
6545 PRINT
6550 PRINT TAB(5); "X"; : PRINT TAB(17); "Y OBS."; : PRINT TAB(27); " Y CALC.";
: PRINT TAB(40); "ERROR"
6555 PRINT
6560 FOR i = 1 TO N
6565 IF ((i - 1) / 10 - INT((i - 1) / 10)) < .05 AND i <> 1 THEN PRINT "PRESS
RETURN FOR REST OF DATA & MENU"; : INPUT k$
6570 PRINT TAB(5); INT(1000 * x(i)) / 1000; TAB(17); INT(1000 * y(i)) / 1000;
TAB(27); INT(1000 * (A2 + S * (x(i) - A1))) / 1000; TAB(40); INT(1000 * ((y(i) - A2) - S
* (x(i) - A1))) / 1000;
6580 NEXT i
6590 PRINT : PRINT
6600 PRINT " SUM OF ERRORS SQUARED = "; INT(1000 * E2) / 1000: PRINT
6610 PRINT
6620 COLOR 14, 4: PRINT TAB(20); "Press any key to continue "; : COLOR 14, 0
k$ = ""
WHILE k$ = ""
    k$ = INKEY$
WEND
END SUB

SUB PrinterCheck
COLOR 14, 0: CLS : COLOR 14, 4
20000 REM check login mode
20010 PRINT
20020 PRINT TAB(5); "In order to be able to print to a the Epson laser printer      "
20030 PRINT TAB(5); "you must run QBasic from the Menu system                      "
20040 PRINT
20050 PRINT
20060 PRINT TAB(5); "If you have run QBasic from the Windows' Icon then this program
"
20070 PRINT TAB(5); " may not be able to print out your results !                    "
20080 PRINT
20090 PRINT TAB(5); "You must exit from the Windows environment by                  "
20100 PRINT
20110 PRINT TAB(5); " 1. Quitting this program                                "
20120 PRINT TAB(5); " 2. Exiting from Windows using ALT/F4 or double-clicking      "
20130 PRINT TAB(5); "      on the top, left-hand box of the window.                            "
20140 PRINT
20150 PRINT TAB(5); "      Restart QBASIC via the PhysChem menu item                            "
20160 PRINT
20170
LOCATE 20, 10: COLOR 14, 1
20180 PRINT " Press key [A] to accept and continue running the program "
LOCATE 21, 10
20190 PRINT "      (or press key [Q] to quit the program)          "; : COLOR 14, 0

```

```

20200 k$ = INKEY$: IF k$ = "" THEN 20200
20210 IF k$ = "A" OR k$ = "a" THEN 20240
20220 IF k$ = "q" OR k$ = "Q" THEN END
20230 GOTO 20170
20240 REM finished checking

```

```

END SUB

```

```

SUB PrintHeader

```

```

    SHARED username$
    DIM month$(13)
    month$(1) = "January": month$(2) = "February": month$(3) = "March"
    month$(4) = "April": month$(5) = "May": month$(6) = "June"
    month$(7) = "July": month$(8) = "August": month$(9) = "September"
    month$(10) = "October": month$(11) = "November": month$(12) = "December":
    currdate$ = DATE$
    currmonth$ = " " + month$(VAL(LEFT$(DATE$, 2))) + " 19"
    fulldate$ = MID$(DATE$, 4, 2) + currmonth$ + RIGHT$(DATE$, 2)
    Bold$ = CHR$(27) + "E"           ' set to enhanced print
    NoBold$ = CHR$(27) + "F"        ' cancel enhanced print

    LPRINT CHR$(27) + CHR$(64)      ' resets printer (#64 = @)
    LPRINT CHR$(27) + "I" + CHR$(6) ' sets left margin to 6
    LPRINT Bold$; username$; " : "; fulldate$; NoBold$
    LPRINT

    ' Add any other relevant information here.....

```

```

END SUB

```

```

SUB ProgramDescription

```

```

    CLS : LOCATE 5, 22: PRINT "A PROGRAM TO FIT A STRAIGHT LINE
    THROUGH ": LOCATE 7, 32: PRINT " A SET OF POINTS X,Y "
    PRINT TAB(22); " _____ "
    PRINT

```

```

END SUB

```

```

SUB Quit

```

```

    COLOR 14, 0: CLS
    COLOR 14, 4
    LOCATE 10, 18
    PRINT "Exit the program ? (Y/N)";
    k$ = ""
    WHILE k$ = ""

```

```

k$ = INKEY$
IF k$ = "Y" OR k$ = "y" THEN k$ = "Y": COLOR 15, 0: CLS : END
IF k$ = "N" OR k$ = "n" THEN EXIT SUB
k$ = ""
WEND

```

```

END SUB

```

```

SUB ReplaceLine

```

```

    REM - Replace an existing line of data

```

```

    LOCATE 23, 5: PRINT "Type LINENUMBER of data to be replaced ";
    INPUT i$
    i = VAL(i$)

```

```

    IF i < 1 OR i > N THEN
        LOCATE 23, 5: PRINT "must be 1 - "; N; " Press a key to continue";
        WHILE k$ = ""
            k$ = INKEY$
        WEND
        EXIT SUB
    END IF

```

```

    LOCATE 23, 5: PRINT "Type a new X value, then press [Enter] "; : INPUT x(i)
    LOCATE 23, 5: PRINT "Now the new Y value, then press [Enter] "; : INPUT y(i)
    1860
    CalcFlag$ = "Not Done"
    PrintFlag$ = "Disabled"

```

```

END SUB

```

```

SUB SuperSubString (specialstring$)

```

```

' This routine prints the "specialstring$" containing superscript and
' subscript characters on a printer (not on the screen).

```

```

' The string prints character-by-character while looking for the
' following special control characters embedded in the string:

```

```

'   "^" : means switch on superscript
'   "_" : means switch on subscript
'   "|" : means cancel superscript & subscript

```

```

    subscript$ = CHR$(27) + "S" + CHR$(1)
    superscript$ = CHR$(27) + "S" + CHR$(0)
    cancel$ = CHR$(27) + "T"

```

```

    FOR i = 1 TO LEN(specialstring$)
        ch$ = MID$(specialstring$, i, 1)
        SELECT CASE ch$

```

```

        CASE "^": LPRINT superscript$;
        CASE "_": LPRINT subscript$;
        CASE "|": LPRINT cancel$;
        CASE ELSE: LPRINT ch$;
    END SELECT
NEXT i

END SUB

SUB TestData
SHARED N
N = 5

FOR i = 1 TO 5
x(i) = i
NEXT i
y(1) = 1: y(2) = 1.8: y(3) = 3.2: y(4) = 3.7: y(5) = 5.4
DataFlag$ = "Data Present"
Xaxis$ = "X"
Yaxis$ = "Y"
Comment$ = "Test Data"
END SUB

SUB TimeOut (numsecs%)
' Ends after a key press or time "numsecs" elapsed.

    CALL ClearKeyboard
    start& = TIMER
    DO

        LOOP WHILE (TIMER - start& < numsecs%) AND (INKEY$ = "")

END SUB

SUB TitleScreen
COLOR 0, 0: CLS
COLOR 14, 1:
LOCATE 8, 23: PRINT " LINEAR REGRESSION "
COLOR 14, 1
LOCATE 11, 25: PRINT " Dr. M. S. Beevers - March 1995 "
COLOR 14, 4
LOCATE 16, 21: PRINT " Any Key to Continue "

k$ = ""
WHILE k$ = ""
k$ = INKEY$
WEND

```

END SUB

SUB TooFewDataCheck

PRINT

IF N > 2 THEN EXIT SUB

LOCATE 21, 8

PRINT " Calculation void - (N<3). Press a key to continue";

k\$ = ""

WHILE k\$ = ""

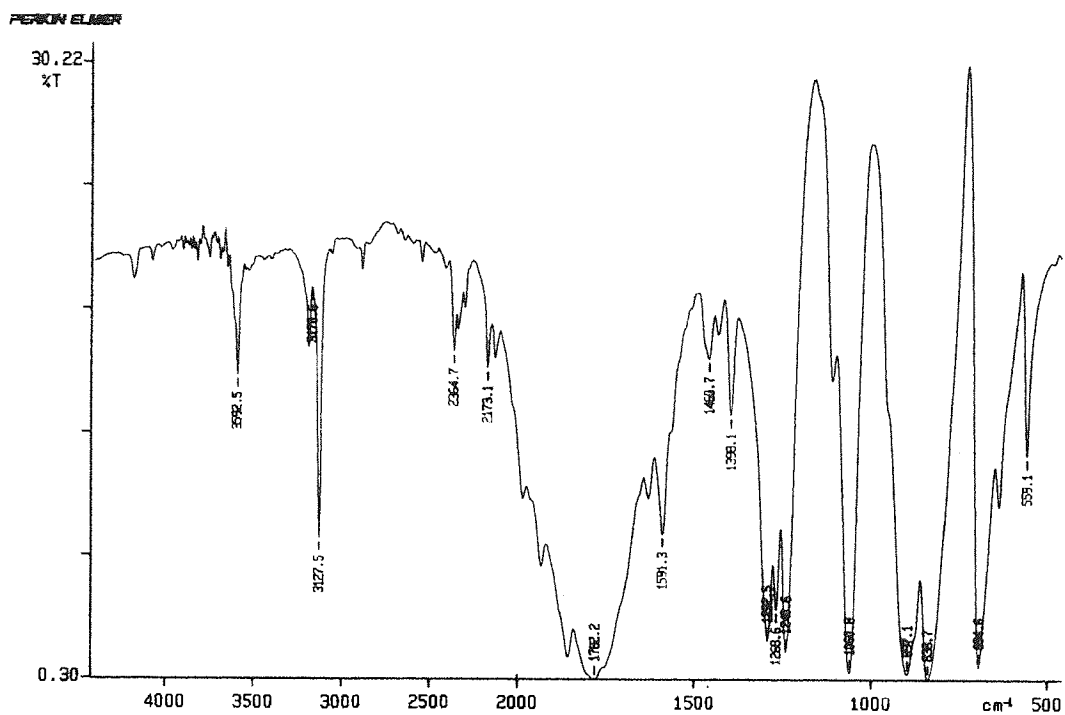
k\$ = INKEY\$

WEND

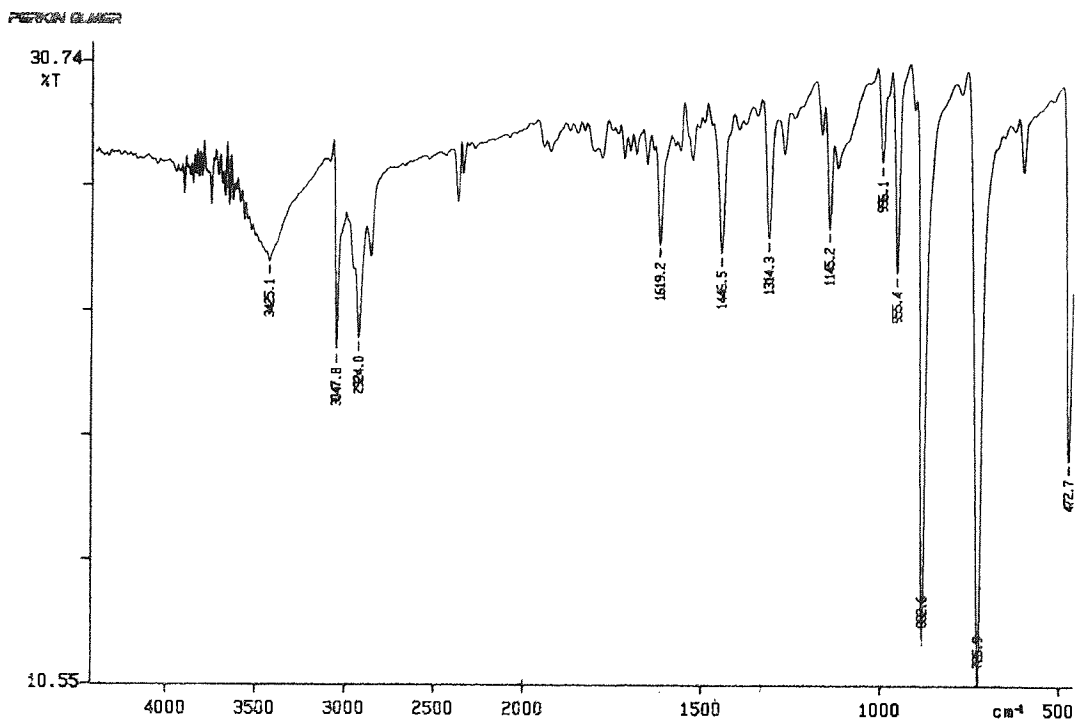
END SUB

### Appendix 3: The Analysis of Precipitate by Infra-Red Spectroscopy.

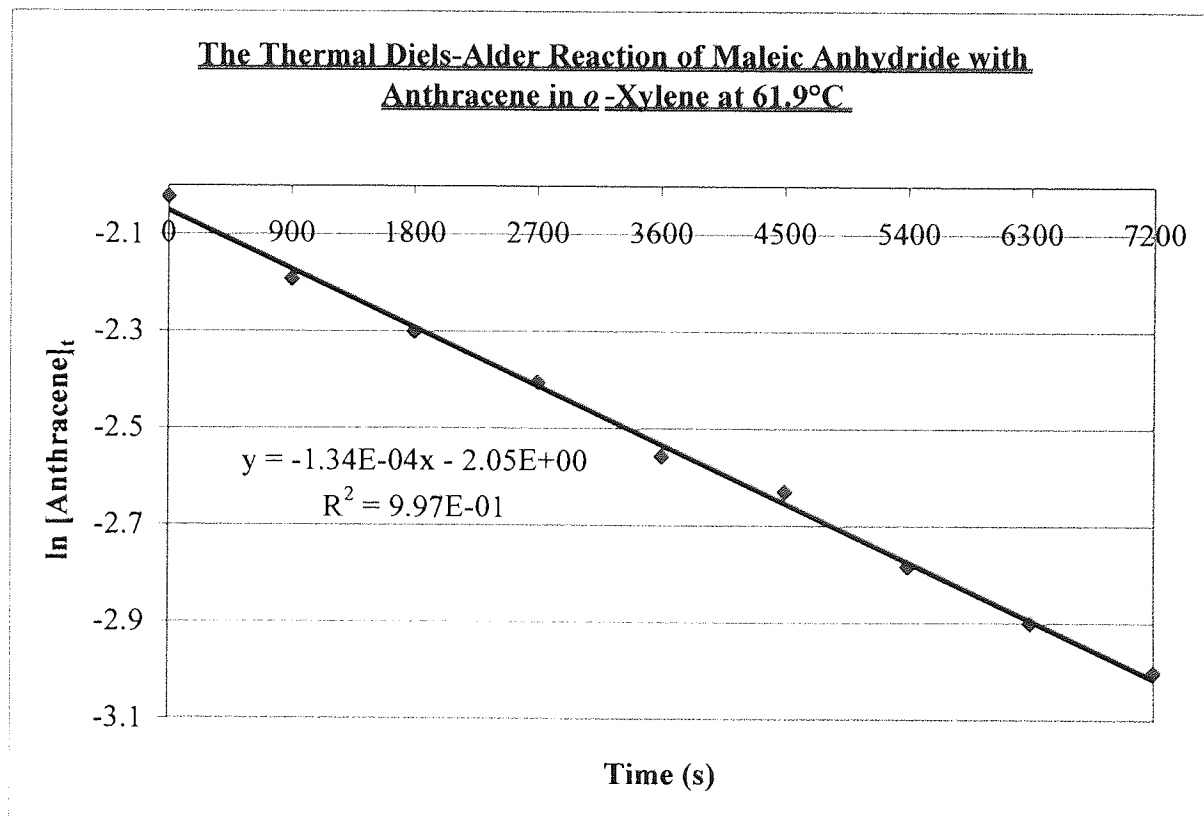
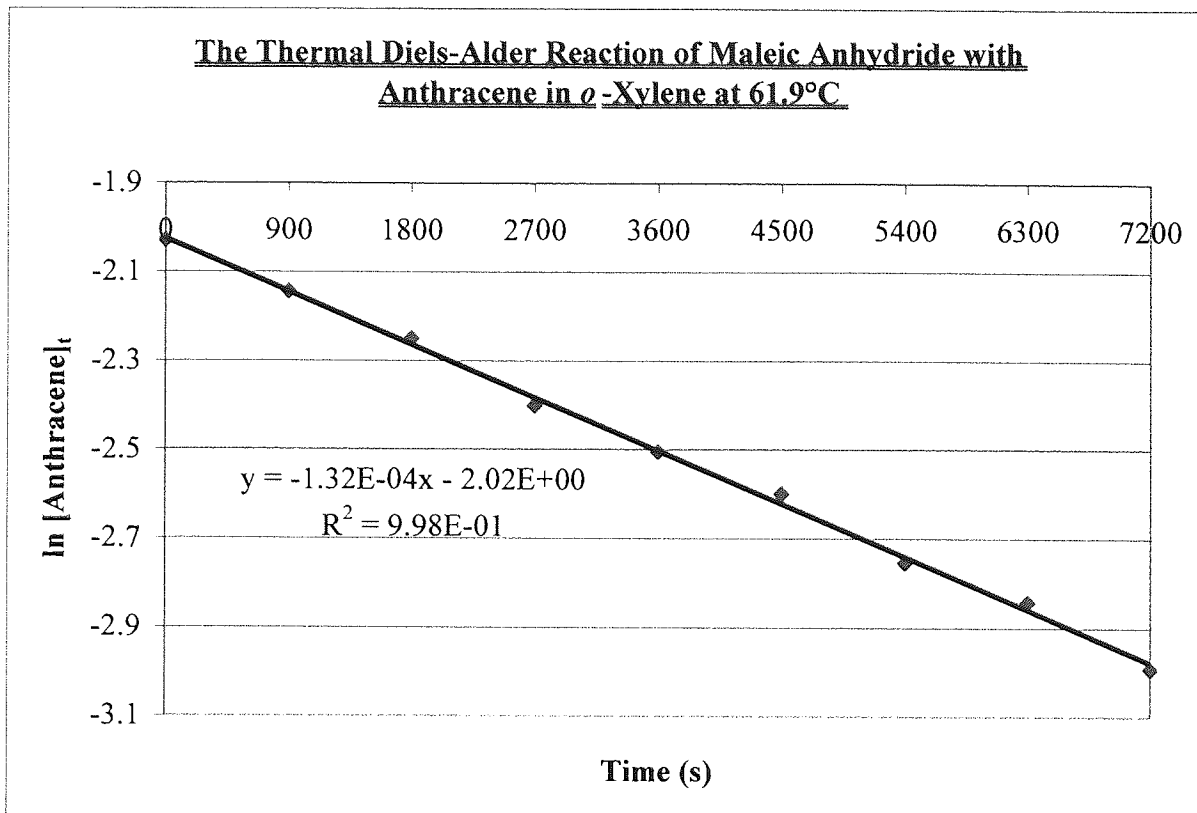
Infrared spectrum of Maleic Anhydride



Infrared spectrum of Anthracene

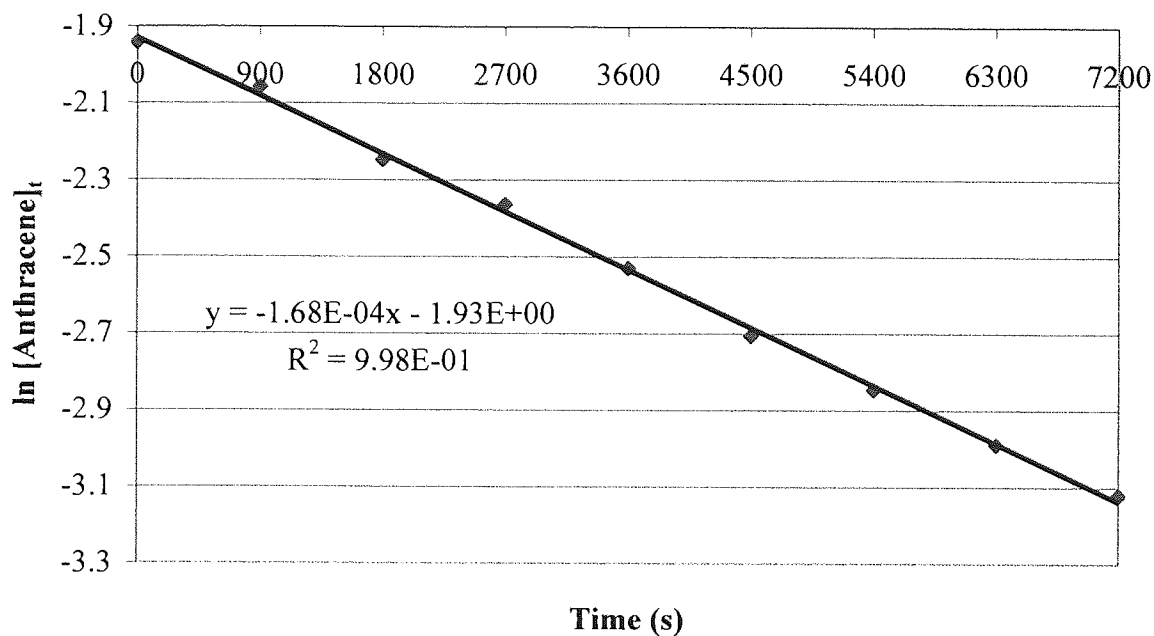


**Appendix 4:** The Thermally Induced Diels-Alder Reaction of Maleic Anhydride with Anthracene in *o*-Xylene.

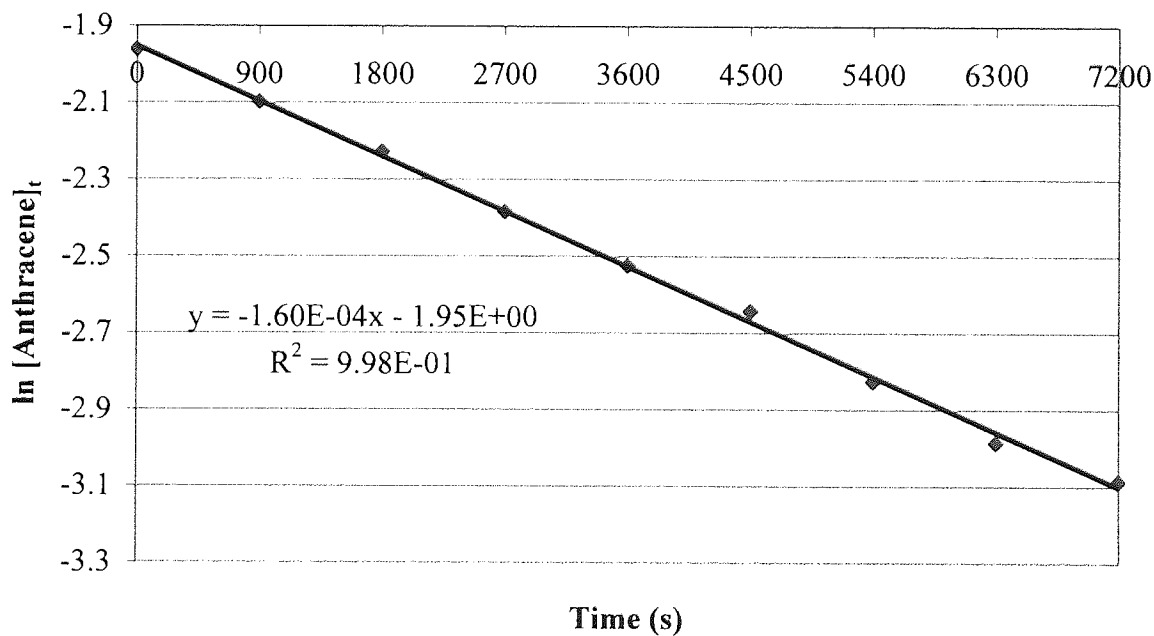




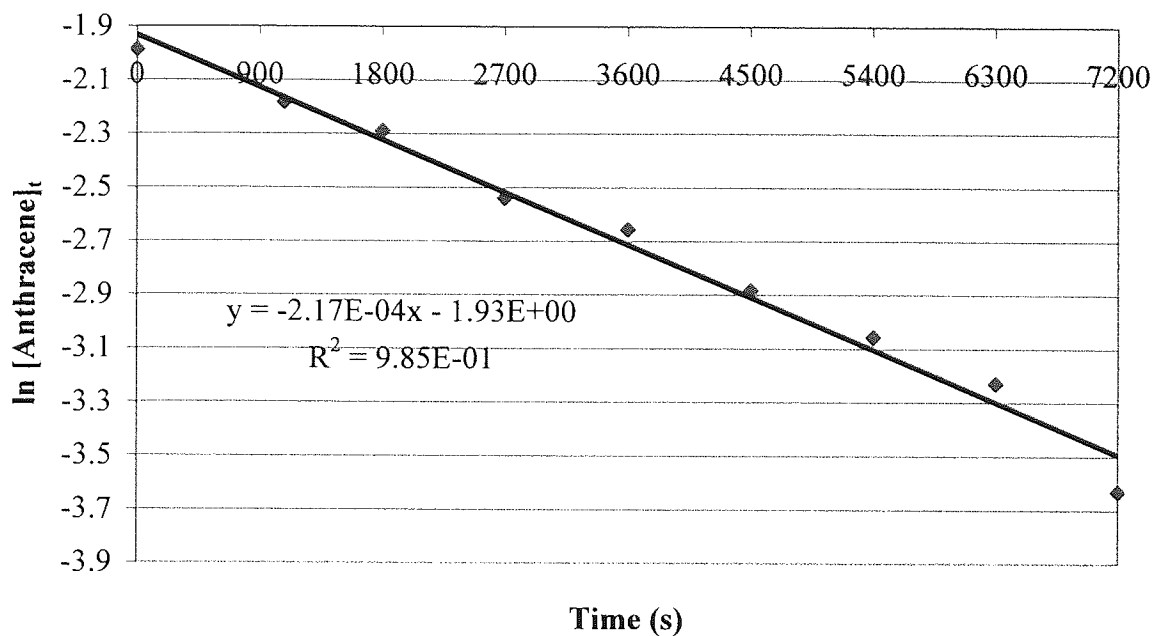
**The Thermal Diels-Alder Reaction of Maleic Anhydride with Anthracene in *o*-Xylene at 65.5°C**



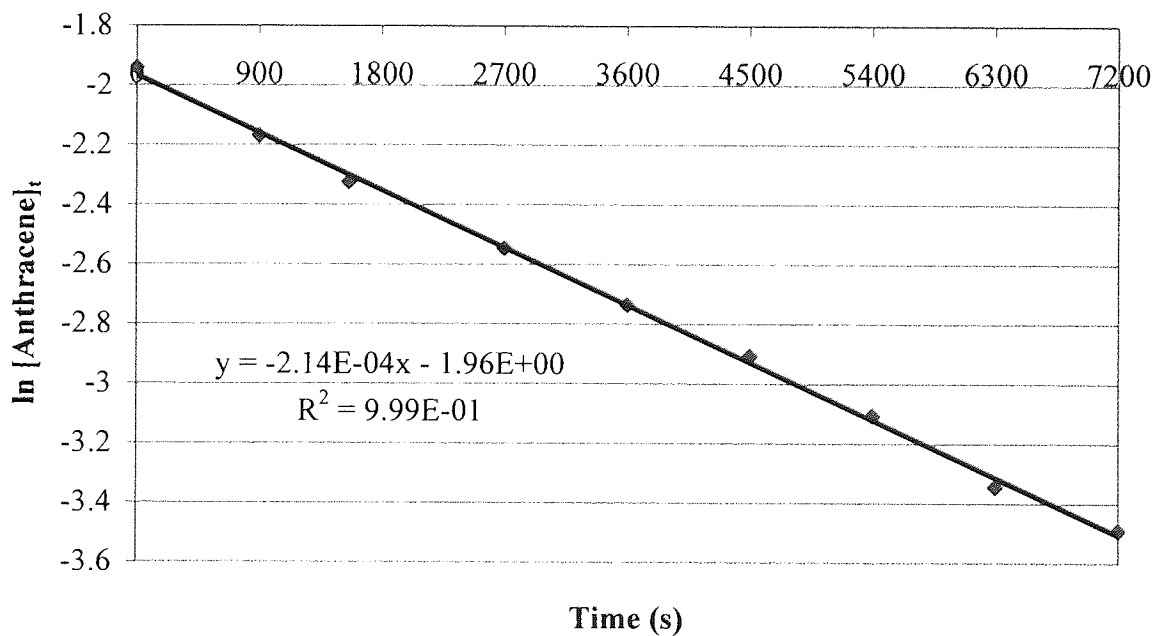
**The Thermal Diels-Alder Reaction of Maleic Anhydride with Anthracene in *o*-Xylene at 65.5°C**



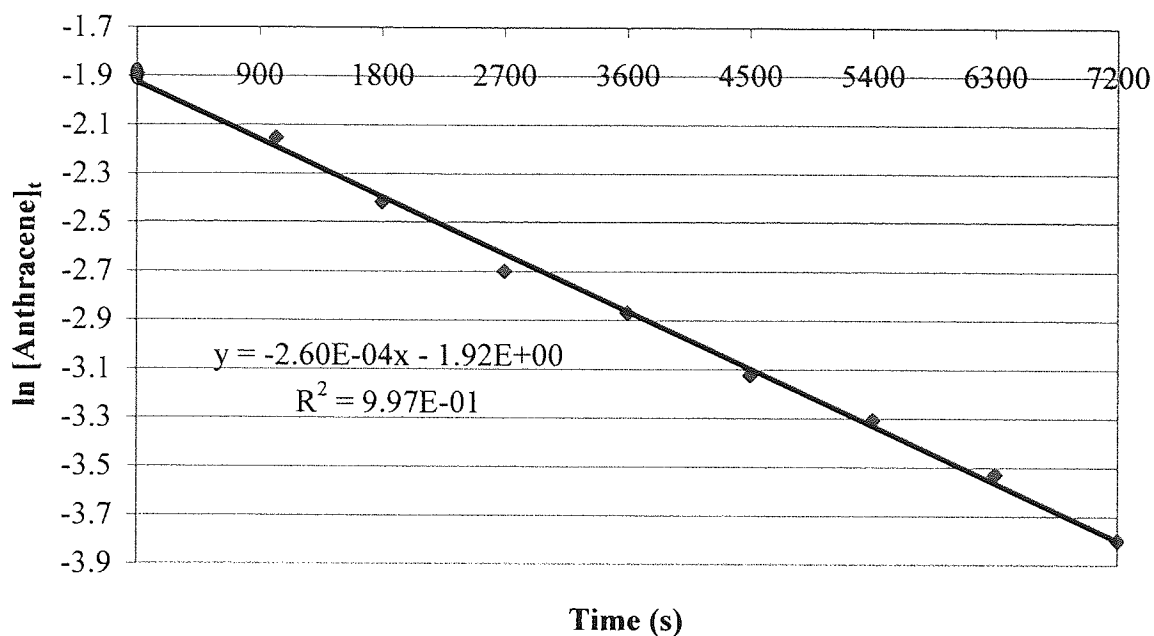
**The Thermal Diels-Alder Reaction of Maleic Anhydride with Anthracene in *o*-Xylene at 68.5°C**



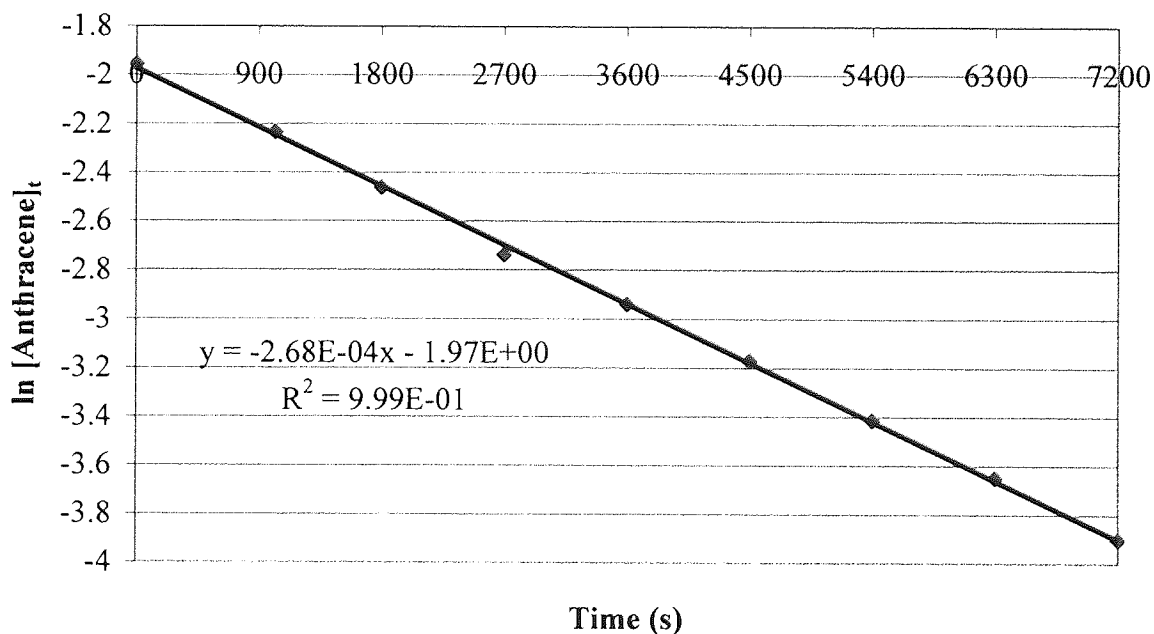
**The Thermal Diels-Alder Reaction of Maleic Anhydride with Anthracene in *o*-Xylene at 68.5°C**



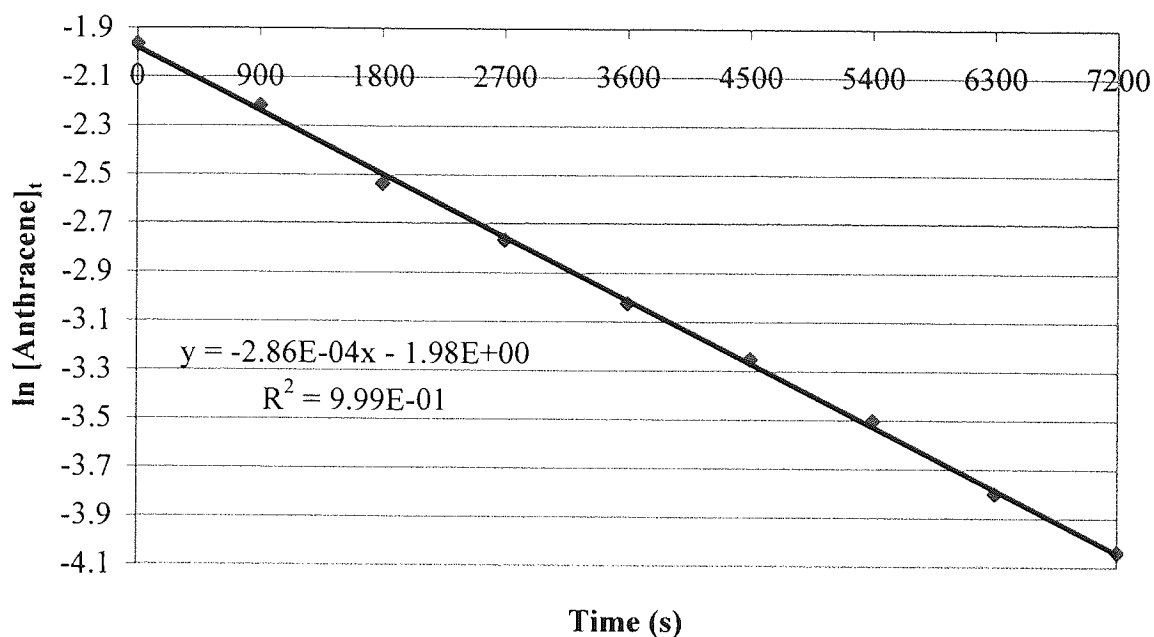
**The Thermal Diels-Alder Reaction of Maleic Anhydride with Anthracene in *o*-Xylene at 73.8°C**



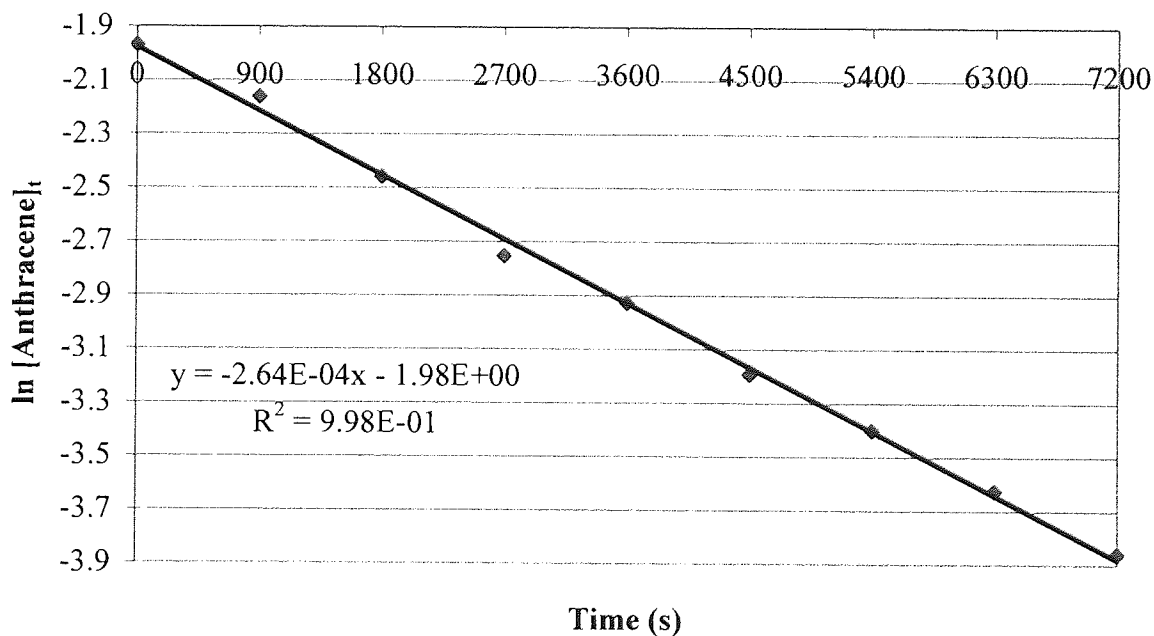
**The Thermal Diels-Alder Reaction of Maleic Anhydride with Anthracene in *o*-Xylene at 73.8°C**



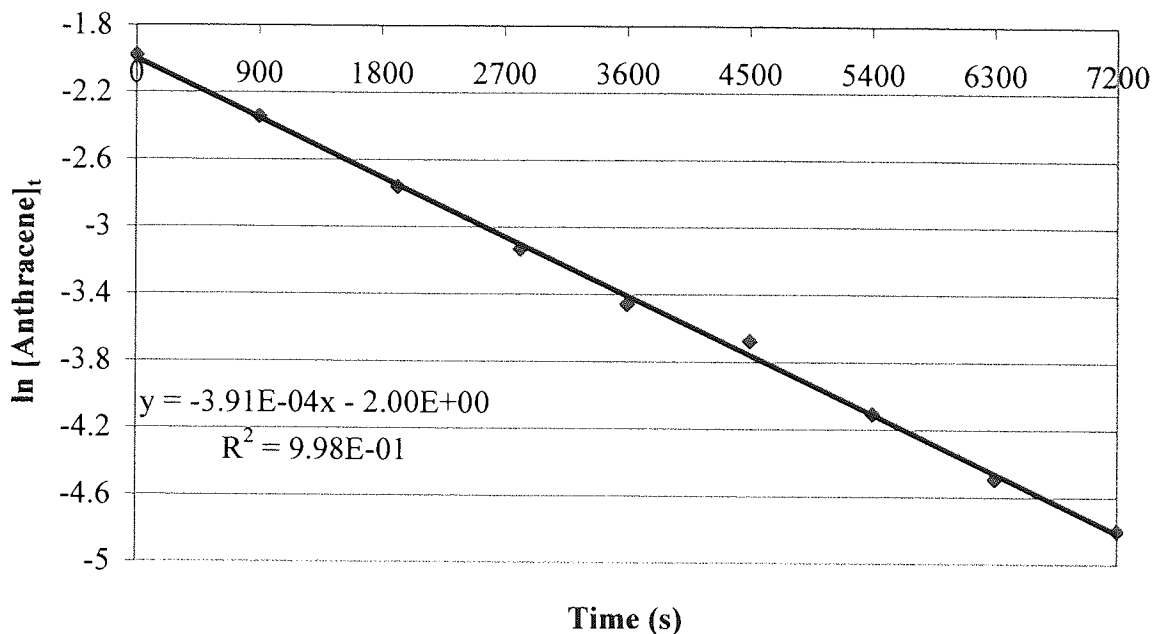
The Thermal Diels-Alder Reaction of Maleic Anhydride with Anthracene in *o*-Xylene at 74.9°C



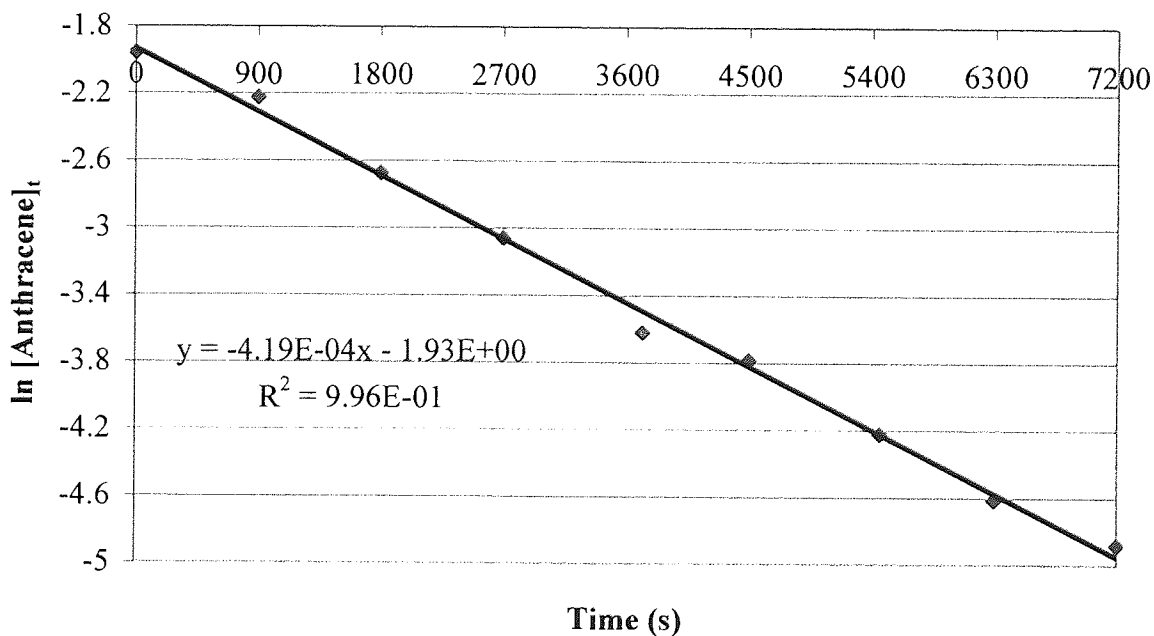
The Thermal Diels-Alder Reaction of Maleic Anhydride with Anthracene in *o*-Xylene at 74.9°C



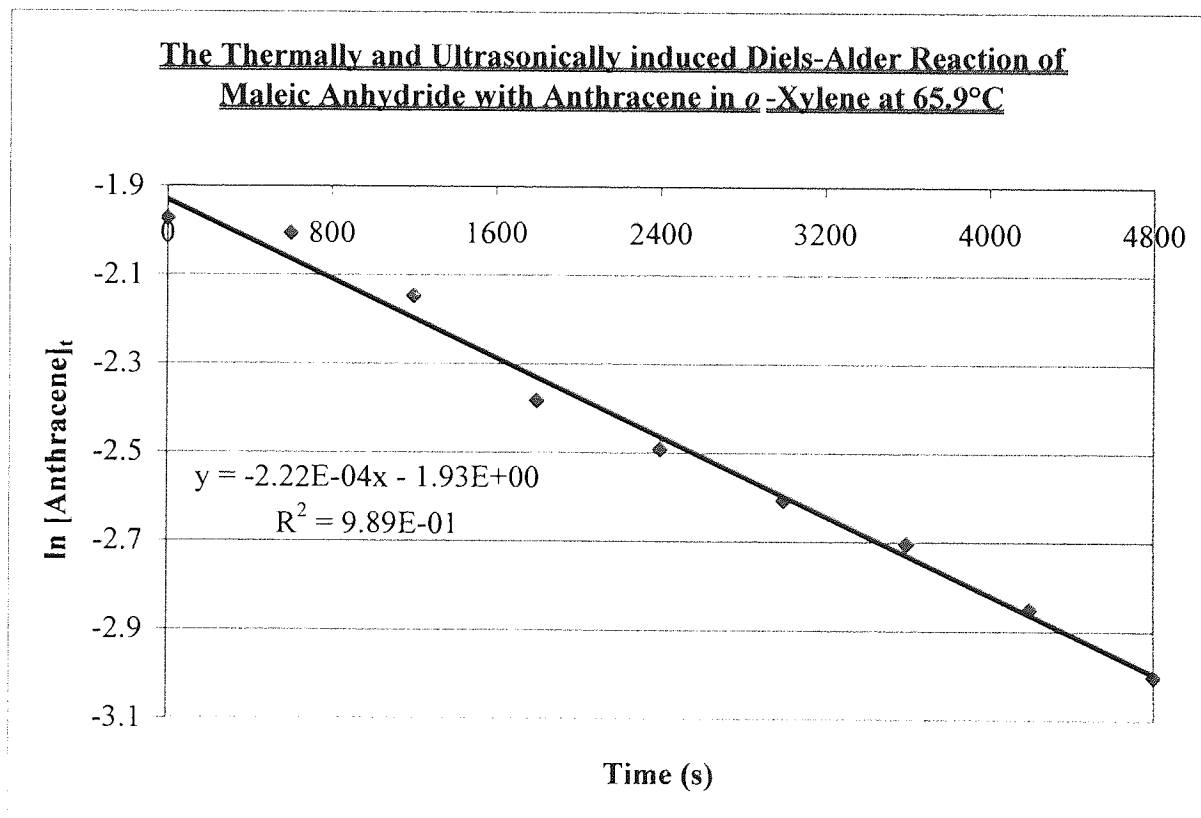
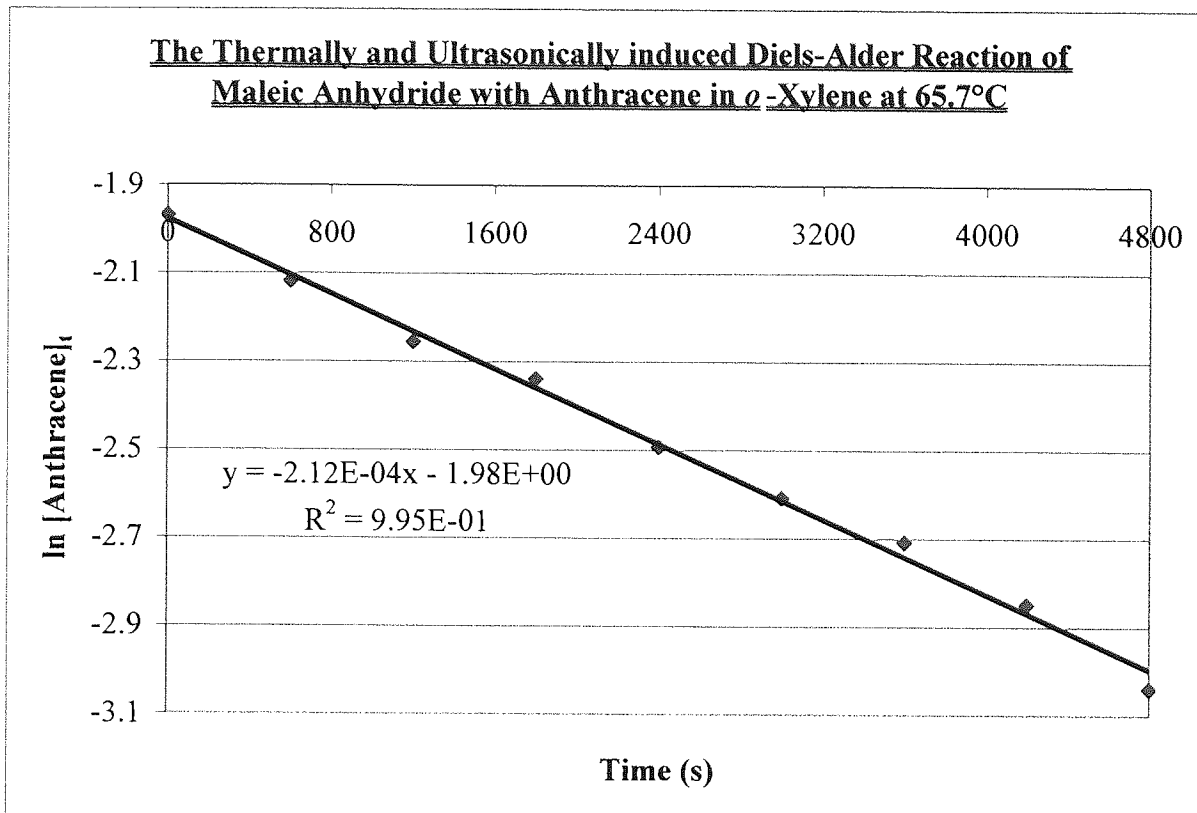
**The Thermal Diels-Alder Reaction of Maleic Anhydride with Anthracene in *o*-Xylene at 79.7°C**



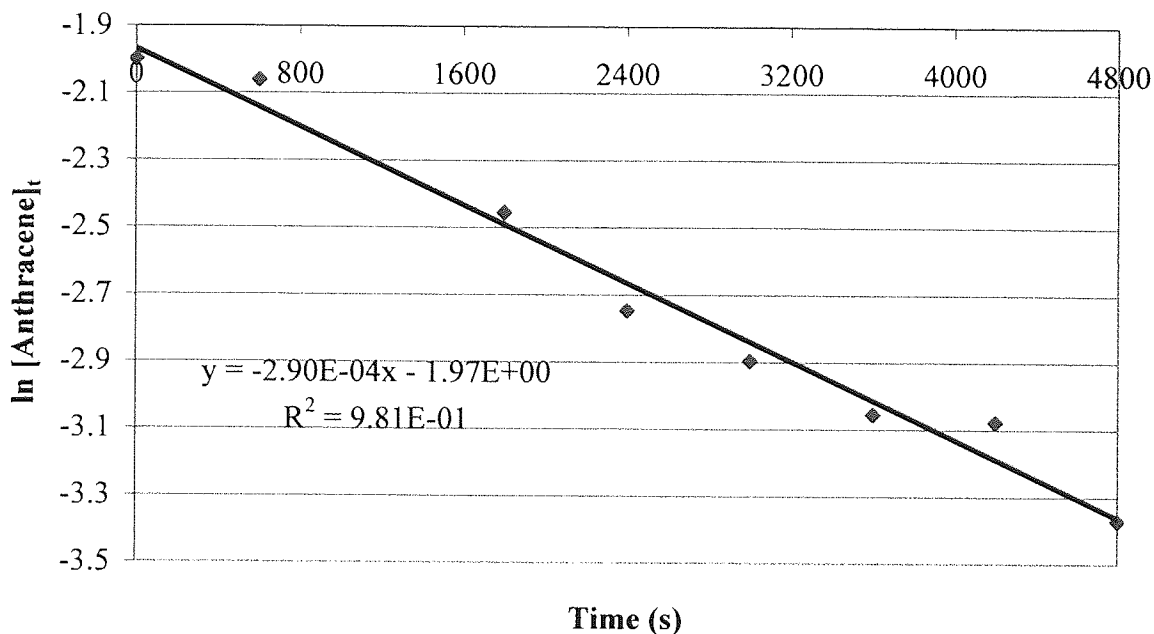
**The Thermal Diels-Alder Reaction of Maleic Anhydride with Anthracene in *o*-Xylene at 80.7°C**



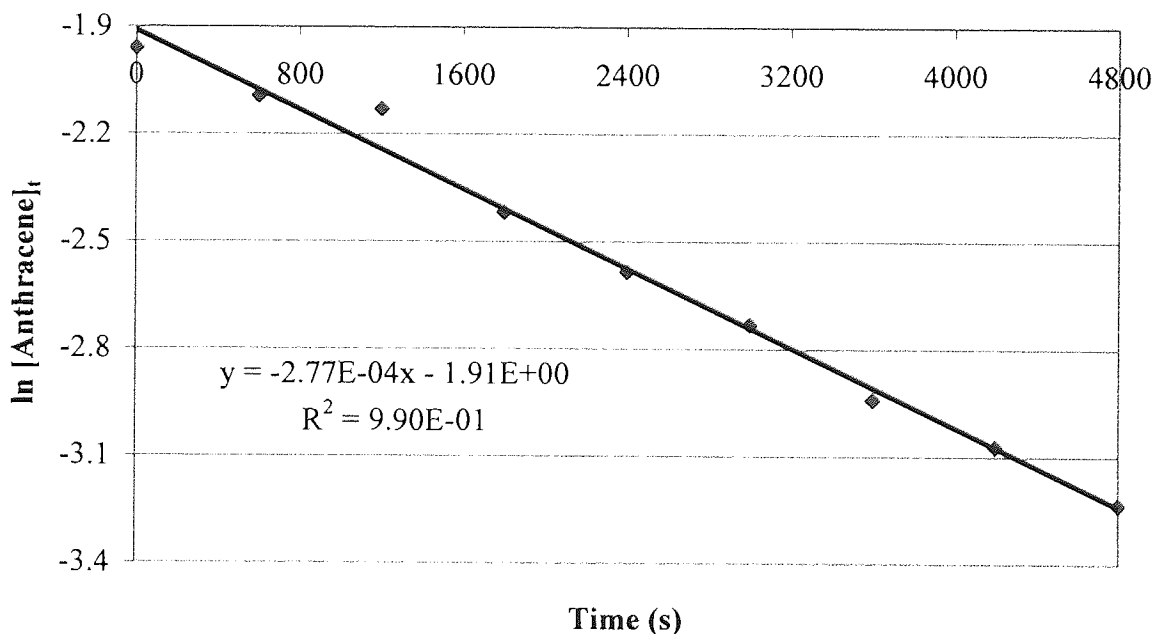
**Appendix 5:** The Ultrasonically Induced Diels-Alder Reaction of Maleic Anhydride with Anthracene in *o*-Xylene.



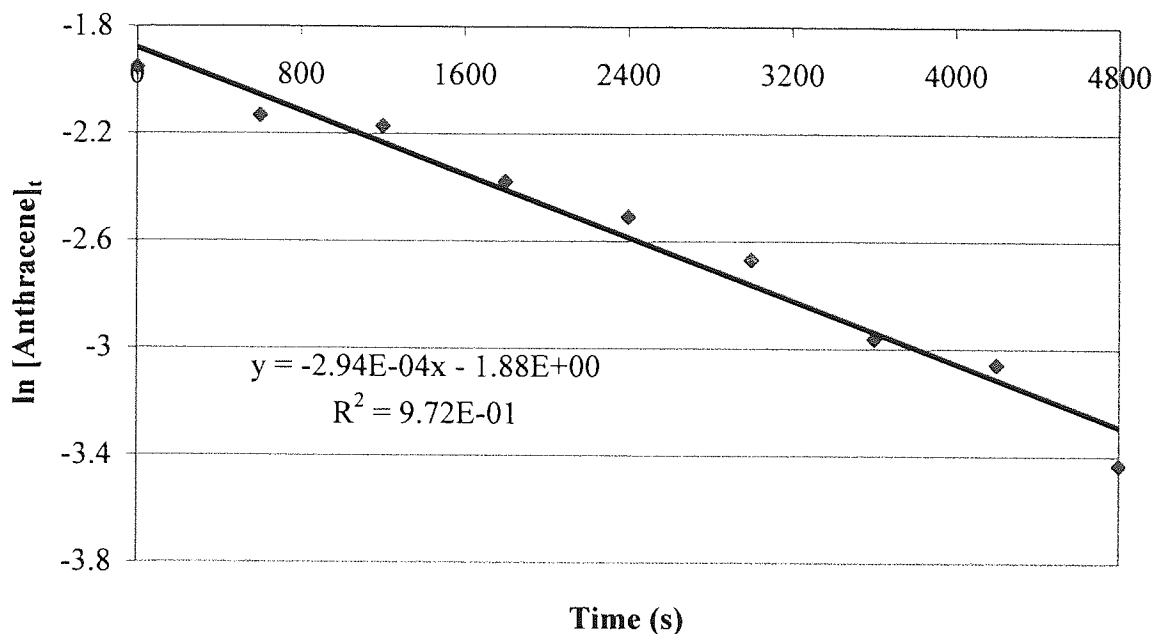
**The Thermally and Ultrasonically induced Diels-Alder Reaction of Maleic Anhydride with Anthracene in *o*-Xylene at 69.5°C**



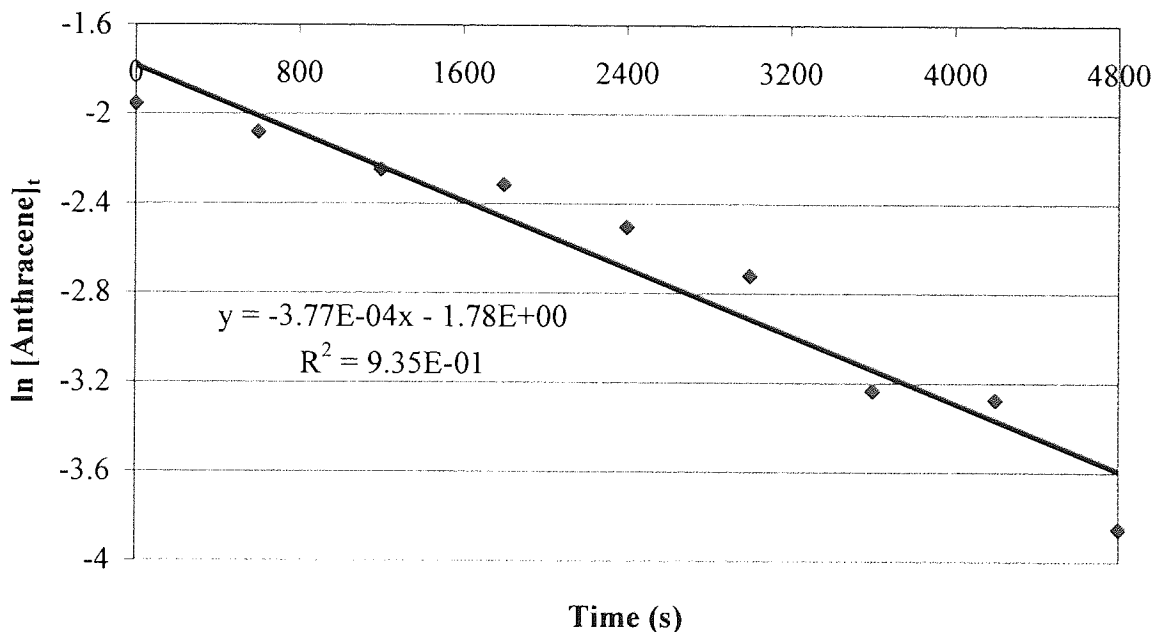
**The Thermally and Ultrasonically induced Diels-Alder Reaction of Maleic Anhydride with Anthracene in *o*-Xylene at 71.6°C**



**The Thermally and Ultrasonically induced Diels-Alder Reaction of Maleic Anhydride with Anthracene in *o*-Xylene at 72.2°C**

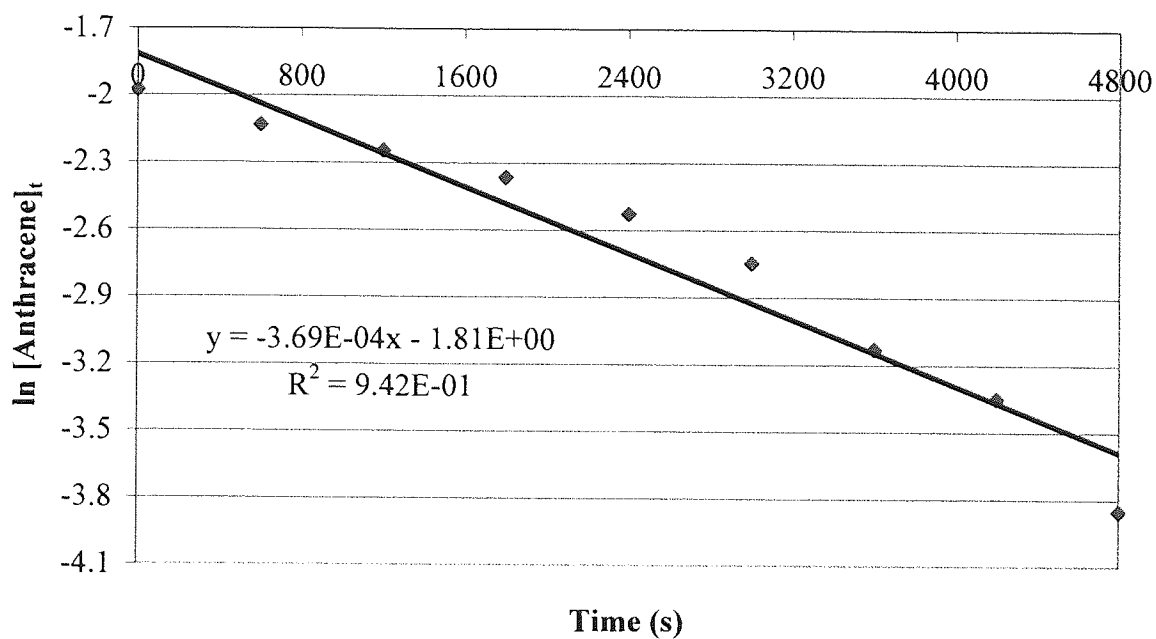


**The Thermally and Ultrasonically induced Diels-Alder Reaction of Maleic Anhydride with Anthracene in *o*-Xylene at 75.6°C**





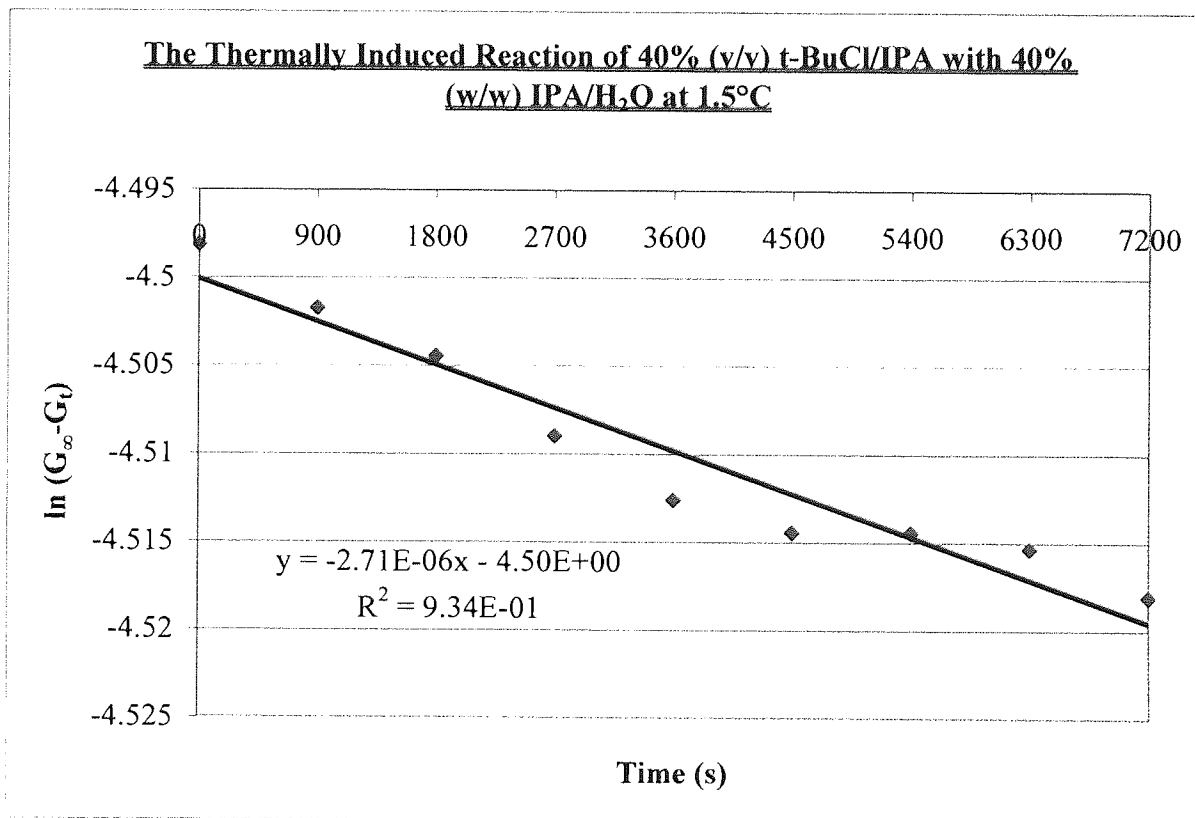
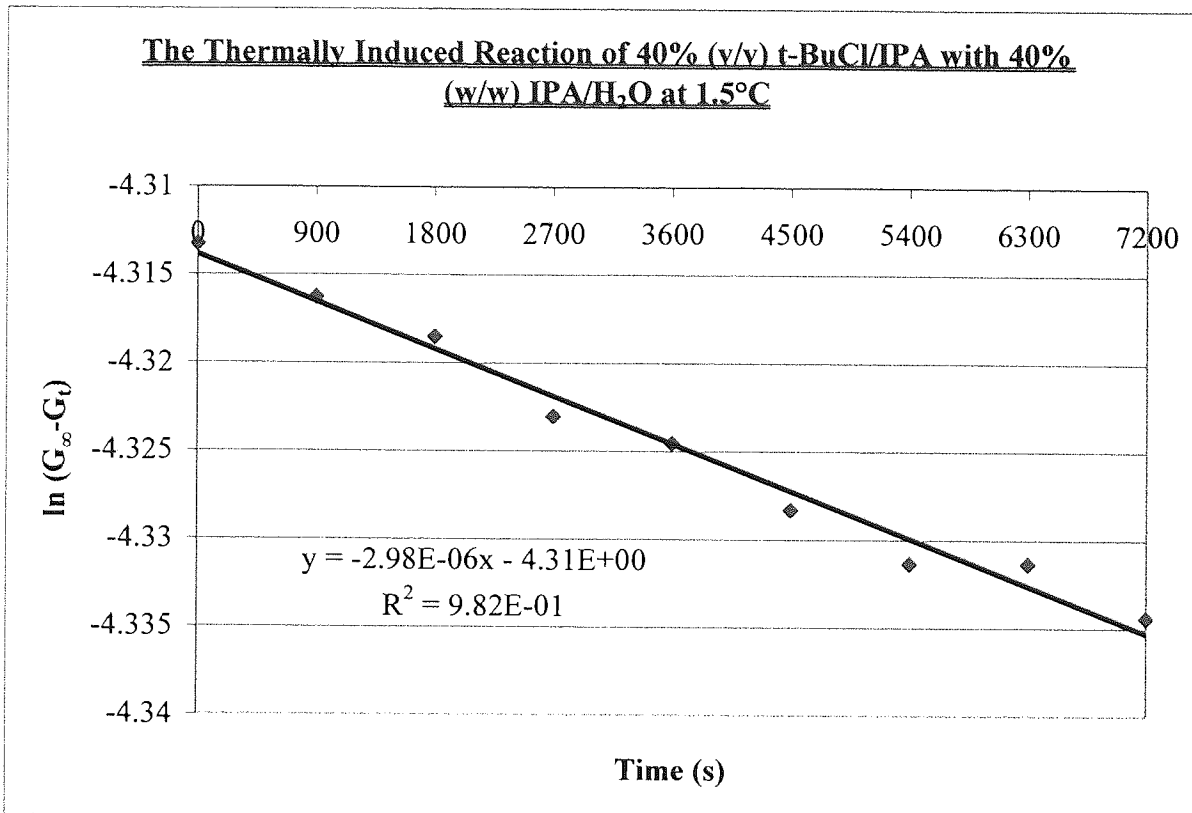
The Thermally and Ultrasonically induced Diels-Alder Reaction of Maleic Anhydride with Anthracene in *o*-Xylene at 76.2°C



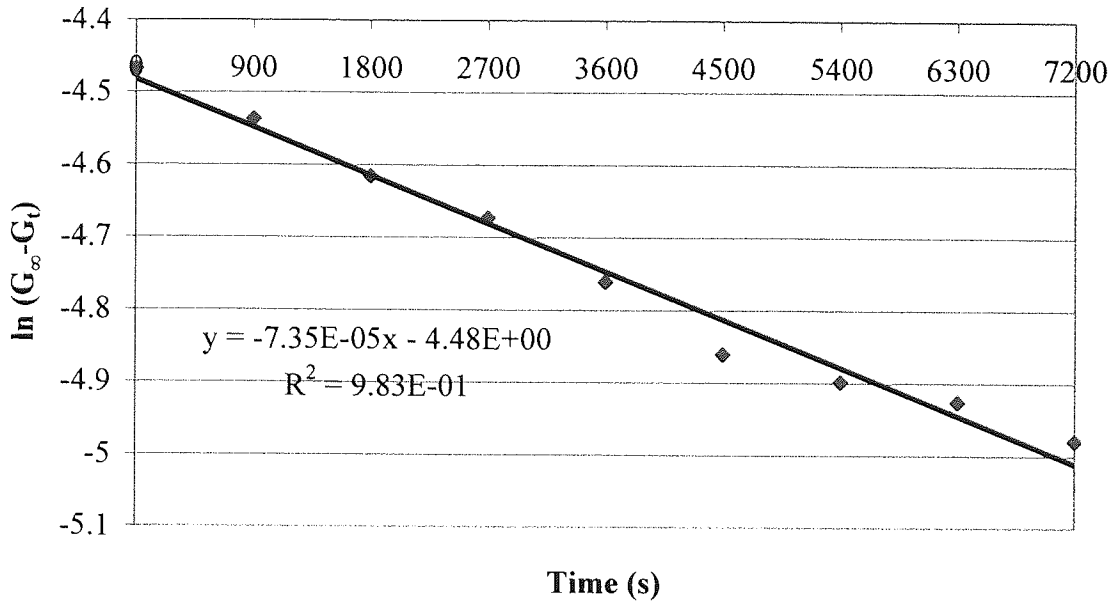
**Appendix 6:**      The DEPT Pulse Programme.

1 ZE  
2 WR DA  
3 IF DA  
4 LO TO 2 TIMES C  
5 RF DA.001  
6 RE DA  
7 D1 S1 DO  
8 (P1 PH1 D2):D  
9 (P2 PH2):D(P3 PH4 D2)  
10 (P0 PH3):D(P4 PH5 D2 S2)  
11 GO=7 PH7 BB  
12 WR DA  
13 IF DA  
14 IN=6  
15 D2 DO  
16 EXIT

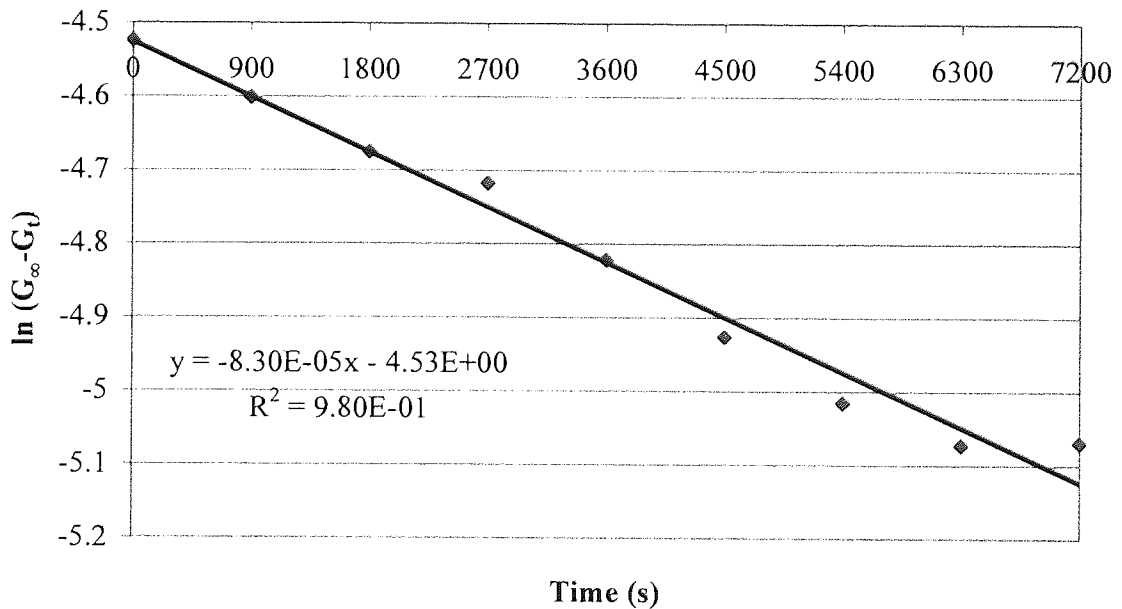
**Appendix 7:** The Thermally Induced Reaction of 40% (v/v) t-BuCl/IPA with 40% (w/w) IPA/H<sub>2</sub>O.



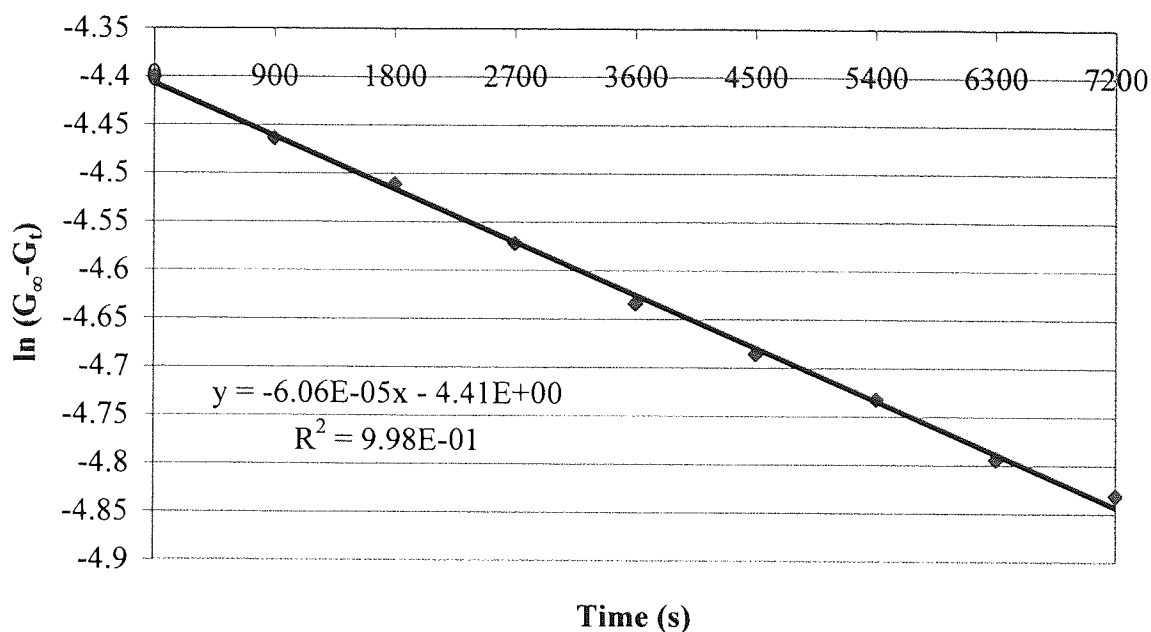
**The Thermally Induced Reaction of 40% (v/v) t-BuCl/IPA with  
40% (w/w) IPA/H<sub>2</sub>O at 25.8°C**



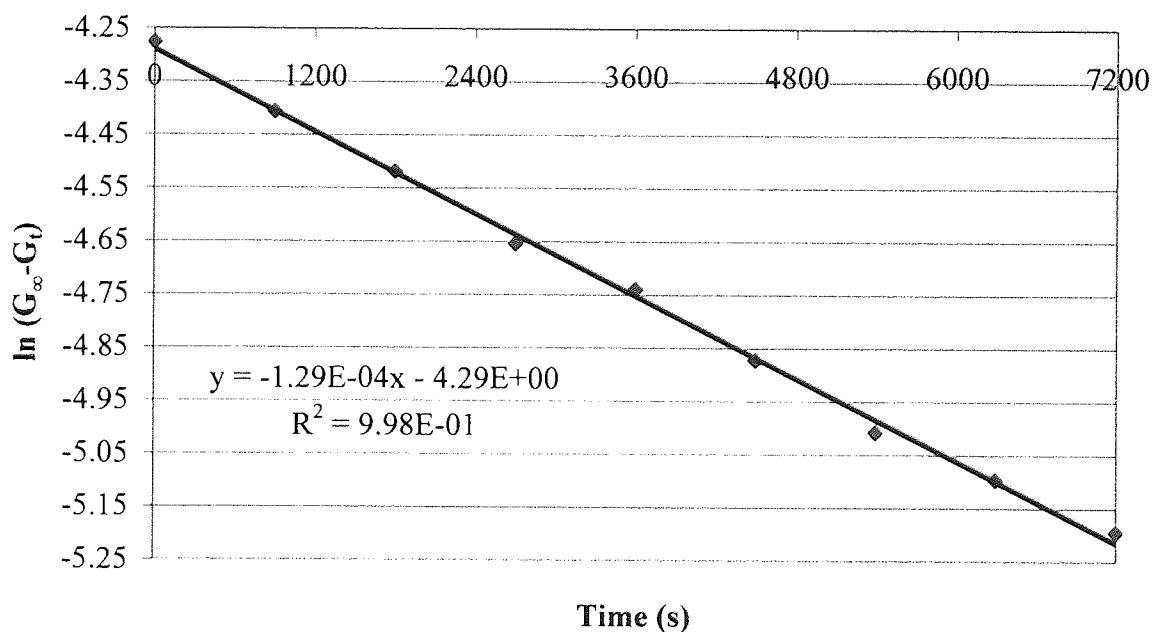
**The Thermally Induced Reaction of 40% (v/v) t-BuCl/IPA with 40%  
(w/w) IPA/H<sub>2</sub>O at 25.9°C**



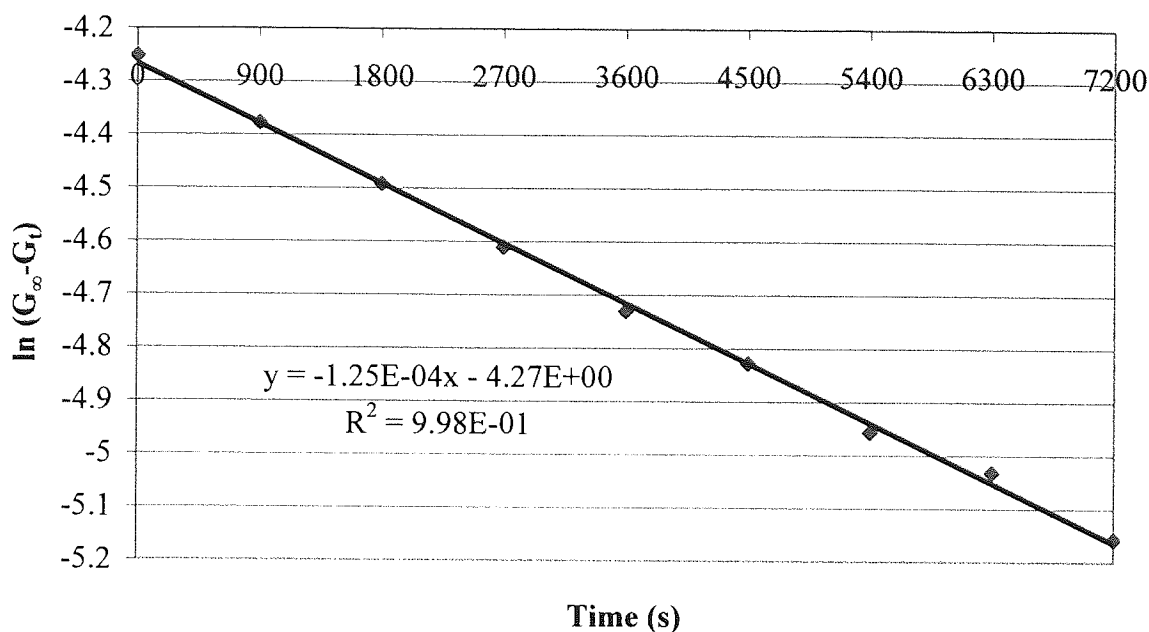
**The Thermally Induced Reaction of 40% (v/v) t-BuCl/IPA with 40% (w/w) IPA/H<sub>2</sub>O at 26.2°C**



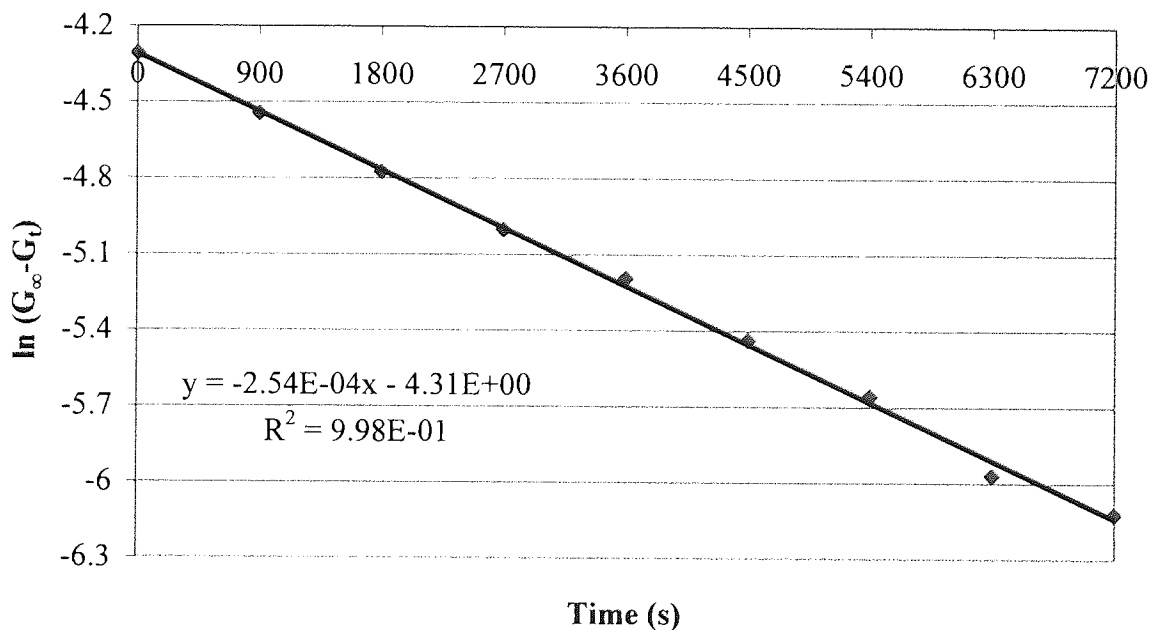
**The Thermally Induced Reaction of 40% (v/v) t-BuCl/IPA with 40% (w/w) IPA/H<sub>2</sub>O at 31.6°C**



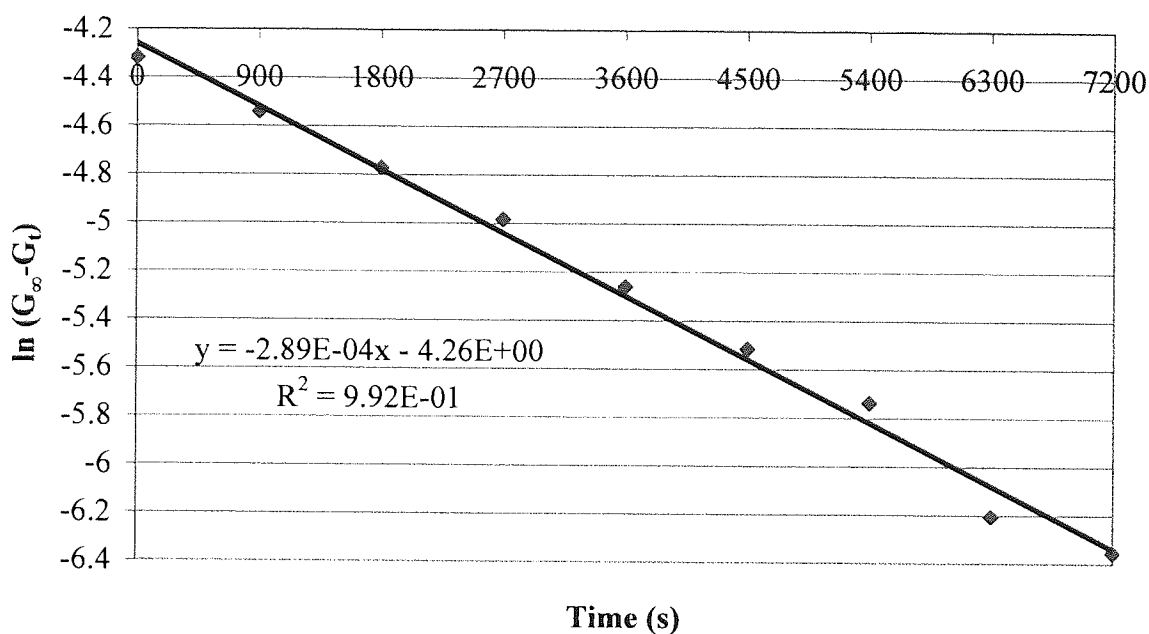
**The Thermally Induced Reaction of 40% (v/v) t-BuCl/IPA with 40% (w/w) IPA/H<sub>2</sub>O at 31.6°C**



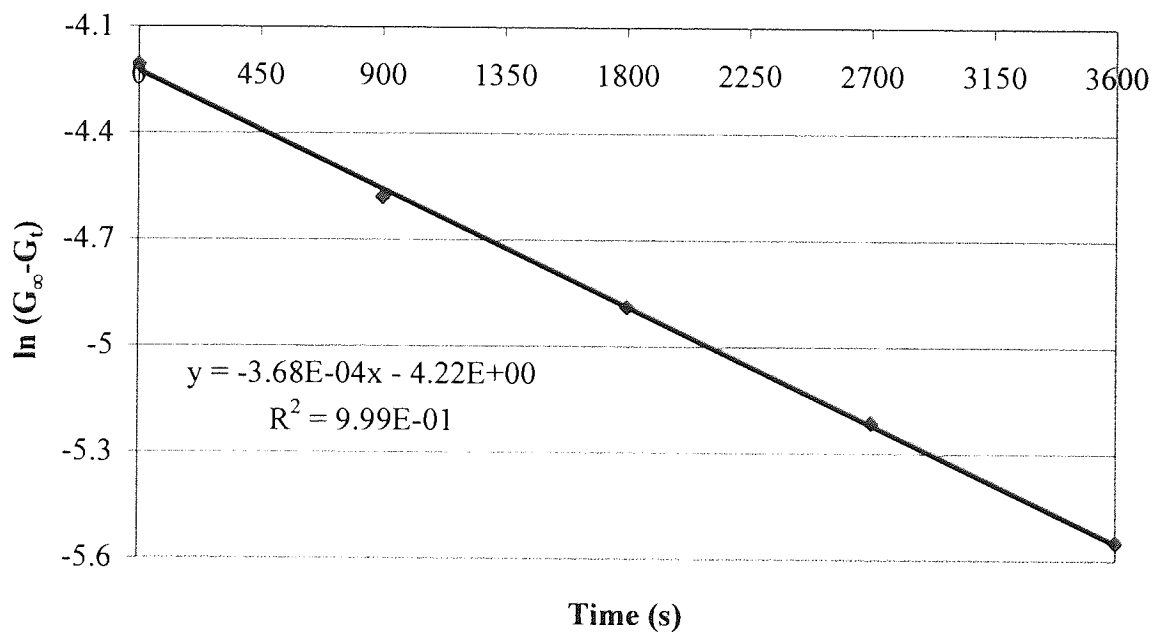
**The Thermally Induced Reaction of 40% (v/v) t-BuCl/IPA with 40% (w/w) IPA/H<sub>2</sub>O at 36.9°C**



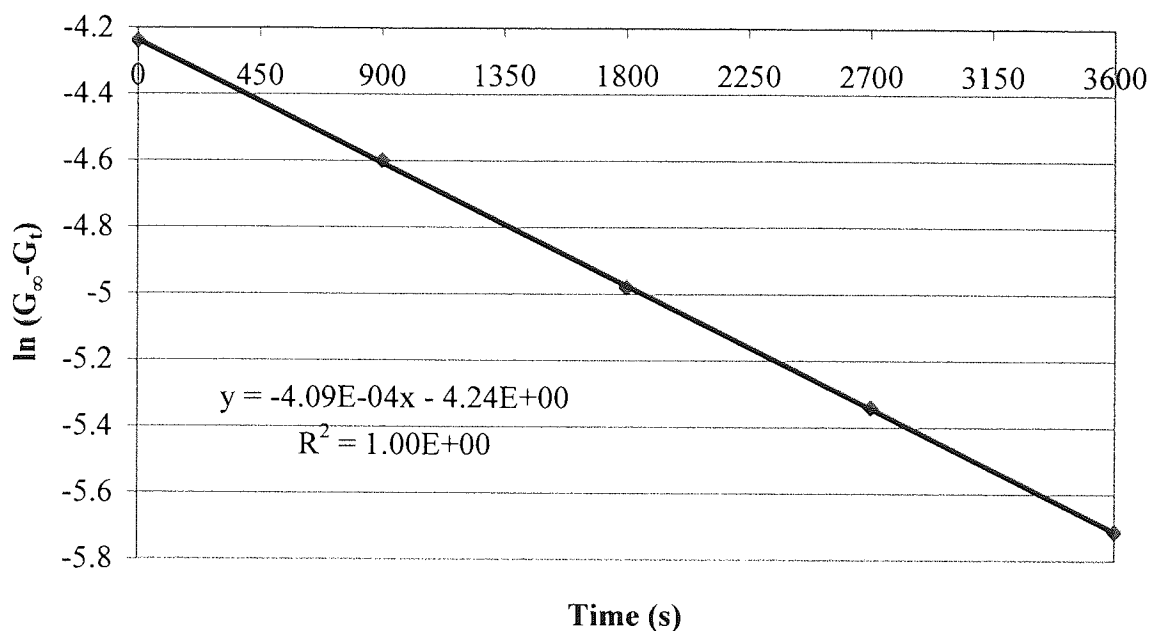
**The Thermally Induced Reaction of 40% (v/v) t-BuCl/IPA with 40% (w/w) IPA/H<sub>2</sub>O at 36.9°C**



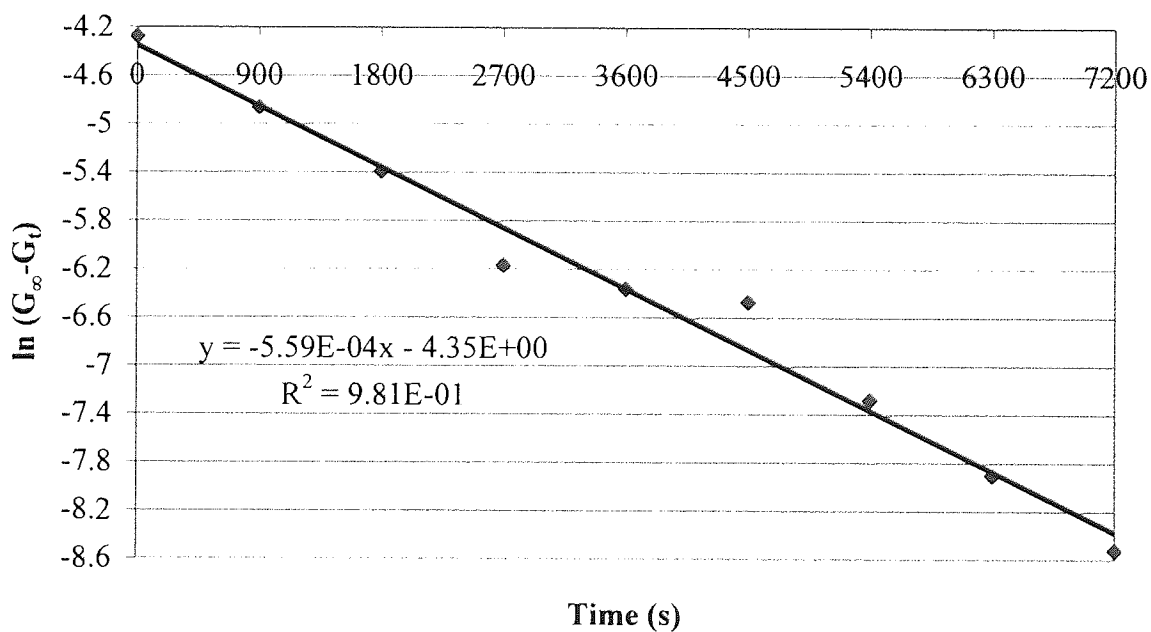
**The Thermally Induced Reaction of 40% (v/v) t-BuCl/IPA with 40% (w/w) IPA/H<sub>2</sub>O at 41.3°C**



**The Thermally Induced Reaction of 40% (v/v) t-BuCl/IPA with 40% (w/w) IPA/H<sub>2</sub>O at 41.3°C**

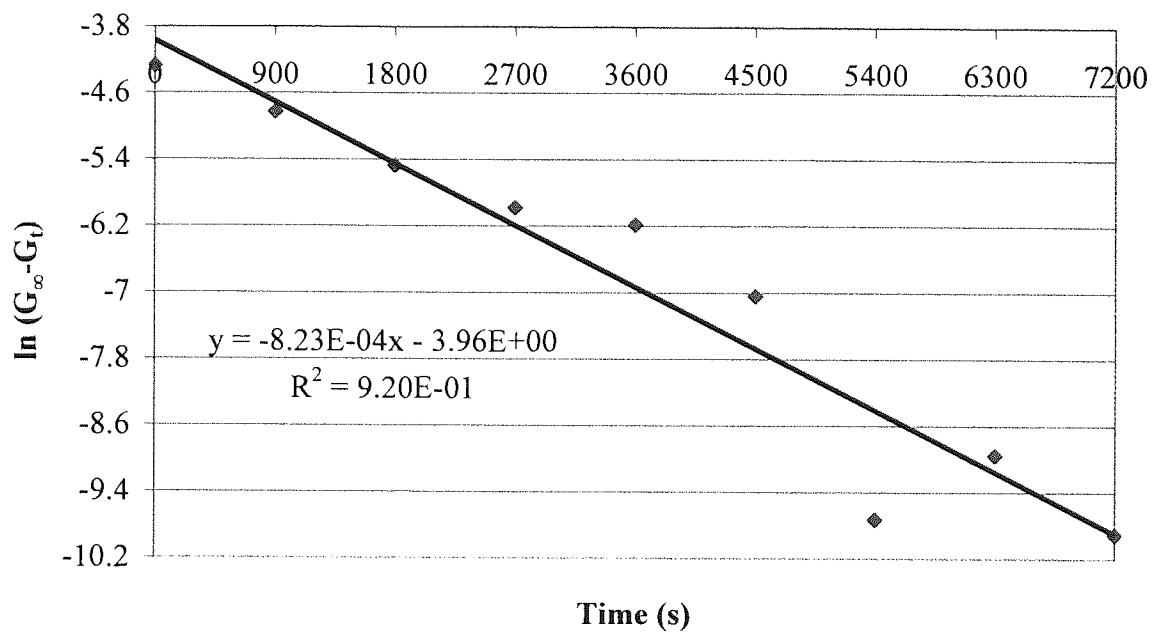


**The Thermally Induced Reaction of 40% (v/v) t-BuCl/IPA with 40% (w/w) IPA/H<sub>2</sub>O at 45.6°C**

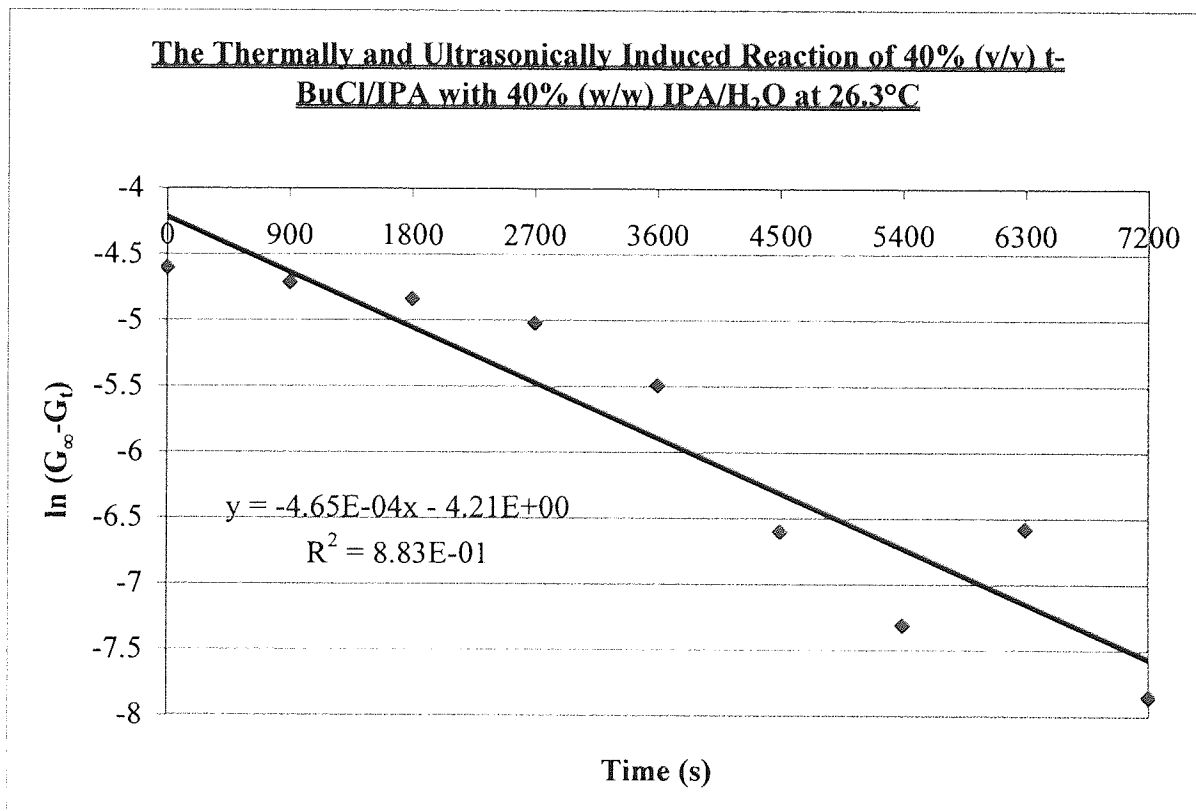
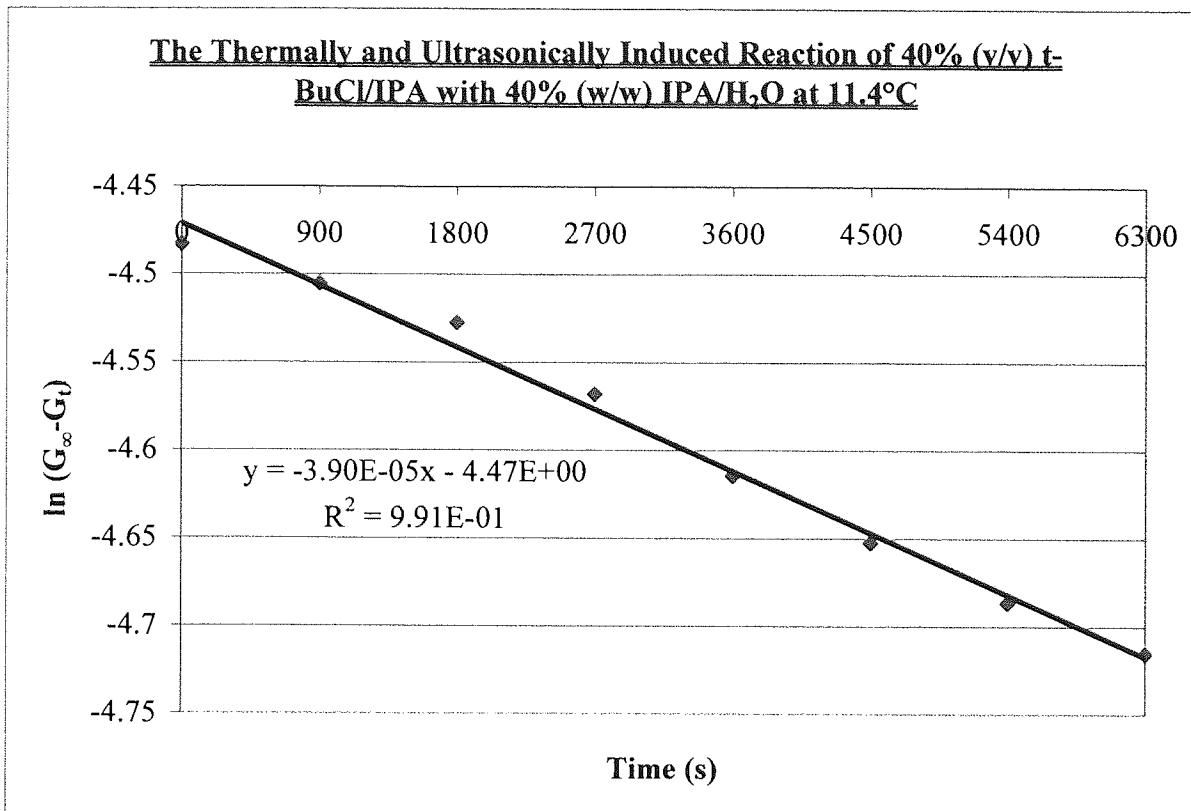




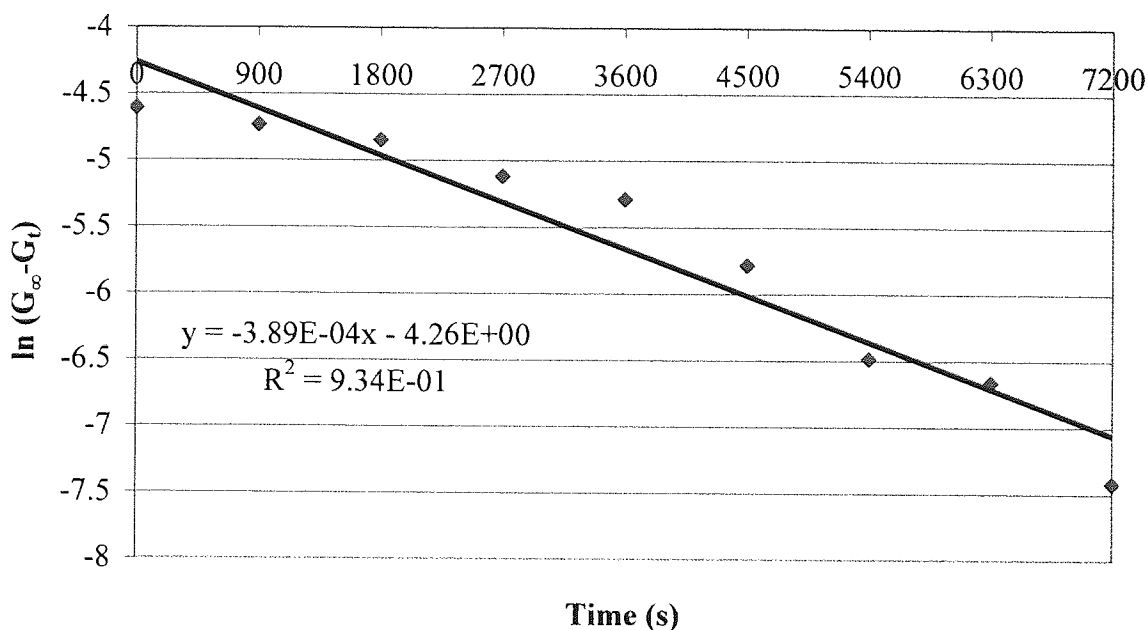
**The Thermally Induced Reaction of 40% (v/v) t-BuCl/IPA with 40% (w/w) IPA/H<sub>2</sub>O at 45.6°C**



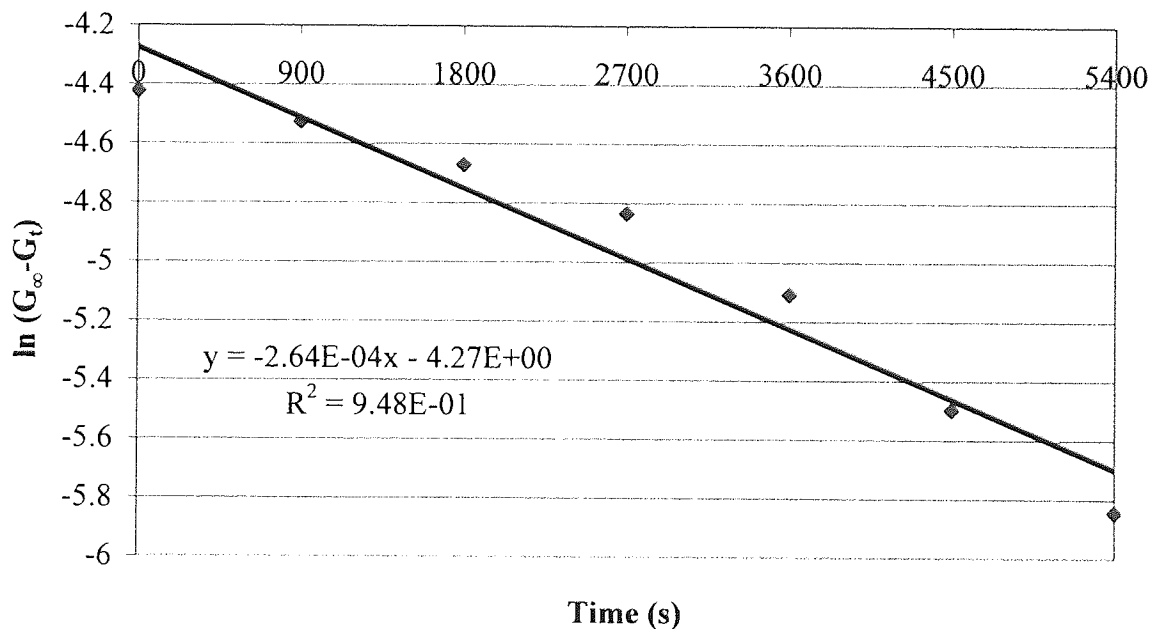
**Appendix 8:** The Thermally and Ultrasonically Induced Reaction of 40% (v/v) t-BuCl/IPA with 40% (w/w) IPA/H<sub>2</sub>O.



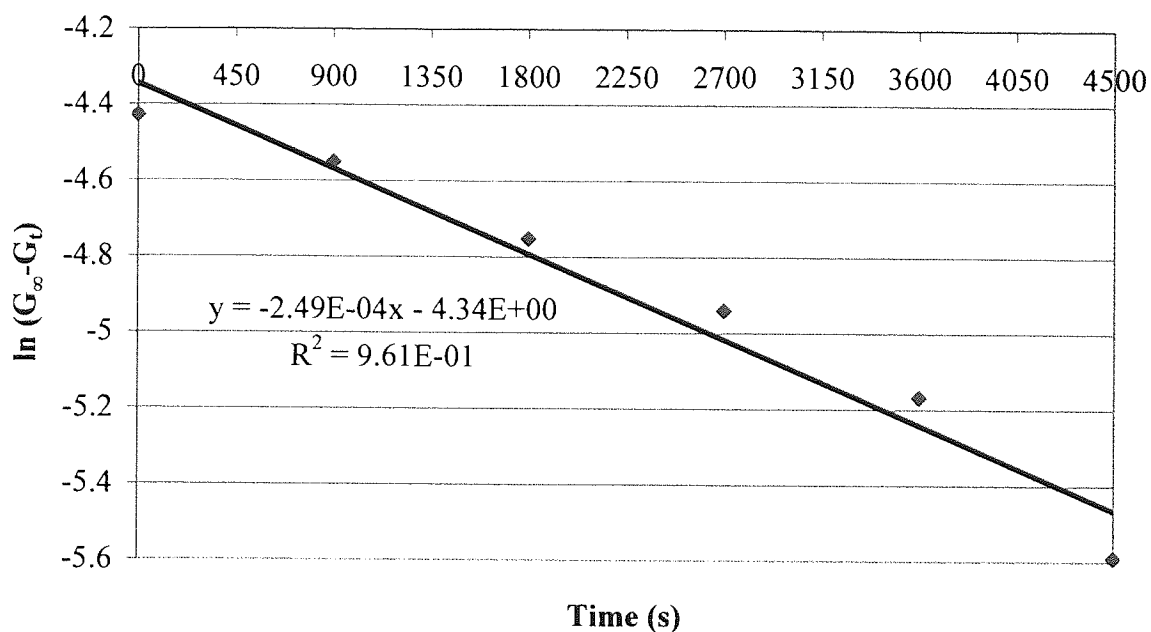
**The Thermally and Ultrasonically Induced Reaction of 40% (v/v) t-BuCl/IPA with 40% (w/w) IPA/H<sub>2</sub>O at 28.6°C**



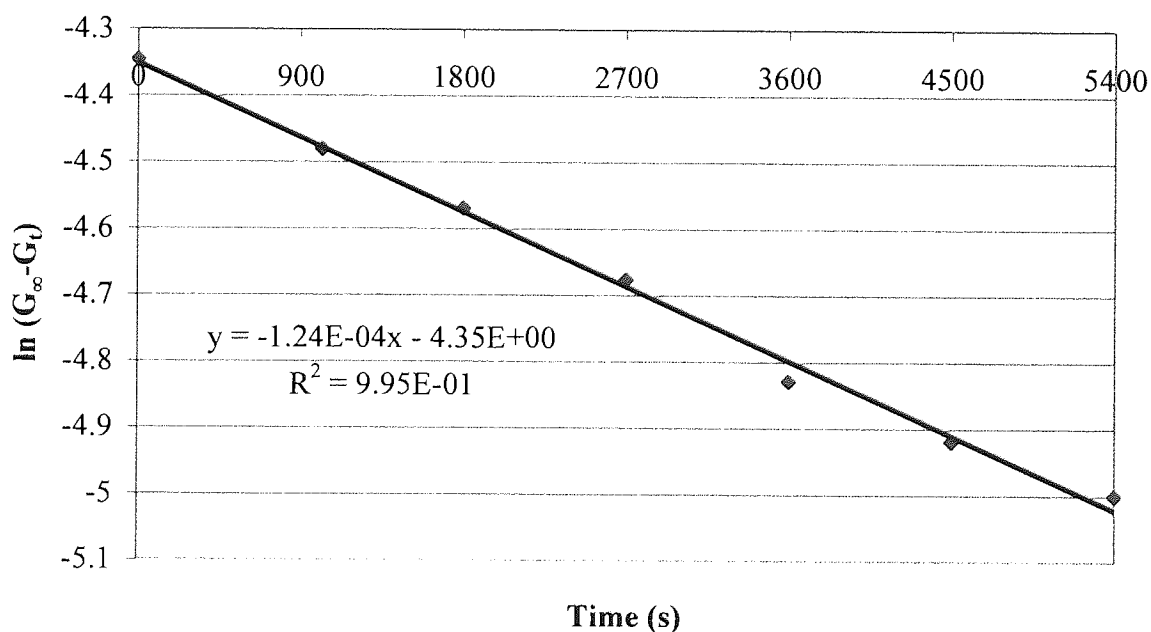
**The Thermally and Ultrasonically Induced Reaction of 40% (v/v) t-BuCl/IPA with 40% (w/w) IPA/H<sub>2</sub>O at 29.1°C**



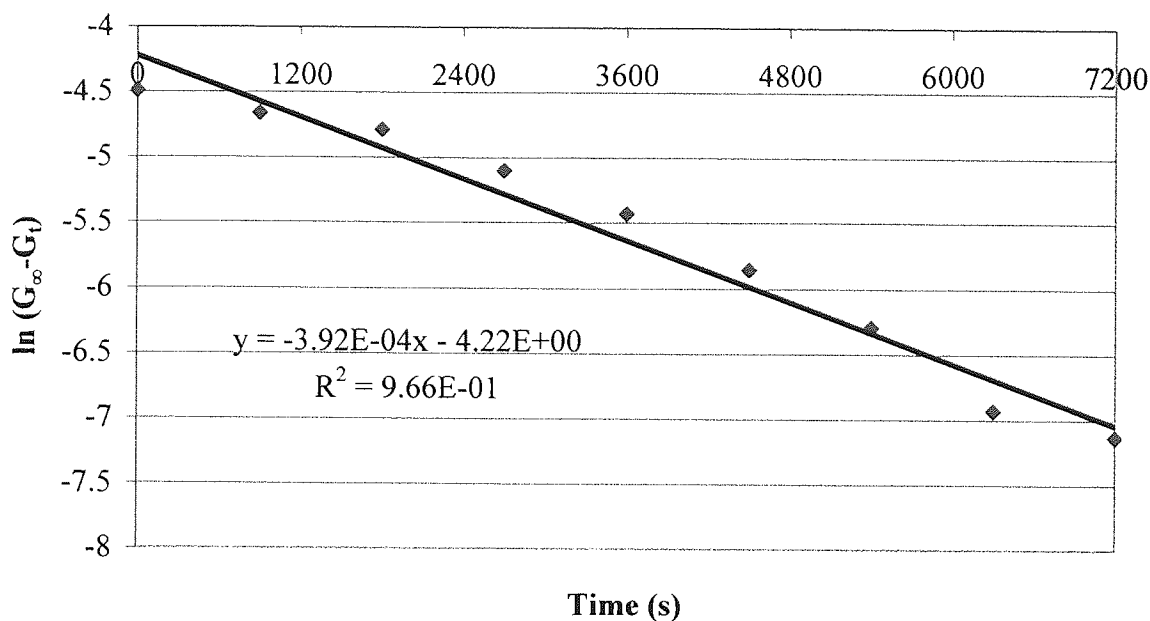
**The Thermally and Ultrasonically Induced Reaction of 40% (v/v) t-BuCl/IPA with 40% (w/w) IPA/H<sub>2</sub>O at 29.6°C**



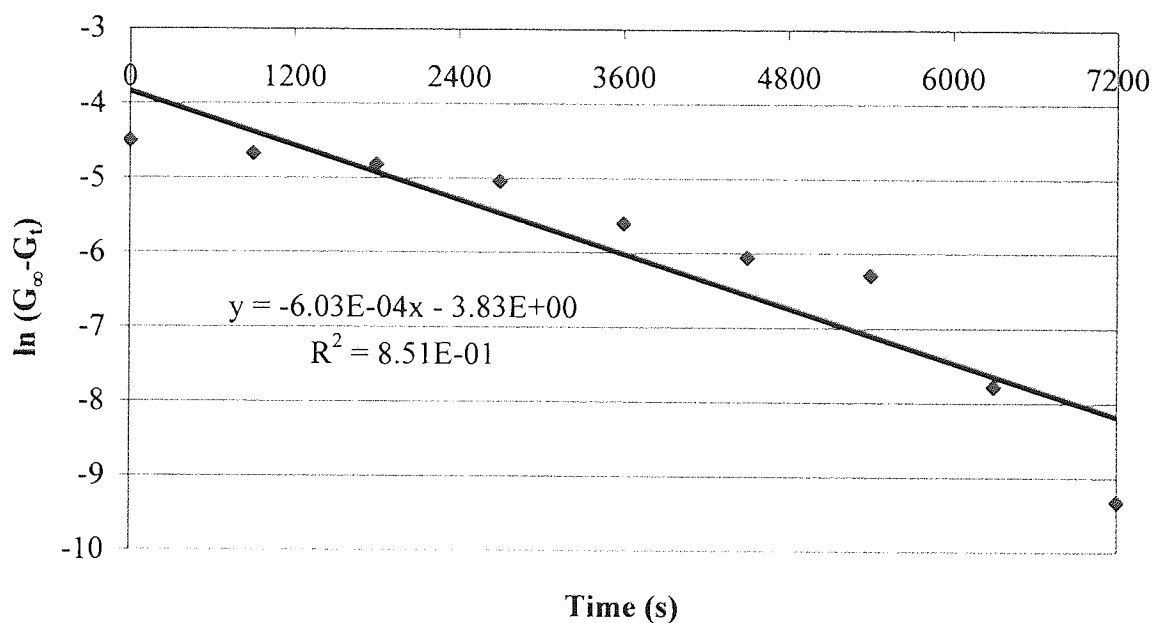
**The Thermally and Ultrasonically Induced Reaction of 40% (v/v) t-BuCl/IPA with 40% (w/w) IPA/H<sub>2</sub>O at 29.9°C**



**The Thermally and Ultrasonically Induced Reaction of 40% (v/v) t-BuCl/IPA with 40% (w/w) IPA/H<sub>2</sub>O at 32.1°C**



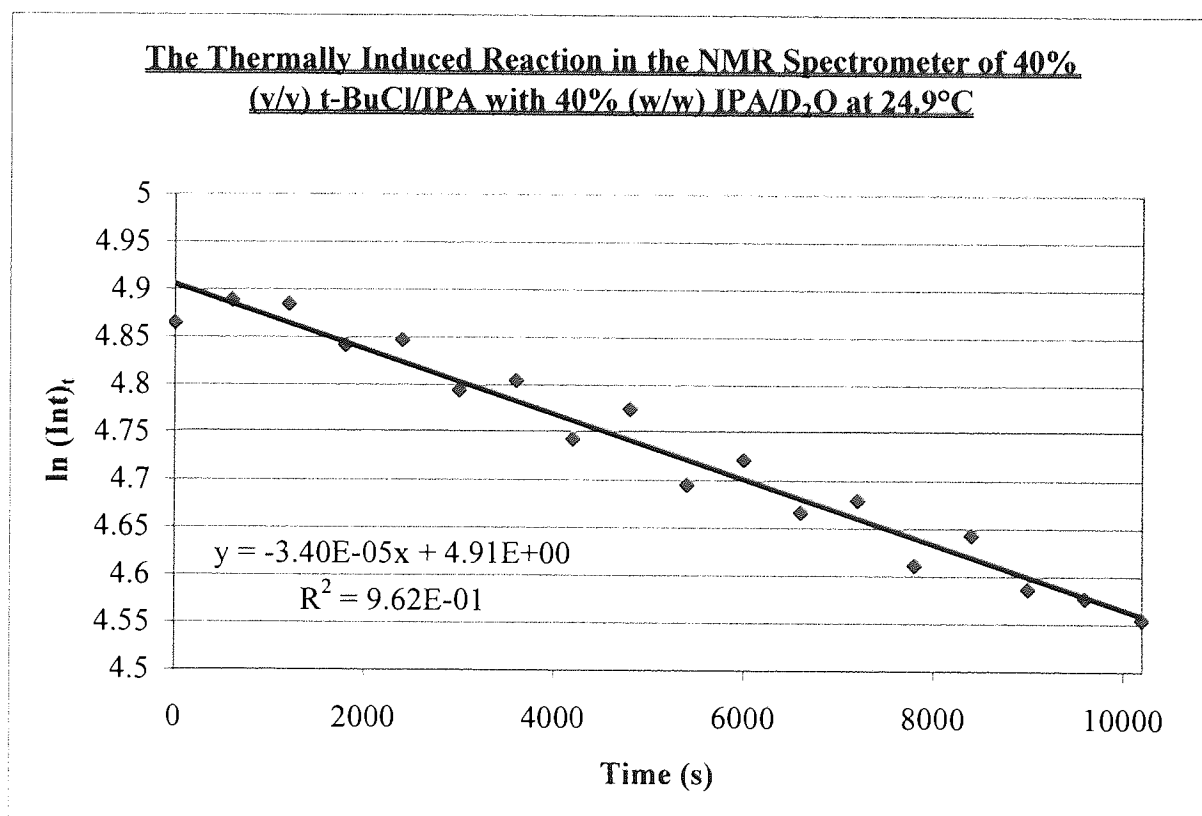
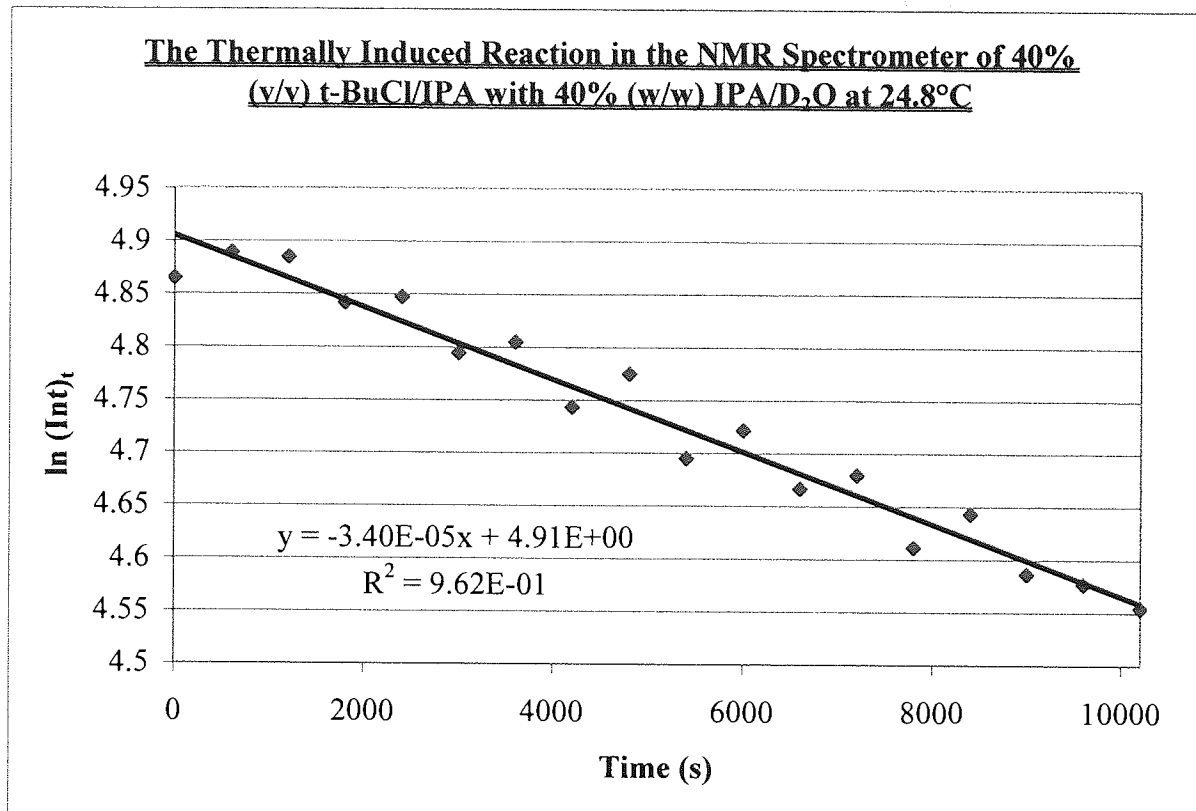
**The Thermally and Ultrasonically Induced Reaction of 40% (v/v) t-BuCl/IPA with 40% (w/w) IPA/H<sub>2</sub>O at 39.6°C**



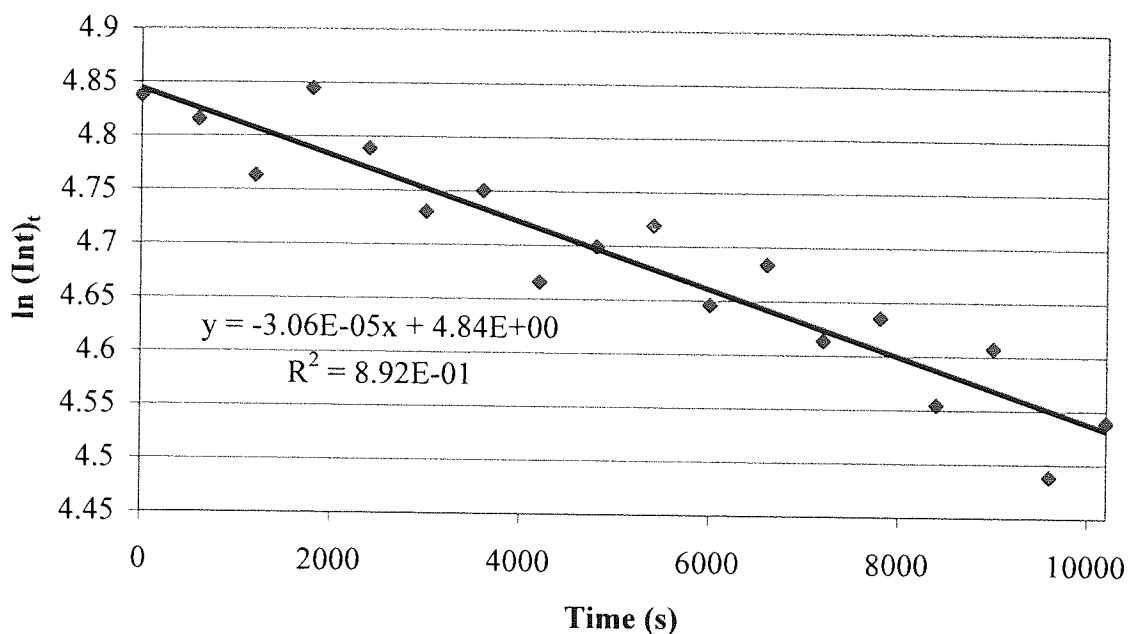
**Appendix 9:** Microprogramme for the in-situ detection of the Reaction of 40% (v/v) t-BuCl/IPA with 40% (w/w) IPA/H<sub>2</sub>O by <sup>1</sup>H NMR Spectroscopy.

1 ZE  
2 WR FA  
3 IF FA  
4 LO TO 2 TIMES C  
5 RF FA.001  
6 RE FA  
7 GO=7  
8 WR FA  
9 IF FA  
10 IN=6  
11 D4 DO  
12 EXIT  
NS=16

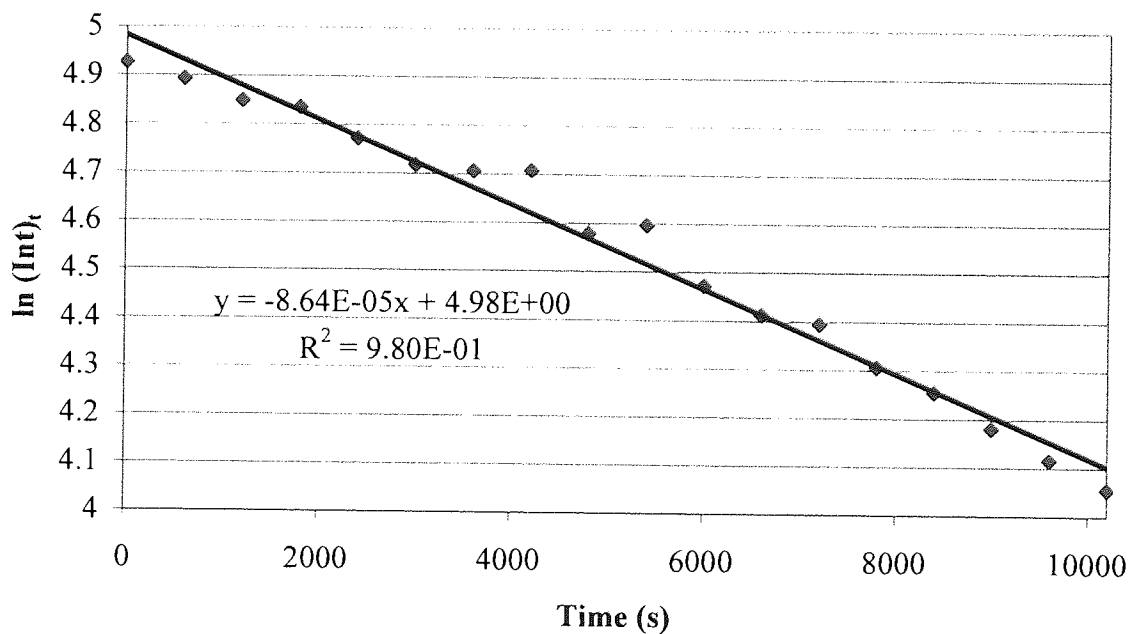
**Appendix 10:** The Thermally Induced Reaction in the NMR Spectrometer of 40% (v/v) t-BuCl/IPA with 40% (w/w) IPA/D<sub>2</sub>O.



**The Thermally Induced Reaction in the NMR Spectrometer of 40% (v/v) t-BuCl/IPA with 40% (w/w) IPA/D<sub>2</sub>O at 24.9°C**

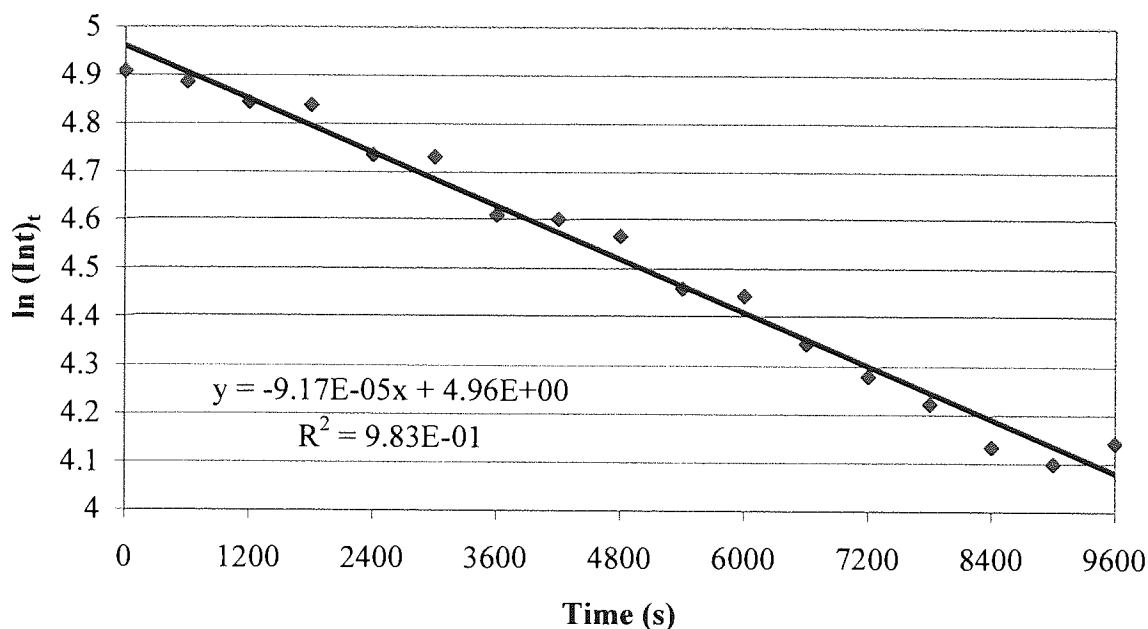


**The Thermally Induced Reaction in the NMR Spectrometer of 40% (v/v) t-BuCl/IPA with 40% (w/w) IPA/D<sub>2</sub>O at 32.2°C**

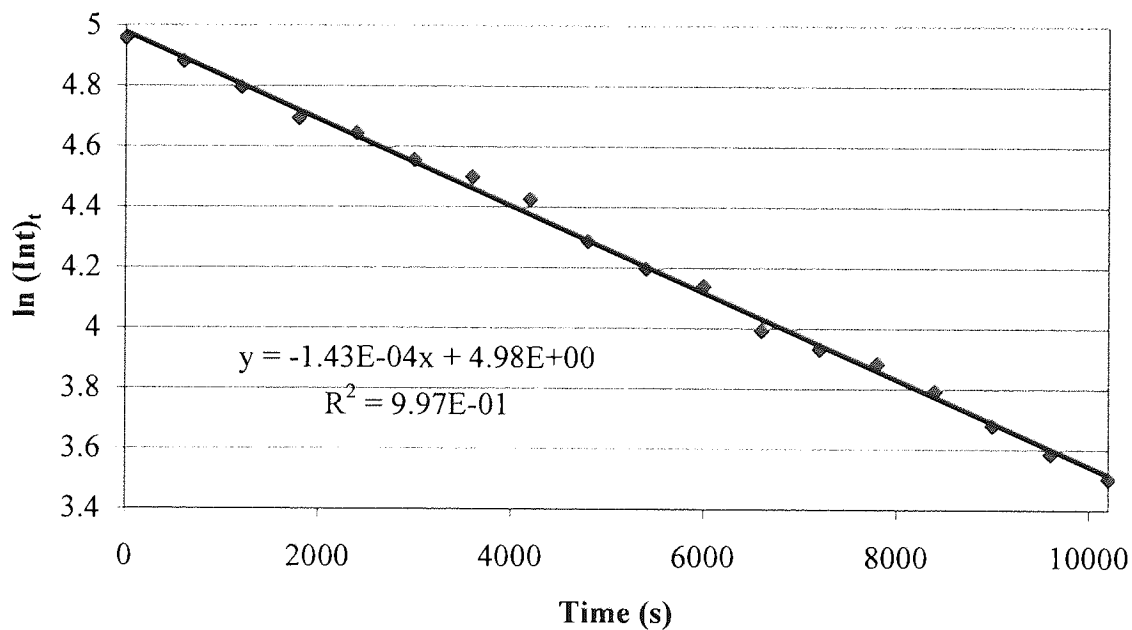




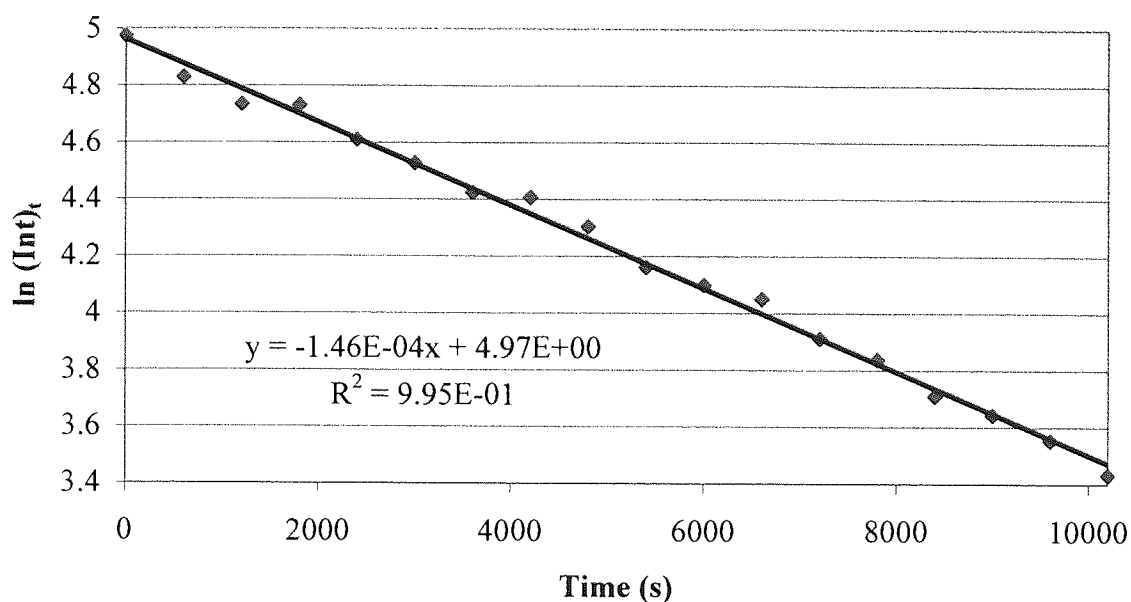
**The Thermally Induced Reaction in the NMR Spectrometer of 40% (v/v) t-BuCl/IPA with 40% (w/w) IPA/D<sub>2</sub>O at 32.8°C**



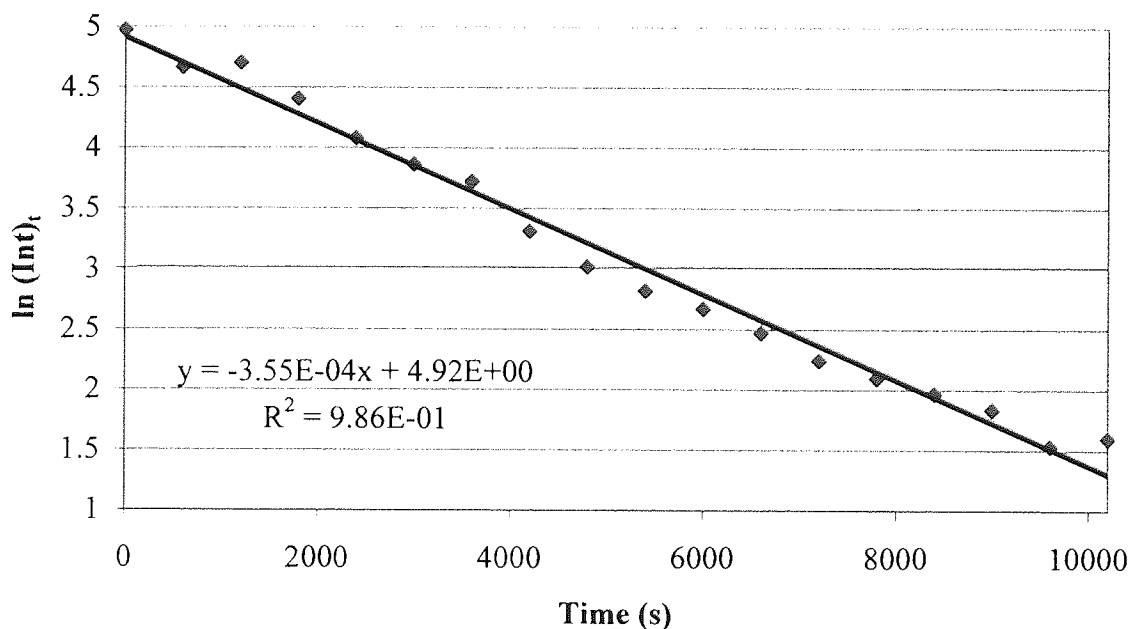
**The Thermally Induced Reaction in the NMR Spectrometer of 40% (v/v) t-BuCl/IPA with 40% (w/w) IPA/D<sub>2</sub>O at 35.5°C**



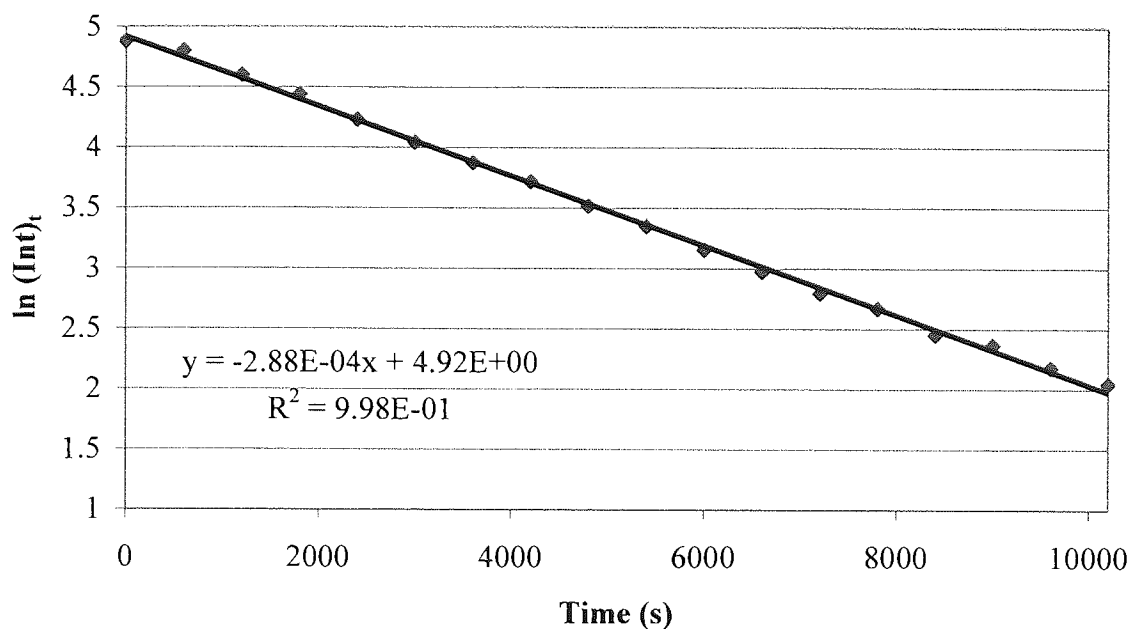
**The Thermally Induced Reaction in the NMR Spectrometer of 40% (v/v) t-BuCl/IPA with 40% (w/w) IPA/D<sub>2</sub>O at 35.5°C**



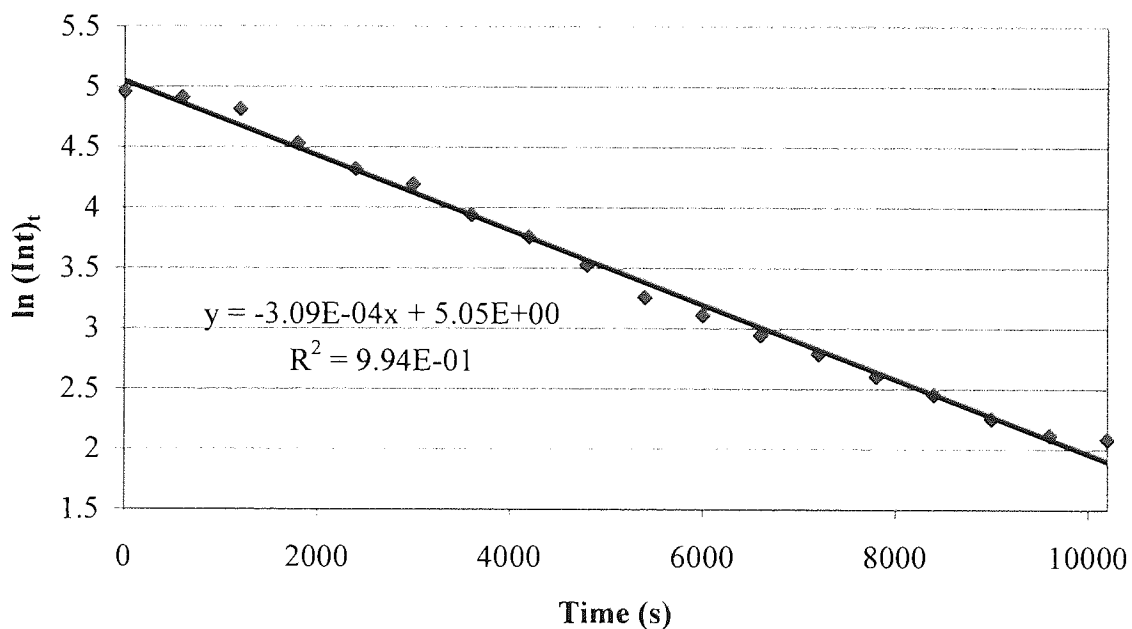
**The Thermally Induced Reaction in the NMR Spectrometer of 40% (v/v) t-BuCl/IPA with 40% (w/w) IPA/D<sub>2</sub>O at 41.9°C**



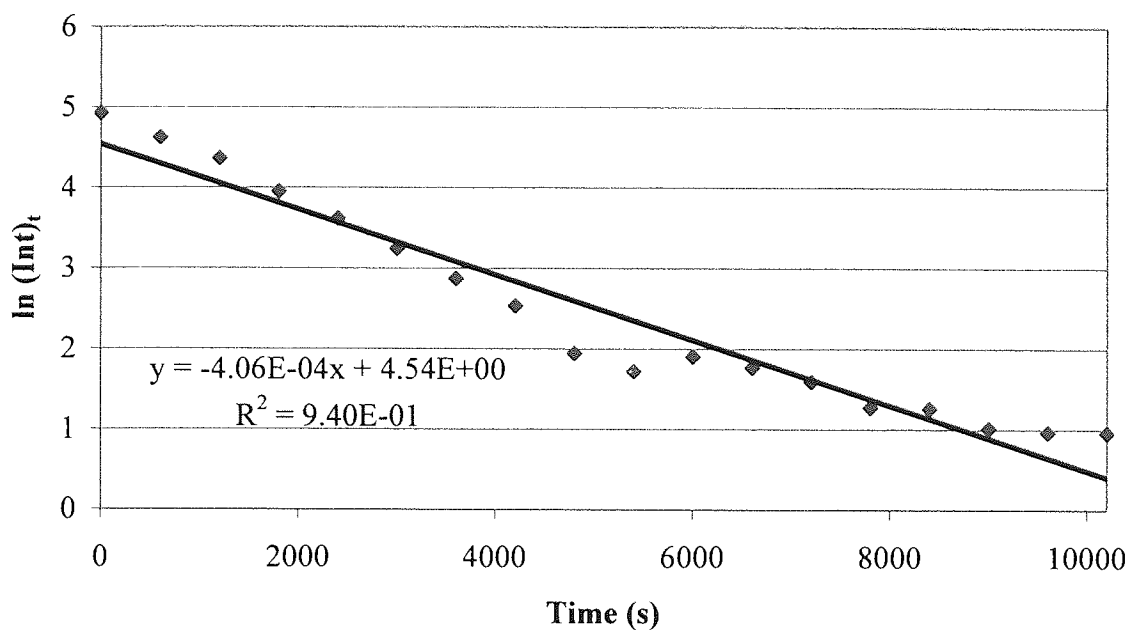
**The Thermally Induced Reaction in the NMR Spectrometer of 40% (v/v) t-BuCl/IPA with 40% (w/w) IPA/D<sub>2</sub>O at 42.2°C**



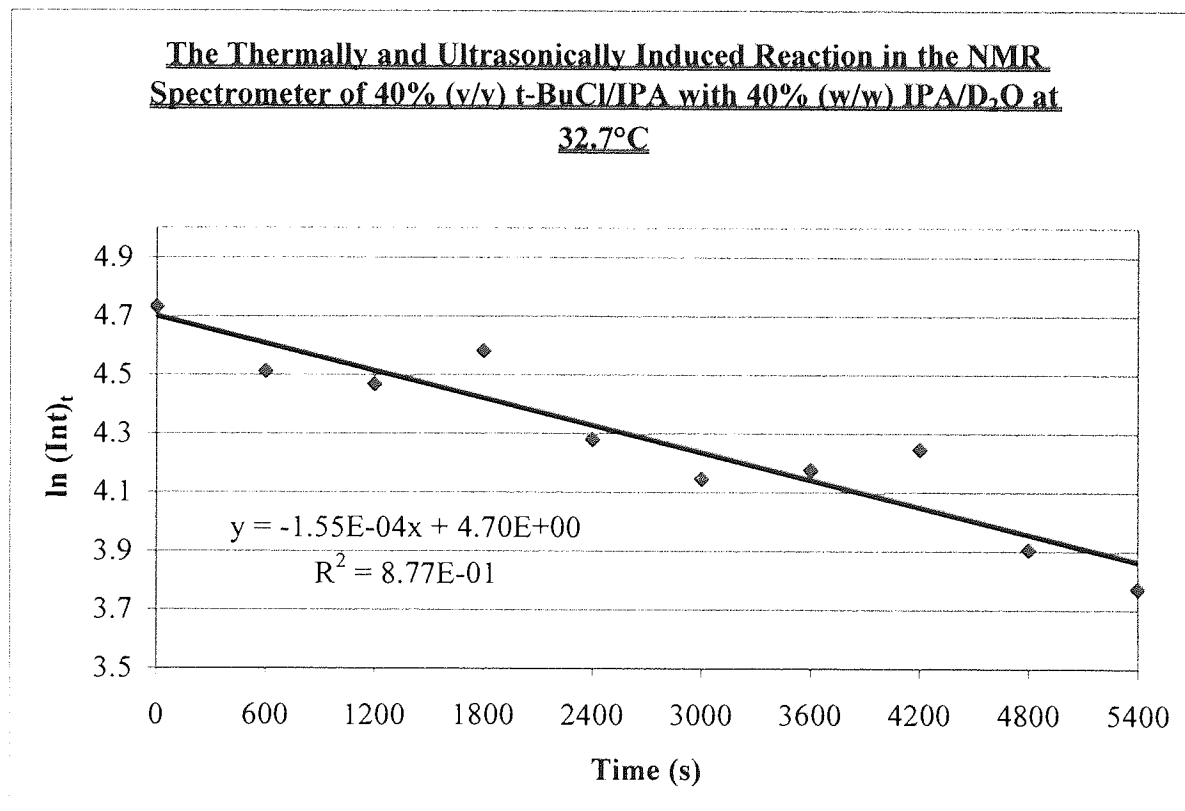
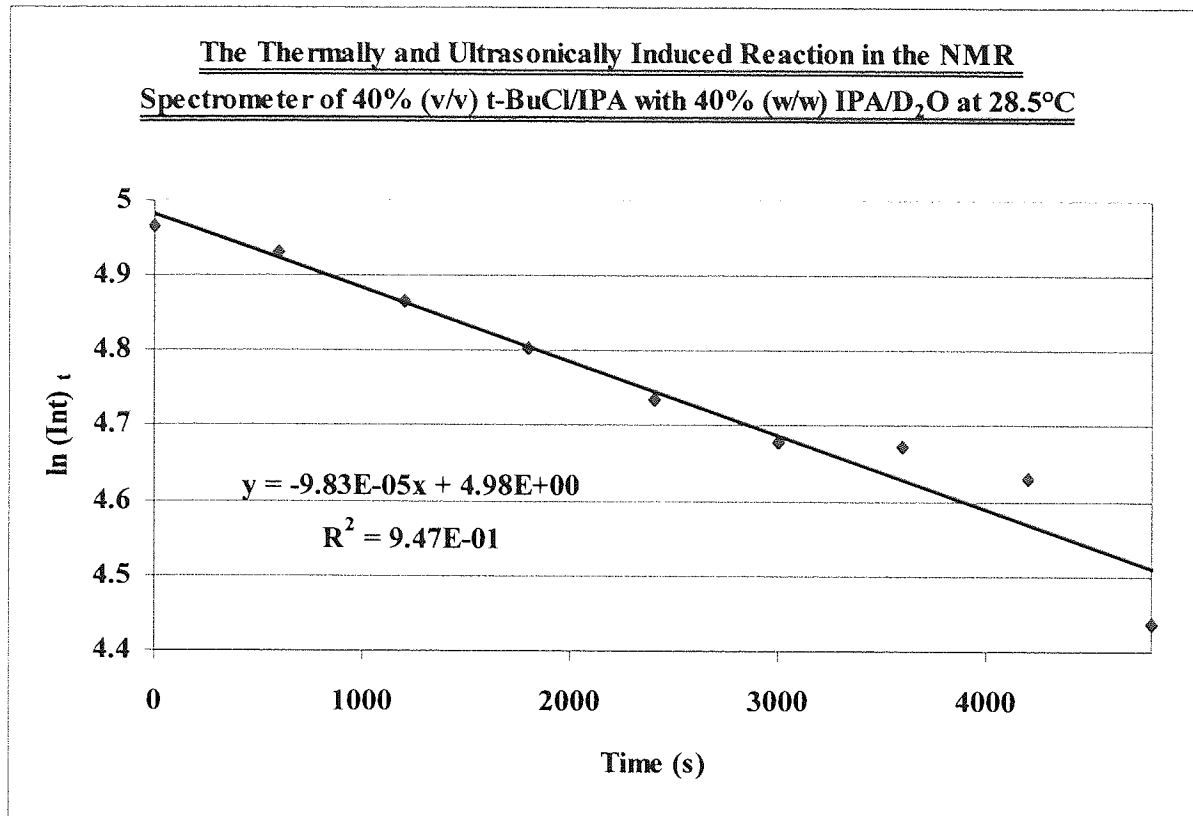
**The Thermally Induced Reaction in the NMR Spectrometer of 40% (v/v) t-BuCl/IPA with 40% (w/w) IPA/D<sub>2</sub>O at 42.3°C**



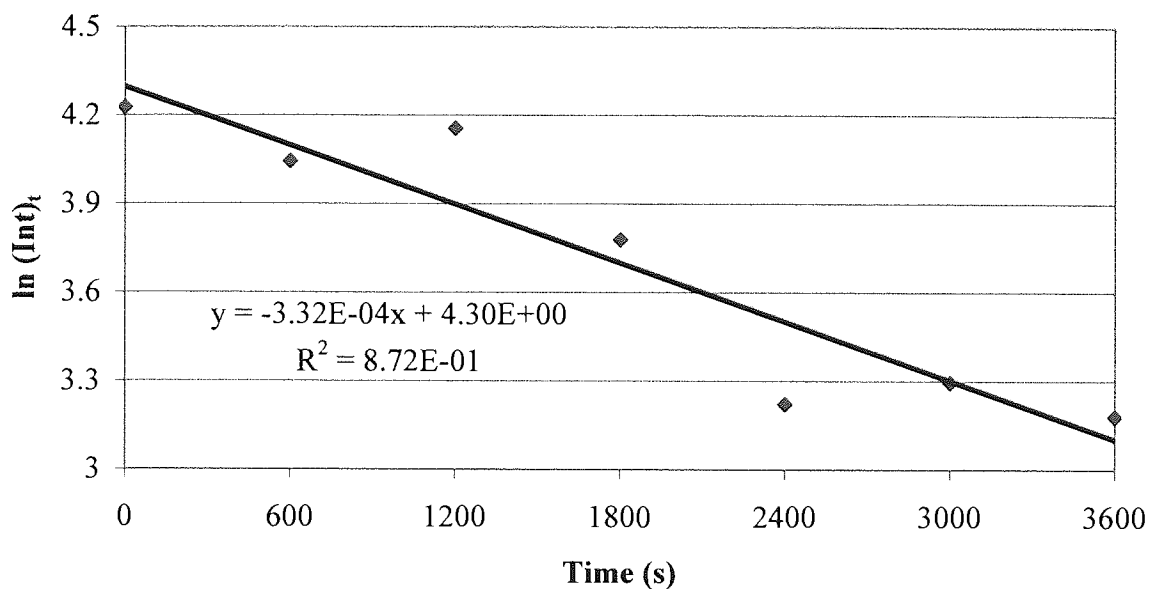
**The Thermally Induced Reaction in the NMR Spectrometer of 40%  
(v/v) t-BuCl/IPA with 40% (w/w) IPA/D<sub>2</sub>O at 45.1°C**



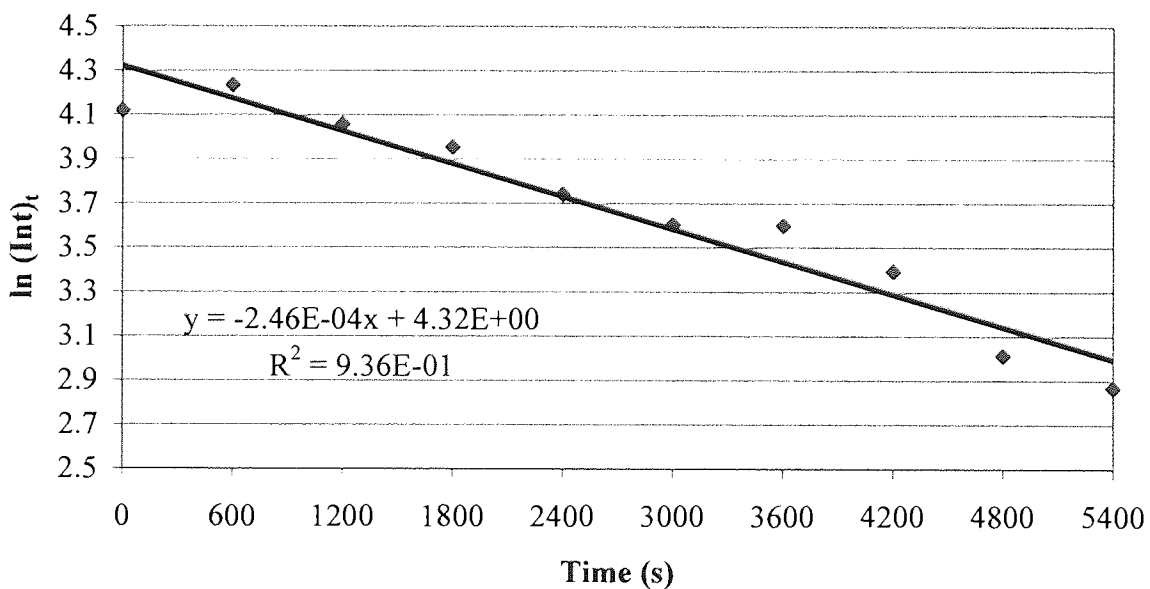
**Appendix 11:** The Ultrasonically Induced Reaction in the NMR Spectrometer of 40% (v/v) t-BuCl/IPA with 40% (w/w) IPA/D<sub>2</sub>O.



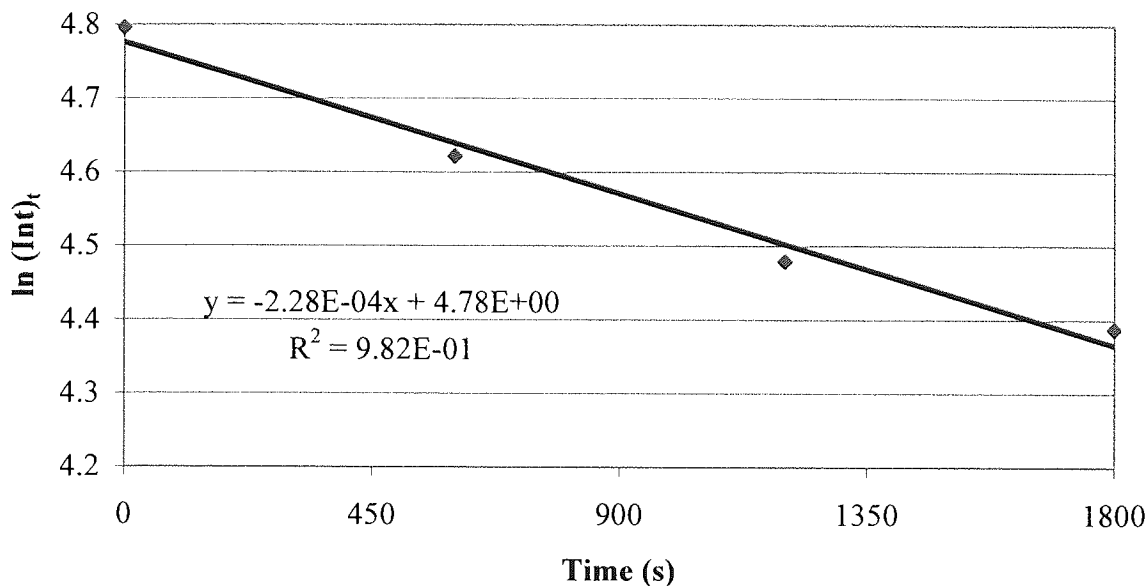
**The Thermally and Ultrasonically Induced Reaction in the NMR Spectrometer of 40% (v/v) t-BuCl/IPA with 40% (w/w) IPA/D<sub>2</sub>O at 32.8°C**



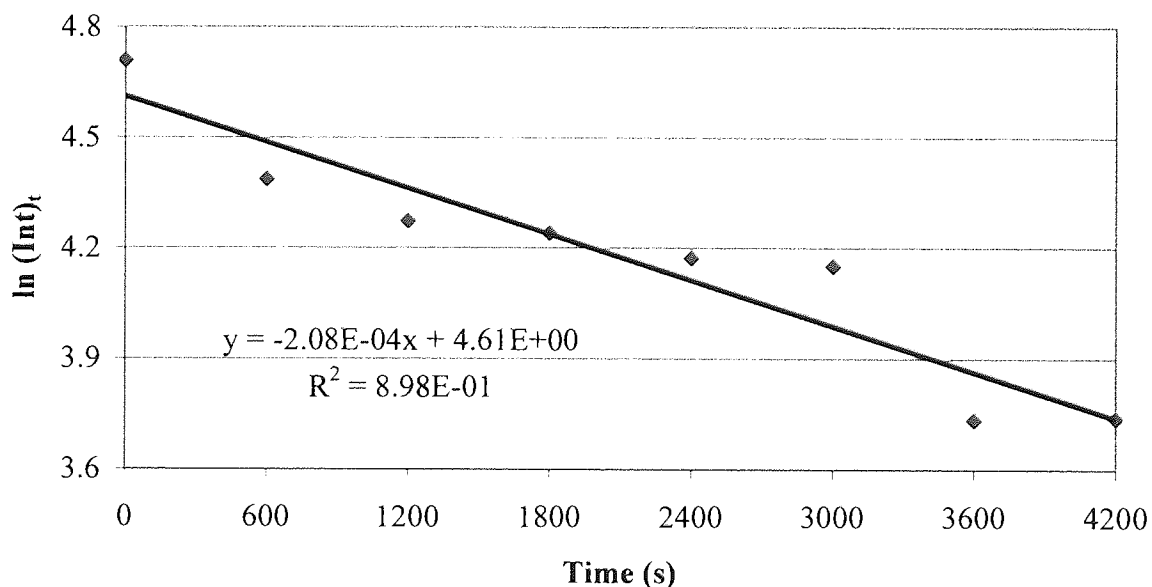
**The Thermally and Ultrasonically Induced Reaction in the NMR Spectrometer of 40% (v/v) t-BuCl/IPA with 40% (w/w) IPA/D<sub>2</sub>O at 34.2°C**



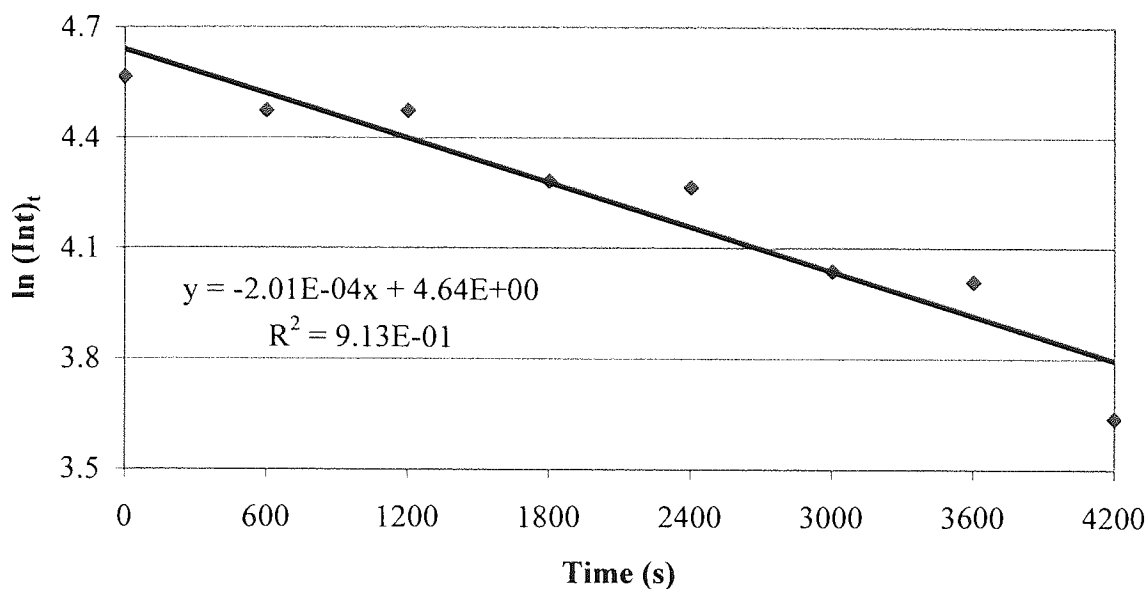
**The Thermally and Ultrasonically Induced Reaction in the NMR Spectrometer of 40% (v/v) t-BuCl/IPA with 40% (w/w) IPA/D<sub>2</sub>O at 34.3°C**



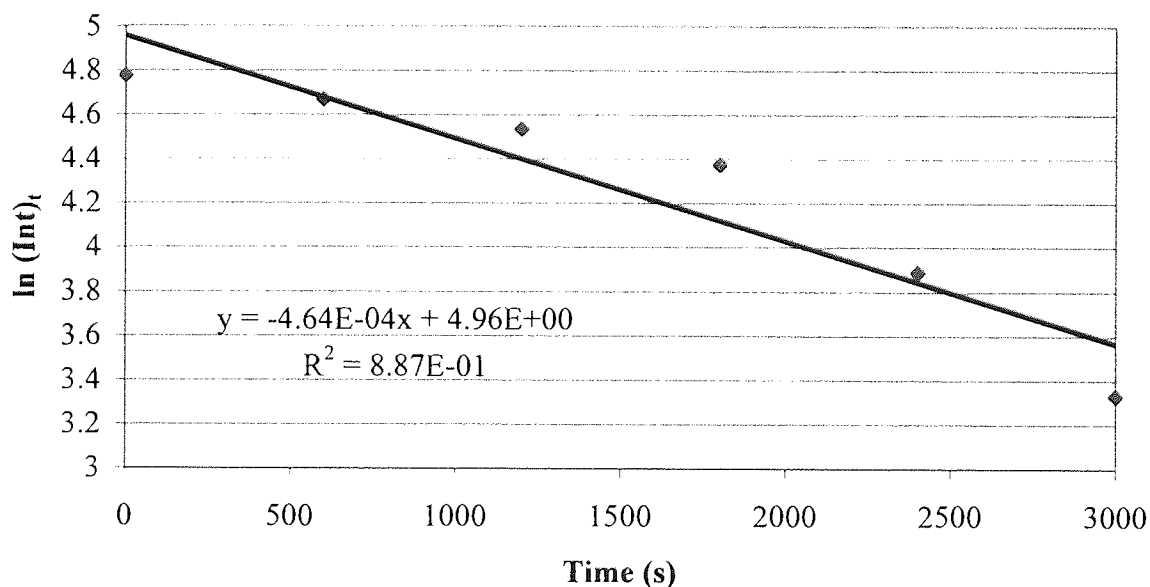
**The Thermally and Ultrasonically Induced Reaction in the NMR Spectrometer of 40% (v/v) t-BuCl/IPA with 40% (w/w) IPA/D<sub>2</sub>O at 35.4°C**



**The Thermally and Ultrasonically Induced Reaction in the NMR Spectrometer of 40% (v/v) t-BuCl/IPA with 40% (w/w) IPA/D<sub>2</sub>O at 37.0°C**

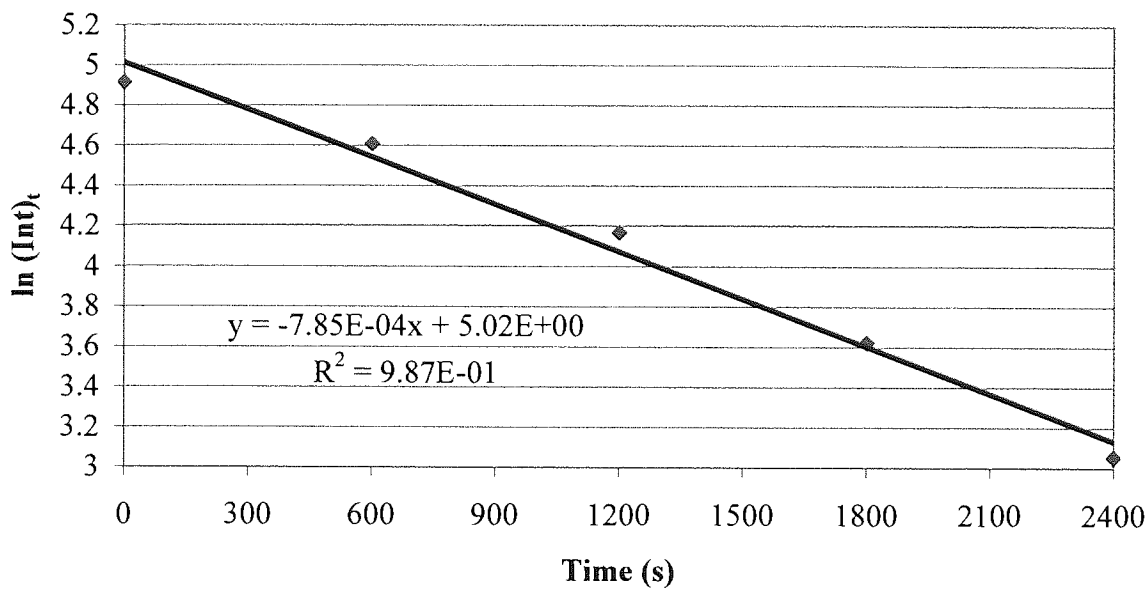


**The Thermally and Ultrasonically Induced Reaction in the NMR Spectrometer of 40% (v/v) t-BuCl/IPA with 40% (w/w) IPA/D<sub>2</sub>O at 43.5°C**

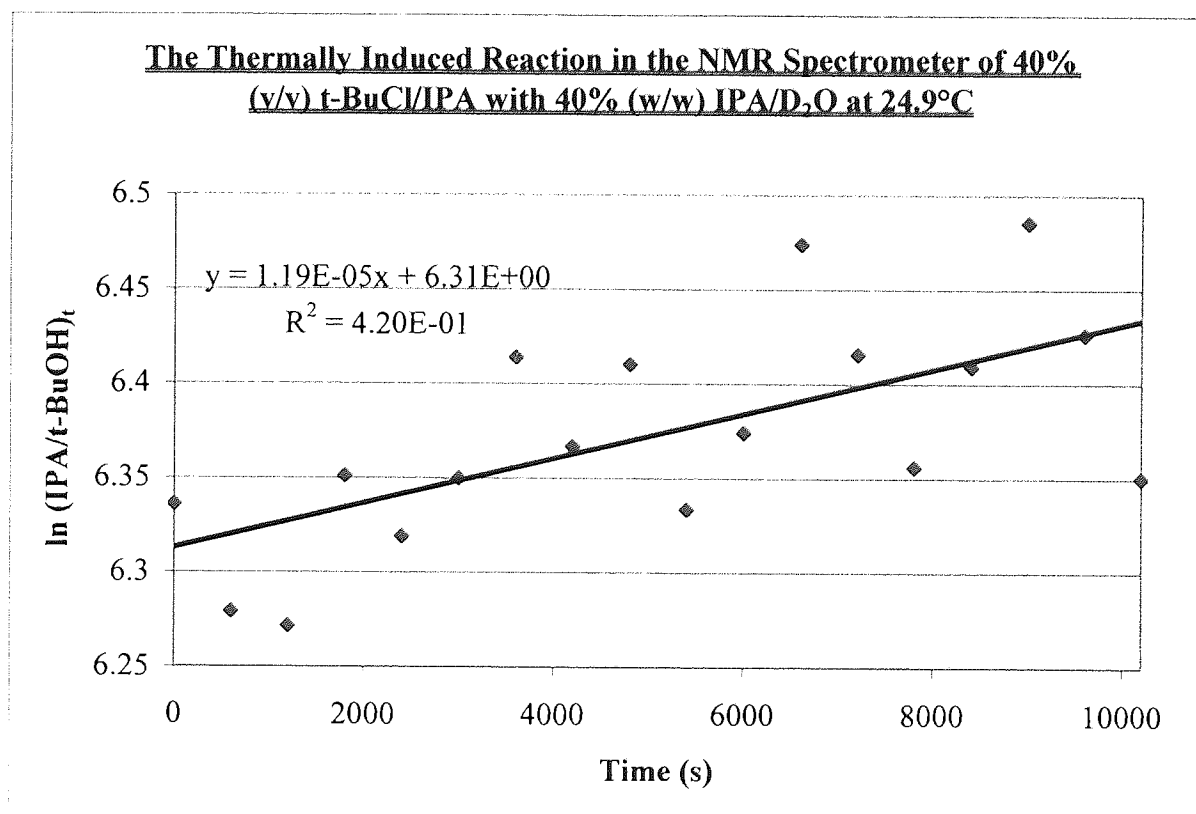
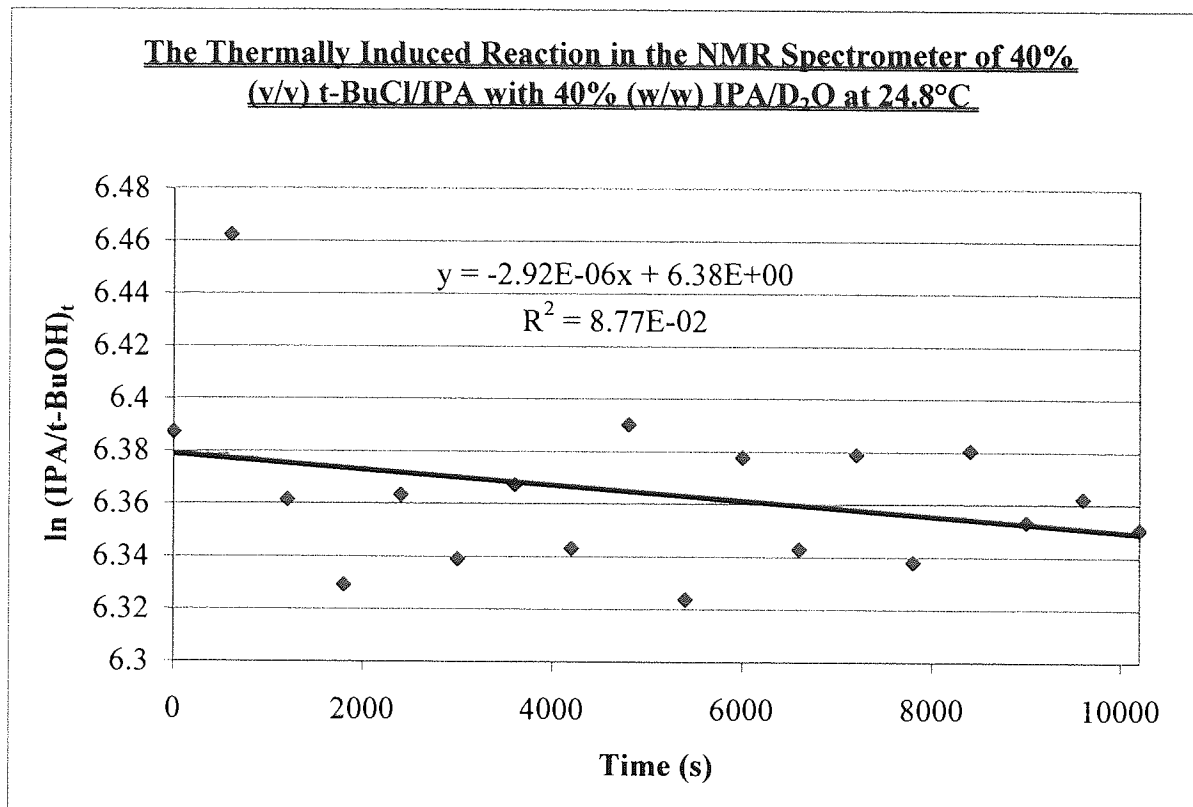




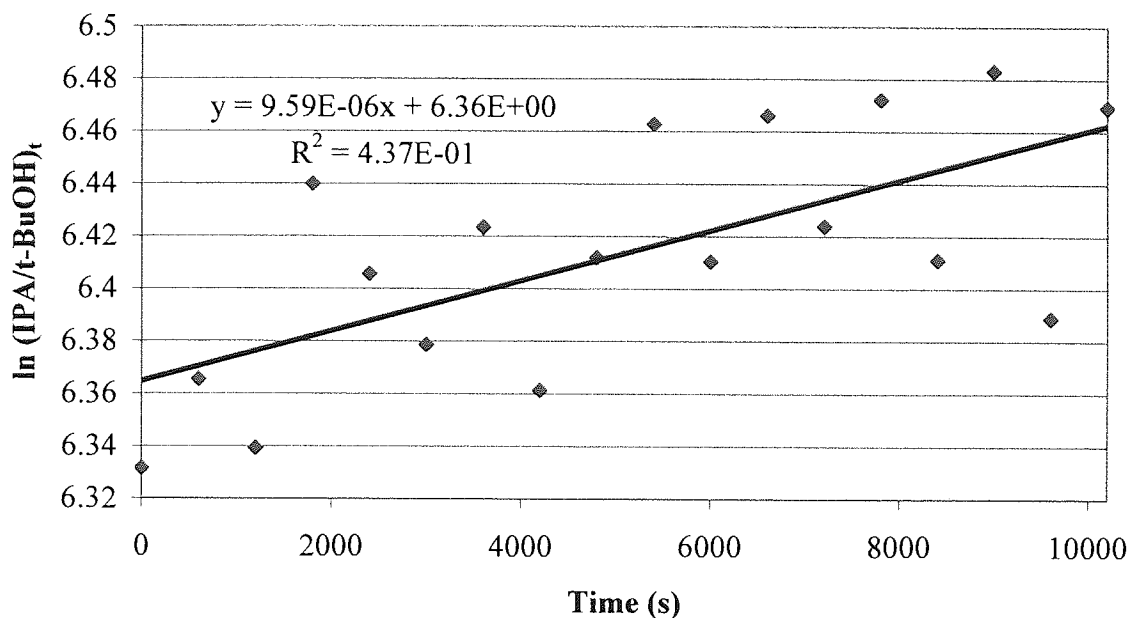
**The Thermally and Ultrasonically Induced Reaction in the NMR Spectrometer of 40% (v/v) t-BuCl/IPA with 40% (w/w) IPA/D<sub>2</sub>O at 45.9°C**



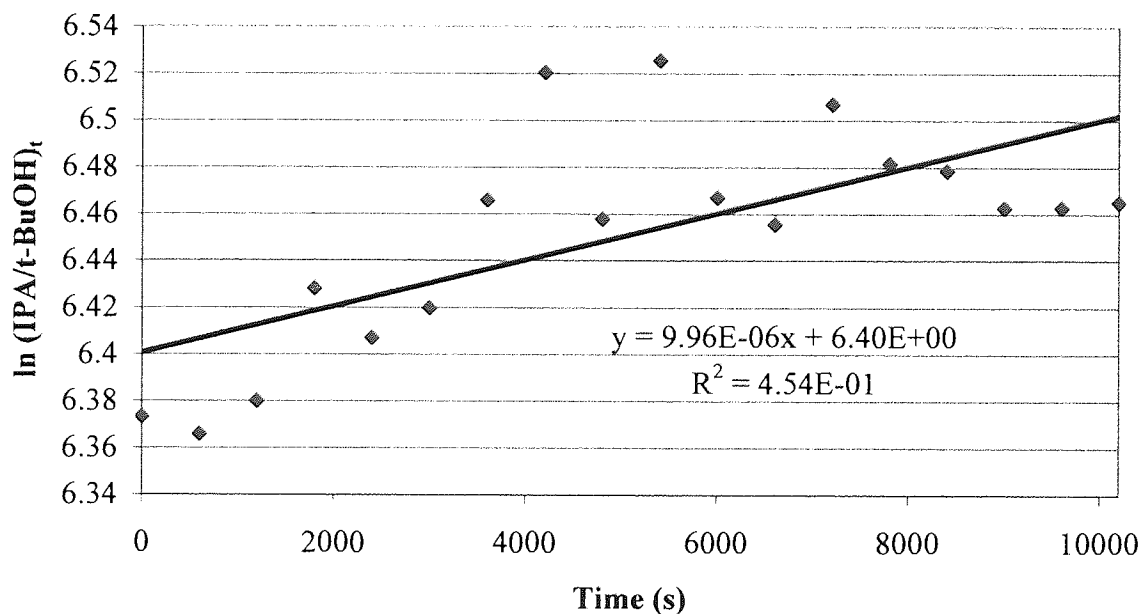
**Appendix 12:** The Thermally Induced Reaction in the NMR Spectrometer of 40% (v/v) t-BuCl/IPA with 40% (w/w) IPA/D<sub>2</sub>O.



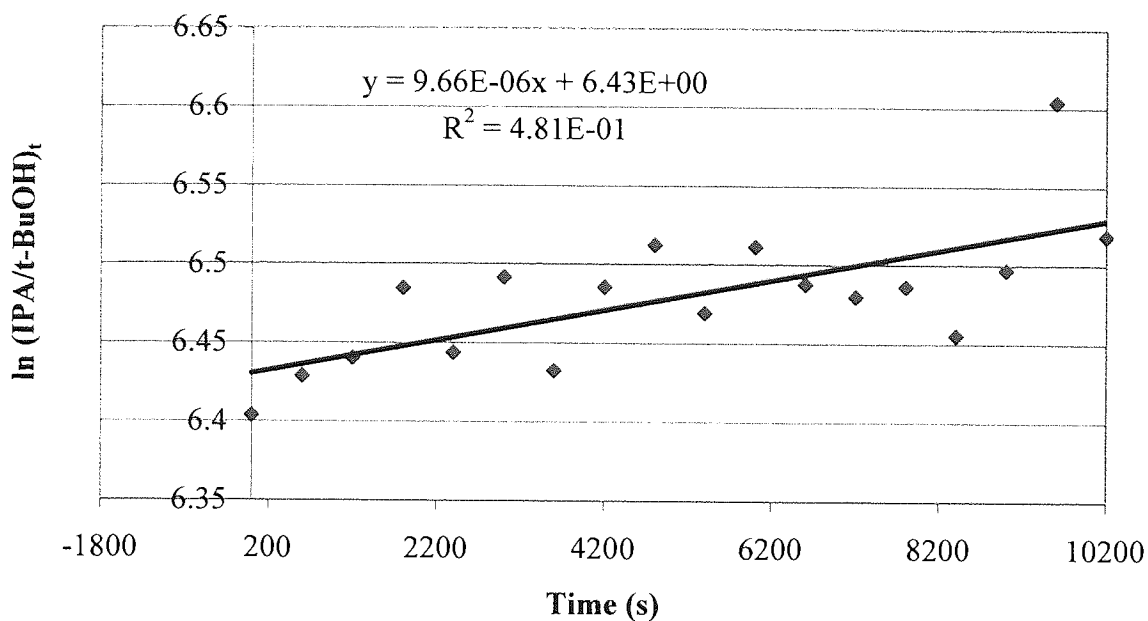
**The Thermally Induced Reaction in the NMR Spectrometer of 40% (v/v) t-BuCl/IPA with 40% (w/w) IPA/D<sub>2</sub>O at 24.9°C**



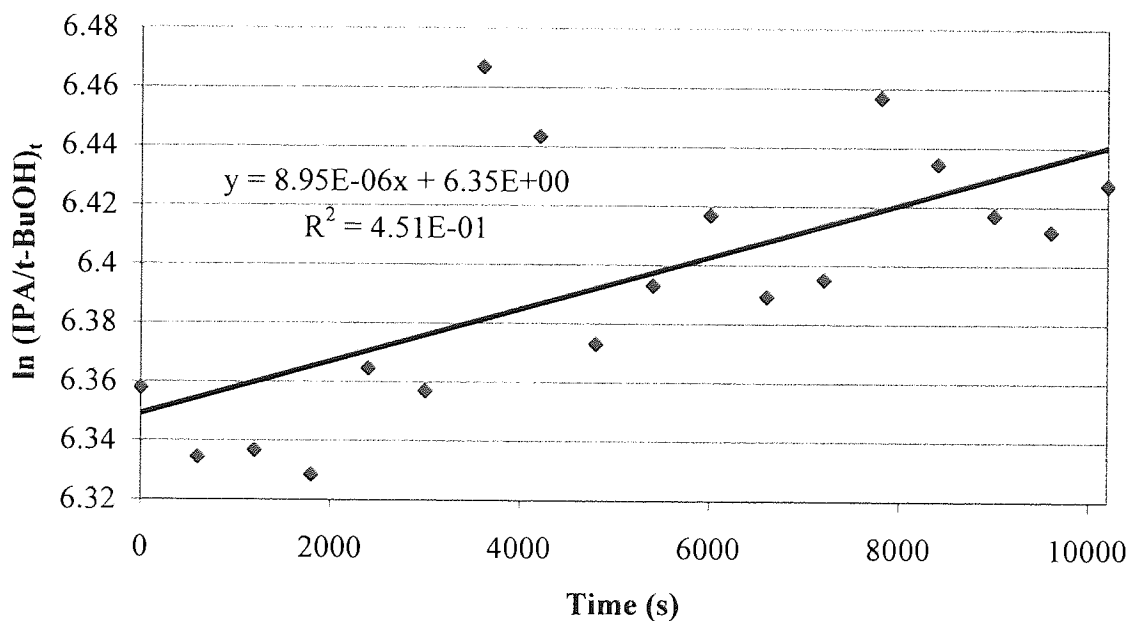
**The Thermally Induced Reaction in the NMR Spectrometer of 40% (v/v) t-BuCl/IPA with 40% (w/w) IPA/D<sub>2</sub>O at 32.2°C**



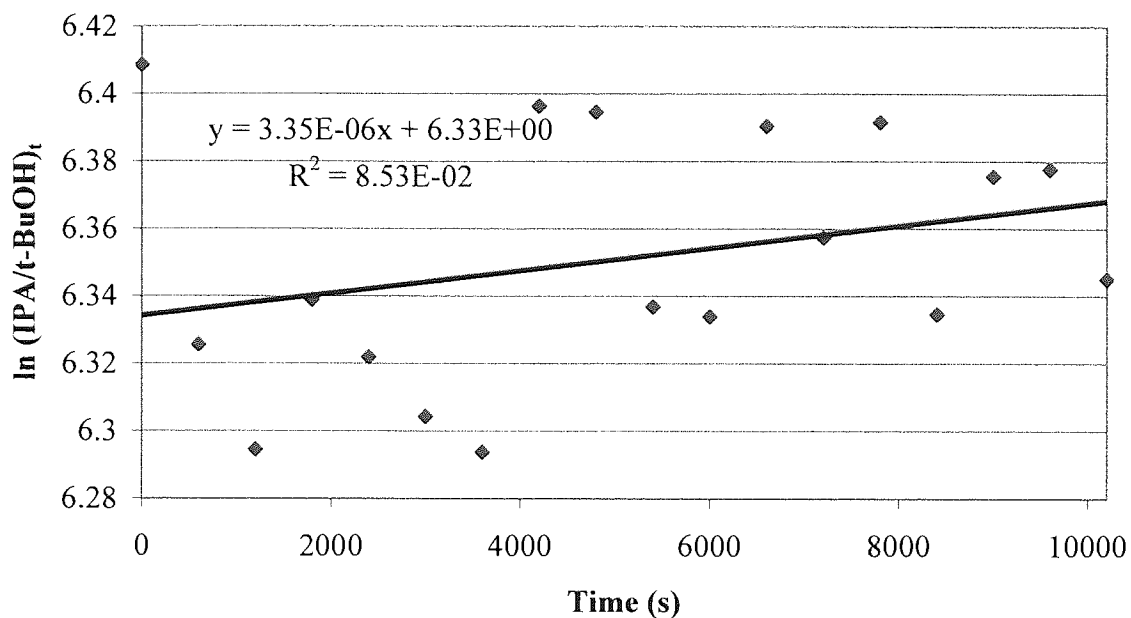
**The Thermally Induced Reaction in the NMR Spectrometer of 40% (v/v) t-BuCl/IPA with 40% (w/w) IPA/D<sub>2</sub>O at 32.8°C**



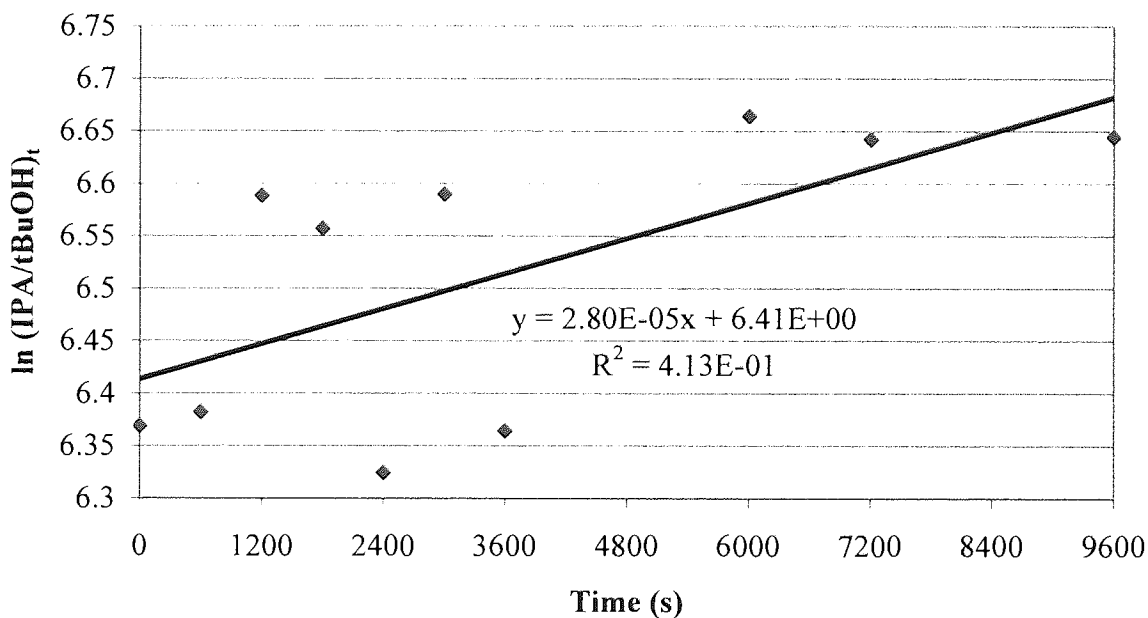
**The Thermally Induced Reaction in the NMR Spectrometer of 40% (v/v) t-BuCl/IPA with 40% (w/w) IPA/D<sub>2</sub>O at 35.5°C**



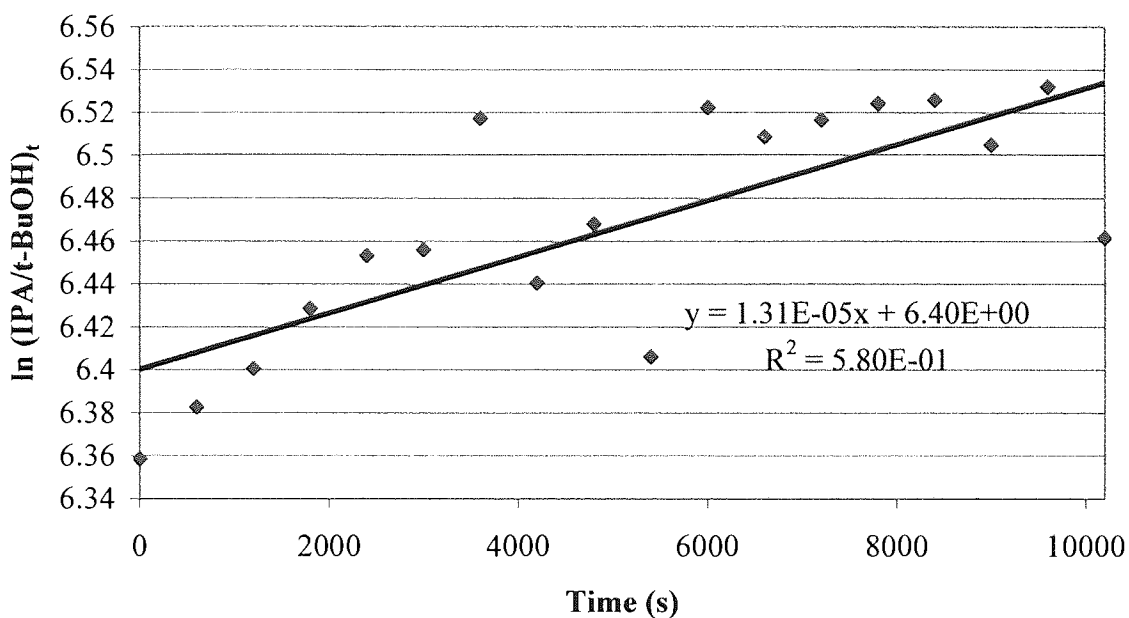
**The Thermally Induced Reaction in the NMR Spectrometer of 40% (v/v) t-BuCl/IPA with 40% (w/w) IPA/D<sub>2</sub>O at 35.5°C**



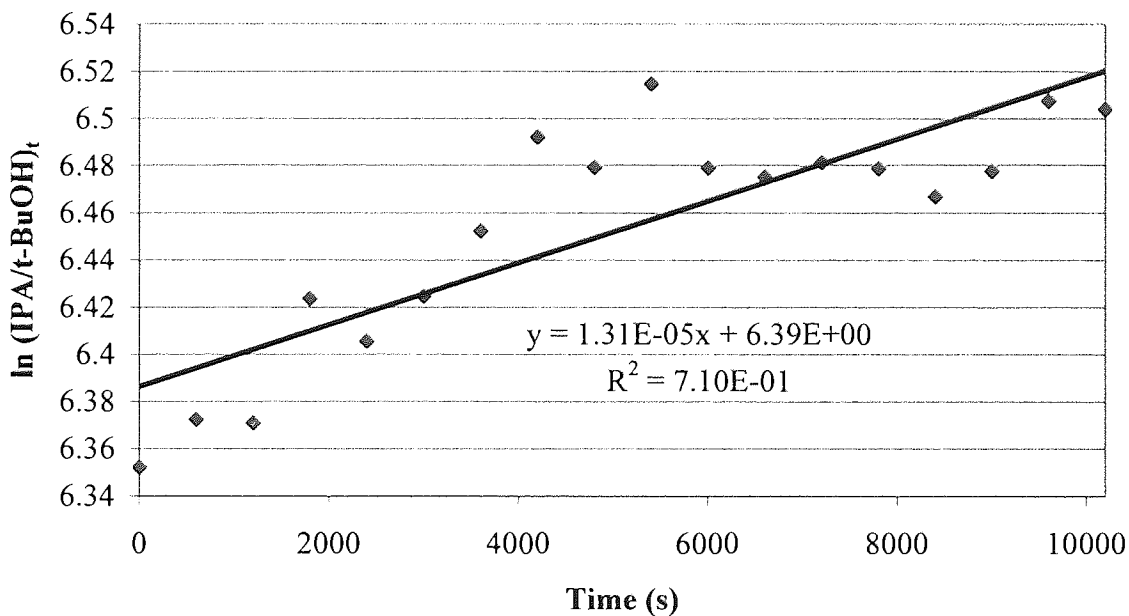
**The Thermally Induced Reaction in the NMR Spectrometer of 40% (v/v) t-BuCl/IPA with 40% (w/w) IPA/D<sub>2</sub>O at 41.9°C**



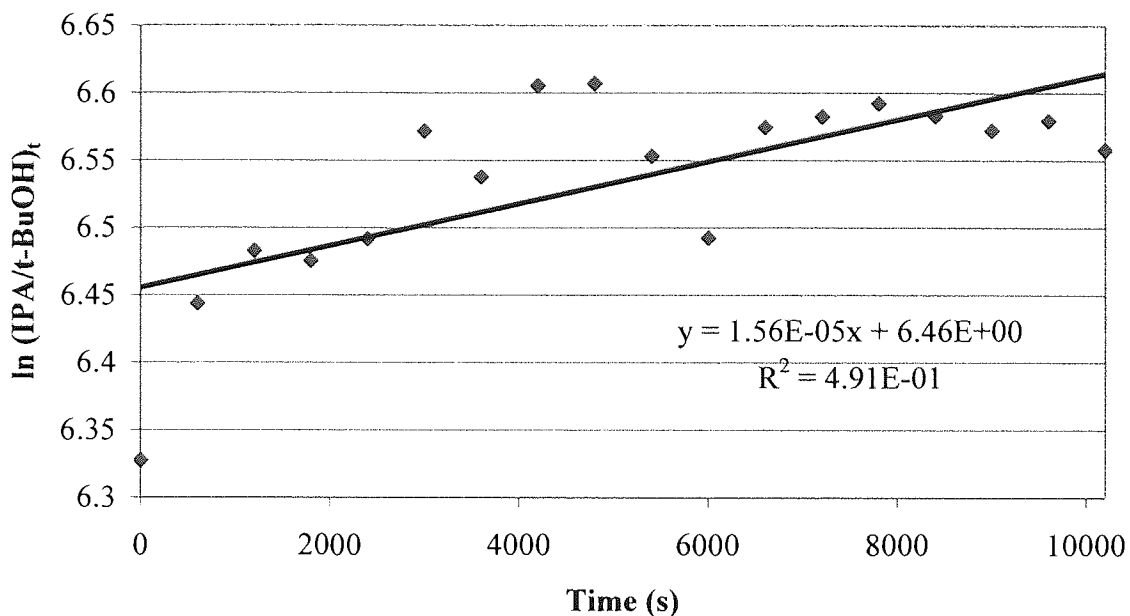
**The Thermally Induced Reaction in the NMR Spectrometer of 40% (v/v) t-BuCl/IPA with 40% (w/w) IPA/D<sub>2</sub>O at 42.0°C**



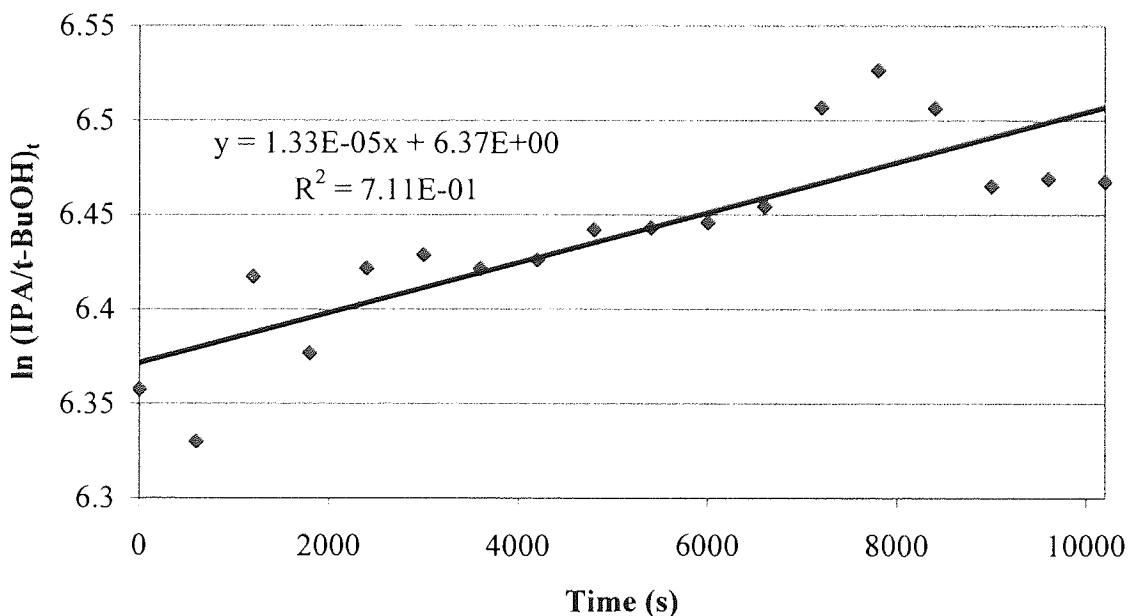
**The Thermally Induced Reaction in the NMR Spectrometer of 40% (v/v) t-BuCl/IPA with 40% (w/w) IPA/D<sub>2</sub>O at 42.2°C**



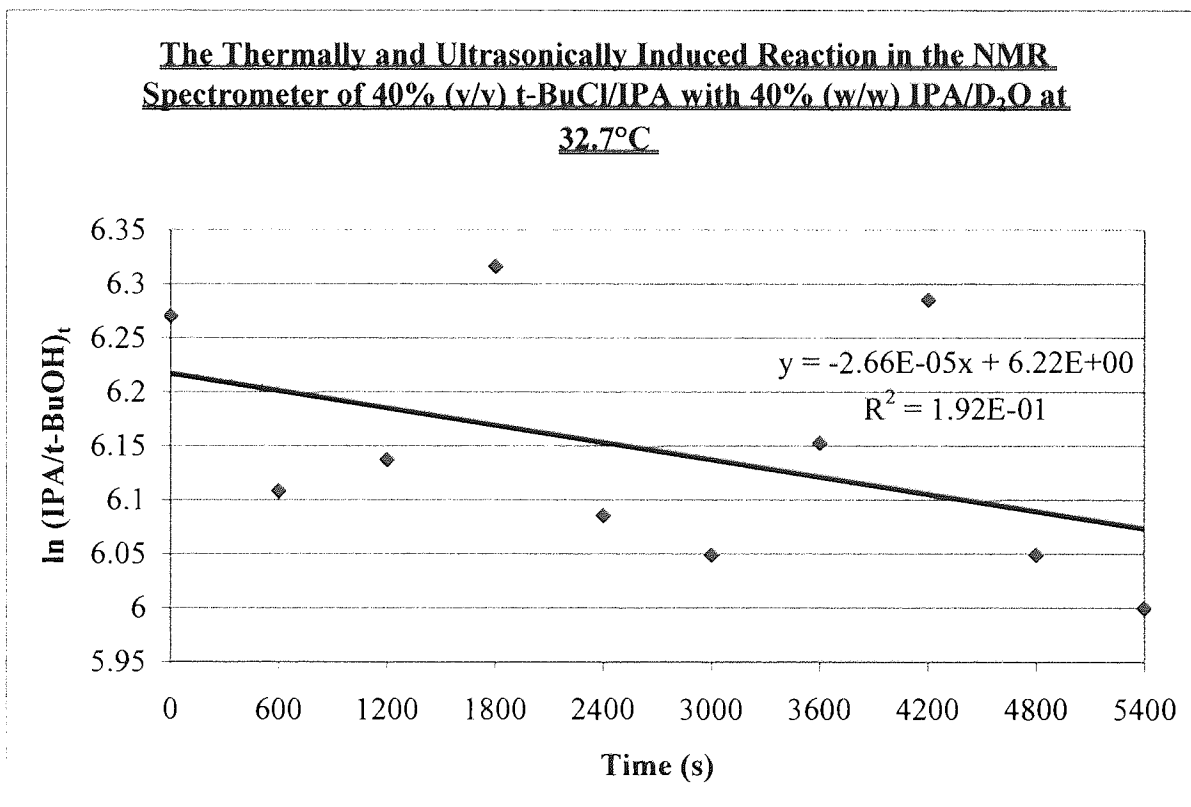
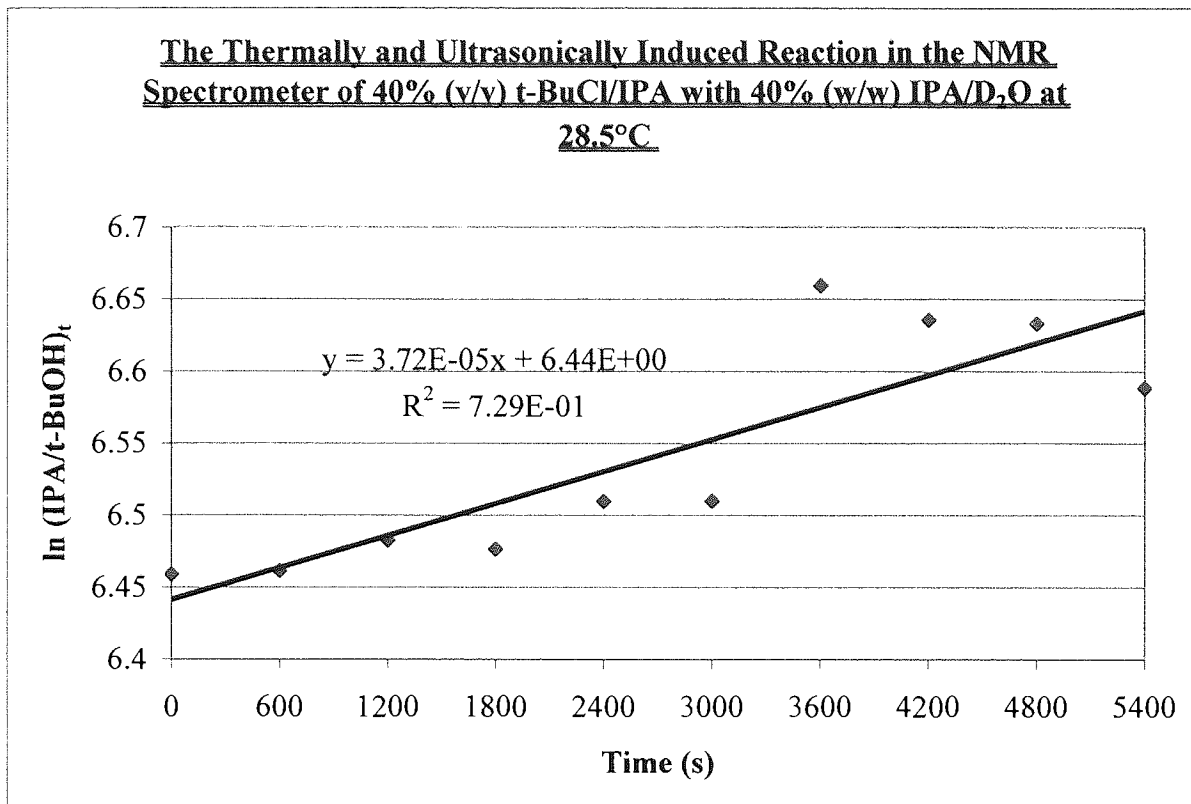
The Thermally Induced Reaction in the NMR Spectrometer of 40% (v/v) t-BuCl/IPA with 40% (w/w) IPA/D<sub>2</sub>O at 42.3°C



The Thermally Induced Reaction in the NMR Spectrometer of 40% (v/v) t-BuCl/IPA with 40% (w/w) IPA/D<sub>2</sub>O at 45.1°C

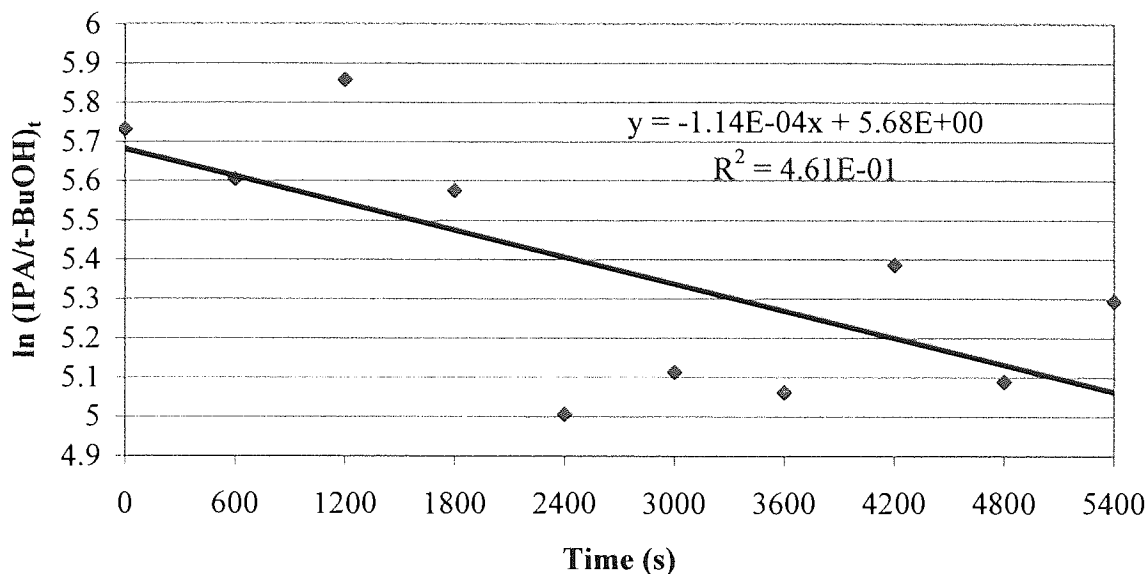


**Appendix 13:** The Ultrasonically Induced Reaction in the NMR Spectrometer of 40% (v/v) t-BuCl/IPA with 40% (w/w) IPA/D<sub>2</sub>O.

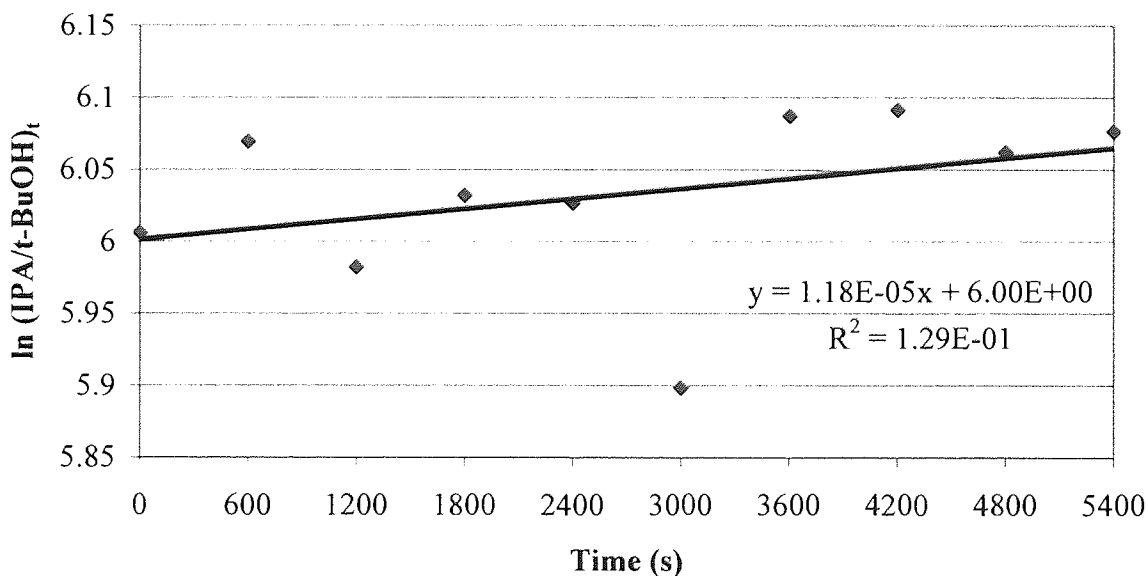




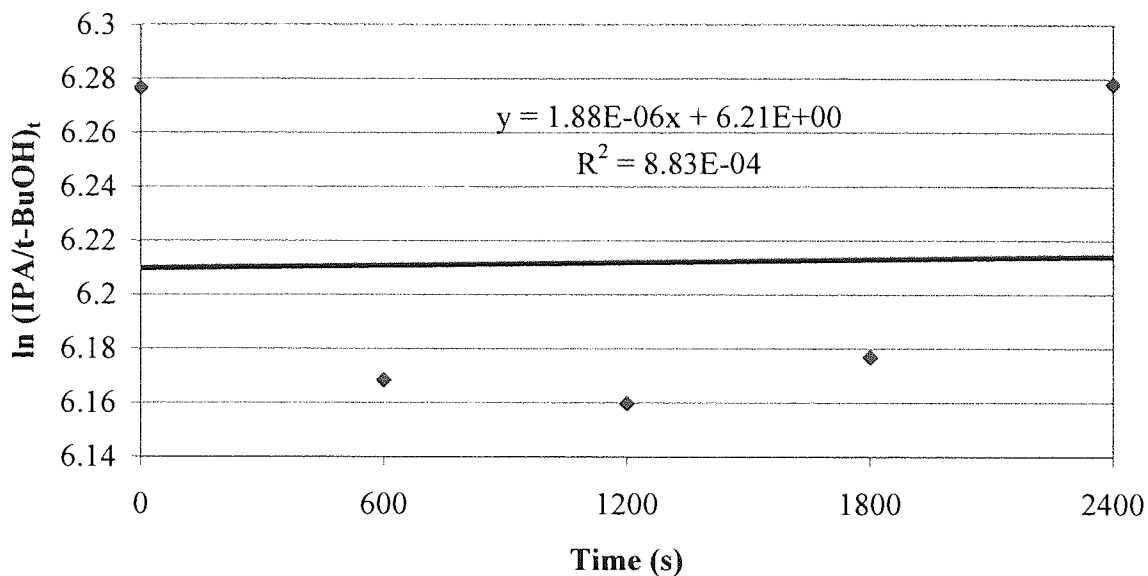
**The Thermally and Ultrasonically Induced Reaction in the NMR Spectrometer of 40% (v/v) t-BuCl/IPA with 40% (w/w) IPA/D<sub>2</sub>O at 32.8°C**



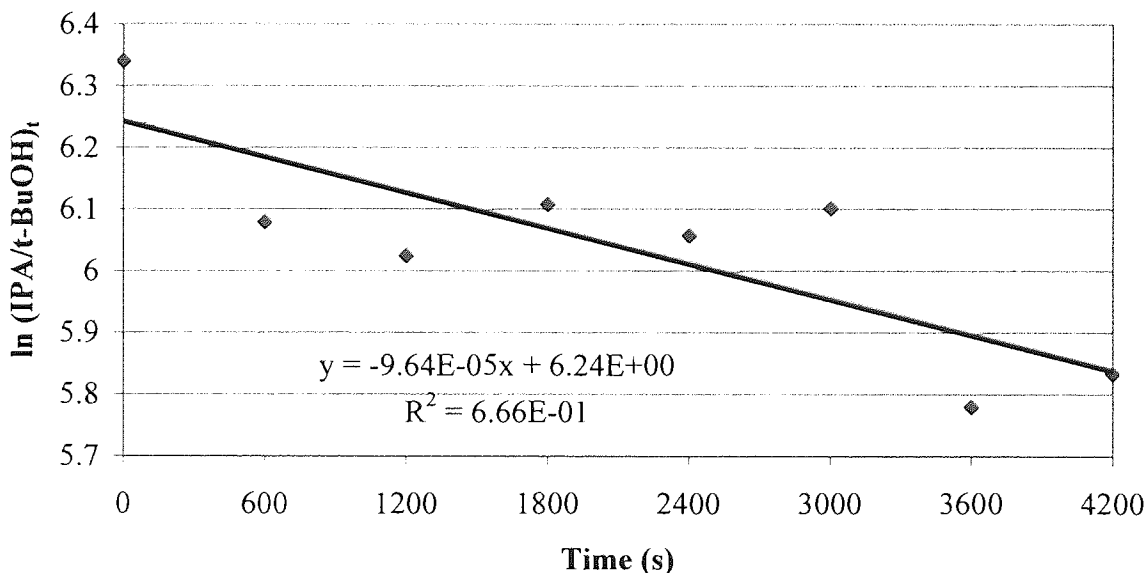
**The Thermally and Ultrasonically Induced Reaction in the NMR Spectrometer of 40% (v/v) t-BuCl/IPA with 40% (w/w) IPA/D<sub>2</sub>O at 34.2°C**



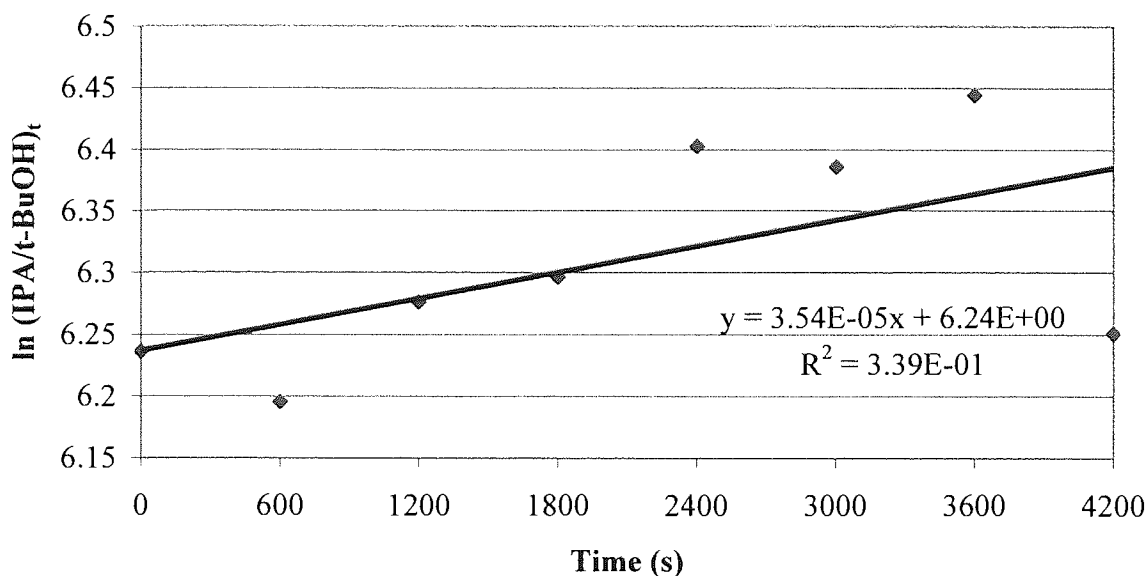
**The Thermally and Ultrasonically Induced Reaction in the NMR Spectrometer of 40% (v/v) t-BuCl/IPA with 40% (w/w) IPA/D<sub>2</sub>O at 34.3°C**



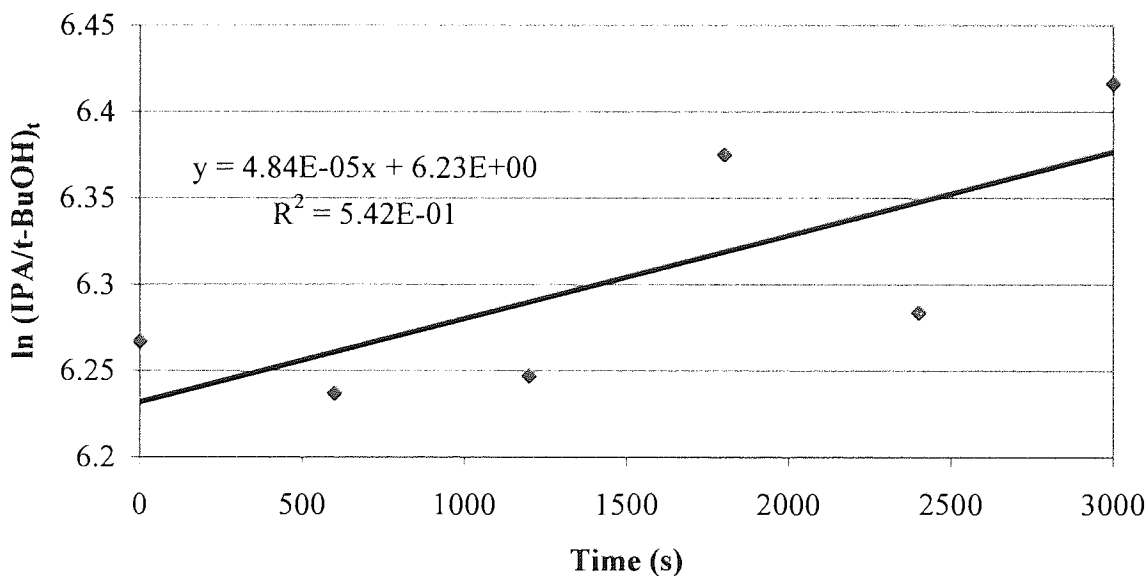
**The Thermally and Ultrasonically Induced Reaction in the NMR Spectrometer of 40% (v/v) t-BuCl/IPA with 40% (w/w) IPA/D<sub>2</sub>O at 35.4°C**



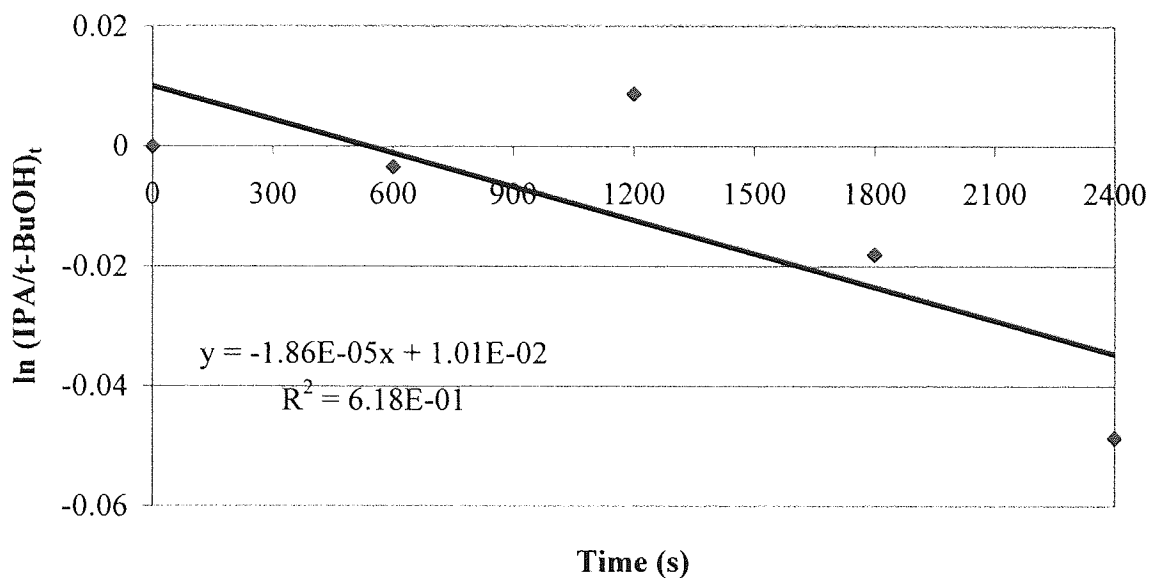
**The Thermally and Ultrasonically Induced Reaction in the NMR Spectrometer of 40% (v/v) t-BuCl/IPA with 40% (w/w) IPA/D<sub>2</sub>O at 37.0°C**



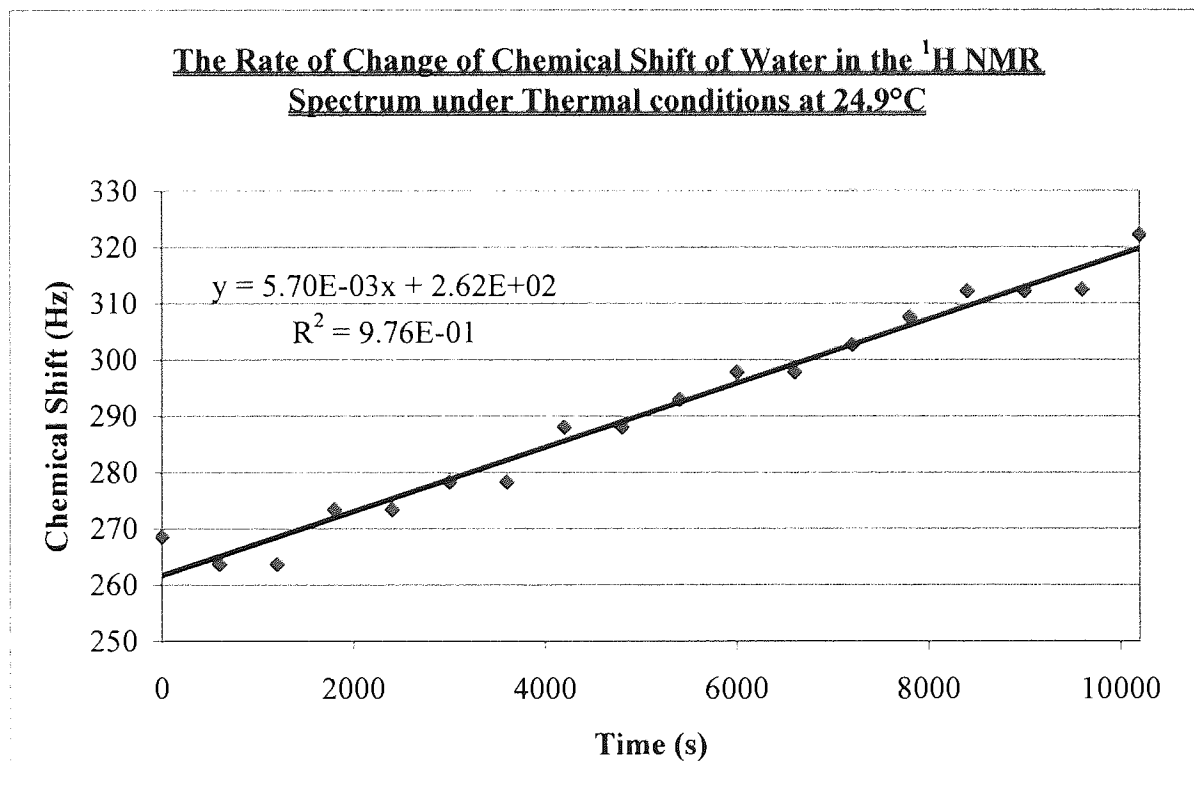
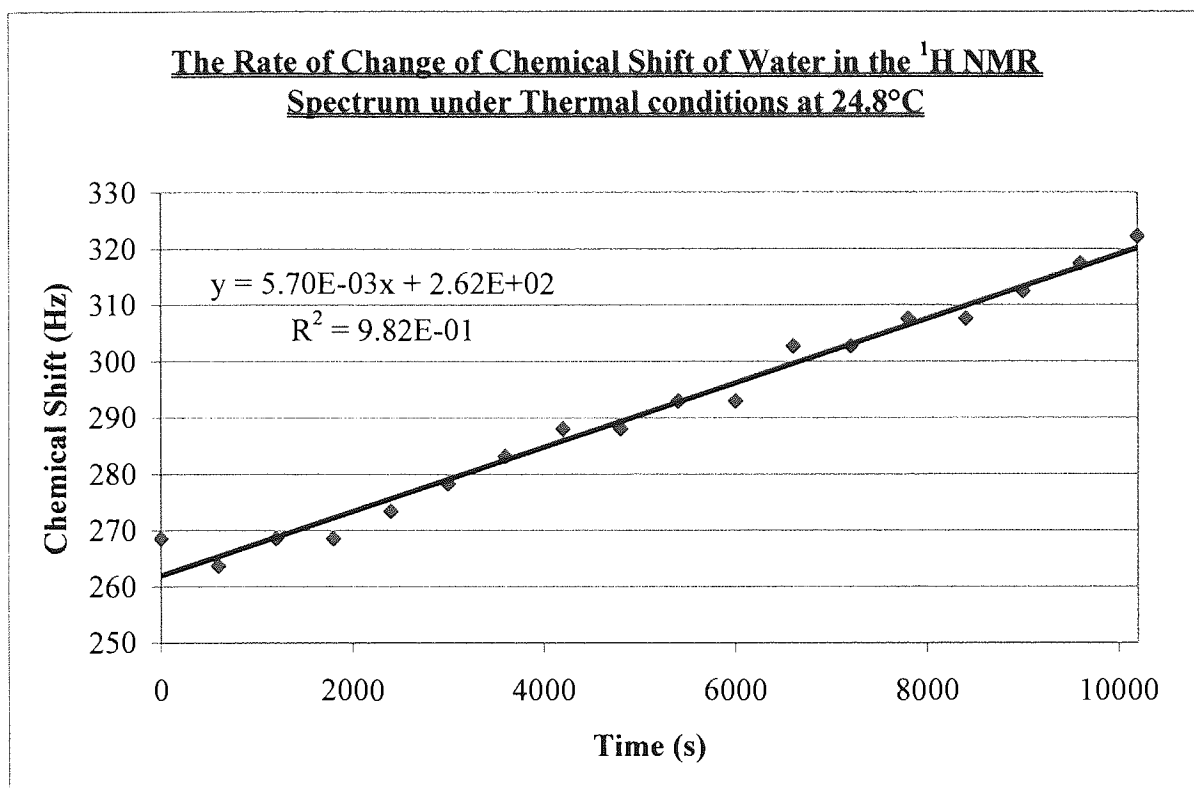
**The Thermally and Ultrasonically Induced Reaction in the NMR Spectrometer of 40% (v/v) t-BuCl/IPA with 40% (w/w) IPA/D<sub>2</sub>O at 43.5°C**



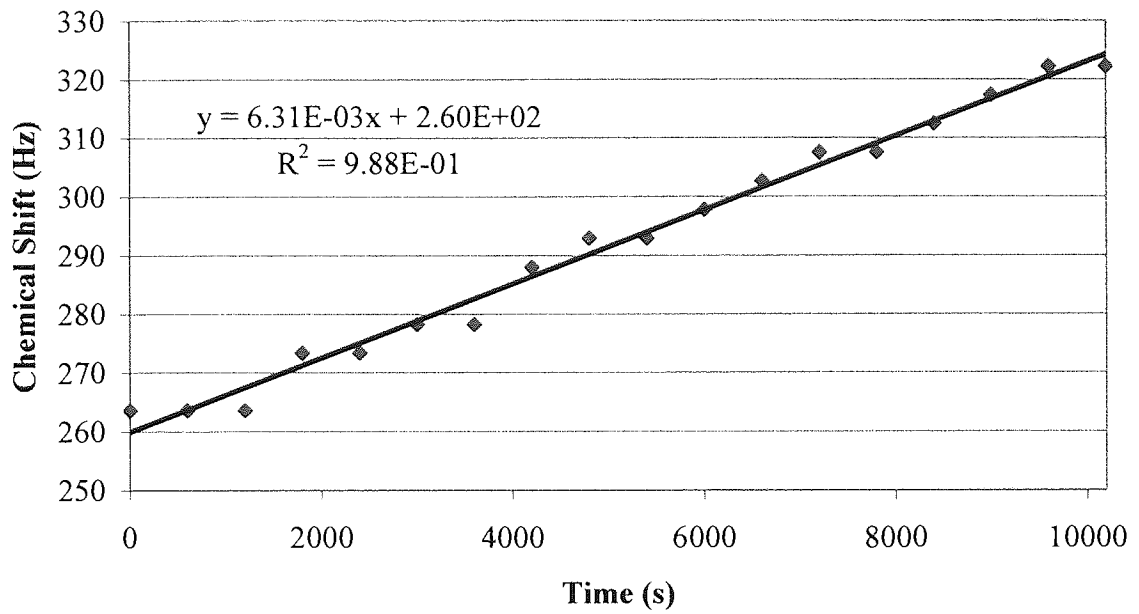
The Thermally and Ultrasonically Induced Reaction in the NMR Spectrometer of 40% (v/v) t-BuCl/IPA with 40% (w/w) IPA/D<sub>2</sub>O at 45.9°C



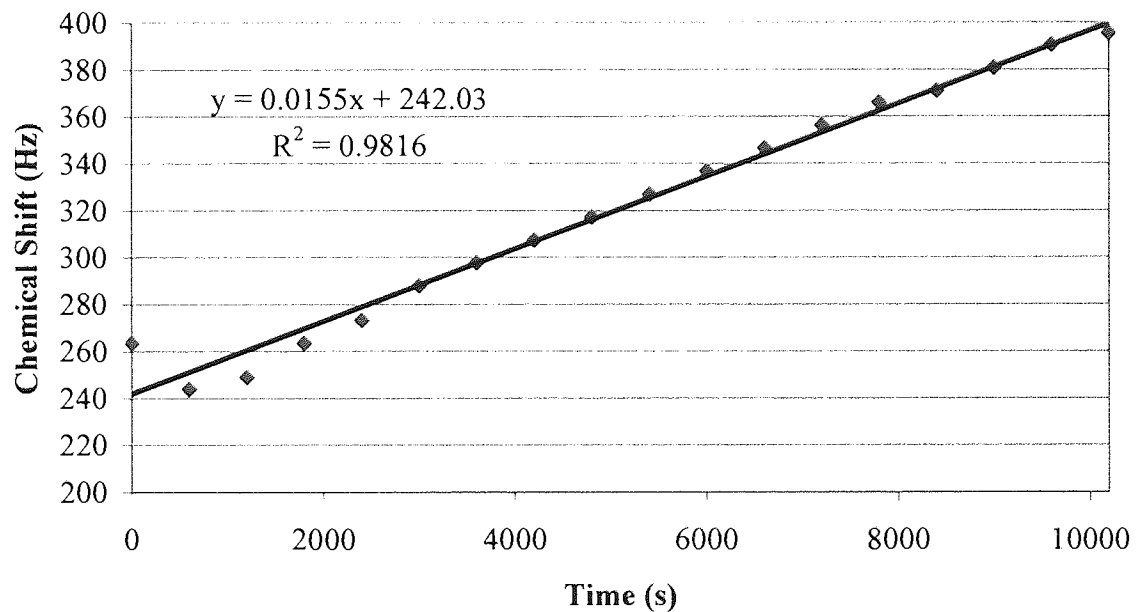
**Appendix 14:** The Rate of Change of the Chemical Shift of Water for the Thermally Induced Reaction in the NMR Spectrometer of 40% (v/v) t-BuCl/IPA with 40% (w/w) IPA/D<sub>2</sub>O.



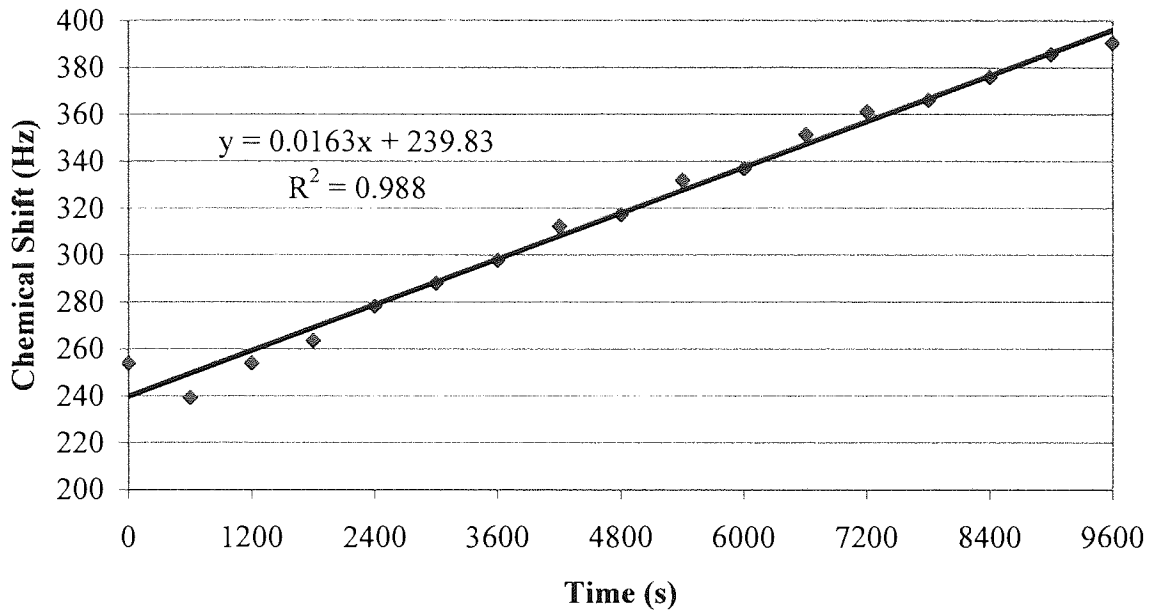
The Rate of Change of Chemical Shift of Water in the  $^1\text{H}$  NMR Spectrum under Thermal conditions at 24.9°C



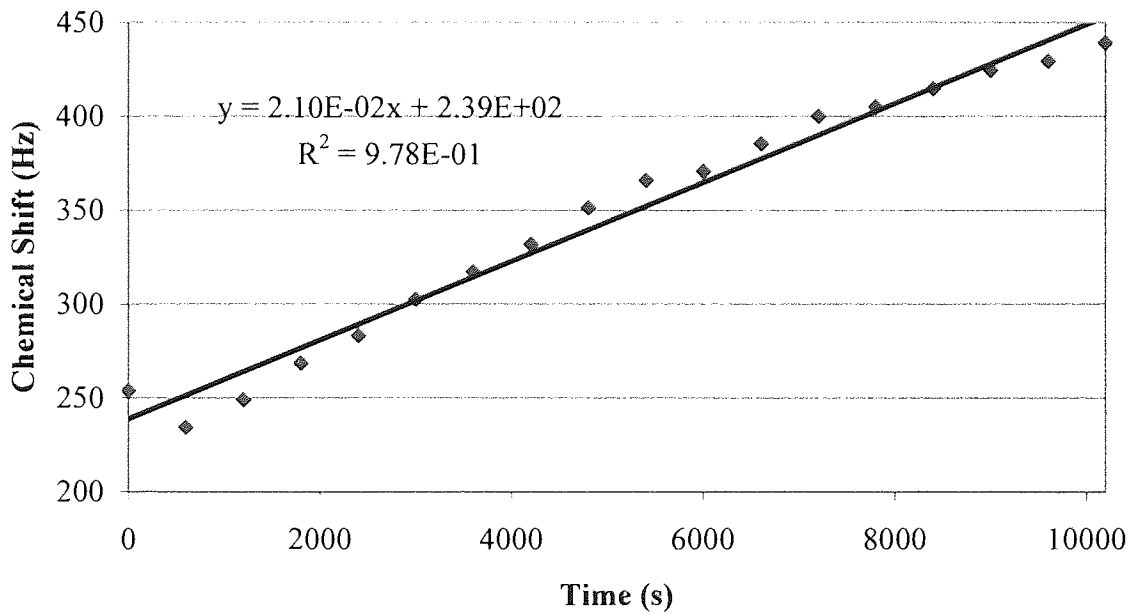
The Rate of Change of Chemical Shift of Water in the  $^1\text{H}$  NMR Spectrum under Thermal conditions at 32.2°C



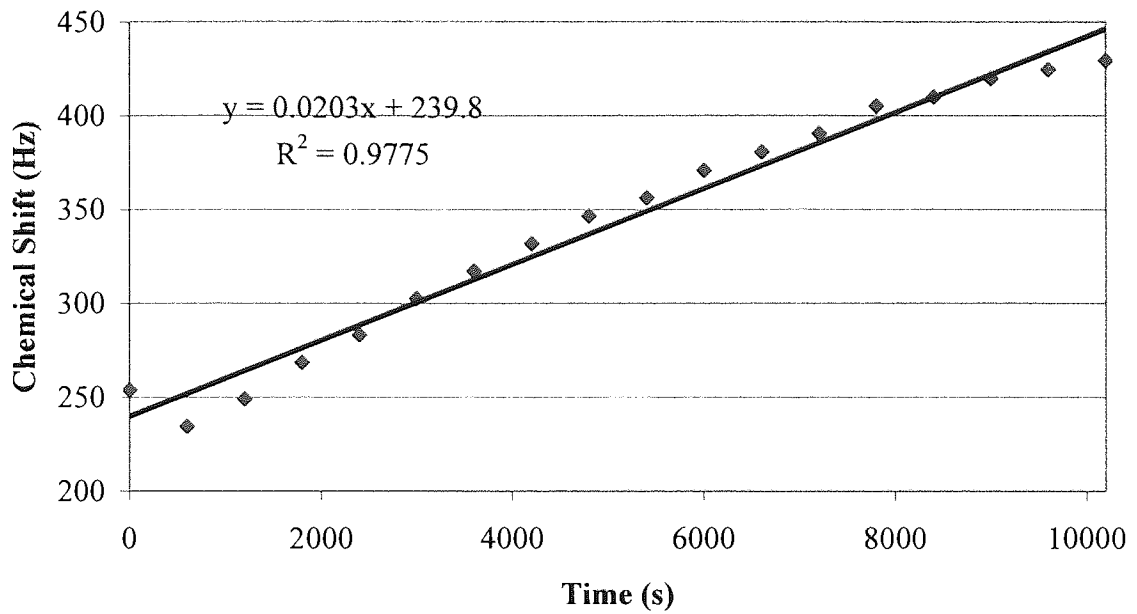
**The Rate of Change of Chemical Shift of Water in the  $^1\text{H}$  NMR Spectrum under Thermal conditions at 32.8°C**



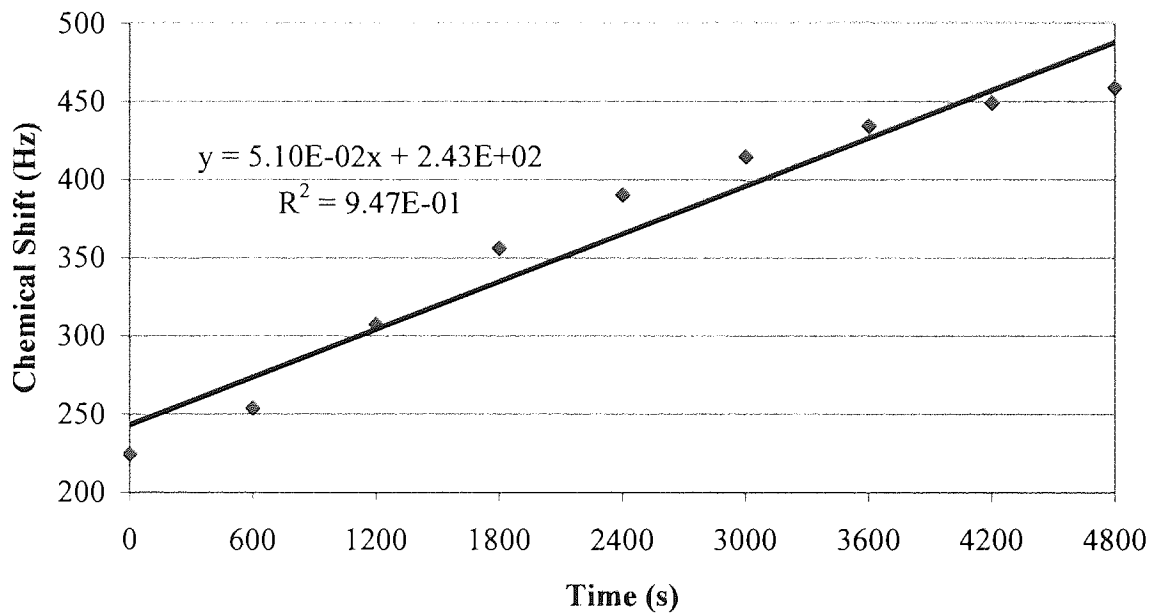
**The Rate of Change of Chemical Shift of Water in the  $^1\text{H}$  NMR Spectrum under Thermal conditions at 35.5°C**



The Rate of Change of Chemical Shift of Water in the  $^1\text{H}$  NMR Spectrum under Thermal conditions at 35.5°C

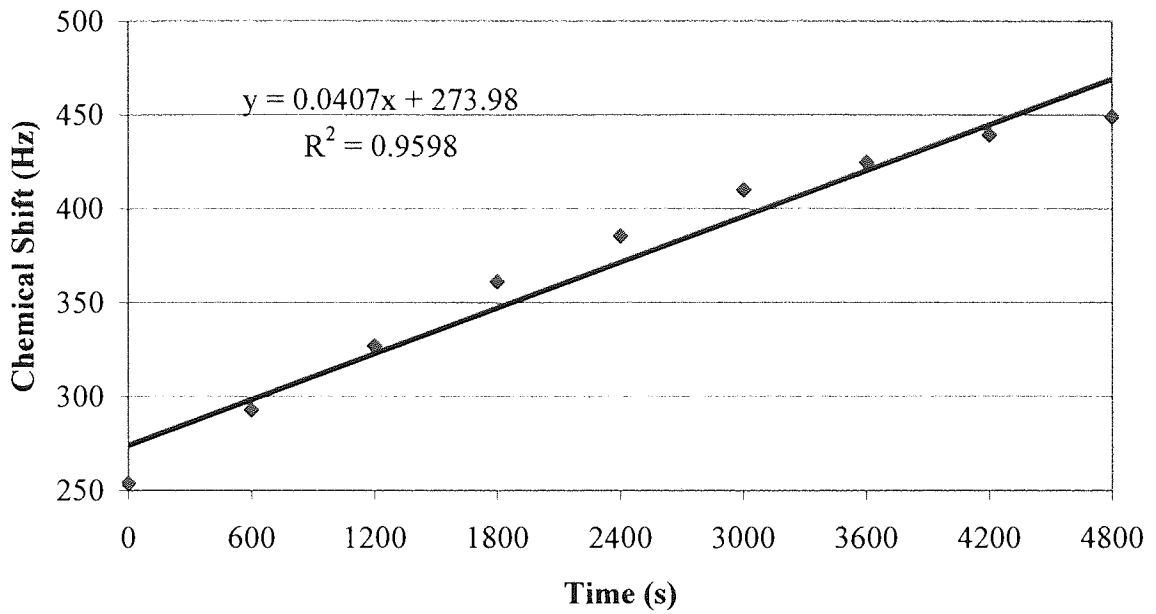


The Rate of Change of Chemical Shift of Water in the  $^1\text{H}$  NMR Spectrum under Thermal conditions at 41.9°C

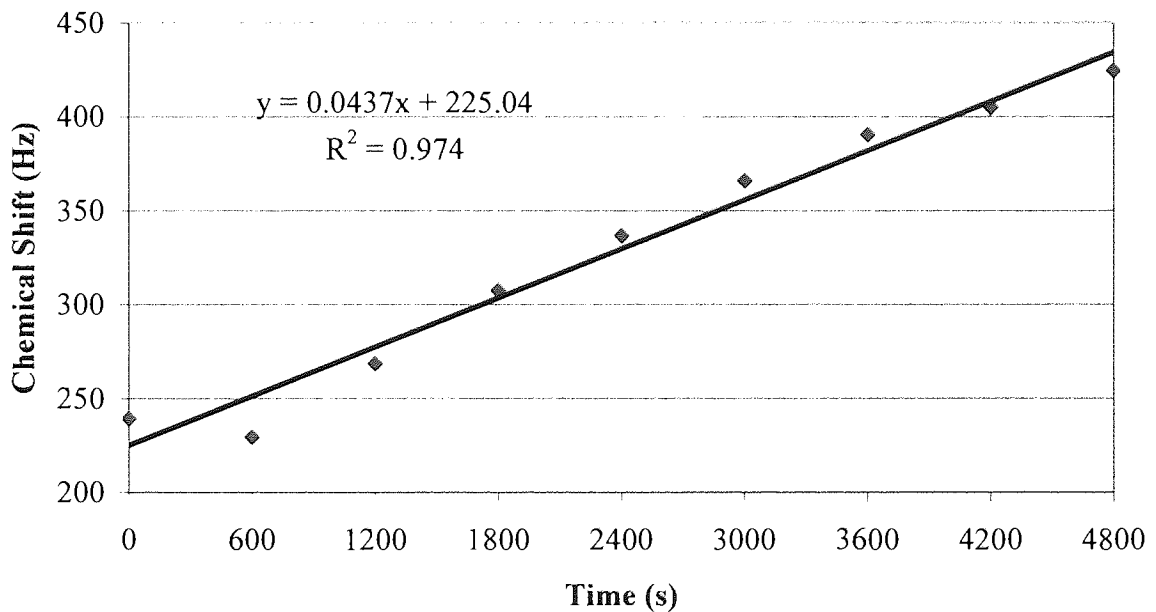




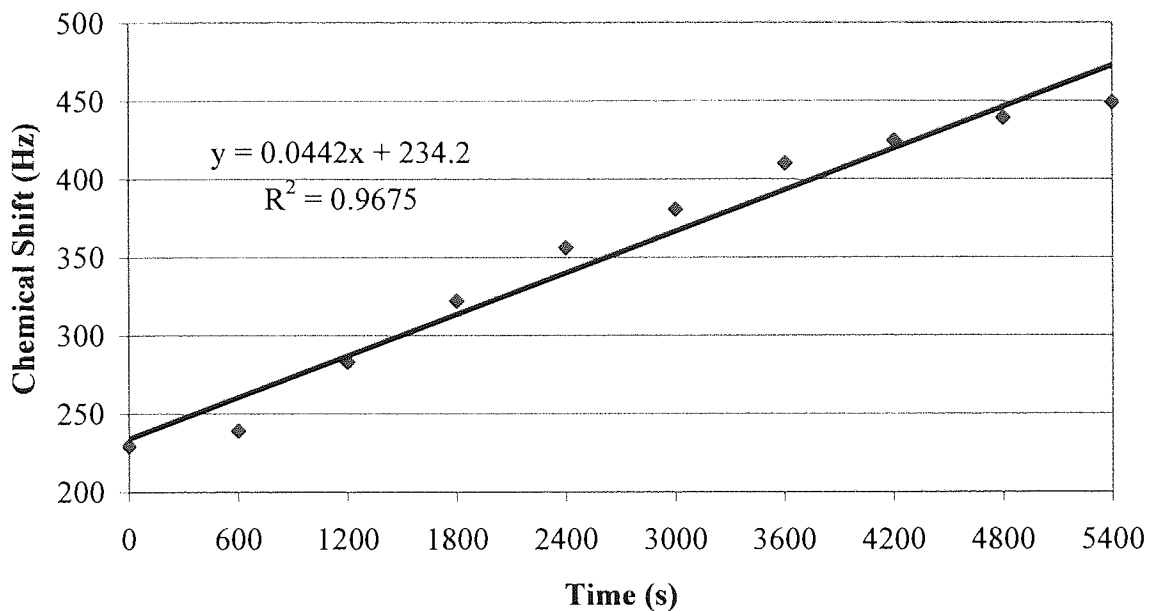
**The Rate of Change of Chemical Shift of Water in the  $^1\text{H}$  NMR Spectrum under Thermal conditions at 42.0°C**



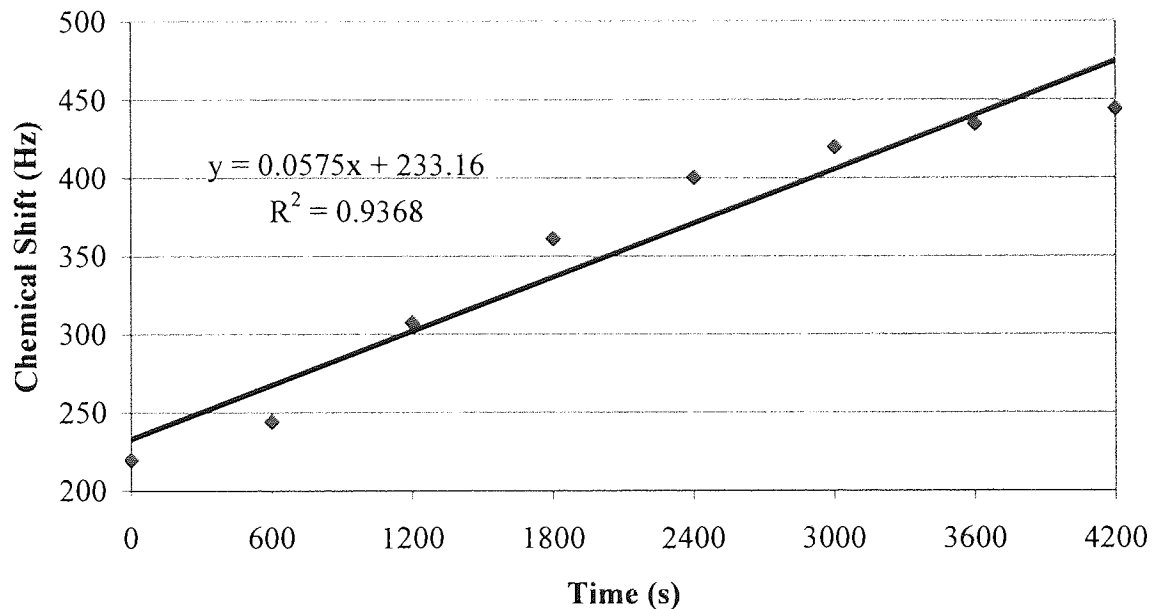
**The Rate of Change of Chemical Shift of Water in the  $^1\text{H}$  NMR Spectrum under Thermal conditions at 42.2°C**



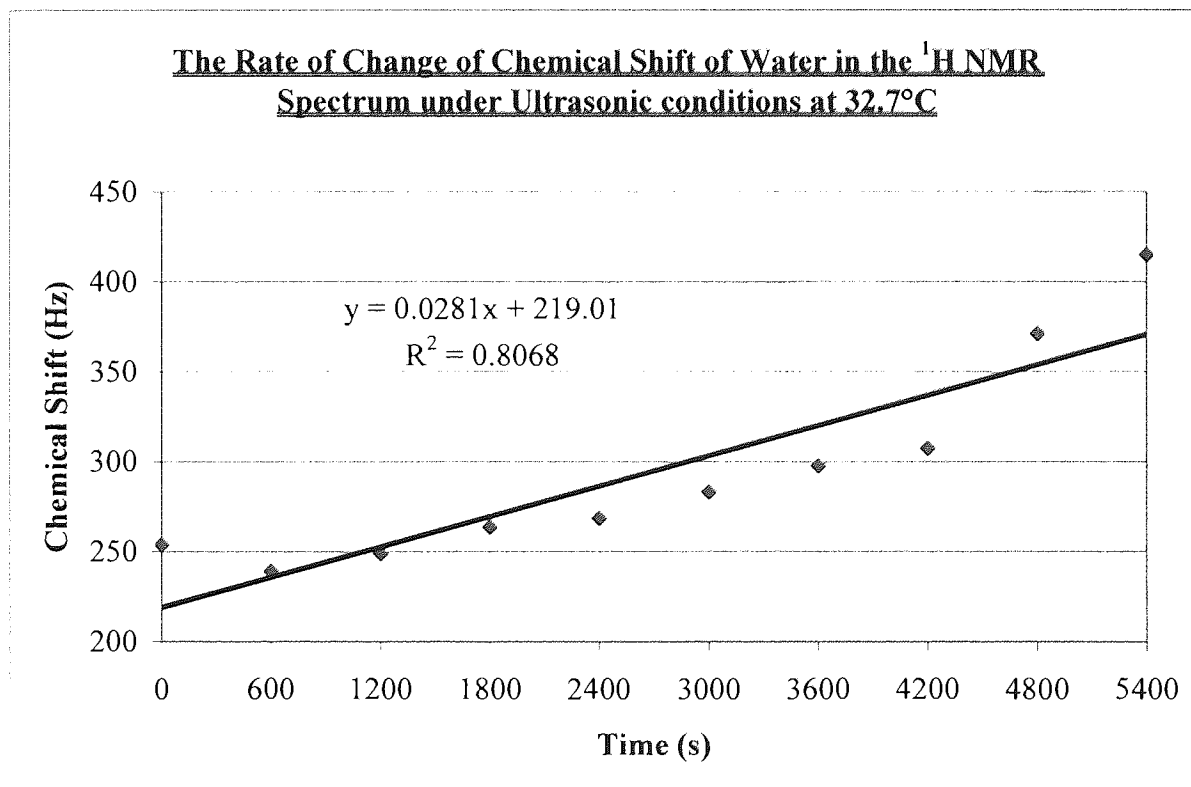
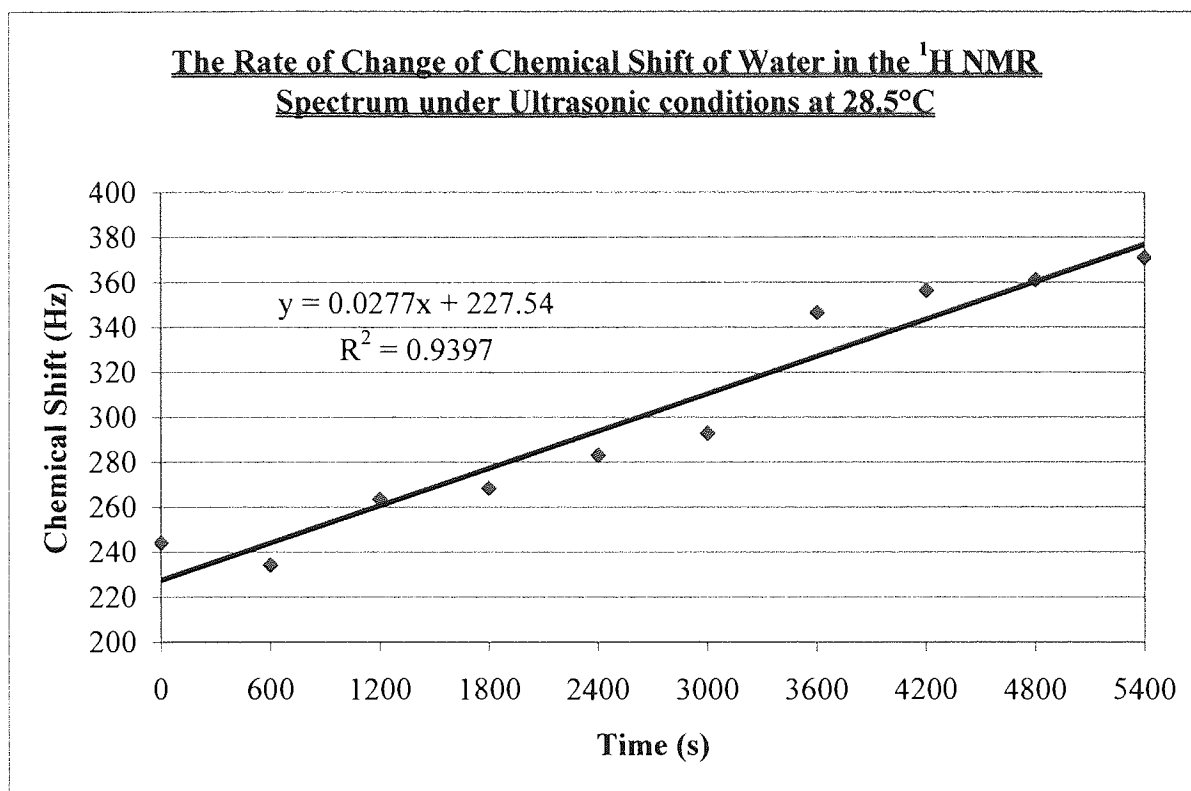
**The Rate of Change of Chemical Shift of Water in the  $^1\text{H}$  NMR Spectrum under Thermal conditions at 42.3°C**



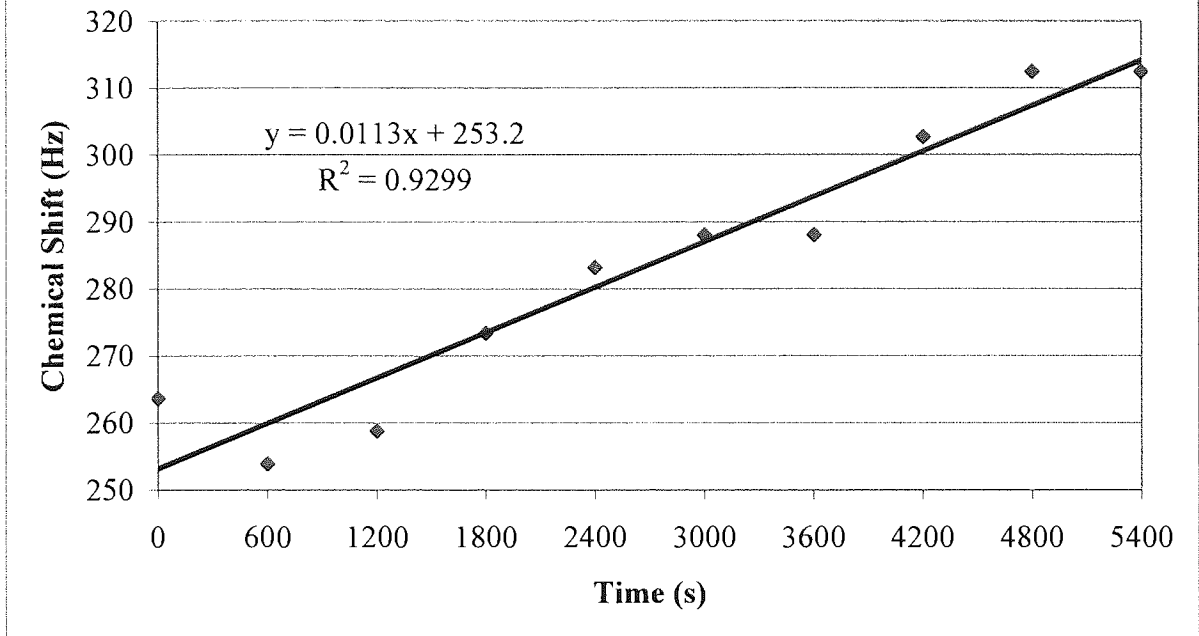
**The Rate of Change of Chemical Shift of Water in the  $^1\text{H}$  NMR Spectrum under Thermal conditions at 45.1°C**



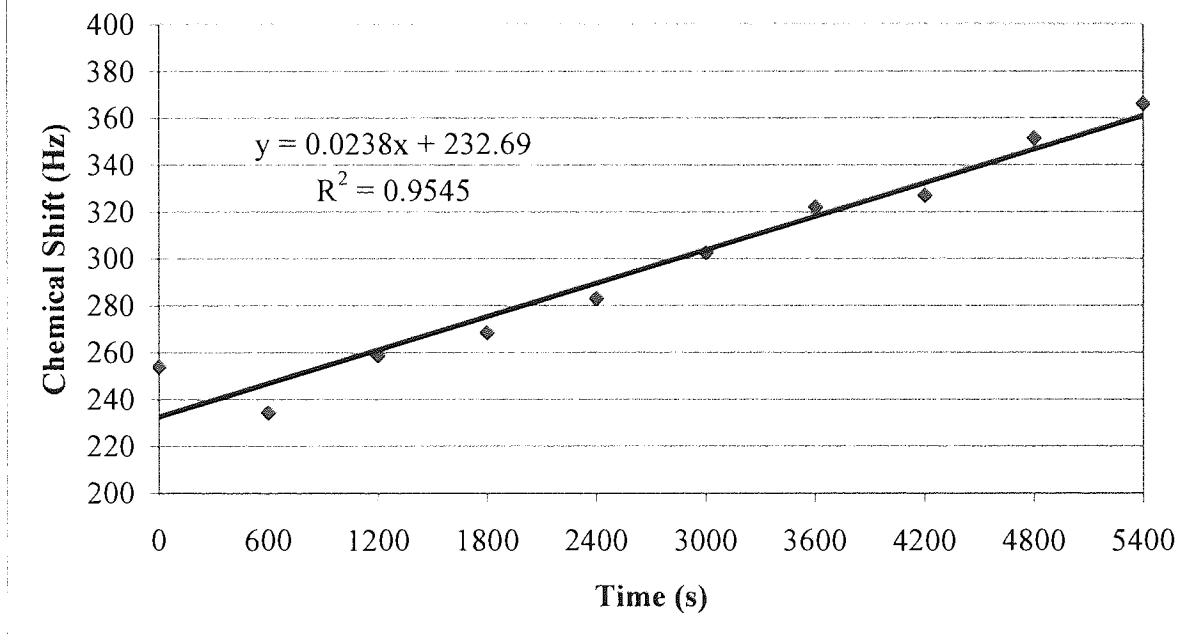
**Appendix 15:** The Rate of Change of the Chemical Shift of Water for the Ultrasonically Induced Reaction in the NMR Spectrometer of 40% (v/v) t-BuCl/IPA with 40% (w/w) IPA/D<sub>2</sub>O.



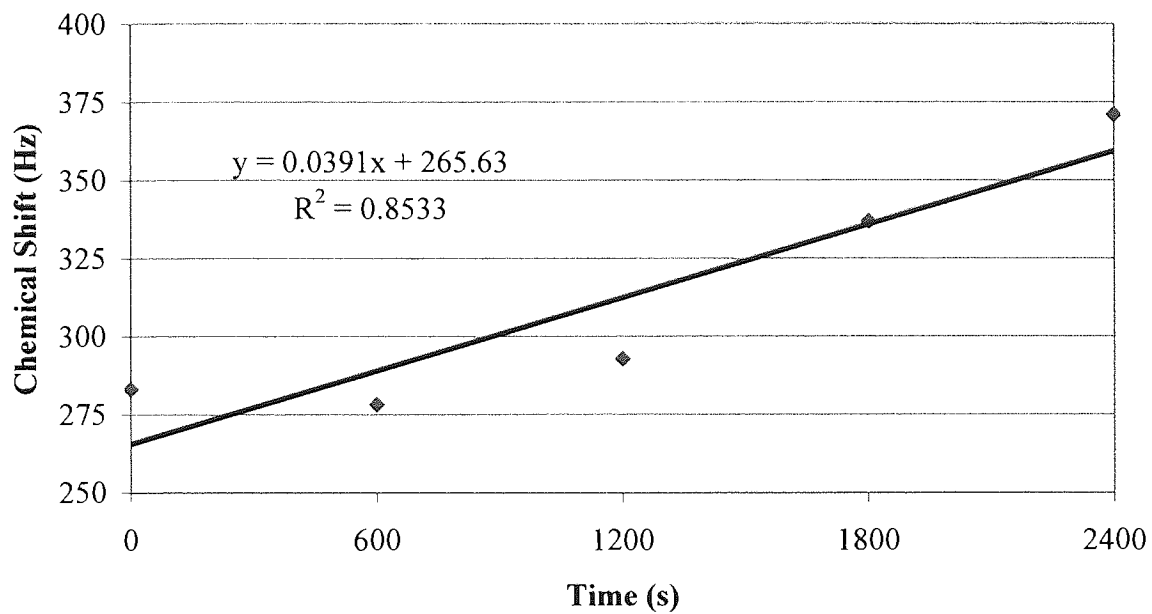
**The Rate of Change of Chemical Shift of Water in the  $^1\text{H}$  NMR Spectrum under Ultrasonic conditions at 32.8°C**



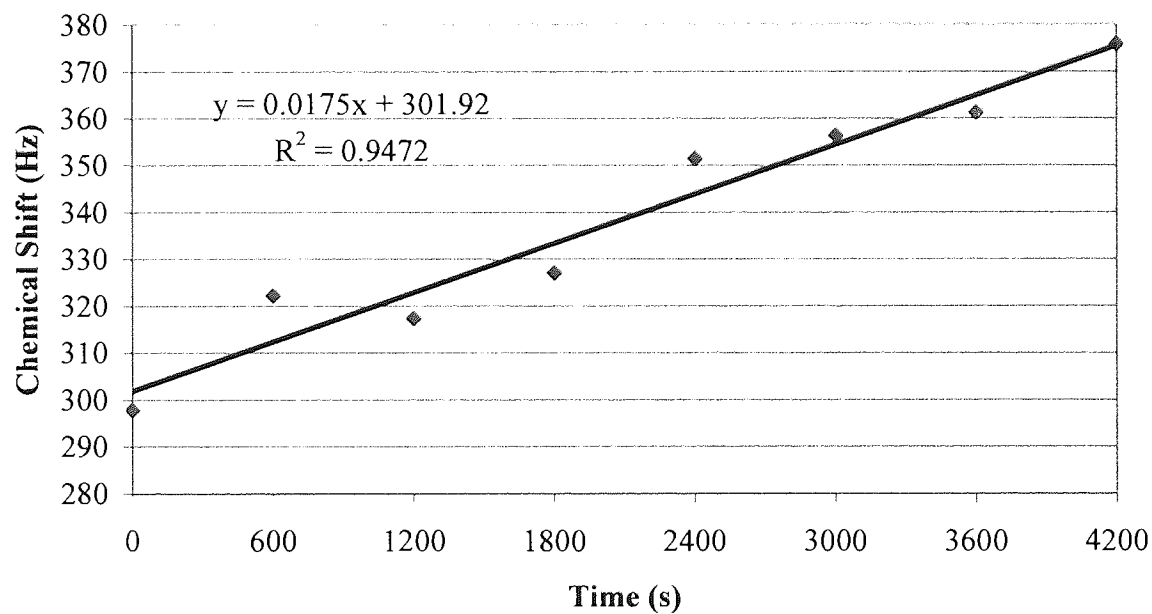
**The Rate of Change of Chemical Shift of Water in the  $^1\text{H}$  NMR Spectrum under Ultrasonic conditions at 34.2°C**



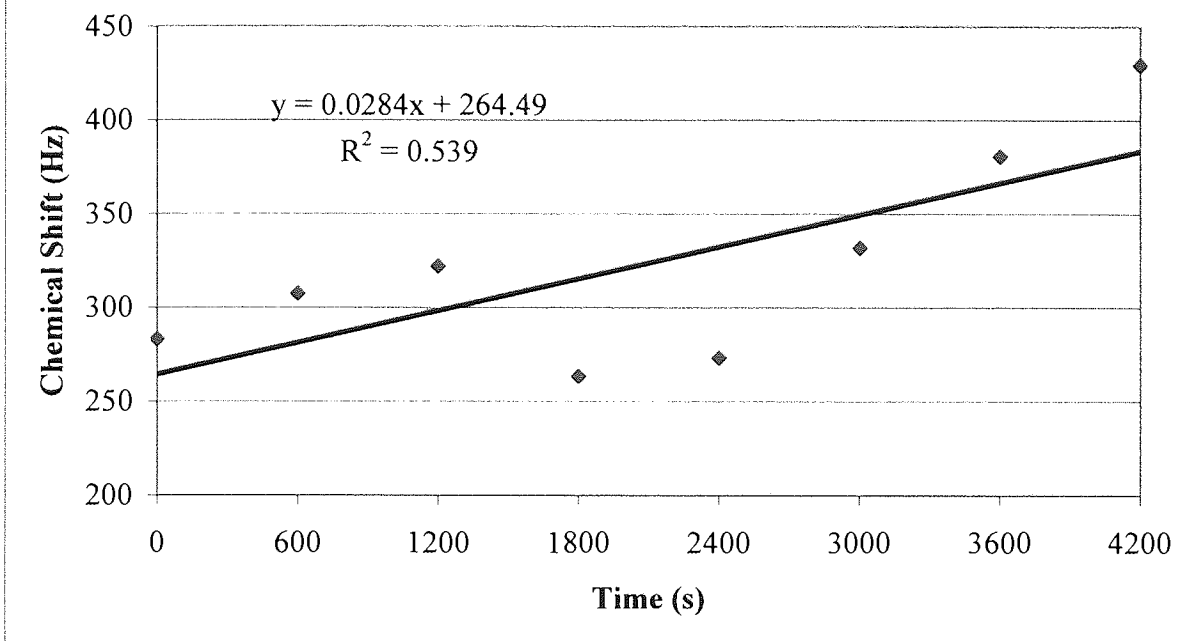
**The Rate of Change of Chemical Shift of Water in the  $^1\text{H}$  NMR Spectrum under Ultrasonic conditions at 34.3°C**



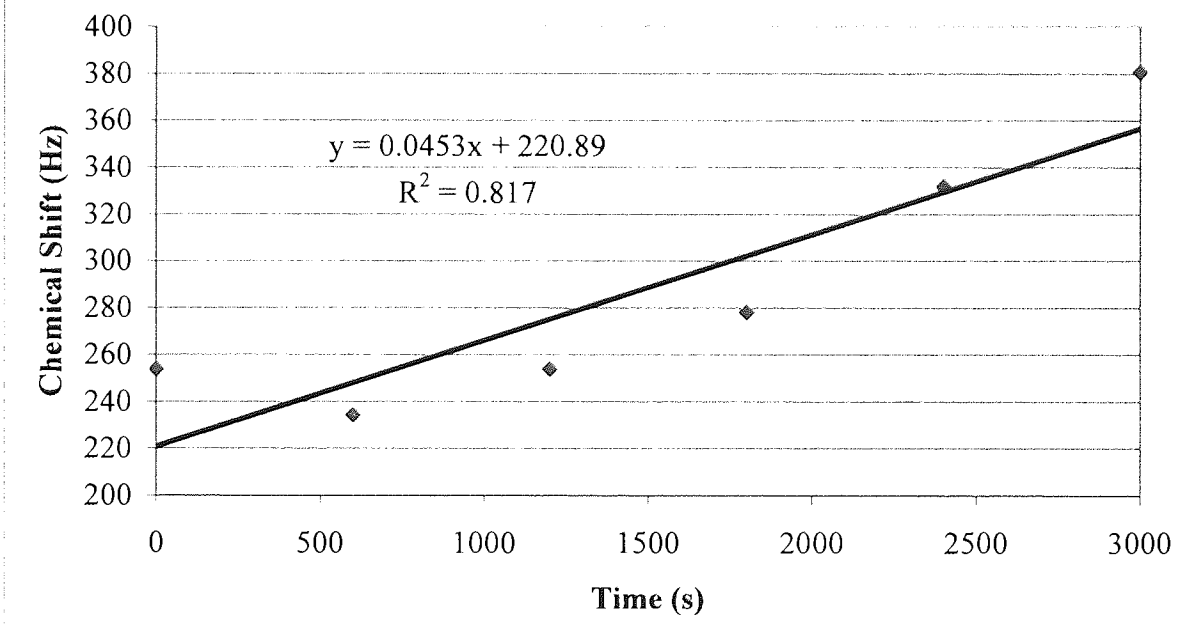
**The Rate of Change of Chemical Shift of Water in the  $^1\text{H}$  NMR Spectrum under Ultrasonic conditions at 35.4°C**



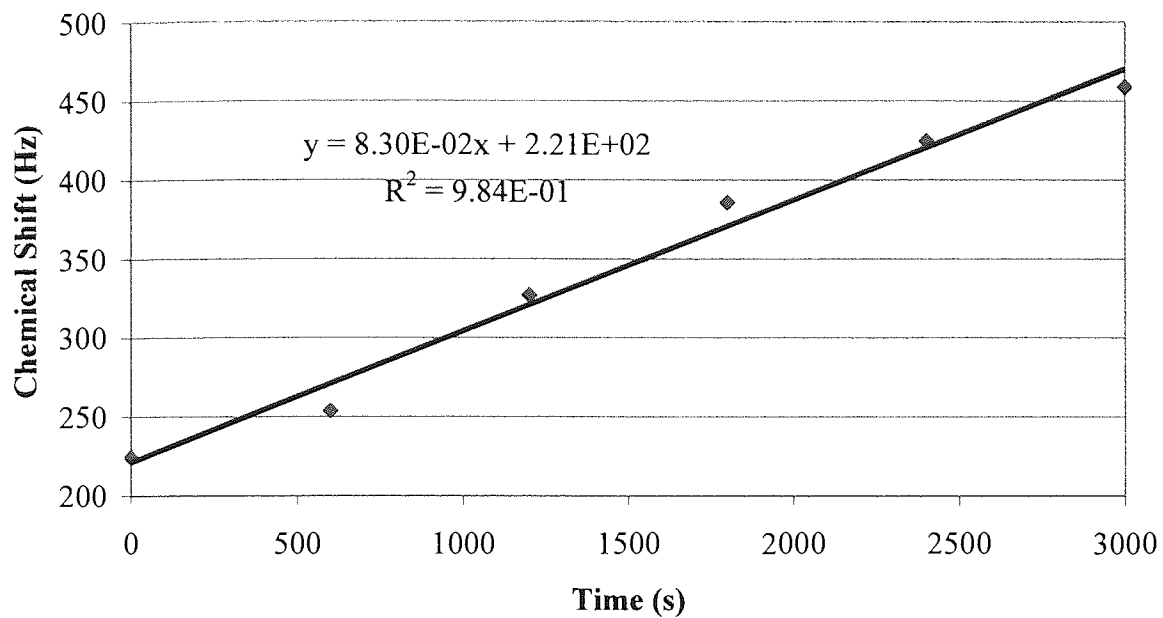
The Rate of Change of Chemical Shift of Water in the  $^1\text{H}$  NMR Spectrum under Ultrasonic conditions at 37.0°C



The Rate of Change of Chemical Shift of Water in the  $^1\text{H}$  NMR Spectrum under Ultrasonic conditions at 43.5°C



**The Rate of Change of Chemical Shift of Water in the  $^1\text{H}$  NMR Spectrum under Ultrasonic conditions at 45.9°C**



---

## References

- 1 F. Bloch, W. W. Hansen and M. Packard, Nuclear Induction, *Phys. Rev.*, 1946, **69**, 127.
- 2 E. M. Purcell, H. C. Torrey and R. V. Pound, Resonance Absorption by Nuclear Magnetic Moments in a Solid, *Phys. Rev.*, 1946, **69**, 37-38.
- 3 W. E. Lamb, Jr., Internal Diamagnetic Fields, *Phys. Rev.*, 1941, **60**, 818-819.
- 4 H. M. McConnell, Reaction Rates by Nuclear Magnetic Resonance, *J. Chem. Phys.*, 1958, **28**, 430.
- 5 D. M. Doddrell, D. T. Pegg and M. R. Bendall, Distortionless Enhancement of NMR Signals by Polarisation Transfer, *J. Magn. Reson.*, 1982, **48**, 323-327.
- 6 J. Homer, and M. C. Perry, New Method for NMR Signal Enhancement by polarization Transfer, and Attached Nucleus Testing, *J. Chem. Soc., Chem. Commun.*, 1994, 373-374.
- 7 F. Galton, "Inquiries into Human Faculty and its Development" MacMillan, London 1883, 26-28.
- 8 M. S Plesset and R. B. Chapman, Collapse of an Initially Spherical Vapour Cavity in the Neighbourhood of a Solid Boundary, *J. Fluid Mech.*, 1971, **47**, 283-290.
- 9 B. E. Noltingk and E. A. Neppiras, Cavitation Produced by Ultrasonics: Theoretical condition for the Onset of Cavitation, *Proc. Phys. Soc. B. (Lond.)*, 1951, **64B**, 1032-1038.
- K. S. Suslick, D. A. Hammerton and R. E. Cline, The Sonochemical Hot Spot, *J. Am. Chem. Soc.*, 1986, **108**, 5641-5642.
- 10 M. E. Fitzgerald, V. Griffing and J. Sullivan, Chemical Effects of Ultrasonics – "Hot Spot" Chemistry, *J. Chem. Phys.*, 1956, **25**, 926-933.
- 11 M. A. Margulis, Study of Electrical Phenomena Associated with Cavitation. II. Theory of the Development of Sonoluminescence in Acoustochemical Reactions, *Russian J. Phys. Chem.*, 1985, **59**, 882-885.
- 12 T. Lepoint, and F. Mullie, What Exactly is Cavitation Chemistry?, *Ultrasonics Sonochem.*, 1994, **1**, 13-22.
- 13 F. Franks and D. J. G. Ives, The Structural Properties of Alcohol-Water Mixtures, *Quart. Rev. (London)*, 1966, **20**, 1-44.
- 14 K. S. Suslick, J. W. Gawienowski, P. F. Schubert and H. H. Wang, Alkane Sonochemistry, *J. Phys. Chem.*, 1983, **87**, 2299-2301.



- 
- 15 T. Lepoint, F. Mullie, N. Voglet, D. H. Yang, J. Vandercammen and J. Reisse, Perfluorocarbons as Inert Gases in Homogeneous Sonochemistry, *Tetrahedron Lett.*, 1992, **33**, 1055-1056.
- 16 Cum, G., Gallo, R., Spadaro, A. and Galli, G., Effect of Static Pressure on the Ultrasonic Activation of Chemical Reactions. Selective Oxidation of Benzylic Carbon in the Liquid Phase, *J. Chem. Soc., Perkin Trans.* 1988, **11**, 376.
- 17 J. C. De Souza-Barboza, C. Pétrier and J-L. Luche, Ultrasound in Organic Synthesis, Some Fundamental Aspects of the Sonochemical Barbier Reaction, *J. Org. Chem.*, 1988, **53**, 1212-1218.
- 18 The Concise Oxford English Dictionary 9<sup>th</sup> ed. Oxford University Press 1995.
- 19 B. Jaffe, R. S. Roth and S. Marzullo, Piezoelectric Properties of Lead Zirconate-Lead Titanate Solid-Solution Ceramics, *Letters to the editor*, 1954, 809-810.
- 20 J. P. Perkins, Power Ultrasonic Equipment for Sonochemistry Research, Based on a paper presented at the Sonochemistry symposium annual chemical congress, held at Warwick University, 8-11 April 1986.
- 21 A. Weissler, Sonochemistry: The Production of Chemical Changes with Sound Waves, *J. Acoust. Chem. Soc. Amer.*, 1953, **25**, 651-657.
- 22 T. J. Mason, "Sonochemistry", Oxford Chemistry Primers, Oxford University Press, 1999, 36.
- 23 A. Kotronarou, G. Mills and M. R. Hoffmann, Ultrasonic Irradiation of *p*-Nitrophenol in Aqueous Solution, *J. Phys. Chem.*, 1991, **95**, 3630-3638.
- 24 N. Miller, Chemical Action of Sound Waves on Aqueous Solutions, *Trans. Faraday Soc.*, 1950, **46**, 546.
- 25 C. Pétrier, A. Jeunet, J-L. Luche and G. Reverdy, Unexpected Frequency Effects on the Rate of Oxidative Processes Induced by Ultrasound, *J. Am. Chem. Soc.*, 1992, **114**, 3148-3150.
- 26 J. Homer and M. Beevers, Driven-Equilibrium Single-Pulse Observation of T<sub>1</sub> Relaxation. A Reevaluation of a Rapid "New" Method for Determining NMR Spin-Lattice Relaxation Times, *J. Mag. Res.*, 1985, **63**, 287-297.
- J. Homer and S. Patel, Preliminary Observations on High-Resolution Nuclear Magnetic Resonance for Liquids Subjected to Ultrasound, *J. Chem. Soc. Faraday Trans.*, 1990, **86**(1), 215-216.
- J. Homer, P. McKeown, W. R. McWhinnie, S. Patel and G. J. Tilstone, Sonically Induced Narrowing of Solid-State Nuclear Magnetic Resonance Spectra: A Possible Alternative to

---

Magic Angle Spinning Nuclear Magnetic Resonance, *J. Chem. Soc. Faraday Trans.*, 1991, **87**(14), 2253-2254.

J. Homer and M. Howard, Studies on the Origin of Sonically Induced Narrowing of Solid-State Nuclear Magnetic Resonance Spectra, *J. Chem. Soc. Faraday Trans.*, 1993, **89**(16), 3029-3038.

J. Homer and M. Howard, SINNMR Studies of Acoustically Induced Rotation of Suspended Particles, *Ultrasonics Sonochemistry*, 1999, **5**, 141-148.

27 O. T. Benfey, E. D. Hughes and C. K. Ingold, Mechanism of Substitution at a Saturated Carbon Atom, *J. Chem. Soc.*, 1952, 2488-2498.

28 L. T. Bateman, E. D. Hughes and C. K. Ingold, Mechanism of Substitution at a saturated Carbon Atom, *J. Chem. Soc.*, 1940, 960-966.

29 The solvent in the experiments was 70/80% (v/v) aqueous acetone.

30 S. Winstein, E. Grunwald and H. W. Jones, The Correlation of Solvolysis Reactions into Mechanistic Categories, *J. Amer. Chem. Soc.*, 1951, **73**, 2700-2707.

31 S. Winstein and R. E. Buckles, The Role of Neighbouring Groups in Replacement Reactions, *J. Amer. Chem. Soc.*, 1942, **64**, 2780-2785.

32 A. Bentley, A. G. Evans and J. Halpern, Ionisation of Triphenyl Methyl Chloride in Nitroalkanes, *Trans. Faraday Soc.*, 1951, **47**, 711-716.

A. G. Evans, A. G. Jones and G. O. Osborne, The Ionisation of Organic Halides in Nitroalkanes, *Trans. Faraday Soc.*, 1954, **50**, 16-23.

33 L. P. Hammett, "Physical Organic Chemistry", McGraw-Hill, New York, 1<sup>st</sup> ed., 1940.

34 S. Winstein, E. Clippinger, A. H. Fainberg, R. Heck and G. C. Robinson, Salt Effects and Ion Pairs in Solvolysis and Related Reactions, *J. Am. Chem. Soc.*, 1956, **78**, 328-335.

35 For a summary of complete references see P. D. Bartlett, The Scientific Work of Saul Winstein, *J. Amer. Chem. Soc.*, 1972, **94**, 2161-2169.

36 S. Winstein, Ion Pairs in Elimination, *J. Am. Chem. Soc.*, 1963, **85**, 1702-1703.

37 S. Winstein and G. C. Robinson, Salt Effects and Ion Pairs in Solvolysis and Related Reactions, *J. Amer. Chem. Soc.*, 1958, **80**, 169-181.

38 V. J. Shiner Jr. and R. D. Fisher,  $\alpha$ -Deuterium Effects on the Rates of Solvolysis of a 2-Adamantyl Sulfonate Ester, *J. Amer. Chem. Soc.*, 1971, **93**, 2553-2554.

39 P. Walden, Über die vermeintliche optische Activität der Chlorfumarsäure und über optisch active Halogenbernsteinsäure, *Ber.*, 1893, **26**, 210-215.

- 
- 40 P. Walden, Über die gegenseitige Umwandlung optischer Antipoden, *Ber.*, 1896, **29**, 133-138.
- 41 P. Walden, Über die gegenseitige Umwandlung optischer Antipoden, *Ber.*, 1899, **32**, 1855-1864.
- 42 W. A. Cowdrey, E. D. Hughes, C. K. Ingold, S. Masterman and A. D. Scott, Reaction Kinetics and the Walden Inversion. Part VI. Relation of Steric Orientation to Mechanism in Substitutions involving Halogens Atoms and Simple or Substituted Hydroxyl Groups, *J. Chem. Soc.*, 1937, 1252-1271.
- 43 H. Philips, Investigations on the Dependence of Rotatory Power on Chemical Constitution, *J. Chem. Soc.*, 1923, **123**, 44-59.
- 44 E. D. Hughes and C. K. Ingold, Mechanism of Substitution at a Saturated Carbon Atom. Part IV. A discussion of Constitutional and Solvent Effects on the Mechanism, Kinetics, Velocity and Orientation of Substitution, *J. Chem. Soc.*, 1935, 244-255.
- 45 R. G. Pearson, Influence of the Solvent on Rates of Ionisation, Entropies and Heats of Activation, *J. Chem. Phys.*, 1952, **20**, 1478-1480.
- 46 C. J. M. Stirling, Some Quantitative Effects of Strain on Reactivity, *Pure Appl. Chem.*, 1984, **56**, 1781-1796.
- 47 H. C. Brown and R. S. Fletcher, Chemical Effects of Steric Strains. I. The Effect of Structure upon the Hydrolysis of Tertiary Aliphatic Chlorides, *J. Am. Chem. Soc.*, 1949, **71**, 1845-1854.
- 48 H. C. Brown and M. Borkowski, The Effect of Ring Size on the Rate of Solvolysis of the 1-Chloro-1-methylcycloalkanes, *J. Am. Chem. Soc.*, 1952, **74**, 1894-1902.
- 49 G. S. Hammond, A Correlation of Reaction Rates, *J. Am. Chem. Soc.*, 1955, **77**, 334-338.
- 50 O. E. Edwards and C. Grieco, S<sub>N</sub>2 Displacement at Tertiary Carbon, *Can J. Chem.*, 1974, **52**, 3561-3562.
- 51 O. Diels and K. Alder, Synthesen in der hydroaromatischen Reihe, *Ann.*, 1928, **460**, 98-122.
- 52 Th. Zincke and H. Günther, Überführung von Pentenderivaten in Indenderivate, *Ann.*, 1893, **272**, 243-252.
- 53 R. B. Woodward, F. E. Bader, H. Bickel, A. J. Frey and R. W. Kierstead, The Total Synthesis of Reserpine, *J. Am. Chem. Soc.*, 1956, **78**, 2023-2025.
- 54 M. C. Kloetzel 'The Diels-Alder Reaction With Maleic Anhydride' *Organic Reactions* 1948, **4**, 1-60.

- 
- 55** H. Stockmann, On the Titrimetric Determination of the Configuration of Bridged Diels-Alder Adducts, *J. Org. Chem.*, 1961, **26**, 2025-2032.
- 56** F. Bergmann and H. E. Eschinazai, The Sterical Course and the Mechanism of the Diene Reaction, *J. Am. Chem. Soc.*, 1943, **65**, 1405-1411.
- 57** For a review see R. G. Pearson, Orbital Topology and Reaction Mechanisms, *J. Chem. Educ.*, 1981, **58**, 753-757.
- 58** K. Fukui and H. Fujimoto, The Stereoselection Rule for Electrocyclic Interactions, *Bull. Chem. Soc. Jpn.*, 1967, **40**, 2018-2025.
- K. Fukui and H. Fujimoto, The MO-theoretical Interpretation of the Nature of Chemical Reactions. II. The Governing Principles, *Bull. Chem. Soc. Jpn.*, 1969, **42**, 3399-3409.
- 59** I. Fleming, "Pericyclic Reactions", Oxford Chemistry Primers, Oxford University Press, 1999, 44.
- 60** I. Fleming, "Pericyclic Reactions", Oxford Chemistry Primers, Oxford University Press, 1999, 44.
- 61** G. Jenner and J. Rimmelin, High Pressure (4+2) Cyclodimerisation of 2,3-Dimethyl-1,3-Butadiene Possible Competition between Concerted and Stepwise Mechanisms, *Tetrahedron Lett.*, 1980, **21**, 3039-3042.
- 62** P. G. Gassman and D. B. Gorman, Use of Alkyl Substitution to Control Ring Size in the Intramolecular Ionic Diels-Alder Reaction, *J. Am. Chem. Soc.*, 1990, **112**, 8624-8625.
- 63** M. J. S. Dewar, S. Olivella and J. J. P. Stewart, Mechanism of the Diels-Alder Reaction: Reactions of Butadiene with Ethylene and Cyanoethylenes, *J. Am. Chem. Soc.*, 1986, **108**, 5771-5779.
- 64** R. O. C. Norman, "Principles of Organic Synthesis", 2<sup>nd</sup> Ed. Chapman and Hall Ltd., 1978, 282.
- 65** E. Clar, Über die Verteilung der Doppelbindungen in kondensierten aromatischen Kohlenwasserstoffen (Zur Kenntnis mehrkerniger aromatischer Kohlenwasserstoffe XII Mittel), *Ber.*, 1932, **65**, 503-519.
- 66** O. Diels and K. Alder, Synthesen in der Hydroaromatischen Reihe. II. Mitteilung: Über Cantharidin, *Ber.*, 1929, **62**, 554-562.
- 67** W. E. Bachmann and M. C. Kloetzel, The Reaction between Maleic Anhydride and Polycyclic Hydrocarbons, *J. Am. Chem. Soc.*, 1938, **60**, 481-485.

- 68 O. C. Dermer and J. King, Purification of Anthracene, *J. Am. Chem. Soc.*, 1941, **63**, 3232.
- 69 D. P. Dolata and R. Bergmann, Acceleration of a Diels-Alder Reaction in an Ultracentrifuge, *Tetrahedron Lett.*, 1987, **28**, 707-708.
- 70 J. Berlan, P. Giboreau, S. Lefeuvre and C. Marchand, Synthèse Organique sous Champ Microondes: Premier Exemple D'activation Spécifique en Phase Homogène, *Tetrahedron Lett.*, 1991, **32**, 2363-2366.
- 71 R. Breslow and C. J. Rizzo, Chaotropic Salt Effects in a Hydrophobically Accelerated Diels-Alder Reaction, *J. Am. Chem. Soc.*, 1991, **113**, 4340-4341.
- 72 M. A. Forman and W. P. Dailey, The Lithium Perchlorate-Diethyl Ether Rate Acceleration of the Diels-Alder Reaction: Lewis Acid Catalysis by Lithium Ion, *J. Am. Chem. Soc.*, 1991, **113**, 2761-2762.
- 73 V. V. Veselovsky, A. S. Gybin, A. V. Lozanova, A. M. Moiseenkov, W. A. Smit and R. Caple, Dramatic Acceleration of the Diels-Alder Reaction by Adsorption on Chromatography Adsorbents, *Tetrahedron Lett.*, 1988, **29**, 175-178.
- 74 L. Bauld, D. J. Bellville, R. Pabon, R. Chelsky and G. Green, Theory of Cation-Radical Pericyclic Reactions, *J. Am. Chem. Soc.*, 1983, **105**, 2378-2382.
- 75 B. E. Noltingk and E. A. Neppiras, Cavitation Produced by Ultrasonics, *Proc. Phys. Soc. B. (Lond.)*, 1950, **63B**, 674-685.
- 76 P. A. Grieco, P. Garner and Z. He, Micellar Catalysis in the Aqueous Intermolecular Diels-Alder Reaction: Rate Acceleration and Enhanced Selectivity, *Tetrahedron Lett.*, 1983, **24**, 1897-1900.
- J. Elguero, P. Guoya, J. Paez, C. Cativiela and J. Mayorol, Study of the Influence of Ultrasound and Aqueous Solvent on the Diels-Alder Reaction: The Case of Cyclopentadiene and Acetamidoacrylates, *Synth. Commun.*, 1989, **19**, 473-476.
- 77 J-L. Luche, C. Einhorn, J. Einhorn and J. V. Sinisterra-Gago, Organic Sonochemistry: A New Interpretation and its Consequences, *Tetrahedron Lett.*, 1990, **31**, 4125-4128.
- C. Einhorn, J. Einhorn, M. J. Dickens and J-L. Luche, Organic Sonochemistry – Some Illustrative Examples of a New Fundamental Approach, *Tetrahedron Lett.*, 1990, **31**, 4129-4130.
- M. J. Dickens and J-L. Luche, Further Evidence for the Effect of Ultrasonic Waves on Electron Transfer Processes - The Case of the Kornblum-Russell Reaction, *Tetrahedron Lett.*, 1991, **32**, 4709-4712.

- 78 M. Haiza, J. Lee and J. K. Snyder, Asymmetric Syntheses of Saliva Miltiorrhiza Abietanoid *o*-Quinones: Methyl Tanshinonate, Tanshinone IIB, Tanshindiol B and 3-Hydroxytanshinone, *J. Org. Chem.*, 1990, **55**, 5008-5016.
- A. Bourgeois-Cury and J. Goré, Reaction de Diels-Alder en Phase Aqueuse derives du 2,5-diméthylpyrrole, *Bull. Soc. Chim. Fr.*, 1992, **129**, 490-495.
- 79 J. Lee and J. K. Snyder, Ultrasound-Promoted Cycloadditions in the Synthesis of Saliva Miltiorrhiza Abietanoid *o*-Quinones, *J. Org. Chem.*, 1990, **55**, 4995-5008.
- J. Lee and J. K. Snyder, Ultrasound-Promoted Diels-Alder Reactions: Syntheses of Tanshinone IIA, Nortanshinone and ( $\pm$ )-Tanshindiol B, *J. Am. Chem. Soc.*, 1989, **111**, 1522-1524.
- J. Lee, H. S. Mei and J. K. Snyder, Synthesis of Miltirone by an Ultrasound-Promoted Cycloaddition, *J. Org. Chem.*, 1990, **55**, 5013-5016.
- 80 M. Villacampa, J. M. Perez, C. Avendano and J. C. Menedez, Ultrasound Assisted Diels-Alder Reactions of 1-Azadienes with "Normal" Electronic Demand, *Tetrahedron*, 1994, **50**, 10047-10054.
- 81 C. M. Low, 'Current Trends in Sonochemistry' (Ed. Price, G. J.) Royal Society of Chemistry Cambridge 1992, 66.
- 82 P. Nebois, Z. Bouaziz, H. Fillion, L. Moeini, M. J. Aurell Piquer, J-L. Luche, A. Riera, A. Moyano and M. A. Pericàs, The Diels-Alder Cycloaddition, an intriguing Problem in Organic Sonochemistry, *Ultrasonics Sonochemistry*, 1996, **3**, 7-13.
- 83 L. Da Cunha, and B. Garrigues, Une Nouvelle Étude sur la Reaction de Diels-Alder Entre L'Anthracene et L'Ahydride Maleique sous Ultrasons, *Bull. Soc. Chim. Belg.*, 1997, **12**, 817-823.
- 84 W. F. K. Wynne-Jones and H. Eyring, The Absolute Rate of Reactions in Condensed Phases, *J. Chem. Phys.*, 1935, **3**, 492-502.
- 85 E. D. Hughes, Mechanism of Substitution at a Saturated Carbon Atom. Part V. Hydrolysis of *tert*-Butyl Chloride, *J. Chem. Soc.*, 1935, 255-258.
- 86 D. J. Raber, R. C. Bingham, J. M. Harris, J. L. Fry and P. v. R. Schleyer, The Role of the Solvent in the Solvolysis of *t*-Alkyl Halides, *J. Am. Chem. Soc.*, 1970, **92**, 5977-5981.
- 87 D. N. Kevill, K. C. Kolwyck, and F. L. Weitzl, Correlation of Solvolysis Rates of 1-Adamantyl *p*-Toluenesulfonate, *J. Am. Chem. Soc.*, 1970, **92**, 7300-7306.
- 88 T. W. Bentley and P. v. R. Schleyer, The S<sub>N</sub>2-S<sub>N</sub>1 Spectrum. 1. Role of Nucleophilic Solvent Assistance and Nucleophilicity Solvated Ion Pair Intermediates in Solvolyses of Primary and Secondary Arenesulfonates, *J. Am. Chem. Soc.*, 1976, **98**, 7685-7666.

- 
- 89 M. H. Abraham, R. W. Taft, and M. J. Kamlet, Linear Solvation Energy Relationships. 15. Heterolytic Decomposition of the *tert*-Butyl Halides, *J. Org. Chem.*, 1981, **46**, 3053-3056.
- 90 M. J. Blandamer, J. M. W. Scott and R.E. Robertson, Solvolysis Revisited, *Prog. Phys. Org. Chem.*, 1985, **15**, 149-196.
- 91 M. J. Blandamer, J. Burgess, P. P. Duce, M.C.R. Symons, R.E. Robertson and J. W. M. Scott, Two-Stage Mechanism for the Solvolysis of *t*-Butyl Chloride in Aqueous Solutions, *J. Chem. Res. (S)*, 1982, 130.
- 92 I. M. Strauss and M. C. R. Symons, Low Temperature Infrared Spectroscopic Study of the Solvation of Ions in Water, *J. Chem. Soc., Faraday Trans. 1*, 1978, **74**, 2518-2529.
- 93 M. C. R. Symons, J. M. Harvey and S. E. Jackson, Spectroscopic Studies of Water-Aprotic-Solvent Interactions in the Water-Rich Region, *J. Chem. Soc., Faraday Trans. 1*, 1980, **76**, 256-265.
- 94 E. M. Arnett and C. Petro, Stabilities of Carbonium Ions in Solution. 8. Heats of Ionisation of some Simple Alkyl Halides in Superacidic Media, *J. Am. Chem. Soc.*, 1978, **100**, 5408-5416.
- 95 G. A. Olah and J. Lukas, Stable Carbonium Ions. XLVII. Alkylcarbonium Ion Formation from Alkanes via Hydride (Alkide) Ion Abstraction in Fluorosulfonic Acid-Antimony Pentafluoride-Sulfuryl Chlorofluoride Solution, *J. Am. Chem. Soc.*, 1967, **89**, 4739-4744.
- 96 R. A. McClelland, V. M. Kanagasabapathy and S. Streenken, Nanosecond Laser Flash Photolytic Generation and Lifetimes in Solvolytic Media of Diarylmethyl and *p*-Methoxyphenethyl Cations, *J. Am. Chem. Soc.*, 1988, **110**, 6913-6914.
- 97 R. N. Young, Spectroscopy of Carbanions and Carbocations, *Prog. Nucl. Magn. Reson. Spec.*, 1979, **12**, 261-286.
- 98 A. H. Fainberg and S. Winstein, Correlation Rates. III. *t*-Butyl Chloride in a Wide Range of Solvent Mixtures, *J. Am. Chem. Soc.*, 1956, **78**, 2770-2777.
- 99 S. Winstein and A. H. Fainberg, Correlation Rates. IV. Solvent Effects on Enthalpy and Entropy of Activation for the Solvolysis of *t*-Butyl Chloride, *J. Am. Chem. Soc.*, 1957, **79**, 5937-5950.
- 100 R. E. Robertson and S E Sougamori, Heat Capacity Changes Associated with the Solvolysis of *t*-Butyl Chloride in Binary Alcohol-Water Systems, *J. Am. Chem. Soc.*, 1969, **91**, 7254-7259.

- 
- 101 R. E. Robertson and S E Sougamori, The Hydrolysis of *t*-Butyl Chloride in Aquo-Organic Mixtures: Heat Capacity of Activation and Solvent Structure, *Can. J. Chem. Soc.*, 1972, **50**, 1353-1360.
- 102 V. A. Mikhailov, Changes of Structure in Aqueous Solutions of Nanoelectrolytes, *J. Struct. Chem.*, 1961, **2**, 625-628.
- 103 A. G. Mitchell and W. F. K. Wynne-Jones, Thermodynamic and Other Properties of Solutions Involving Hydrogen Bonding, *Disc. Faraday Soc.*, 1953, **15**, 161-168.
- 104 M. J. Blandamer, M. C. R. Symons and M. J. Wooten, Solvation Spectra, *Trans. Faraday Soc.*, 1967, **63**, 2337-2341.
- 105 E. M. Arnett, W. G. Bentrude, J. J. Burke and P. McC. Duggleby, Solvent Effects in Organic Chemistry. V. Molecules, Ions and Transition States in Aqueous Ethanol, *J. Am. Chem. Soc.*, 1965, **87**, 1541-1553.
- 106 E. M. Arnett, W. G. Bentrude and P. McC. Duggleby, Salt-Like Behaviour of the *t*-Butyl Chloride Solvolysis Transition State, *J. Am. Chem. Soc.*, 1965, **87**, 2048-2050.
- 107 J. A. V. Butler, The Energy and Entropy of Hydration of Organic Compounds, *Trans. Faraday Soc.*, 1937, **33**, 229-238.
- 108 E. Grunwald and S. Winstein, The Correlation of Solvolysis Rates, *J. Am. Chem. Soc.*, 1948, **70**, 846-854.
- 109 S. Winstein, E. Grunwald and H. W. Jones, The Correlation of Solvolysis Rates and the Classification of Solvolysis Reactions into Mechanistic Categories, *J. Am. Chem. Soc.*, 1951, **73**, 2700-2707.
- 110 S. G. Smith, A. H. Fainberg and S. Winstein, Correlation of Solvolysis Rates. IX. *p*-Methoxyneophyl Toluene-sulfonate in a Variety of Solvents. Ionising Power of Hydroxylic and Non-hydroxylic Solvents, *J. Am. Chem. Soc.*, 1961, **83**, 618-625.
- 111 H. S. Franks and W. Y. Wen, Structural Aspects of Ion-Solvent Interaction in Aqueous Solutions: A Suggested Picture of Water Structure, *Disc. Faraday Soc.*, 1957, **24**, 133-140.
- 112 D. Eisenberg and W. Kauzmann, "The Structure and Properties of Water". Oxford University Press, Oxford, 1969.
- 113 M. J. Blandamer, "Introduction to Chemical Ultrasonics", Academic Press, New York, 1973, 109.
- 114 T. J. Mason, J. P. Lorimer and B. P. Mistry, The Effect of Ultrasound on the Solvolysis of 2-Chloro-2-Methylpropane in Aqueous Alcoholic Media, *Tetrahedron Lett.*, 1982, **23**, 5363-5364.



- 
- 115 T. J. Mason, J. P. Lorimer and B. P. Mistry, The Effect of Temperature on the Ultrasonically Enhanced Reaction Rates of the 2-Chloro-2-Methylpropane in Aqueous Ethanol Mixtures, *Tetrahedron Lett.*, 1983, **24**, 4371-4372.
- 116 T. J. Mason, J. P. Lorimer and B. P. Mistry, The Effect of Ultrasound on the Solvolysis of 2-Chloro-2-Methylpropane in Aqueous Ethanol, *Tetrahedron Lett.*, 1985, **41**, 5201-5204.
- 117 T. J. Mason, J. P. Lorimer and B. P. Mistry, Observations on the Heat Capacity of Activation ( $\Delta C_p^\ddagger$ ) for the Ultrasonically Enhanced Solvolyses of 2-Chloro-2-Methylpropane in Aqueous Ethanol Mixtures, *J. Chem. Soc., Chem. Commun.*, 1986, **8**, 611-612.
- 118 C. J. Burton, A Study of Ultrasonic Velocity and Absorption in Liquid Mixtures, *J. Acoust. Soc. Amer.*, 1948, **20**, 186-199.
- 119 J. Hore, A New Method for Water Suppression in the Proton NMR Spectra of Aqueous Solutions, *J. Magn. Res.*, 1983, **54**, 539-542.
- 120 The suggested concentration referred to may be found in T. J. Mason, "Sonochemistry", Oxford Chemistry Primers, Oxford University Press, 1999, 36.
- 121 A. Weekes, "Design and Construction of an Ultrasonic Probe for use in a Cryomagnet NMR Spectrometer", Aston University, Aston Birmingham B4 7ET, 1998.
- 122 M. Beevers, "Linear Regression Analysis", Aston University, Aston Birmingham B4 7ET, 1995.
- 123 D. A. Skoog and J. J. Leary, "Principles of Instrumental Analysis" Saunders College Publishing, 1992, 278.
- 124 J. C. Lindon and A. G. Ferrige, Digitisation and Data Processing in Fourier Transform NMR, *Prog. NMR Spectrosc.*, 1980, **14**, 49.
- 125 Reproduced from L. Stryer, "Biochemistry", W. H. Freeman and Co., 1988, 203.
- 126 Reproduced from T. W. G. Solomons, "Organic Chemistry", 5<sup>th</sup> Ed., John Wiley and Sons Inc., 1992, 1126.